



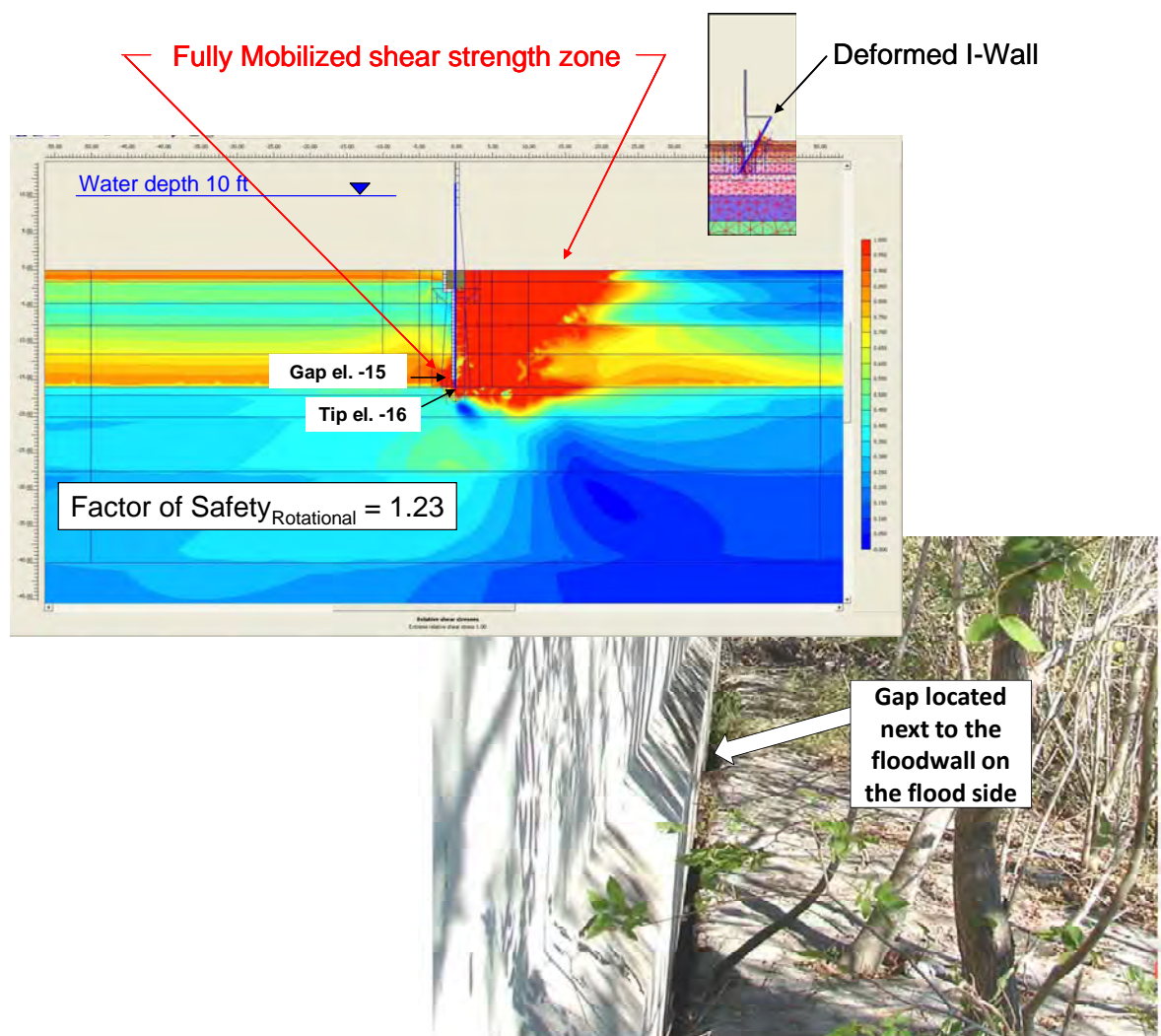
**US Army Corps
of Engineers®**
Engineer Research and
Development Center

Flood and Coastal Storm Damage Reduction Program

Complete Soil-Structure Interaction (SSI) Analyses of I-walls Embedded in Level Ground During Flood Loading

Michael E. Pace, Kevin Abraham, and Robert M. Ebeling

September 2012



Complete Soil-Structure Interaction Analyses of I-walls Embedded in Level Ground During Flood Loading

Michael E. Pace, Kevin Abraham, and Robert M. Ebeling

*Information Technology Laboratory
U.S. Army Engineer Research and Development Center
3909 Halls Ferry Road
Vicksburg, MS 39180-6199*

Final report

Approved for public release; distribution is unlimited.

Prepared for U.S. Army Corps of Engineers
Washington, DC 20314-1000

Under Work Unit L04956

Abstract

This report extends the 2007 investigation of I-wall performance during flood loading to I-walls located in regions of the United States outside New Orleans, Louisiana. Specifically, this study investigates I-walls embedded in level ground consisting of four different soils that are stronger and stiffer than the fine-grained New Orleans soils that were inspected during the 2007 Interagency Performance Evaluation Task Force (IPET) study. A focus of the study summarized in this report is the investigation of the development of a zone of separation along the flood side of the soil-to-I-wall interface. The effects of this zone of separation on the resulting deformation and stress conditions in the soil regime on both the flood side and landside of the I-wall system were then examined. This study is restricted to level soil floodwall sites. The landside is referred to as the protected side in some figures in this report.

This investigation relies on a complete soil-structure interaction (SSI) method of analysis. In this procedure, the soil foundation, I-wall, and interface between the I-wall and the soil (on both sides of the I-wall) all are modeled using finite elements; both the soil and interface properties are modeled as nonlinear materials; and flood loadings are incrementally raised to the design flood pool elevation. A hydraulic fracturing criterion is applied to determine if a gap develops on the flood side of the I-wall and if it propagates down the soil-to-I-wall interface during the incremental flood loadings.

Soil stresses, the level of mobilized shear strength, gap depth, I-wall deflections, shear forces, and bending moments internal to the sheet piling are computed in the complete SSI analyses at the incremental flood elevations.

Results presented in this report will be used to prepare a U.S. Army Corps of Engineers (USACE) guidance document for flood I-walls.

DISCLAIMER: The contents of this report are not to be used for advertising, publication, or promotional purposes. Citation of trade names does not constitute an official endorsement or approval of the use of such commercial products. All product names and trademarks cited are the property of their respective owners. The findings of this report are not to be construed as an official Department of the Army position unless so designated by other authorized documents.

DESTROY THIS REPORT WHEN NO LONGER NEEDED. DO NOT RETURN IT TO THE ORIGINATOR.

Contents

Abstract.....	ii
Figures and Tables.....	vii
Preface.....	xx
Unit Conversion Factors.....	xxi
1 Description of the Complete Soil-Structure Interaction (SSI) Analyses of Flood I-walls Embedded in Level Ground.....	1
1.1 Introduction.....	1
1.2 Terminology.....	2
1.3 Phase III: Research and development in support of USACE guidance document.....	3
1.4 The complete SSI method of analysis used in this research study	3
1.5 Gap initiation and propagation used in the complete SSI analyses.....	4
1.6 Report content.....	4
2 Analyses of I-wall Site Founded in an Overconsolidated Lean Clay	8
2.1 Purpose of analyses	8
2.2 Overview of flood-site I-wall being analyzed.....	8
2.3 Shear strength and conventional design of cantilever I-wall	9
2.4 Shear strength and stiffness properties used in the complete SSI analysis	14
2.5 Discussion of finite element analyses.....	19
2.5.1 Conceptual model	19
2.5.2 Gap initiation and propagation criterion.....	20
2.5.3 Finite element model	20
2.6 Results of the finite element analyses	22
2.6.1 Initial stresses	22
2.6.2 Gap initiation and propagation results	24
2.6.3 Performance of interface elements	24
2.6.4 Discussion of displacements and stresses	25
3 Analyses of I-Wall Site Founded in Clay with High Plasticity	33
3.1 Purpose of analyses	33
3.2 Overview of problem analyzed.....	33
3.3 Conventional design of cantilever I-wall	37
3.3.1 Modeling a total stress problem in CWALSHT with consideration of a gap.....	37
3.3.2 Computation of active and passive earth pressures	38
3.3.3 Criteria for gap initiation and propagation	39
3.3.4 Material properties for use with CWALSHT.....	40
3.3.5 Computed gap depth	42
3.3.6 CWALSHT design results.....	42

3.4	PLAXIS finite element analyses	44
3.4.1	Conceptual model	44
3.4.2	Finite element mesh	45
3.4.3	Total stress analysis procedure in PLAXIS.....	45
3.4.4	Tracking the progression of the gap	47
3.4.5	Shear strength and stiffness properties used in the finite element analyses	48
3.4.6	Initial stresses	54
3.4.7	Performance of interface elements	55
3.4.8	Comparison of HS and MC models	55
3.4.9	Progression of gap propagation for MC model analyses	56
3.4.10	Sheet-pile wall displacements for MC model.....	58
3.4.11	Total displacements of finite element mesh for maximum water condition.....	63
3.4.12	Moments in sheet-pile wall for MC model.....	65
3.4.13	Shear stresses in soil for MC model.....	65
3.4.14	Horizontal earth pressures for MC model.....	68
3.4.15	Comparison of finite element analysis results to conventional analysis results and field measurements	75
4	Analyses of I-wall Site Founded on a Clay with Undrained Shear Strength (S_u) of 300 psf.....	77
4.1	Purpose of analyses	77
4.2	Overview of problem analyzed	77
4.3	Conventional design of cantilever I-wall	79
4.3.1	Modeling a total stress problem in CWALSHT with consideration of a gap.....	79
4.3.2	Computation of active and passive earth pressures	79
4.3.3	Criteria for gap initiation and propagation	81
4.3.4	Material properties for use with CWALSHT.....	83
4.3.5	Computed gap depth	83
4.3.6	CWALSHT design results.....	84
4.3.7	CWALSHT design moments and selection of sheet-pile section	86
4.4	PLAXIS finite element analyses	87
4.4.1	Conceptual model	87
4.4.2	Finite element mesh	87
4.4.3	Total stress analysis procedure in PLAXIS.....	89
4.4.4	Tracking the progression of the gap	90
4.4.5	Shear strength and stiffness properties used in the finite element analyses	91
4.4.6	Initial stresses	95
4.4.7	Performance of interface elements	95
4.4.8	Comparison of HS and MC models	96
4.4.9	Progression of the gap for MC analyses	100
4.4.10	Sheet-pile wall displacements for MC model.....	100
4.4.11	Total displacements of finite element mesh for maximum water condition.....	107
4.4.12	Moments in sheet-pile wall for MC model.....	107
4.4.13	Shear stresses in soil for MC model.....	110
4.4.14	Horizontal earth pressures for MC model.....	110
4.5	Final observations and conclusions for the finite element analyses	118

5	Analyses of I-wall Site Founded on a Silt of Low Plasticity	121
5.1	Purpose of analyses	121
5.2	Overview of problem analyzed	121
5.3	Shear strength and stiffness properties used in the finite element analyses	123
5.4	Material properties governing transient seepage	124
5.5	Conventional design of cantilever I-wall	130
5.6	Discussion of loading	135
5.7	Discussion of finite element analyses	136
5.7.1	<i>Conceptual model</i>	136
5.7.2	<i>Finite element mesh</i>	137
5.7.3	<i>Three-stage analysis procedure</i>	137
5.8	Results of the finite element analyses	140
5.8.1	<i>Gap progression</i>	140
5.8.2	<i>Performance of interface elements</i>	140
5.8.3	<i>Comparison of pore pressures for low and high permeabilities</i>	142
5.8.4	<i>Discussion of stresses and displacements</i>	149
6	Initial Investigation of the Effects of Geometry on I-wall Performance	153
6.1	Purpose of the analyses	153
6.2	Overview of flood-site I-wall being analyzed	153
6.3	Shear strength and stiffness values used in the analysis	155
6.4	Shear strength and stiffness properties used in the complete SSI analysis	159
6.5	Discussion of finite element analyses	162
6.5.1	<i>Finite element model</i>	162
6.5.2	<i>Gap initiation and propagation criterion</i>	163
6.6	Results of the finite element analyses	163
6.6.1	<i>Initial stresses</i>	163
6.6.2	<i>Gap initiation and propagation results</i>	165
6.6.3	<i>Discussion of displacements and stresses</i>	166
7	Summary and Conclusions of the Complete Soil-Structure Interaction (SSI)	
	Analyses of Flood I-walls Embedded in Level Ground	173
7.1	Summary	173
7.1.1	<i>Level ground</i>	173
7.1.2	<i>Influence of geometry on I-wall performance</i>	174
7.2	Conclusions	176
	References	178
	Appendix A: Analyses of I-wall Site Founded in an Overconsolidated Lean Clay Using	
	Minimum Values of Both Undrained Shear Strength (S_u) and Undrained Secant	
	Stiffness (E_u)	180
	Appendix B: Analyses of I-wall Site Founded in an Overconsolidated Lean Clay Using	
	Minimum Values of Undrained Shear Strength (S_u) and Maximum Values of	
	Undrained Secant Stiffness (E_u)	200

Appendix C: Analyses of I-wall Site Founded in an Overconsolidated Lean Clay Using Maximum Values of Undrained Shear Strength (S_u) and Minimum Values of Undrained Secant Stiffness (E_u)	220
Appendix D: Analyses of I-wall Site Founded in an Overconsolidated Lean Clay Using Maximum Values of Undrained Shear Strength (S_u) and Maximum Values of Undrained Secant Stiffness (E_u)	241
Appendix E: Analyses of E-99 Sheet-pile Wall Field Load Test Using Minimum Values of Both Undrained Shear Strength (S_u) and Undrained Secant Stiffness (E_u)	261
Appendix F: Analyses of E-99 Sheet-pile Wall Field Load Test Using Minimum Values of Undrained Shear Strength (S_u) and Maximum Values of Undrained Secant Stiffness (E_u).....	282
Appendix G: Analyses of E-99 Sheet-pile Wall Field Load Test Using Maximum Values of Undrained Shear Strength (S_u) and Minimum Values of Undrained Secant Stiffness (E_u).....	303
Appendix H: Analyses of E-99 Sheet-pile Wall Field Load Test Using Maximum Values of Undrained Shear Strength (S_u) and Maximum Values of Undrained Secant Stiffness (E_u).....	325
Appendix I: Notation	346
Report Documentation Page	

Figures and Tables

Figures

Figure 1.1. I-wall failures in London Canal during Hurricane Katrina.....	1
Figure 1.2. Development of a zone of separation between the I-wall and the soil interface on the flood side of the I-wall following Hurricane Katrina.....	2
Figure 2.1. Geometry of the problem.	9
Figure 2.2. USCS plasticity chart for fine-grained soils. CL, clay with low plasticity; ML, silt with low plasticity; CH, clay of high plasticity; MH, silt of high plasticity; OL, organic silt, organic clay (LL < 50%); and OH, organic silt, organic clay (LL ≥ 50%).....	9
Figure 2.3. OCR variation with depth for Tell City site.	12
Figure 2.4. Variation in undrained shear strength with depth.	13
Figure 2.5. Estimation of E_{us} for clay (Duncan and Bursey 2007).....	16
Figure 2.6. Conceptual model.....	19
Figure 2.7. Gap propagation beside I-wall.....	21
Figure 2.8. Two-dimensional cross-section model used in the SSI analyses.	21
Figure 2.9. Finite element mesh used in the analyses.....	22
Figure 2.10. Enlarged view of finite element mesh around the I-wall.	22
Figure 2.11. Fraction of mobilized shear strength for initial conditions.....	23
Figure 2.12. Progression of gap versus water elevation.	25
Figure 2.13. Behavior of interface versus soil elements at flood el 2 ft.	25
Figure 2.14. Total exaggerated displacements for a water elevation of 9 ft and gap elevation of -15 ft.	26
Figure 2.15. Horizontal sheet-pile deflection versus water elevation.	27
Figure 2.16. Relative horizontal sheet-pile deflection at the ground surface el 0 ft versus water elevation.	27
Figure 2.17. Comparison of total normal stresses on the interface elements adjacent to the wall on the flood side and landside for flood el 6 ft and gap el -15 ft.....	29
Figure 2.18. Comparison of total normal stresses on the interface elements adjacent to the wall on the flood side and landside for flood el 9 ft and gap el -15 ft.....	29
Figure 2.19. Comparison of total normal stresses on the interface elements adjacent to the wall on the flood side and landside for flood el 10 ft and gap el -15 ft.....	30
Figure 2.20. Fraction of mobilized shear strength at various loading phases.	31
Figure 2.21. Rotational factor of safety using Φ/c reduction for peak flood elevation of 10 ft.	32
Figure 3.1. Soil geometry of E-99 field load test).	34
Figure 3.2. Idealized problem geometry.	34
Figure 3.3. Location of instrumented sections of I-wall).	35
Figure 3.4. USCS plasticity chart for fine-grained soils.....	36
Figure 3.5. Equivalent CWALSHT model to account for gap.	38

Figure 3.6. Soil layering and design strengths assumed for the E-99 field load test.....	41
Figure 3.7. Conceptual model.	45
Figure 3.8. Finite element mesh used in the analyses.....	46
Figure 3.9. Enlargement of finite element mesh around the I-wall.....	46
Figure 3.10. Location and propagation of gap beside I-wall.	47
Figure 3.11. Soil layering and material numbers used in the finite element analyses.	49
Figure 3.12. Variation of horizontal displacement of top of pile with K	53
Figure 3.13. Variation of relative horizontal displacement of top of pile with K	53
Figure 3.14. Behavior of interface versus soil elements for water el 14.5 ft and gap el -10 ft	55
Figure 3.15. Comparison of normal pressures for the HS and MC models.	57
Figure 3.16. Comparison of the deflections of the sheet-pile wall for the HS and MC models.....	57
Figure 3.17. Comparison of the moments in the sheet-pile wall for the HS and MC models.	58
Figure 3.18. Comparison of mobilized shear strength for the HS and MC models for water el 14.5 ft and gap tip el -10 ft.	59
Figure 3.19. Progression of gap versus water elevation along flood side of I-wall.	60
Figure 3.20. Sheet-pile horizontal displacements for various water elevations.	60
Figure 3.21. Sheet-pile horizontal displacements around the tip of the sheet pile for various water elevations.....	61
Figure 3.22. Sheet-pile horizontal displacements for selected locations.....	62
Figure 3.23. Relative horizontal displacements of the sheet pile at the ground surface.	62
Figure 3.24. Total displacements for a water elevation of 16.5 ft and a gap tip elevation of -11 ft.	63
Figure 3.25. Total displacements for a water elevation of 16.5 ft and a gap tip elevation of -11 ft, windowed view.....	64
Figure 3.26. Vectors of total incremental displacements showing the movement of the soil during the final increment of loading.	64
Figure 3.27. Vectors of total displacements showing the movement of the soil.....	65
Figure 3.28. Comparison of moments as various water elevations.....	66
Figure 3.29. Relative shear stress after placement of I-wall.	66
Figure 3.30. Relative shear stress for water at el 10.5 ft and gap tip elevation of 1 ft.....	67
Figure 3.31. Relative shear stress for the design conditions of a water elevation of 14.5 ft and gap tip elevation of -10 ft.	67
Figure 3.32. Relative shear stress for water at el 14.5 ft and gap tip elevation of -8 ft.....	68
Figure 3.33. Relative shear stress for water at el 16.5 ft and gap tip elevation of -11 ft.	69
Figure 3.34. Relative shear stress for water at el 17.5 ft and gap tip elevation of -12.5 ft.	69
Figure 3.35. Horizontal earth pressures for a water elevation of 10.5 ft and gap tip elevation of 1 ft.....	70
Figure 3.36. Horizontal earth pressures for a water elevation of 14.5 ft and gap tip elevation of -8 ft.....	70
Figure 3.37. Horizontal earth pressures for the design condition of a water elevation of 14.5 ft and gap tip elevation of -10 ft.	71

Figure 3.38. Horizontal earth pressures for a water elevation of 16.5 ft and gap tip elevation of -11 ft.	71
Figure 3.39. Horizontal earth pressures for a water elevation 17.5 ft and gap tip elevation of -12.5 ft.	72
Figure 3.40. Comparison of net earth pressures computed from limiting earth pressures and PLAXIS results for a water elevation of 16.5 ft.	72
Figure 3.41. Comparison of net earth pressures computed from limiting earth pressures and PLAXIS results for a water elevation of 17.5 ft.	73
Figure 4.1. Problem geometry.	78
Figure 4.2. USCS plasticity chart for fine-grained soils.	78
Figure 4.3. Equivalent CWALSHT model to account for gap.	80
Figure 4.4. Conceptual model.	88
Figure 4.5. Finite element mesh used in the analyses.	88
Figure 4.6. Enlargement of finite element mesh around the I-wall.	89
Figure 4.7. Location and propagation of gap beside I-wall.	90
Figure 4.8. Soil layering and material numbers used in the finite element analyses.	92
Figure 4.9. Behavior of interface versus soil elements for a water elevation at 9 ft and a gap elevation at -13 ft.	96
Figure 4.10. Full mobilization of shear strength on the landside of the wall due to a water elevation of 3 ft and a gap tip elevation of -11 ft.	97
Figure 4.11. Comparison of normal pressures for the HS and MC models.	98
Figure 4.12. Comparison of the deflections of the sheet-pile wall for the HS and MC models.	98
Figure 4.13. Comparison of the moments in the sheet-pile wall for the HS and MC models.	99
Figure 4.14. Comparison of mobilized shear strength for the HS and MC models for a water elevation of 9 ft and a gap tip elevation of -13 ft.	99
Figure 4.15. Progression of gap versus water elevation along flood side of I-wall.	101
Figure 4.16. Sheet-pile horizontal displacements for various water elevations.	101
Figure 4.17. Sheet-pile horizontal displacements around the tip of the sheet pile for various water elevations.	102
Figure 4.18. Sheet-pile horizontal displacements for selected locations.	103
Figure 4.19. Relative horizontal displacements of the sheet pile at the ground surface.	104
Figure 4.20. Sheet-pile horizontal displacements for various water elevations for an increased soil stiffness.	105
Figure 4.21. Sheet-pile horizontal displacements for selected locations for an increased soil stiffness.	106
Figure 4.22. Relative horizontal displacements of the sheet pile at the ground surface for an increased soil stiffness.	107
Figure 4.23. Total displacements for a water elevation of 13 ft and a gap tip elevation of 22 ft.	108
Figure 4.24. Enlarged view of total displacements for a water elevation of 13 ft and a gap tip elevation of 22 ft.	108
Figure 4.25. Vectors of total incremental displacements showing the movement of the soil during the final increment of loading.	109

Figure 4.26. Comparison of moments at various water elevations.	109
Figure 4.27. Relative shear stress after placement of I-wall.	111
Figure 4.28. Relative shear stress for water at el 4 ft and gap tip at el -15 ft.	111
Figure 4.29. Relative shear stress for the design conditions of water at el 9 ft and gap tip at el -13 ft.	112
Figure 4.30. Relative shear stress for water at el 9 ft and gap tip at el -18 ft.	112
Figure 4.31. Relative shear stress for water at el 13 ft and gap tip at el -22 ft.	113
Figure 4.32. Relative shear stress for water at el 13 ft and gap tip at el -22 ft for a Φ/c reduction analysis.	113
Figure 4.33. Horizontal earth pressures for water at el 4 ft and gap tip at el 15 ft.	114
Figure 4.34. Horizontal earth pressures for the design condition for water at el 9 ft and a gap tip at el 13 ft.	114
Figure 4.35. Horizontal earth pressures for water at el 9 ft and a gap tip at el -18 ft.	115
Figure 4.36. Horizontal earth pressures for water at el 12 ft and a gap tip at el -21 ft.	115
Figure 4.37. Horizontal earth pressures for water at el 13 ft and a gap tip at el -22 ft.	116
Figure 4.38. Comparison of net earth pressures computed from limiting earth pressures and PLAXIS results.	116
Figure 4.39. Horizontal earth pressures for water el 9 ft and gap tip el -13 ft.	119
Figure 4.40. Horizontal earth pressures for water el 13 ft and gap tip el -22 ft.	119
Figure 4.41. Relative of net earth pressures computed from limiting earth pressures and PLAXIS results for an increased soil stiffness.	120
Figure 5.1. Problem geometry.	122
Figure 5.2. USCS plasticity chart for fine-grained soils.	123
Figure 5.3. Relative permeability (k_r) versus the saturation.	128
Figure 5.4. Water coefficient of permeability (K_w) versus the matric suction head (ϕ_p) or the soil-water characteristic curve.	129
Figure 5.5. OCR variation with depth for ML-SM site with a 5-ft-thick crust.	132
Figure 5.6. Variation in undrained shear strength with depth for a 15-ft-deep water table.	133
Figure 5.7. Long-duration hydrograph, scaled for 9-ft pool, Mississippi River.	135
Figure 5.8. Conceptual model.	136
Figure 5.9. Gap propagation beside I-wall.	137
Figure 5.10. Finite element mesh used in the analyses.	138
Figure 5.11. Enlargement of finite element mesh around the I-wall.	138
Figure 5.12. Progression of gap versus water elevation along flood side of I-wall.	141
Figure 5.13. Behavior of interface versus soil elements.	141
Figure 5.14. Total head values for the case of $k_x = 1 \times 10^{-4}$ cm/sec at various times.	143
Figure 5.15. Saturation for water at el 4, gap at el -22, time equal to 60.7 days, $k_x = 1 \times 10^{-4}$ cm/sec.	144
Figure 5.16. Total head values at water el 4 ft, gap el -22 ft, 31 days, $k_x = 1 \times 10^{-5}$ cm/sec.	144
Figure 5.17. Total head values at water el 9 ft, gap el -32.5 ft, 105 days, $k_x = 1 \times 10^{-5}$ cm/sec.	145
Figure 5.18. Saturation for a water elevation of 9 ft, gap elevation of -32.5 ft, 105 days, and $k_x = 1 \times 10^{-5}$ cm/sec.	146

Figure 5.19. Comparison of total head on the flood side to the bounding initial and steady states for several times and associated water elevations.	146
Figure 5.20. Comparison of total head on the protected side (landside) to the bounding initial and steady states for several times and associated water elevations.	147
Figure 5.21. Comparison of total heads on the flood side to the drained and undrained conditions for water at el 9 ft.	148
Figure 5.22. Comparison of total heads on the protected side (landside) to the drained and undrained conditions for water at el 9 ft.	149
Figure 5.23. Normal effective stresses on the interface elements adjacent to the wall on the flood side and protected side (landside), 31 days.....	150
Figure 5.24. Normal effective stresses on the interface elements adjacent to the wall on the flood side and protected side (landside), 60.7 days.	150
Figure 5.25. Relative shear stress for a water elevation of 9 ft, gap elevation of -32.5 ft, 105 days, and $k_x = 1 \times 10^{-5}$ cm/sec.	151
Figure 5.26. Total displacements for a water elevation of 9 ft, gap elevation of -32.5 ft, 105 days, and $k_x = 1 \times 10^{-5}$ cm/sec.	152
Figure 5.27. Total horizontal pile displacements versus water elevations.....	152
Figure 6.1. Modified New Tiger Island geometry and initial water table elevation of the problem.	154
Figure 6.2. Variation in undrained shear strength (S_u) within the soil strata.	154
Figure 6.3. Sections used to estimate OCR and undrained stiffness variations.	158
Figure 6.4. Variation in OCR with depth at selected cross sections.....	160
Figure 6.5. Variation in undrained stiffness (E_u) with depth at different modified New Tiger Island I-wall sections.	161
Figure 6.6. PLAXIS finite element mesh of the I-wall, levee, and foundation.	163
Figure 6.7. Exaggerated displaced mesh plot at initial stress conditions.....	164
Figure 6.8. Fraction of relative shear stresses at initial conditions.....	165
Figure 6.9. Progression of gap versus water elevation.....	166
Figure 6.10. Exaggerated deformed mesh after flood elevation to 21.9 ft (top of I-wall), and the gap extends to pile tip (el 0.6 ft).	167
Figure 6.11. Displacement results versus flood elevations at three locations along the wall.	168
Figure 6.12. Relative horizontal displacement results versus flood elevations at the ground surface.	169
Figure 6.13. Horizontal displacement vectors after Phi/c reduction; computed factor of safety = 1.595, recall: (pile tip at el 0.6) $d/h = 2.0$	171
Figure 6.14. Incremental shear strains after Phi/c reduction.	171
Figure 6.15. Original New Tiger Island floodwall (pile tip at el -13 ft) $d/h = 4.0$; SlopeW results, FS = 1.68.....	172
Figure 6.16. UTexas4 slope stability results.	172
Figure 7.1. Summary of extent of gap propagation for level ground analyses and I-wall in levee analysis.....	175
Figure 7.2. Summary of mean analysis result of extent of gap propagation for level ground analyses and I-wall in levee analysis.	176
Figure A.1. Variation in minimum computed values of undrained shear strength (S_u) with depth.....	184

Figure A.2. Two-dimensional (2-D) cross-section model using minimum computed values of undrained shear strength (S_u) used in the SSI analyses.	189
Figure A.3. Fraction of mobilized shear strength for initial conditions using minimum computed values of undrained shear strength (S_u) and undrained stiffness (E_u).	190
Figure A.4. Progression of gap versus water elevation using minimum computed values of undrained shear strength (S_u) and undrained stiffness (E_u).	191
Figure A.5. Total exaggerated displacements for a water elevation of 9 ft and gap elevation of -15 ft using minimum computed values of undrained shear strength (S_u) and undrained stiffness (E_u).	192
Figure A.6. Horizontal sheet-pile deflection versus water elevation using minimum computed values of undrained shear strength (S_u) and undrained stiffness (E_u).	193
Figure A.7. Relative horizontal sheet-pile deflection at the ground surface el 0 ft versus water surface elevation using minimum computed values of undrained shear strength (S_u) and undrained stiffness (E_u).	194
Figure A.8. Comparison of total normal stresses on the interface elements adjacent to the wall on the flood side and protected side (landside) for flood 6 ft and gap el -15 ft using minimum computed values of undrained shear strength (S_u) and undrained stiffness (E_u).	196
Figure A.9. Comparison of total normal stresses on the interface elements adjacent to the wall on the flood side and protected side (landside) for flood el 9 ft and gap el -15 ft using minimum computed values of undrained shear strength (S_u) and undrained stiffness (E_u).	196
Figure A.10. Fractions of mobilized shear strength at various loading phases using minimum computed values of undrained shear strength (S_u) and undrained stiffness (E_u).	198
Figure A.11. Rotational factor of safety using Phi/c reduction for design peak flood elevation of 9 ft using minimum computed values of undrained shear strength (S_u) and undrained stiffness (E_u).	199
Figure B.1. Variation in minimum computed values of undrained shear strength (S_u) with depth.	204
Figure B.2. Two-dimensional (2-D) cross-section model using the minimum computed values of undrained shear strength (S_u) and maximum computed undrained secant stiffness (E_u) used in the SSI analyses.	209
Figure B.3. Fraction of mobilized shear strength for initial conditions using the minimum computed values of undrained shear strength (S_u) and the maximum computed values of undrained secant stiffness (E_u).	210
Figure B.4. Progression of gap versus water elevation using the minimum computed values of undrained shear strength (S_u) and the maximum computed values of undrained secant stiffness (E_u).	211
Figure B.5. Total exaggerated displacements for a water elevation of 9 ft and gap elevation of -15 ft using the minimum computed values of undrained shear strength (S_u) and the maximum computed values of undrained secant stiffness (E_u).	212
Figure B.6. Horizontal sheet-pile deflection versus water elevation using the minimum computed values of undrained shear strength (S_u) and the maximum computed values of undrained secant stiffness (E_u).	213
Figure B.7. Relative horizontal sheet-pile deflection at the ground surface el 0 ft versus water elevation using the minimum computed values of undrained shear strength (S_u) and the maximum computed values of undrained secant stiffness (E_u).	214
Figure B.8. Comparison of total normal stresses on the interface elements adjacent to the wall on the flood side and protected side (landside) for flood el 7 ft and gap el -15 ft	

using the minimum computed values of undrained shear strength (S_u) and the maximum computed values of undrained secant stiffness (E_u).	216
Figure B.9. Comparison of total normal stresses on the interface elements adjacent to the wall on the flood side and protected side (landside) for flood el 9 ft and gap el -15 ft using the minimum computed values of undrained shear strength (S_u) and the maximum computed values of undrained secant stiffness (E_u).	216
Figure B.10. Comparison of total normal stresses on the interface elements adjacent to the wall on the flood side and protected side (landside) for flood el 10 ft and gap el -15 ft using the minimum computed values of undrained shear strength (S_u) and the maximum computed values of undrained secant stiffness (E_u).	217
Figure B.11. Fraction of mobilized shear strength at various loading phases using minimum computed values of undrained shear strength (S_u) and the maximum computed values of undrained secant stiffness (E_u).	219
Figure B.12. Rotational factor of safety using Phi/c reduction for design peak flood elevation of 10 ft using minimum computed values of undrained shear strength (S_u) and the maximum computed values of undrained secant stiffness (E_u).	219
Figure C.1. Variation in maximum computed values of undrained shear strength (S_u) with depth.	224
Figure C.2. Two-dimensional (2-D) cross-section model using the maximum computed values of undrained shear strength (S_u) and minimum computed undrained secant stiffness (E_u) used in the SSI analyses.	229
Figure C.3. Fraction of mobilized shear strength for initial conditions using the maximum computed values of undrained shear strength (S_u) and the minimum computed values of undrained secant stiffness (E_u).	230
Figure C.4. Progression of gap versus water elevation using the maximum computed values of undrained shear strength (S_u) and the minimum computed values of undrained secant stiffness (E_u).	232
Figure C.5. Total exaggerated displacements for a water elevation of 9 ft and gap elevation of -15 ft using the maximum computed values of undrained shear strength (S_u) and the minimum computed values of undrained secant stiffness (E_u).	232
Figure C.6. Horizontal sheet-pile deflection versus water elevation using the maximum computed values of undrained shear strength (S_u) and the minimum computed values of undrained secant stiffness (E_u).	233
Figure C.7. Relative horizontal sheet-pile deflection at the ground surface el 0.0 versus water elevation using the maximum computed values of undrained shear strength (S_u) and the minimum computed values of undrained secant stiffness (E_u).	234
Figure C.8. Comparison of total normal stresses on the interface elements adjacent to the wall on the flood side and protected side (landside) for flood el 6 and gap el -15 using the maximum computed values of undrained shear strength (S_u) and the minimum computed values of undrained secant stiffness (E_u).	237
Figure C.9. Comparison of total normal stresses on the interface elements adjacent to the wall on the flood side and protected side (landside) for flood el 9 ft and gap el -15 ft using the maximum computed values of undrained shear strength (S_u) and the minimum computed values of undrained secant stiffness (E_u).	237
Figure C.10. Comparison of total normal stresses on the interface elements adjacent to the wall on the flood side and protected side (landside) for flood el 10 ft and gap el -15 ft using the maximum computed values of undrained shear strength (S_u) and the minimum computed values of undrained secant stiffness (E_u).	238

Figure C.11. Fraction of mobilized shear strength at various loading phases using maximum computed values of undrained shear strength (S_u) and the minimum computed values of undrained secant stiffness (E_u).....	239
Figure C.12. Rotational factor of safety using Phi/c reduction for design peak flood elevation of 10 ft using maximum computed values of undrained shear strength (S_u) and the minimum computed values of undrained secant stiffness (E_u).....	240
Figure D.1. Variation in maximum computed values of undrained shear strength (S_u) with depth.....	245
Figure D.2. Two-dimensional (2-D) cross-section model using the maximum computed values of undrained shear strength (S_u) and maximum computed undrained secant stiffness (E_u) used in the SSI analyses.....	250
Figure D.3. Fraction of mobilized shear strength for initial conditions using the maximum computed values of undrained shear strength (S_u) and the maximum computed values of undrained secant stiffness (E_u).	251
Figure D.4. Progression of gap versus water elevation using the maximum computed values of undrained shear strength (S_u) and the maximum computed values of undrained secant stiffness (E_u).	252
Figure D.5. Total exaggerated displacements for a water elevation of 9 ft and gap elevation of -15 ft using the maximum computed values of undrained shear strength (S_u) and the maximum computed values of undrained secant stiffness (E_u).	253
Figure D.6. Horizontal sheet-pile deflection versus water elevation using the maximum computed values of undrained shear strength (S_u) and the maximum computed values of undrained secant stiffness (E_u).	254
Figure D.7. Relative horizontal sheet-pile deflection at the ground surface el 0 ft versus water elevation using the maximum computed values of undrained shear strength (S_u) and the maximum computed values of undrained secant stiffness (E_u).	255
Figure D.8. Comparison of total normal stresses on the interface elements adjacent to the wall on the flood side and protected side (landside)for flood el 9 ft and gap el -15 ft using the maximum computed values of undrained shear strength (S_u) and the maximum computed values of undrained secant stiffness (E_u).....	257
Figure D.9. Comparison of total normal stresses on the interface elements adjacent to the wall on the flood side and protected side (landside)for flood el 11 ft and gap el -15 ft using the maximum computed values of undrained shear strength (S_u) and the maximum computed values of undrained secant stiffness (E_u).....	257
Figure D.10. Fraction of mobilized shear strength at various loading phases using maximum computed values of undrained shear strength (S_u) and the maximum computed values of undrained secant stiffness (E_u).....	259
Figure D.11. Rotational factor of safety using Phi/c reduction for design peak flood elevation of 10 ft using maximum computed values of undrained shear strength (S_u) and the maximum computed values of undrained secant stiffness (E_u).	260
Figure E.1. Progression of gap versus water elevation along flood side of I-wall.	271
Figure E.2. Sheet-pile horizontal displacements for various water elevations.....	272
Figure E.3. Sheet-pile horizontal displacements for selected locations.	273
Figure E.4. Relative horizontal displacements of the sheet pile at the ground surface.....	273
Figure E.5. Total displacements for water el 14.5 ft and gap tip el -9 ft.	274
Figure E.6. Enlarged view of total displacements for water el 14.5 ft and gap tip el -9 ft.	275

Figure E.7. Vectors of total incremental displacements showing the movement of the soil during the final increment of loading.	275
Figure E.8. Vectors of total displacements showing the movement of the soil.....	276
Figure E.9. Comparison of moments at various water elevations.....	276
Figure E.10. Relative shear stress after placement of I-wall.	277
Figure E.11. Relative shear stress for water at el 10 ft and gap tip el 1.5 ft.....	278
Figure E.12. Relative shear stress for water at el 14.5 ft and gap tip el -9 ft.....	278
Figure E.13. Horizontal earth pressures for water el 10.5 ft and gap tip el 1.5 ft.....	279
Figure E.14. Horizontal earth pressures for water el 14.5 ft and gap tip el -9 ft.	279
Figure E.15. Comparison of net earth pressures computed from limiting earth pressures and PLAXIS results for water el 14.5 ft.....	280
Figure F.1. Progression of gap versus water elevation along flood side of I-wall.....	293
Figure F.2. Sheet-pile horizontal displacements for various water elevations.	293
Figure F.3. Sheet-pile horizontal displacements for selected locations.....	295
Figure F.4. Relative horizontal displacements of the sheet pile at the ground surface.	295
Figure F.5. Total displacements for water el 14.5 ft and gap tip el -9 ft.	296
Figure F.6. Enlarged view of total displacements for water el 14.5 ft and gap tip el -9 ft.	296
Figure F.7. Vectors of total incremental displacements showing the movement of the soil during the final increment of loading.	297
Figure F.8. Vectors of total displacements showing the movement of the soil.	297
Figure F.9. Comparison of moments at various water elevations.	298
Figure F.10. Relative shear stress after placement of I-wall.	299
Figure F.11. Relative shear stress for water at el 10.5 ft and gap tip at el 0 ft.....	299
Figure F.12. Relative shear stress for water at el 14.5 ft and gap tip at el -9 ft.....	300
Figure F.13. Horizontal earth pressures for water el 10.5 ft and gap tip el 0 ft.....	300
Figure F.14. Horizontal earth pressures for water el 14.5 ft and gap tip el -9 ft.	301
Figure F.15. Comparison of net earth pressures computed from limiting earth pressures and PLAXIS results for water el 14.5 ft.....	301
Figure G.1. Progression of gap versus water elevation along flood side of I-wall.....	314
Figure G.2. Sheet-pile horizontal displacements for various water elevations.	315
Figure G.3. Sheet-pile horizontal displacements for selected locations.....	316
Figure G.4. Relative horizontal displacements of the sheet pile at the ground surface.	317
Figure G.5. Total displacements for water el 22.5 ft and gap tip el -14.5 ft.....	318
Figure G.6. Enlarged view of total displacements for water el 22.5 ft and gap tip el -14.5 ft.	318
Figure G.7. Vectors of total incremental displacements showing the movement of the soil during the final increment of loading.	319
Figure G.8. Vectors of total displacements showing the movement of the soil.	319
Figure G.9. Comparison of moments at various water elevations.	320
Figure G.10. Relative shear stress after placement of I-wall.	321
Figure G.11. Relative shear stress for water at el 14.5 ft and gap tip el -9 ft.	321
Figure G.12. Relative shear stress for water at el 22.5 ft and gap tip el -14.5 ft.	322
Figure G.13. Horizontal earth pressures for water el 14.5 ft and gap tip el -9 ft.....	322

Figure G.14. Horizontal earth pressures for water el 22.5 ft and gap tip el -14.5 ft	323
Figure G.15. Comparison of net earth pressures computed from limiting earth pressures and PLAXIS results for water el 22.5 ft.	323
Figure H.1. Progression of gap versus water elevation along flood side of I-wall.....	335
Figure H.2. Sheet-pile horizontal displacements for various water elevations.	336
Figure H.3. Sheet-pile horizontal displacements for selected locations.....	338
Figure H.4. Relative horizontal displacements of the sheet pile at the ground surface.	338
Figure H.5. Total displacements for water el 22.5 ft and gap tip el -15 ft.	339
Figure H.6. Enlarged view of total displacements for a water elevation of 22.5 ft and a gap tip elevation of -15 ft.	339
Figure H.7. Vectors of total incremental displacements showing the movement of the soil during the final increment of loading.	340
Figure H.8. Vectors of total displacements showing the movement of the soil.	340
Figure H.9. Comparison of moments at various water elevations.	341
Figure H.10. Relative shear stress after placement of I-wall.	341
Figure H.11. Relative shear stress for water at el 14.5 ft and gap tip el -7 ft.	342
Figure H.12. Relative shear stress for water at el 22.5 ft and gap tip el -15 ft.....	342
Figure H.13. Horizontal earth pressures for water el 14.5 ft and gap tip el -7 ft.....	343
Figure H.14. Horizontal earth pressures for water el 22.5 ft and gap tip el -15 ft.....	344
Figure H.15. Comparison of net earth pressures computed from limiting earth pressures and PLAXIS results for water el 22.5 ft.	344

Tables

Table 1.1. Combinations of minimum and maximum undrained shear strength (S_u) and undrained secant stiffness (E_u) distributions analyzed for an overconsolidated lean clay	5
Table 1.2. Combinations of minimum and maximum undrained shear strength (S_u) and undrained secant stiffness (E_u) distributions analyzed, level ground clay, E-99 I-wall.....	6
Table 2.1. Computation of S_u variation with depth.	11
Table 2.2. Summary of CWALSHT design cases, 12-ft wall height, 9-ft water height.	14
Table 2.3. Computation of undrained secant modulus (E_{us}).....	17
Table 2.4. HS model strength and stiffness properties for the soil layers.....	18
Table 2.5. Selected interface friction values for the interface elements.....	18
Table 2.6. Properties of the concrete cap.....	18
Table 2.7. Properties of the plate elements representing the concrete I-wall.....	18
Table 2.8. Properties of the plate elements representing the sheet pile.	18
Table 2.9. Summary of at-rest coefficients used.	23
Table 2.10. Summary of relative horizontal displacements (U_x) of I-wall at the ground surface.....	28
Table 3.1. Material properties for analyses.	41
Table 3.2. Results of design computations using CWALSHT.....	43
Table 3.3. Type and number of elements used in the finite element mesh.....	47
Table 3.4. Strength and stiffness properties for the soil layers used in the hardening soil model.....	49

Table 3.5. Strength and stiffness properties for the soil layers used in the Mohr-Coulomb soil model.....	50
Table 3.6. Properties of the plate elements representing the sheet pile.	50
Table 3.7. Variation of displacements of the top of the pile with K	52
Table 3.8. Observed displacements of top of sheet pile and maximum moments.....	54
Table 3.9. Poisson's ratio and at-rest horizontal earth pressure coefficients used for analyses.	54
Table 3.10. Pile displacements for MC model.	61
Table 3.11. PLAXIS finite element results for various water elevations.	75
Table 3.12. CWALSHT results for various water elevations.....	75
Table 3.13. Measured field results for instrumented locations.....	76
Table 4.1. Material properties for analyses.	83
Table 4.2. Factor of safety for design of cantilever I-walls.....	85
Table 4.3. Results of design computations using CWALSHT.....	85
Table 4.4. Type and number of elements used in the finite element mesh.....	89
Table 4.5. Strength and stiffness properties for the soil layers used in the HS model.	92
Table 4.6. Strength and stiffness properties for the soil layers used in the MC soil model.....	94
Table 4.7. Strength and stiffness properties for the soil layers used in the MC soil model with increased E_{ref}	94
Table 4.8. Properties of the plate elements representing the sheet pile.	95
Table 4.9. Poisson's ratio and at-rest horizontal earth pressure coefficients used for analyses.	95
Table 4.10. Pile displacements for MC model.	103
Table 4.11. Pile displacements for MC model with increased soil stiffness.	105
Table 4.12. Increase in displacements due to a reduction in soil stiffness.	106
Table 5.1. Strength and stiffness properties for the soil layers using undrained soil with unsaturated unit weight 120 lb/ft ³ and saturated unit weight 125 lb/ft ³	124
Table 5.2. Selected interface friction values (ψ) for the interface elements.....	125
Table 5.3. Properties of the concrete wall.	125
Table 5.4. Properties of the plate elements representing the sheet pile.	125
Table 5.5. Range of permeabilities for soils.	125
Table 5.6. Permeabilities used in the analyses.....	126
Table 5.7. PLAXIS data sets for examination of van Genuchten properties.	127
Table 5.8. PLAXIS data sets for ML-SM material.	128
Table 5.9. Computation of S_u (DSS) for short-term (undrained) loading.....	133
Table 5.10. Summary of CWALSHT design cases, 12-ft wall height, 9-ft water height.	134
Table 6.1.a. Summary of variations of $E_{u(oc)}$; near free field on landside - Section AA.....	156
Table 6.1.b. Summary of variations of $E_{u(oc)}$; near landside toe - Section BB.....	156
Table 6.1.c. Summary of variations of $E_{u(oc)}$; near landside crest - Section CC.	156
Table 6.1.d. Summary of variations of $E_{u(oc)}$; near free field flood side - Section DD.....	157
Table 6.2. Comparison of shear strength (S_u) and stiffness values (E_u) for various New Orleans I-wall and levee sections.....	162

Table 6.3. Summary of relative horizontal displacements (U_x) of I-wall at the ground surface.	170
Table A.1. Computation of minimum (S_u) variation with depth.	182
Table A.2. Computation of minimum undrained secant modulus (E_{us}).	186
Table A.3. Minimum HS model strength and stiffness properties for the soil layers.	187
Table A.4. Summary of relative horizontal displacements (U_x) of I-wall at the ground surface using minimum computed values of undrained shear strength (S_u) and undrained stiffness (E_u).	194
Table A.5. Comparison of relative horizontal displacements of I-wall at the ground surface using both the B.E. and minimum values of undrained shear strength (S_u) and undrained stiffness (E_u).	195
Table B.1. Computation of minimum S_u variation with depth.	202
Table B.2. Computation of maximum undrained secant modulus (E_{us}).	206
Table B.3. Minimum HS model strength and maximum stiffness properties for the soil layers.	207
Table B.4. Summary of relative horizontal displacements (U_x) of I-wall at the ground surface using minimum computed values of undrained shear strength (S_u) and maximum computed values undrained secant stiffness (E_u).	214
Table B.5. Comparison of relative horizontal displacements of I-wall at the ground surface using both the best-estimate and minimum computed values of undrained shear strength (S_u) and maximum computed values undrained secant stiffness (E_u).	215
Table C.1. Computation of maximum S_u variation with depth.	222
Table C.2. Computation of minimum undrained secant modulus (E_{us}).	226
Table C.3. Maximum HS model strength and minimum stiffness properties for the soil layers.	227
Table C.4. Summary of relative horizontal displacements (U_x) of I-wall at the ground surface using maximum computed values of undrained shear strength (S_u) and minimum computed values undrained secant stiffness (E_u).	235
Table C.5. Comparison of relative horizontal displacements of I-wall at the ground surface using both the best estimate and maximum computed values of undrained shear strength (S_u) and minimum computed values undrained secant stiffness (E_u).	235
Table D.1. Computation of maximum S_u variation with depth.	243
Table D.2. Computation of maximum undrained secant modulus (E_{us}).	247
Table D.3. Maximum HS model strengths and maximum stiffness properties for the soil layers.	248
Table D.4. Summary of relative horizontal displacements (U_x) of I-wall at the ground surface using maximum computed values of undrained shear strength (S_u) and maximum computed values undrained secant stiffness (E_u).	255
Table D.5. Comparison of relative horizontal displacements of I-wall at the ground surface using both the B.E. and maximum computed values of undrained shear strength (S_u) and maximum computed values undrained secant stiffness (E_u).	256
Table E.1. Mean and standard deviation values for the clay layers.	263
Table E.2. Factors of safety for various multiples of the standard deviation.	264
Table E.3. Material properties for analyses.	265
Table E.4. Results of analysis computations using CWALSHT.	266

Table E.5. Strength and stiffness properties for the soil layers used in the MC soil model for the case of a minimum S_u and minimum E_{ref} .	269
Table E.6. Pile displacements for MC model.	272
Table F.1. Mean and standard deviation values for the clay layers.	284
Table F.2. Factors of safety for various multiples of the standard deviation.	286
Table F.3. Material properties for analyses.	286
Table F.4. Results of analysis computations using CWALSHT.	288
Table F.5. Strength and stiffness properties for the soil layers used in the MC soil model for the case of a minimum (S_u) and maximum (E_{ref}).	291
Table F.6. Pile displacements for MC model.	294
Table G.1. Mean and standard deviation values for the clay layers.	305
Table G.2. Factors of safety for various multiples of the standard deviation.	307
Table G.3. Material properties for analyses.	308
Table G.4. Results of analysis computations using CWALSHT.	309
Table G.5. Strength and stiffness properties for the soil layers used in the MC soil model for the case of a maximum (S_u) and minimum (E_{ref}).	312
Table G.6. Pile displacements for MC model.	315
Table H.1. Mean and standard deviation values for the clay layers.	327
Table H.2. Material properties for analyses.	328
Table H.3. Results of analysis computations using CWALSHT.	330
Table H.4. Strength and stiffness properties for the soil layers used in the MC soil model for the case of a maximum (S_u) and (E_{ref}).	333
Table H.5. Pile displacements for MC model.	336

Preface

The investigation reported herein was authorized by Headquarters, U.S. Army Corps of Engineers (HQUSACE), and was performed from January 2009 to September 2010 under the Water Resources Infrastructure Research Program. The HQUSACE Technical Monitor was Anjana Chudgar. The Technical Director for the Water Resources Infrastructure Research Program was Dr. Michael K. Sharp, U.S. Army Engineer Research and Development Center (ERDC), Geotechnical and Structures Laboratory (GSL). Dr. Maureen Corcoran, GSL, was Associate Technical Director. The research discussed in this report was led by Dr. Robert M. Ebeling, Computational Science and Engineering Division, Information Technology Laboratory (ITL), ERDC, under the general supervision of Dr. Reed L. Mosher, Director, ITL; Dr. Deborah F. Dent, Deputy Director, ITL; and Dr. Robert M. Wallace, Chief of the Computational Science and Engineering Division. The research was conducted and the report written by Michael E. Pace and Dr. Kevin Abraham, both of the ITL's Computational Analysis Branch, and Ebeling. Chris A. Merrill was Chief of the Computational Analysis Branch during this R&D effort.

The research described in this report was supplemented by results from a companion (2011-2012) study of the response of an I-wall embedded in a levee and subjected to flood loading. Funding for this complete SSI analysis was provided by Reliability Model for Major Rehabilitation. Final data reduction and writing of this report were funded by the Improving Flood Risk Management and Water Control Infrastructure Resiliency and Reliability Program under the Flood and Coastal Storm Damage Reduction (FCDR) Research and Development Program in the focus area titled I-wall Analysis. William Curtis was the Technical Director of the Coastal and Hydraulics Laboratory (CHL) for the FCDR program. The Program Manager for FCDR was Dr. Cary A. Talbot, CHL. Corcoran was the Program Manager for the Improving Flood Risk Management and Water Control Infrastructure Resiliency and Reliability Program.

Kent D. Hokens and Neil T. Schwanz, both of the USACE St. Paul District, and Chudgar were team members providing oversight and guidance for this research.

At the time of publication, Ken Pathak was Acting Deputy Director, ITL. COL Kevin J. Wilson was Commander and Executive Director of ERDC. Dr. Jeffery P. Holland was Director.

Unit Conversion Factors

Multiply	By	To Obtain
cubic inches	1.6387064 E-05	cubic meters
feet	0.3048	meters
foot-pounds force	1.355818	joules
inches	0.0254	meters
pounds (force) per foot	14.59390	newtons per meter
pounds (force) per square foot	47.88026	pascals
pounds (force) per square inch	6.894757	kilopascals
pounds (mass) per cubic foot	16.01846	kilograms per cubic meter
square inches	6.4516 E-04	square meters

1 Description of the Complete Soil-Structure Interaction (SSI) Analyses of Flood I-walls Embedded in Level Ground

1.1 Introduction

On August 29, 2005, Hurricane Katrina came ashore in the New Orleans, Louisiana, area, causing severe flooding of significant sections of the city and its surrounding communities. Some of the levees containing I-walls suffered failures at flood pools lower than their design height. Early on in the post-Katrina investigations by the U.S. Army Corps of Engineers (USACE) of these flood retention systems, it was recognized that a contributing factor to I-wall failures (an example of one is shown in Figure 1.1) was the development of a zone of separation that can develop between the I-wall and the soil interface on the flood side of the I-wall. This phenomenon is illustrated in Figure 1.2. The Interagency Performance Evaluation Task Force (IPETF) study (IPETF 2007) summarizes the results of the investigation of this behavior as well as the overall performance of representative I-walls embedded in New Orleans levees during Hurricane Katrina.



Figure 1.1. I-wall failures in London Canal during Hurricane Katrina.



Figure 1.2. Development of a zone of separation between the I-wall and the soil interface on the flood side of the I-wall following Hurricane Katrina.

This report extends the IPET (2007) investigation of I-wall performance during flood loading to I-walls located in regions of the United States outside New Orleans. Specifically, this study investigates I-walls embedded in level ground consisting of soils with different strength properties (overconsolidated lean clay, clay of high plasticity, clay with constant undrained shear strength of 300 psi, and silt of low plasticity) that are stronger and stiffer than the fine-grained soils in New Orleans investigated during the IPET studies. The primary focus of the study summarized in this report is to investigate the development of a zone of separation along the flood side of the soil-to-I-wall interface. The effects of this zone of separation on the resulting deformation and stress conditions in the soil regime on both the flood side and landside of the I-wall system then were examined. This study is restricted to level soil floodwall sites.

1.2 Terminology

The zone of separation that can develop between an I-wall and the soil interface on the flood side of the I-wall has been referred to as a gap, a crack, and sometimes as a flaw. There is no universal agreement on the terminology. The majority of this report uses the term gap to describe this separation zone. No matter which of the three terms is used, they all

describe this same separation zone. In this report, the terms are interchangeable.

1.3 Phase III: Research and development in support of USACE guidance document

Investigations of the hurricane protection systems in Louisiana after Katrina identified possible deficiencies in the USACE guidance used to design I-walls. The deficiencies centered on designs related to the phenomenon of a gap between the sheet pile and the soil on the flood side of the wall that can form under flood loading. This gap phenomenon was attributed to several I-wall failures in New Orleans related to global instability or seepage. USACE, therefore, issued guidance regarding these deficiencies in a memorandum to Major Subordinate Commands dated 23 May 2006. The compilation of data and site inspections required in that memorandum was considered Phase I of an approach to evaluate existing I-walls under the USACE jurisdiction throughout the United States. Phase II interim guidance then was prepared and deployed to assist USACE districts to evaluate and identify projects that might be at risk of poor performance. This effort resulted in the identification of more than 50 projects with potential performance concerns. Most of the projects not meeting the criteria of the Phase II guidance failed to meet factors of safety for rotational stability or the check of a minimum ratio of 2.5 for depth of penetration (5 ft) to stickup (2 ft). The Phase III study summarized in this report supports the development of the next phase of USACE guidance documents for use in the design of I-walls.

1.4 The complete SSI method of analysis used in this research study

This investigation relies on the use of a complete SSI method of analysis. In this procedure, the soil foundation, I-wall and interface between the I-wall and the soil (on both sides of the I-wall) all are modeled using finite elements; soil and the interface properties are modeled as nonlinear materials; and the flood loadings are incrementally raised to the design flood pool elevation. The Plasticity Axi-Symmetry (PLAXIS) software, a two-dimensional (2-D) nonlinear incremental construction finite element program, is used for the complete SSI analyses discussed in this report.

1.5 Gap initiation and propagation used in the complete SSI analyses

A hydraulic fracturing criterion is applied to determine if a gap develops and if it spreads down the soil-to-I-wall interface.¹ In this procedure of analysis, the total horizontal stress (computed by PLAXIS) at the ground surface soil-to-I-wall interface, is compared to the hydrostatic water pressure developing at the top of the ground surface from the presence of the specified flood pool elevation. If the hydrostatic water pressure of the flood pool (the demand) exceeds the total horizontal stress (the capacity) at the ground surface, a gap will initiate at the ground surface, along the soil-to-I-wall interface.² After hydraulic fracturing commences at the ground surface, the next or lower soil (or interface) element at the soil-to-I-wall interface then is checked for hydraulic fracturing. Its total horizontal stress is compared to a hydrostatic water pressure for the same flood pool elevation that initiated a gap above the current soil/interface element in question. If the hydrostatic water pressure of the flood pool exceeds the total horizontal stress at this soil or interface element, a gap will propagate through this element and down to the next soil or interface element along the soil-to-I-wall interface. This check for gap propagation proceeds until a depth is reached for which the total horizontal stress at the soil-to-I-wall interface (capacity) exceeds the hydrostatic water pressure of the flood pool (demand) and, thus, the gap is arrested by the horizontal total stresses contained within that soil element.

1.6 Report content

Chapter 2 summarizes the findings of a series of complete nonlinear SSI finite element analyses performed on an I-wall section founded in an overconsolidated lean clay. The focus of this complete SSI analysis was to investigate the phenomena of gap initiation and propagation along the soil-to-structure interface on the landside of the I-wall, and to study the effects of gap initiation and propagation on the resulting deformation and stress conditions in the soil regime on both the flood and landside of the I-wall. A description of the engineering characterization of the soil used in the analysis, the soil stiffness and shear strength parameters, the conventional design of the I-wall, and the results of the complete nonlinear SSI analyses

¹ This hydraulic fracturing type of analysis has been adapted from the procedure used to estimate the potential for crack formation in earthen dams with a clay core (e.g. Nobari et al. 1973; Widjaja et al. 1984; Sherard 1973 and 1986; and Independent Panel to Review Cause of Teton Dam Failure 1976).

² Zero tensile strength capability is assumed along this soil-to-I-wall interface.

are discussed. A design flood depth of 9 ft¹ above level ground was used in the conventional design of this I-wall. Following USACE design criteria given in Engineer Manual (EM) 1110-2-2504 (Headquarters, USACE (HQUSACE) 1994); a depth of embedment of 16 ft was obtained for the undrained shear strength profile used for this soil site. This corresponds to a ratio of 1.78 for depth of penetration to stickup. The complete SSI analyses follow I-wall performance, gap development, wall deformations, and soil-to-I-structure stress distributions along the I-wall-to-soil interface for both the landside and flood side of the I-wall with a flood pool rising from 1 to 9 ft in 1-ft increments. Results for the companion parametric complete SSI analyses, using the four combinations of minimum and maximum undrained shear strength (S_u) distributions with depth and undrained secant modulus (E_u) distributions with depth, are discussed in Appendices A through D. Table 1.1 shows the combinations of minimum and maximum undrained shear strength and undrained secant stiffness distributions used in the parametric study. These results will be used in a companion research effort focusing on risk and reliability assessments of I-walls.

Table 1.1. Combinations of minimum and maximum undrained shear strength (S_u) and undrained secant stiffness (E_u) distributions analyzed for an overconsolidated lean clay.

Report Section	S_u Distribution	E_u Distribution
Chapter 2	μ	μ
Appendix A	$\mu - 2\sigma$	$\mu - 2\sigma$
Appendix B	$\mu - 2\sigma$	$\mu + 4\sigma$
Appendix C	$\mu + 4\sigma$	$\mu - 2\sigma$
Appendix D	$\mu + 4\sigma$	$\mu + 4\sigma$

Note: μ = mean; σ = standard deviation.

Chapter 3 summarizes the findings of a series of complete nonlinear SSI finite element analyses. These analyses were performed on an I-wall section founded in a level ground clay site with soil material properties consistent with the soils found at the site of the E-99 sheet pile wall field load test conducted as part of the E-99 East Atchafalaya Basin Protection Levee Sheet Pile Floodwall construction contract, from May through September 1985 (U.S. Army Engineer Division, Lower Mississippi Valley, 1988). The foundation for this test site consisted of soft, highly plastic clays. A flood depth of 8 ft above level ground was used in the analyses based on the highest pool in this full-scale, I-wall field experiment. The

¹ A table of factors for converting non-SI units of measure to SI units is on Page xxi.

sheet-pile wall had a depth of embedment of 23 ft. This corresponds to a ratio of 2.9 for the depth of penetration to stickup. Results for the companion parametric complete SSI analyses using the four combinations of minimum and maximum undrained shear strength (S_u) distributions with depth and undrained secant modulus (E_u) distributions with depth are discussed in Appendices E through H. Table 1.2 shows the combinations of minimum and maximum undrained shear strength and undrained secant stiffness distributions used in the parametric study. These results will be used in a companion research effort focusing on risk and reliability assessments of I-walls.

Table 1.2. Combinations of minimum and maximum undrained shear strength (S_u) and undrained secant stiffness (E_u) distributions analyzed, level ground clay, E-99 I-wall.

Report Section	S_u Distribution	E_u Distribution
Chapter 3	μ	μ
Appendix E	$\mu - 1.6\sigma$	$\mu - 1.6\sigma$
Appendix F	$\mu - 1.6\sigma$	$\mu + 4\sigma$
Appendix G	$\mu + 4\sigma$	$\mu - 1.6\sigma$
Appendix H	$\mu + 4\sigma$	$\mu + 4\sigma$

Note: μ = mean; σ = standard deviation.

Chapter 4 summarizes the findings of a series of complete nonlinear SSI finite element analyses performed on an I-wall section founded in a level ground clay site with constant undrained shear strength of 300 psf. A design flood depth of 9 ft above level ground was used in the conventional design of this I-wall. Following USACE design criteria given in HQUSACE (1994), a depth of embedment of 30 ft was obtained for the constant undrained shear strength profile used for this soil site. This corresponds to a ratio of 3.3 for depth of penetration to stickup.

Chapter 5 summarizes the findings of a series of complete nonlinear SSI finite element analyses performed on an I-wall section founded in a level ground in a silt of low plasticity or a silty sand classified as an ML and SM, respectively, by the Unified Soil Classification System (USCS). A design flood depth of 9 ft above level ground was used in the conventional design of this I-wall. Following USACE design criteria given in HQUSACE (1994), a depth of embedment of 38 ft was obtained for the constant undrained shear strength profile used for this soil site. This corresponds to a ratio of 4.2 for depth of penetration to stickup. Two different permeabilities for the ML and SM were assumed to study the time-dependent effects of the problem,

including loading, transient seepage, induced excess pore pressures, and dissipation of the excess pore pressures with time. These time-dependent effects control whether the problem can be considered drained, undrained, or partially drained. For these analyses, the long duration hydrograph was chosen to ascertain if the soil performed as drained or undrained. The loading was performed in PLAXIS in 1-ft increments of water with the associated time duration taken from the hydrograph. A three-stage incremental analysis procedure was conducted in this series of complete SSI analyses: a transient seepage analysis, a deformation analysis, and a consolidation analysis.

Chapter 6 summarizes the findings of an initial complete nonlinear SSI finite element analysis performed on an I-wall section embedded in a levee section. The objective was to investigate the effects that levee geometry (nonlevel ground surface) has on the phenomena of gap initiation and propagation along the soil-to-structure interface on the flood side of the I-wall. Additionally, the effects that levee geometry have on the resulting deformation and stress conditions in the soil regime, both on the flood side and landside of the I-wall, were examined.

Chapter 7 discusses the summary and conclusions of the complete SSI analyses of flood I-walls embedded in level ground and the initial conclusions of the effects that levee geometry has on I-wall performance.

2 Analyses of I-wall Site Founded in an Overconsolidated Lean Clay

2.1 Purpose of analyses

This chapter summarizes the findings of a series of complete nonlinear SSI finite element analyses performed on an I-wall section founded in an overconsolidated lean clay. The focus of this study was to investigate the phenomena of gap initiation and propagation along the soil-to-structure interface on the flood side of the I-wall. The effects of this gap initiation and propagation on the resulting deformation and stress conditions in the soil regime on both the flood side and landside of the I-wall then were examined.

The following sections will describe the soil used in the analyses, the selection of stiffness and shear strength parameters, the conventional design of the I-wall, the procedures employed for the analyses, and the results of the complete nonlinear SSI analyses.

2.2 Overview of flood-site I-wall being analyzed

The geometry of the problem analyzed is shown in Figure 2.1. The site was assumed to be a level plan site with a maximum floodwater elevation (el) of 9 ft. Two soil layers were assumed in the analyses. The top 20 ft of soil represented an overconsolidated layer, while the underlying soil was assumed to be normally consolidated. The elevation of the soil surface was assumed to be 0 ft.

The I-wall was composed of a sheet-pile wall with its tip at el -16 ft. The top of the I-wall was composed of a concrete cap 2.5 sq ft (embedded to el -2.5 ft), with the top of the cap level with the ground surface. The wall above the top of the soil was composed of a tapered concrete section 2.5 ft at the base and 1 ft at the top of the wall (el 9 ft). The water table for this problem was at the pile tip (el -16 ft).

The designation for the soil used in the analyses is clay with low plasticity (CL), based on the Unified Soil Classification System (USCS). This soil has a liquid limit (LL) of less than 50% and a plasticity index from 7 to 38% (Figure 2.2). The objective was to have a soil with enough plasticity to hold open a gap along the interface of the flood side soil and I-wall. Figure 2.2 shows the region where CL falls on the USCS plasticity chart.

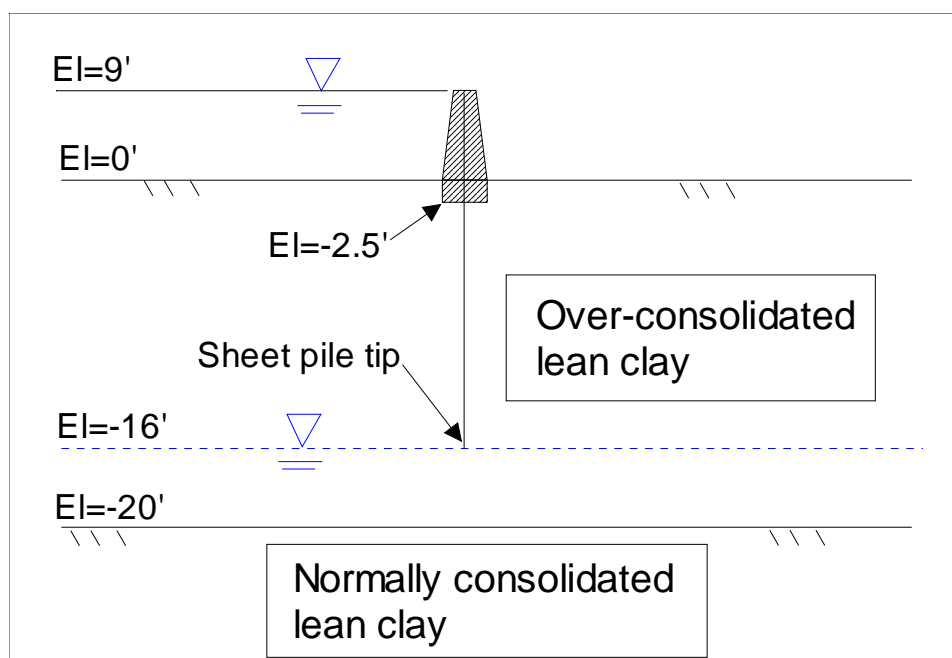


Figure 2.1. Geometry of the problem.

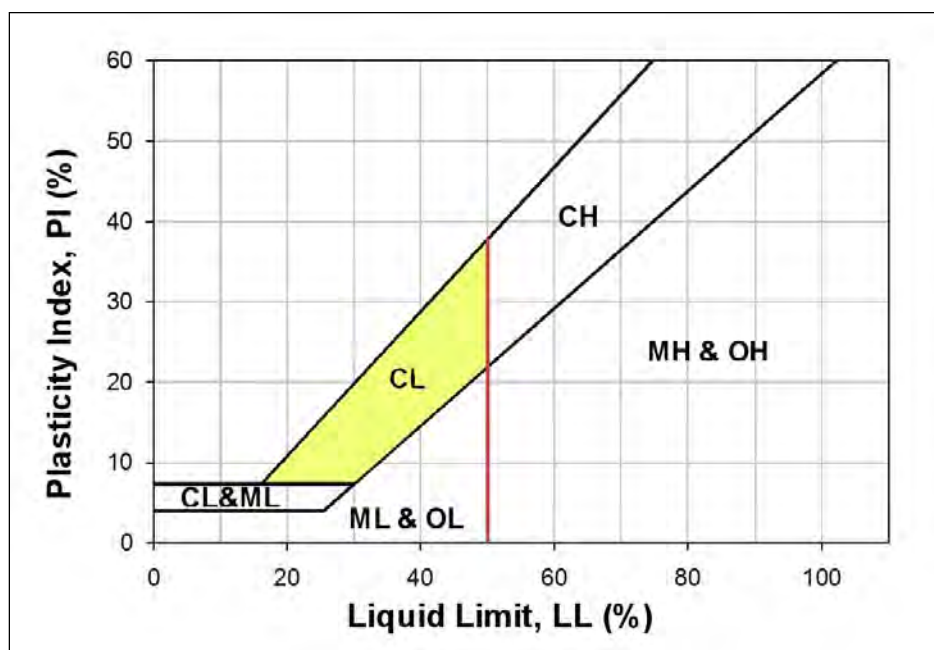


Figure 2.2. USCS plasticity chart for fine-grained soils. CL , clay with low plasticity; ML , silt with low plasticity; CH , clay of high plasticity; MH , silt of high plasticity; OL , organic silt, organic clay ($LL < 50\%$); and OH , organic silt, organic clay ($LL \geq 50\%$).

2.3 Shear strength and conventional design of cantilever I-wall

The design depth of penetration of the sheet-pile section of the I-wall was determined using the Computer-Aided Structural Engineering (CASE) Computer Program for Design and Analysis of Sheet Pile Walls

(CWALSHT) (Dawkins 1991) and procedures outlined in HQUSACE (1994). The initial design depth of penetration of the sheet pile was computed to be -16 ft, without consideration of a gap forming between the concrete cap and the soil or between the sheet pile and soil on the flood side of the I-wall. However, the finite element analysis conducted for this design depth considered the potential for gap initiation and propagation. It should be noted that the inclusion of a gap beside the wall also would affect the design depth. This analysis provides useful information for a high ratio of embedment to flood height. It is important to recognize that the factor of safety for this system based on complete SSI results for a flood elevation of 9 ft would not correspond to the factor of safety used for design in CWALSHT because a gap was not assumed in the CWALSHT analysis.

To perform a CWALSHT analysis of the I-wall system, two designs were performed based on short-term and long-term loading conditions. This required the use of effective stress (drained) strength parameters for the long-term design and total stress (undrained) strength parameters for the short-term design. Effective stress strength parameters were estimates of medium-range values of the clay soil. The total stress (undrained) shear strength parameters were determined using the Stress History and Normalized Soil Engineering Parameters (SHANSEP) procedure (Ladd and Foott 1974). It assumes that the soil shear strength can be normalized by the effective overburden pressure. The effective overburden pressure is calculated at midlayer for each of the layers identified in Table 2.1 using a preflood water table elevation of -16 ft. The ratio of shear strength to effective overburden pressure (S_u/σ'_{vo}) is dependent on the overconsolidation ratio (OCR) and a fitting parameter (m), assumed to be 0.8 as shown in Equation 2.1:

$$\left(\frac{S_u}{\sigma'_{vo}} \right)_{OC} = \left(\frac{S_u}{\sigma'_{vo}} \right)_{NC} \bullet OCR^m, \quad (2.1)$$

where

$(S_u/\sigma'_{vo})_{NC}$ = ratio of the undrained shear strength to effective overburden pressure for the normally consolidated condition;

$(S_u/\sigma'_{vo})_{OC}$ = ratio of the undrained shear strength to effective overburden pressure for the over-consolidated condition.

Table 2.1. Computation of S_u variation with depth.

Layer			Short-Term (Undrained) Loading				
No.	Top el, ft	Bottom el, ft	Depth, ft	σ'_{vo} , psf	OCR	$(S_u/\sigma'_{vo})_{oc}$	S_u , psf
1	0	-1.5	1	122	7	1.043521	127
2	-1.5	-4.5	2	244	7	1.043521	255
			3	366	7	1.043521	382
			4	488	7	1.043521	509
3	-4.5	-7.5	5	610	6.4	0.97133	593
			6	732	5.5	0.860425	630
			7	854	4.8	0.771642	659
4	-7.5	-11.5	8	976	3.6	0.613006	598
			9	1098	2.9	0.515633	566
			10	1220	2.3	0.428356	523
			11	1342	2	0.383042	514
5	-11.5	-17.5	12	1464	1.7	0.336343	492
			13	1586	1.6	0.320419	508
			14	1708	1.4	0.287955	492
			15	1830	1.35	0.279698	512
			16	1952	1.3	0.27138	530
			17	2011.5	1.25	0.262997	529
6	-17.5	-20	18	2071	1.2	0.254547	527
			19	2130.5	1.15	0.246026	524
			20	2190	1.1	0.237431	520
7	-20	-27.5	25	2487.5	1	0.22	547
8	-27.5	-40	30	2785	1	0.22	613
			35	3082.5	1	0.22	678
			40	3380	1	0.22	744
9	-40	-60	45	3677.5	1	0.22	809
			50	3975	1	0.22	875
			55	4272.5	1	0.22	940
			60	4570	1	0.22	1005
10	-60	-80	65	4867.5	1	0.22	1071
			70	5165	1	0.22	1136
			75	5462.5	1	0.22	1202
			80	5760	1	0.22	1267
11	-80	-100	85	6057.5	1	0.22	1333
			90	6355	1	0.22	1398
			95	6652.5	1	0.22	1464
			100	6950	1	0.22	1529

From Ladd (1991), a value of 0.22 was assigned to $(S_u/\sigma'_v)_{NC}$ and a value of 0.8 for (m) based on undrained Direct Simple Shear (DSS) test results. DSS results were chosen because they represented the predominant type of loading stress state of a passive soil wedge. Undrained triaxial compression tests (TX) better represent the loading stress state for an active wedge. Because the passive wedge was deemed more important for the stability of the wall, DSS strengths were used. To compute the effective overburden pressures, 122 pcf was used for both the moist and the saturated unit weight.

To characterize this site, OCR variation with depth was adapted from a recent testing program of OCR clay at the I-wall at Tell City, Indiana, shown in Figure 2.3. The OCR is the ratio of the preconsolidation pressure (P'_c) to the effective overburden pressure, σ'_v (P'_c/σ'_v). As shown in Figure 2.3, the OCR varies from 7 near the ground surface to 1.7 at el -14 ft to 1 ft at el -20 ft for the Tell City site.

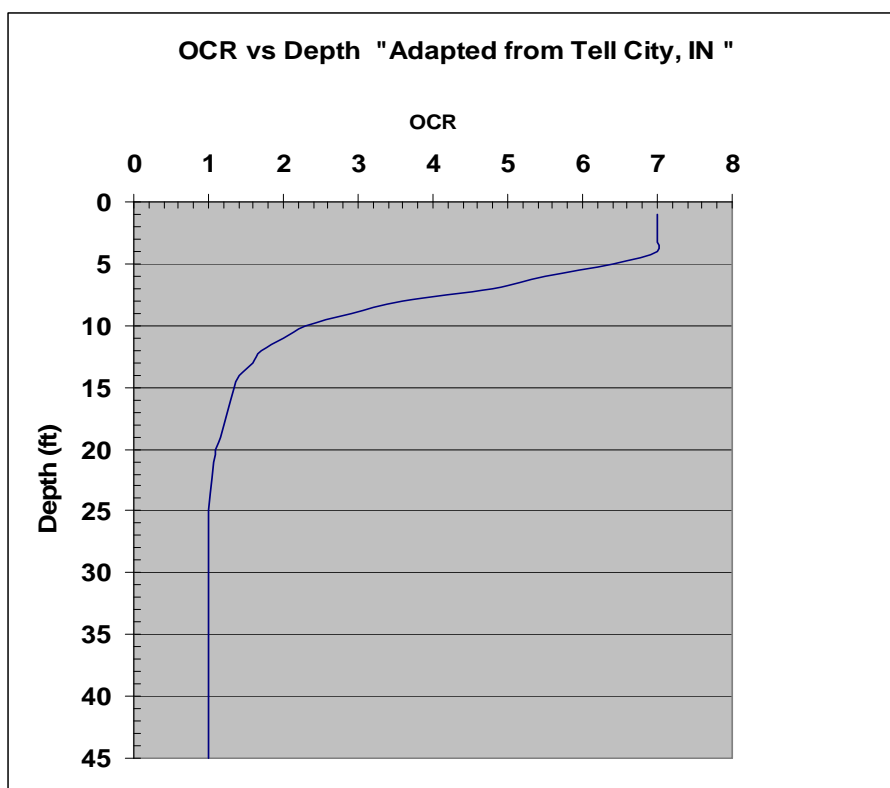


Figure 2.3. OCR variation with depth for Tell City site.

The resulting variation in the undrained shear strength (S_u) with depth is shown in blue in Figure 2.4. Average values of (S_u) were estimated to be constant over a given depth, as shown in Figure 2.4. These constant values

were used both in the conventional design and the complete SSI analysis to approximate to variation in (S_u) with depth.

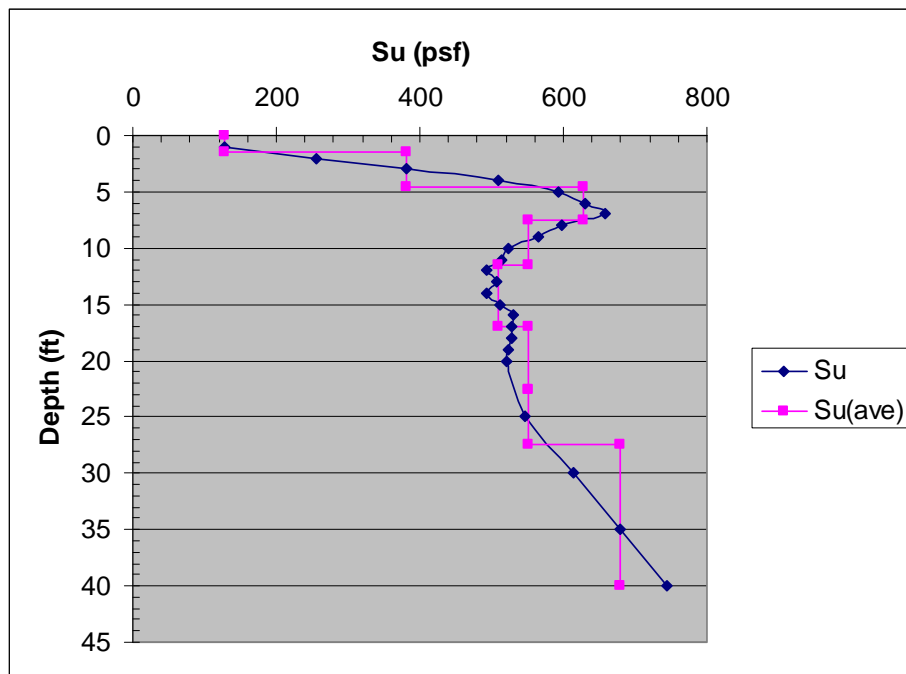


Figure 2.4. Variation in undrained shear strength with depth.

Table 2.2 summarizes four CWALSHT-based conventional designs and their respective shear strength assignments. The short-term, total stress case with adhesion equal to zero was the governing design case. It had a corresponding design depth of penetration of -16 ft (in italics). For this design depth of penetration, the chosen pile section for the maximum bending moment was a PZ22.

When a CWALSHT-based design/analysis is performed for a short-term (undrained) condition, caution must be taken to account properly for the water loadings. For the short-term condition, using a total stress method of analysis, pore pressures should not be calculated within the soil regime. External water loadings on both the wall and soil surface must be accounted for in the analysis. Therefore, uniform vertical and horizontal boundary pressure loads must be used to represent the external loading due to the water rather than associating a water table elevation in the CWALSHT analysis.

Table 2.2. Summary of CWALSHT design cases, 9-ft wall height (h), 9-ft water height.

Analysis Type	Design Case	Soil Layer	Shear Strength				CWALSHT Penetration, depth (d), ft	d/h
			ϕ , deg	δ , deg	c, psf	Adhesion, psf		
Long-term effective stress	1	Upper	28	0	300	0	16	1.78
		Middle	29	0	150	0		
		Lower	30	0	0	0		
	2	Upper	28	14	300	0	13.3	1.48
		Middle	29	14.5	150	0		
		Lower	30	15	0	0		
Short-term total stress	3	Multiple	0	0	Increased with depth (127-625)	0	16.1	1.79
	4	Multiple	0	0	Increased with depth (127-625)	0.25(S_u)	13.4	1.49

Lastly, the I-wall also was checked for stability against a bearing capacity failure. Both the bearing capacity of the concrete wall and the side friction along the sheet pile were inspected to ensure adequate bearing. The wall was found to have an adequate factor of safety against a bearing capacity failure due to its own weight.

2.4 Shear strength and stiffness properties used in the complete SSI analysis

A complete SSI analysis of the I-wall section shown in Figure 2.1 was performed using the 2-D version of the personal computer-based finite element program PLAXIS. A complete SSI analysis is considered to provide the most reasonable estimate for deformation response of a soil-structural system involving nonlinear material behavior. Soil stresses, I-wall deflections, shear forces, and bending moments internal to the sheet piling also are computed in complete SSI analyses. The finite element method employed required certain input material properties for the selected soil constitutive models. The PLAXIS nonlinear Hardening Soil (HS) constitutive model was used to model all soil elements. This model provides for nonlinear stress-strain response for soil elements during loading. Elastic plate elements were used to model the steel sheet-pile and the concrete I-wall section. Plate elements were used to model the concrete I-wall to process bending moment and shear distribution results

more efficiently. Two-dimensional elastic elements were used to represent the concrete cap (the concrete region in which the sheet pile is embedded).

PLAXIS can perform analyses in terms of effective or total stress soil strength parameters. For the analysis described herein, total stress soil strength parameters were used to characterize the overconsolidated lean clay site. The average of values of (S_u) , assumed to be constant over a given depth as shown in Figure 2.4, also was used in the complete SSI analysis to approximate variation in (S_u) with depth. Figure 2.4 shows that at a depth of 1 ft, (S_u) is equal to 127 psf. From 2 to 7 ft in depth, (S_u) increases in value from 255 psf to 659 psf. Between 8 and 14 ft, (S_u) decreases in value from 598 to 492 psf. Between 14 and 20 ft, S_u increases in value from 492 to 579 psf. The correlation by Duncan and Bursey (2007) shown in Figure 2.5 was used to estimate the variation of undrained secant modulus in clay with depth. The correlation is based on its undrained shear strength, plasticity index, and overconsolidation ratio using:

$$E_{us} = K \times S_u, \quad (2.2)$$

where

E_{us} = undrained secant modulus;

K = a factor determined from field measurements and shown in Figure 2.5;

S_u = undrained shear strength.

Table 2.3 summarizes the computation of (E_{us}) with depth using the average values of the variation of (S_u) with depth from Table 2.1 and Equation 2.2. These values of (E_{us}) were used to estimate the variation in the PLAXIS input stiffness parameter $(E_{50,ref})$, which is a secant modulus at 50 percent of the principal stress difference $(\sigma_1 - \sigma_3)$. A literature search was performed to collect typical parameters of overconsolidated clay used in PLAXIS finite element analyses. Three additional HS parameters were assigned: the unload-reload stiffness $(E_{ur,ref})$, which is set equal to 3 times $(E_{50,ref})$; the exponent $m=0.8$; and the failure ratio $R_f=0.9$. From the review, an average set of soil properties was selected to represent the CL soils used in the analyses. These properties are shown in Table 2.4 for the HS constitutive soil model. Values of the coefficient of friction between the sheet pile and the soil and between the concrete cap and the soil were selected from values published by Potyondy (1961) and shown in Table 2.5. The value of the coefficient of friction (f_c) is defined by:

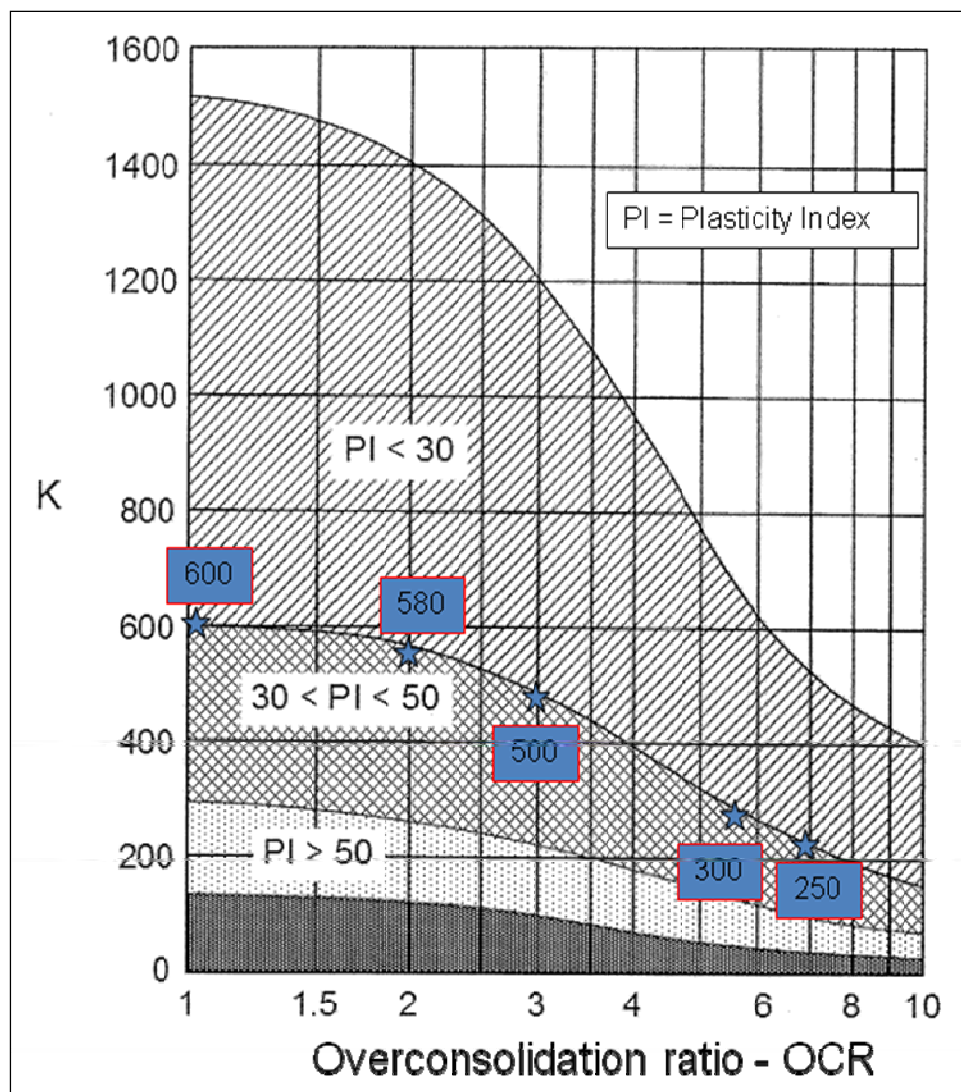


Figure 2.5. Estimation of E_{us} for clay (Duncan and Bursey 2007).

$$f_c = \frac{c_a}{c}, \quad (2.3)$$

where c_a is adhesion and c is cohesion.

The properties of the concrete cap were represented by elastic elements, and the properties of the concrete I-wall section were modeled by elastic plate elements with the properties given in Tables 2.6 and 2.7. The sheet pile was represented by elastic plate elements with the properties given in Table 2.8.

Table 2.3. Computation of undrained secant modulus (E_{us}).

Short-Term (Undrained) Loading					E_u/S_u	E_u , psf
Depth, ft	σ'_{vo} , psf	OCR	$(S_u/\sigma'_{vo})_{oc}$	S_u , psf		
1	122	7	1.043521	127	250	3.18E+04
2	244	7	1.043521	255	250	6.37E+04
3	366	7	1.043521	382	250	9.55E+04
4	488	7	1.043521	509	250	1.27E+05
5	610	6.4	0.97133	593	270	1.60E+05
6	732	5.5	0.860425	630	300	1.89E+05
7	854	4.8	0.771642	659	350	2.31E+05
8	976	3.6	0.613006	598	450	2.69E+05
9	1098	2.9	0.515633	566	500	2.83E+05
10	1220	2.3	0.428356	523	550	2.87E+05
11	1342	2	0.383042	514	580	2.98E+05
12	1464	1.7	0.336343	492	590	2.91E+05
13	1586	1.6	0.320419	508	590	3.00E+05
14	1708	1.4	0.287955	492	600	2.95E+05
15	1830	1.35	0.279698	512	600	3.07E+05
16	1952	1.3	0.27138	530	600	3.18E+05
17	2011.5	1.25	0.262997	529	600	3.17E+05
18	2071	1.2	0.254547	527	600	3.16E+05
19	2130.5	1.15	0.246026	524	600	3.14E+05
20	2190	1.1	0.237431	520	600	3.12E+05
25	2487.5	1	0.22	547	600	3.28E+05
30	2785	1	0.22	613	600	3.68E+05
35	3082.5	1	0.22	678	600	4.07E+05
40	3380	1	0.22	744	600	4.46E+05
45	3677.5	1	0.22	809	600	4.85E+05
50	3975	1	0.22	875	600	5.25E+05
55	4272.5	1	0.22	940	600	5.64E+05
60	4570	1	0.22	1005	600	6.03E+05
65	4867.5	1	0.22	1071	600	6.43E+05
70	5165	1	0.22	1136	600	6.82E+05
75	5462.5	1	0.22	1202	600	7.21E+05
80	5760	1	0.22	1267	600	7.60E+05
85	6057.5	1	0.22	1333	600	8.00E+05
90	6355	1	0.22	1398	600	8.39E+05
95	6652.5	1	0.22	1464	600	8.78E+05
100	6950	1	0.22	1529	600	9.17E+05

Table 2.4. HS model strength and stiffness properties for the soil layers.

Layer			C_{ref} , lb/ft ²	$E_{50,ref}$, lb/ft ²	$E_{oed,ref}$, lb/ft ²	$E_{ur,ref}$, lb/ft ²
No.	Top el, ft	Bottom el, ft				
1	0.0	0.0	127	3.18E+04	3.18E+04	9.55E+04
2	-1.5	-4.5	382	9.55E+04	9.55E+04	2.86E+05
3	-4.5	-7.5	627	2.10E+05	2.10E+05	3.78E+05
4	-7.5	-11.5	550	2.84E+05	2.84E+05	8.53E+05
5	-11.5	-17.0	510	3.02E+05	3.02E+05	9.06E+05
6	-17.0	-20.0	524	3.14E+05	3.14E+05	9.43E+05
7	-20.0	-27.5	547	3.28E+05	3.28E+05	9.85E+05
8	-27.5	-40.0	678	4.07E+05	4.07E+05	1.22E+06
9	-40.0	-60.0	907	5.44E+05	5.44E+05	1.63E+06
10	-60.0	-80.0	1169	7.01E+05	7.01E+05	2.10E+06
11	-80.0	-100.0	1431	8.58E+05	8.58E+05	2.58E+06

Note: drained material behavior, γ_{unsat} and $\gamma_{sat} = 122$ lb/ft³, $m = 0.8$, and $R_f = 0.9$.

Table 2.5. Selected interface friction values for the interface elements.

Values Inferred from a Database by Potyondy (1961)	f_c	f_{cmax}	Values Used in Analyses
Rough steel (sheet pile)	0.5	0.8	0.8
Rough concrete (I-wall)	0.6	1.0	0.8

Table 2.6. Properties of the concrete cap.

Name	Type	γ_{unsat} , lb/ft ³	ν	E_{ref} , lb/ft ²
Concrete cap	Nonporous	150	0.2	3.15E+06

Table 2.7. Properties of the plate elements representing the concrete I-wall.

Name	Type	EA, lb/ft	EI, lbft ² /ft	Weight, lb/ft ²	ν
Concrete plate to el 3.0	Elastic	1.02E+09	4.31E+08	197.1	0.2
Concrete plate to el 6.0	Elastic	7.94E+08	2.03E+08	153.3	0.2
Concrete plate to el 9.0	Elastic	5.67E+08	7.38E+07	109.5	0.2

Table 2.8. Properties of the plate elements representing the sheet pile.

Name	Material Behavior	EA, lb/ft	EI, lbft ² /ft	Weight, lb/ft ²	ν
Sheet pile	Elastic	2.30E+08	3.71E+07	20.29	0.25
Embedded sheet pile	Elastic	2.30E+08	3.71E+07	18.73	0.25

2.5 Discussion of finite element analyses

2.5.1 Conceptual model

The finite element analysis was performed using the 2-D version of the nonlinear incremental construction finite element program PLAXIS. The conceptual model of the finite element mesh is shown in Figure 2.6. The geometry is the same as explained previously (Figure 2.1); however, several modeling features should be noted. The sheet-pile wall and the concrete I-wall section were modeled by elastic plate elements. As mentioned, plate elements were used to model the concrete I-wall to process bending moment and shear distribution results more efficiently. Two-dimensional elastic elements were used to represent the concrete cap. Interface elements were placed around the concrete cap and along both sides of the sheet-pile wall. Extensions of the interface elements are provided both horizontally and vertically at the corners of the concrete cap at el -2.5 ft and at the bottom of the sheet-pile wall at el -16 ft. This was done to alleviate stress concentrations that occur at the corners of the geometry during loading. A 2-D element extension was added above the wall to provide for additional flood loading height. The 2-D elements in the cap region of the I-wall were assigned properties of concrete. The mesh was structured to provide nodal points at 1-ft raises of the water table. Soil elements beside the sheet-pile wall on the flood side were 1/2 ft in height. This allowed for the assignment of 1-ft raises in water and modeling of the gap to within 1/2 ft.

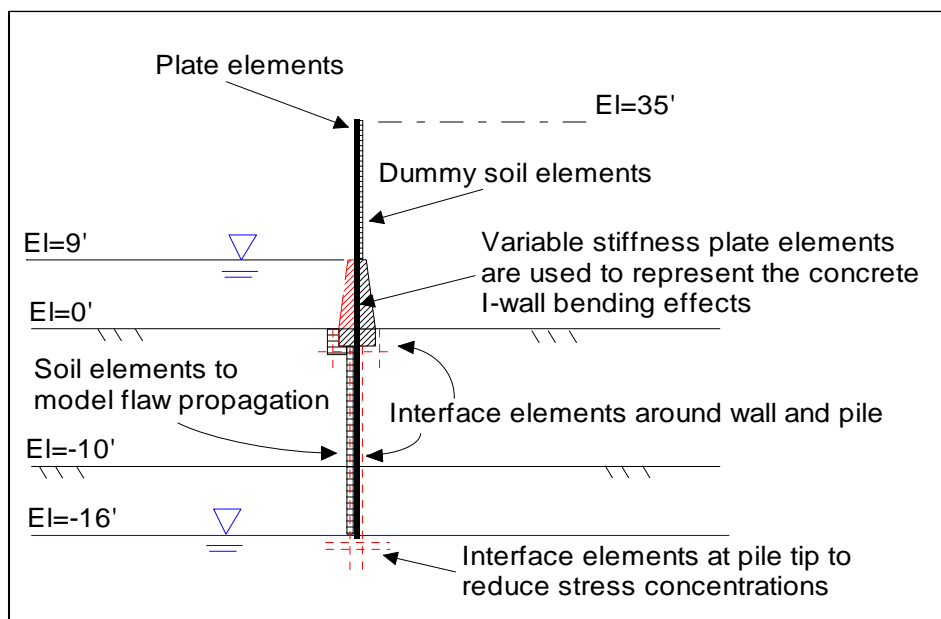


Figure 2.6. Conceptual model.

2.5.2 Gap initiation and propagation criterion

A hydraulic fracturing criterion was applied to determine if a gap develops and if it propagates down the soil-to-I-wall interface.¹ In this procedure of analysis, the total horizontal stress (computed by PLAXIS) at the ground surface soil-to-I-wall interface is compared to the hydrostatic water pressure developing at the top of the ground surface caused by the presence of the specified flood pool elevation. If the hydrostatic water pressure of the flood pool (the demand) exceeds the total horizontal stress (the capacity), a gap will initiate at the ground surface, along the soil-to-I-wall interface.² After hydraulic fracturing commences at the ground surface, the next soil-to-I-wall interface element down the soil-to-I-wall interface then is checked for hydraulic fracturing. Its total horizontal stress is compared to a hydrostatic water pressure for the same flood pool elevation that initiated a gap above the current soil/interface element in question. If the hydrostatic water pressure of the flood pool exceeds the total horizontal stress of this soil (or interface) element, a gap will propagate through this element and down to the next soil (or interface) element along the soil-to-I-wall interface. This check for gap propagation proceeds until a depth is reached for which the total horizontal stress at the soil-to-I-wall interface (capacity) exceeds the hydrostatic water pressure of the flood pool (demand). Thus, the gap is arrested by the horizontal total stresses contained within that soil element. The gap (when it develops from the ground surface down along the flood side of the I-wall) is modeled in PLAXIS by deactivating soil clusters (elements), effectively creating a void beside the wall. Hydrostatic water pressures (based on the flood elevation) are applied within this void and are manually checked against the hydraulic fracturing criterion to determine if the gap progresses (additional soil clusters are deactivated). Figure 2.7 shows the potential path for and progression of the gap beside the sheet-pile wall.

2.5.3 Finite element model

A 2-D cross section used to model the variation of undrained shear strength and soil stiffness with depth by the PLAXIS program is shown in Figure 2.8. The regions of uniform color reflect soil clusters used to define the mesh and assign soil regions with common properties. The inset figure shows the

¹ This hydraulic fracturing type of analysis has been adapted from the procedure used to estimate the potential for crack formation in earthen dams with a clay core (Nobari et al. 1973; Widjaja et al. 1984; Sherard 1973 and 1986; and the Independent Panel to Review Cause of Teton Dam Failure 1976).

² Zero tensile strength capability is assumed along this soil-to-I-wall interface.

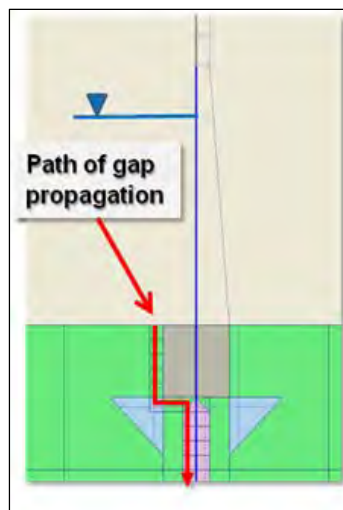


Figure 2.7. Gap propagation beside I-wall.

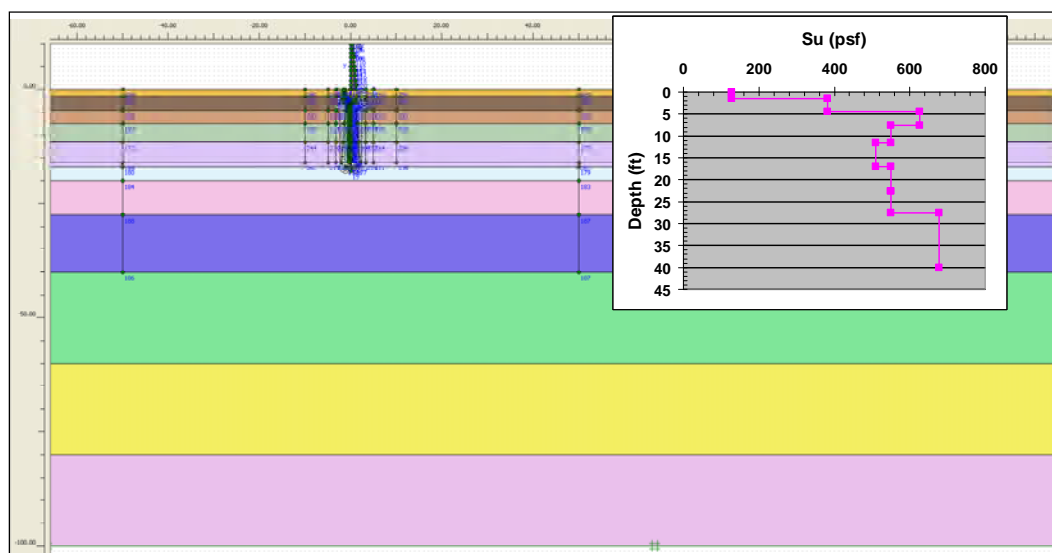


Figure 2.8. Two-dimensional cross-section model used in the SSI analyses.

average undrained shear strengths assigned to the upper eight layers. The finite element mesh used in the analysis is shown in Figure 2.9. The mesh is composed of 4,187 elements, 34,408 nodes, with 50,244 stress points. The mesh consists of 15-node triangular elements to model the soil, plate elements to model the bending effects of the I-wall and sheet-pile wall, and interface elements to model SSI between the sheet-pile wall and the adjacent soil elements. The analyses are executed as a plane strain problem. Figure 2.10 shows an enlarged view of the area around the wall and its mesh.

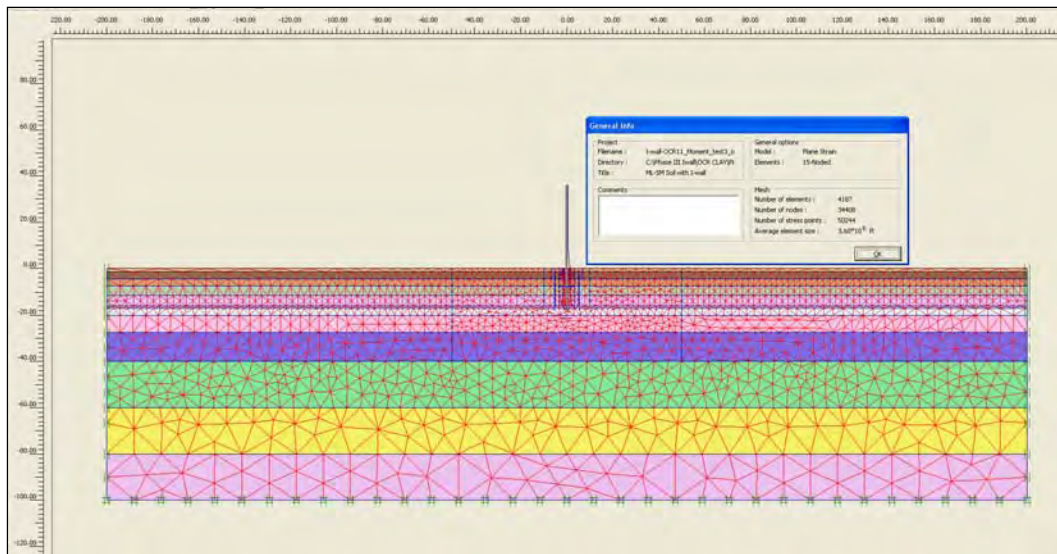


Figure 2.9. Finite element mesh used in the analyses.

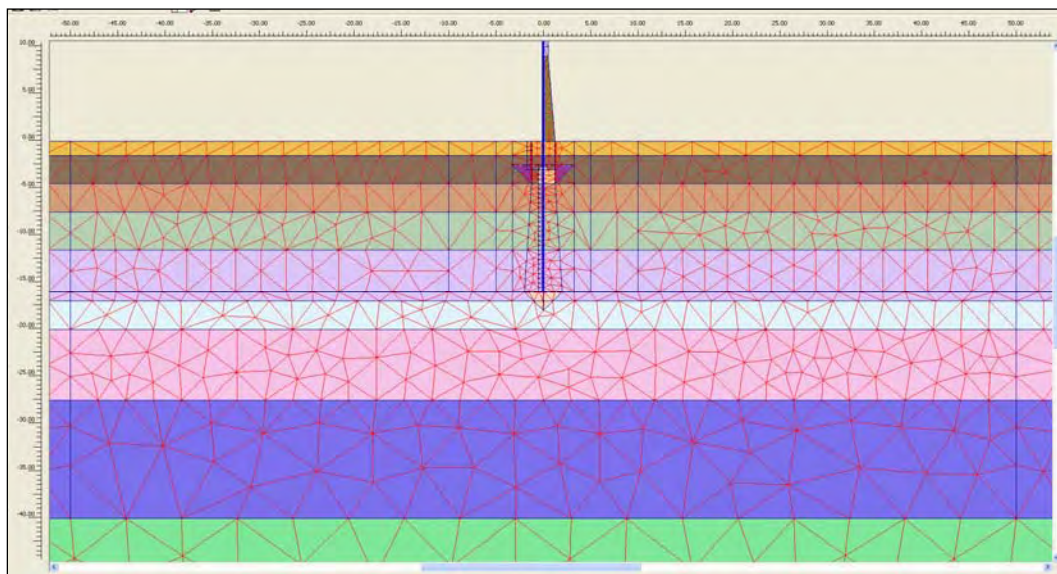


Figure 2.10. Enlarged view of finite element mesh around the I-wall.

2.6 Results of the finite element analyses

2.6.1 Initial stresses

The initial total stress state within the finite element mesh was established using the at-rest soil conditions for a level ground surface. Horizontal at-rest soil stresses were estimated using the interrelationship between the at-rest earth pressure coefficient (K_0) and the soil Poisson's ratio (ν), given as

$$K_o = \frac{v}{1-v}. \quad (2.4)$$

The assumed groundwater elevation was at the sheet-pile tip (el -16 ft). Table 2.9 shows a summary of the assigned values of (ν) and the corresponding (K_o) values used to compute the horizontal earth pressures for the initial conditions.

Table 2.9. Summary of at-rest coefficients used.

Soil Condition	Elevation Range, ft	ν	K_o
Unsaturated	0 to -16	0.4	0.67
Saturated	-16 to -100	0.495	≈ 1.0

For this level ground site the at-rest stress is computed using the total overburden pressure (for each integration point in every soil element) times (K_o). Figure 2.11 shows the computed fraction of mobilized shear strength (referred to as relative shear stress in PLAXIS output) from the initial total stress condition. The resulting fraction of mobilized shear strength (1.0 indicates full mobilization of shear strength) is less than or equal to 0.63 for all soil clusters. These results indicate reserve shear capacity in the soil regime and, thus, a stable numerical model at this initial stage of construction.

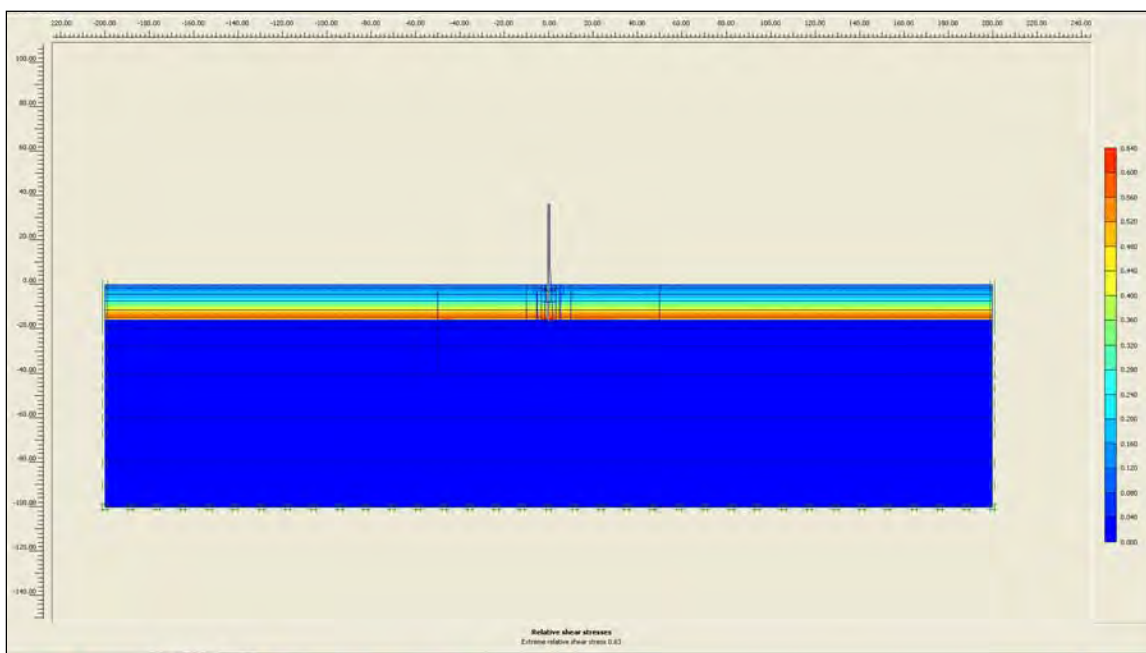


Figure 2.11. Fraction of mobilized shear strength for initial conditions.

2.6.2 Gap initiation and propagation results

As mentioned, the focus of this study was to investigate the phenomena of gap initiation and propagation along the flood side of the soil-to-I-wall interface and to study the effects of gap initiation and propagation on the resulting deformation and stress conditions in the soil regime on both the flood side and landside of the I-wall system.

Modeling of the flood loading commenced in the complete SSI analysis after the total initial stresses state was established within the mesh for an assumed steady-state water elevation at the ground surface (el 0). The flood loading was applied in 1-ft incremental raises of the water level in order to track the formation and propagation of a gap. Hydraulic fracturing criterion was used to estimate a gap formation and its propagation. This procedure compares the total normal earth pressures due to the flood pool acting on the wall at a given depth to the hydrostatic water pressure acting at the corresponding depth. Recall that a gap is formed when the total horizontal earth pressure (the capacity) is less than the water pressure due to the flood pool acting at the corresponding depth (the demand). Next, hydrostatic water pressure is applied over the depth of gap, and this pressure at the new, deeper gap depth is compared to the total horizontal earth pressure. Gap propagation is terminated at the depth at which the demand is less than the capacity. Complete SSI analysis results were examined for various water elevations and gap depths. Figure 2.12 shows the progression of the gap as the water level against the I-wall is increased. As shown, the gap initiates when the water is at the shallow elevation of 2 ft and extends to a depth of -1.0 ft. The gap extends to el -7 ft at water el 3 ft. At water el 6 ft, the gap extends to el -15 ft and gap elevation remains constant until water el 10 ft. Observe that the gap is within 1 ft of the sheet-pile tip for flood water levels at and above el 6 ft.

2.6.3 Performance of interface elements

The performance of the interface elements was compared to the performance of the soil elements adjacent to the wall to ascertain whether the results for the interface elements could be used to accurately characterize the computed results of the analyses. Figure 2.13 shows that the total horizontal stresses computed within the interface and soil elements agree closely for the selected flood elevation of 2 ft. Therefore, interface element results were used to summarize computed results from this complete SSI analysis.

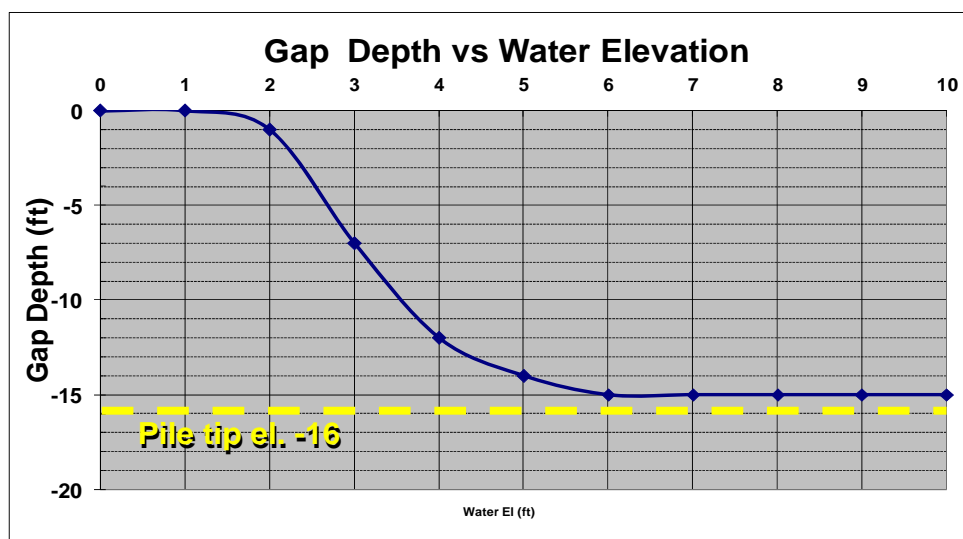


Figure 2.12. Progression of gap versus water elevation.

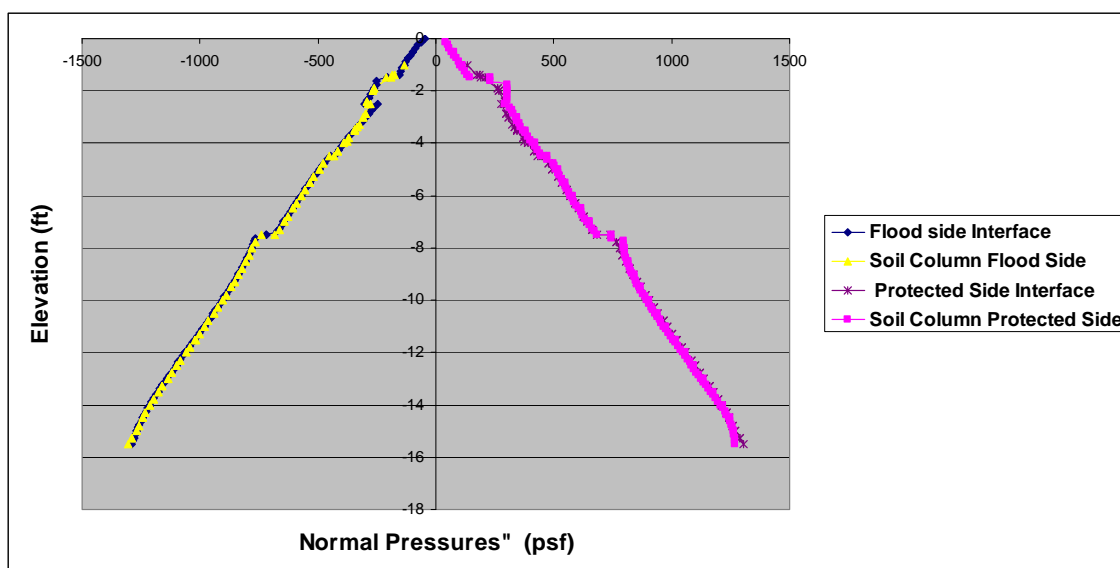


Figure 2.13. Behavior of interface versus soil elements at flood el 2 ft.

2.6.4 Discussion of displacements and stresses

The total (exaggerated) nodal displacements within the finite element mesh (both soil and wall) are shown in Figure 2.14. These displacements are for the design water elevation of 9 ft with a gap depth to el -15 ft. Note that the nodal displacements are increased by a factor of 50 to show the deformed mesh relative to its initial position and to show the extent of the gap. The gap is modeled by deactivating the soil elements adjacent to the wall. The general trend of the deflections was toward the landside because of the applied boundary water pressures on the flood side. The wall has a greater movement than the soil at this loading phase. The

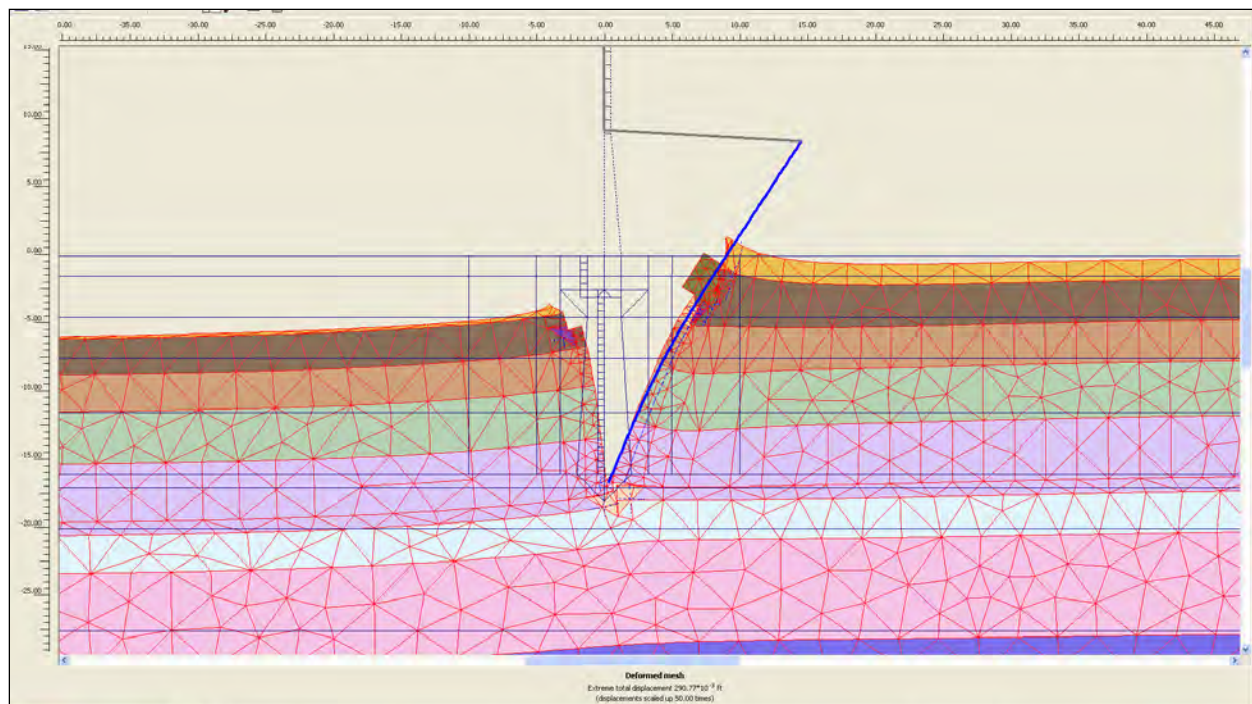


Figure 2.14. Total exaggerated displacements for a water elevation of 9 ft and gap elevation of -15 ft.

maximum wall displacement is approximately 3.5 in. at the top of the wall. The displacement of the wall consists of both horizontal and vertical movements. The tip of the wall has moved slightly upward and toward the landside.

Figure 2.15 shows a plot of horizontal displacements of I-wall versus floodwater elevation at three points along the wall. The points monitored in the analysis were the top of the I-wall at el 9 ft, at the ground surface el 0 ft, and at the sheet-pile tip el -16 ft. As shown, the deflection of the wall up to flood el 3 ft (after gap initiation) is primarily uniform translation. As the water elevation increases, the top of the wall has larger deformations compared to the ground and much larger deformations than the pile tip. This implies that the wall is undergoing rotation along with translation. Also, above water el 8 ft, the deflection of the pile tip was directed toward the flood side soil, which indicates kickback of the pile tip. This behavior is consistent with the behavior assumed in limit equilibrium design procedures for the design of cantilever sheet-pile walls.

Figure 2.16 shows a plot of relative horizontal displacements of I-wall versus floodwater elevation at the ground surface. Relative displacements were computed at this location to provide results to a companion research effort reported in HQUSACE (2011) focusing on risk and reliability assessments of

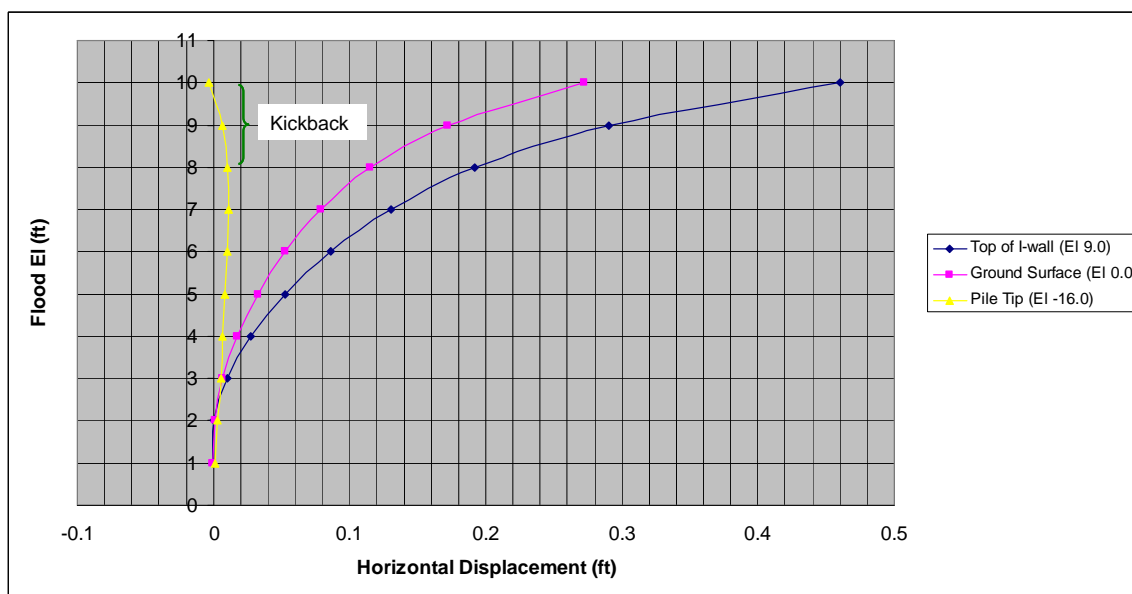


Figure 2.15. Horizontal sheet-pile deflection versus water elevation.

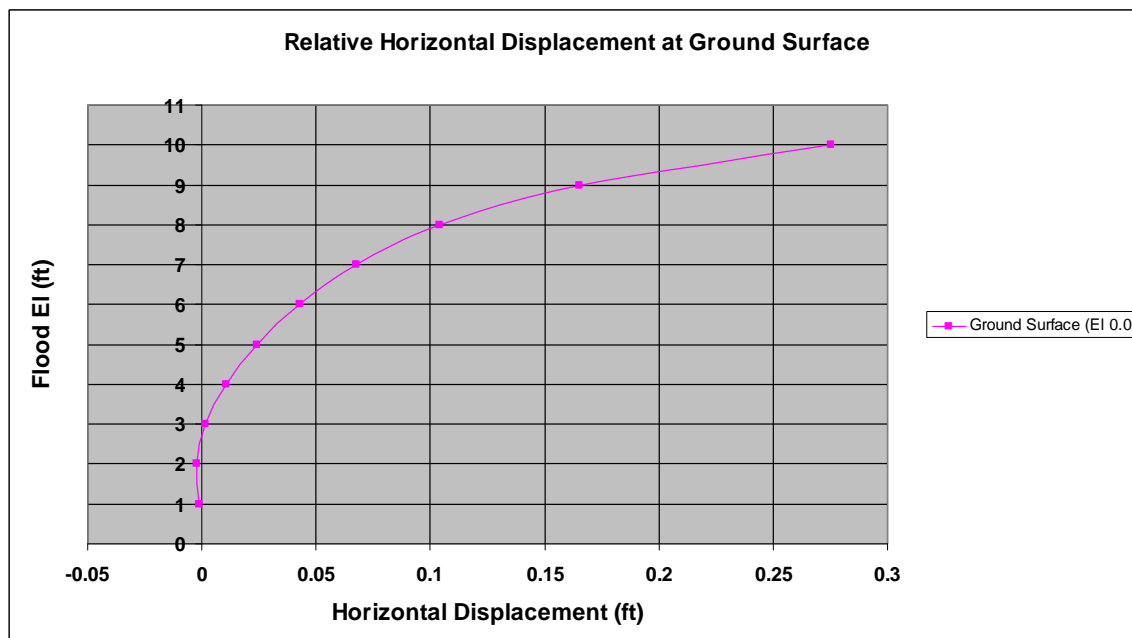


Figure 2.16. Relative horizontal sheet-pile deflection at the ground surface el 0 ft versus water elevation.

I-walls. The relative displacements were computed by subtracting the displacements of the sheet-pile tip from the sheet-pile displacements at the ground surface for a given floodwater elevation. The maximum computed relative horizontal displacement of the wall at the ground was approximately 3.3 in. These computed relative horizontal displacements also are reported in Table 2.10.

Table 2.10. Summary of relative horizontal displacements (U_x) of I-wall at the ground surface.

U_x at Ground Surface, ft	U_x at Pile Tip, ft	Relative Displacement at Ground Surface, ft	Flood el, ft	Gap depth, ft
0.0012	0.0034	-0.0021	2.0	1.5
0.0070	0.0054	0.0017	3.0	7.0
0.0176	0.0070	0.0106	4.0	12.0
0.0326	0.0084	0.0243	5.0	14.0
0.0527	0.0098	0.0428	6.0	15.0
0.0785	0.0108	0.0677	7.0	15.0
0.1146	0.0105	0.1041	8.0	15.0
0.1721	0.0069	0.1652	9.0	15.0
0.2720	-0.0031	0.2751	10.0	15.0

The total horizontal pressures acting on the interface elements adjacent to the wall on the flood side and landside for three flood elevations (6 ft, 9 ft, and 10 ft) and a corresponding gap elevation of -15 ft for each flood elevation are shown in Figures 2.17 through 2.19, respectively. These pressure results were compared to limiting stress states (active and passive) for varying factors of safety applied to the undrained shear strength values. The flood elevation of 6 ft corresponds to the shallowest water level to which the gap propagated at el -15 ft. The flood elevation of 9 ft corresponds to the water height used in the conventional design. The flood elevation of 10 ft corresponds to the peak flood level that was specified in the PLAXIS SSI analysis while maintaining numerical stability. As shown in Figure 2.17 for the flood elevation of 6 ft, the SSI earth pressures on the landside fall between at-rest pressures and passive pressures (with a factor of safety of 1.5) down to el -14 ft. Below el -14 ft, the earth pressures reduce to near active earth pressure (with a factor of safety of 1.0) at the sheet-pile tip (i.e., at el -16 ft). On the flood side, the complete SSI analysis computes hydrostatic water pressures acting down to the gap tip elevation of -15 ft, which is 1 ft above the pile tip el -16 ft. In Figure 2.18 for design flood el 9 ft, the results show that on the landside of the wall the complete SSI earth pressure results more closely match passive earth pressures computed with a factor of safety of 1.5 applied to the undrained shear strength values. On the flood side, the complete SSI analysis computes hydrostatic water pressures acting down to the gap tip elevation of -15 ft, 1 ft above the pile tip elevation -16 ft. Below the gap tip elevation, the kickback of the I-wall into the flood side soil allows for the comparison of horizontal pressures computed by complete SSI analysis to limiting earth passive pressures over this 1-ft depth. For all points but the point at el -16 ft, these computed horizontal pressures were less than the limiting passive earth

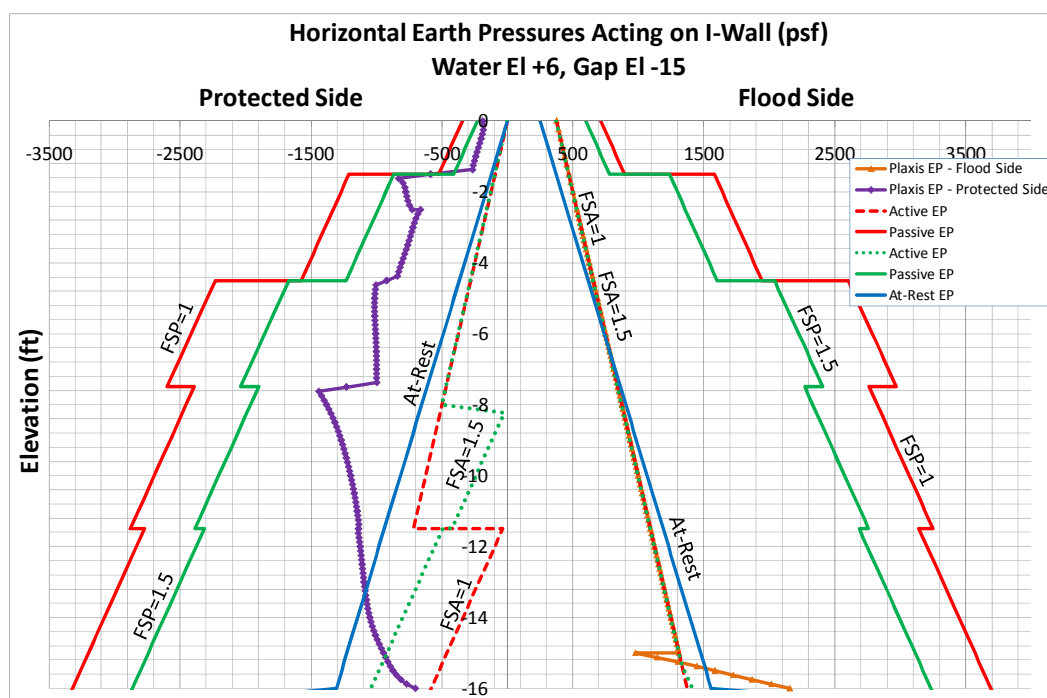


Figure 2.17. Comparison of total normal stresses on the interface elements adjacent to the wall on the flood side and landside for flood el 6 ft and gap el -15 ft (FSP is the factor of safety applied to passive earth pressures, and FSA is the factor of safety applied to active earth pressures).

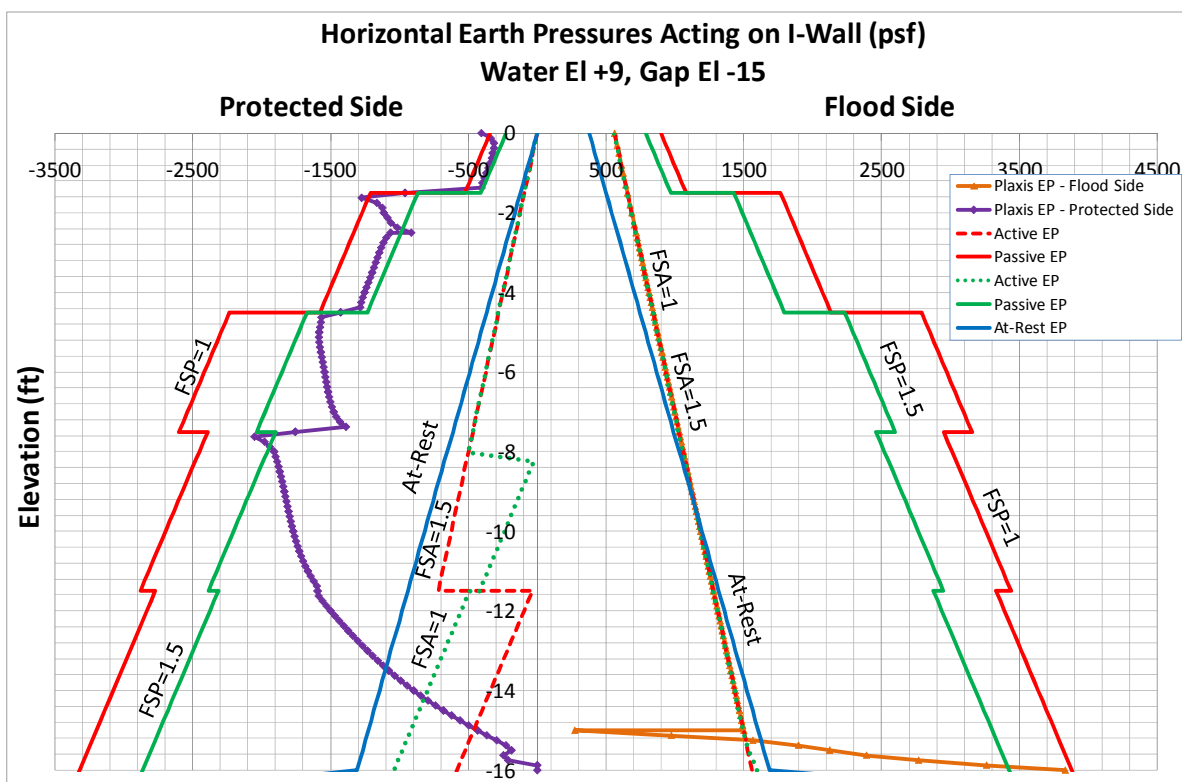


Figure 2.18. Comparison of total normal stresses on the interface elements adjacent to the wall on the flood side and landside for flood el 9 ft and gap el -15 ft.

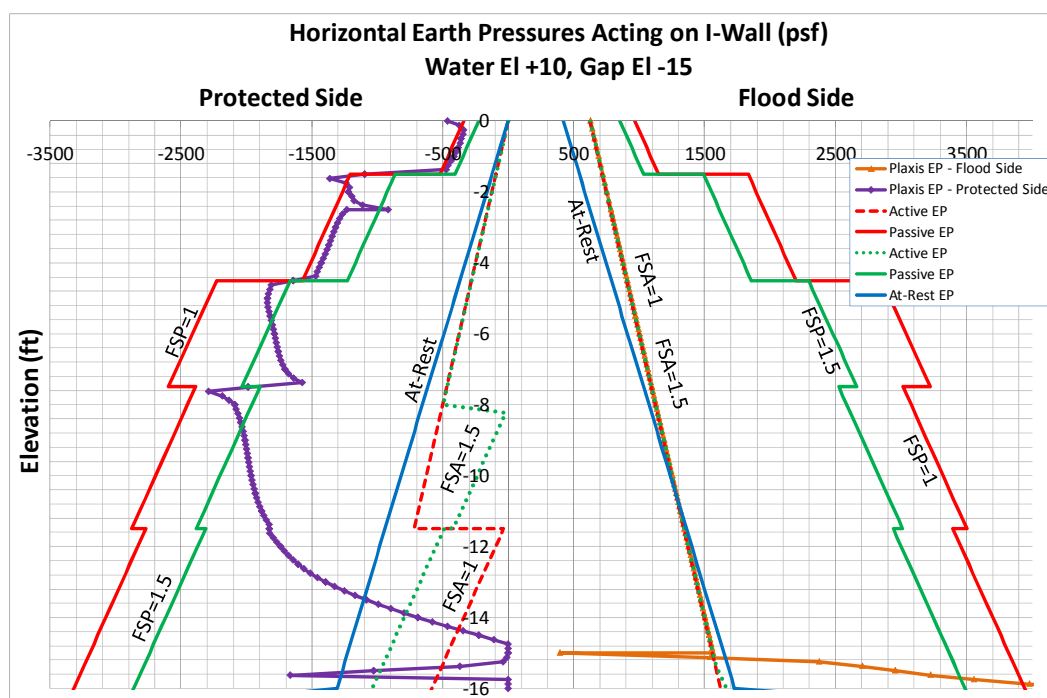


Figure 2.19. Comparison of total normal stresses on the interface elements adjacent to the wall on the flood side and landside for flood el 10 ft and gap el -15 ft.

pressure values computed using a factor of safety equal to 1.5. Figure 2.19 shows the pressure results for the peak flood elevation of 10 ft. On the landside, the pressure results more closely match the passive pressures (with a factor of safety of 1.0) down to el -4 ft because of the increased flood loading. Again, the complete SSI analysis computes hydrostatic water pressures acting on the flood side, down to the gap tip elevation of -15 ft. Kickback of the I-wall into the flood side soil again is observed near the pile tip. This behavior is consistent with conventional force equilibrium procedures.

The computed fraction of mobilized shear strength for selected floodwater elevations and gap depths is shown in Figure 2.20. As mentioned, a fraction of mobilized shear strength equal to 1 indicates full mobilization of shear strength. As shown in Figures 2.20(a) and 2.20(b), for the specified flood elevation and gap depth, there are no regions of full mobilization of shear strength. These results indicated there is reserve shear capacity in the soil regime and, thus, a stable numerical model at these stages of construction. Figure 2.20c, with the design flood depth of 9 ft and gap depth of -15 ft, shows small regions of full mobilization of shear strength on the landside near the concrete cap. However, there is no indication of a fully developed failure mechanism at the stage of loading.

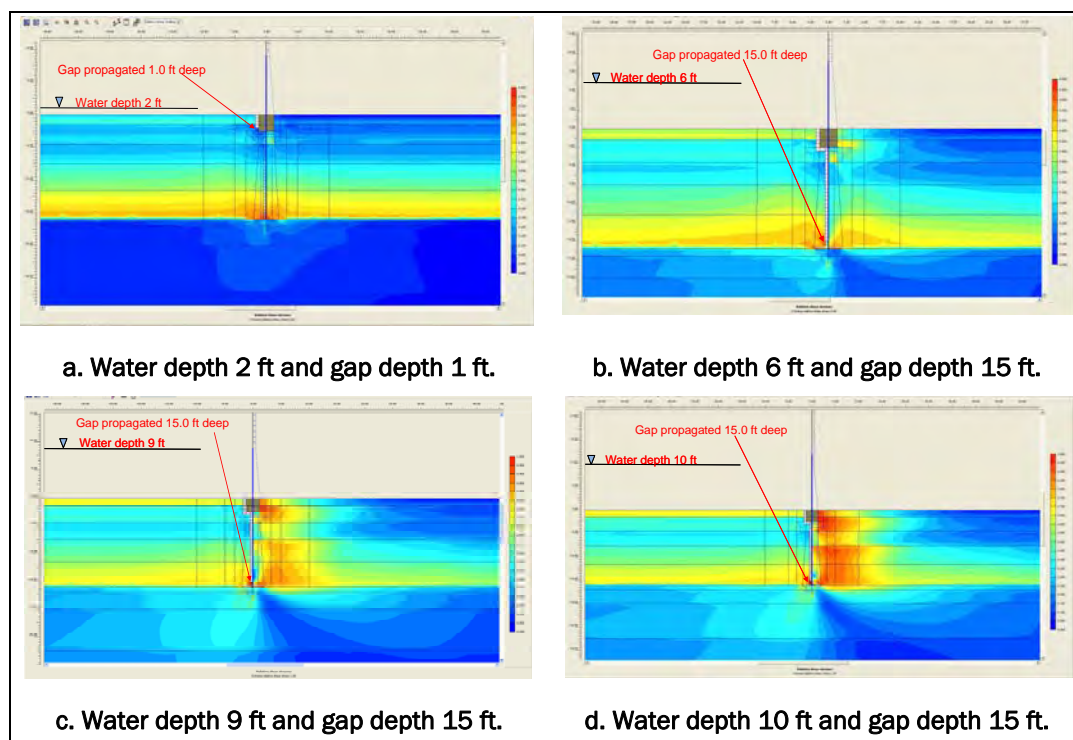


Figure 2.20. Fraction of mobilized shear strength at various loading phases.

Figure 2.20(d), with peak flood elevation of 10 ft and gap depth of -15 ft, shows larger regions of full mobilization of shear strength. An additional loading phase with a flood elevation at 11 ft was attempted, but it resulted in numerical instability. A subsequent PLAXIS analysis was performed at the peak flood elevation of 10 ft and gap depth at elevation of -15 ft to compute a factor of safety against a possible rotational failure mechanism. Figure 2.16 indicated that the wall was rotating about a point near the pile tip. Figure 2.21 shows a failure mechanism based on the PLAXIS Phi/c reduction procedure. The resulting rotational factor of safety was computed to be equal to 1.23.

However, at intermediate flood elevations, less than el 9 ft, rotation of the wall was not indicated. It is believed that the Phi/c reduction procedure would compute factors of safety based on localized shear failures with the active driving wedge only. Therefore, for this analysis, the Phi/c reduction procedure was not further used to compute factors of safety resulting from rotational failure mechanisms (as is performed in limit equilibrium procedures) for intermediate flood elevations.

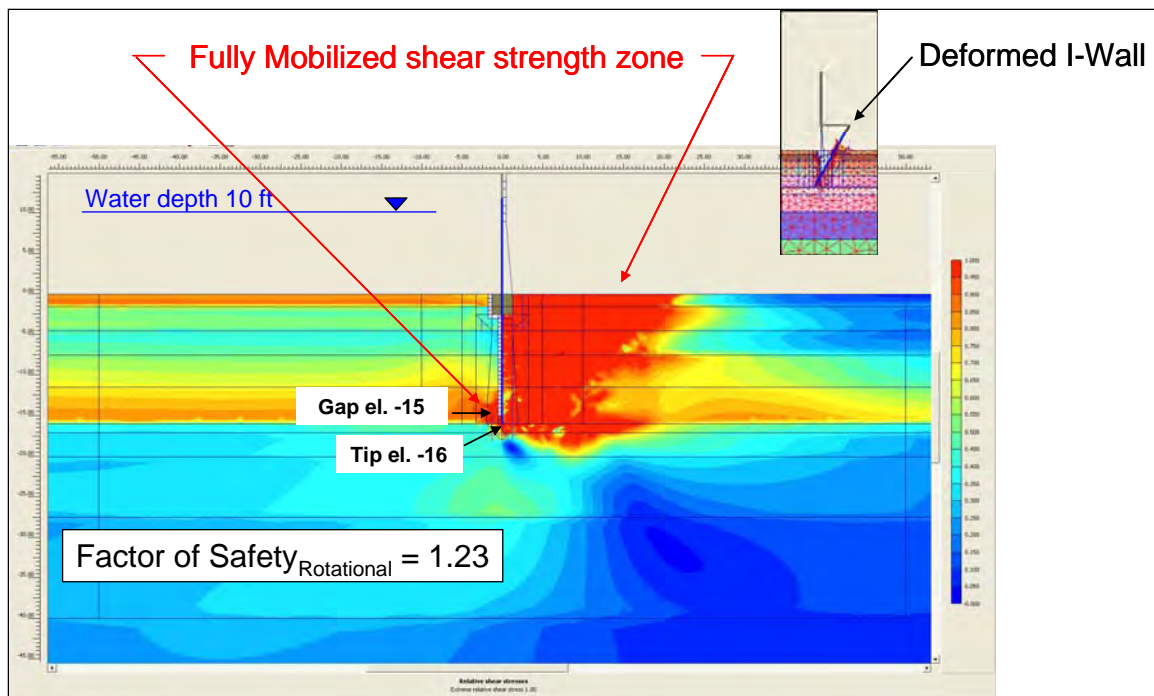


Figure 2.21. Rotational factor of safety using Phi/c reduction for peak flood elevation of 10 ft.

3 Analyses of I-Wall Site Founded in Clay with High Plasticity

3.1 Purpose of analyses

This chapter summarizes the results of nonlinear SSI finite element analyses of the E-99 sheet-pile wall field load test as described by Jackson (1988). This analysis included the formation and propagation of a gap beside the sheet-pile wall on the flood side. This gap affected the resulting deformation and stress conditions of the soil regime on both the flood side and landside of the I-wall. The results from this complete nonlinear SSI finite element analysis were compared to the results from the actual field load test.

The following sections will describe the soil used in the analyses, the selection of stiffness and shear strength parameters, the conventional analysis and design of the I-wall, the analysis procedures employed, and the results of the finite element analyses.

3.2 Overview of problem analyzed

The E-99 field load test consisted of a 200-ft section of floodwall constructed on the landside berm of the Item E-99 East Atchafalaya Basin Protection Levee (EABPL) on Avoca Island, just south of Morgan City, Louisiana. The test was performed between July and September of 1985 (Jackson 1988).

The soil geometry, maximum water height, and pile geometry of the field load test are shown in Figure 3.1. The sheet pile is located on the landside of the existing levee. The water loading was applied between the existing levee and the sheet-pile wall. The geometry was idealized as shown in Figure 3.2 and is assumed to be a flat (level) site. The elevation of the top soil layer is 6.5 ft.

The sheet pile used was a PZ-27. The section properties of the PZ27 are:

- Driving distance = 18 in.;
- Weight per foot = 40.5 lb/ft;
- Section modulus $S = 30.2 \text{ in.}^3/\text{ft}$ Area = 11.91 in.^2 ;

- Moment of inertia $I = 184.2 \text{ in}^4/\text{ft}$
- Height = 12 in.;
- Width = 18 in.

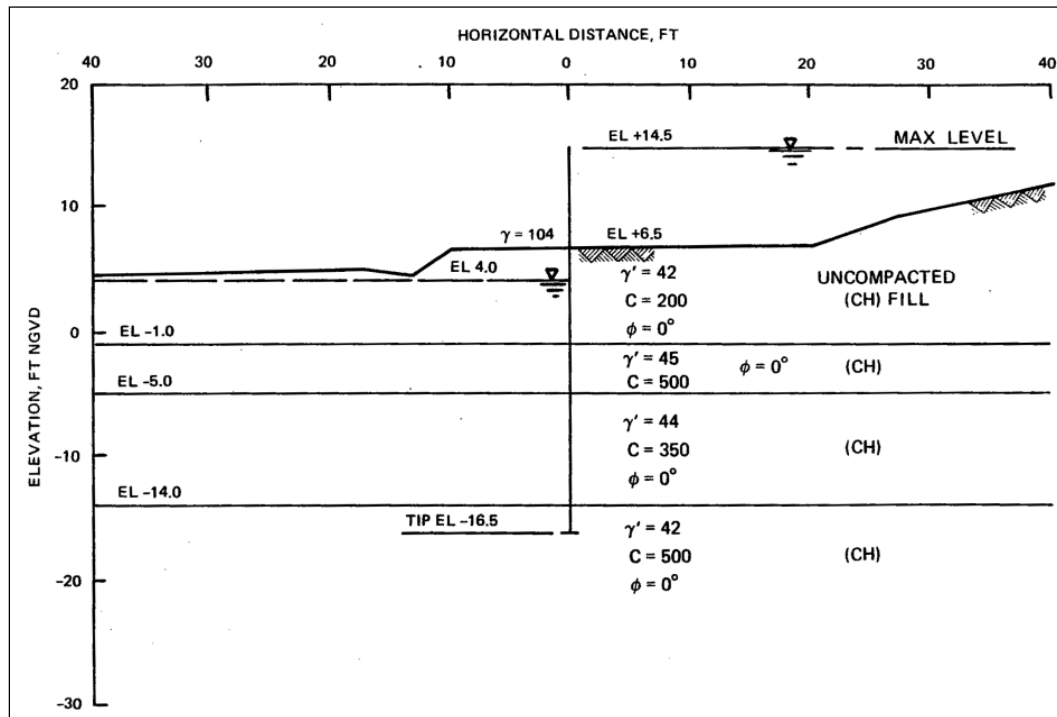


Figure 3.1. Soil geometry of E-99 field load test (Jackson 1988).

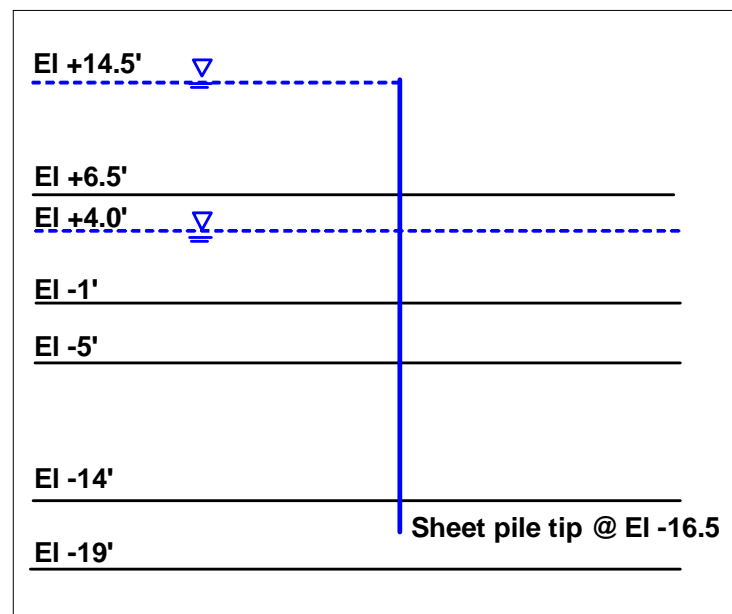


Figure 3.2. Idealized problem geometry.

The top of the sheet-pile wall was at el 14.5 ft, and the tip of the sheet-pile wall was at el -16.5 ft. Four sections along the I-wall were instrumented with strain gauges and inclinometers to measure moments and deflections in the I-wall. Piezometers were used to measure pore pressures. The locations of the instrumented sections and inclinometers are shown in Figure 3.3. The sections are labeled Test Pile A, Test Pile B, Test Pile C, and Test Pile D.

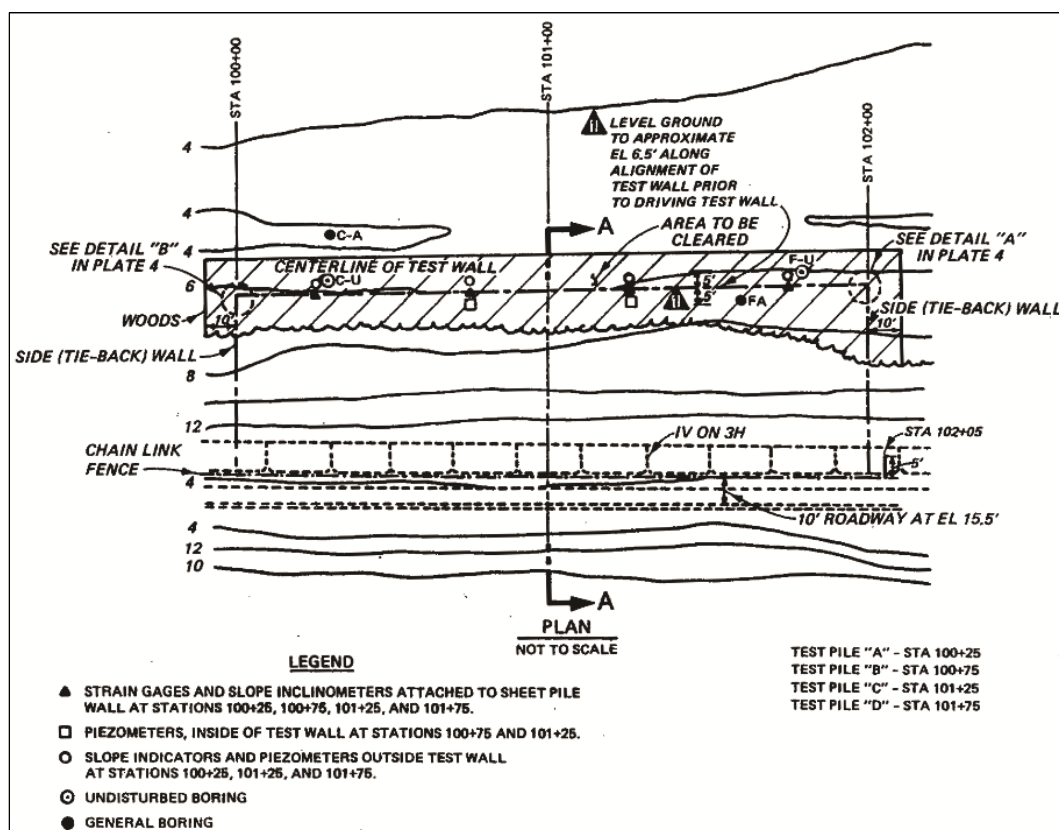


Figure 3.3. Location of instrumented sections of I-wall (Jackson 1988).

Both unconsolidated undrained (UU) and unconfined compression (UC) tests were performed, and design strengths that ranged from 200 to 500 psf in the region of the sheet-pile wall were chosen. The soils at the site were clays of high plasticity designated as a clay of high plasticity (CH) in the Unified Soil Classification System (USCS). From the classification chart shown in Figure 3.4, the plasticity index (PI) of a CH material has a value of 22 and greater. The soil was normally consolidated with LLs between 76 and 114 percent and natural water contents between 40 and 80 percent.

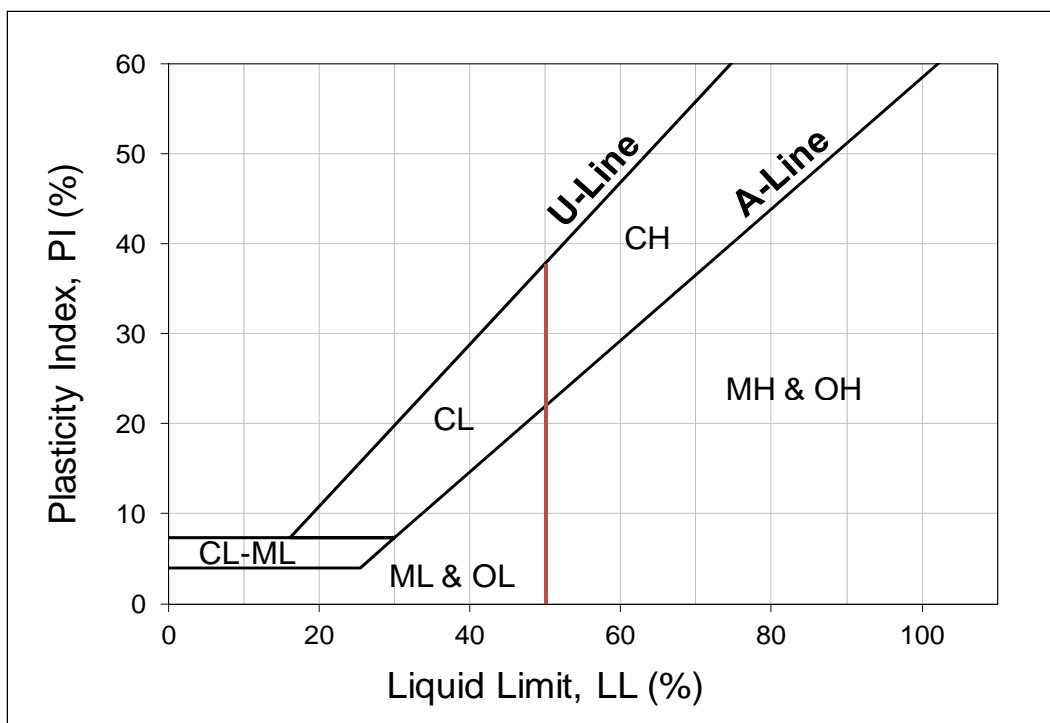


Figure 3.4. USCS plasticity chart for fine-grained soils (see Figure 2.2 on page 9 for explanation of soils).

In the field test, the level of the floodwater was raised in increments over several months, allowing time for the displacements of the wall to stabilize before additional loading was added. Displacements of the wall measured at the instrumented locations increased approximately the same, to a head level of 6 ft. Beyond 6 ft of head, the I-wall was reported to experience plastic deformations as seen from the resulting load deflection data. At 7 ft of head, the instrumented locations experienced differing amounts of deflection at the top of the wall, with the greatest at locations A and B and least at locations C and D. The deflections stabilized after a few days for locations C and D, but kept increasing at locations A and B for two weeks before the addition of more loading. When the wall was loaded to 8 ft of head, the displacements at all locations still were increasing after nine days with the most displacement at A and lower displacements at B, C, and D. On the ninth day at a head of 8 ft, seals at the ends of the walls ruptured allowing the pool to drain.

For the analyses explained in this chapter, the permeability of the clay layers was assumed to be small enough that the soil would not become fully saturated as the floodwater level was increased. Therefore, as shown in Figure 3.2, two zones of soil were considered: a partially saturated zone

above the water table elevation of 4 and a saturated zone of soil below the water table.

3.3 Conventional design of cantilever I-wall

3.3.1 Modeling a total stress problem in CWALSHT with consideration of a gap

CWALSHT is designed to analyze effective stress (drained) problems. That is, both the input and computations conform to the procedure that would be used to analyze an effective stress (drained) analysis. Most notably, water levels are input to account for the effects of water (both hydrostatic and seepage). To properly account for the water loadings, care must be taken when performing a CWALSHT analysis for a short-term (undrained) condition. For the short-term condition using a total stress method of analysis, pore pressures should not be calculated nor used within the soil layers. External water loadings must be accounted for in the analysis. Therefore, vertical uniform and horizontal boundary pressure loads must be used to represent the external loading due to the water. Water levels would not be input and, therefore, pore pressures within the soil would not be computed.

Also, for a short-term analysis with a soil having an angle of internal friction (ϕ) of 0, a gap will form on the flood side of the wall, as shown in Figure 3.5. The depth of the gap must be computed before CWALSHT is run and is based on a hydraulic fracturing concept as discussed in Section 3.3.3. To model this gap and the external pressures due to the water, the input for the CWALSHT model will be different from the actual geometry, as shown in Figure 3.5. The soil down to the elevation of the bottom of the computed gap will be replaced by two external pressure loadings. A horizontal pressure loading will represent the water pressure against the wall above the level of the soil and down to the bottom of the gap. A vertical pressure loading will replace the effects of the total vertical overburden of the flood pool and the soil down to the bottom elevation of the gap. No water levels will be input in CWALSHT and, therefore, no pore pressures will be generated within the soil. The unit weights of the soil used in the analysis would correspond to moist and saturated unit weights. Buoyant unit weights are not input. These input conditions adequately represent a total stress analysis in CWALSHT.

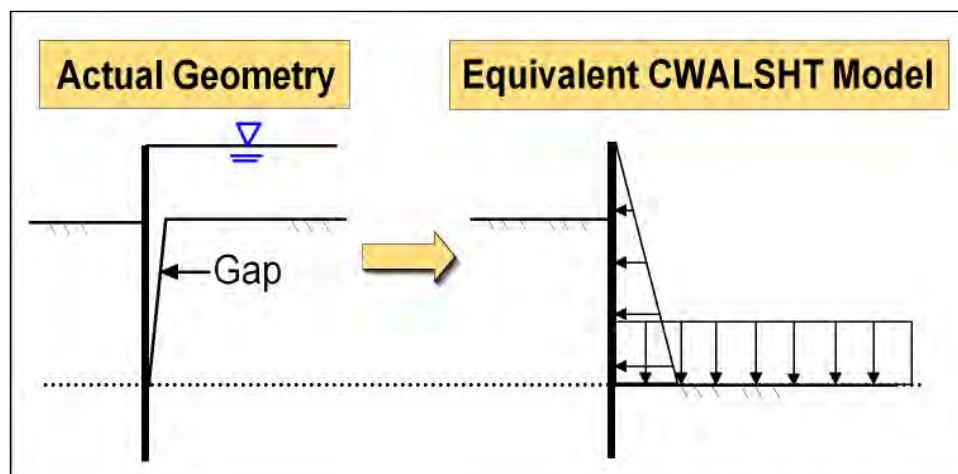


Figure 3.5. Equivalent CWALSHT model to account for gap.

3.3.2 Computation of active and passive earth pressures

For a conventional design, horizontal earth pressures against the cantilever wall must be computed. Both active and passive earth pressures on both the flood side and landside of the wall are used to design the depth of penetration and size the sheet-pile wall section. Coulomb or Rankine earth pressure coefficients can be used to compute the earth pressures, depending on the applicable conditions (Clayton et al. 1993; Craig 1997). Using the active earth pressure coefficient (K_a), the horizontal active earth pressure (σ_{ha}) can be computed using Equation 3.1 (Clayton et al. 1993):

$$\sigma_{ha} = K_a (\gamma z + q) - 2c\sqrt{K_a}, \quad (3.1)$$

where

- γ = the saturated or moist unit weight of the soil for a total stress analysis and the buoyant unit weight for an effective stress analysis (units of force/length³);
- z = the depth at which the pressure is computed (units of length);
- q = surcharges on the soil surface (units of force/length²).

This equation is applied to an I-wall in level ground and can be used for a soil having both a cohesion (c) and an angle of internal friction (ϕ).

K_a includes the effects of wall friction. If the effects of adhesion against the I-wall are to be considered, Equation 3.1 can be expanded to include adhesion by the addition of an adhesion factor (r) as given by Equation 3.2:

$$\sigma_{ha} = K_a(\gamma z + q) - 2c\sqrt{K_a}r. \quad (3.2)$$

The adhesion factor is given by Equation 3.3:

$$r = \sqrt{1 + \frac{c_a}{c}}, \quad (3.3)$$

where

c_a = adhesion between soil and sheet-pile wall (force/length²);

c = cohesion of soil (force/length²).

The horizontal passive earth pressures can be computed using the passive earth pressure coefficient (K_p) and Equation 3.4:

$$\sigma_{hp} = K_p(\gamma z + q) + 2c\sqrt{K_p}r. \quad (3.4)$$

For the case of a soil with $\phi=0$, the values of (K_a) and (K_p) are equal to 1.0. Also, the critical failure angle of the soil wedge corresponding to the minimum active or maximum passive earth pressure is equal to 45 deg for level ground. Therefore, for a soil with $\phi=0$, Equations 3.2 and 3.4 reduce to, respectively:

$$\sigma_{ha} = (\gamma z + q) - 2cr \quad (3.5)$$

$$\sigma_{hp} = (\gamma z + q) + 2cr. \quad (3.6)$$

3.3.3 Criteria for gap initiation and propagation

Two criteria are used to determine if a gap initiates in the soil adjacent to the sheet-pile wall and how far the gap will propagate, one for the flood side and another for the landside. A hydraulic fracturing criterion is used for the flood side of the I-wall (Criterion 1). A negative horizontal stress criterion is used for the landside of the I-wall (Criterion 2).

3.3.3.1 Criterion 1

When the hydraulic fracturing criterion is used, a gap will initiate on the flood side when the hydrostatic water pressures due to the flood loading

(of the pool) exceed the total horizontal earth pressures at the interface between the sheet-pile wall and the soil. The hydrostatic water pressure is computed as the height below the floodwater times the unit weight of water. The depth of the gap will proceed until the total horizontal earth pressure equals the hydrostatic water pressure of the flood pool.

For a layered system as shown in Figure 3.2, the total horizontal stress is computed using Equation 3.5 for points along a vertical section extending down to the pile tip. For the flood side, the total vertical stress at a point is computed taking into account all soil layers and external water loads above the point in question. The total horizontal stress is computed using this value of the total vertical stress in Equation 3.5 and compared to the hydrostatic water pressure computed based on the height of the floodwater and the distance to the point in question. If the water pressure is greater than the horizontal earth pressure, the soil is assumed to form a gap. This criterion for predicting gap depth is discussed in Brandon et al. (2008).

3.3.3.2 Criterion 2

The depth of gap computed using this criterion is based on whether the computed total horizontal stress is less than zero. The total horizontal stress at a point is computed using Equation 3.5. If the result is a negative or tensile value, the soil is assumed to form a gap. The gap extends down to a point where the horizontal earth pressures become positive.

3.3.4 Material properties for use with CWALSHT

The undrained shear strength of the clay layers was determined from unconsolidated undrained (UU) tests and unconfined compression (UC) tests. The design strengths used for the conventional and finite element analyses are shown in Figure 3.6 and Table 3.1. These strengths were used to perform an undrained short-term design of the wall. The material property values consist of the saturated (γ_{sat}) and moist (γ_{moist}) unit weights of the soil, the undrained shear strength (S_u), and adhesion (c_a). The angle of internal friction (ϕ) and wall friction (δ) are zero because this was an undrained analysis. The same value of the unit weight was used for both saturated and moist conditions. A value of 0.8 for f_{cmax} , which is the adhesion (c_a) divided by the cohesion (c) of the soil, was assumed for the total stress analysis and was taken from values cited in Potyondy (1961) for a cohesive soil against rough steel.

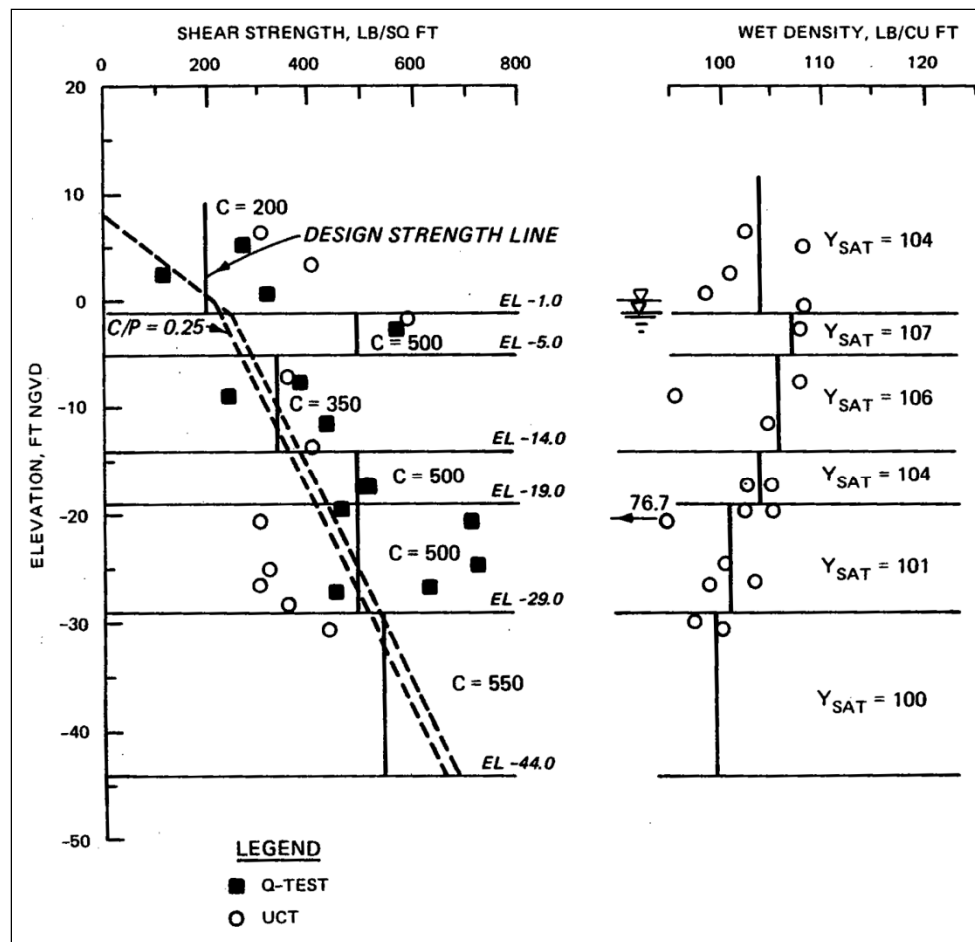


Figure 3.6. Soil layering and design strengths assumed for the E-99 field load test (Jackson 1988).

Table 3.1. Material properties for analyses.

Material	Elevation of Top of Layer, ft	γ_{moist} , lb/ft ³	γ_{sat} , lb/ft ³	S_u , lb/ft ²	C_u , lb/ft ²	Φ , deg	δ , deg
1	6.5	104	104	200	160	0	0
2	-1	107	107	500	400	0	0
3	-5	106	106	350	280	0	0
4	-14	104	104	500	400	0	0
5	-19	101	101	500	400	0	0
6	-29	100	100	550	440	0	0
7	-44	100	100	675	540	0	0
8	-72	100	100	925	740	0	0

3.3.5 Computed gap depth

CWALSHT uses the negative horizontal stress criterion discussed in Section 3.3.3 to compute whether a gap forms in the soil. Negative computed earth pressures imply that the soil-to-sheet-pile interface is in tension. Because the soil-to-sheet-pile interface cannot sustain a tensile load, the soil is assumed to form a gap and CWALSHT sets any negative (tensile) earth pressures to zero. CWALSHT applies water pressures within a gap below the input water level. If the gap is above the water level, CWALSHT does not fill the gap with water.

CWALSHT always computes effective stresses based on the input material properties and the level of the water in the soil. To perform a total stress (undrained) analysis, the procedure discussed in Section 3.3.1 should be followed. This requires that the gap depth is known before the analysis is run because the gap affects the modeling of the problem. If the gap depth is computed assuming no adhesion, the computed elevation of the bottom of the gap is -9.8 ft. If the gap depth is computed assuming an adhesion equal to $0.8 * c$ (from Potyondy's values), the elevation of the bottom of the gap is -25.3 ft, which is below the tip of the sheet pile.

The adhesion factor (r) in Equation 3.5 is computed as:

$$r = \sqrt{1 + \frac{c_a}{c}} = \sqrt{1 + 0.8} = 1.34. \quad (3.7)$$

These values of gap depths will be used in the CWALSHT analyses discussed in the next section.

3.3.6 CWALSHT design results

The elevation of the tip of the sheet pile for this analysis was -16.5 ft. A short-term analysis was performed with CWALSHT using the material properties given in Table 3.1. The analyses performed with CWALSHT are shown in Table 3.2.

Table 3.2. Results of design computations using CWALSHT.

Design Case		Adhesion, psf	Elevation of Bottom of Gap, ft	Elevation of Tip of Sheet Pile			Maximum Moment Computed Using $FS_{Active}=1.0$ $FS_{Passive}=1.0$ ft-lb
				FS_{Active}	$FS_{Passive}$	Elevation, ft	
1	Short term with surcharge loads	0	-9.8	1	?	No solution ¹	-
2	Short term with water levels	0	-9.8	1	1.5	-17.56	-
3	Short term with water levels	0	-9.8	1	1.4	-16.5	-
4	Short term with water levels	$0.8 \cdot S_u$	Below wall	1	1.89	-16.5	-
5	Short term with water levels	$0.8 \cdot S_u$	Below wall	1	1.5	-13.46	-
6	Short term with water levels	0	-9.8	1	1	-	21609
7	Short term with water levels	$0.8 \cdot S_u$	Below wall	1	1	-	16961

Note: S_u are design values, $\phi=0$, $\delta=0$.

¹ A stable solution in CWALSHT requires a loading that produces a counterclockwise wall rotation.

Several analyses were run with various combinations of parameters. Case 1 in Table 3.2 is an analysis with CWALSHT using the procedure described in Section 3.3.1. This case requires the depth of the gap beforehand and uses this information to replace the soil in the region of the gap with horizontal and vertical surcharges. This case would not converge to a solution.

Cases 2 through 7 were modeled with the actual soil layer geometry with input water levels. It was found that for a problem involving all clay layers, a total stress (short-term) analysis with $c = S_u$ and $\phi = 0$ could be performed with CWALSHT in this manner. This gives a correct total stress analysis because, even though CWALSHT computes effective stresses based on the input water levels, the pore pressures are added to the effective stresses to arrive at total stresses. Because the value of the horizontal earth pressure coefficient is equal to 1.0 for a soil with only cohesion, the total stress computed in this manner is correct. The determination of the depth of the gap also conforms to the hydraulic fracturing criterion described in Section 3.3.3. This is because CWALSHT computes effective stresses and uses the effective stresses to determine the tensile zone. The hydraulic fracturing criterion uses total stresses and compares these to static pore pressures, which end up being numerically equivalent.

Case 3 shows a factor of safety of 1.4 computed using CWALSHT for the actual elevation of the tip of the sheet pile of -16.5 ft. This run does not include adhesion. If adhesion is included (Case 4), then the factor of safety is equal to 1.89. Execution of the program Corps_I-wall, in a proper total stress analysis for this problem with a factor of safety equal to 1.4, results in a sheet-pile tip elevation of -16.5 ft, which is consistent with the results shown in Case 3.

The design guidance for cantilever walls states that the maximum moment used for sizing the sheet-pile section should be computed using a factor of safety for the active and passive earth pressures of 1.0 as shown in Cases 6 and 7. The maximum moment for Case 6 (no adhesion) is 21,609 ft-lb at an elevation of -2.84 ft, and the maximum moment for Case 7 (including adhesion) is 16,961 ft-lb at an elevation of -1.53 ft.

From these analyses, why the procedure described in Section 3.3.1 and the procedure described in this section do not yield the same results needs further investigation.

3.4 PLAXIS finite element analyses

3.4.1 Conceptual model

The finite element analyses were performed with PLAXIS, a 2-D nonlinear incremental construction finite element program. The conceptual model of the finite element mesh is shown in Figure 3.7. The geometry is the same as described previously, but several modeling features should be noted. The sheet-pile wall was represented by plate elements. Interface elements were placed on both sides of the plate elements from the ground surface down to the tip of the sheet pile. Extensions of the interface elements, both horizontally and vertically, were provided at the tip of the sheet-pile wall at el -16.5 ft. This was done to alleviate stress concentrations at the corners of the geometry. A plate element extension and dummy soil elements were added above the wall to provide for additional loading height, if needed. The mesh was structured to provide node points at 1-ft raises of the water table. The soil elements beside the sheet-pile wall on the flood side were 0.5 ft in height. This enabled the inputting of 1-ft raises in water and modeling of the gap to within 0.5 ft.

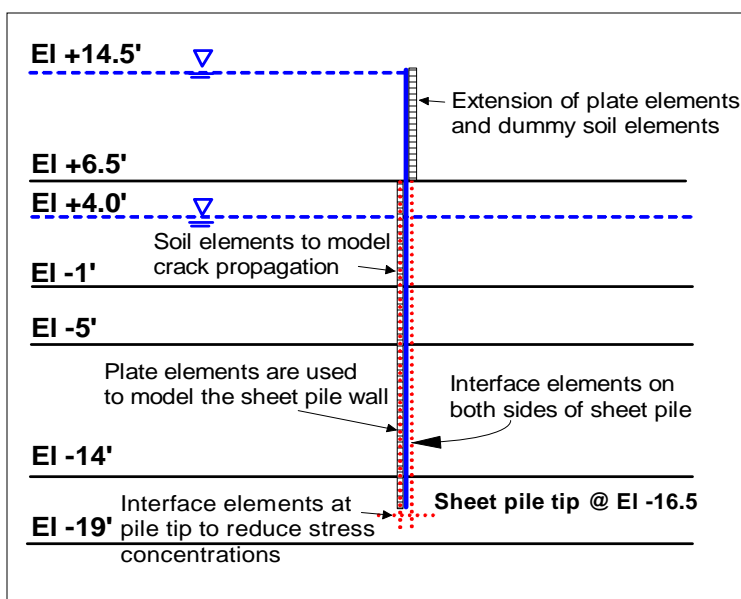


Figure 3.7. Conceptual model.

3.4.2 Finite element mesh

The finite element mesh used in the analyses is shown in Figure 3.8. Figure 3.9 shows an enlargement of the area around the wall and the detail of the mesh. The mesh is composed of 2,396 elements and 19,917 nodes with 28,752 stress points. The type and number of elements used in the mesh are shown in Table 3.3. The mesh consists of 15-node triangular elements to model the soil, 5-node plate elements to model the sheet-pile wall, and 5-node interface elements to model the soil-structure interaction effects between the sheet-pile wall and the adjacent soil elements. The problem was run as a plane strain problem.

3.4.3 Total stress analysis procedure in PLAXIS

The E-99 field test was analyzed as a short-term (undrained) analysis. To perform a short-term (undrained) analysis using PLAXIS, total unit weights of the soil and boundary water pressures were used. All materials were designated as drained, which in PLAXIS terminology means that no excess pore-water pressures will be generated from applied loads. The general phreatic surface was used in PLAXIS to apply the boundary water pressures on the soil surface and within the gap. All soil layers were associated with a cluster phreatic surface that was input below the minimum elevation of the mesh. Because the water surface is below all soil layers, no internal water pressures are generated within the soil layers. This procedure results in a total stress analysis with the computed effective stresses being equal to the total stresses (i.e., no internal pore pressures are present).

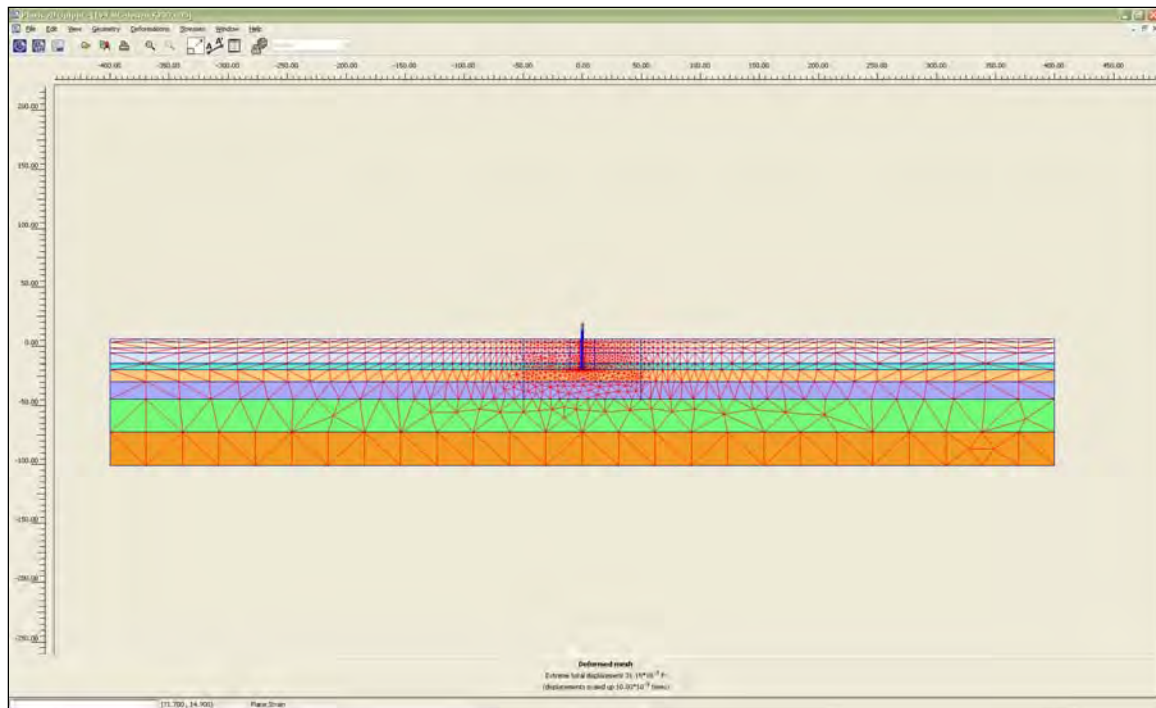


Figure 3.8. Finite element mesh used in the analyses.

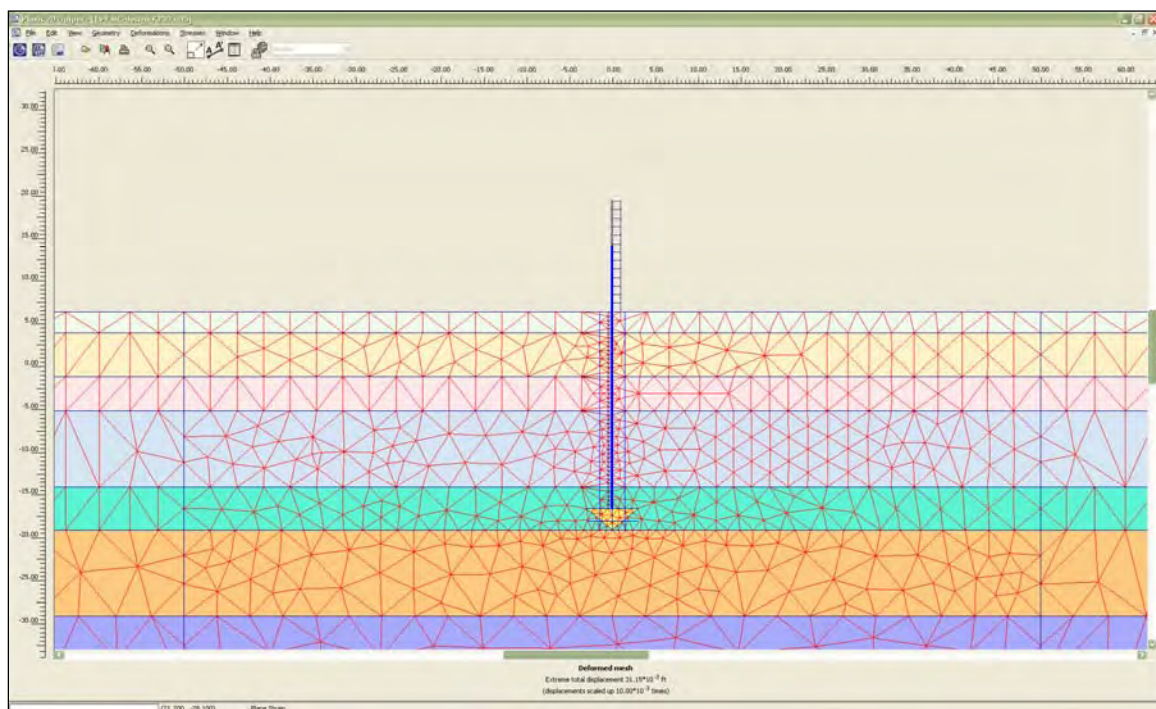


Figure 3.9. Enlargement of finite element mesh around the I-wall.

Table 3.3. Type and number of elements used in the finite element mesh.

Type	Type of Element	Type of Integration	Total Number
Soil	15-node triangular	12-point Gauss	2396
Plate	5-node line	4-point Gauss	59
Interface	5-node line	4-point Newton-Cotes	106

It is assumed that the permeability of the soil is small enough that any time-dependent effects, such as seepage, can be ignored and that the undrained shear strengths may be used to determine the behavior of the system.

3.4.4 Tracking the progression of the gap

The I-wall deflects as the flood loading increases, and eventually a gap forms beside the I-wall on the flood side of the wall. The gap begins at the ground surface and progresses downward as shown in Figure 3.10. The gap along the flood side of the I-wall-to-soil interface is modeled by deactivating soil clusters (elements), effectively creating a void beside the wall. As water pressures are applied within this void, the gap progresses downward. Modeling of the flood loading commenced in the finite element analysis after the total initial stress state was computed based on an assumed steady-state water elevation of 4 ft. The flood loading was applied in 1-ft incremental raises of the water level in order to track the formation and propagation of the gap.

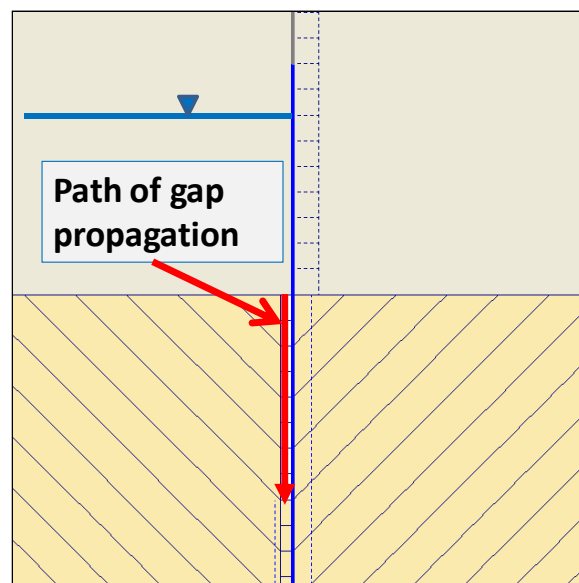


Figure 3.10. Location and propagation of gap beside I-wall.

The criterion used to estimate the formation and propagation of the gap is based on the hydraulic fracturing concept discussed in Section 3.3.3. The procedure used to estimate the gap depth:

1. For each rise in water level, the total horizontal stresses against the sheet-pile wall are compared against the hydrostatic water pressures acting on the wall, given the current water elevation. A gap is formed when the horizontal earth pressure is less than the water pressure at a given depth.
2. Soil elements are deactivated within the computed region of the gap, and hydrostatic water pressures are applied within the deactivated elements.
3. The analysis is rerun for the current water level, and Steps 1 and 2 are repeated until the depth of the gap ceases to increase.
4. The water level is increased, and Steps 1 through 3 are repeated. The water level is raised until instability in the analyses is encountered.

3.4.5 Shear strength and stiffness properties used in the finite element analyses

The finite element analyses required certain material properties for the selected soil models. All finite element analyses were performed with the PLAXIS finite element program. Separate analyses were performed using two different soil constitutive models to represent the behavior of the soil elements: the Hardening Soil (HS) model, which uses a nonlinear stress-strain relationship; and the Mohr-Coulomb (MC) soil model, which uses an elastic-perfectly plastic stress-strain relationship. Elastic plate elements were used to model the steel sheet pile, and interface elements were used to capture the soil-structure interaction effects between the sheet-pile wall and the soil. PLAXIS can perform analyses using either effective or total stress soil parameters. For the analyses described herein, total stress soil parameters were used.

Figure 3.11 shows the material numbering and soil layering used in the finite element analyses. The soil was divided into layers below the tip of the pile to provide for an increasing undrained shear strength and stiffness below the elevation of the pile tip. The values of the undrained shear strength for Materials 9 and 10 were computed by assuming a value of 0.25 for the ratio of the undrained shear strength to the effective overburden stress (S_u/σ'_{vo}), as shown in Figure 3.6. The increase in vertical stress above the vertical stress at el -44 ft was computed at the center of each layer. This stress increment was multiplied by $S_u/\sigma'_{vo}=0.25$, and the result added to the constant (S_u) equal to 550 psf to arrive at the undrained shear strength of each layer.

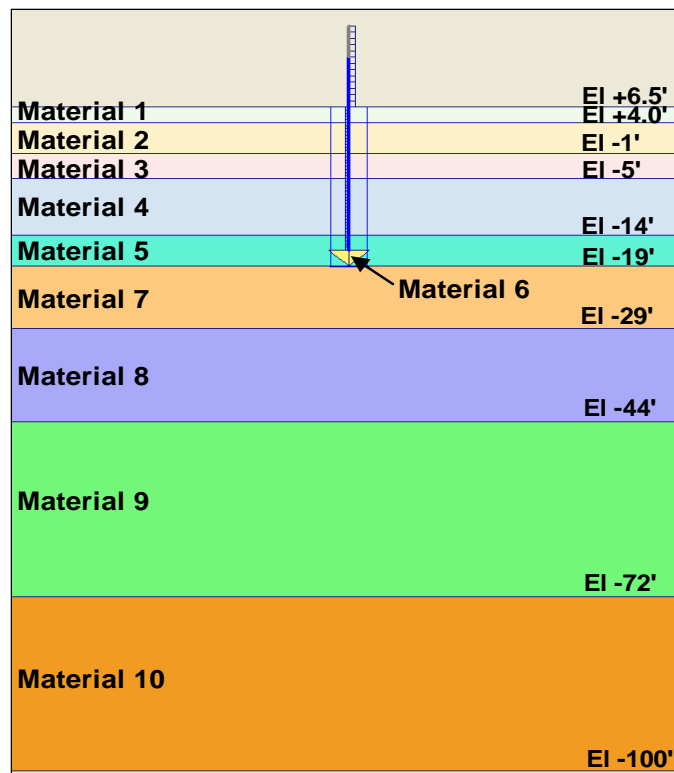


Figure 3.11. Soil layering and material numbers used in the finite element analyses.

The material properties used for the HS model are given in Table 3.4. The material properties used for the MC model are given in Table 3.5. The sheet pile was represented by elastic plate elements with the properties given in Table 3.6, where EA is the axial stiffness and EI is the flexural rigidity.

Table 3.4. Strength and stiffness properties for the soil layers used in the hardening soil model.

Material Number	Material Description	γ_{moist} , lb/ft ³	γ_{sat} , lb/ft ³	S_u , lb/ft ²	$E_{50,ref}$, lb/ft ²	$E_{oed,ref}$, lb/ft ²	$E_{ur,ref}$, lb/ft ²	$R_{interface}$
1	Clay_1_6.5_200_Rinit=0.8	104	104	200	120,000	120,000	360,000	0.8
2	Clay_2_4_200_Rinit=0.8	104	104	200	120,000	120,000	360,000	0.8
3	Clay_3_-1_500_Rinit=0.8	107	107	500	300,000	300,000	900,000	0.8
4	Clay_4_-5_350_Rint=0.8	106	106	350	210,000	210,000	630,000	0.8
5	Clay_5_-14_500_Rinit=0.8	104	104	500	300,000	300,000	900,000	0.8
6	Clay_5a_-14_500_Rinit=1.0	104	104	500	300,000	300,000	900,000	1
7	Clay_6_-19_500_Rinit=0.8	101	101	500	300,000	300,000	900,000	0.8
8	Clay_7_-29_550_Rinit=0.8	100	100	550	330,000	330,000	990,000	0.8
9	Clay_8_-44_675_Rinit=0.8	100	100	675	405,000	405,000	1,215,000	0.8
10	Clay_9_-72_925_Rinit=0.8	100	100	925	555,000	555,000	1,665,000	0.8

Note: properties are given for drained material, with ϕ and the dilation angle (Ψ) set to 0, as this is a total stress analysis. The unload/reload Poisson's ratio (ν_{ur}) is set to 0.2, and the interface strength (R_i) is set to 0.9.

Table 3.5. Strength and stiffness properties for the soil layers used in the Mohr-Coulomb soil model.

Material Number	Material Description	γ_{moist} , lb/ft ³	γ_{sat} , lb/ft ³	S_u , lb/ft ²	E_{ref} , lb/ft ²	ν	$R_{interface}$
1	Clay_1_6.5_200_Rinit=0.8	104	104	200	40,000	0.4	0.8
2	Clay_2_4_200_Rinit=0.8	104	104	200	40,000	0.495	0.8
3	Clay_3_1_500_Rinit=0.8	107	107	500	100,000	0.495	0.8
4	Clay_4_5_350_Rinit=0.8	106	106	350	70,000	0.495	0.8
5	Clay_5_14_500_Rinit=0.8	104	104	500	100,000	0.495	0.8
6	Clay_5a_14_500_Rinit=1.0	104	104	500	100,000	0.495	1
7	Clay_6_19_500_Rinit=0.8	101	101	500	100,000	0.495	0.8
8	Clay_7_29_550_Rinit=0.8	100	100	550	110,000	0.495	0.8
9	Clay_8_44_675_Rinit=0.8	100	100	675	135,000	0.495	0.8
10	Clay_9_72_925_Rinit=0.8	100	100	925	185,000	0.495	0.8

Note: properties are given for drained material, with ϕ and the dilation angle (Ψ) set to 0, as this is a total stress analysis.

Table 3.6. Properties of the plate elements representing the sheet pile.

Name	Material Behavior	EA, lb/ft	EI, lb-ft ²	Weight, lb/ft ²	ν
Sheet pile	Elastic	2.30E+08	3.71E+07	20.95	0.25

The $R_{interface}$ value was assumed to be 0.8, which is equal to the f_{cmax} value discussed in Section 3.3.4, taken from values cited in Potyondy (1961) for a cohesive soil against rough steel. This controls the amount of adhesion along the soil-to-wall interface. Material 6 in Table 3.4 has an $R_{interface}$ value of 1.0 because this material represents a soil-to-soil interface. The R_f value controls the shear strength at failure and is a percentage of the maximum shear strength.

The HS model uses a secant reference stiffness ($E_{50,ref}$), an oedometer reference stiffness ($E_{oed,ref}$), and an unload/reload reference stiffness ($E_{ur,ref}$), as shown in Table 3.4. Equations 3.8 and 3.9 show the assumed relationship between the E_{50} reference stiffness and the oedometer and unload/reload reference stiffnesses:

$$E_{oed,ref} = E_{50,ref} \quad (3.8)$$

$$E_{ur,ref} = 3 \cdot E_{50,ref} \quad (3.9)$$

The E_{50} stiffness is dependent on the reference stiffness ($E_{50,ref}$), a reference pressure (p_{ref}), the confining stress (σ_3'), the cohesion (c), the angle of internal friction (ϕ), and a fitting parameter (m), as shown in Equation 3.10:

$$E_{50} = E_{50,ref} \left(\frac{c \cdot \cos f - \sigma_3' \sin f}{c \times \cos f - p_{ref} \sin f} \right)^m. \quad (3.10)$$

For ϕ equal to zero, Equation 3.10 reduces to Equation 3.11:

$$E_{50} = E_{50,ref}. \quad (3.11)$$

The value of m does not make a difference when ϕ is equal to zero.

To compute the initial value of the E_{50} stiffness, a chart developed by Duncan and Buchignani (1976) relating the plasticity index, the over-consolidation ratio, and a factor K defined in Equation 3.12 is used:

$$K = \frac{E_u}{S_u}. \quad (3.12)$$

With a K value from the chart and the undrained shear strength of the soil layer, Equation 3.13 can be used to compute the stiffness of the soil layer:

$$E_u = E_{50}^{ref} = KS_u. \quad (3.13)$$

The material properties for the MC model given in Table 3.5 are identical to those of the HS model, except not as many properties are required. The reference stiffness values for the MC model in Table 3.5 are set equal to the $E_{50,ref}$ stiffness values from the HS model.

Initial $E_{50,ref}$ stiffness values were assigned to the HS and MC models based on the assumption that the soil layers had a plasticity index (PI) of 50 and were normally consolidated. Using the chart from Duncan and Buchignani (1976), an initial value of (K) of 300 was selected, and Equation 3.13 was used to compute the stiffness of the soil layers. This gave a starting point for comparison of the displacements from the HS and MC analyses with the

actual displacements observed in the field. The displacements, as well as the relative displacements of the top of the sheet pile, were compared to the observed field results. The relative displacement at the top of the sheet pile is the displacement of the top of the sheet pile minus the tip displacement. Table 3.7 shows these displacements for various values of K . Figure 3.12 shows the horizontal displacement of the top of the pile versus K , and Figure 3.13 shows the relative displacement of the top of the pile versus K . As K increases, the stiffness of the soil layers increase and, thus, the horizontal displacements decrease.

Analyses were run for the case of water at el 14.5 ft and the bottom of the gap at el -10 ft. This case corresponded to design Case 3 in Table 3.2. The gap progression was not tracked in these analyses. The loading was applied in one construction step. PLAXIS applies the load increment in many substeps for convergence. Previous experience with I-wall analyses has shown that the results of a complete analysis tracking the gap progression and this simplified procedure are comparable as long as the gap depth does not vary greatly and no unloading of the system occurs.

Table 3.7. Variation of displacements of the top of the pile with K .

HS						
K	Top		Tip		Relative - Top	
	ft	in.	ft	in.	ft	in.
100	0.6230	7.4763	0.0715	0.8583	0.5515	6.6180
150	0.5013	6.0161	0.0418	0.5019	0.4595	5.5142
200	0.3351	4.0211	0.0379	0.4552	0.2972	3.5659
250	0.2952	3.5424	0.0313	0.3757	0.2639	3.1668
600	0.1782	2.1380	0.0137	0.1645	0.1645	1.9735
MC						
K	Top		Tip		Relative - Top	
	ft	in.	ft	in.	ft	in.
100	-	-	-	-	-	-
150	0.7080	8.4956	0.2641	3.1690	0.4439	5.3265
200	0.5495	6.5935	0.1992	2.3901	0.3503	4.2034
250	0.4545	5.4541	0.1601	1.9216	0.2944	3.5325
600	0.2313	2.7762	0.0685	0.8220	0.1628	1.9541

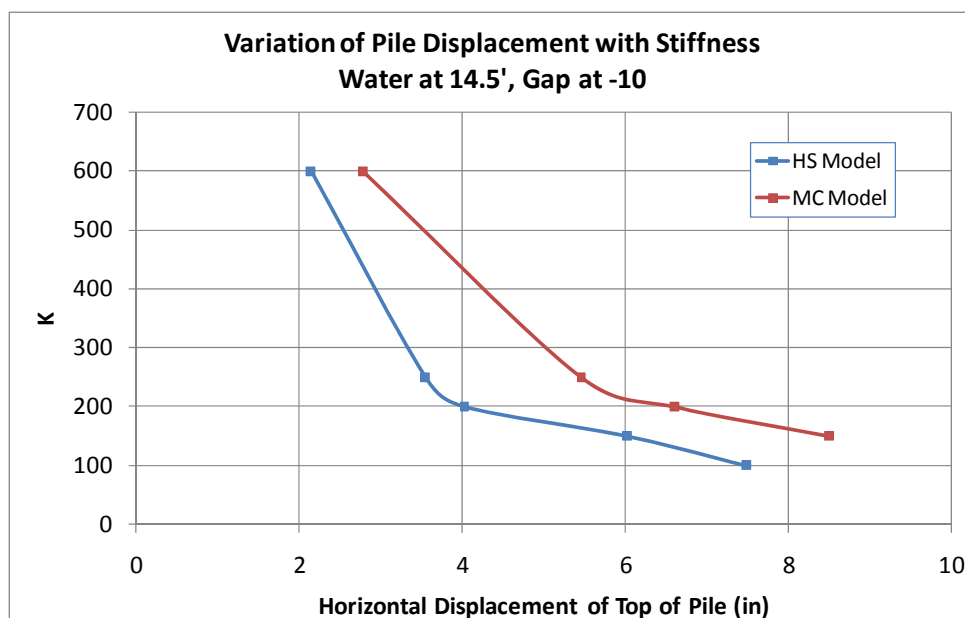


Figure 3.12. Variation of horizontal displacement of top of pile with K .

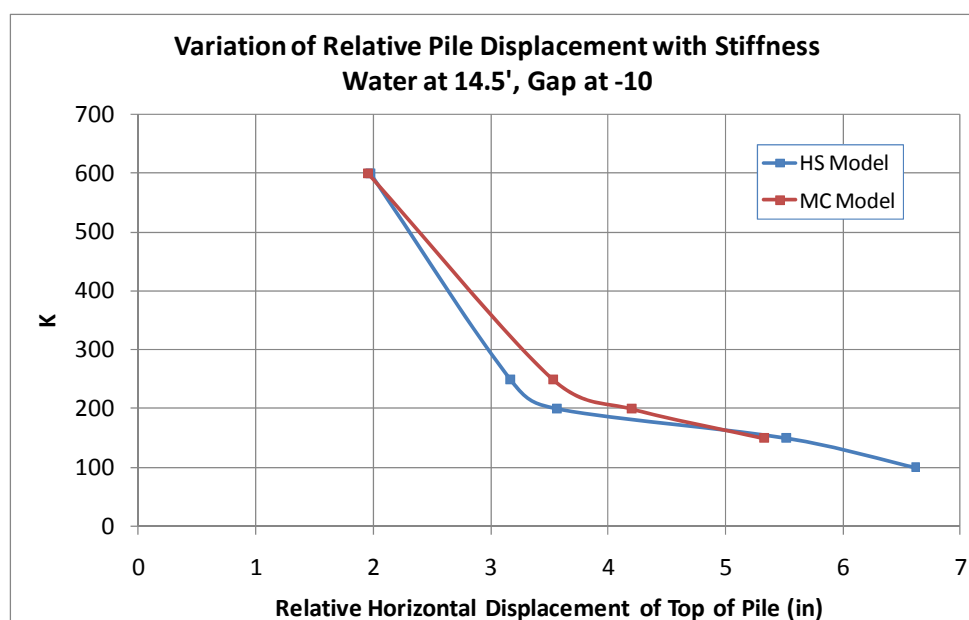


Figure 3.13. Variation of relative horizontal displacement of top of pile with K .

Table 3.8 shows the observed data at four instrumented locations parallel to the sheet-pile wall. The ground varied along the wall; therefore, the values of head applied to the sections of the wall varied as shown in Table 3.8. Sections C and D were chosen as the most appropriate locations to try to match the displacements of the sheet-pile wall, as they were close to the same soil elevation and water loading used in the finite element model. The tip displacements observed in the field varied between 0.25 and 0.50 in. The HS model with a K of 200 resulted in a displacement of the top of the pile

Table 3.8. Observed displacements of top of sheet pile and maximum moments (Jackson 1988).

Test Pile	Head, ft	Lateral Deflection, in.	Maximum Stress, psi	Maximum Moment, ft-lb	EI of Maximum Moment, ft NGVD
A	8.3	8	9800	25100	-5.5
B	8.1	6	7200	18400	-5.5
C	7.8	4	6500	16500	-5.5
D	7.8	4	7500	19200	-3.5

of 4.02 in. and a displacement of the tip of the sheet pile of 0.46 in. The MC model with a K of 200 resulted in a displacement of the top of the pile of 6.59 in. and a tip displacement of 2.39 in. For the MC case, the relative displacement was compared to the field results. Because the head applied in the analyses was slightly more than in the field, the value of 4.20 in. for the relative displacement compared to 3.5 to 3.75 in. in the field was considered acceptable. The relative displacements for the HS and MC models are close at the upper and lower values of K in Table 3.7. The value of 200 for K is in agreement with the value reported by Oner et al. (1997).

3.4.6 Initial stresses

The initial total stress state within the finite element mesh was established using the at-rest soil conditions for a level ground surface. Horizontal at-rest soil stresses were estimated using the following relationship between the at-rest earth pressure coefficient (K_o) and the soil's Poisson's ratio (ν):

$$K_o = \frac{\nu}{1 - \nu} \quad (3.14)$$

The assumed groundwater elevation was 4 ft. Table 3.9 summarizes the K_o values used to compute the horizontal earth pressures for the initial conditions. The Poisson's ratio (ν) for the partially saturated soil layer is 0.4, which corresponds to a K_o of 0.67. This value is less than the value of K_o for a fully saturated material, which is 1.0.

Table 3.9. Poisson's ratio and at-rest horizontal earth pressure coefficients used for analyses.

Soil Condition	Elevation Range, ft	ν	K_o
Partially saturated	6.5 to 4	0.4	0.67
Saturated	4 to -100	0.495	1

3.4.7 Performance of interface elements

The performance of the interface elements was examined to determine if the normal stresses in the interface elements corresponded closely to the normal stresses in the adjacent soil elements. Results for the case of flood pool at el 14.5 ft and gap tip at el -10 ft were used for this comparison. Figure 3.14 shows that the stresses within the interface elements agree very closely with the stresses in the adjacent soil elements and that the processing of results could be done using either data set. Most of the results presented use the stresses extracted from the soil elements adjacent to the sheet-pile wall.

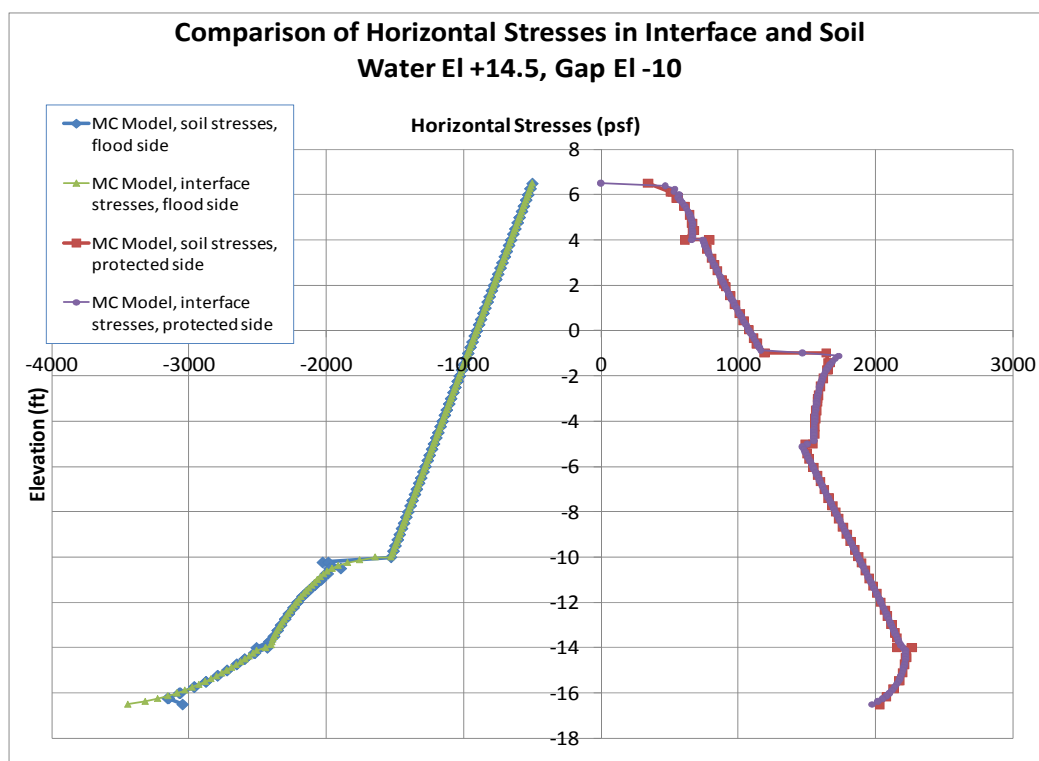


Figure 3.14. Behavior of interface versus soil elements for water el 14.5 ft and gap el -10 ft.

3.4.8 Comparison of HS and MC models

As stated, analyses were conducted using both the HS and MC models in PLAXIS to represent the soil response. When the progression of the gap was tracked, as detailed in Section 3.4.4, for lower water levels than the design flood height of 14.5 ft, the HS model produced large relative shear stresses on the flood side. The externally applied hydrostatic water loads caused by settlement of the soil caused the wall to deflect toward the flood side. As the water levels increased, the wall was pushed into the landside.

The MC model did not exhibit these same characteristics, and the procedure detailed in Section 3.4.4 could be followed to track the gap progression as the water level was increased. Because the HS model captures nonlinear stress-strain behavior and the MC model does not, a comparison of the models was performed to determine if the results from the MC model could be used reliably to determine the behavior of the system.

Figures 3.15 through 3.18 compare results from the HS and MC models and are based on results for the design flood condition of water el 14.5 ft and gap tip el -10 ft. Figure 3.15 compares the normal stresses in the interface elements on each side of the sheet-pile wall for both the HS and MC models. As can be seen from the figure, the normal stresses are in fair agreement on both the flood side (left) and protected side (right), or landside.

The displacements of the sheet-pile wall are shown in Figure 3.16. The displacements from the MC model were greater than those from the HS model at both the top and tip of the sheet pile. If the difference between the tip displacements of the MC model and the HS model are subtracted from the MC model, the resulting displacements of the MC model match the HS model within 19 percent.

Figure 3.17, which compares the moments in the sheet-pile wall, shows that the value of the maximum moment of the MC model exhibits less than 1 percent error compared to that of the HS model. As can be seen from Figure 3.18, the magnitude and distribution of the mobilized shear strength of the MC and HS models are similar.

From this comparison, it was determined that the results of the MC model are consistent with the results from the HS model and would be used to report the post-processing results.

3.4.9 Progression of gap propagation for MC model analyses

Figure 3.19 shows the progression of the gap as the water level against the I-wall increases from 1 ft (el 6.5 ft) up to 11 ft (el 17.5 ft). The gap initiates at a water elevation of 7.5 ft and extends to a depth of 4 ft. The gap essentially increases linearly as depicted by the black dotted line in Figure 3.19. The depth of the gap extends to el -12.5 ft at a water elevation of 17.5 ft. The tip of the sheet pile is at el -16.5 ft.

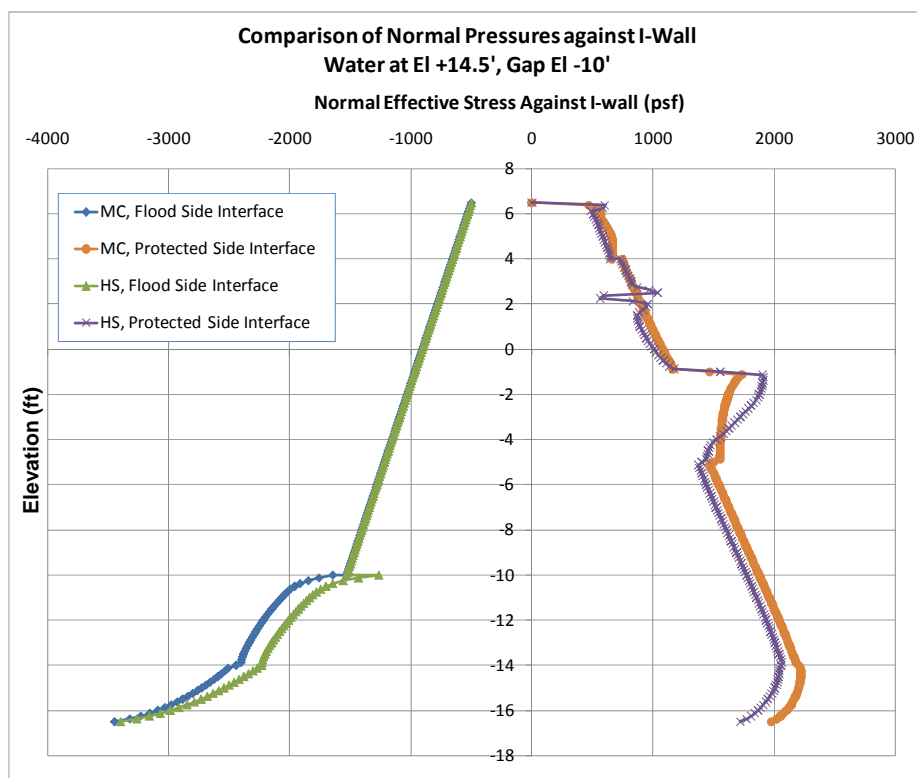


Figure 3.15. Comparison of normal pressures for the HS and MC models.

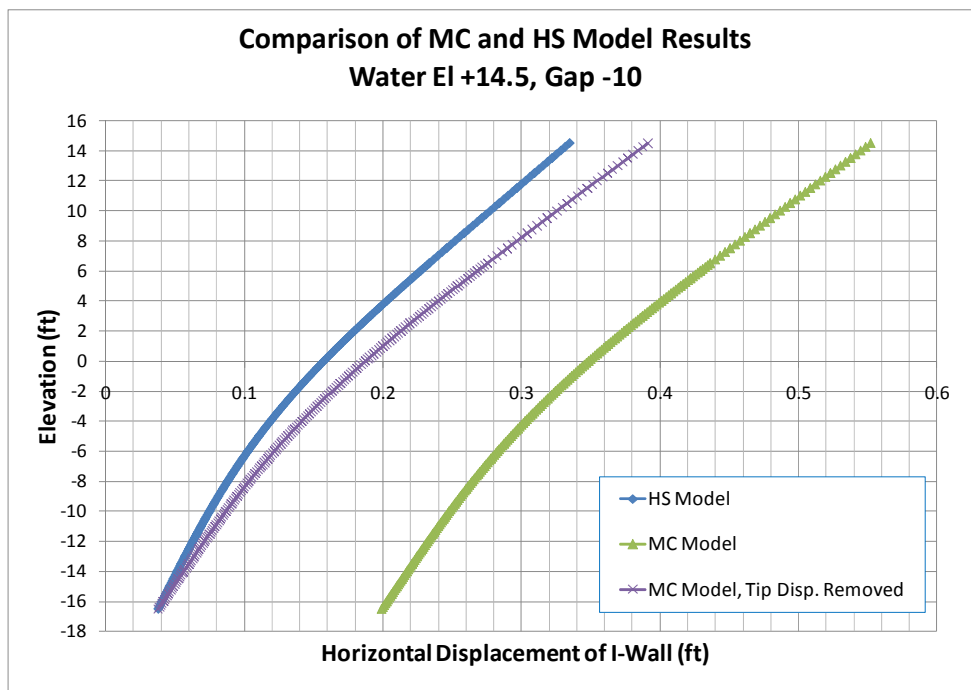


Figure 3.16. Comparison of the deflections of the sheet-pile wall for the HS and MC models.

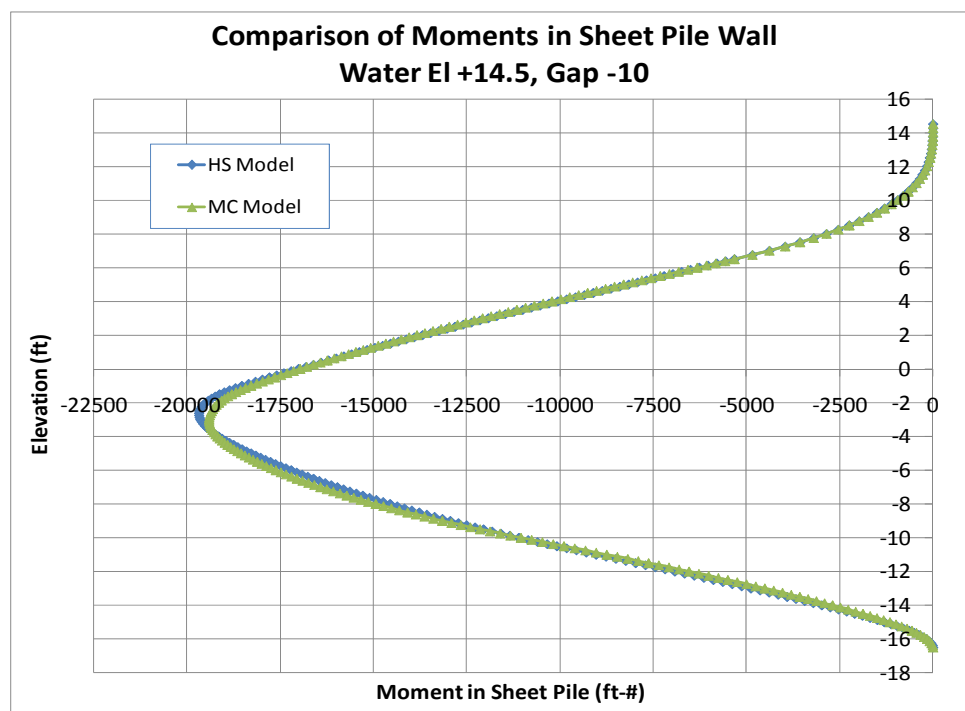


Figure 3.17. Comparison of the moments in the sheet-pile wall for the HS and MC models.

3.4.10 Sheet-pile wall displacements for MC model

Figures 3.20 and 3.21 show the horizontal displacements of the sheet-pile wall for various water elevations. The horizontal displacements at the top of the pile increase with a rising water elevation, as seen from Figure 3.20. For the last two water elevations, 16.5 ft and 17.5 ft, the displacements at the top of the pile almost quadruple for a 1-ft rise in water. From Table 3.10, the displacement of the top of the sheet pile for a water elevation of 16.5 ft is 12.9 in., while the displacement at the ground surface is 9.7 in. The displacement at the top of the pile for a water elevation of 17.5 is 50.7 in., and the displacement at the ground surface is 36.7 in.

Figure 3.21, an enlargement of the area around the tip of the sheet pile, shows that the displacements of the tip are relatively constant with an increasing water elevation and progressively translate into the landside of the I-wall. The displacements of the tip can be seen to decrease dramatically for a water elevation of 16.5 ft and to kick back into the flood side for a water elevation of 17.5 ft. The maximum tip displacement was 2.6 in. at a water elevation of 16.5 ft, and the tip moved 0.67 in. back into the landside at a water elevation of 17.5 ft. This large movement is due to the large area of highly stressed soil adjacent to the sheet-pile wall as discussed in Section 3.4.13.

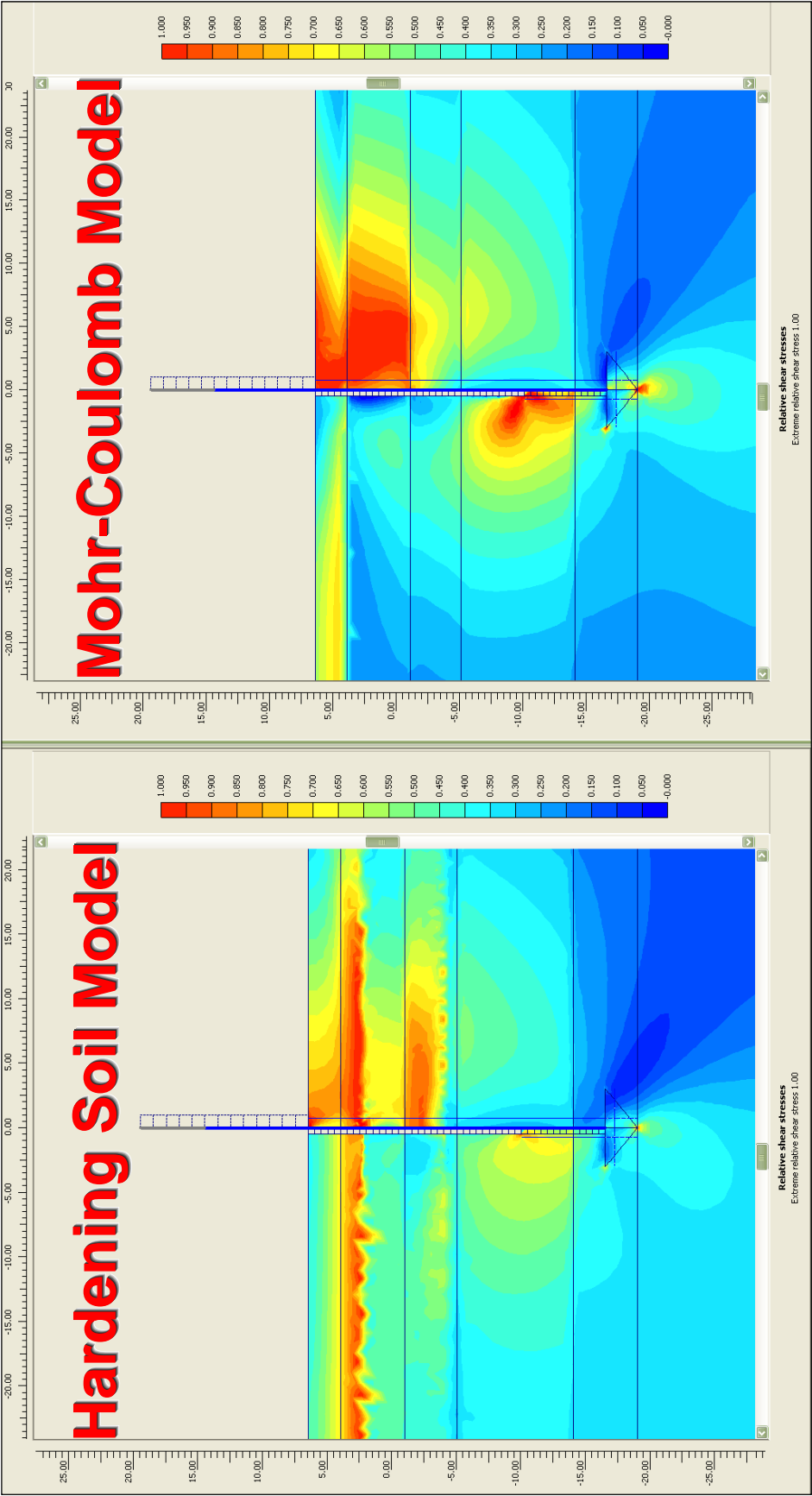


Figure 3.18. Comparison of mobilized shear strength for the HS and MC models for water el 14.5 ft and gap tip el -10 ft.

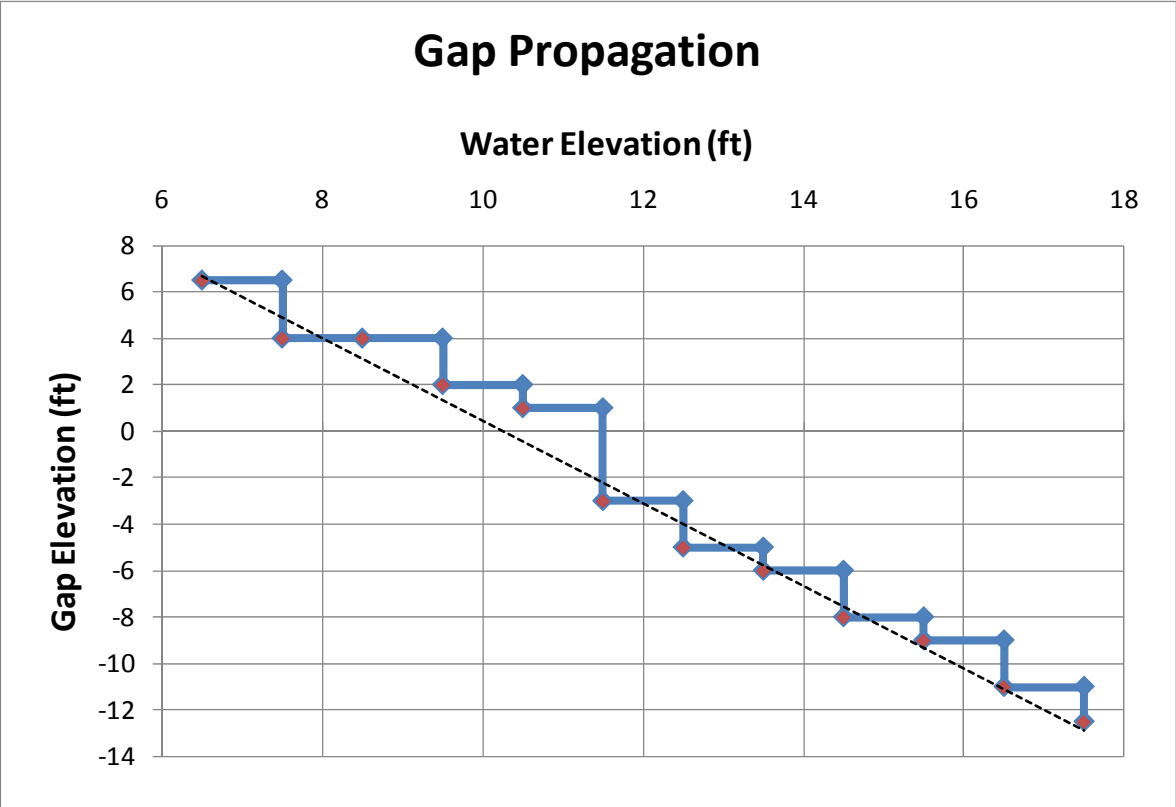


Figure 3.19. Progression of gap versus water elevation along flood side of I-wall.

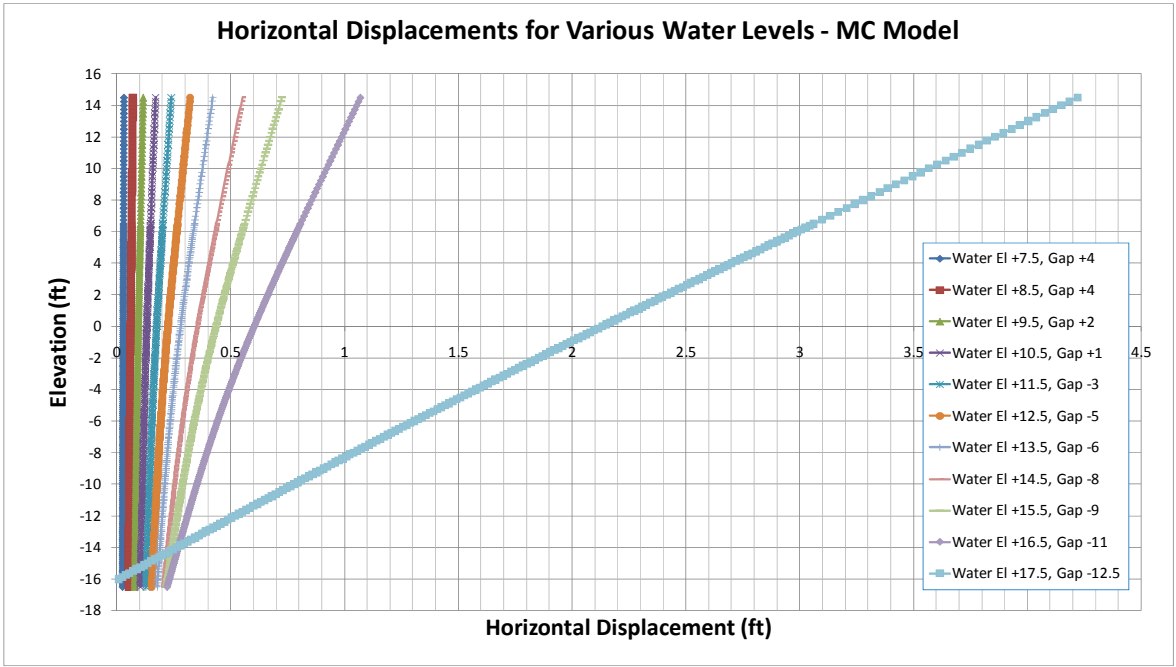


Figure 3.20. Sheet-pile horizontal displacements for various water elevations.

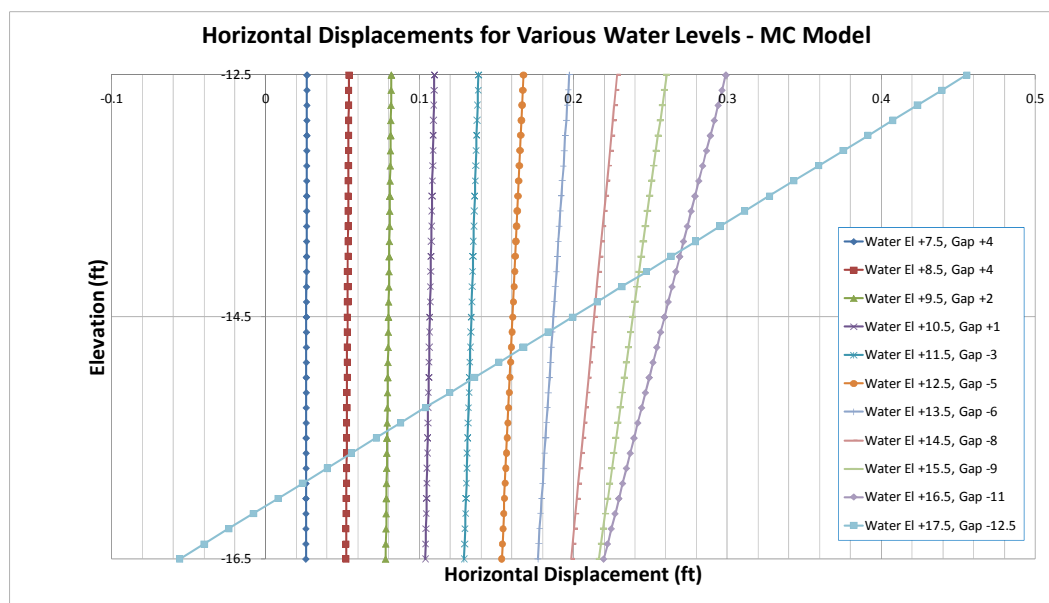


Figure 3.21. Sheet-pile horizontal displacements around the tip of the sheet pile for various water elevations.

Table 3.10. Pile displacements for MC model.

Water Elevation, ft	Top of I-Wall, el 14.5 ft		Ground Surface, el 6.5 ft		Tip of Sheet Pile, el -16.5 ft		Relative Pile Displacement at Ground Surface (Ground Surface minus Tip Displacement)	
	ft	in.	ft	in.	ft	in.	ft	in.
6.5	0.0000	0.0000	0.0000	0.0000	0.0000	0.0000	0.0000	0.0000
7.5	0.0324	0.3882	0.0306	0.3674	0.0261	0.3135	0.0045	0.0539
8.5	0.0709	0.8511	0.0652	0.7829	0.0522	0.6268	0.0130	0.1561
9.5	0.1170	1.4040	0.1046	1.2553	0.0781	0.9377	0.0265	0.3175
10.5	0.1704	2.0454	0.1487	1.7839	0.1039	1.2464	0.0448	0.5375
11.5	0.2388	2.8655	0.2026	2.4306	0.1291	1.5487	0.0735	0.8820
12.5	0.3228	3.8735	0.2670	3.2038	0.1534	1.8414	0.1135	1.3624
13.5	0.4219	5.0634	0.3414	4.0968	0.1768	2.1217	0.1646	1.9751
14.5	0.5519	6.6224	0.4363	5.2360	0.1986	2.3834	0.2377	2.8526
15.5	0.7264	8.7169	0.5613	6.7361	0.2168	2.6014	0.3446	4.1347
16.5	1.0713	12.8552	0.8067	9.6803	0.2198	2.6376	0.5869	7.0427
17.5	4.2211	50.6532	3.0612	36.7344	-0.0557	-0.6688	3.1169	37.4032

Phi/c reduction analyses were performed for water elevations of 16.5 ft and 17.5 ft. At a water elevation of 16.5 ft, the factor of safety was 1.15 and, for a water elevation of 17.5 ft, the factor of safety was 0.96.

Values of horizontal displacements for the sheet pile at the top, ground surface, and tip are tabulated in Table 3.10 and displayed in Figure 3.22. As shown in Figure 3.22, the pile tip displacements increase by a constant amount until finally reducing and kicking back into the flood side. Figure 3.23 shows the relative displacement of the sheet pile at the ground surface, which is computed as the displacement of the sheet pile at the ground surface minus the displacement of the tip of the sheet pile.

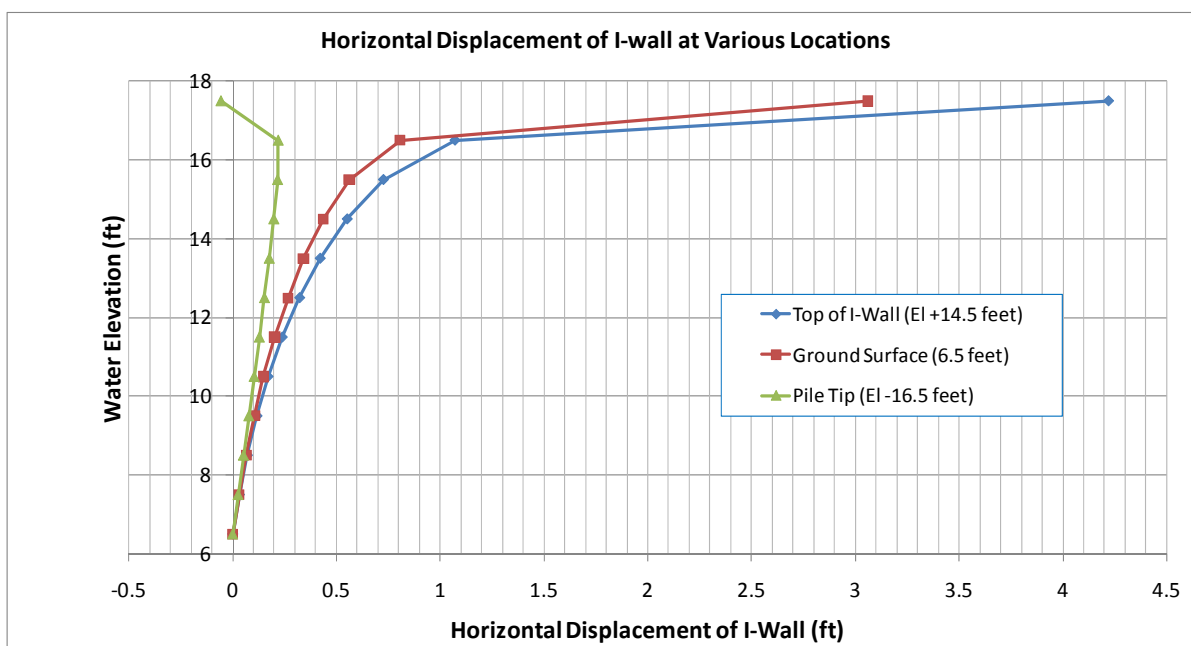


Figure 3.22. Sheet-pile horizontal displacements for selected locations.

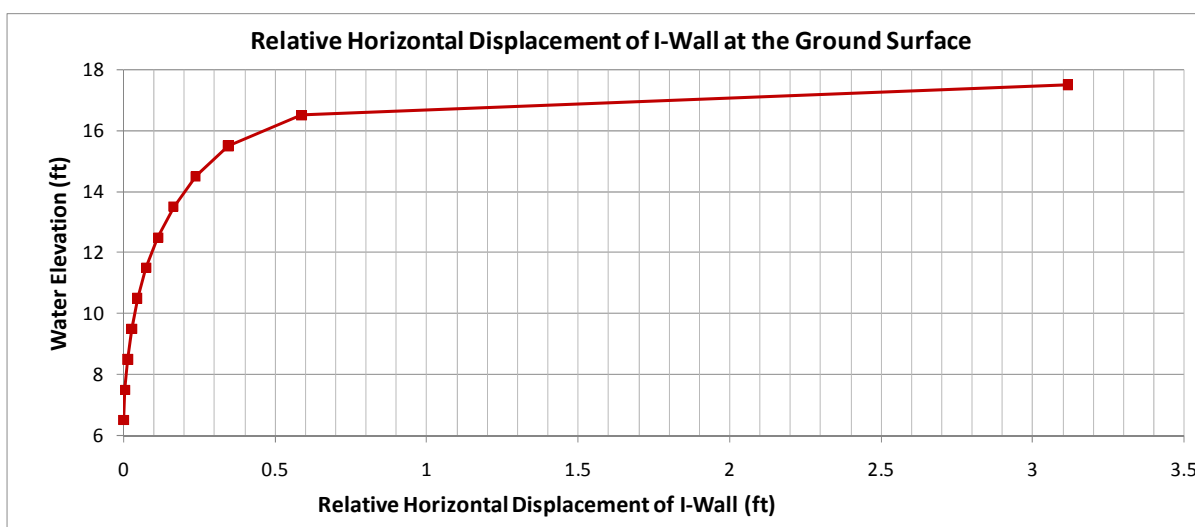


Figure 3.23. Relative horizontal displacements of the sheet pile at the ground surface.

3.4.11 Total displacements of finite element mesh for maximum water condition

Figures 3.24 and 3.25 show the total deflection of the finite element mesh for the water elevation of 16.5 ft. The gap at this water height propagated down to el -11 ft. There is some settlement on the flood side of the wall and some heave on the landside, as shown in Figure 3.25.

The left side of Figure 3.26 shows the total incremental displacements for a water elevation of 16.5 ft, and the right side for a water elevation of 17.5 ft. The incremental displacements give the movements during the last increment of loading, that is, the last part of the load that completes the total load added to the system. From Figure 3.26, for a water elevation of 16.5 ft, the soil is moving downward on the flood side and upward on the landside. A small zone of soil on the landside at el -13.5 ft is beginning to rotate. For a water elevation of 17.5 ft, the soil around the tip and the soil on the landside are moving upward. There is a zone of soil rotating about a point approximately at el -13.5 ft at a distance of 1.5 ft on the landside of the wall. In contrast, Figure 3.27 shows the total displacements of the system for the applied loads. The displacements are similar but, for the water elevation of 17.5 ft, the soil around the tip is seen to have some slight rotation.

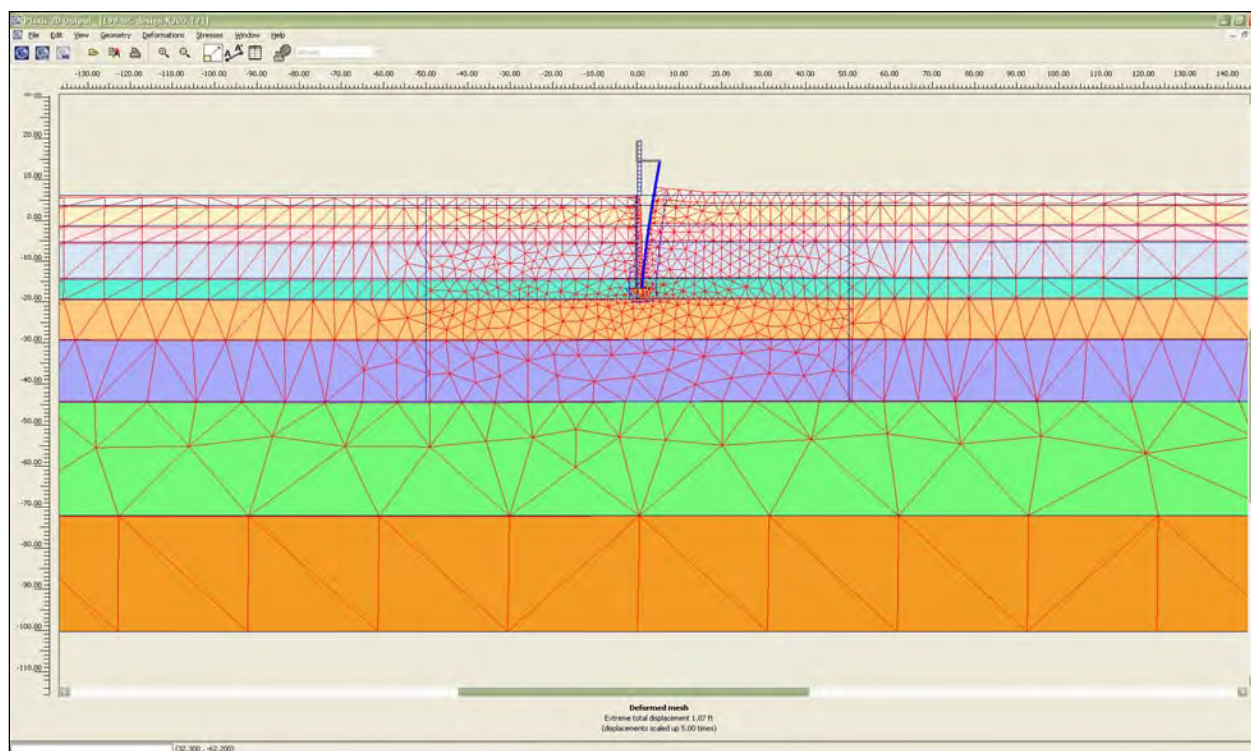


Figure 3.24. Total displacements for a water elevation of 16.5 ft and a gap tip elevation of -11 ft.

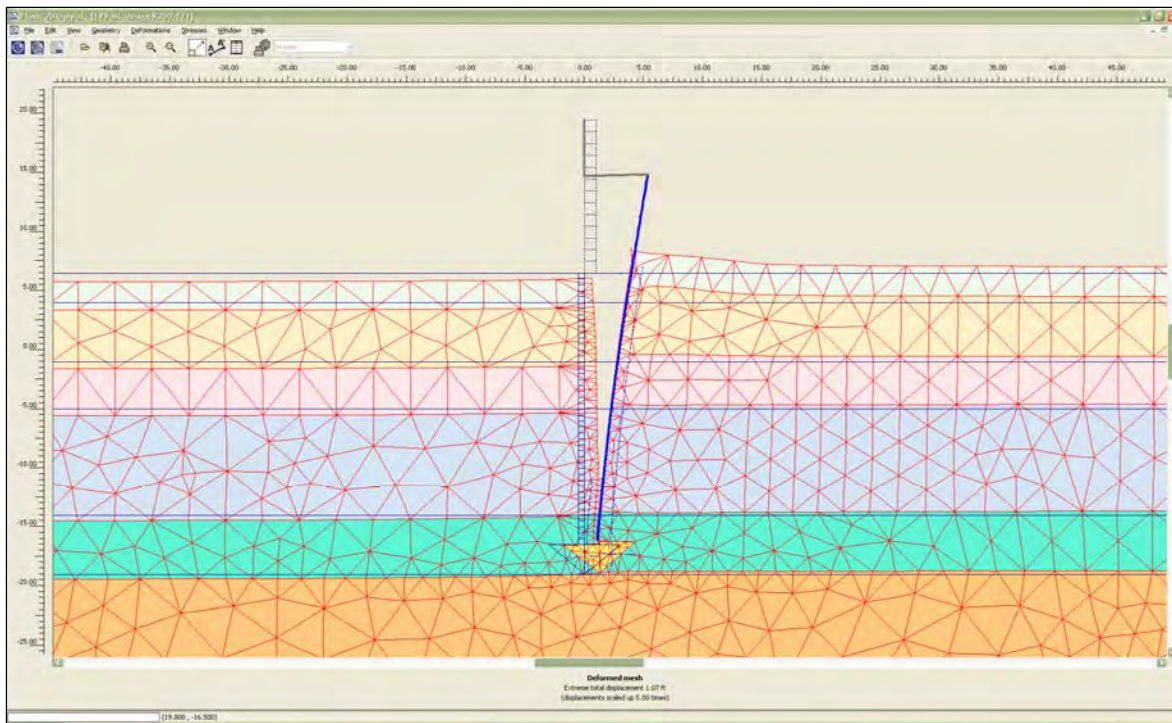


Figure 3.25. Total displacements for a water elevation of 16.5 ft and a gap tip elevation of -11 ft, windowed view.

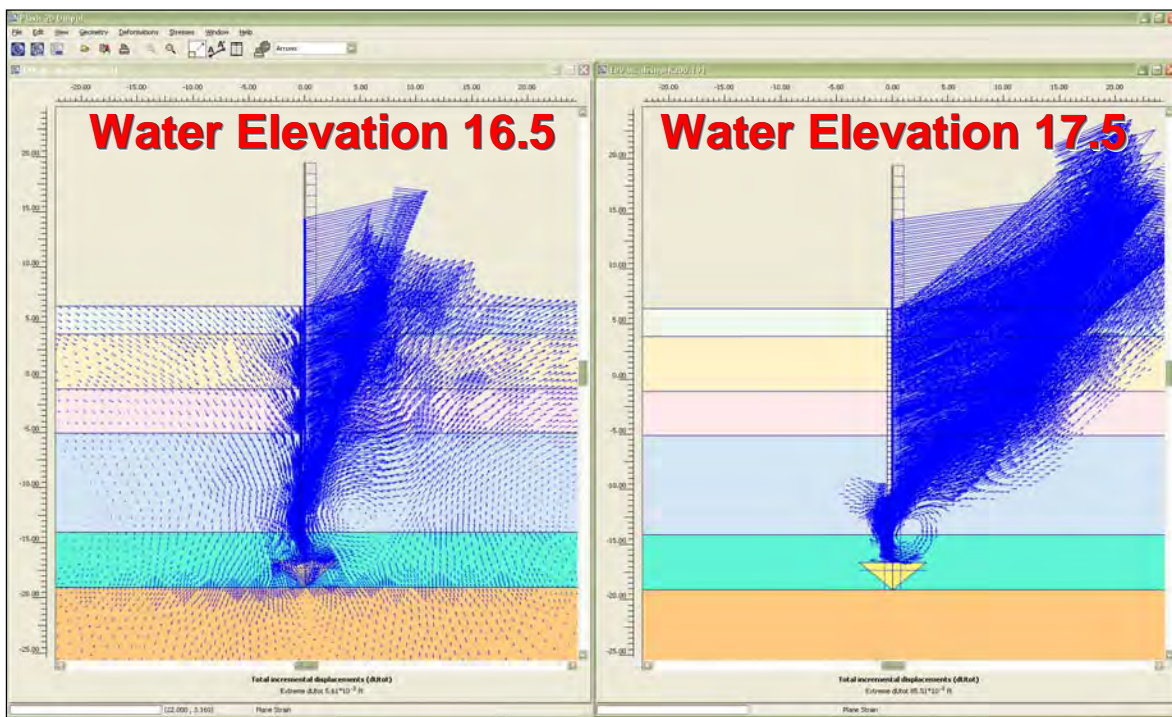


Figure 3.26. Vectors of total incremental displacements showing the movement of the soil during the final increment of loading.

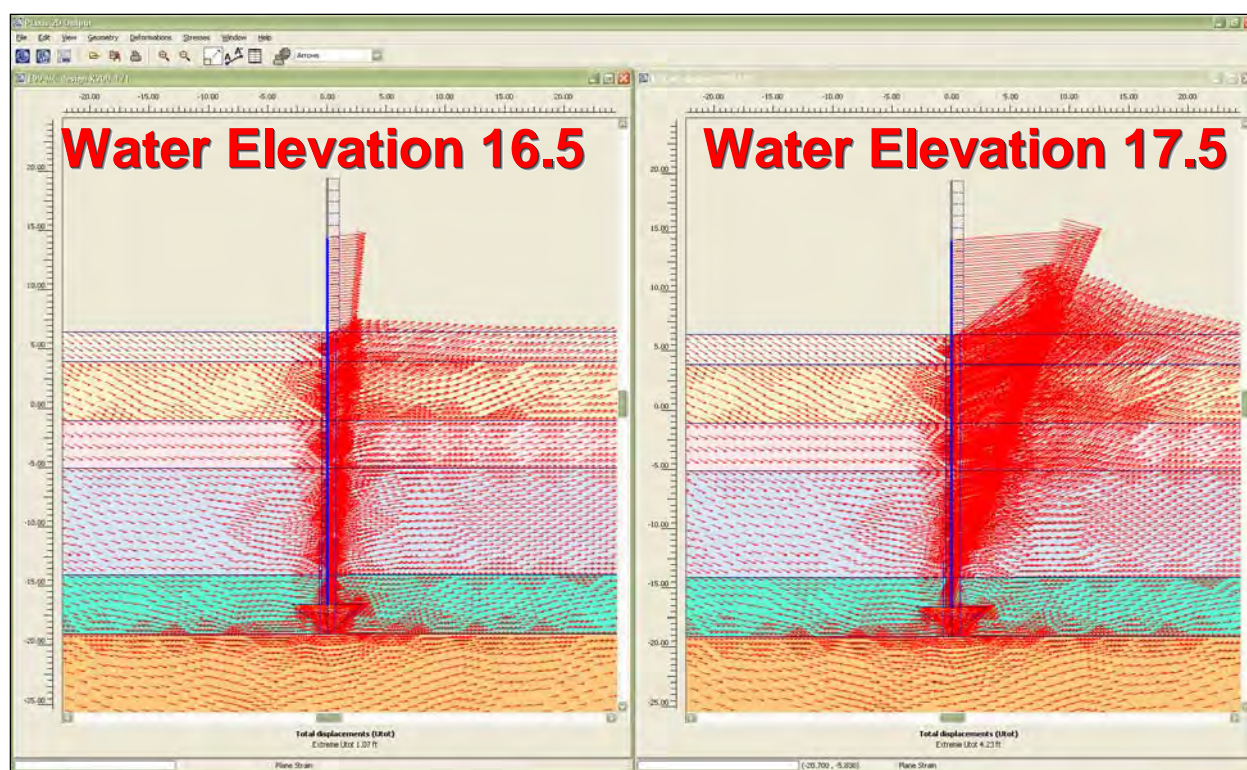


Figure 3.27. Vectors of total displacements showing the movement of the soil.

3.4.12 Moments in sheet-pile wall for MC model

A comparison of moments in the sheet pile for various water elevations is shown in Figure 3.28. The moment increases as the water elevation increases, and reaches a maximum at a water elevation of 17.5 ft. The moment for a water elevation 16.5 ft is 35,814 ft-lb at el -3.8 ft. The moment at a water elevation of 14.5 ft is 19,094 ft-lb at el -2.9. In comparison, the moment from the short-term CWALSHT analysis was 28,386 ft-lb at el -4.98 ft.

3.4.13 Shear stresses in soil for MC model

Figures 3.29 through 3.32 show the relative shear stress in the soil for various water elevations and the associated gap depths. The relative shear stress is a measure of the shear stress in the soil compared to the maximum available shear stress at failure. The shear stress in the soil increases as the water elevation increases. The shear stress increases in the upper unsaturated layer first, then progresses downward toward the tip of the pile. The shear stresses are greatest on the landside of the sheet-pile wall and at the bottom of the gap. For a water elevation of 14.5 ft, as shown in Figures 3.31 and 3.32, the highly stressed region does not extend below the

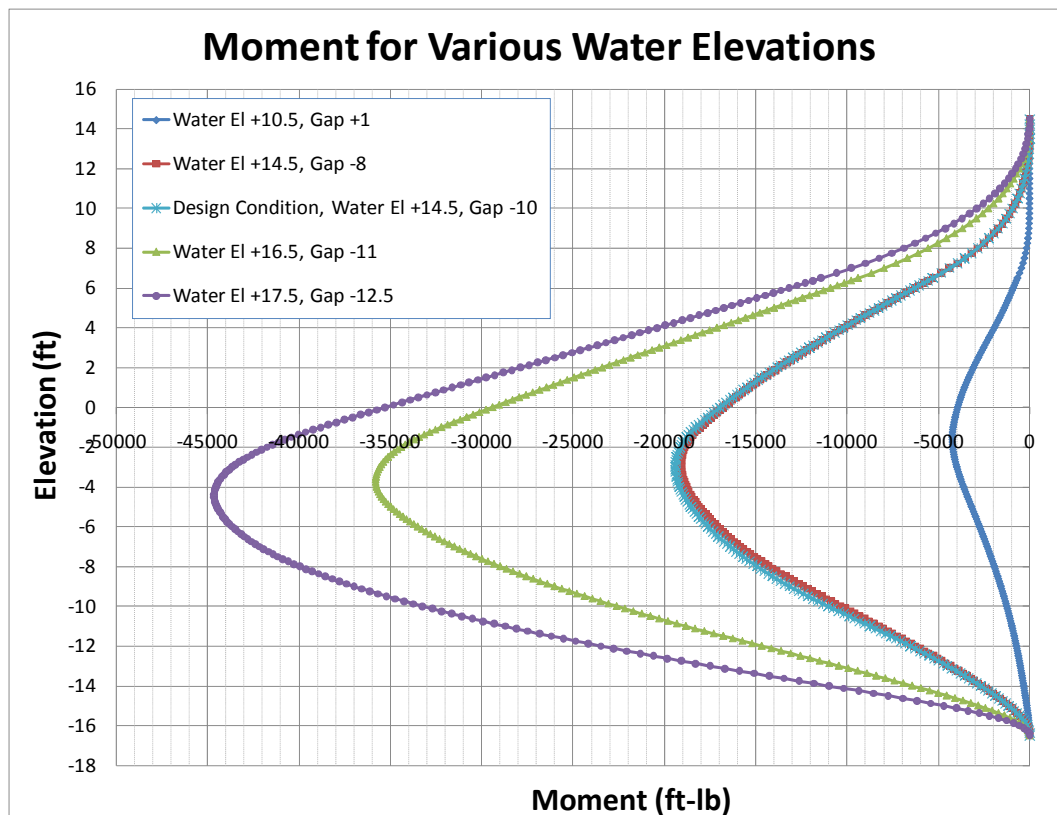


Figure 3.28. Comparison of moments as various water elevations.

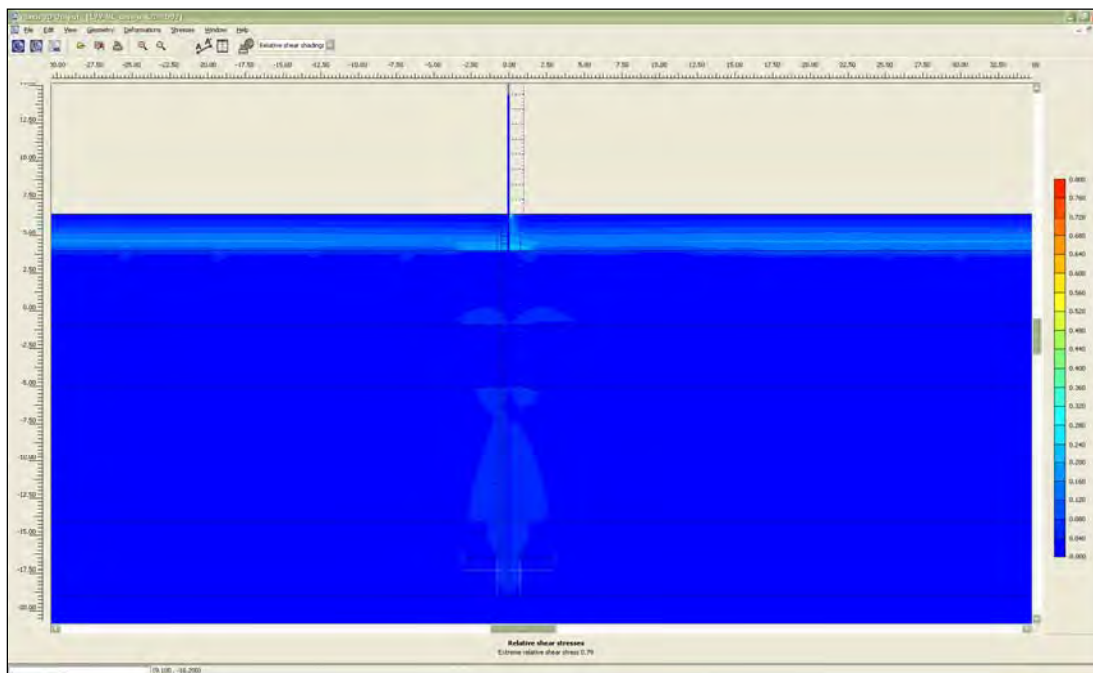


Figure 3.29. Relative shear stress after placement of I-wall.

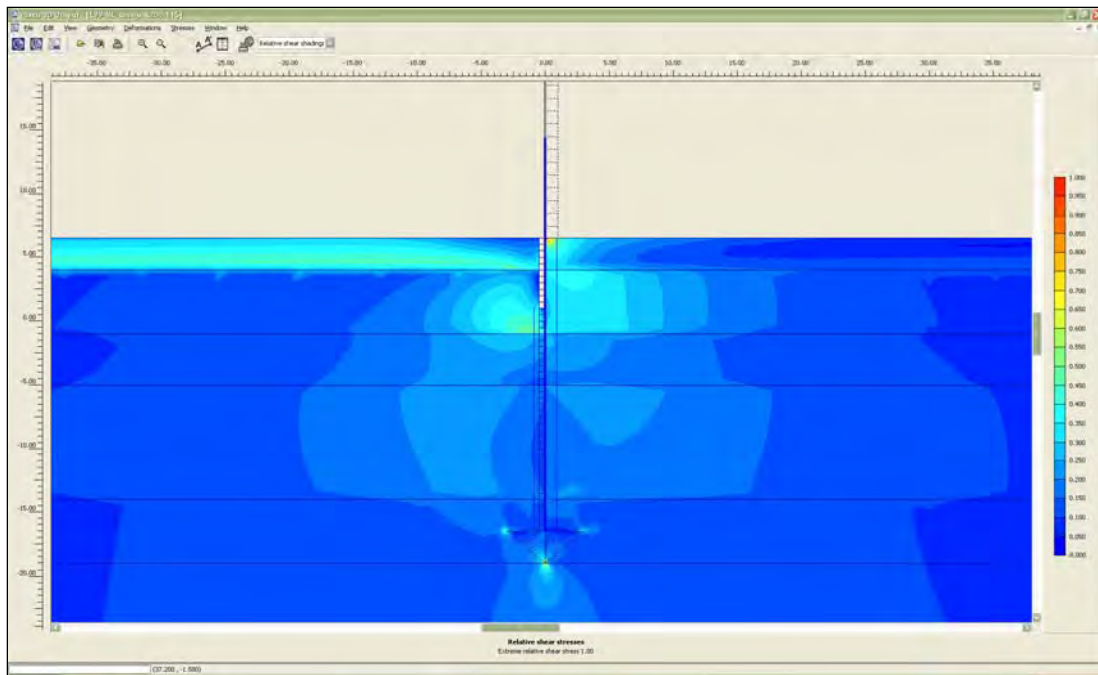


Figure 3.30. Relative shear stress for water at el 10.5 ft and gap tip elevation of 1 ft.

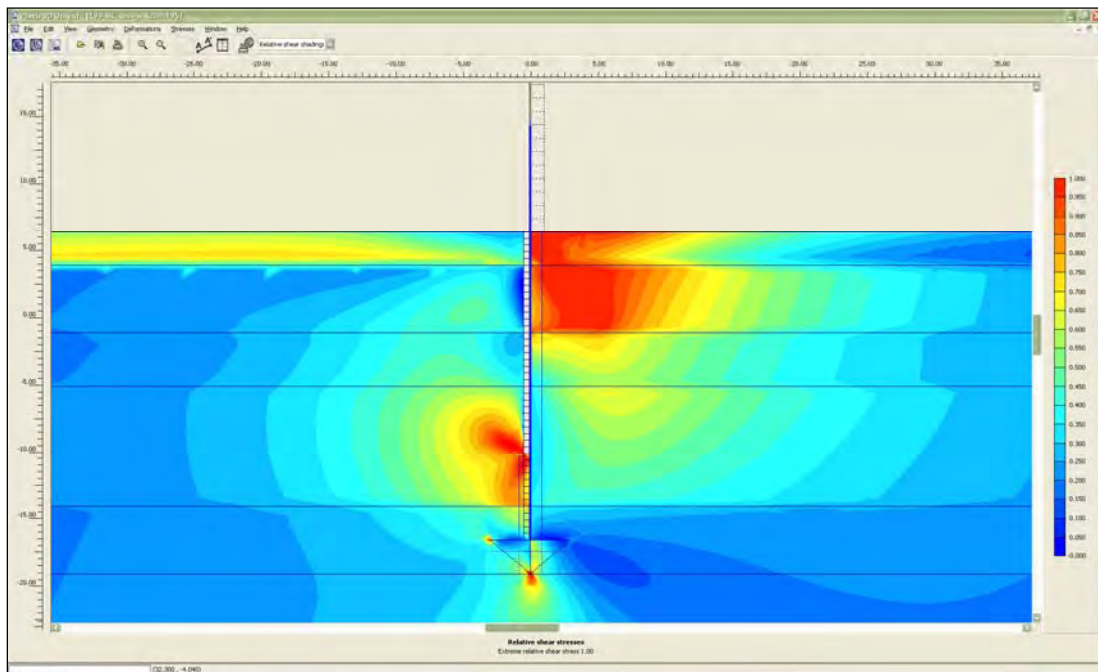


Figure 3.31. Relative shear stress for the design conditions of a water elevation of 14.5 ft and gap tip elevation of -10 ft.

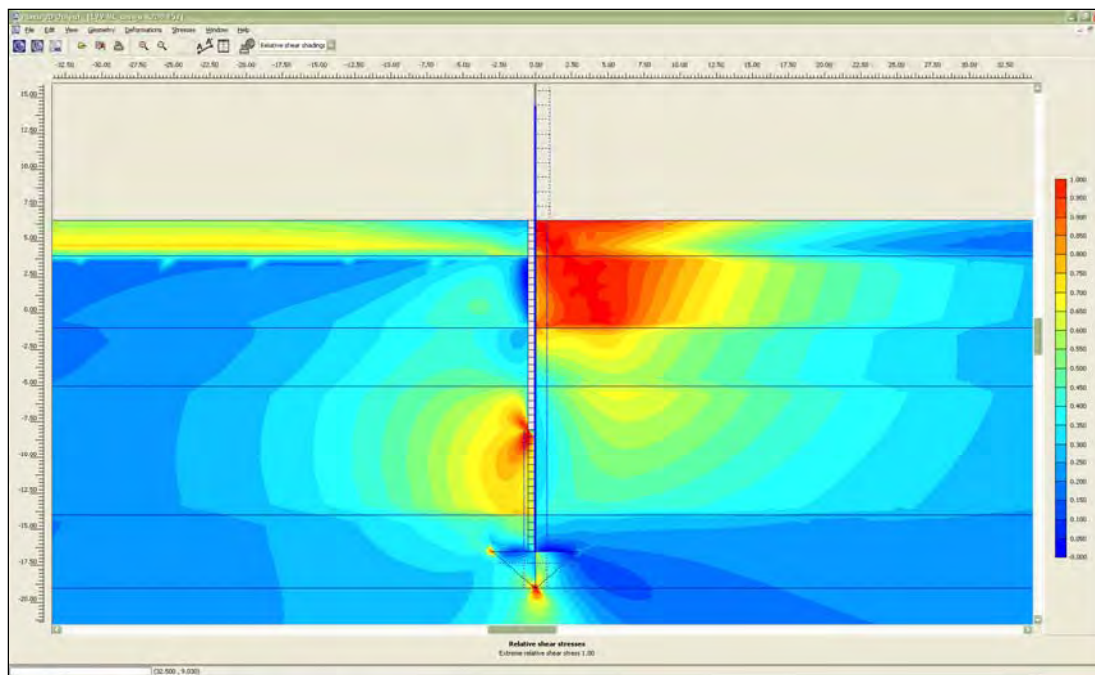


Figure 3.32. Relative shear stress for water at el 14.5 ft and gap tip elevation of -8 ft.

bottom of the gap. For water elevations of 16.5 ft and 17.5 ft as shown in Figures 3.33 and 3.34, respectively, the highly stressed region extends below the depth of the gap. For the maximum water elevation of 17.5 ft, the highly stressed region encompasses almost the entire length of the sheet pile.

3.4.14 Horizontal earth pressures for MC model

For Figures 3.35 through 3.41, the flood side is on the right side of the figure and the landside is on the left side of the figure. This corresponds to the input convention CWALSHT uses.

Figures 3.35 through 3.39 compare the horizontal earth pressures from PLAXIS acting against the sheet-pile wall to the limiting active and passive earth pressures computed using adhesion, as shown in Equations 3.5 and 3.6. The value of adhesion used is 80 percent of the cohesion, as discussed in Section 3.3.4. The limiting earth pressures in the figures are computed for factors of safety equal to 1.0 and 1.5. A factor of safety of 1.0 results in full active and passive earth pressures, while a factor of safety of 1.5 results in increased active and decreased passive earth pressures.

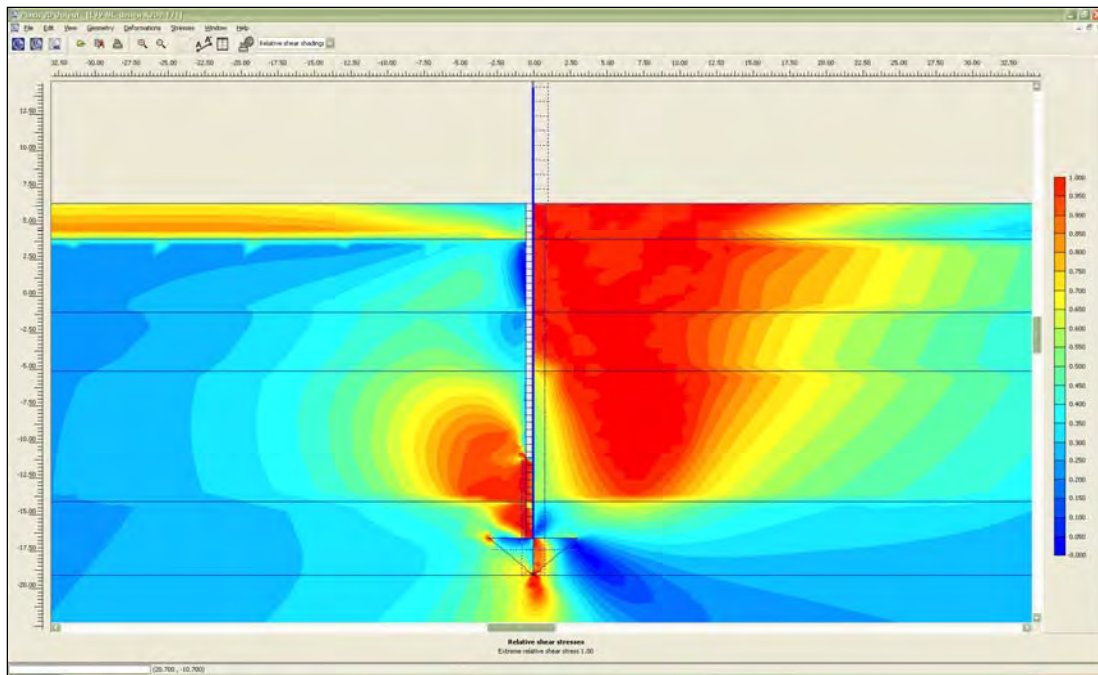


Figure 3.33. Relative shear stress for water at el 16.5 ft and gap tip elevation of -11 ft.

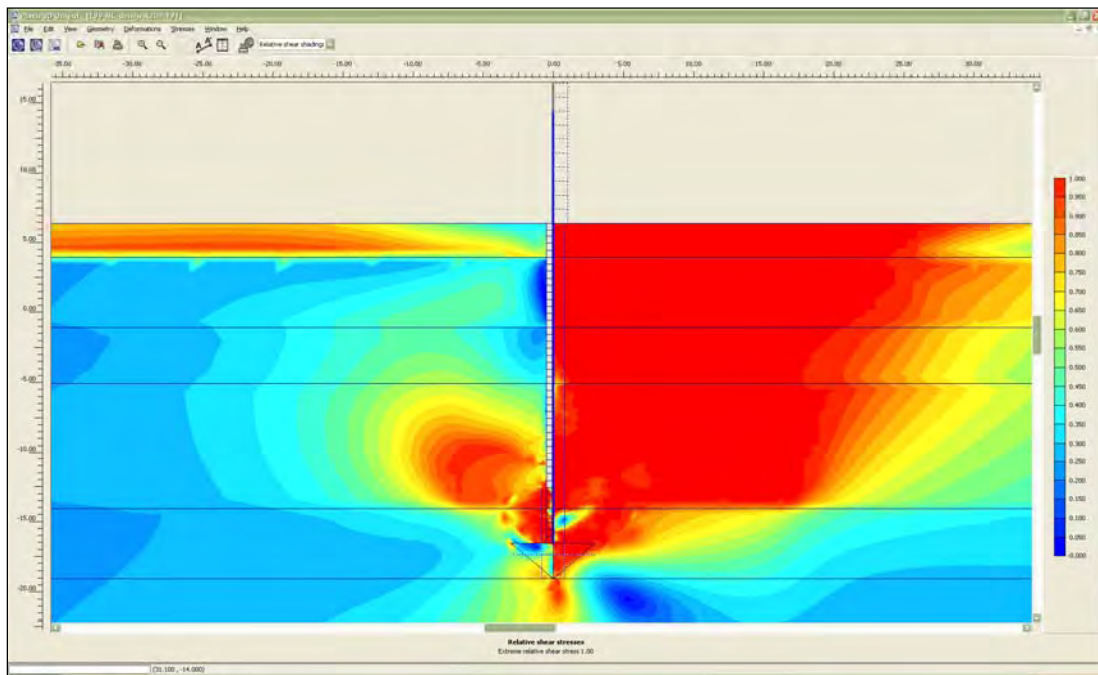


Figure 3.34. Relative shear stress for water at el 17.5 ft and gap tip elevation of -12.5 ft.

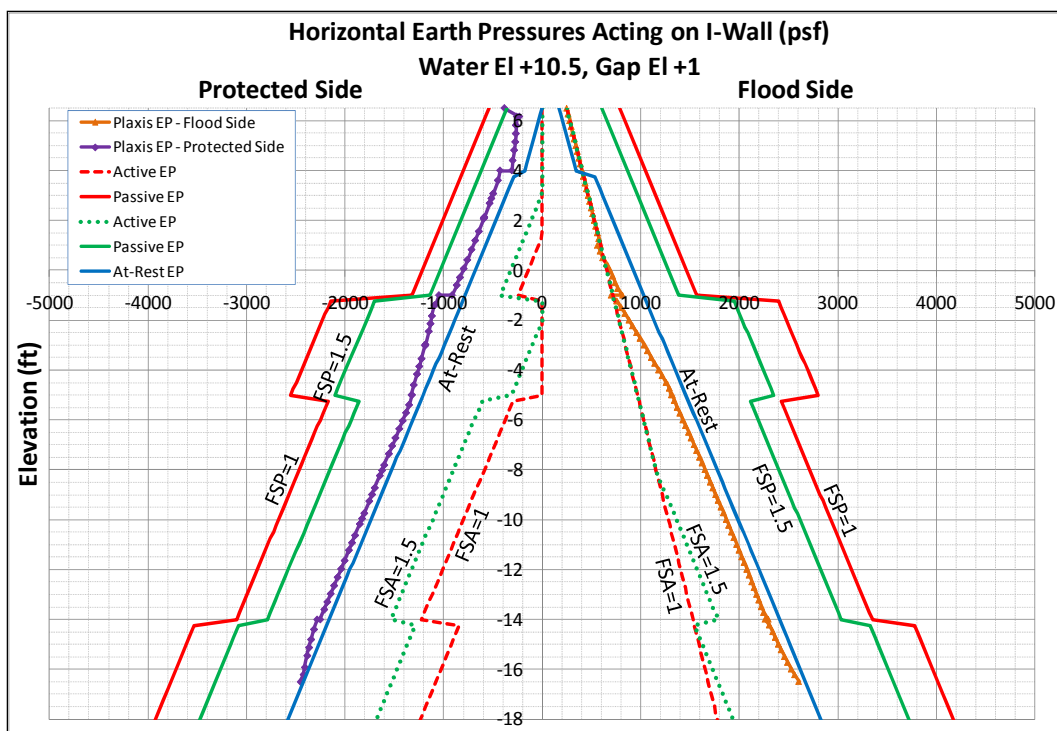


Figure 3.35. Horizontal earth pressures for a water elevation of 10.5 ft and gap tip elevation of 1 ft.

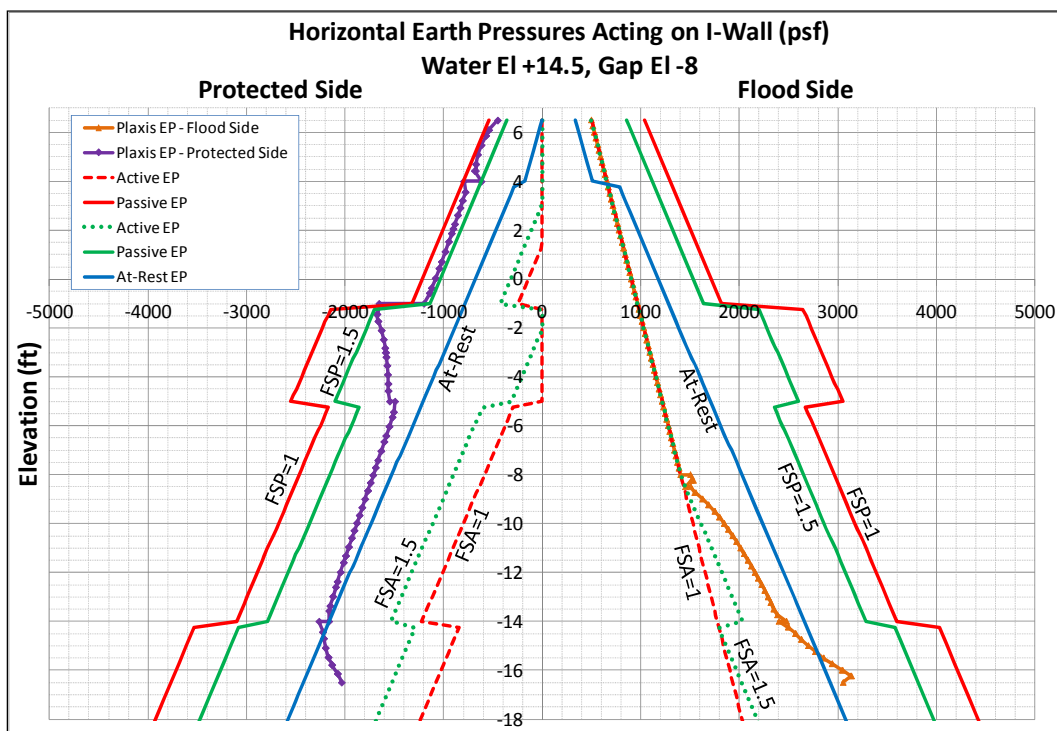


Figure 3.36. Horizontal earth pressures for a water elevation of 14.5 ft and gap tip elevation of -8 ft.

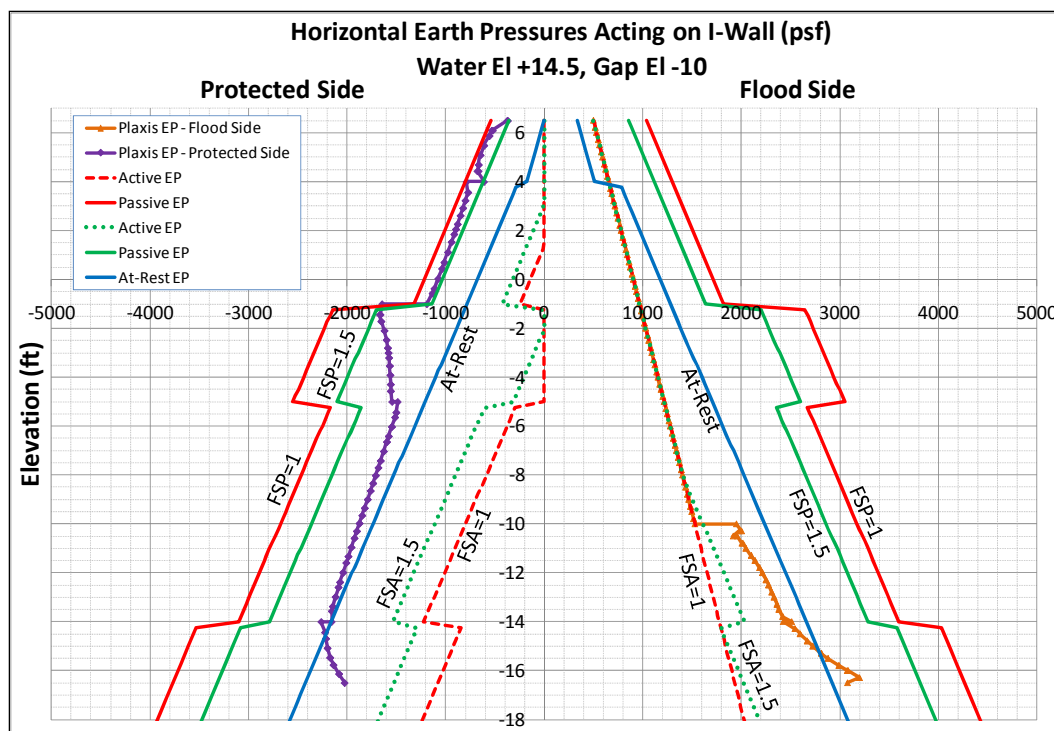


Figure 3.37. Horizontal earth pressures for the design condition of a water elevation of 14.5 ft and gap tip elevation of -10 ft.

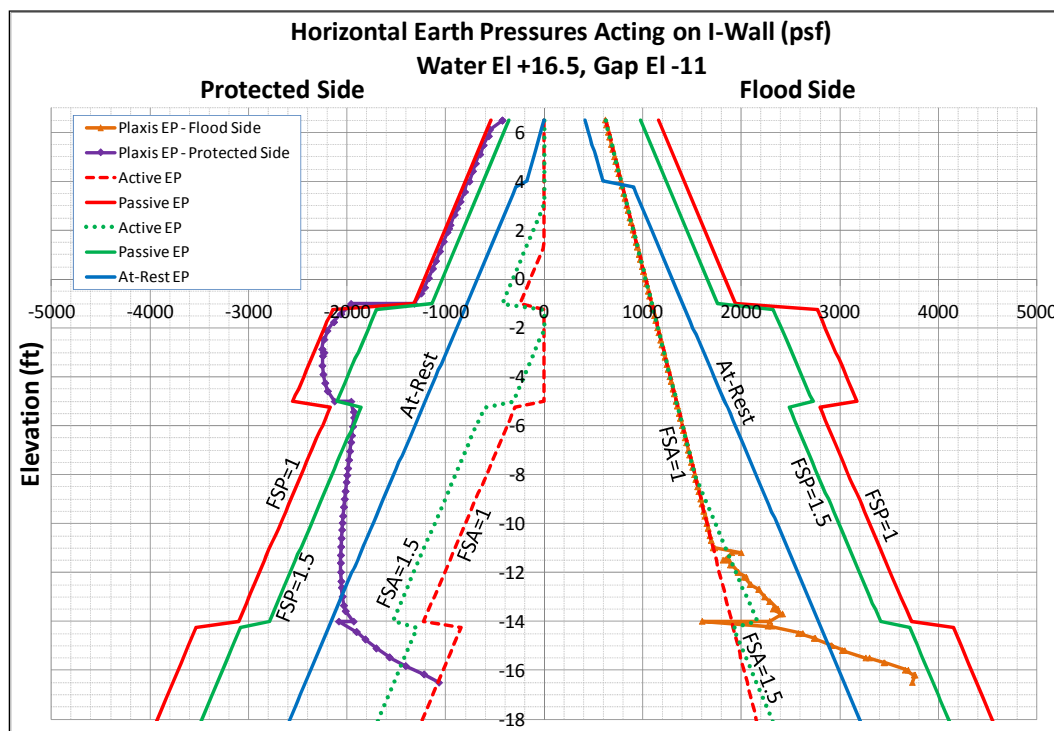


Figure 3.38. Horizontal earth pressures for a water elevation of 16.5 ft and gap tip elevation of -11 ft.

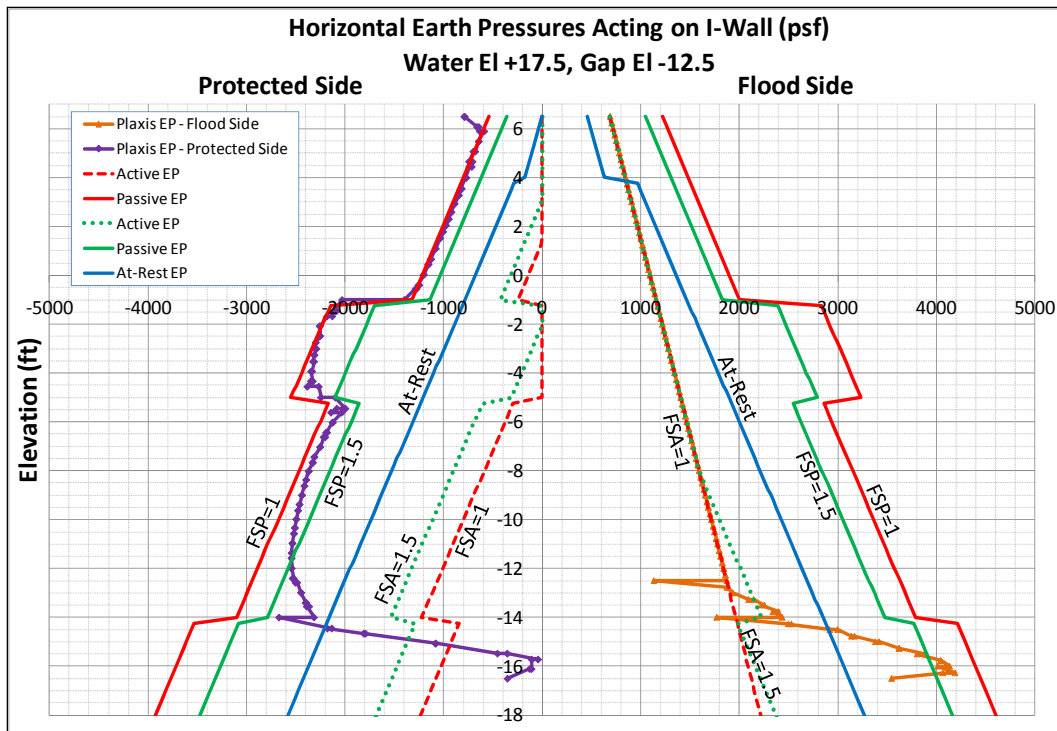


Figure 3.39. Horizontal earth pressures for a water elevation 17.5 ft and gap tip elevation of -12.5 ft.

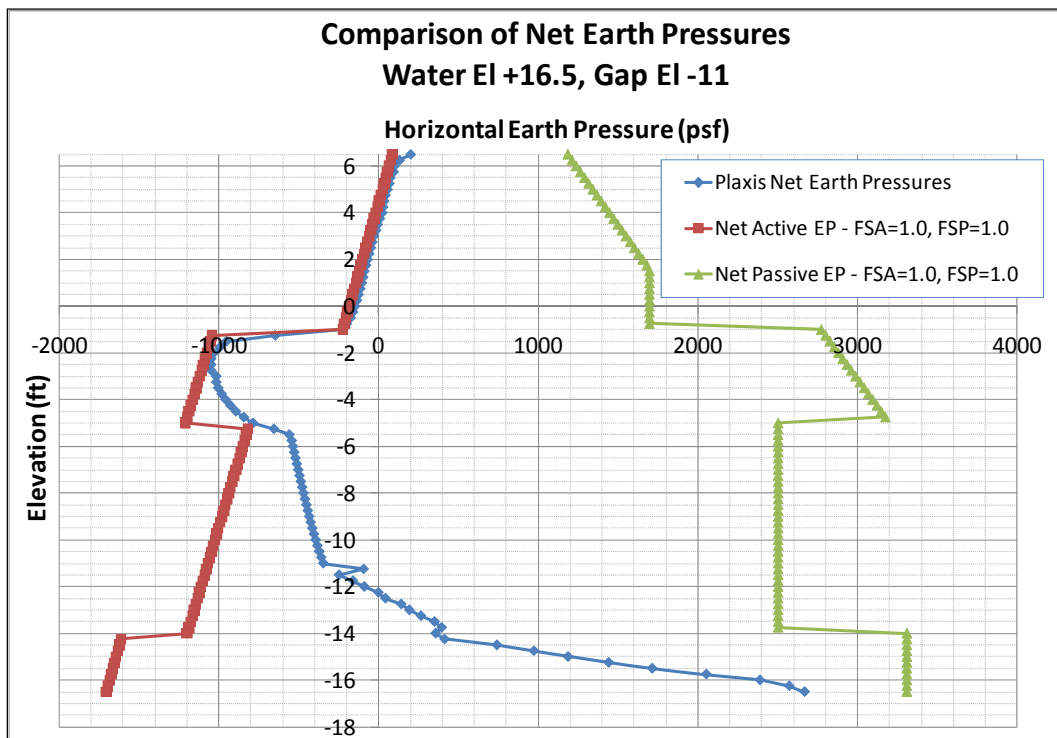


Figure 3.40. Comparison of net earth pressures computed from limiting earth pressures and PLAXIS results for a water elevation of 16.5 ft.

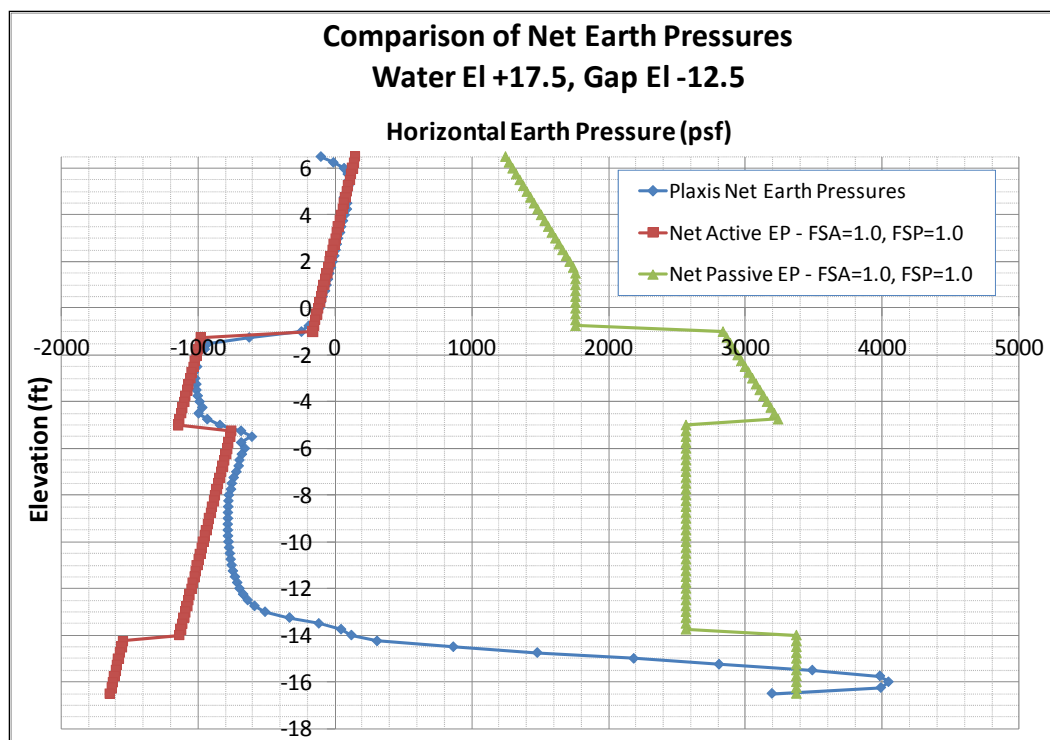


Figure 3.41. Comparison of net earth pressures computed from limiting earth pressures and PLAXIS results for a water elevation of 17.5 ft.

Originally, the net pressure diagram computed from CWALSHT was to be compared to the net pressure diagram computed from the PLAXIS results. The intent was to increase or decrease the factors of safety applied to the active and passive earth pressures to cause the computed net pressure diagram from CWALSHT to match the net pressure diagram computed using PLAXIS results. This approach did not work because, although changing the factors of safety on the earth pressures in CWALSHT will change the values of the net pressures, the penetration depth and point of rotation of the pile also are affected. Therefore, the results from PLAXIS were compared to the earth pressures computed by CWALSHT using limiting earth pressures computed with two different factors of safety.

Figure 3.35 displays the earth pressures for a water elevation of 10.5 ft and a gap tip elevation of 1 ft. For the flood side, the pressures are equal to hydrostatic pressures down to the bottom of the gap. Below the gap, the pressures are close to at-rest earth pressures computed using the assumed values of K_0 given in Table 3.9. On the landside, the earth pressures are very close to at-rest earth pressures.

Figure 3.36 shows horizontal earth pressures for the water elevation at 14.5 ft. The gap in this case extends to el -8 ft. The earth pressures on the flood side are equal to hydrostatic pressures down to the bottom of the gap. Below the gap, the earth pressures are less than the at-rest condition caused by the wall moving away from the soil. On the landside, the earth pressures are greater than the at-rest condition above el -5 ft. From el 6.5 ft down to el 0 ft, the earth pressures approach the fully passive values. Below el 0 ft, the earth pressures on the landside tend toward the at-rest condition. Figure 3.37, which is the design condition for CWALSHT with no adhesion, exhibits similar characteristics to those in Figure 3.36. The only difference in the analyses between Figures 3.36 and 3.37 is the depth of the gap.

For Figures 3.38 and 3.39, the earth pressures continue to decrease below the at-rest condition on the flood side below the gap. The magnitude of the earth pressures tends back toward an active state. The lower portion of the pile on the flood side experiences an increase in earth pressures up to a passive value defined using a factor of safety between 1.0 and 1.5. This agrees with the movements experienced by the pile in that a rotation point exists above the tip of the pile. The passive pressures acting on the lower portion of the pile are due to the rotation and kickback of the tip of the pile into the flood side.

Figures 3.38 and 3.39 show the earth pressures on the landside increasing from the at-rest condition to the passive condition computed using a factor of safety equal to 1.0. The factor of safety of 1.0 produces earth pressures that are greater than those assumed in the CWALSHT design. The lower portion of the pile experiences a decrease in earth pressures that agrees with the movement of the pile. The earth pressures around the tip of the pile on the landside decrease below active pressures computed using a factor of safety equal to 1.0 (the factor of safety assumed in CWALSHT).

Figures 3.40 and 3.41 compare the net earth pressures computed using limiting earth pressures and the results from PLAXIS for water elevations of 16.5 ft and 17.5 ft, respectively. The limiting earth pressures are computed using a factor of safety of 1.0 for both the active and passive earth pressures for both the flood side and landside of the wall. Net pressures were compared for this water elevation because the movements of the wall were sufficient to produce values of full active and passive earth pressures. As can be seen from the figure, the net earth pressures on the landside compare

fairly well to the net active earth pressures. Toward the tip of the pile, the net earth pressures transition from the net active to the net passive and compare fairly well.

3.4.15 Comparison of finite element analysis results to conventional analysis results and field measurements

This section compares the results from the finite element analyses to conventional (CWALSHT) results and to the E-99 field test measurements. Tables 3.11 through 3.13 contain data for the finite element, conventional, and field results, respectively.

Table 3.11. PLAXIS finite element results for various water elevations.

Analysis	Water Elevation, ft	Elevation of Bottom of Gap, ft	FS	Maximum Moment, ft-lb	Elevation of Maximum Moment, ft	Relative Horizontal Displacement of Pile at Ground Surface, in.
1	14.5	-8	1.78	19,094	-2.9	2.9
2	14.5	-10	1.77	19,340	-3.0	2.9
3	15.5	-9	1.42	19,400	-3.0	4.1
4	16.5	-11	1.15	35,817	-3.6	7.0
5	17.5	-12.5	0.96	44,636	-4.5	37.4

Table 3.12. CWALSHT results for various water elevations.

Analysis	Water Elevation, ft	Adhesion, psf	Elevation of Bottom of Gap, ft	FS _A	FS _P	Maximum Moment, ft-lb	Elevation of Maximum Moment, ft	Horizontal Displacement of Pile at Ground Surface, in.
1	14.5	0	-9.8	1.00	1.00	21,609	-	-
2	14.5	0.8*S _u	Below wall	1.00	1.00	16,961	-	-
3	14.5	0	-9.8	1.00	1.40	28,386	-4.98	1.4
4	15.5	0	-9.8	1.00	1.08	34,344	-4.70	1.7
5	16.5	0	-9.8	1.00	0.87	41,048	-4.45	2.0
6	17.5	0	-9.8	1.00	0.71	48,644	-4.24	2.4
7	14.5	0.8*S _u	Below wall	1.00	1.89	28,906	-5.08	1.5
8	15.5	0.8*S _u	Below wall	1.00	1.45	34,833	-4.75	1.7
9	16.5	0.8*S _u	Below wall	1.00	1.16	41,575	-4.48	2.1
10	17.5	0.8*S _u	Below wall	1.00	0.95	49,171	-4.25	2.4

Table 3.13. Measured field results for instrumented locations.

Test Pile	Head, ft	Horizontal Displacement at top of Pile, in.	Maximum Moment, ft-lb	Elevation of Maximum Moment, ft	Horizontal Displacement of Pile at Ground Surface, in.
A	8.3	8	25,100	-5.5	5.7
B	8.1	6	18,400	-5.5	4.1
C	7.8	4	16,500	-5.5	2.6
D	7.8	4	19,200	-3.5	2.5

Table 3.11 shows results for finite element analyses for various water elevations. It should be noted that the finite element analyses include the effects of adhesion. As the water elevation is increased, the factor of safety computed from a Φ/c reduction analysis decreases. These factors of safety are slightly lower than the factors of safety shown for the conventional analyses for the same analysis case, except for Analysis 5 in Table 3.11 that has a slightly higher factor of safety.

For the design condition (Analysis 2, Table 3.11), the factor of safety is equal to 1.77 for the finite element results versus 1.89 for the conventional results (Analysis 7, Table 3.12). The water elevation for these analyses corresponds to the top of the wall. The gap elevation for the finite element analysis extends to -10 ft, while the gap elevation for the conventional analysis is below the tip of the sheet pile. Both analyses include the effects of adhesion.

The maximum moment for Analysis 2 shown in Table 3.11 is 19,340 ft-lb, compared to a moment of 28,906 ft-lb for Analysis 7 shown in Table 3.12. Current guidance states that the moment should be computed for a factor of safety on the active and passive earth pressures of 1.0. This is Analysis 2 in Table 3.12, and the maximum moment is equal to 16,961 ft-lb. The measured moments from the field test are shown in Table 3.14, with the greatest moment equal to 25,100 ft-lb and the least equal to 16,500 ft-lb.

The relative horizontal displacement of the pile at the ground surface for the design condition (Analysis 2) in Table 3.11 is 2.9 in. CWALSHT reports 1.5 in. for the same condition (Analysis 7) in Table 3.12. Note that the CWALSHT pile deflections are computed for a pile modeled as a cantilever wall with “fixity” imposed at the pile tip. Field measurements vary from 5.7 to 2.5 in. as shown in Table 3.13. The test locations C and D are closer to the actual analysis conditions, and the horizontal displacements at these locations are 2.6 and 2.5 in., respectively.

4 Analyses of I-wall Site Founded on a Clay with Undrained Shear Strength (S_u) of 300 psf

4.1 Purpose of analyses

This chapter summarizes the findings of nonlinear SSI finite element analyses of an I-wall founded in a clay soil with constant undrained shear strength of 300 psf. The focus of this chapter is to analyze the initiation and propagation of a gap beside an I-wall and to study the effects of this gap on the resulting deformation and stress conditions on the soil regime on both the flood side and landside of the I-wall.

The following sections will describe the soil used in the analyses, the selection of stiffness and shear strength parameters, the conventional analysis and design of the I-wall, the procedures employed in the analysis, and the results of the finite element analyses.

4.2 Overview of problem analyzed

The geometry of the problem analyzed is shown in Figure 4.1. The site was assumed to be flat (level) with a maximum floodwater elevation of 9 ft; the groundwater level assumed to be at el -15 ft; and the elevation of the soil surface assumed to be at 0 ft. The I-wall was composed of a sheet-pile wall with the top of the wall at el 9 ft and the tip at el -30 ft. The tip elevation was determined by performing both short-term and long-term designs using CWALSHT. These design computations are discussed later in this chapter.

The designation according to the Unified Soil Classification System (USCS) for the soil used in the analyses is CL (clay with low plasticity). From the classification chart shown in Figure 4.2, the plasticity index (PI) of a CL ranges from 7 to 38. The soil was assumed to be normally consolidated. The permeability of the clay was assumed to be small enough that the soil would not become fully saturated as the floodwater level was increased. Therefore, as shown in Figure 4.1, two zones of soil were considered in the analysis: a partially saturated zone above the water table elevation of -15 ft and a saturated zone of soil below the water table.

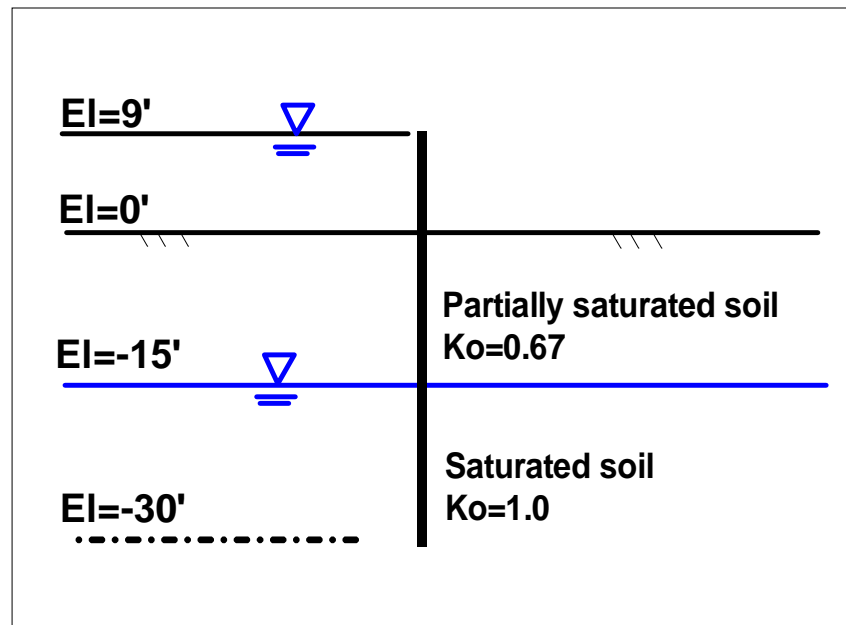


Figure 4.1. Problem geometry.

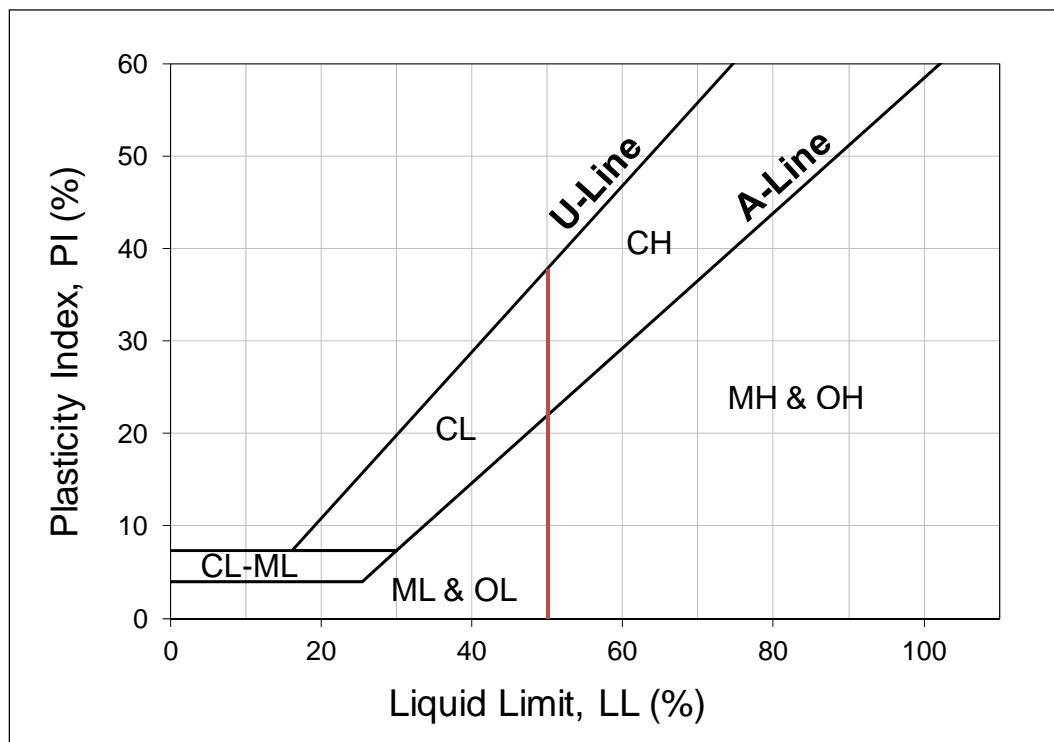


Figure 4.2. USCS plasticity chart for fine-grained soils (see Figure 2.2 on page 9 for explanation of soils).

4.3 Conventional design of cantilever I-wall

4.3.1 Modeling a total stress problem in CWALSHT with consideration of a gap

CWALSHT is designed to analyze effective stress (drained) problems. That is, both the input and computations conform to the procedure that would be used to analyze an effective stress (drained) analysis. Most notably, water levels are input to account for the effects of water (both hydrostatic and seepage effects). When performing a CWALSHT analysis for a short-term (undrained) condition, care must be taken to account properly for the water loadings. For the short-term condition using a total stress method of analysis, pore pressures should not be calculated within the soil. External water loadings must be accounted for in the analysis. Therefore, vertical uniform and horizontal boundary pressure loads must be used to represent the external loading due to the water. Water levels would not be input and, therefore, pore pressures within the soil would not be computed.

Also, for a short-term analysis with a soil with $\phi=0$, a gap will form on the flood side of the wall, as shown in Figure 4.3. The depth of the gap must be computed prior to running CWALSHT and is based on a hydraulic fracturing concept as discussed in Section 4.3.3. To model this gap and the external pressures due to the water, the input for the CWALSHT model will be different from the actual geometry, as shown in Figure 4.3. The soil down to the elevation of the bottom of the computed gap will be replaced by two external pressure loadings. A horizontal pressure loading will represent the water pressure against the wall above the level of the soil and down to the bottom of the gap. A vertical pressure loading will replace the effects of the total vertical overburden of the flood pool and the soil down to the bottom elevation of the gap. Because no water levels will be input in CWALSHT, no pore pressures will be generated within the soil. The unit weights of the soil used in the analysis would correspond to moist and saturated unit weights. Buoyant unit weights are not input. These input conditions adequately represent a total stress analysis in CWALSHT.

4.3.2 Computation of active and passive earth pressures

For a conventional design, horizontal earth pressures against the cantilever wall must be computed. Both active and passive earth pressures on both the flood side and landside of the wall are used to design the depth of penetration and size the sheet-pile wall section. Coulomb or Rankine earth

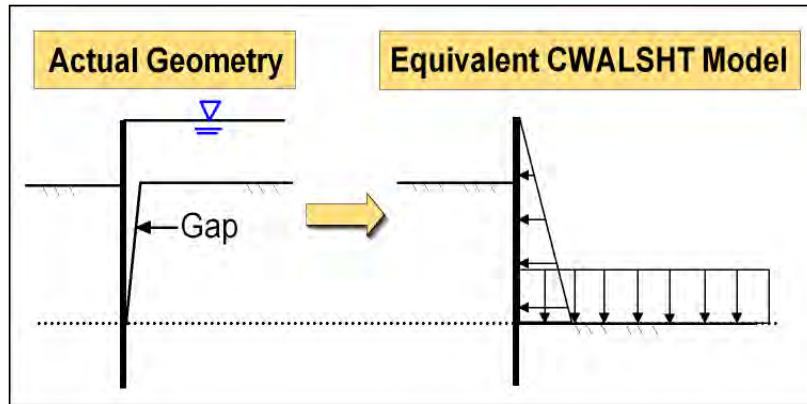


Figure 4.3. Equivalent CWALSHT model to account for gap.

pressure coefficients can be used to compute the earth pressures depending on the applicable conditions (Clayton et al. 1993; Craig 1998). Using the active earth pressure coefficient (K_a), the horizontal active earth pressure (σ_{ha}) can be computed using Equation 4.1 (Clayton et al. 1993):

$$\sigma_{ha} = K_a(\gamma z + q) - 2c\sqrt{K_a}, \quad (4.1)$$

where

- γ = the saturated or moist unit weight of the soil for a total stress analysis and the buoyant unit weight for an effective stress analysis (units of force/length³);
- z = the depth at which the pressure is computed (units of length);
- q = surcharges on the soil surface (units of force/length²);
- K_a = the active earth pressure coefficient.

This equation is applied to an I-wall in level ground and can be used for a soil having both a cohesion (c) and an angle of internal friction (ϕ).

K_a includes the effects of wall friction. If the effects of adhesion against the I-wall are to be considered, Equation 4.1 can be expanded to include adhesion by the addition of an adhesion factor (r) as given by Equation 4.2:

$$\sigma_{ha} = K_a(\gamma z + q) - 2c\sqrt{K_a}r. \quad (4.2)$$

The adhesion factor is given by Equation 4.3:

$$r = \sqrt{1 + \frac{c_a}{c}}, \quad (4.3)$$

where

c_a = adhesion between soil and sheet-pile wall (force/length²);
 c = cohesion of soil (force/length²).

The horizontal passive earth pressures can be computed using the passive earth pressure coefficient (K_p) and Equation 4.4:

$$\sigma_{hp} = K_p(\gamma z + q) + 2c\sqrt{K_p}r. \quad (4.4)$$

For the case of a soil with $\phi=0$, the values of K_a and K_p are equal to 1.0. The critical failure angle of the soil wedge corresponding to the minimum active or maximum passive earth pressure is equal to 45 deg for level ground. Therefore, for a soil with $\phi=0$, Equations 4.2 and 4.4 reduce to, respectively:

$$\sigma_{ha} = (\gamma z + q) - 2cr \quad (4.5)$$

$$\sigma_{hp} = (\gamma z + q) + 2cr. \quad (4.6)$$

4.3.3 Criteria for gap initiation and propagation

Two different criteria, one for the flood side and one for the landside, are used to determine whether a gap will initiate in the soil adjacent to the sheet-pile wall and how far the gap will propagate. A hydraulic fracturing criterion is used for the flood side of the I-wall (Criterion 1). A negative horizontal stress criterion is used for the landside of the I-wall (Criterion 2).

4.3.3.1 Criterion 1

When the hydraulic fracturing criterion (Criterion 1) is used, a gap will initiate on the flood side when the hydrostatic water pressures from the flood loading (of the pool) exceed the total horizontal earth pressures at the interface between the sheet-pile wall and the soil. The hydrostatic water pressure is computed as the height below the floodwater times the unit weight of water. The depth of gap will proceed until the total horizontal earth pressure equals the hydrostatic water pressure of the flood pool.

For a system as shown in Figure 4.1, the total horizontal stress is computed using Equation 4.5 for points along a vertical section extending down to the pile tip. For the flood side, the total vertical stress at a point is computed taking into account all soil layers and external water loads above the point in question. The total horizontal stress is computed using this value of the total vertical stress in Equation 4.5 and compared to the hydrostatic water pressure computed based on the height of the floodwater and the distance to the point in question. If the water pressure is greater than the horizontal earth pressure, the soil is assumed to form a gap. This criterion for predicting gap depth is discussed in Brandon et al. (2008).

4.3.3.2 Criterion 2

The depth of gap computed using this criterion is based on whether the computed total horizontal stress is less than zero. The total horizontal stress at a point is computed using Equation 4.5. If the result is a negative or tensile value, the soil is assumed to form a gap. The gap extends down to a point where the horizontal earth pressures become positive. In this unique case of a constant undrained shear strength with depth for this clay site, a convenient equation for determining the depth of the gap (d_c) from Craig (1997) for a soil containing both cohesion and an internal angle of friction is

$$d_c = \frac{2c\sqrt{1 + \frac{c_a}{c}}}{\gamma\sqrt{K_a}}, \quad (4.7)$$

where γ is the saturated unit weight of the soil if the water table is at or above the top of the ground surface and the moist unit weight of the soil if the water table is below the ground surface. Note that this is not a hydraulic fracturing-based criterion.

For a cohesive soil ($\phi = 0$) with zero adhesion ($c_a = 0$), the depth of the gap d_c is

$$d_c = \frac{2c}{\gamma}. \quad (4.8)$$

From Brandon et al. (2008), for a homogeneous system with water at or above the ground surface, the depth of the gap can be computed using

Equation 4.8 (for constant c only) with γ equal to the buoyant unit weight of the soil.

4.3.4 Material properties for use with CWALSHT

The depth of the sheet-pile wall was determined using the CWALSHT computer program and procedures from the sheet-pile wall engineering manual as given in HQUSACE (1994). To perform a CWALSHT design of the I-wall system, two designs were performed based on short-term and long-term conditions. This required the use of effective stress (drained) strength parameters for the long-term design and total stress (undrained) strength parameters for the short-term design. The soil properties for both analyses are shown in Table 4.1.

Table 4.1. Material properties for analyses.

Analysis Type	γ_{moist} , lb/ft ³	γ_{sat} , lb/ft ³	S_u , lb/ft ²	c_a , lb/ft ²	ϕ , deg	δ , deg
Total stress	110	110	300	240	0	0
Effective stress	110	110	0	0	28	0

The material property values were chosen to represent a soft clay and consisted of the saturated (γ_{sat}) and moist (γ_{moist}) unit weights of the soil, the undrained shear strength (S_u), adhesion (c_a), and the angle of internal friction (ϕ). The same value of the unit weight was used for both saturated and moist conditions. A value of 0.8 for f_{cmax} , which is the adhesion (c_a) divided by the cohesion (c) of the soil, was assumed for the total stress analysis, and was taken from values cited in Potyondy (1961) for a cohesive soil against rough steel.

4.3.5 Computed gap depth

For the effective stress (drained) analysis, the depth of the gap is automatically computed by CWALSHT using the negative horizontal effective stress criterion (Criterion 2) discussed in Section 4.3.3. If the computed earth pressures are negative, this implies that the soil-to-sheet-pile interface is in tension. Because the soil-to-sheet-pile interface cannot sustain a tensile load, the soil is assumed to form a gap. CWALSHT sets any negative (tensile) earth pressures to zero and applies water pressures within a gap below the input water level. If the gap is above the water level, CWALSHT does not fill the gap with water.

For the total stress (undrained) analysis, the gap depth must be computed and used to develop the input for the CWALSHT analysis. Because the soil is homogeneous, the depth of the gap can be computed using Equation 4.8 with γ equal to the buoyant unit weight of the soil and the cohesion (c) equal to the undrained shear strength. If adhesion (c_a) is ignored, the following gap depth is computed:

$$d_c = \frac{2c}{\gamma} = \frac{2(300)}{47.6} = 12.6 \text{ ft.} \quad (4.9)$$

If adhesion is accounted for, the value of the adhesion factor is

$$r = \sqrt{1 + \frac{c_a}{c}} = \sqrt{1 + 0.8} = 1.34. \quad (4.10)$$

The value of 0.8 in Equation 4.10 is obtained by dividing the adhesion (c_a) by the cohesion (c) of the soil. The depth of the gap considering adhesion is therefore

$$d_c = \frac{2c\sqrt{1 + \frac{c_a}{c}}}{\gamma\sqrt{K_a}} = \frac{2(300)\sqrt{1 + 0.8}}{47.6(1.0)} = 16.9 \text{ ft.} \quad (4.11)$$

These values of gap depths will be used in the CWALSHT analyses discussed in the next section.

4.3.6 CWALSHT design results

Both short-term and long-term designs were performed with CWALSHT using the material properties given in Table 4.1. For the designs, the required factors of safety on the active and passive pressures, as given in HQUSACE (1994), are shown in Table 4.2.

The results of the design computations are given in Table 4.3.

Table 4.2. Factor of safety for design of cantilever l-walls.

Design Case	Factor of Safety	
	Active Pressures	Passive Pressures
Short term	1	1.5
Long term	1	1.1

Table 4.3. Results of design computations using CWALSHT.

Design Case		S_u , psf	ϕ , deg	Adhesion, psf	Wall Friction, deg	Gap Depth, ft	Wall Depth, ft	Maximum Moment Computed Using $FS_{Active}=1.0$, $FS_{Passive}=1.0$ ft-lb	Notes ¹
1	Short term	200	0	0	0	8.4	No solution	-	No sign change in net pressure
2	Short term	300	0	0	0	12.6	29.85	No solution	$FS_A=1.0$, $FS_P=1.35$, $M=3.29 \times 10^4$ ft-lb
3	Short term	300	0	240	0	16.91	No solution	-	Wall is rotating clockwise
4	Short term	300	0	0	0	16.91	No solution	-	-
5	Short term	300	0	20	0	13.02	No solution	-	Design bottom of cantilever wall is above el -14 ft
6	Short term	300	0	15	0	12.92	28.98	-	-
7	Short term	400	0	0	0	16.8	No solution	-	Wall is rotating clockwise
8	Long term	0	28	0	0	0	25.89	4.59×10^4	$FS_A=1.0$, $FS_P=1.1$, $M=5.06 \times 10^4$ ft-lb
9	Long term	0	28	0	22.4	0	17.63	No solution	$FS_A=1.0$, $FS_P=1.1$, $M=3.11 \times 10^4$ ft-lb

¹ A stable solution in CWALSHT requires a loading that produces a counterclockwise wall rotation.

Short-term Case 2, highlighted in red in Table 4.3, is the case that governs the depth of penetration of the sheet pile (a penetration depth equal to 29.85 ft). The short-term case exceeds the penetration requirements of the long-term cases.

The CWALSHT program reported that a solution was not possible for various values of the undrained shear strength and the adhesion. As shown in Table 4.3, solutions were not possible for values of the undrained shear strength of 200 psf (Case 1) and 400 psf (Case 7). Both of these analyses reported different reasons for the inability to compute a depth of penetration.

A penetration depth was computed for the value of the undrained shear strength equal to 300 psf (Case 2 in Table 4.3). This case did not include the effect of adhesion on the penetration depth. Cases 3 through 6 varied the amount of adhesion. As seen from Equation 4.7, the amount of the adhesion affects the depth of the gap. Case 3 includes the amount of adhesion ($c_a = 0.8 * c$), and a solution was not obtained. When the case of no adhesion (Case 4) was run with the gap at a depth of 16.91 ft (computed using an adhesion of 240 psf), a solution was not obtained.

Case 5 used an adhesion of 20 psf with a computed gap depth of 13.01 ft, and a solution was not obtained. CWALSHT reported that the design bottom of the cantilever wall was above el -14 ft and, therefore, no penetration was required. Case 6 used an adhesion of 15 psf and a computed gap depth of 12.92 ft. CWALSHT reported a design penetration of 28.98 ft. Therefore, there appear to be some inconsistencies in the design computations in CWALSHT that warrant additional examination.

4.3.7 CWALSHT design moments and selection of sheet-pile section

The design guidance (HQUSACE 1994) for cantilever walls states that the maximum moment used for sizing the sheet-pile section should be computed using a factor of safety for the active and passive earth pressures of 1.0 as shown in Table 4.3. From Table 4.3, the maximum moment equal to 4.59×10^4 ft-lb from long-term Case 8 was used for sizing the sheet pile. The moment for Case 2 for a factor of safety on the active and passive earth pressures of 1.0 could not be computed. The moment for a factor of safety of 1.35 for the passive pressures was computed to be 3.29×10^4 ft-lb. The moment for a factor of safety of 1.0 for the passive earth pressure for Case 2 would result in a smaller moment than reported for the factor of safety of 1.35. Therefore, the short-term case controlled the penetration depth, but the long-term case controlled the maximum moment in the sheet pile.

Using the maximum moment of 4.59×10^4 ft-lb, a PZ27 section was found to satisfy the needed section modulus using an allowable yield stress for A328 steel of 38,500 psi. The section properties of the PZ27 are:

- Driving distance = 18 in.;
- Weight per foot = 40.5 lb/ft;
- Section modulus $S = 30.2$ in.³/ft;
- Area = 11.91 in.²;
- Moment of inertia $I = 184.2$ in.⁴/ft;

- Height = 12 in.;
- Width = 18 in.

4.4 PLAXIS finite element analyses

4.4.1 Conceptual model

The finite element analyses were performed with PLAXIS. The conceptual model of the finite element mesh is shown in Figure 4.4. The geometry is the same as explained previously, but several modeling features should be noted. The sheet-pile wall was represented by plate elements, and the concrete wall was represented by 2-D elastic elements. Interface elements were placed on both sides of the plate elements from the ground surface down to the tip of the sheet pile. Both horizontal and vertical extensions of the interface elements were provided at the tip of the sheet-pile wall at el -30 ft. This was done to alleviate stress concentrations at the corners of the geometry. A plate element extension and dummy soil elements were added above the wall to provide for additional loading height if needed. The mesh was structured to provide node points at 1-ft raises of the water table. The soil elements beside the sheet-pile wall on the flood side were 1 ft high. This enabled the inputting of 1-ft raises in water and modeling of the gap to within 1 ft.

4.4.2 Finite element mesh

The finite element mesh used in the analyses is shown in Figure 4.5. Figure 4.6 shows an enlargement of the area around the wall and the detail of the mesh. The mesh is composed of 1,953 elements, 16,371 nodes, with 23,436 stress points. The type and number of elements used in the mesh are shown in Table 4.4. The mesh consists of 15-node triangular elements to model the soil, 5-node plate elements to model the sheet-pile wall, and 5-node interface elements to model the soil-structure interaction effects between the sheet-pile wall and the adjacent soil elements. The problem was run as a plane strain problem.

The 45-deg lines emanating from the tip of the sheet-pile wall to the top of the ground surface shown in Figures 4.5 and 4.6 were included in case the need arose to alter material properties adjacent to the wall within the regions of active and passive soil pressures. This modeling also provided some mesh refinement adjacent to the wall.

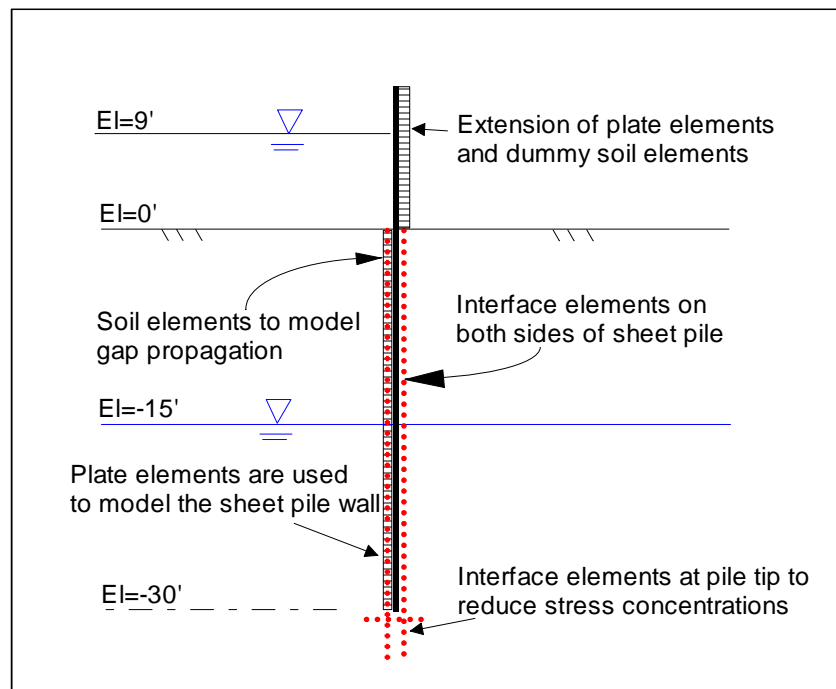


Figure 4.4. Conceptual model.

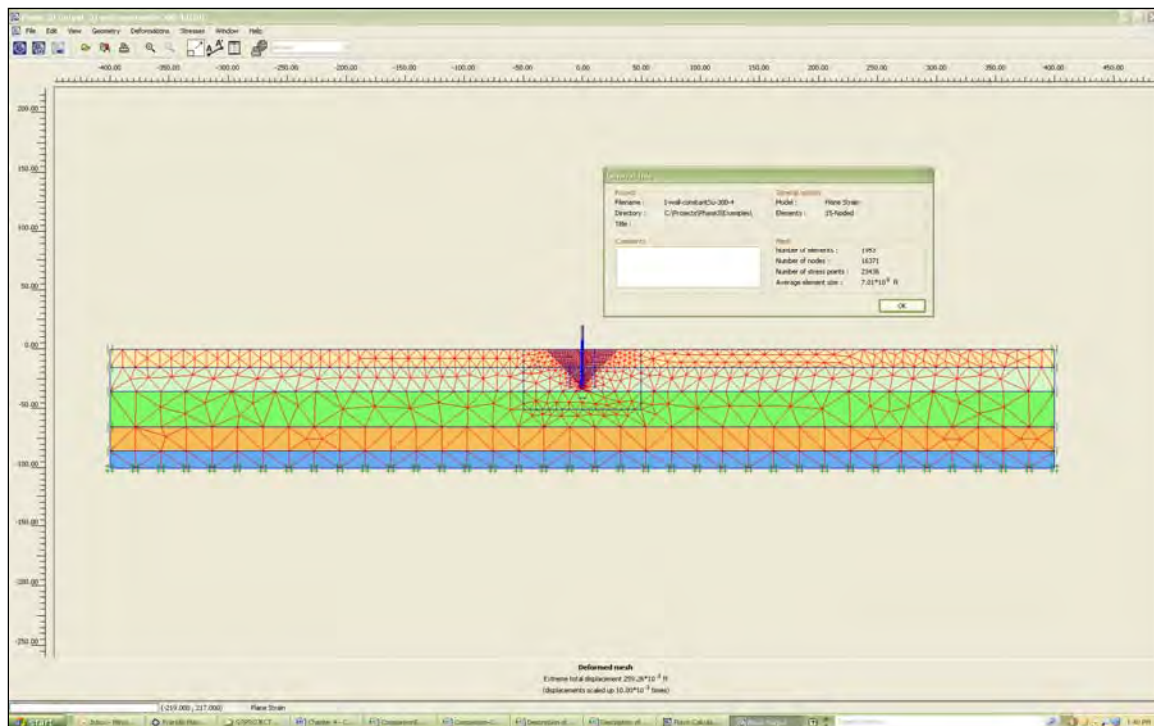


Figure 4.5. Finite element mesh used in the analyses.

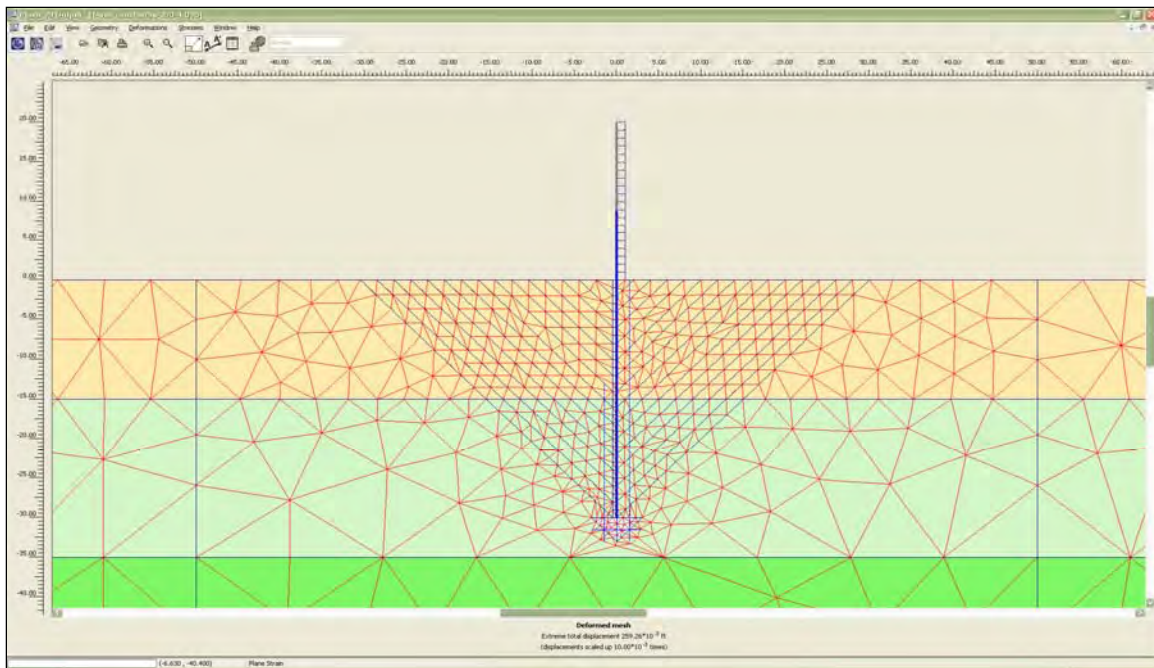


Figure 4.6. Enlargement of finite element mesh around the I-wall.

Table 4.4. Type and number of elements used in the finite element mesh.

Type	Type of Element	Type of Integration	Total Number
Soil	15-node triangular	12-point Gauss	1953
Plate	5-node line	4-point Gauss	50
Interface	5-node line	4-point Newton-Cotes	77

4.4.3 Total stress analysis procedure in PLAXIS

The results from the CWALSHT design computations show that the short-term (undrained) case produced the greater sheet-pile wall tip penetration as shown in Table 4.3. Therefore, the short-term condition was the case analyzed by the finite element method. To perform a short-term (undrained) analysis using PLAXIS, total unit weights of the soil and boundary water pressures were used. All materials were designated as drained, which in PLAXIS terminology means that no excess pore-water pressures will be generated from applied loads. The general phreatic surface was used in PLAXIS to apply the boundary water pressures on the soil surface and within the gap. All soil layers were associated with a cluster phreatic surface that was input below the minimum elevation of the mesh. Because the water surface is below all soil layers, no internal water pressures are generated within the soil layers. This procedure results in a total stress analysis with the computed effective stresses being equal to the total stresses (i.e., no internal pore pressures are present).

It is assumed that the permeability of the soil is small enough that any time-dependent effects, such as seepage, can be ignored and that the undrained shear strengths can be used to determine the behavior of the system.

4.4.4 Tracking the progression of the gap

The I-wall will deflect as the flood loading is increased and, eventually, a gap forms beside the I-wall on the flood side of the wall. The gap begins at the ground surface and progresses downward as shown in Figure 4.7. The gap along the flood side of the I-wall-to-soil interface is modeled by deactivating soil clusters (elements), effectively creating a void beside the wall. As water pressures are applied within this void, the gap progresses downward. Modeling of the flood loading commenced in the finite element analysis after the total initial stress state was computed based on an assumed steady-state water elevation of -15 ft. The flood loading was applied in 1-ft incremental raises of the water level to track the formation and propagation of the gap.

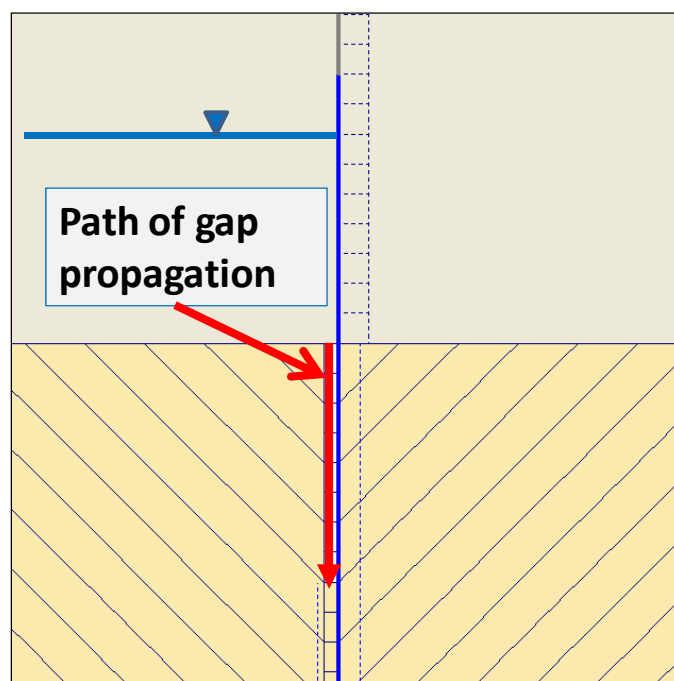


Figure 4.7. Location and propagation of gap beside I-wall.

The criterion used to estimate the formation and propagation of the gap is based on the hydraulic fracturing concept discussed in Section 4.3.3. The procedure used to estimate the gap depth:

1. For each rise in water level, the total horizontal stresses against the sheet-pile wall are compared against the hydrostatic water pressures acting on the wall given the current water elevation. A gap is formed when the horizontal earth pressure is less than the water pressure at a given depth.
2. Soil elements are deactivated within the computed region of the gap, and hydrostatic water pressures are applied within the deactivated elements.
3. The analysis is rerun for the current water level, and Steps 1 and 2 are repeated until the depth of the gap ceases to increase.
4. The water level is increased, and Steps 1 through 3 are repeated. The water level is raised until instability in the analyses is encountered.

4.4.5 Shear strength and stiffness properties used in the finite element analyses

The finite element analyses required certain material properties for the selected soil models. All finite element analyses were performed with the PLAXIS finite element program. Separate analyses were performed using two different soil constitutive models to represent the behavior of the soil elements: the Hardening Soil (HS) model, which uses a nonlinear stress-strain relationship; and the Mohr-Coulomb (MC) soil model, which uses an elastic-perfectly plastic stress-strain relationship. Elastic plate elements were used to model the steel sheet pile, and interface elements were used to capture the soil-structure interaction effects between the sheet-pile wall and the soil. PLAXIS can perform analyses using either effective or total stress soil parameters. For the analyses described herein, total stress soil parameters were used.

Figure 4.8 shows the material numbering and soil layering used in the finite element analyses. The soil was divided into layers to provide for an increasing undrained shear strength and stiffness below the elevation of the pile tip. This was done to alleviate excessive settlements caused by using a constant undrained shear strength and stiffness for the entire 100-ft soil depth.

The soil properties used for the HS analyses are shown in Table 4.5. The material numbers in the tables match the material numbers in Figure 4.8. The values of the undrained shear strength (for Figure 4.8 Materials 4, 5, and 6) were computed by assuming a value of 0.22 for the ratio of the undrained shear strength to the effective overburden stress, (S_u/σ'_{vo}) . The increase in vertical stress above the vertical stress at el -35 ft was computed at the center of each layer. This stress increment was multiplied by $S_u/\sigma'_{vo}=0.22$ and the result added to the constant (S_u) equal to 300 psf to arrive at the undrained shear strength of each layer.

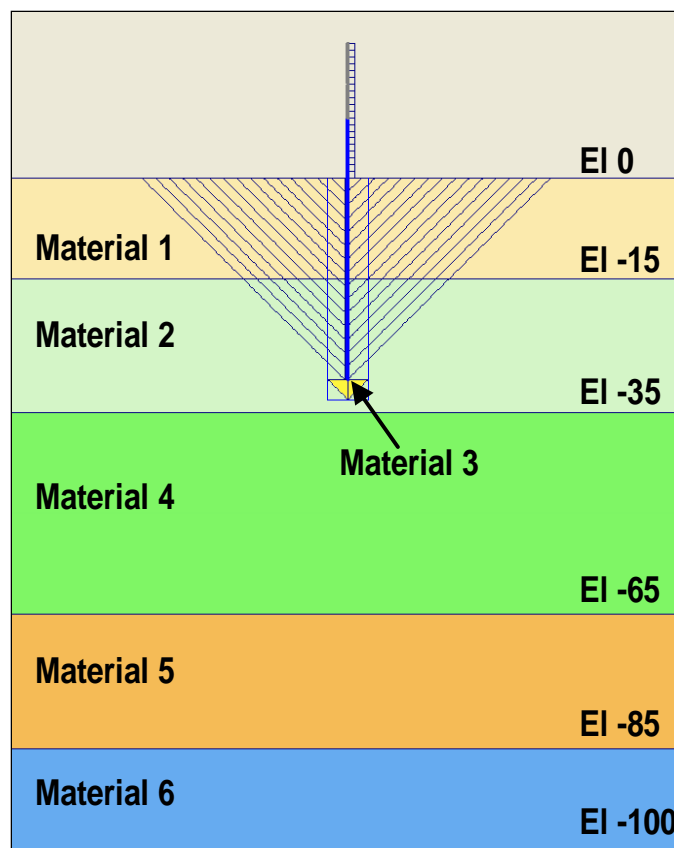


Figure 4.8. Soil layering and material numbers used in the finite element analyses.

Table 4.5. Strength and stiffness properties for the soil layers used in the HS model.

Material Number	Material Description	S_{ur} lb/ft ²	$E_{50,ref}$ lb/ft ²	$E_{oed,ref}$ lb/ft ²	$E_{ur,ref}$ lb/ft ²	$R_{interface}$
1	Clay-300-Rint=0.8	300	180,000	180,000	462,857	0.8
2	Clay-300-Rinit=0.8	300	180,000	180,000	432,000	0.8
3	Clay-300-Rint=1.0	300	180,000	180,000	433,445	1
4	Clay-500-Rint=0.8	500	300,000	300,000	900,000	0.8
5	Clay-700-Rint=0.8	700	420,000	420,000	1,260,000	0.8
6	Clay-900-Rint=0.8	900	540,000	540,000	1,620,000	0.8

Note: properties are given for drained material, with ϕ and the dilation angle (ψ) set to 0, as this is a total stress analysis. γ_{sat} and γ_{moist} are set to 110 lb/ft³, unload/reload Poisson's ratio (ν) is set to 0.2, and the interface strength (R_f) is set to 0.9.

The $R_{interface}$ value is from those cited by Potyondy (1961) as discussed in Section 4.3.4. This controls the amount of adhesion along the soil-to-wall interface. Material 3 in Table 4.5 has an $R_{interface}$ value of 1.0 since this material represents a soil-to-soil interface. The R_f value controls the shear strength at failure and is a percentage of the maximum shear strength.

The HS model uses a secant reference stiffness ($E_{50,ref}$), an oedometer reference stiffness ($E_{oed,ref}$), and an unload/reload reference stiffness ($E_{ur,ref}$), as shown in Table 4.5. Equations 4.12 and 4.13 show the assumed relationship between the E_{50} reference stiffness and the oedometer and unload/reload reference stiffnesses:

$$E_{OED,ref} = E_{50,ref} \quad (4.12)$$

$$E_{ur,ref} = 3 \cdot E_{50,ref} \quad (4.13)$$

The E_{50} stiffness is dependent on the reference stiffness ($E_{50,ref}$), a reference pressure (p_{ref}), the confining stress (σ_3'), the cohesion (c), the angle of internal friction (ϕ), and a fitting parameter (m), as shown in Equation 4.14:

$$E_{50} = E_{50,ref} \left(\frac{c \cdot \cos f - \sigma_3' \sin f}{c \cdot \cos f - p_{ref} \sin f} \right)^m \quad (4.14)$$

For ϕ equal to zero, Equation 4.14 reduces to Equation 4.15:

$$E_{50} = E_{50,ref} \quad (4.15)$$

The value of m does not make a difference when ϕ is equal to zero.

To compute the value of the E_{50} stiffness, the soil was assumed to have a PI of 30 and be normally consolidated. Duncan and Buchignani (1976) developed a chart relating the PI, the overconsolidation ratio (OCR), and a factor (K) defined in Equation 4.16:

$$K = \frac{E_u}{S_u} \quad (4.16)$$

Using Figure 5 from Duncan and Buchignani (1976), K was assigned a value of 600. This constant was used with the values of the undrained shear strength to compute the undrained secant stiffness as shown in Equation 4.17 for each soil layer:

$$E_u = E_{50}^{ref} = K S_u \quad (4.17)$$

Differences in the computed values of $E_{ur,ref}$ and the values reported in Table 4.6 are due to automatic adjustments by PLAXIS to the stiffnesses upon data entry. The adjustments are made any time the value of the Poisson's ratio is changed.

Table 4.6. Strength and stiffness properties for the soil layers used in the MC soil model.

Material Number	Material Description	S_u , lb/ft ²	E_{ref} , lb/ft ²	ν	$R_{interface}$
1	Clay-300- $R_{int}=0.8$	300	180,000	0.4	0.8
2	Clay-300- $R_{int}=0.8$	300	180,000	0.495	0.8
3	Clay-300- $R_{int}=1.0$	300	180,000	0.495	1
4	Clay-500- $R_{int}=0.8$	500	300,000	0.495	0.8
5	Clay-700- $R_{int}=0.8$	700	420,000	0.495	0.8
6	Clay-900- $R_{int}=0.8$	900	540,000	0.495	0.8

Note: properties are given for drained material, with ϕ and the dilation angle (ψ) set to 0, as this is a total stress analysis. γ_{sat} and γ_{moist} are set to 110 lb/ft³.

Two sets of material properties were used for the MC analyses as shown in Tables 4.6 and 4.7. The properties are identical to the HS model, except that not as many properties are required. The reference stiffness for the MC model (E_{ref}) in Table 4.6 is set equal to the $E_{50,ref}$ stiffness values from the HS model. The reference stiffnesses in Table 4.7 are set equal to the unload/reload stiffnesses from the HS model. These stiffnesses range from 2.4 to 3.0 times the $E_{50,ref}$ stiffnesses. The Table 4.7 material properties were used in a parametric analysis.

Table 4.7. Strength and stiffness properties for the soil layers used in the MC soil model with increased E_{ref} .

Material Number	Material Description	S_u , lb/ft ²	E_{ref} , lb/ft ²	ν	$R_{interface}$	E_{ref} Increase
1	Clay-300- $R_{int}=0.8$	300	462,857	0.4	0.8	2.6
2	Clay-300- $R_{int}=0.8$	300	432,000	0.495	0.8	2.4
3	Clay-300- $R_{int}=1.0$	300	433,445	0.495	1	2.4
4	Clay-500- $R_{int}=0.8$	500	900,000	0.495	0.8	3.0
5	Clay-700- $R_{int}=0.8$	700	1,207,500	0.495	0.8	2.9
6	Clay-900- $R_{int}=0.8$	900	1,620,000	0.495	0.8	3.0

Note: properties are given for drained material, with ϕ and the dilation angle ψ set to 0, as this is a total stress analysis.

The sheet pile was represented by elastic plate elements with the properties given in Table 4.8, where EA is the axial stiffness and EI is the flexural rigidity.

Table 4.8. Properties of the plate elements representing the sheet pile.

Name	Material Behavior	EA, lb/ft	EI, lb-ft ²	Weight, lb/ft ²	ν
Sheet pile	Elastic	2.30E+08	37,100,000	20.95	0.25

4.4.6 Initial stresses

The initial total stress state within the finite element mesh was established using the at-rest soil conditions for a level ground surface. Horizontal at-rest soil stresses were estimated using the relationship between the at-rest earth pressure coefficient (K_o) and the soil's Poisson's ratio (ν) given in Equation 4.18:

$$K_o = \frac{\nu}{1 - \nu}. \quad (4.18)$$

The assumed groundwater elevation was at el -15 ft. Table 4.9 summarizes the K_o values used to compute the horizontal earth pressures for the initial conditions. The Poisson's ratio for the partially saturated soil layer is 0.4, and this corresponds to a K_o of 0.67. This value is less than the value for a fully saturated material, which has a K_o of 1.0.

Table 4.9. Poisson's ratio and at-rest horizontal earth pressure coefficients used for analyses.

Soil Condition	Elevation Range, ft	ν	K_o
Partially saturated	0 to -15	0.4	0.67
Saturated	-15 to -100	0.495	1

4.4.7 Performance of interface elements

The performance of the interface elements was examined to determine if the normal stresses in the interface elements corresponded closely to the normal stresses in the adjacent soil elements. Results for the case of flood pool at el 9 ft and gap to el -13 ft were used for this comparison. Figure 4.9 shows that the stresses within the interface elements agree very closely with the stresses in the adjacent soil elements and that the processing of results could be done using either data set. There were some small irregularities in the stresses in the interface elements at the soil surface, the bottom of the

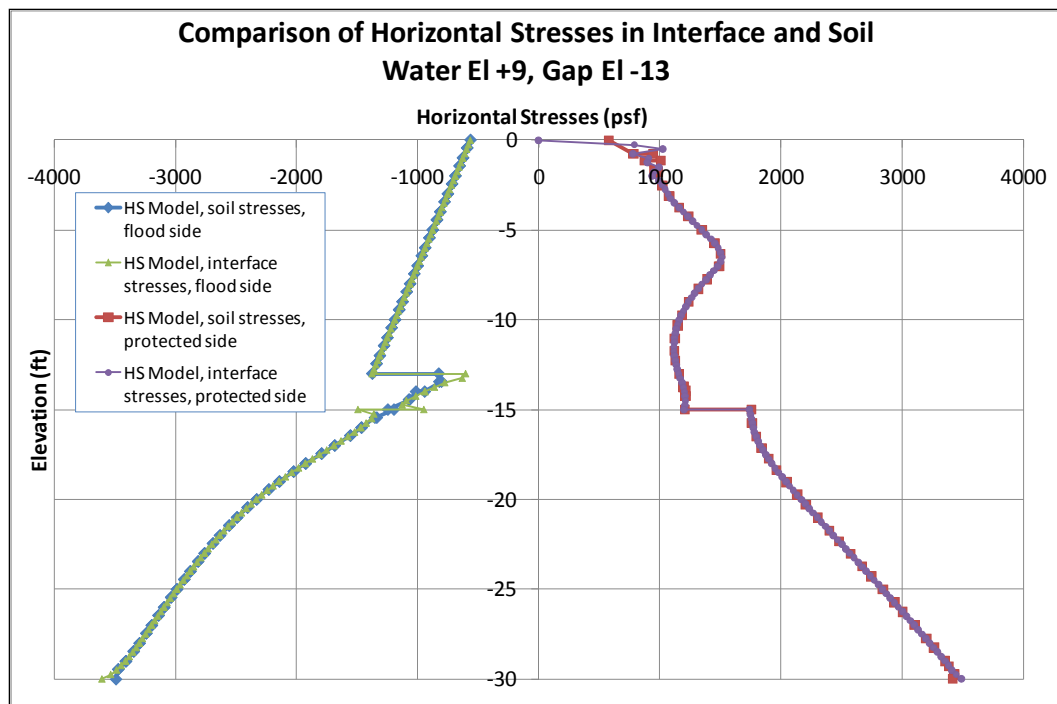


Figure 4.9. Behavior of interface versus soil elements for a water elevation at 9 ft and a gap elevation at -13 ft.

gap adjacent to the flood side of the wall, and at the interface between changes in Poisson's ratio at el -15 ft. For this reason, most of the results presented use the stresses extracted from the soil elements adjacent to the sheet-pile wall.

4.4.8 Comparison of HS and MC models

As stated, analyses were conducted using both the HS and MC models contained in PLAXIS to represent the soil response. Initially, only the HS model was used, but problems were encountered with the stability of the problem. When the progression of the gap was tracked, as detailed in Section 4.4.4, convergence of a solution could not be obtained for water levels lower than the design flood height of 9 ft. Figure 4.10 shows the relative shear stress around the sheet-pile wall for a water level of 3 ft and a gap tip elevation of -11 ft. As can be seen from the figure, a large portion of the soil on the landside (right side) of the wall is at full mobilization of the shear strength (i.e., a relative shear stress of 1.0). This occurred because the externally applied hydrostatic water loads caused the wall to deflect toward the flood side due to settlements of the soil. As the water levels increased, the wall was pushed into the landside and the instability was alleviated.

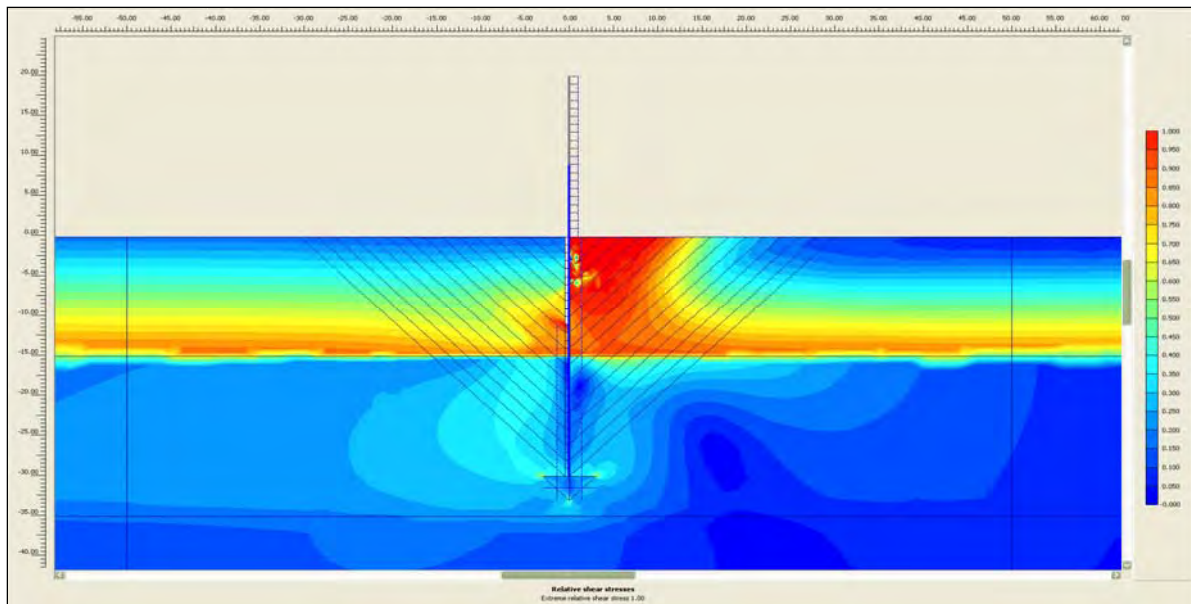


Figure 4.10. Full mobilization of shear strength on the landside of the wall due to a water elevation of 3 ft and a gap tip elevation of -11 ft.

The MC model did not exhibit these same instabilities, and the procedure detailed in Section 4.4.4 could be followed to track the gap progression as the water level was increased. Because the HS model captures nonlinear stress-strain behavior and the MC model does not, a comparison of the models was performed to determine if the results from the MC model could be used reliably to determine the behavior of the system.

Figures 4.11 through 4.14 compare results from the HS and MC models and are based on results for the design flood condition of a water elevation at 9 ft and a gap tip elevation at -13 ft. Figure 4.11 compares the normal stresses in the interface elements on each side of the sheet-pile wall for both the HS and MC models. As can be seen from the figure, the normal stresses are very close to each other on the flood side (left side) and in good agreement on the landside (right side).

The displacements of the sheet-pile wall are shown in Figure 4.12. The MC model with an increased E_{ref} resulted in displacements less than those from the HS model. The displacements from the MC model with stiffnesses equal to those of the HS model resulted in displacements greater than those of the HS model. The displacements exhibit a 28-percent error for the maximum value of the wall displacement. The stiffer MC model resulted in tip displacements about equal to the HS model, while the softer MC model resulted in larger tip displacements than the HS model. If the

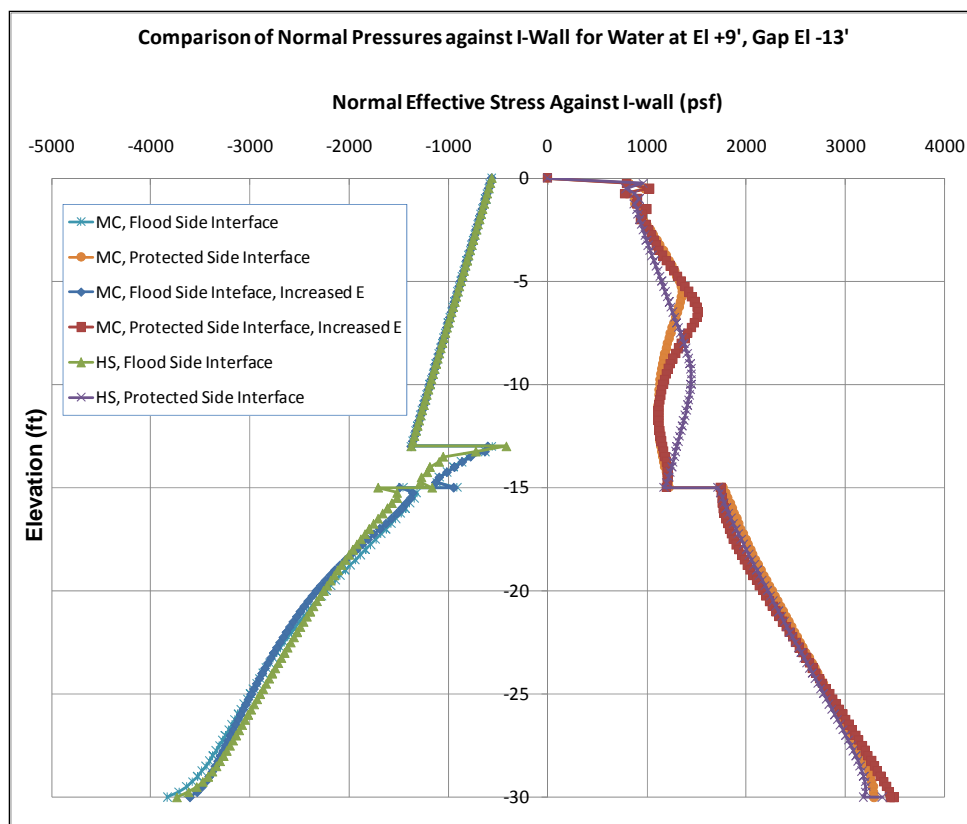


Figure 4.11. Comparison of normal pressures for the HS and MC models.

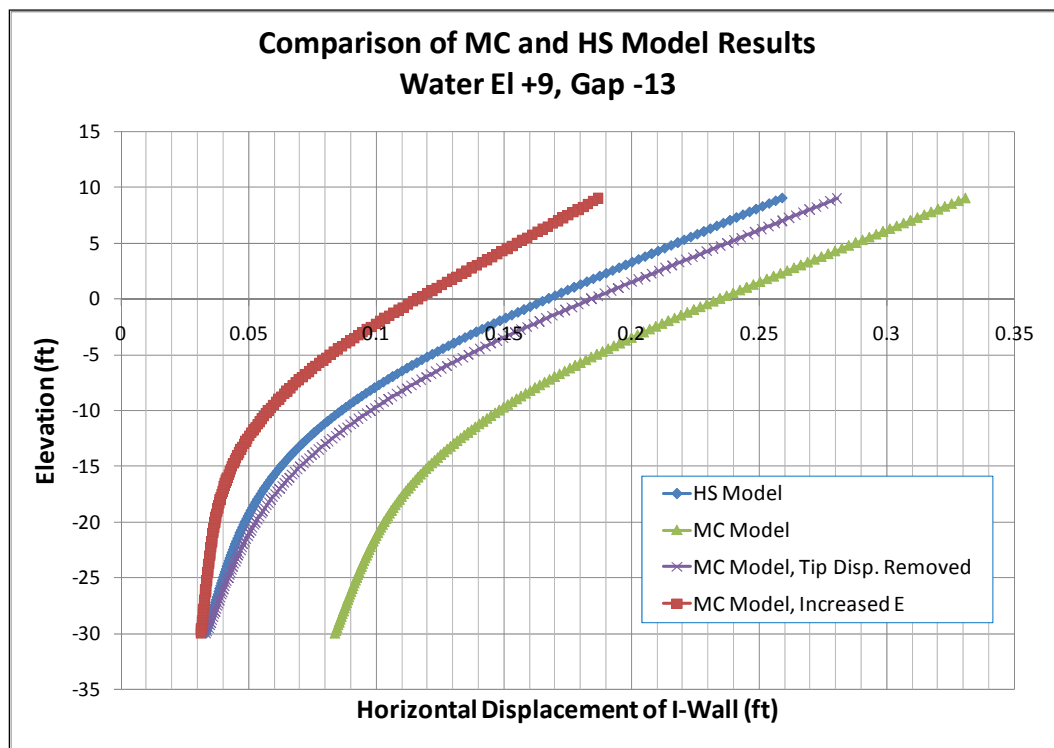


Figure 4.12. Comparison of the deflections of the sheet-pile wall for the HS and MC models.

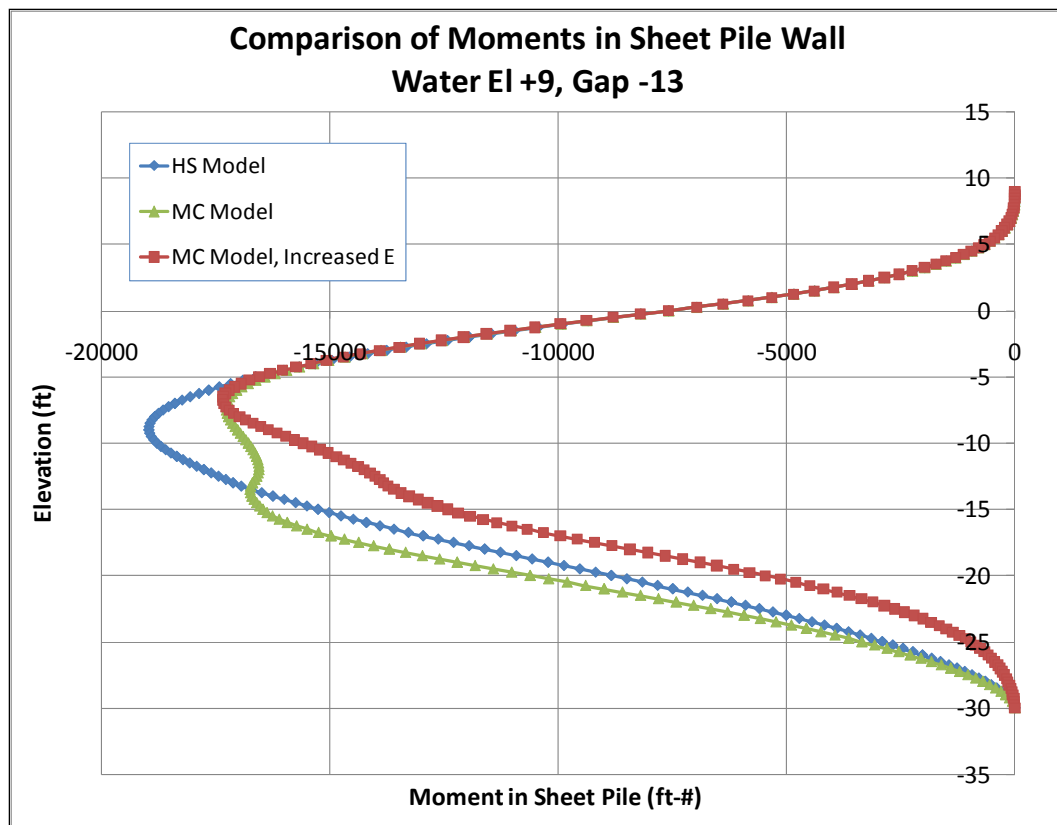


Figure 4.13. Comparison of the moments in the sheet-pile wall for the HS and MC models.

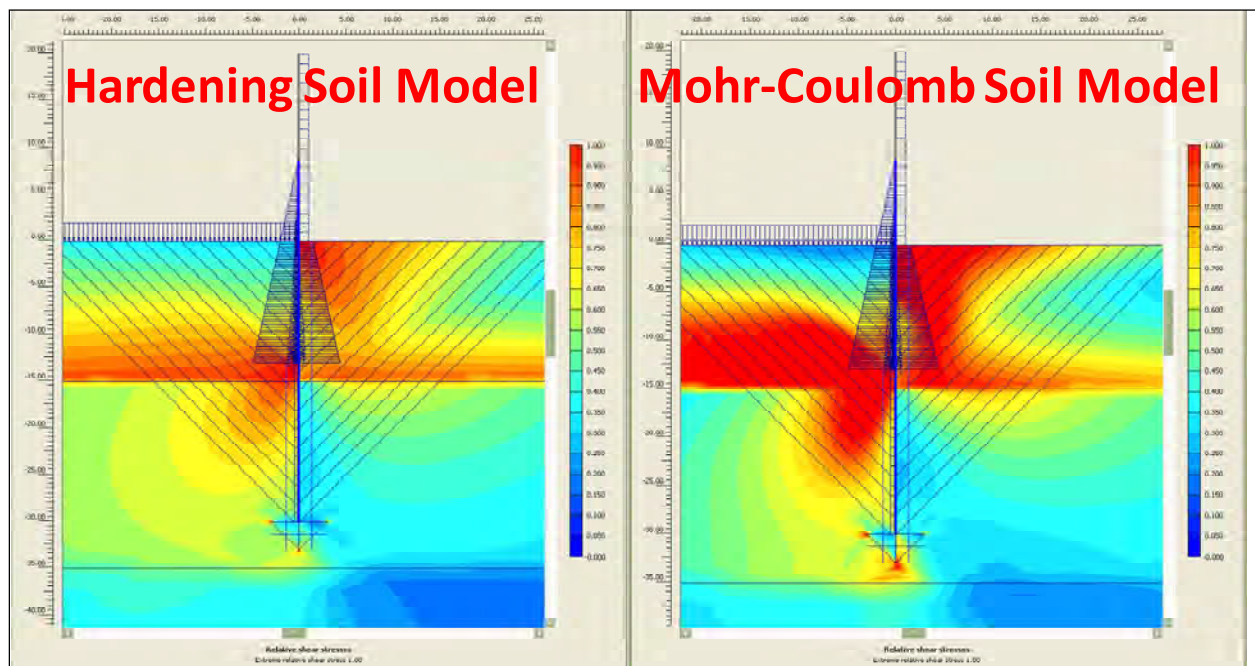


Figure 4.14. Comparison of mobilized shear strength for the HS and MC models for a water elevation of 9 ft and a gap tip elevation of -13 ft.

difference between the tip displacements of the softer MC model and the HS model are subtracted from those of the softer MC model, the resulting displacements of the MC model match the HS model within 13 percent.

Figure 4.13 compares the moments in the sheet-pile wall and exhibits an 8.5-percent error for the value of the maximum moment of the MC model compared to that of the HS model. Figure 4.14 compares the mobilized shear strength and, as can be seen from the figure, the magnitude and distribution of the mobilized shear strength are similar for the MC and HS models.

From this comparison, it was determined that the results of the MC model would be used to report the post-processing results.

4.4.9 Progression of the gap for MC analyses

Figure 4.15 shows the progression of the gap as the water level against the I-wall is increased from 1 ft to 13 ft. The gap initiates at a water elevation of 1 ft and extends to a depth of -4 ft. Upon a rise in water elevation to 2 ft, the gap extends another 7 ft to el -11 ft. At a water elevation of 3 ft, the gap extends to el -15 ft. At this point, another 8 ft of water results in only 4 ft more of gap formation to an elevation of -19 ft. The final 2 ft of water elevation from 11 to 13 ft results in 3 ft more of gap formation. Therefore, the rate of gap increase is rapid to begin with at the lower water elevations, then slows at the higher water elevations until finally increasing again as the system approaches instability.

The progression of the gap was essentially identical in the low and high soil stiffness analyses.

4.4.10 Sheet-pile wall displacements for MC model

Figures 4.16 and 4.17 show the horizontal displacements of the sheet-pile wall for various water elevations. The horizontal displacements at the top of the pile increase with a rising water elevation as seen from Figure 4.16. For the last two water elevations of 12 ft and 13 ft, the displacements at the top of the pile almost double for each 1-ft rise in water. The displacement of the top of the sheet pile for a water elevation of 13 ft is 22.7 in., while the displacement at the ground surface is 16.0 in.

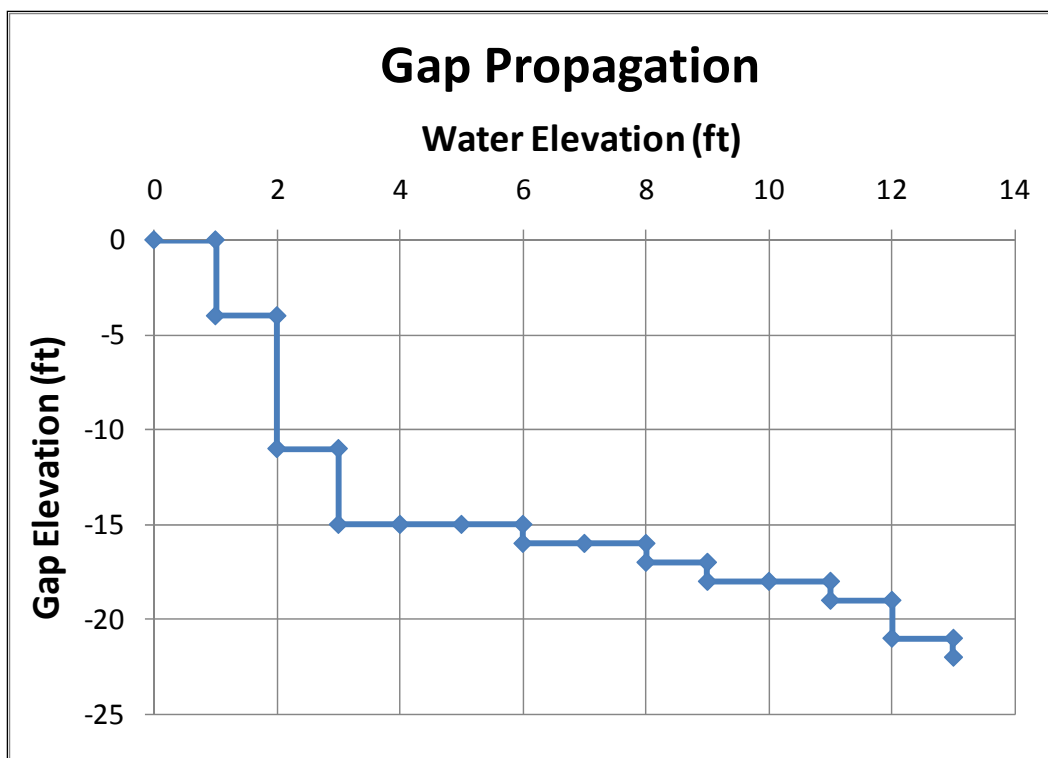


Figure 4.15. Progression of gap versus water elevation along flood side of I-wall.

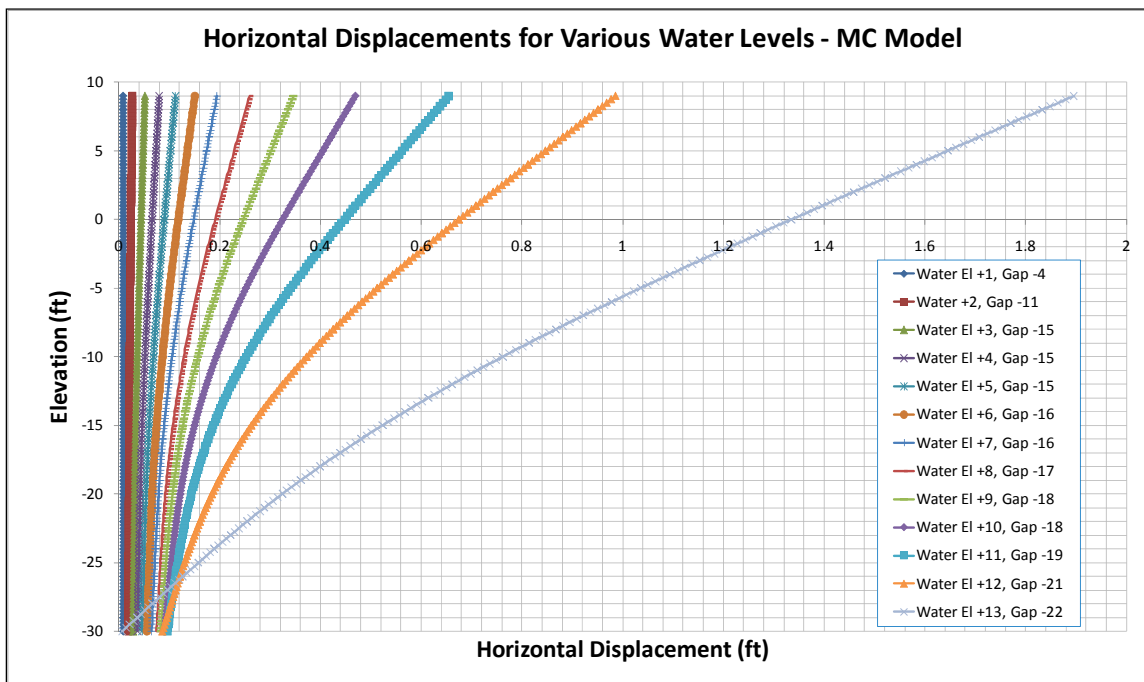


Figure 4.16. Sheet-pile horizontal displacements for various water elevations.

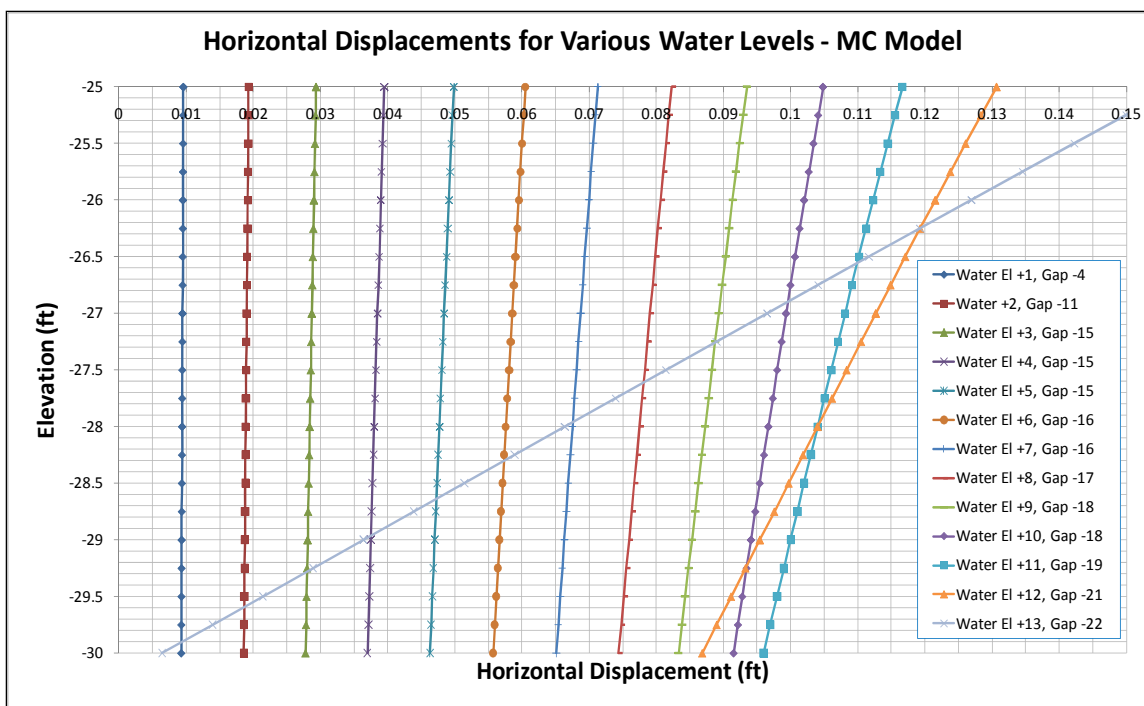


Figure 4.17. Sheet-pile horizontal displacements around the tip of the sheet pile for various water elevations.

Figure 4.17 is an enlargement of the area around the tip of the sheet pile and shows that the displacements of the tip are relatively constant with an increasing water elevation and progressively translate into the landside of the I-wall. The displacements of the tip can be seen to kick back into the flood side for water elevations of 11 ft to 13 ft. The maximum tip displacement was 1.15 in. at a water elevation of 11 ft. At 11 ft, the tip moved back into the flood side. For the final 1-ft rise in water to el 13 ft, the tip moved almost 1 in. back into the flood side to its original position. This large movement is due to the large area of highly stressed soil adjacent to the sheet-pile wall as discussed in Section 4.4.13.

Values of horizontal displacements for the sheet pile at the top, ground surface, and tip are tabulated in Table 4.10 and displayed in Figure 4.18. As shown in Figure 4.18, the pile tip displacements increase by a constant amount until reducing and kicking back into flood side. Figure 4.19 shows the relative displacement of the sheet pile at the ground surface, which is computed as the displacement of the sheet pile at the ground surface minus the displacement of the tip of the sheet pile.

Table 4.10. Pile displacements for MC model.

Water Elevation, ft	Top of I-wall, el 9 ft		Ground Surface, el 0 ft		Tip of Sheet Pile, el -30 ft		Relative Pile Displacement at Ground Surface (Ground Surface minus Tip Displacement)	
	ft	in.	ft	in.	ft	in.	ft	in.
1	0.0088	0.1056	0.0093	0.1112	0.0093	0.1115	0.0000	-0.0002
2	0.0263	0.3153	0.0238	0.2851	0.0186	0.2231	0.0052	0.0620
3	0.0517	0.6207	0.0440	0.5275	0.0278	0.3337	0.0162	0.1938
4	0.0800	0.9606	0.0659	0.7908	0.0370	0.4441	0.0289	0.3467
5	0.1123	1.3470	0.0900	1.0803	0.0463	0.5556	0.0437	0.5247
6	0.1506	1.8069	0.1177	1.4125	0.0557	0.6684	0.0620	0.7441
7	0.1948	2.3372	0.1484	1.7812	0.0651	0.7813	0.0833	0.9999
8	0.2592	3.1104	0.1908	2.2894	0.0744	0.8927	0.1164	1.3967
9	0.3467	4.1605	0.2470	2.9640	0.0833	0.9998	0.1637	1.9642
10	0.4700	5.6398	0.3258	3.9101	0.0915	1.0980	0.2343	2.8121
11	0.6546	7.8548	0.4473	5.3677	0.0960	1.1518	0.3513	4.2159
12	0.9863	11.8351	0.6752	8.1027	0.0868	1.0422	0.5884	7.0606
13	1.8955	22.7465	1.3347	16.0168	0.0064	0.0773	1.3283	15.9395

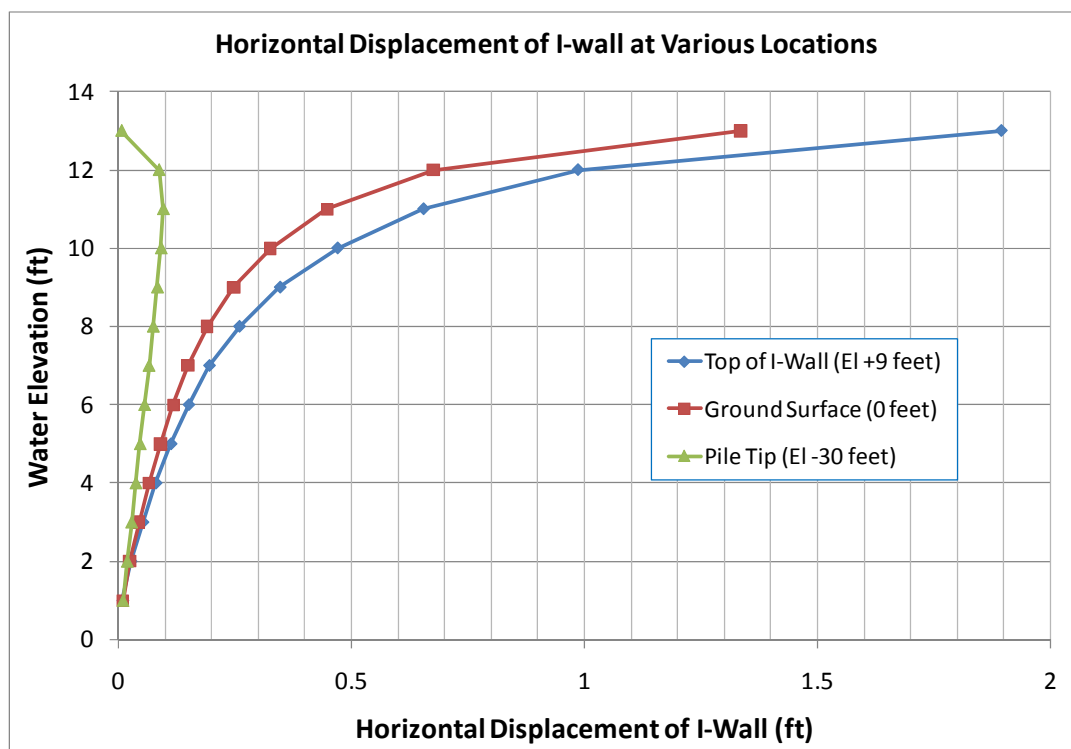


Figure 4.18. Sheet-pile horizontal displacements for selected locations.

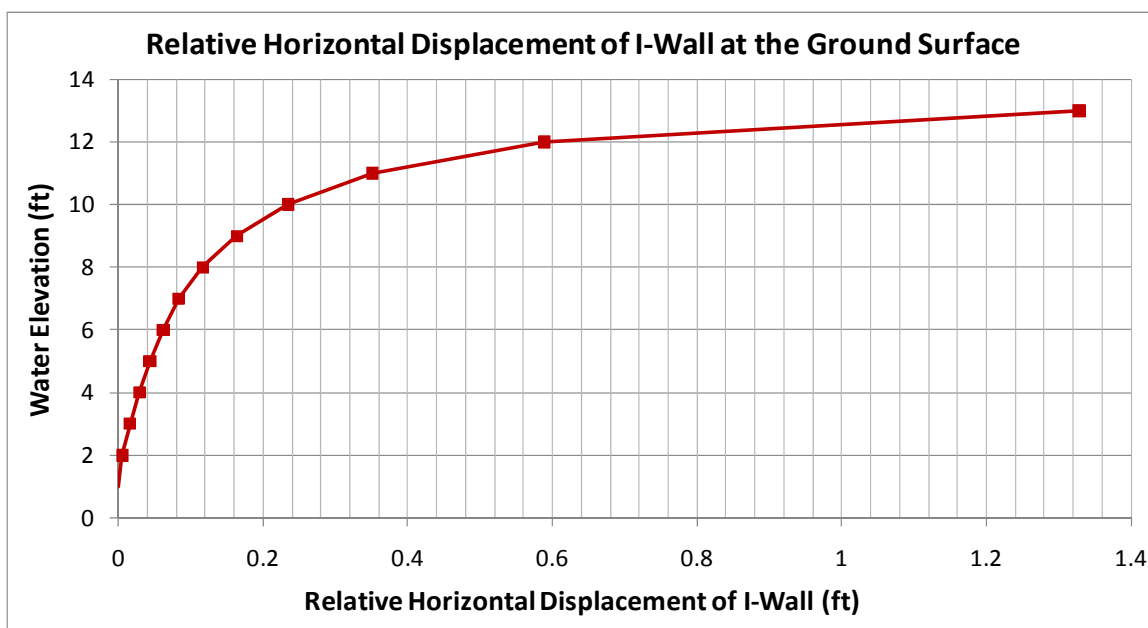


Figure 4.19. Relative horizontal displacements of the sheet pile at the ground surface.

Figure 4.20 shows the horizontal displacements of the sheet pile for an increased stiffness as given in Table 4.7 (i.e., the parametric study material values). The characteristics of the sheet-pile deflections are similar to the previous results shown for the lower soil stiffness. The displacement of the top of the sheet pile for a water elevation of 13 ft is 13.3 in., while the displacement at the ground surface is 8.8 in. as shown in Table 4.11. These displacements are about a factor of 2 less than the displacements reported for the lower soil stiffness as shown in Table 4.12.

The maximum tip displacement was 0.44 in. at a water elevation of 11 ft. At 11 ft, the tip moved back into the flood side. For the final 1-ft rise in water to el 13 ft, the tip moved about 0.4 in. into the flood side to its original position. This sizeable movement is due to the large area of highly stressed soil adjacent to the sheet-pile wall as discussed in Section 4.4.13.

Values of horizontal displacements for the sheet pile at the top, ground surface, and tip are tabulated in Table 4.11 and displayed in Figure 4.21. As shown in Figure 4.21, the pile tip displacements increased a constant amount until reducing and kicking back into the flood side. Figure 4.22 shows the relative displacement of the sheet pile at the ground surface, which is computed as the displacement of the sheet pile at the ground surface minus the displacement of the tip of the sheet pile.

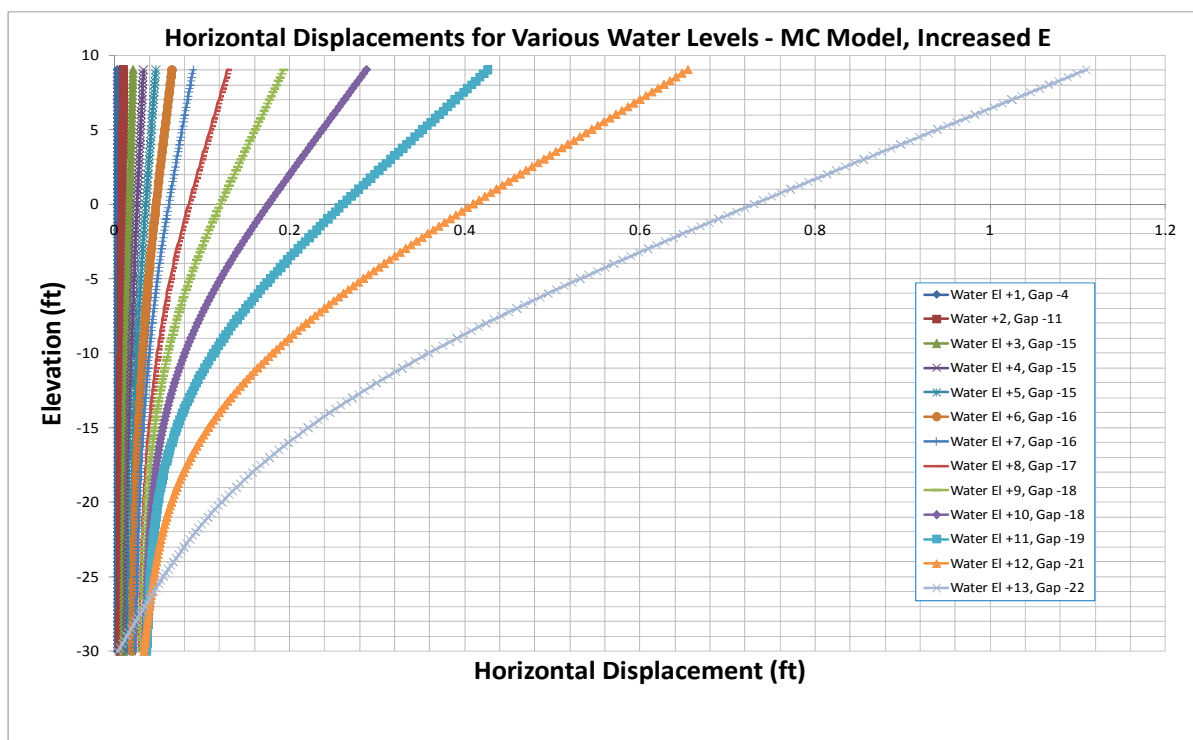


Figure 4.20. Sheet-pile horizontal displacements for various water elevations for an increased soil stiffness.

Table 4.11. Pile displacements for MC model with increased soil stiffness.

Water Elevation, ft	Top of I-wall, el 9 ft		Ground Surface, el 0 ft		Tip of Sheet Pile, el -30 ft		Relative Pile Displacement at Ground Surface (Ground Surface minus Tip Displacement)	
	ft	in.	ft	in.	ft	in.	ft	in.
1	0.0032	0.0382	0.0034	0.0409	0.0033	0.0398	0.0001	0.0011
2	0.0105	0.1260	0.0092	0.1098	0.0067	0.0803	0.0025	0.0295
3	0.0211	0.2527	0.0172	0.2063	0.0101	0.1212	0.0071	0.0850
4	0.0331	0.3970	0.0260	0.3120	0.0135	0.1622	0.0125	0.1498
5	0.0473	0.5676	0.0358	0.4301	0.0170	0.2037	0.0189	0.2265
6	0.0656	0.7877	0.0477	0.5721	0.0205	0.2460	0.0272	0.3261
7	0.0897	1.0762	0.0622	0.7459	0.0240	0.2885	0.0381	0.4574
8	0.1291	1.5494	0.0847	1.0160	0.0277	0.3318	0.0570	0.6842
9	0.1933	2.3201	0.1212	1.4542	0.0313	0.3757	0.0899	1.0785
10	0.2874	3.4483	0.1759	2.1114	0.0346	0.4153	0.1413	1.6961
11	0.4264	5.1162	0.2612	3.1341	0.0367	0.4400	0.2245	2.6941
12	0.6545	7.8539	0.4095	4.9137	0.0340	0.4080	0.3755	4.5058
13	1.1098	13.3178	0.7304	8.7649	0.0040	0.0480	0.7264	8.7169

Table 4.12. Increase in displacements due to a reduction in soil stiffness.

Water Elevation, ft	Top of I-wall, el 9 ft, ft	Ground Surface, el 0 ft, ft	Tip of Sheet Pile, el -30 ft, ft
1	2.8	2.7	2.8
2	2.5	2.6	2.8
3	2.5	2.6	2.8
4	2.4	2.5	2.7
5	2.4	2.5	2.7
6	2.3	2.5	2.7
7	2.2	2.4	2.7
8	2.0	2.3	2.7
9	1.8	2.0	2.7
10	1.6	1.9	2.6
11	1.5	1.7	2.6
12	1.5	1.6	2.6
13	1.7	1.8	1.6

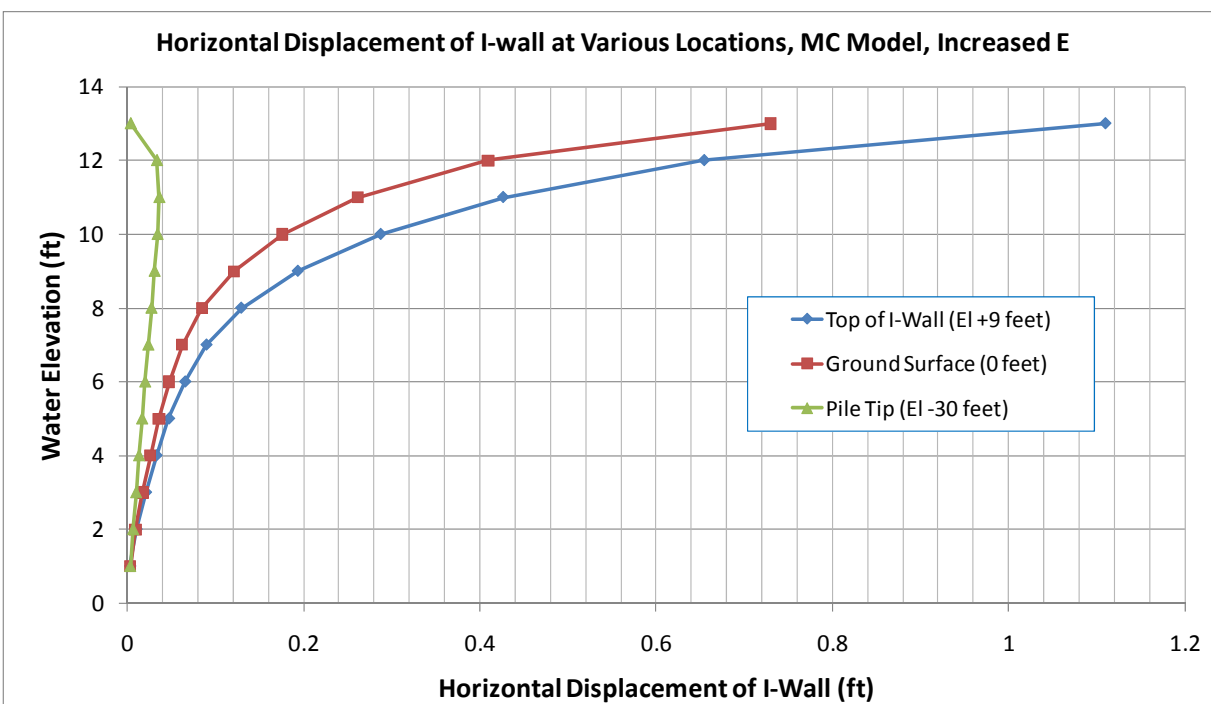


Figure 4.21. Sheet-pile horizontal displacements for selected locations for an increased soil stiffness.

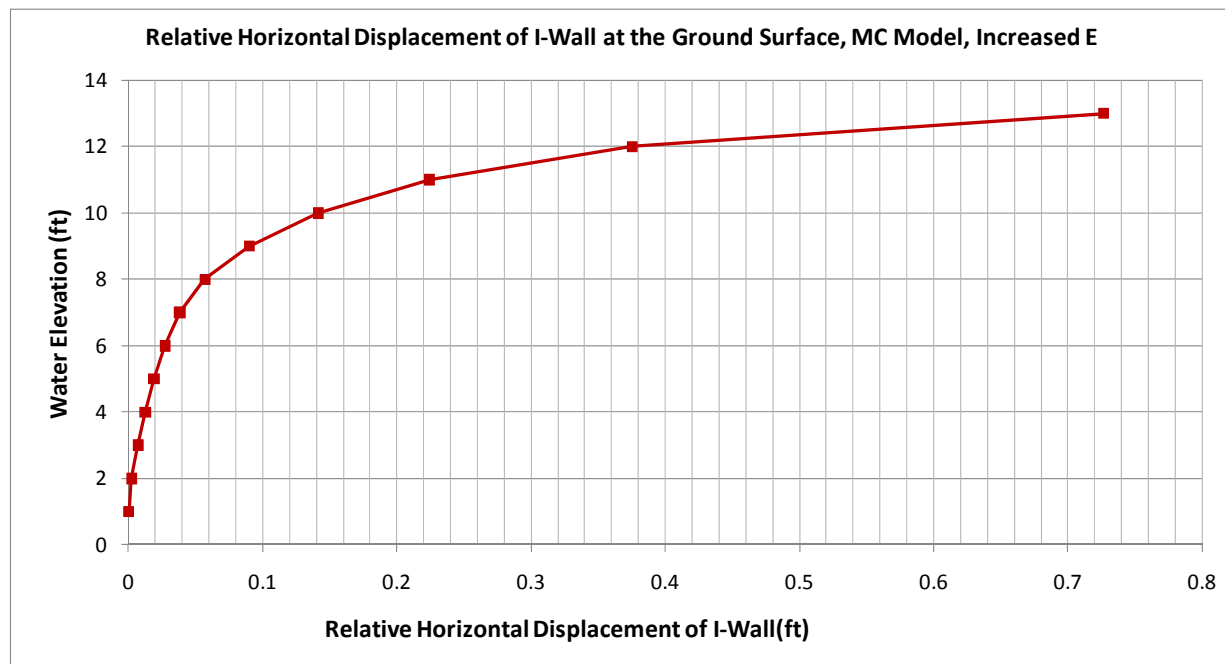


Figure 4.22. Relative horizontal displacements of the sheet pile at the ground surface for an increased soil stiffness.

4.4.11 Total displacements of finite element mesh for maximum water condition

Figures 4.23 and 4.24 show the total deflection of the finite element mesh for the maximum water height of 13 ft. The gap at this water height propagated down to el -22 ft. There were some settlement on the flood side of the wall and some heave on the landside. This pattern of movement can be seen in Figure 4.25 as the soil on the flood side moved downward along a 45-deg line toward the tip of the pile and upward on the landside along a 45-deg line emanating from the tip of the pile. There is a zone of soil rotating about a point at approximately el -25 ft at a distance of 2 ft on the landside of the wall.

4.4.12 Moments in sheet-pile wall for MC model

Shown in Figure 4.26 is a comparison of moments in the sheet pile for various water elevations. The moment increased as the water elevation increased to 13 ft and reached a maximum of 62,974 ft-lb at el -14.5 ft. In contrast, the design moment from the long-term design condition was 45,900 ft-lb for a water elevation of 9 ft. The distribution and maximum moment for the low and high soil stiffness cases are virtually identical. The maximum moment for the design condition of a water elevation of 9 ft and a gap tip elevation of -13 ft was 17,268 ft-lb at el -7.5 ft.

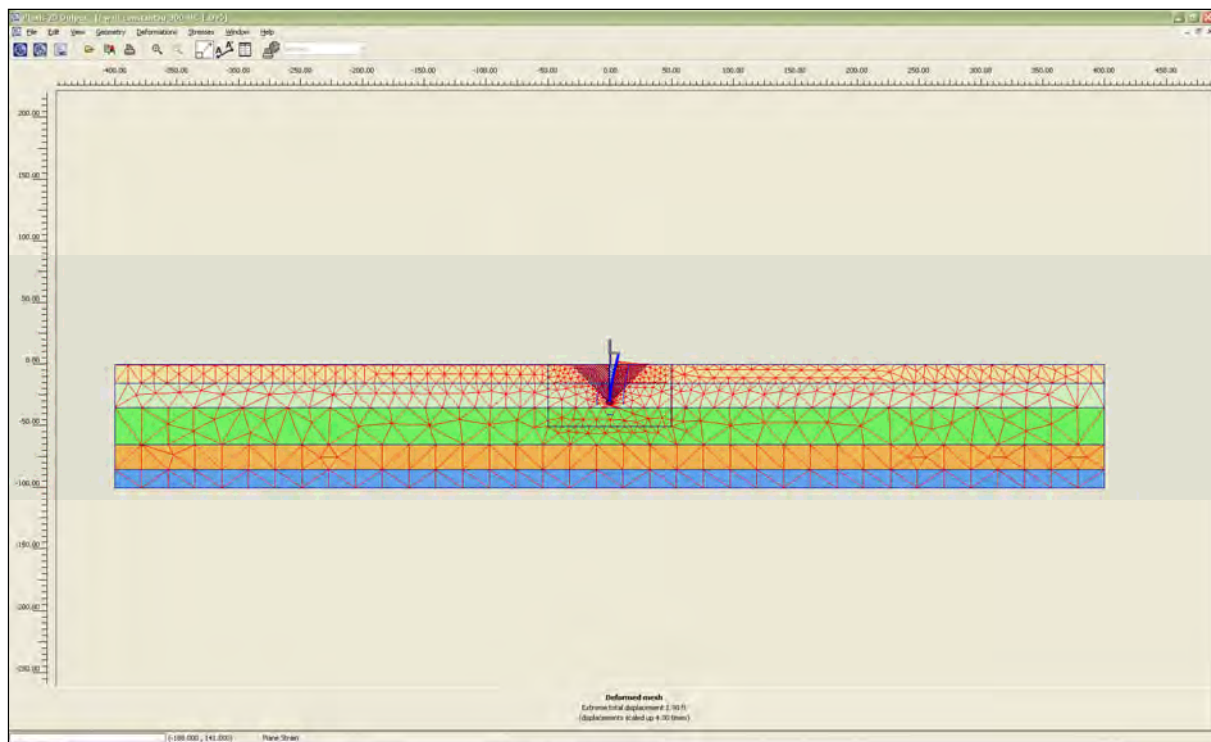


Figure 4.23. Total displacements for a water elevation of 13 ft and a gap tip elevation of 22 ft.

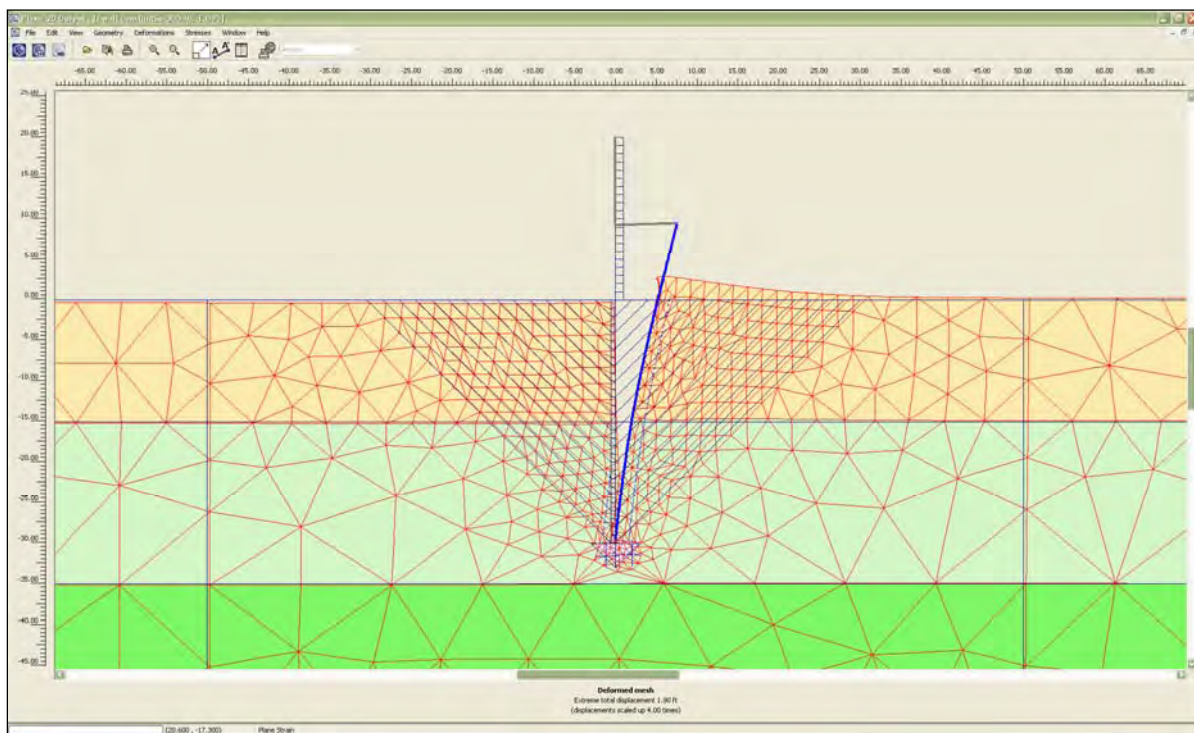


Figure 4.24. Enlarged view of total displacements for a water elevation of 13 ft and a gap tip elevation of 22 ft.

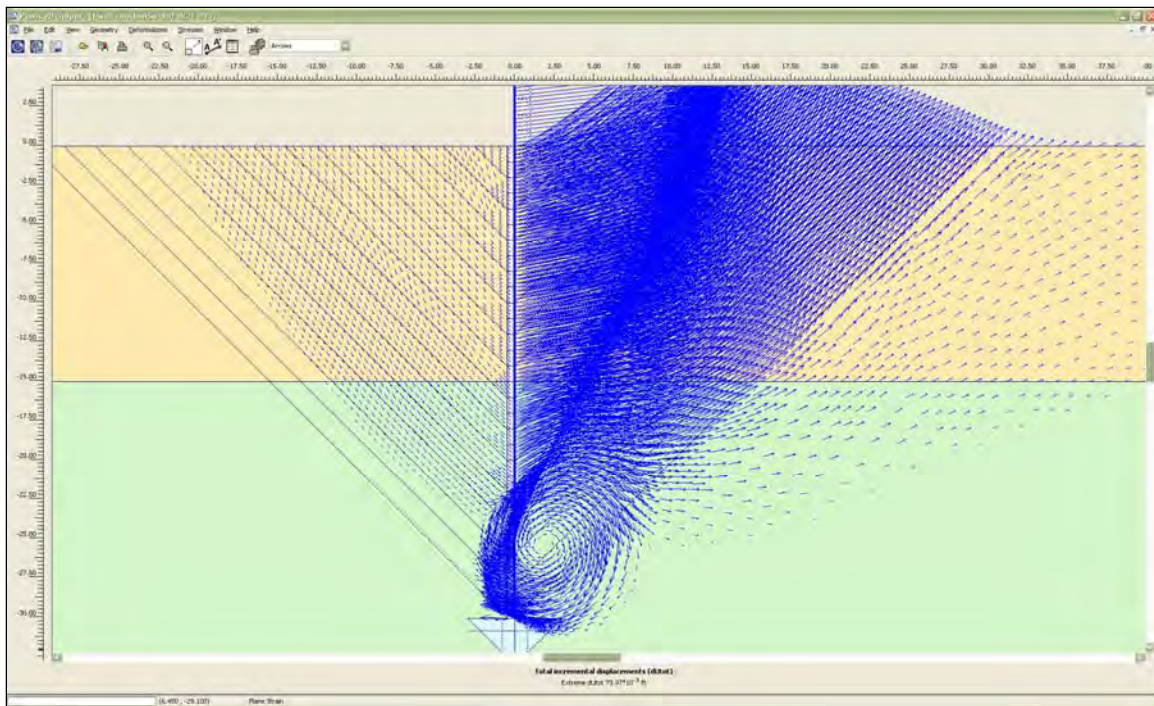


Figure 4.25. Vectors of total incremental displacements showing the movement of the soil during the final increment of loading.

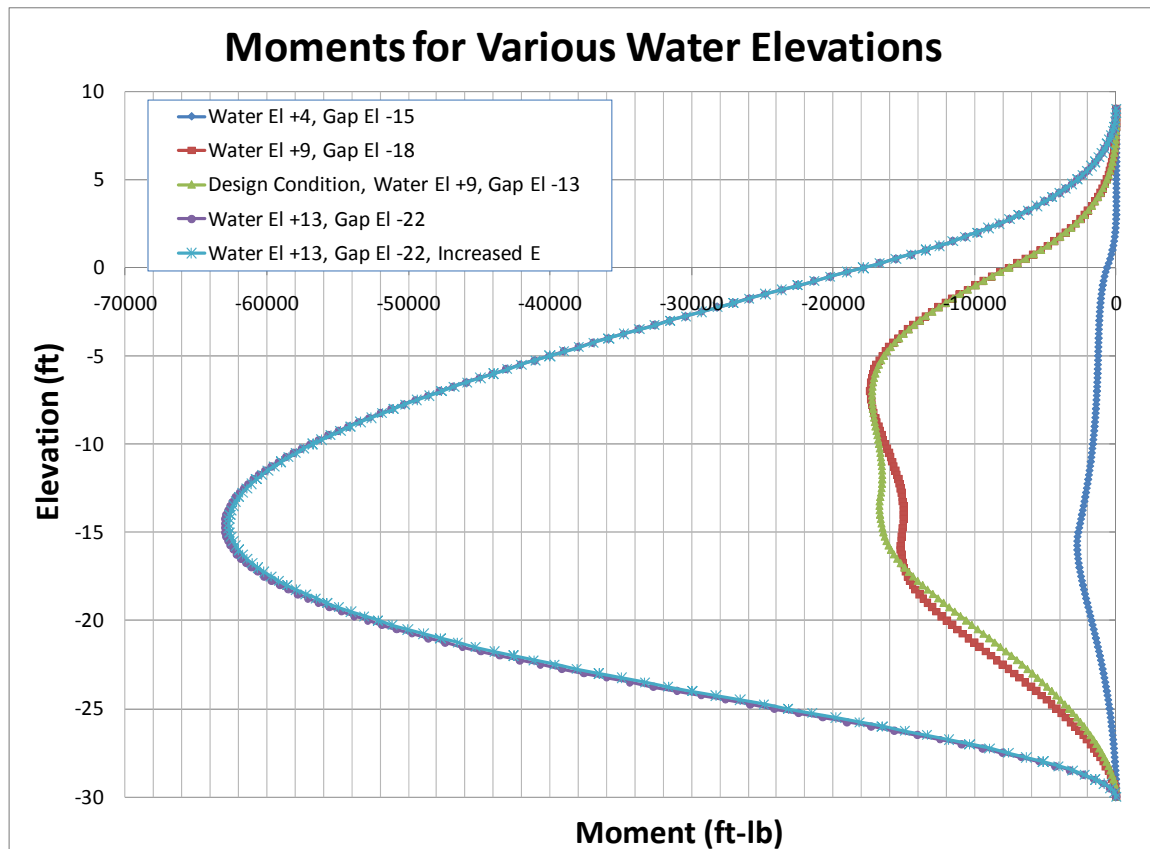


Figure 4.26. Comparison of moments at various water elevations.

4.4.13 Shear stresses in soil for MC model

Figures 4.27 through 4.31 show the relative shear stress in the soil for various water elevations and the associated gap depths. The relative shear stress is a measure of the shear stress in the soil compared to the maximum available shear stress at failure. The shear stress in the soil increases as the water elevation increases, first in the upper unsaturated layer, then downward toward the tip of the pile.

The results of a Φ/c reduction analysis for a water elevation of 13 ft and a gap tip elevation of -22 ft are shown in Figure 4.32, which looks very much like Figure 4.31. The factor of safety from the Φ/c analysis for the case shown in Figure 4.32 is 0.95. In comparison, the factor of safety for a Φ/c analysis for the preceding water level of 12 ft with a gap tip elevation of -21 ft is 1.10.

4.4.14 Horizontal earth pressures for MC model

Figures 4.33 through 4.37 compare the horizontal earth pressures acting against the sheet-pile wall, calculated using PLAXIS, to the limiting active and passive earth pressures computed using adhesion as shown in Equations 4.5 and 4.6. The value of adhesion used is 80 percent of the cohesion, as taken from values cited in Potyondy (1961) for a cohesive soil against rough steel. The limiting earth pressures in the figures are computed for factors of safety equal to 1.0 and 1.5. This corresponds to factors of safety used in the design of the wall using CWALSHT as shown in Table 4.2. For all these figures, the flood side is on the right side of the figure and the landside is on the left. This corresponds to the input convention CWALSHT uses.

Net pressures computed using a factor of safety for active and passive pressures of 1.0 were compared to the net pressures computed from the PLAXIS horizontal earth pressure results as shown in Figure 4.38.

The original intent was to compare the net pressure diagram computed from CWALSHT to the net pressure diagram computed from the PLAXIS results. The objective was to increase or decrease the factors of safety applied to the active and passive earth pressures to cause the computed net pressure diagram from CWALSHT to match the net pressure diagram computed using PLAXIS results. This approach did not work because, although changing the factors of safety on the earth pressures in CWALSHT

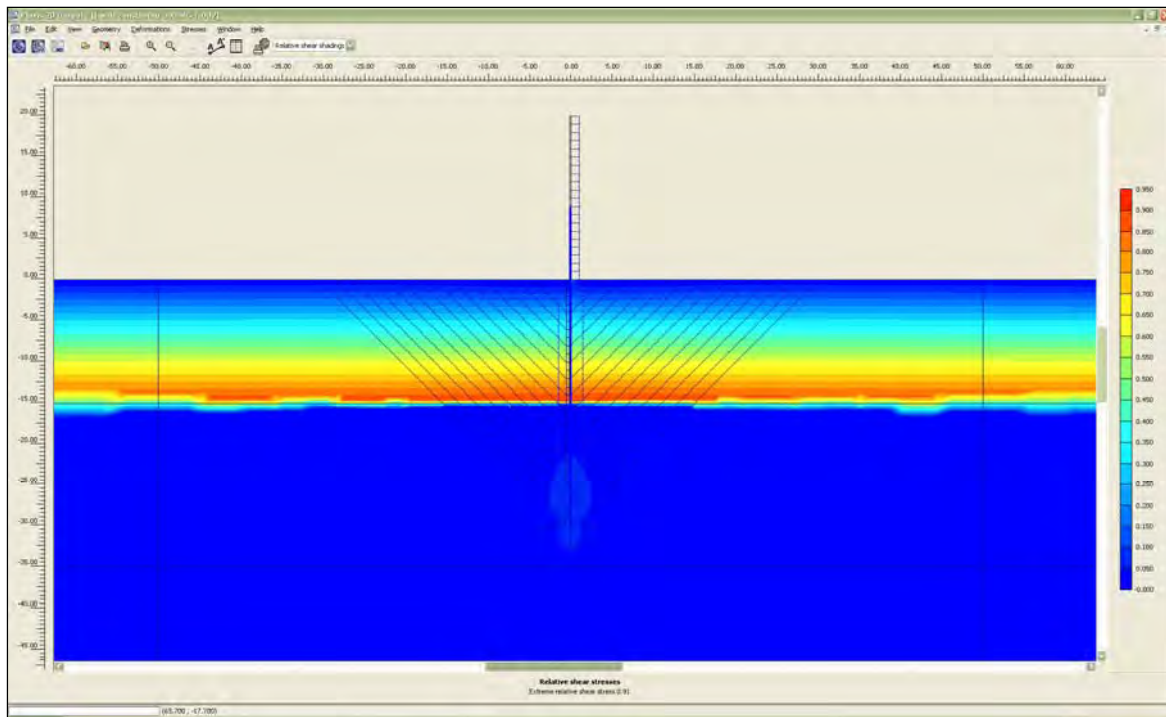


Figure 4.27. Relative shear stress after placement of I-wall.

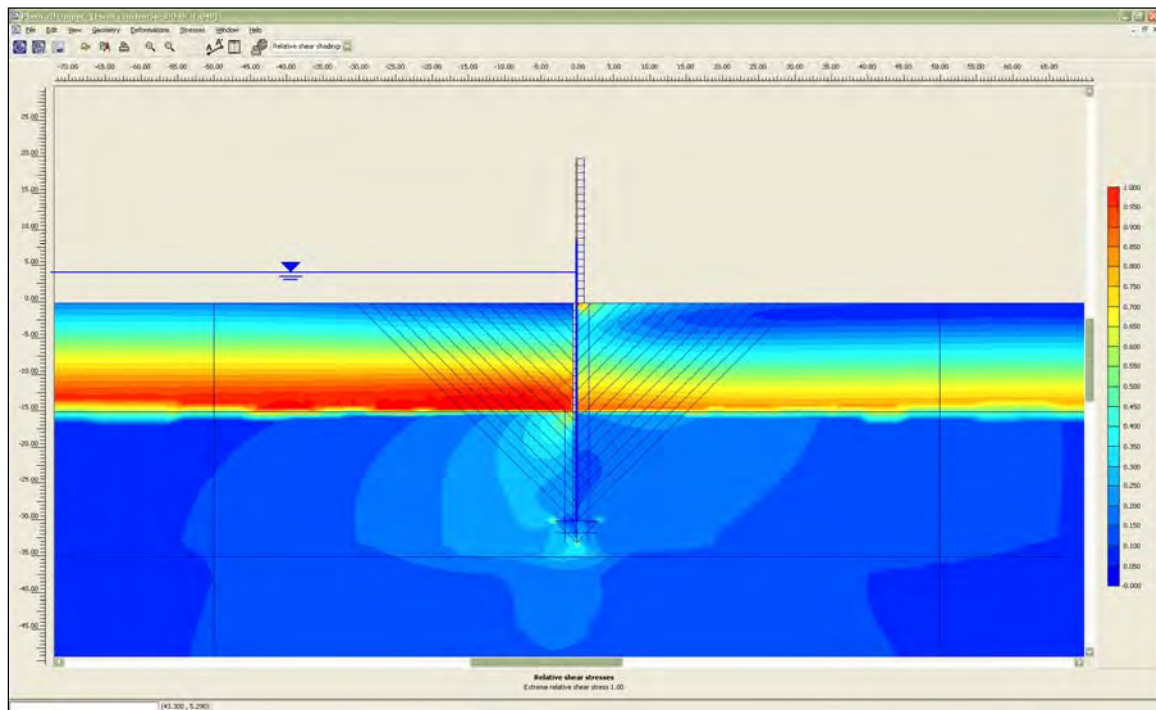


Figure 4.28. Relative shear stress for water at el 4 ft and gap tip at el -15 ft.

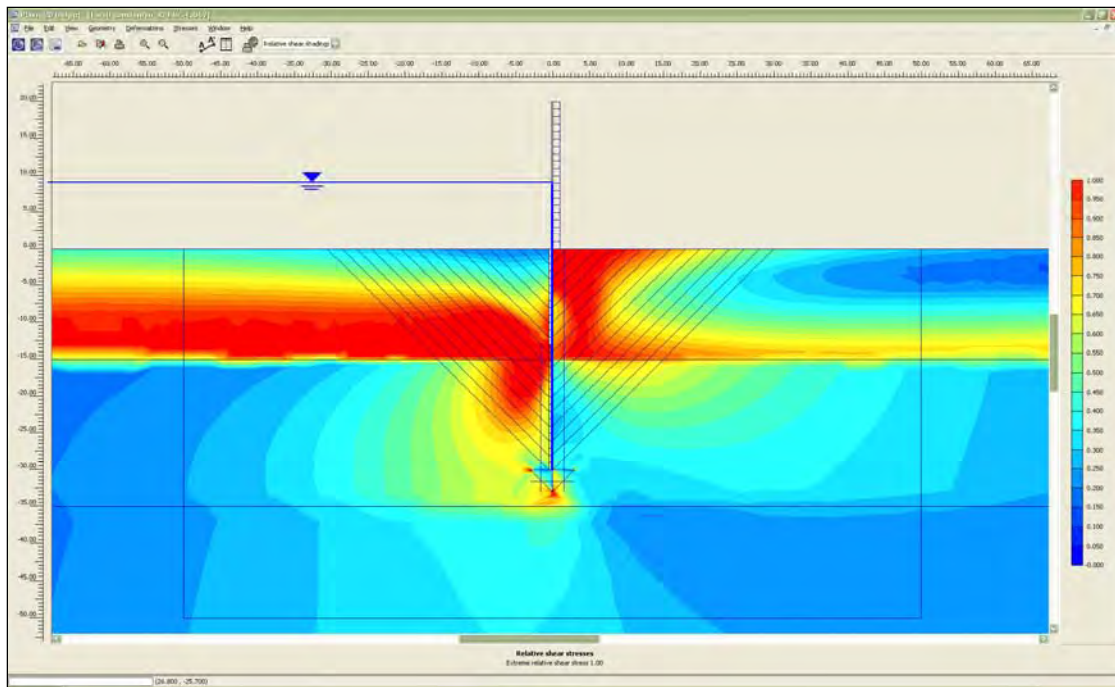


Figure 4.29. Relative shear stress for the design conditions of water at el 9 ft and gap tip at el -13 ft.

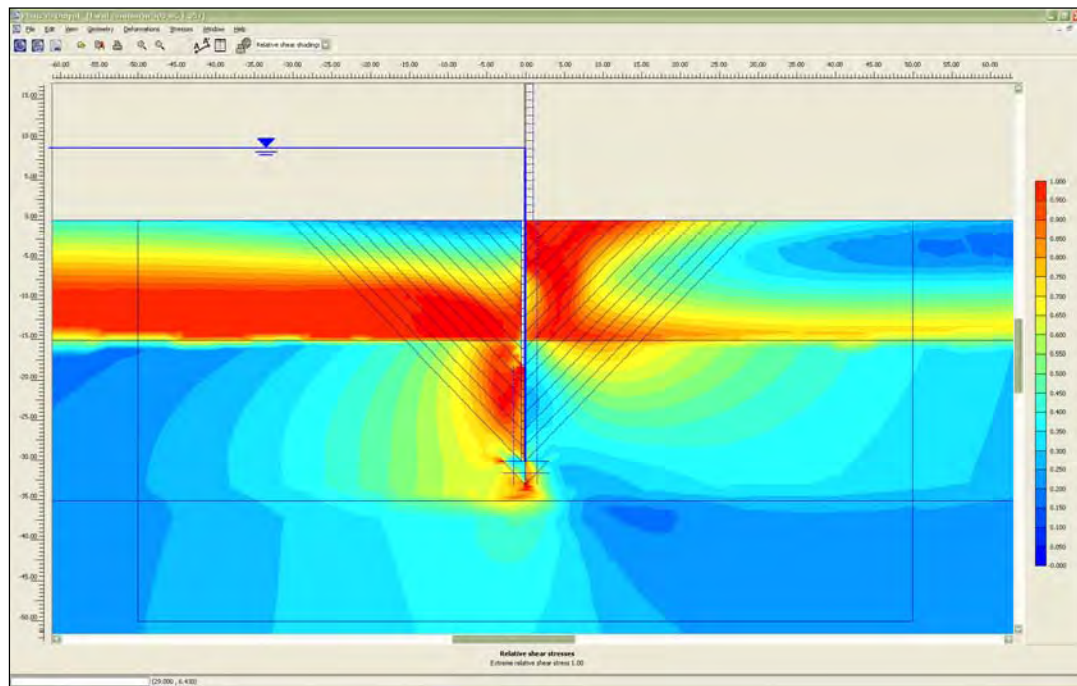


Figure 4.30. Relative shear stress for water at el 9 ft and gap tip at el -18 ft.

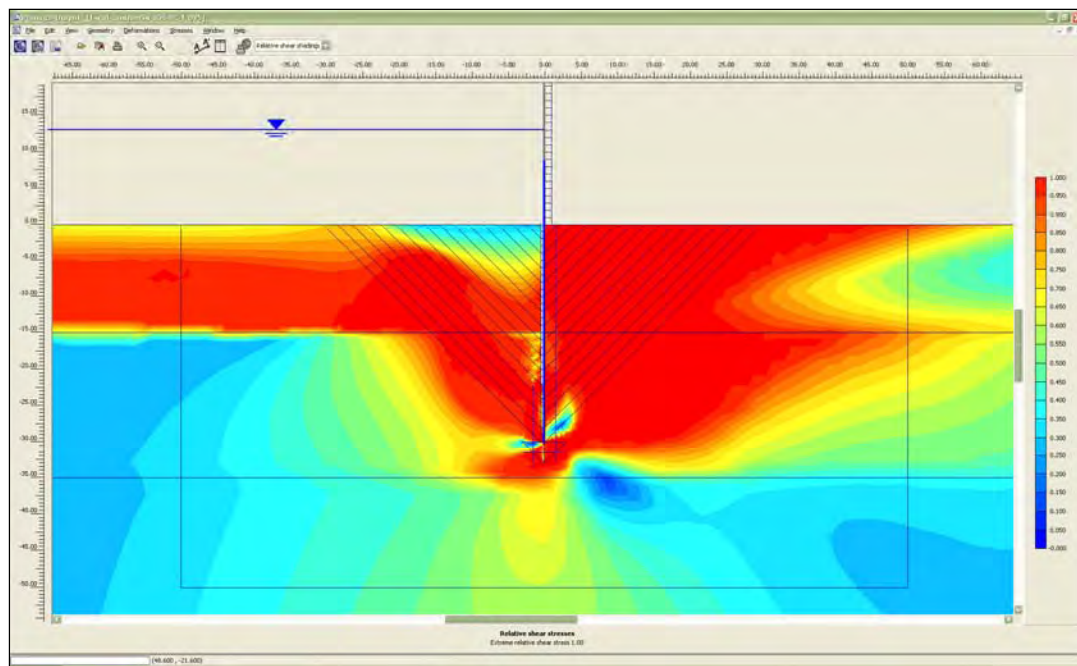


Figure 4.31. Relative shear stress for water at el 13 ft and gap tip at el -22 ft.

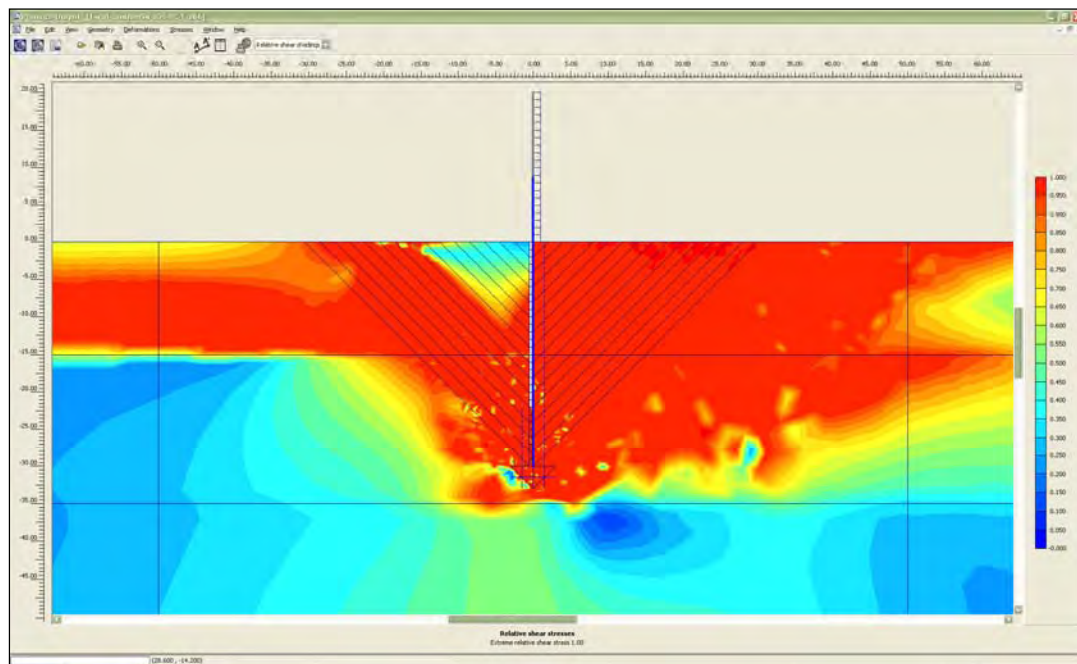


Figure 4.32. Relative shear stress for water at el 13 ft and gap tip at el -22 ft for a Φ/c reduction analysis.

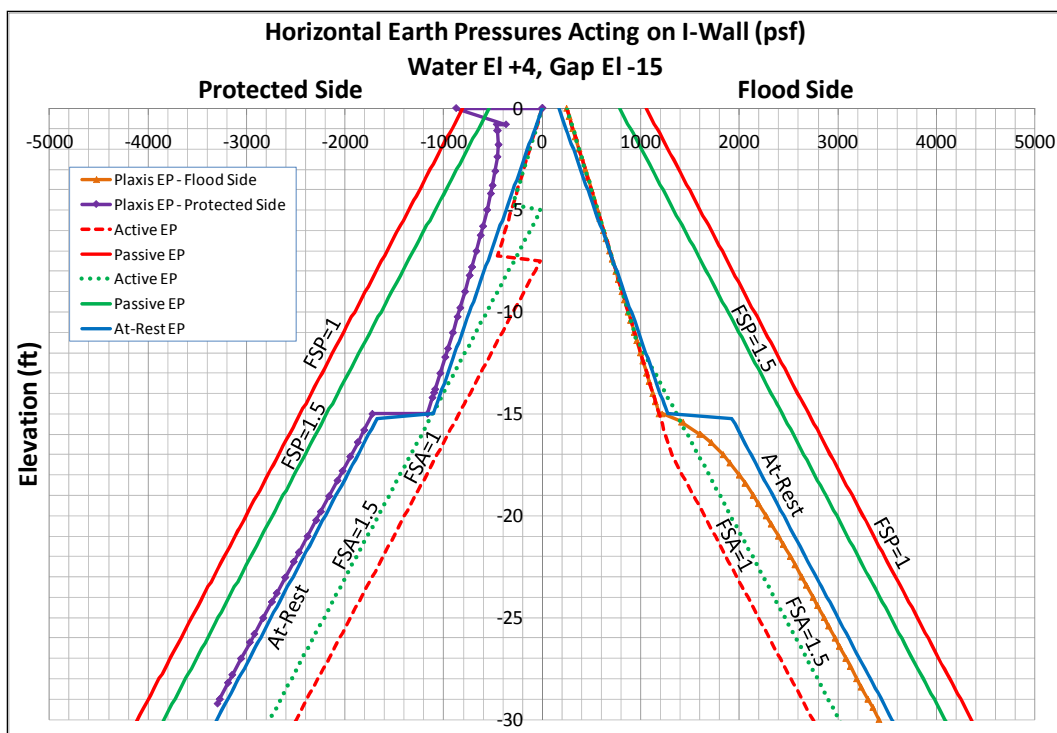


Figure 4.33. Horizontal earth pressures for water at el 4 ft and gap tip at el 15 ft.

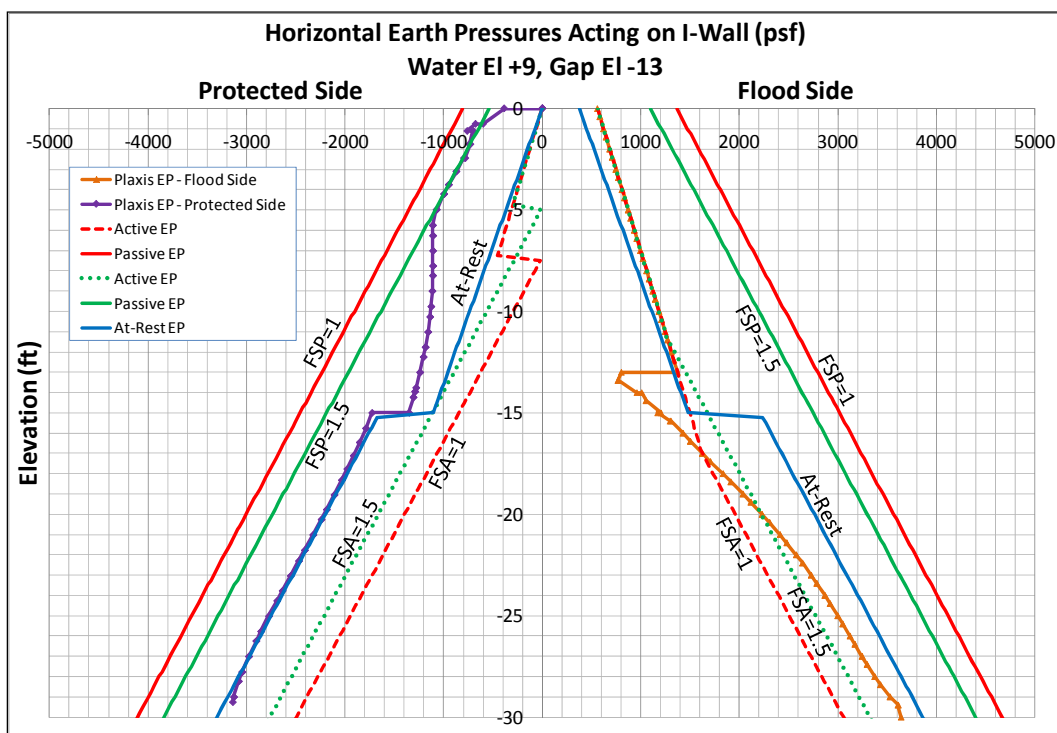


Figure 4.34. Horizontal earth pressures for the design condition for water at el 9 ft and a gap tip at el 13 ft.

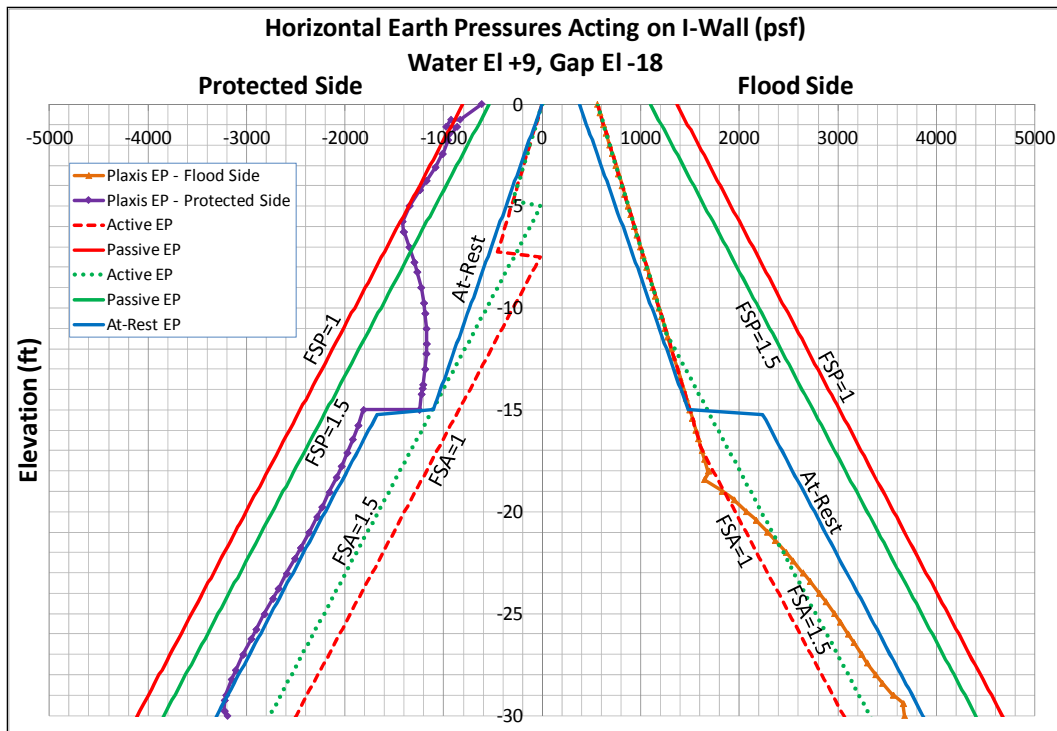


Figure 4.35. Horizontal earth pressures for water at el 9 ft and a gap tip at el -18 ft.

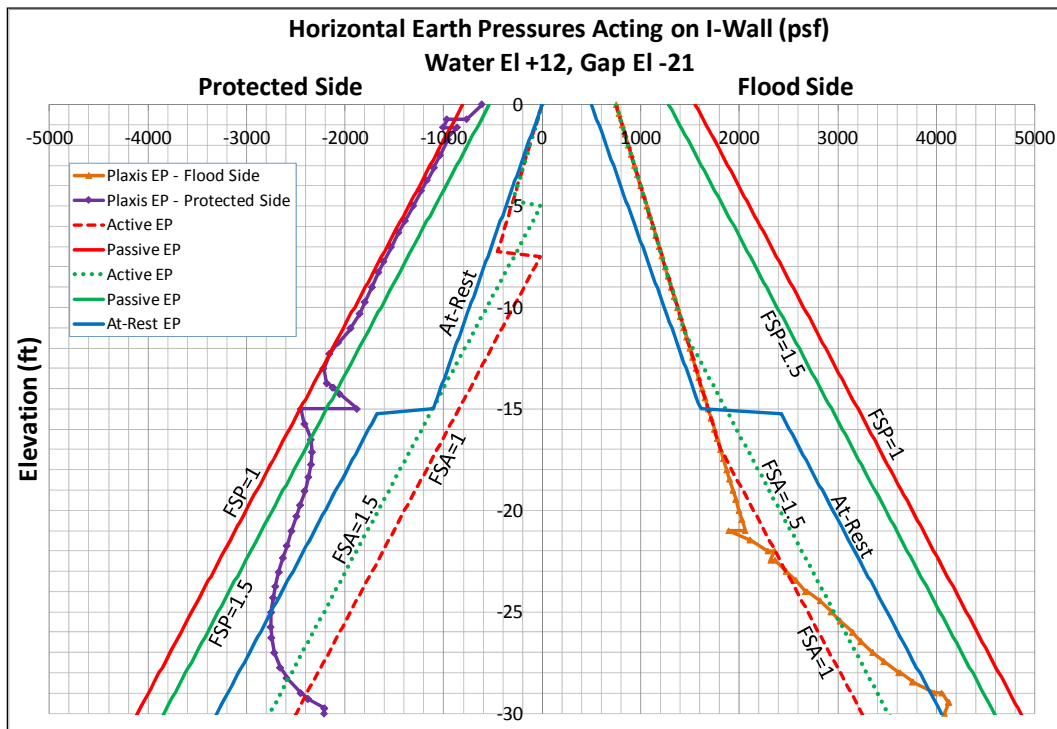


Figure 4.36. Horizontal earth pressures for water at el 12 ft and a gap tip at el -21 ft.

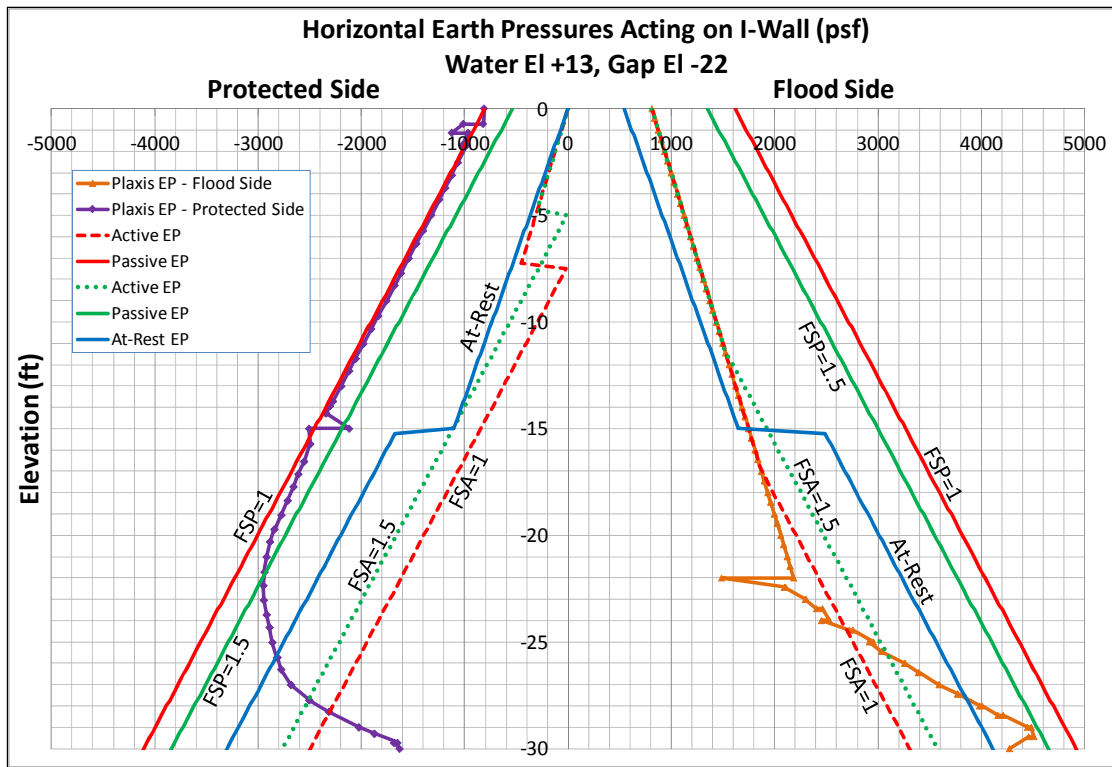


Figure 4.37. Horizontal earth pressures for water at el 13 ft and a gap tip at el -22 ft.

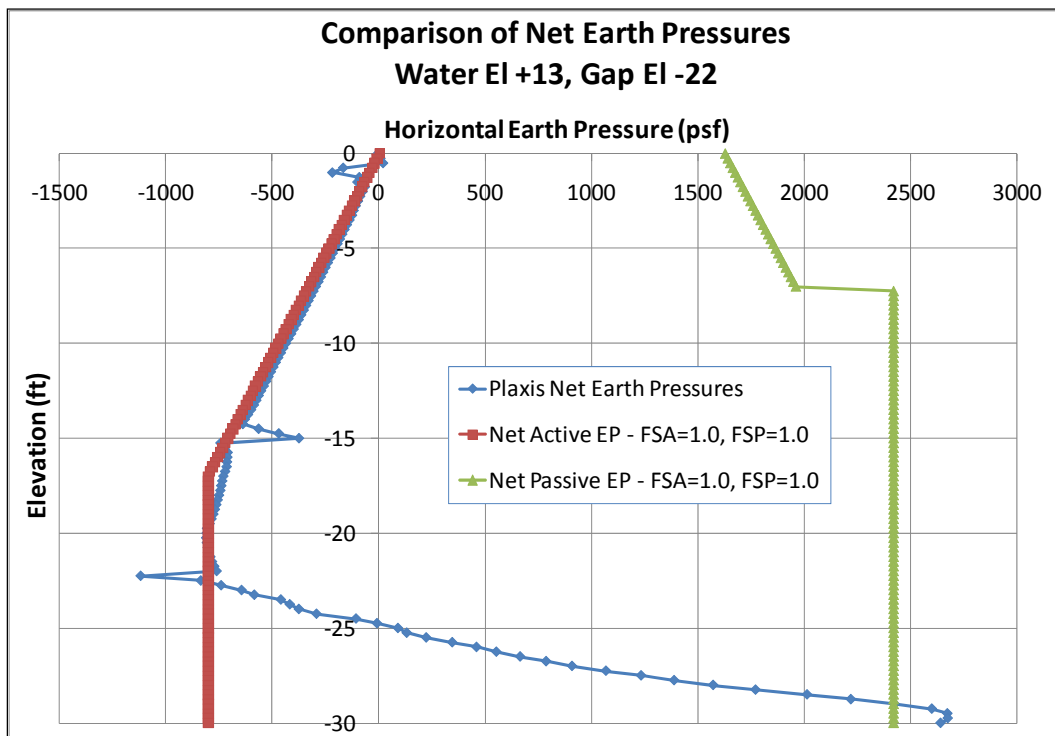


Figure 4.38. Comparison of net earth pressures computed from limiting earth pressures and PLAXIS results.

will change the values of the net pressures, the penetration depth and point of rotation of the pile also are affected. Therefore, the results from PLAXIS were compared to the earth pressures computed by CWALSHT using limiting earth pressures computed using two different factors of safety. This allows one to get a sense of where the PLAXIS earth pressures are in relation to values computed from conventional design procedures.

Figure 4.33 displays the earth pressures for a water elevation of 4 ft and a gap tip elevation of -15 ft. For the flood side, the pressures are equal to hydrostatic pressures down to the bottom of the gap. Below the gap, the pressures are close to at-rest earth pressures computed using the assumed values of K_o given in Table 4.9. On the landside, the earth pressures are very close to at-rest earth pressures.

Figure 4.34 is for the design condition of a water elevation at 9 ft. The gap in this case extends to el -13 ft. This value was computed assuming no adhesion as shown in Equation 4.9. The earth pressures on the flood side are equal to hydrostatic pressures down to the bottom of the gap. Below the gap, the earth pressures are less than the at-rest condition because of the wall moving from the soil. On the landside, the earth pressures are greater than the at-rest condition above el -15 ft and equal to at-rest conditions below this elevation.

For Figures 4.35 through 4.37, the earth pressures continue to decrease below the at-rest condition on the flood side below the gap. The magnitude of the earth pressures approaches the active line defined by a factor of safety equal to 1.0 (the factor of safety value assumed in the CWALSHT design). For higher water elevations, the lower portion of the pile on the flood side experiences an increase in earth pressures up to a passive value defined using a factor of safety of 1.5 (the factor of safety value assumed in the CWALSHT design). The passive pressures acting on the lower portion of the pile are due to the rotation and kickback of the tip of the pile into the flood side.

For Figures 4.35 through 4.37, the earth pressures on the landside increased from the at-rest condition to a value equal to the passive earth pressures computed using a factor of safety equal to 1.0. The factor of safety of 1.0 produced earth pressures greater than those assumed in the CWALSHT design. The lower portion of the pile experienced a decrease in earth pressures as the water level increased. The earth pressures around

the tip of the pile on the landside decreased below active pressures computed using a factor of safety equal to 1.0 (the factor of safety assumed in CWALSHT). For the design condition with a water elevation of 9 ft, the earth pressure values were closer to at-rest values than the values assumed in the CWALSHT design.

Figure 4.38 compares the net earth pressures computed using limiting earth pressures and the results from PLAXIS for a water elevation of 13 ft with a gap tip elevation of -22 ft. The limiting earth pressures were computed using a factor of safety of 1.0 for both the active and passive earth pressures for both the flood side and landside of the wall. Net pressures for this water elevation were compared because the movements of the wall were sufficient to produce values of full active and passive earth pressures. As can be seen from the figure, the net earth pressures on the landside compare fairly well to the net active earth pressures. Toward the tip of the pile, the net earth pressures transition from the net active to the net passive earth pressures and compare fairly well.

Figures 4.39 through 4.41 compare results for an increase in soil stiffness as shown in Table 4.7. The previous discussion for Figures 4.35 through 4.38 applies to the results for the analysis of the system with an increased soil stiffness. The magnitudes of the earth pressures and net earth pressures computed using the lower soil stiffness compare almost identically with the values computed using the higher soil stiffness.

4.5 Final observations and conclusions for the finite element analyses

The results of earth pressures and moments in the sheet pile compared well for the HS and MC models. If the tip displacements are removed from the MC model results, the displacements compared quite well with the HS results.

The progression of the gap was essentially identical in the low and high soil stiffness analyses. Results computed using the lower and higher soil stiffnesses compared almost identically, except for the displacements. The displacements computed for the higher soil stiffness are about two times less than the displacements computed using the lower soil stiffness.

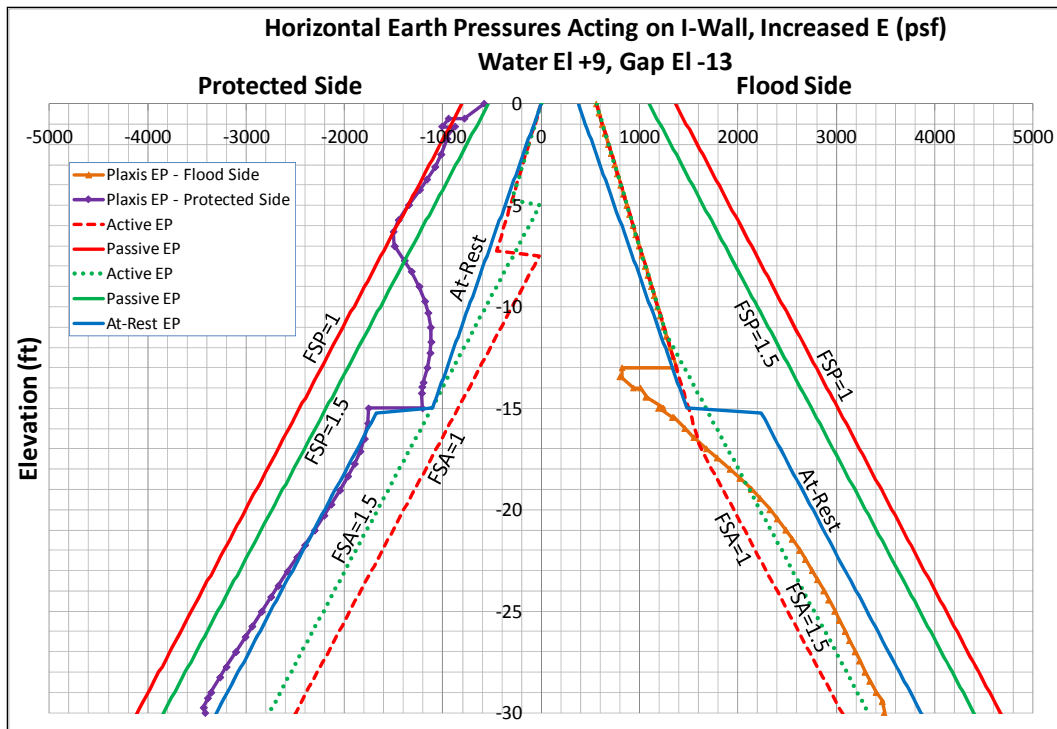


Figure 4.39. Horizontal earth pressures for water el 9 ft and gap tip el -13 ft.

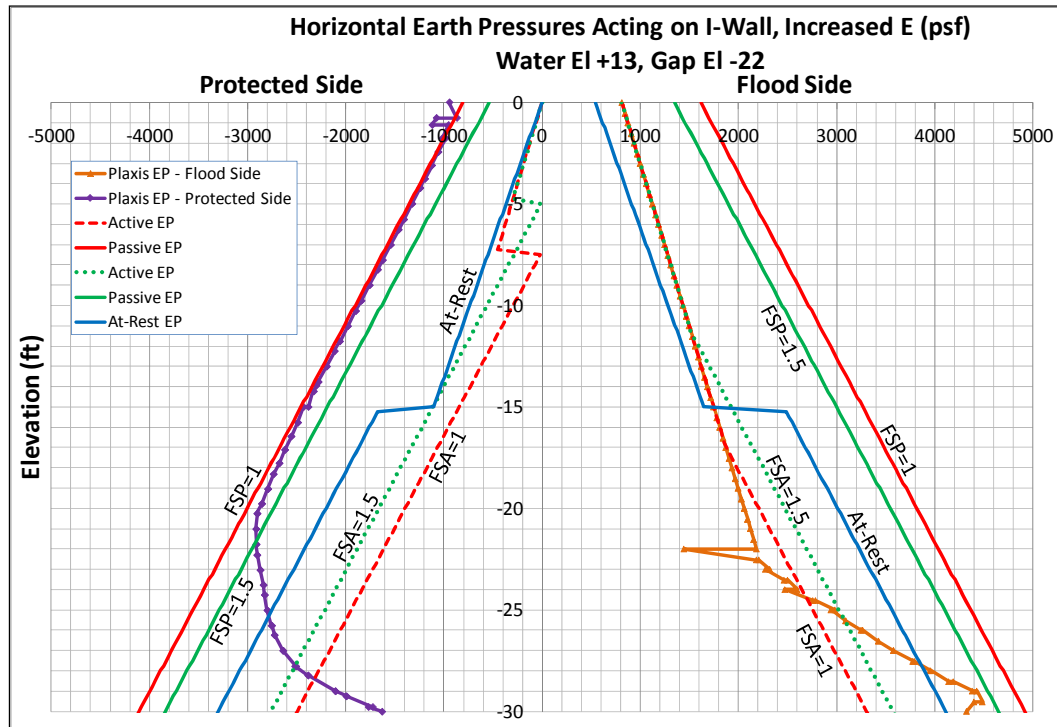


Figure 4.40. Horizontal earth pressures for water el 13 ft and gap tip el -22 ft.

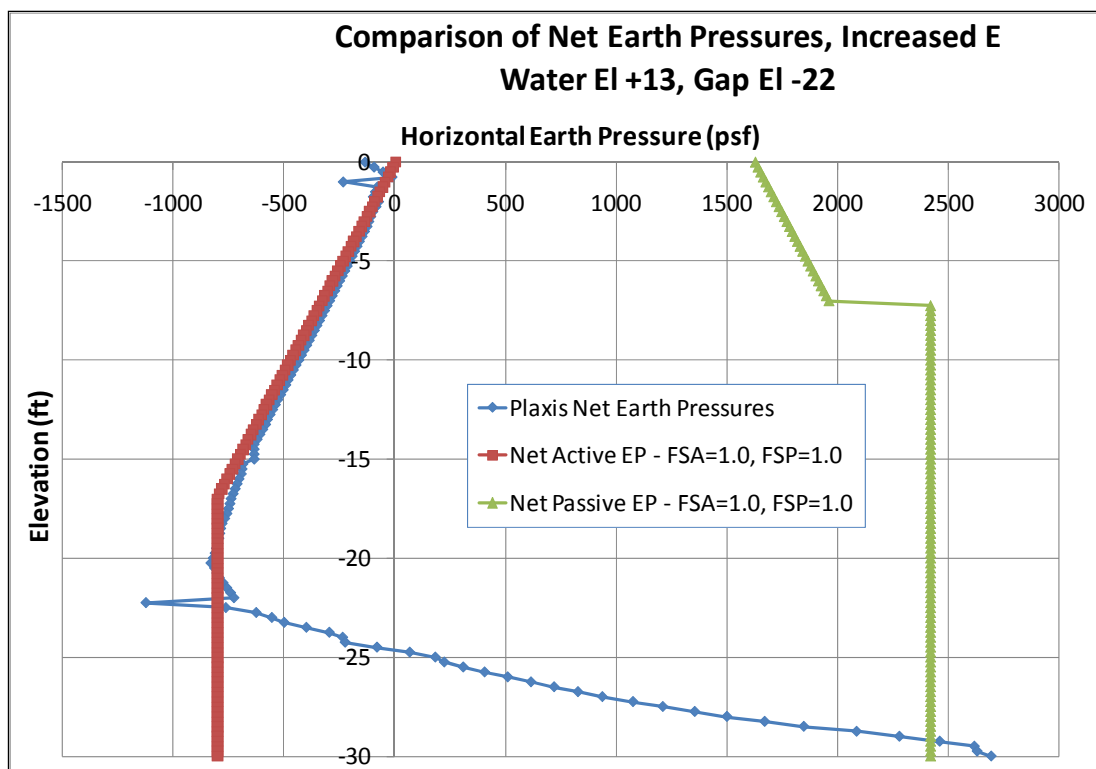


Figure 4.41. Relative of net earth pressures computed from limiting earth pressures and PLAXIS results for an increased soil stiffness.

The differences between the displacements of the top of the sheet pile for adjacent water elevations increased with an increase in water elevation. The differences between the displacements of the tip of the sheet pile for adjacent water elevations remained constant for an increase in water elevation. The tip of the sheet pile eventually kicks back into the flood side at higher water elevations.

At the design condition of 9 ft of water, the maximum moment in the sheet pile from the PLAXIS results is 38 percent of the moment computed using CWALSHT.

The earth pressures from PLAXIS for the design condition (water elevation of 9 ft) are not close to the values assumed in the CWALSHT design. The water elevation must be raised to el 13 ft before the earth pressure values compare well with assumed limiting values. The flood side compared well with active pressures computed assuming a factor of safety of 1.0 and passive pressures computed assuming a factor of safety of 1.5. The landside earth pressures are closer to limiting values computed using a factor of safety of 1.0 instead of 1.5 as assumed in the design.

5 Analyses of I-wall Site Founded on a Silt of Low Plasticity

5.1 Purpose of analyses

The purpose of this chapter is to detail the findings of nonlinear SSI finite element analyses of an I-wall founded in a silt of low plasticity or a silty sand. This study focused on the initiation and propagation of a gap beside an I-wall and the effects of this gap on the resulting deformation and stress conditions on the soil regime on both the flood side and landside of the I-wall.

Two different permeabilities (k), also called hydraulic conductivities, for the soil were assumed to study the time-dependent effects of the problem: loading, transient seepage, induced excess pore pressures, and dissipation of the excess pore pressures with time. These time-dependent effects control whether the problem can be considered drained, undrained, or somewhere in between. The following sections will describe the soil used in the analyses, the selection of stiffness and shear strength parameters, the conventional analysis and design of the I-wall, the analysis procedures employed, and the results of the finite element analyses.

5.2 Overview of problem analyzed

The geometry of the problem analyzed is shown in Figure 5.1. The site was assumed to be flat (el 0 ft) with a maximum floodwater elevation at 9 ft. Two soil layers were assumed in the analyses. The top 10 ft of soil represented a slightly overconsolidated crust, while the lower portion was assumed to be normally consolidated. The elevation of the soil surface was assumed to be at 0 ft.

The I-wall was composed of a sheet-pile wall with the tip at el -38 ft. The top of the I-wall was composed of a concrete cap that was 2.5 sq ft with the top level with the ground surface. The wall above the top of the soil consisted of a tapered concrete section that was 2.5 ft at the base and 1 ft at the top of the wall.

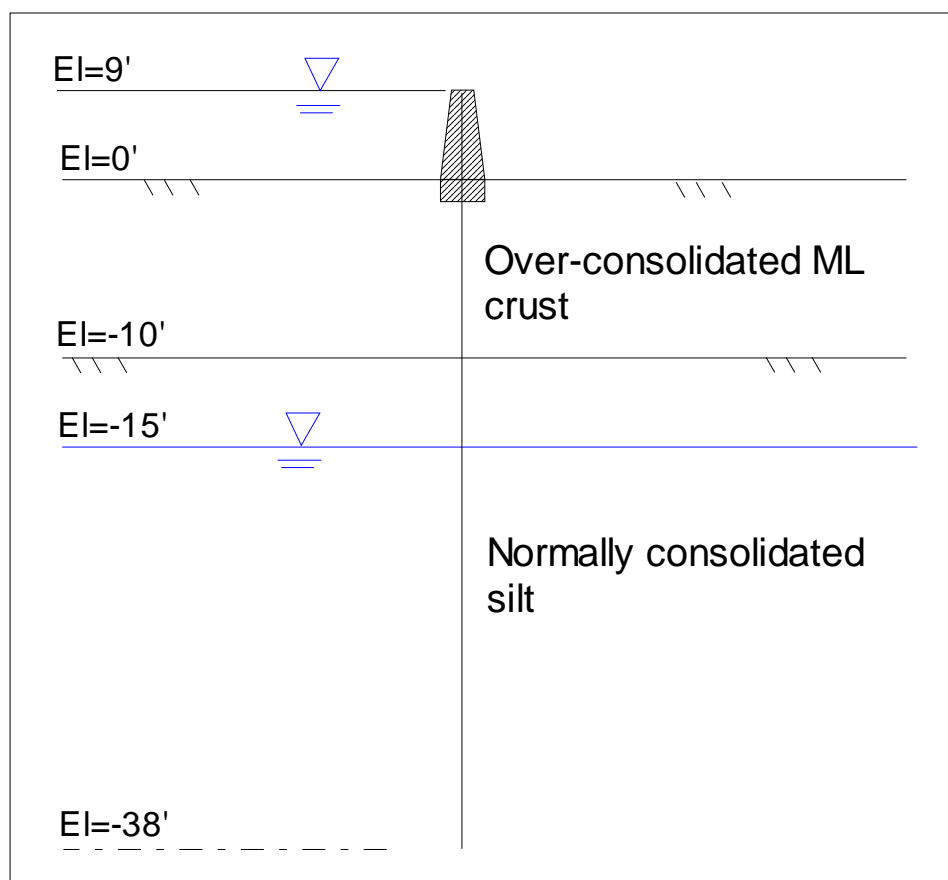


Figure 5.1. Problem geometry.

The water table for the problem was initially at el -15 ft. The water followed a selected hydrograph with a maximum elevation of 9 ft.

The Unified Soil Classification System (USCS) designation for the soil used in the analyses is ML (silt of low plasticity) or SM (silty sand). Both were assumed to have a low percentage of clay fines ($< 2 \mu\text{m}$) of approximately 20 percent or less. The objective was to have a soil with enough plasticity to hold open a gap beside the I-wall.

A soil classified as an ML material has the following characteristics:

1. Greater than 50 percent by weight passing the #200 sieve;
2. $LL < 50$ percent;
3. The PI of the percentage passing the #40 sieve falls below the A-line or the $PI < 4$ percent.

A soil classified as an SM material has the following characteristics:

1. Less than 50 percent by weight passing the #200 sieve;
2. Greater than 50 percent by weight passing #4 sieve;
3. Greater than 12 percent by weight passing the #200 sieve;
4. The PI of the percentage passing the #40 sieve falls below the A-line or the $PI < 4$ percent.

Figure 5.2 shows where ML materials fall on the USCS plasticity chart.

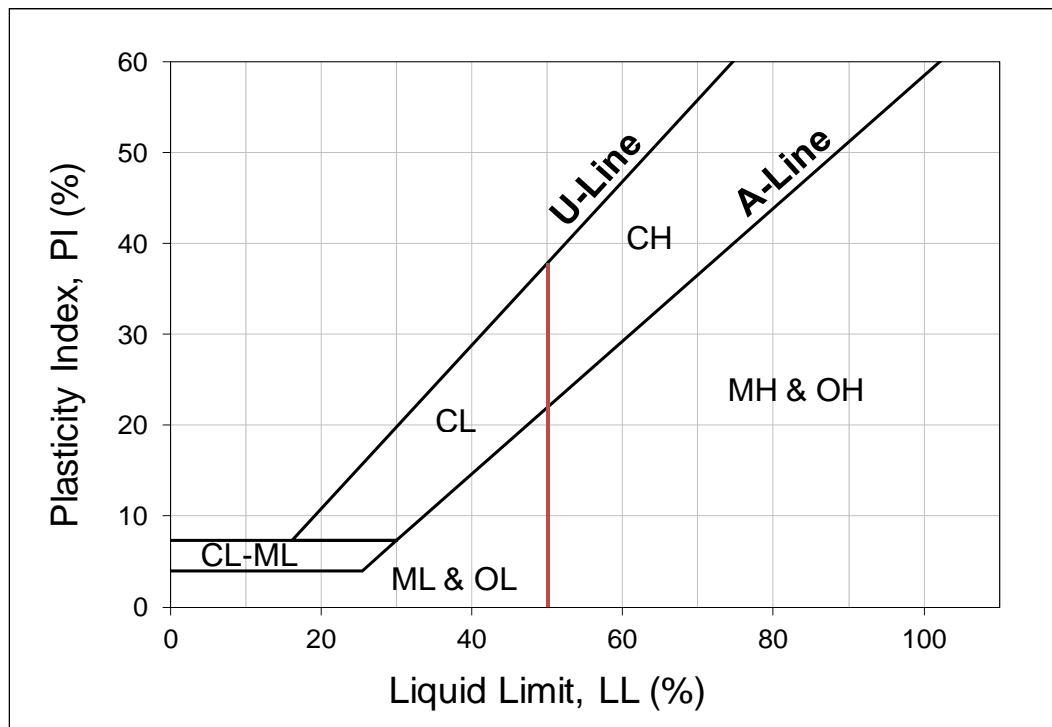


Figure 5.2. USCS plasticity chart for fine-grained soils (see Figure 2.2 on page 9 for explanation of soils).

5.3 Shear strength and stiffness properties used in the finite element analyses

The finite element analyses required certain material properties for the selected soil models. All finite element analyses were performed with the PLAXIS finite element program. The Hardening Soil (HS) model, which has a nonlinear stress-strain relationship, was used for all soil elements. Two-dimensional elastic elements were used to represent the concrete wall, and elastic plate elements were used to model the steel sheet pile.

PLAXIS can perform analyses with either effective or total stress soil parameters. For the analyses described herein, effective stress soil parameters were used, and the material behavior was designated as

undrained, which causes PLAXIS to compute excess pore pressures due to the deformation analysis and to dissipate these excess pore pressures during a consolidation analysis. Based on the permeability of the soil, the rate of loading, the compressibility of the soil, and the length of the drainage path, the behavior of the soil can range from drained to undrained.

A literature search was performed to collect typical parameters of silts used in various finite element analyses. From the review, an average set of soil properties was selected to represent the ML-SM soils used in the analyses. The parameters for the HS model are given in Table 5.1 and consists of the drained angle of internal friction (ϕ), drained cohesion (c), dilation angle (ψ), secant reference stiffness ($E_{50,ref}$), oedometer reference stiffness ($E_{oed,ref}$), and an unload/reload reference stiffness ($E_{ur,ref}$).

Table 5.1. Strength and stiffness properties for the soil layers using undrained soil with unsaturated unit weight 120 lb/ft³ and saturated unit weight 125 lb/ft³.

Layer	c' , lb/ft ²	ϕ' , deg	ψ , deg	$E_{50,ref}$, lb/ft ²	$E_{oed,ref}$, lb/ft ²	$E_{ur,ref}$, lb/ft ²
ML-SM Crust <10'	200	33	3	290,000	290,000	870,000
ML-SM > 10'	1	34	4	290,000	290,000	870,000

Note: unload/reload Poisson's ratio (ν) is set to 0.2, the fitting parameter (m) is set to 0.9, and the interface strength (R_f) is set to 0.85.

Values of friction (δ) between the sheet pile and the soil and between the concrete cap and the soil were selected from values published by Potyondy (1961). Table 5.2 shows the $R_{interface}$ values used in previous studies by Geomatrix (2010) and the values used in the analyses described in this chapter.

The properties of the concrete wall were represented by elastic elements with the properties given in Table 5.3, where E_{ref} is the stiffness of the elastic elements. The sheet pile was represented by elastic plate elements with the properties given in Table 5.4, where EA is the axial stiffness and EI is the flexural rigidity.

5.4 Material properties governing transient seepage

Permeabilities were selected based on a search of the literature for typical values of permeabilities for silty soils. Table 5.5 shows typical ranges for various soils.

Table 5.2. Selected interface friction values (ψ) for the interface elements.

Geomatrix		ϕ	δ/ϕ	$R_{\text{interface}} = \tan \delta / \tan \phi$
Geomatrix	Sheet pile/sand	29	0.85	0.83
	I-wall/sand	32	0.94	0.92
Values Inferred from Potyondy (1961)	Rough steel (sheet pile)	33-34	0.75	0.71
	Rough concrete (I-wall)	33-34	0.9	0.88

Table 5.3. Properties of the concrete wall.

Name	Material Behavior	γ_{unsat} , lb/ft ³	ν	E_{ref} , lb/ft ²
Concrete wall	Nonporous	150	0.2	4.54E+08

Table 5.4. Properties of the plate elements representing the sheet pile.

Name	Material Behavior	EA, lb/ft	EI, lb-ft ²	Weight, lb/ft ²	ν
Sheet pile in cap	Elastic	2.729E+08	4.439E+07	22.24	0.25
Sheet pile	Elastic	2.729E+08	4.439E+07	23.87	0.25

Table 5.5. Range of permeabilities for soils (Duncan 1987).

Soil Type	Value of k , cm/sec
Coarse sands, gravels	$>10^{-1}$
Fine sands	10^{-1} to 10^{-3}
Silty sands	10^{-3} to 10^{-5}
Silts	10^{-5} to 10^{-7}
Clays	$<10^{-7}$

As mentioned, two permeabilities for the soil were examined (Table 5.6). A permeability equal to 1×10^{-4} cm/sec was selected to represent a high permeability. This was done to determine if, even at this high permeability, the behavior of the system was between drained and undrained behavior. A lower permeability equal to 1×10^{-5} cm/sec was chosen as a more reasonable permeability for the silty soil. Both permeabilities were examined to determine if a defining line between drained and undrained behavior would result.

Table 5.6. Permeabilities used in the analyses.

Layer	k_x		$k_y = k_x/4$	
	ft/day	cm/sec	ft/day	cm/sec
ML-SM Crust <10'	0.02835 - 0.2835	1×10^{-5} - 1×10^{-4}	0.00709 - 0.0709	2.5×10^{-6} - 2.5×10^{-5}
ML-SM > 10'	0.02835 - 0.2835	1×10^{-5} - 1×10^{-4}	0.00709 - 0.0709	2.5×10^{-6} - 2.5×10^{-5}

The permeability in the horizontal (k_x) direction is usually the most significant because of layering effects in soils. The permeability in the vertical (k_y) direction was chosen to be one-fourth the value of the horizontal direction.

Because the loading imposed on the soil by the floodwaters varied with time, transient seepage analyses were performed. The pore pressures resulting from the transient seepage analyses were used in the deformation analyses. The pore pressures from the transient seepage analyses were different from the pore pressures for the steady-state condition based on the permeability of the soil. All seepage analyses were performed using the PLAXFLOW (Brinkgreve et al. 2006) finite element seepage program. Additional soil parameters were required to perform a transient seepage analysis.

Because the water level in the soil starts out at an elevation below the top of the soil, unsaturated flow conditions exist. Unsaturated flow in a transient seepage analysis can be performed using van Genuchten properties for the soil. PLAXFLOW contains several soil data sets for use with unsaturated flow. To arrive at typical values for the silty soil, the data sets in PLAXIS were examined to determine which ones could represent a silty soil, and values were chosen for the van Genuchten properties that represented an average behavior of the applicable data sets.

The U.S. Department of Agriculture (USDA) and Hypres data sets in PLAXFLOW were examined to determine applicable data sets to represent an ML-SM site. The data sets are based on the triangular classification chart representing percentages of sand, silt, and clay size particles. Data sets were deemed acceptable if they would classify as an ML or SM material, had an appropriate permeability, and contained less than 20 percent fines by weight. The Activity Ratio defined in Equation 5.1 was used to relate the PI to the percentage of fines in the soil. The activity was assumed to be approximately 1; therefore, the plasticity index (PI) was equal to the amount of clay-sized fines. The value of 20 percent was chosen as a maximum

because the upper bound of the plasticity chart for ML materials is approximately 20 percent (see Figure 5.2). Table 5.7 shows the data sets that were examined, with the acceptable ones in bold print.

Table 5.7. PLAXIS data sets for examination of van Genuchten properties.

PLAXIS Data Set	Soil Description	(% < #200) > 50%	k , ft/sec	(% < 2 μ m) < 20%
USDA	loamy sand	No	11.5 (high)	Yes
USDA	sandy loam	No	3.5 (high)	Yes
USDA	loam	Yes	0.82 (little high)	Yes
USDA	silt	Yes	1.97 (high)	Yes
USDA	silty loam	Yes	0.35 (OK)	Yes
USDA	sandy clayey loam	No	1.03 (high)	No
USDA	clayey loam	Yes	2.05 (high)	No
USDA	silty clayey loam	Yes	0.55 (OK)	No
USDA	sandy clay	Yes	0.94 (little high)	No
USDA	silty clay	Yes	0.0155 (OK)	No
Hypres	coarse	No	2.29 (high)	Yes
Hypres	medium	Yes	0.35 (OK)	Yes
Hypres	medium fine	Yes	0.13 (OK)	Yes
Hypres	fine	Yes	0.28 (OK)	No
Hypres	very fine	Yes	0.27 (OK)	No

$$A = \frac{\text{PI (\%)}}{\text{clay fraction (\%)}} \quad (5.1)$$

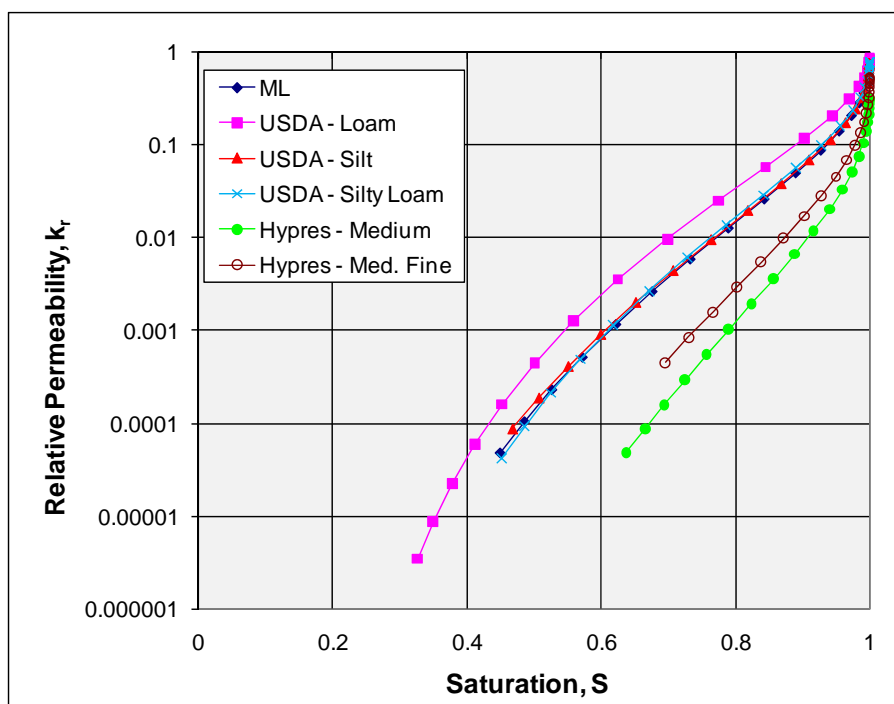
where the clay fraction is the percent of soil by weight with fines < 2 μ m.

The properties of the resulting data sets were examined, and an average set of van Genuchten properties was chosen to represent the silty soils (Table 5.8). The average properties were chosen using plots such as Figures 5.3 and 5.4. The data sets of Table 5.8 were plotted and the properties of the average data set were adjusted until a fit that fell visually between the other data sets was obtained. The variables listed in Table 5.8 are discussed next.

Figures 5.3 and 5.4 were constructed using the values selected for the van Genuchten parameters as listed in Table 5.8. The van Genuchten equation (Equation 5.2) relates the effective saturation (S_e) to the pressure head (ϕ_p) as a function of g_a with units of 1/length, g_m , and g_n .

Table 5.8. PLAXIS data sets for ML-SM material.

	Series					
	1 ML-SM	2 USDA - loam	3 USDA - silt	4 USDA - silty loam	5 Hypres - medium	6 Hypres - medium fine
S_r	0.09	0.1814	0.0739	0.1489	0.02551	0.02427
S_s	1	1	1	1	1	1
g_a (1/ft)	0.6	1.097	0.488	0.6097	0.7591	0.25
g_n	1.37	1.56	1.37	1.41	1.1689	1.2179
g_l	0.5	0.5	0.5	0.5	-0.7437	0.5
k_s (ft/day)	2.84E-01	8.20E-01	1.97E+00	3.54E-01	3.54E-01	1.31E-01
Void ratio	0.75398	0.7544	0.8519	0.8182	0.6447	0.7007

Figure 5.3. Relative permeability (k_r) versus the saturation.

$$S_e = \left[1 + (g_a |\varphi_p|^{g_n})^{-g_m} \right], \quad (5.2)$$

where

S_e = the effective saturation (ranges in value between 0.0 and 1.0);

φ_p = pressure head (units of length);

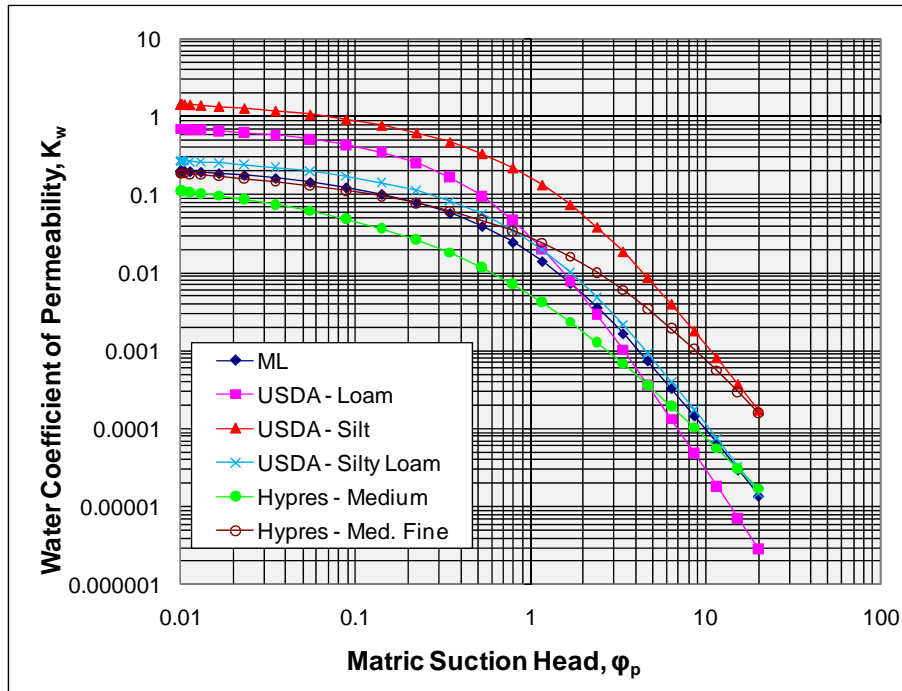


Figure 5.4. Water coefficient of permeability (K_w) versus the matric suction head (ϕ_p) or the soil-water characteristic curve.

and

$$g_m = 1 - \frac{1}{g_n}.$$

The parameters g_a and g_n are fitting parameters and typically are determined experimentally.

The saturation is shown in Equation 5.3. The saturation is a function of the residual saturation (S_r) and the saturation at the maximum moisture content (S_s). The saturation varies between 0 and 1. S_r is the degree of saturation at which an increase in matric suction does not produce a significant change in the degree of saturation. At this matric suction value, some fluid still remains trapped in the voids of the soil. Matric suction is a tensile pressure head. S_s is the saturation at the maximum moisture content and is equal to 1 or very close to 1. S_s can be less than 1 because some air remains trapped in the voids of the soil.

$$S = S_r + (S_s - S_r)S_e \quad (5.3)$$

The relative permeability (K_r) is defined by Equation 5.4 and ranges in value between 0.0 and 1.0 cm/sec.

$$k_r = (S_e)^{g_l} \left[1 - \left(1 - (S_e)^{1/g_m} \right)^{g_m} \right]^2 \quad (5.4)$$

The effective permeability (k_w) is defined by Equation 5.5 and is some percentage of k_s , which is the maximum possible permeability that occurs at a saturation of 100 percent.

$$k_w = k_r k_s, \quad (5.5)$$

where

- k_w = coefficient of permeability with respect to the water phase (length/time);
- k_r = relative permeability with respect to the water phase (ranges in value between 0.0 and 1.0);
- k_s = coefficient of permeability with respect to the water phase at saturation of 100 percent (units of length/time).

5.5 Conventional design of cantilever I-wall

The depth of the sheet-pile wall was determined using the CWALSHT computer program and procedures from EM 1110-2-2504 (HQUSACE 1994). The design depth of the tip of the sheet pile was computed to be -38 ft without consideration of a gap forming between the concrete cap and soil or between the sheet pile and soil on the flood side of the I-wall. Upon later examination of the CWALSHT results, the design depth was found to be in error. Because the finite element analyses were mostly complete for this design depth, the PLAXIS analyses were completed using the original design depth (sheet-pile tip at el -38 ft). However, it should be noted that the inclusion of a gap beside the wall also would affect the design depth. Therefore, these analyses were assumed to provide information for a high ratio of embedment to flood height and, therefore, still are considered useful. The factor of safety for this system for a water elevation of 9 ft would not correspond to the factor of safety used for design in CWALSHT because a gap was not assumed in the analysis.

To create the I-wall system using CWALSHT, two designs were performed based on short-term and long-term conditions. This required the use of effective stress (drained) strength parameters for the long-term design and total stress (undrained) strength parameters for the short-term design.

The effective stress strength parameters were discussed in Section 5.3 and assumed from values taken from a literature review as shown in Tables 5.1 and 5.2. The total stress (undrained) shear strength parameters were determined using the SHANSEP procedure (Ladd and Foott 1974). It assumes that the soil shear strength can be normalized by the effective overburden pressure. The ratio of shear strength to effective overburden pressure (S_u/σ'_{vo}) is dependent on the overconsolidation ratio (OCR) and a fitting parameter (m) assumed to be 0.8, as shown in Equation 5.5:

$$\left(\frac{S_u}{\sigma'_{vo}} \right)_{OC} = \left(\frac{S_u}{\sigma'_{vo}} \right)_{NC} \bullet OCR^m, \quad (5.5)$$

where

- $(S_u/\sigma'_{vo})_{OC}$ = ratio of shear strength to effective overburden pressure for the overconsolidated condition;
 $(S_u/\sigma'_{vo})_{NC}$ = ratio of shear strength to effective overburden pressure for the normally consolidated condition.

From published values (Ladd 1991), a value of 0.25 was assigned to $(S_u/\sigma'_{vo})_{NC}$ and a value of 0.8 for m based on undrained Direct Simple Shear (DSS) test results. DSS results were chosen because this represented the predominant type shear surface of a passive soil wedge. Undrained triaxial compression tests (TX) better represent the shear surface of an active wedge. Because the passive wedge was deemed more important for the stability of the wall, DSS strengths were used. When computing the effective overburden pressures, 120 pcf was used for the moist unit weight of the soil and 125 pcf was used for the saturated unit weight.

A 10-ft-deep crust is assumed to exist for the ML-SM site as shown in Figure 5.1. However, the upper 5 ft of the crust are assumed to be more overconsolidated than the lower 5 ft. This crustal zone is characterized by the OCR shown in Figure 5.5. The OCR is the ratio of the preconsolidation pressure (P'_c) to the effective overburden pressure σ'_v (P'_c/σ'_v). As shown in Figure 5.5, the OCR varies from 5 at 1 ft below the ground surface to 2 at el -5 ft to 1 at el -10 ft.

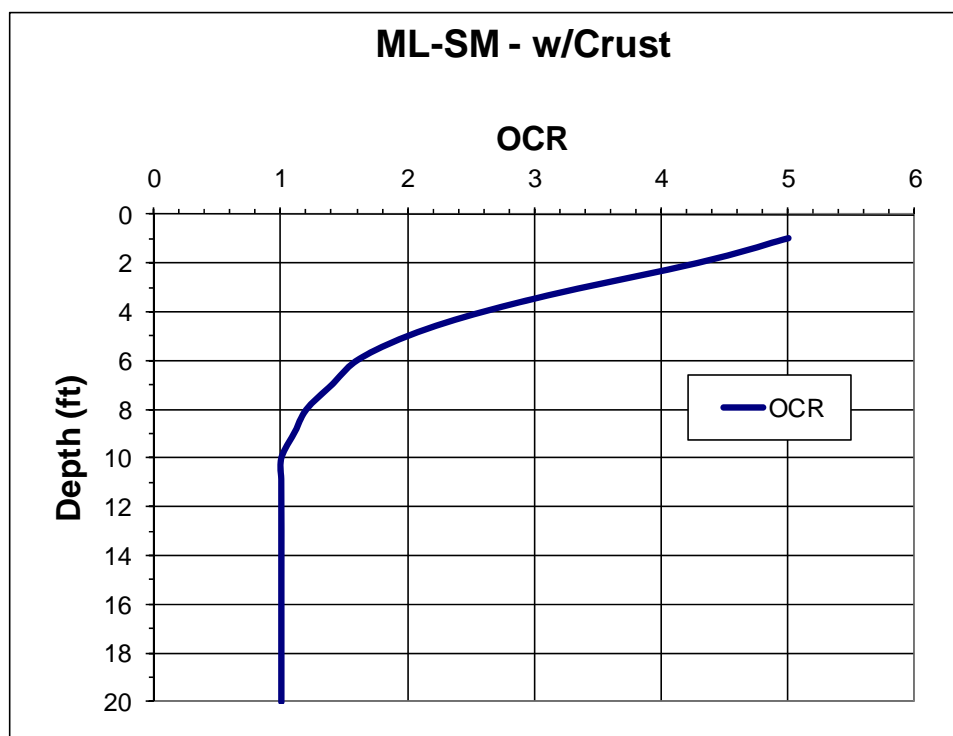


Figure 5.5. OCR variation with depth for ML-SM site with a 5-ft-thick crust.

The resulting variation in S_u with depth is shown in Figure 5.6. Triaxial test results are shown in this figure for comparison purposes only. The triaxial test $(S_u/\sigma'_v)_{NC}$ equals to 0.32 and would be appropriate for the active driving wedge. Figure 5.6 shows that at a depth of 1 ft, S_u is equal to 113 psf. From 2 to 10 ft in depth, S_u increases in value from 200 psf to 313 psf. Between 10 and 13 ft, S_u increases in value from 313 to 400 psf. The computations for S_u are shown in Table 5.9.

The depth of the sheet-pile wall was computed using CWALSHT. Table 5.10 summarizes the initial design cases run and the associated design depths. For the design depth of -38 ft, the chosen pile section for the maximum moment was a PZ32.

To account for the water loadings properly, care must be taken when performing a CWALSHT analysis for a short-term (undrained) condition. For the short-term condition using a total stress method of analysis, pore pressures should not be calculated within the soil. External water loadings must be accounted for in the analysis. Therefore, vertical uniform and horizontal boundary pressure loads must be used to represent the external loading due to the water.

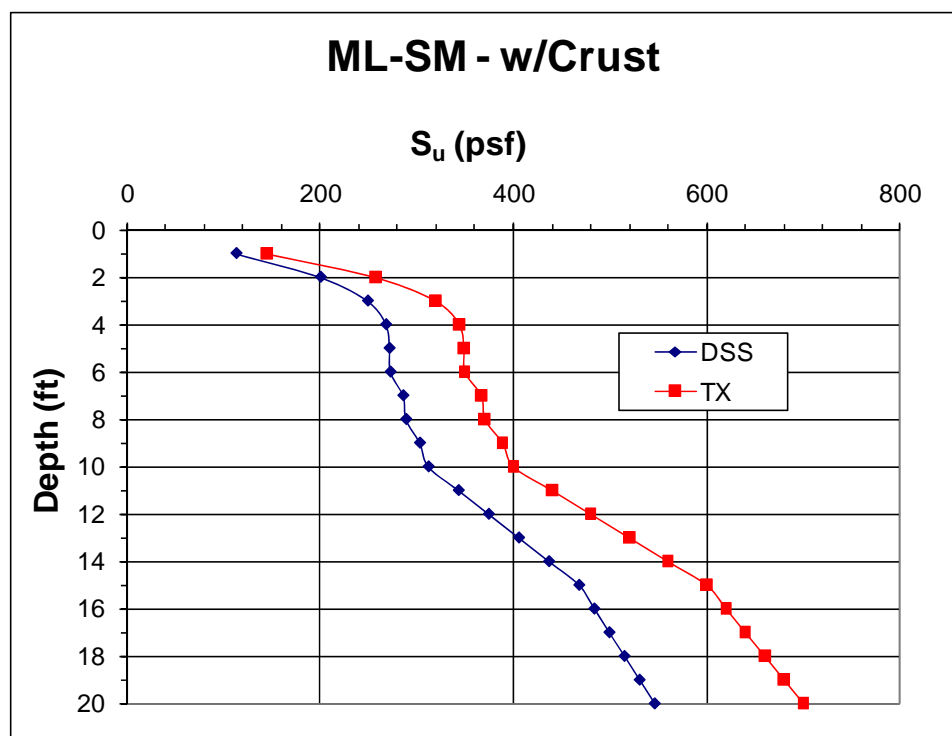


Figure 5.6. Variation in undrained shear strength with depth for a 15-ft-deep water table.

Table 5.9. Computation of S_u (DSS) for short-term (undrained) loading (continued on next page).

Short-Term (Undrained) Loading							α	$\alpha * S_u / FS$ FS=3.0, psf	ST Friction, lbs	$\sigma'_h = K_o \sigma'_v$ $K_o = 0.5$, psf	LT Friction FS=3.0, lbs
Depth, ft	σ'_{vo} , psf	OCR	$(S_u / \sigma'_{vo})_{OC}$	S_u , psf	E_u / S_u	E_u , psf					
1	125	5	0.91	113	500	56,623	1.00	38	113	122	41
2	250	4.3	0.80	201	570	114,427	1.00	67	134	162	54
3	375	3.4	0.67	250	670	167,197	1.00	83	166	244	81
4	500	2.6	0.54	268	780	209,403	1.00	89	179	325	108
5	625	2	0.44	272	900	244,842	1.00	91	181	406	135
6	750	1.6	0.36	273	950	259,430	1.00	91	182	487	162
7	875	1.4	0.33	286	970	277,730	1.00	95	191	568	189
8	1000	1.2	0.29	289	980	283,473	1.00	96	193	649	216
9	1125	1.1	0.27	304	1000	303,534	1.00	101	202	731	244
10	1250	1	0.25	313	1000	312,500	1.00	104	208	812	271
11	1375	1	0.25	344	1000	343,750	1.00	115	229	927	309
12	1500	1	0.25	375	1000	375,000	1.00	125	250	1012	337
13	1625	1	0.25	406	1000	406,250	1.00	135	271	1096	365
14	1750	1	0.25	438	1000	437,500	1.00	146	292	1180	393
15	1875	1	0.25	469	1000	468,750	1.00	156	313	1265	422
16	1938	1	0.25	484	1000	484,400	1.00	161	323	1307	436

Short-Term (Undrained) Loading							α	$\alpha * S_u / FS$ FS=3.0, psf	ST Friction, lbs	$\sigma'_h = K_o \sigma'_v$ $K_o = 0.5$, psf	LT Friction FS=3.0, lbs
Depth, ft	σ'_{vo} , psf	OCR	$(S_u / \sigma'_{vo})_{oc}$	S_u , psf	E_u / S_u	E_u , psf					
17	2000	1	0.25	500	1000	500,050	1.00	167	333	1349	450
18	2063	1	0.25	516	1000	515,700	0.99	171	341	1391	464
19	2125	1	0.25	531	1000	531,350	0.98	174	349	1434	478
20	2188	1	0.25	547	1000	547,000	0.98	178	1068	4427	1476
25	2501	1	0.25	625	1000	625,250	0.94	195	1954	8435	2812
30	2814	1	0.25	704	1000	703,500	0.90	211	2106	9490	3163
35	3127	1	0.25	782	1000	781,750	0.86	224	2239	10,546	3515
40	3440	1	0.25	860	1000	860,000	0.82	235	2351	11,602	3867
45	3753	1	0.25	938	1000	938,250	0.78	244	2442	12,657	4219
50	4066	1	0.25	1017	1000	1,016,500	0.74	251	2513	13,713	4571
55	4379	1	0.25	1095	1000	1,094,750	0.70	256	2564	14,768	4923
60	4692	1	0.25	1173	1000	1,173,000	0.66	259	2594	15,824	5275
65	5005	1	0.25	1251	1000	1,251,250	0.62	260	2604	16,880	5627
70	5318	1	0.25	1330	1000	1,329,500	0.59	259	2594	17,935	5978
75	5631	1	0.25	1408	1000	1,407,750	0.55	256	2563	18,991	6330
80	5944	1	0.25	1486	1000	1,486,000	0.51	251	2511	20,046	6682
85	6257	1	0.25	1564	1000	1,564,250	0.50	261	2607	21,102	7034
90	6570	1	0.25	1643	1000	1,642,500	0.50	274	2738	22,158	7386
95	6883	1	0.25	1721	1000	1,720,750	0.50	287	2868	23,213	7738
100	7196	1	0.25	1799	1000	1,799,000	0.50	300	1499	12,134	4045

Table 5.10. Summary of CWALSHT design cases, 9-ft wall height (h), 9-ft water height.

Seepage (yes, no)	Shear Strength				Required Penetration depth for Side Friction, d , ft	CWALSHT penetration, depth d , ft	d/h	Analysis Case
	ϕ , deg	δ , deg	Adhesion, psf	c , psf				
no	0	0	0	increases with depth (113 - 860)		38	4.22	ST
no	0	0	$0.25 * S_u$	increases with depth (113 - 860)		32	3.56	ST
yes	$33 < 10'$ $34 > 10'$	0	$200 < 10'$ $0 > 10'$	0		15.5	1.72	LT
no	0	0	0	increases with depth (113 - 860), ($S_u * \alpha / FS = 3.0$)	16		1.78	Side Friction - ST
no	$33 < 10'$ $34 > 10'$	0	0	0	15		1.67	Side Friction - LT

The I-wall also was checked for stability against a bearing capacity failure. The bearing capacity of the concrete wall and the side friction along the sheet pile were checked to ensure adequate bearing. The wall was found to have an adequate factor of safety against a bearing capacity failure due to its own weight.

5.6 Discussion of loading

Several hydrographs were considered to define the flood loading for the system. The hydrographs ranged from short-duration loading (30 days or fewer) to long-duration loading (200 days). For these analyses, the long-duration hydrograph was chosen to ascertain if the soil performed as drained or undrained. The hydrograph was scaled to the problem geometry (i.e., a maximum flood elevation of 9 ft). The water elevation began at -15 ft (the starting elevation of the water) and progressed to 9 ft (the top of the I-wall). The chosen hydrograph is shown in Figure 5.7.

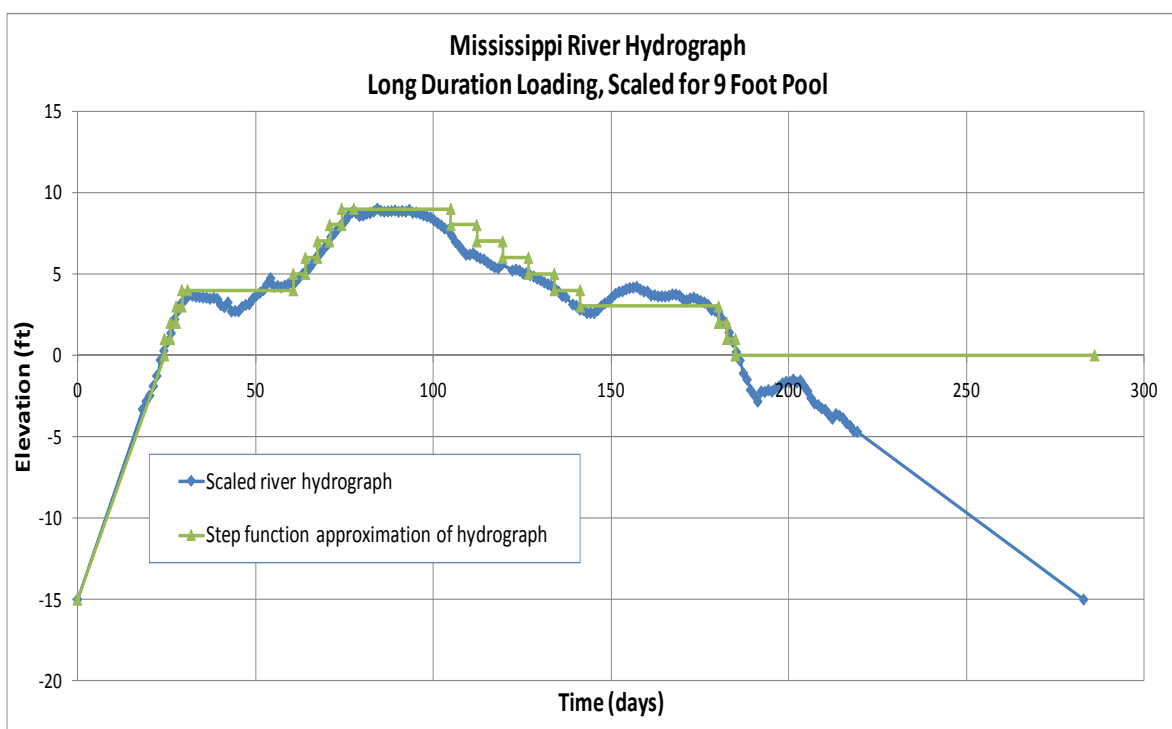


Figure 5.7. Long-duration hydrograph, scaled for 9-ft pool, Mississippi River.

The loading was performed in PLAXIS in 1-ft increments of water, with the associated time duration taken from the hydrograph. This is shown as the step function approximation in Figure 5.7. This was done to simplify the examination of pore pressures, stresses, and displacements as the water was raised against the I-wall.

5.7 Discussion of finite element analyses

5.7.1 Conceptual model

The finite element analyses were performed with PLAXIS, a nonlinear incremental construction finite element program. The conceptual model of the finite element mesh is shown in Figure 5.8. The geometry is the same as explained in Section 5.2, but there are several modeling features that should be noted. The sheet-pile wall is represented by plate elements, and the concrete wall is represented by 2-D elastic elements. Interface elements are placed around the concrete cap and along both sides of the sheet-pile wall. Extensions of the interface elements are provided at the corners of the concrete cap at el -2.5 ft and at the bottom of the sheet-pile wall, both horizontally and vertically. This was done to alleviate stress concentrations at the corners of the geometry. A 2-D element extension was added above the wall to provide for additional loading height. The 2-D elements were given the same properties as the concrete. The mesh was structured to provide node points at 1-ft raises of the water table. The soil elements beside the sheet-pile wall on the flood side were 1/2 ft high. This enabled the inputting of 1-ft raises in water and modeling of the gap to within 1/2 ft.

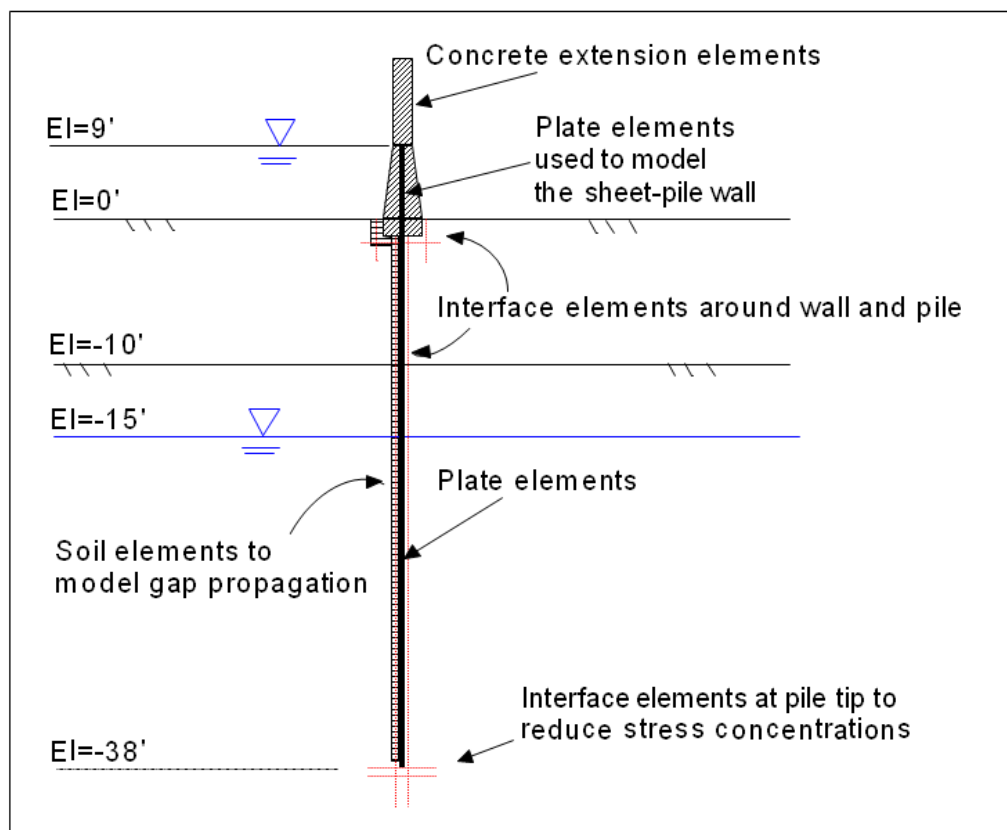


Figure 5.8. Conceptual model.

The gap along the flood side of the interface of the I-wall and soil is modeled by turning soil clusters (elements) off, effectively creating a void beside the wall. Water pressures are applied within this void, and the gap progresses. Figure 5.9 shows the location and progression of the gap beside the sheet-pile wall.

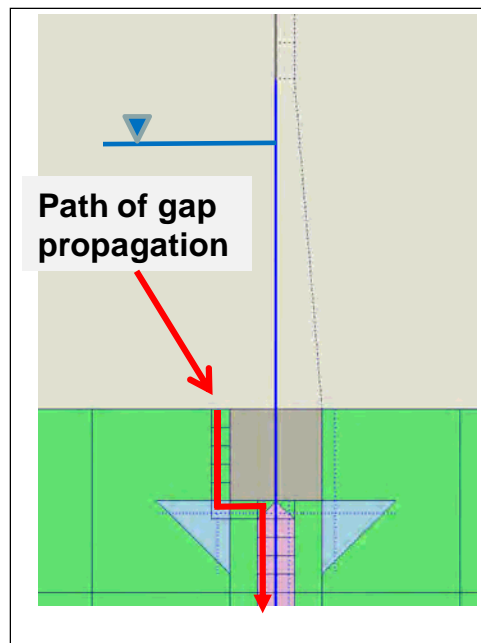


Figure 5.9. Gap propagation beside I-wall.

5.7.2 Finite element mesh

The finite element mesh used in the analyses is shown in Figure 5.10. The mesh is composed of 2,089 elements and 17,836 nodes, with 25,068 stress points. The mesh uses 15-node triangular elements. The problem is run as a plane strain problem. Figure 5.11 shows an enlargement of the area around the wall and the detail of the mesh.

5.7.3 Three-stage analysis procedure

For the ML-SM soil, an effective stress analysis was performed for two values of the horizontal permeability (k_x), as shown in Table 5.6. The effects of the value of the permeability, the compressibility of the soil, the rate of loading, and the length of the drainage path affect whether the problem will act as drained, undrained, or somewhere in between.

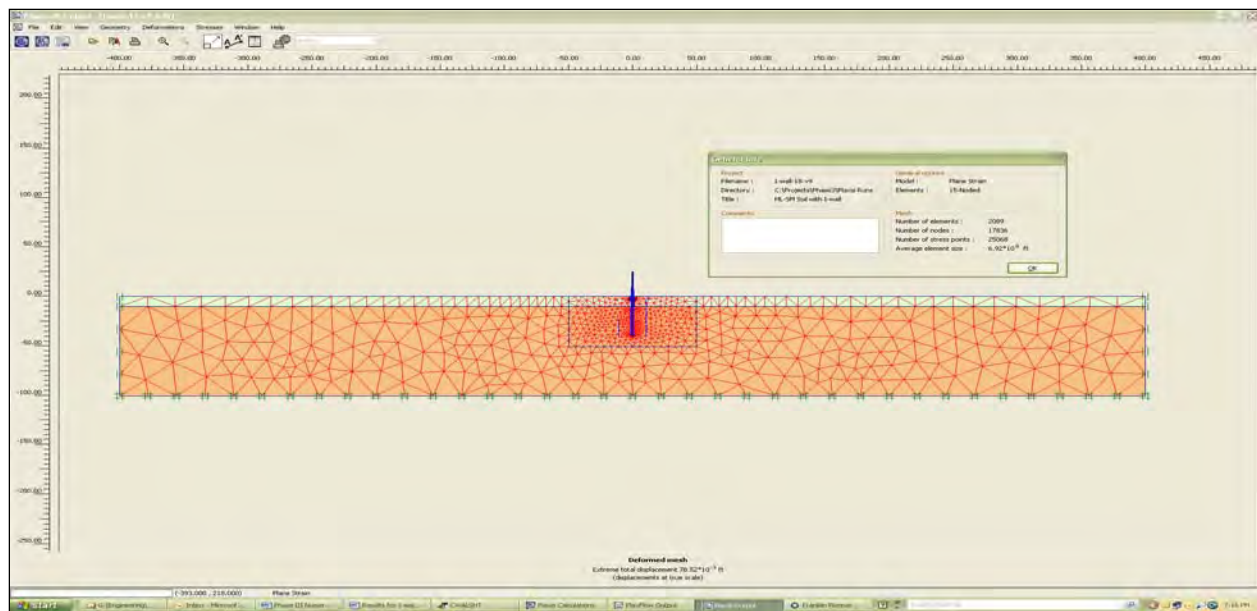


Figure 5.10. Finite element mesh used in the analyses.

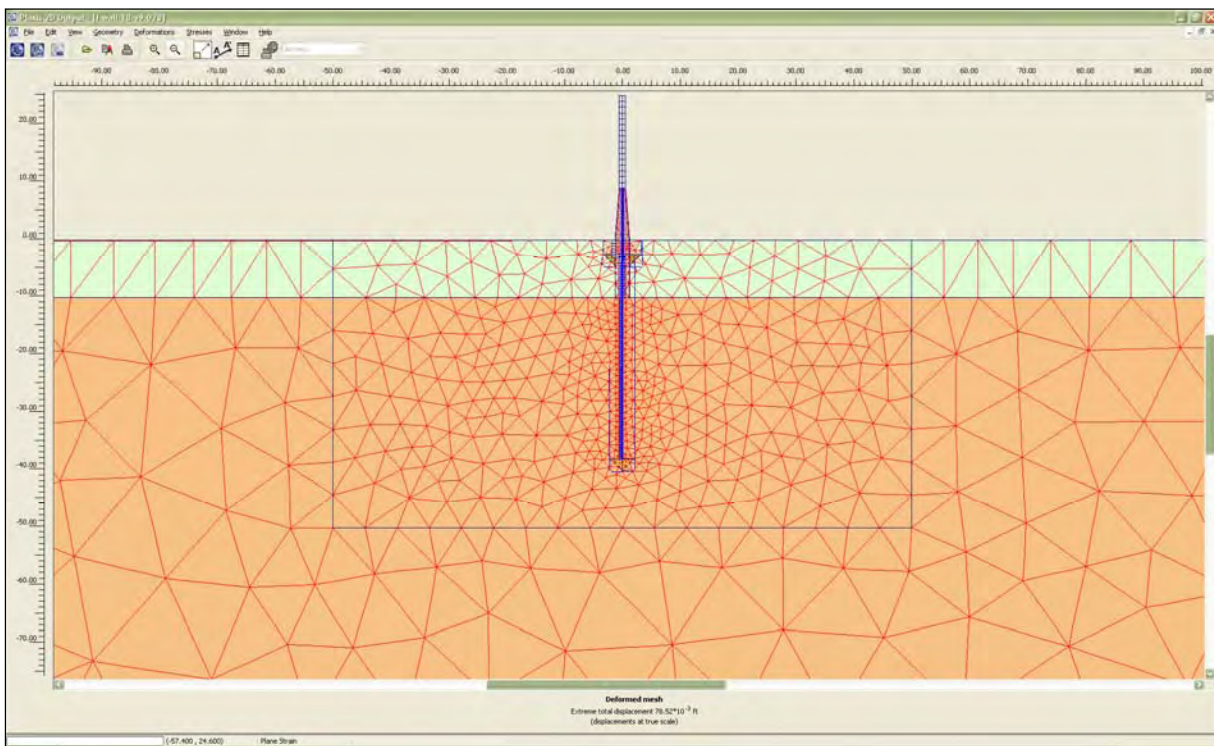


Figure 5.11. Enlargement of finite element mesh around the I-wall.

The PLAXIS analysis using effective stress strength parameters with the designation of the materials as undrained results in the generation of excess pore-water pressures in the soil. The undrained switch in PLAXIS is used specifically to tell the program to generate excess pore-water pressures

caused by computed deformations. The magnitude of the permeability also affects the pore pressures developed during the transient seepage analysis. That is, the flow regime will not be at a steady-state condition (e.g. pore pressures existing at infinite time). For each construction phase (i.e. a level of applied water), the excess pore pressures above the transient condition existing at the particular time of the loading are dissipated through a consolidation analysis. This analysis is coupled with the deformation analysis so, as pore pressures are generated, they simultaneously are being dissipated. The rate of dissipation is dependent upon the permeability, compressibility of the soil, and the length of the drainage path.

The analysis performed in PLAXIS, therefore, has three distinct parts:

1. A transient seepage analysis;
2. A deformation analysis;
3. A consolidation analysis.

This three-stage analysis procedure is performed as follows:

1. For a hydrograph representing a slow rate of rise, the water level is raised in 1-ft increments in the analyses. The step function hydrograph shown in Figure 5.7 is used to determine the times for each 1-ft rise in water.
2. For each 1-ft rise of the water, a transient seepage analysis is performed using the time increment associated with that particular 1-ft rise of water. This results in a set of total heads and pore pressures that feed into the deformation analysis.
3. The deformation analysis is run, and excess pore-water pressures are generated in addition to the transient seepage pore pressures already computed. The excess pore-water pressures are tied to the volumetric strains occurring in the elements.
4. The induced excess pore pressures resulting from the water loading are dissipated in a consolidation analysis that occurs with the deformation analysis.
5. The resulting total normal stresses along the flood side of the pile are examined to determine if a gap has occurred. A gap will occur when the hydrostatic water pressure for the current water level exceeds the total normal stress on the wall.
6. The gap beside the sheet-pile wall is modeled by turning off soil clusters (elements) down to the computed depth of the gap (Figure 5.9).

7. The analysis is repeated with the computed gap in place with the current water elevation. This results in additional deformation and a change in the normal stresses on the wall.
8. Steps 5 through 7 are repeated until the gap depth ceases to change. This usually takes only one to two iterations.
9. The water elevation is increased according to the hydrograph, and Steps 2 through 8 are repeated.
10. The water elevation is increased until instability occurs.

The induced pore pressures and the rate of dissipation are dependent upon the properties of the soil and the rate of loading. The soil may act as drained, undrained, or somewhere in between.

5.8 Results of the finite element analyses

5.8.1 Gap progression

Figure 5.12 shows the progression of the gap as the water level against the I-wall is increased for the two values of the permeability. For k_x equal to 1×10^{-4} cm/sec, the gap first appears when the water is at el 2 ft and extends to a depth of -2.5 ft (the bottom of the concrete cap). The gap extends to el -22 ft at a water elevation of 3 ft. The analysis becomes unstable for k_x equal to 1×10^{-4} cm/sec at a water height of 5 ft.

For k_x equal to 1×10^{-5} cm/sec, the gap first appears when the water is at el 2 ft and extends to a depth of -2.5 ft (the bottom of the concrete cap). The gap extends to el -22 ft at a water elevation of 3 ft. As the water rises, the depth of the gap continues to increase, as shown in Figure 5.12, and eventually reaches a depth of -32.5 ft at a water elevation of 9 ft. Results for various water elevations and gap depths will be examined.

5.8.2 Performance of interface elements

The performance of the interface elements was studied to ascertain whether the results for the soil elements adjacent to the wall or the interface elements could be used to examine the results of the analyses. Figure 5.13 shows that the interface and soil elements agree closely; therefore, the interface elements were used to extract data from the analyses.

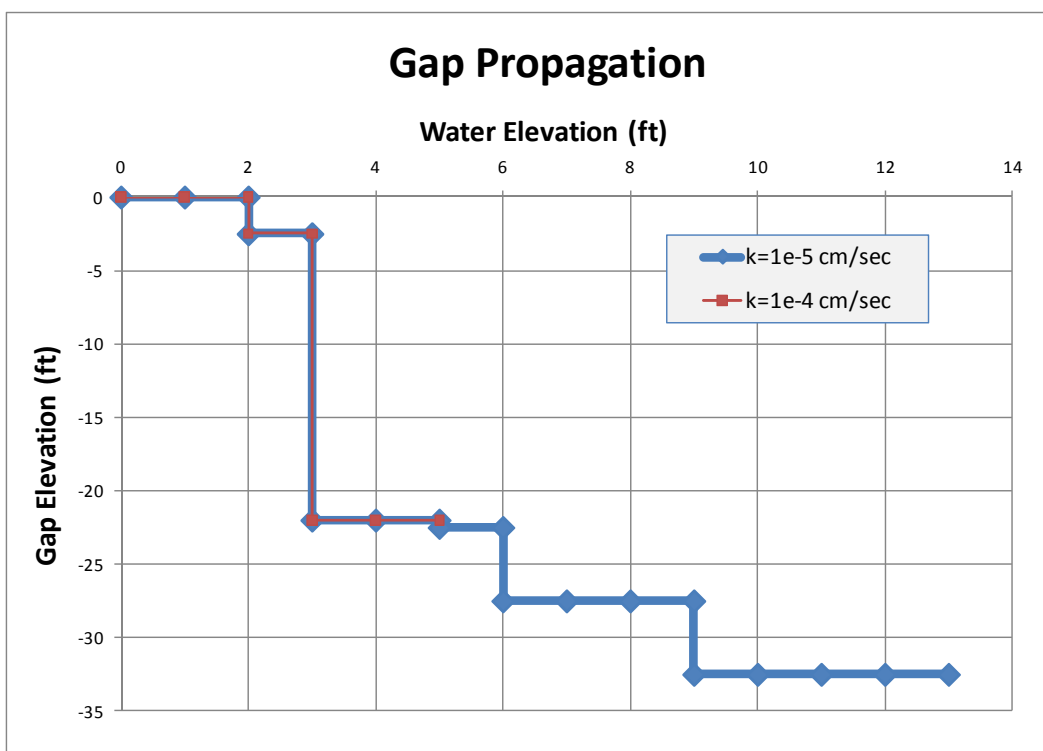


Figure 5.12. Progression of gap versus water elevation along flood side of I-wall.

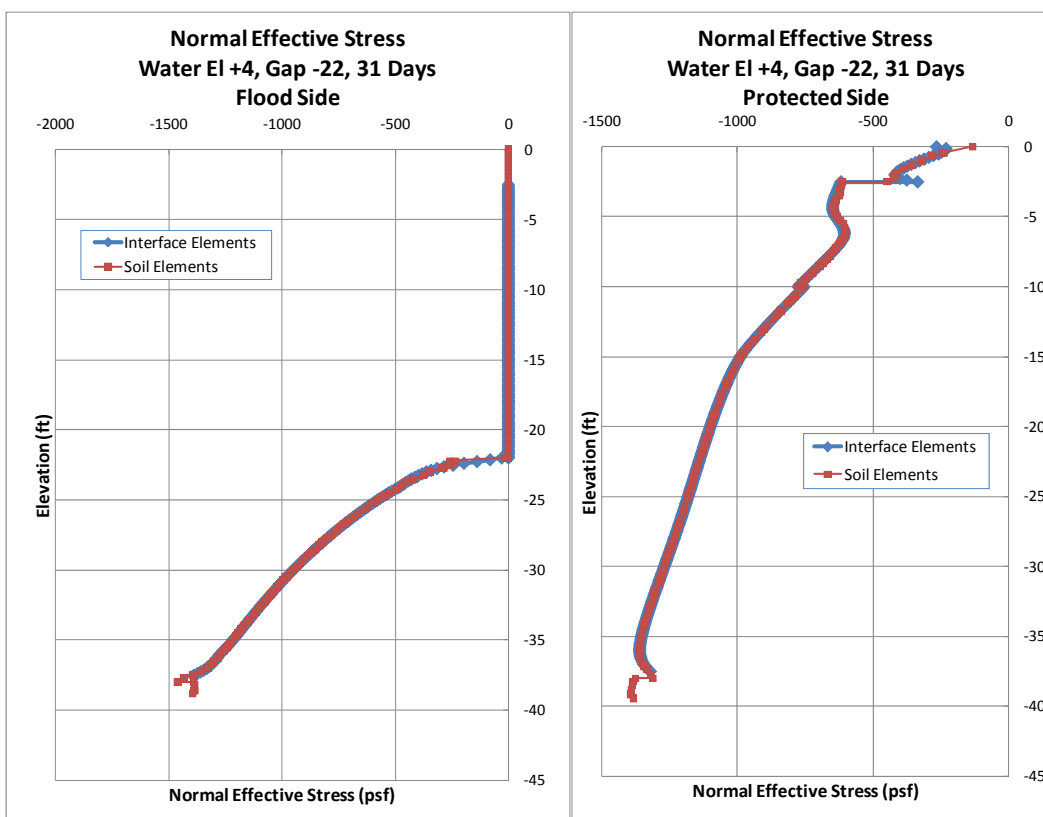


Figure 5.13. Behavior of interface versus soil elements.

5.8.3 Comparison of pore pressures for low and high permeabilities

The pore pressures for several water elevations will be examined to determine how close the flood side and landside of the I-wall are to a drained or undrained condition. The pore pressures are a combination of pore pressures resulting from transient seepage and excess pore pressures generated from the deformation analysis. To compare pore pressures between the two cases of permeabilities used, total head values will be compared. Note that, for all figures, the left side is the flood side and the right is the landside.

Figure 5.14 shows the total head contours for a value of 1×10^{-4} cm/sec for k_x for results at 31 days and 60.7 days compared to the pore pressures existing at the steady-state condition. As can be seen from the figure, the equipotential lines do not have the same shape or values close to the wall as those for the steady-state condition. The gap at the wall on the flood side also influences the total head values. This can be seen from the larger values of head around the wall. The gap provides a boundary condition for the seepage analyses equal to the full hydrostatic head applied down the height of the gap. Therefore, adjacent to the wall on the flood side, the pore pressures are equal to the steady-state pore pressures.

Figure 5.15 shows the saturation of the soil at a water elevation of 4 ft with a gap down to el -22 ft at 60.7 days for a k_x of 1×10^{-4} cm/sec. As can be seen from the figure, the flood side is fully saturated at this time. The landside is still partially saturated, and the water elevation next to the wall has moved up from el -15 ft only a small amount.

Figure 5.16 shows the total head contours for the case of the permeability of 1×10^{-5} cm/sec and a water elevation of 4 ft. The distribution of the contours looks similar to the ones shown in Figure 5.14 at 31 days.

These values of total head do not compare well with the steady-state condition for this depth of gap and water elevation.

The total head contours for k_x of 1×10^{-5} cm/sec, a water elevation of 9 ft, a gap elevation of -32.5 ft, and a time of 105 days are shown in Figure 5.17. As can be seen from this figure, the equipotential lines do not compare well with the steady-state condition computed using the same gap depth and water elevation.

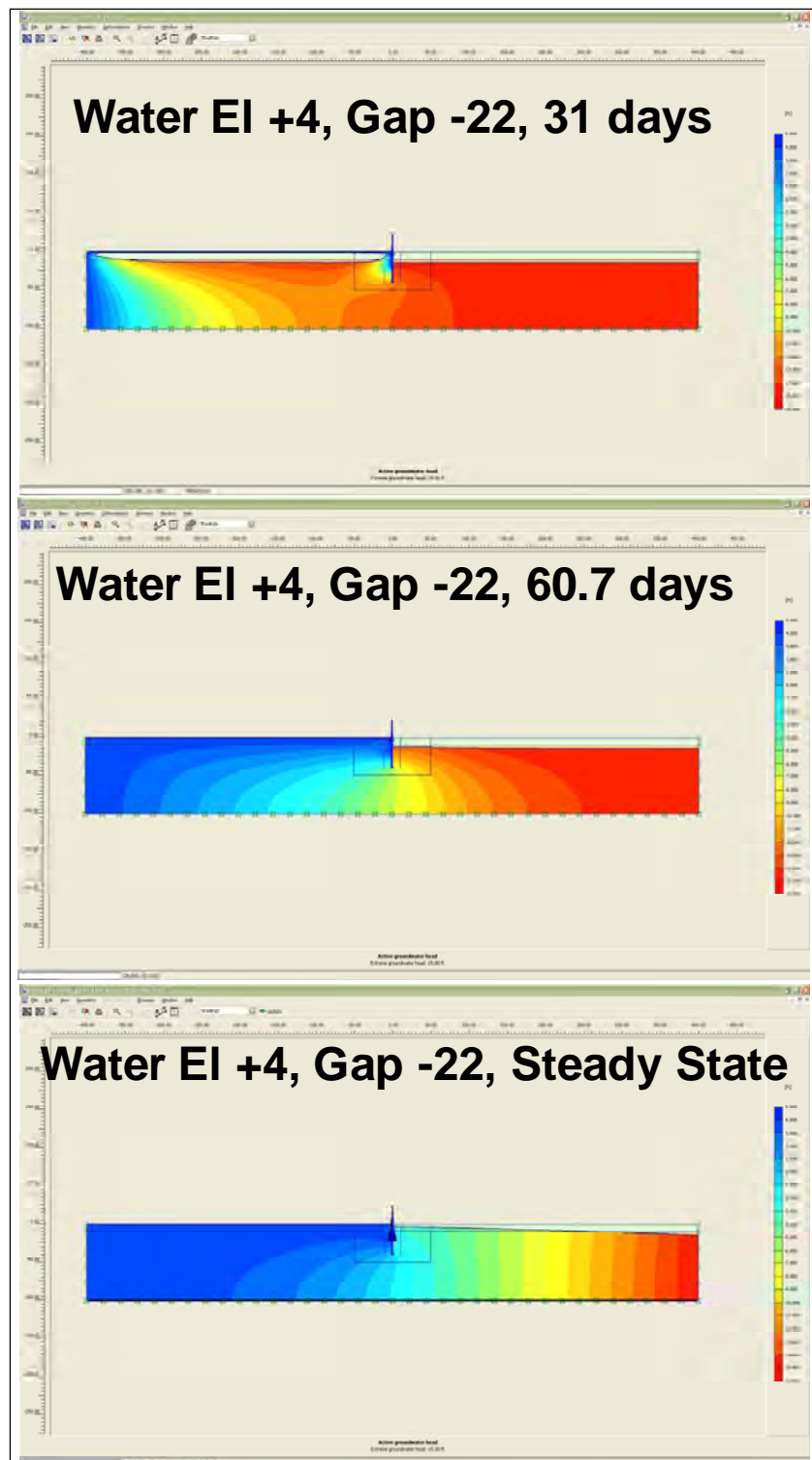


Figure 5.14. Total head values for the case of $k_x = 1 \times 10^{-4}$ cm/sec at various times.

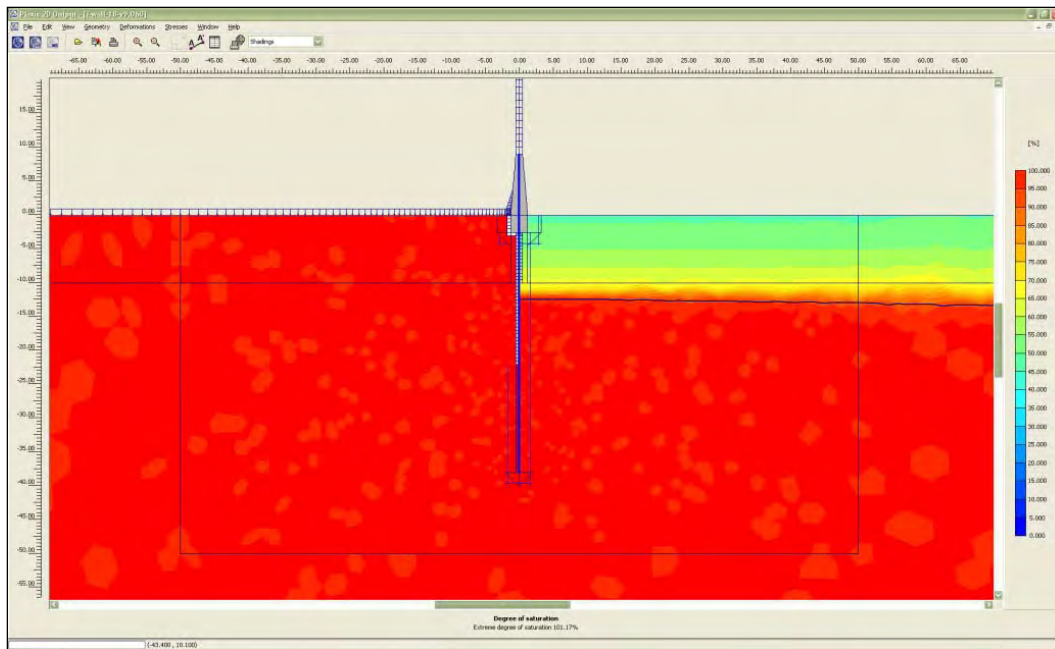


Figure 5.15. Saturation for water at el 4, gap at el -22, time equal to 60.7 days, $k_x = 1 \times 10^{-4}$ cm/sec.

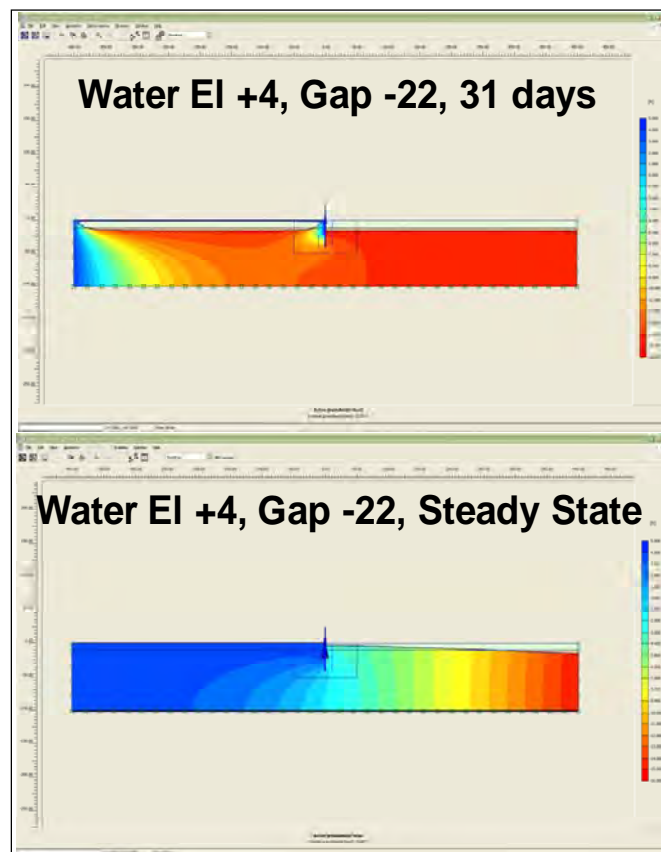


Figure 5.16. Total head values at water el 4 ft, gap el -22 ft, 31 days, $k_x = 1 \times 10^{-5}$ cm/sec.

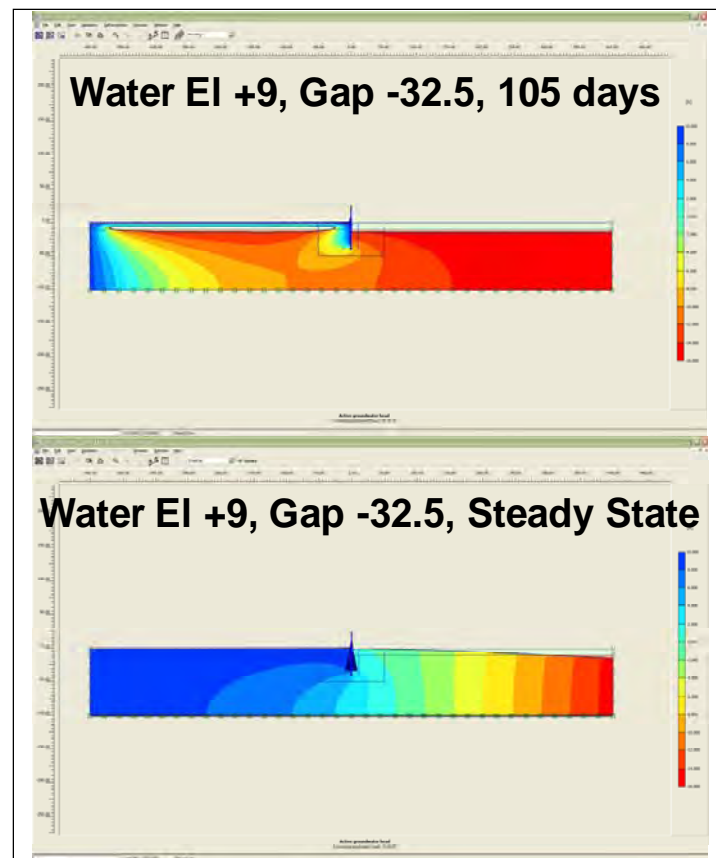


Figure 5.17. Total head values at water el 9 ft, gap el -32.5 ft, 105 days, $k_x = 1 \times 10^{-5}$ cm/sec.

Figure 5.18 shows the saturation of the soil at a water elevation of 9 ft with a gap down to el -32.5 ft at 105 days for a k_x of 1×10^{-5} cm/sec. The flood side has not reached full saturation. The soil is saturated from the top down and from the bottom up, resulting in an isolated interior zone of partially saturated soil. The landside is still partially saturated, and the water elevation next to the wall has moved up from el -15 ft only a small amount.

Figures 5.19 and 5.20 compare the total head values for the flood side and landside, respectively, to the bounding conditions of total head existing at the initial condition and at the steady-state condition for the permeabilities of $k_x = 1 \times 10^{-4}$ and 1×10^{-5} cm/sec. The total head existing for the undrained condition is shown in these figures by a green line. This line represents the total heads existing at the initial condition of the water at el -15 ft. Therefore, the line starts at 0 ft of total head at the ground surface and decreases to -15 ft of total head at a depth of -15 ft. Essentially, the total head is equal to the elevation head above the water elevation and a constant

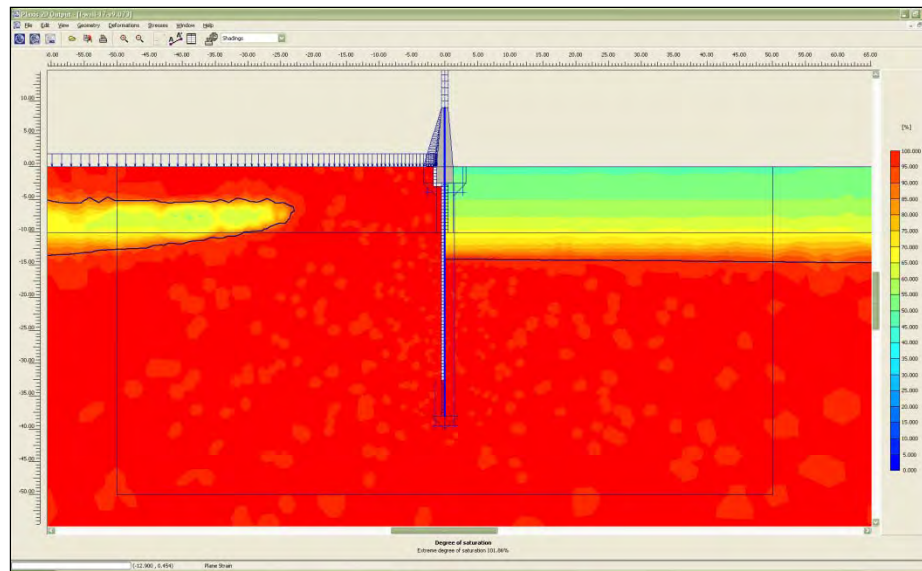


Figure 5.18. Saturation for a water elevation of 9 ft, gap elevation of -32.5 ft, 105 days, and $k_x = 1 \times 10^{-5}$ cm/sec.

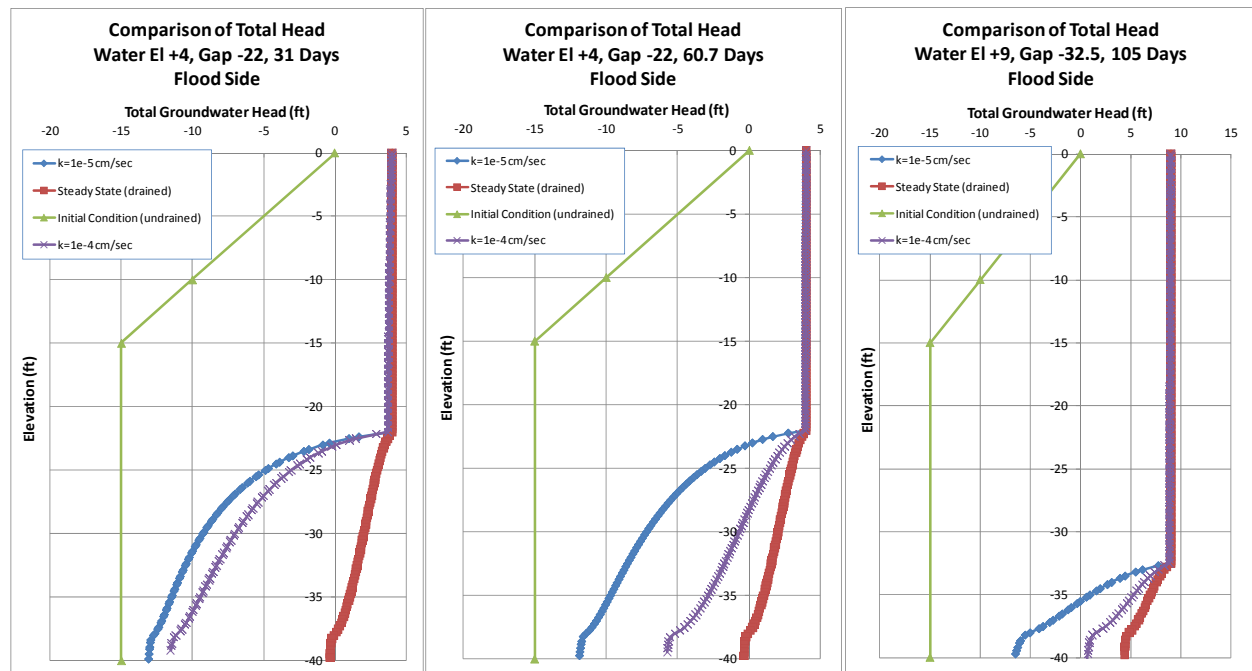


Figure 5.19. Comparison of total head on the flood side to the bounding initial and steady states for several times and associated water elevations.

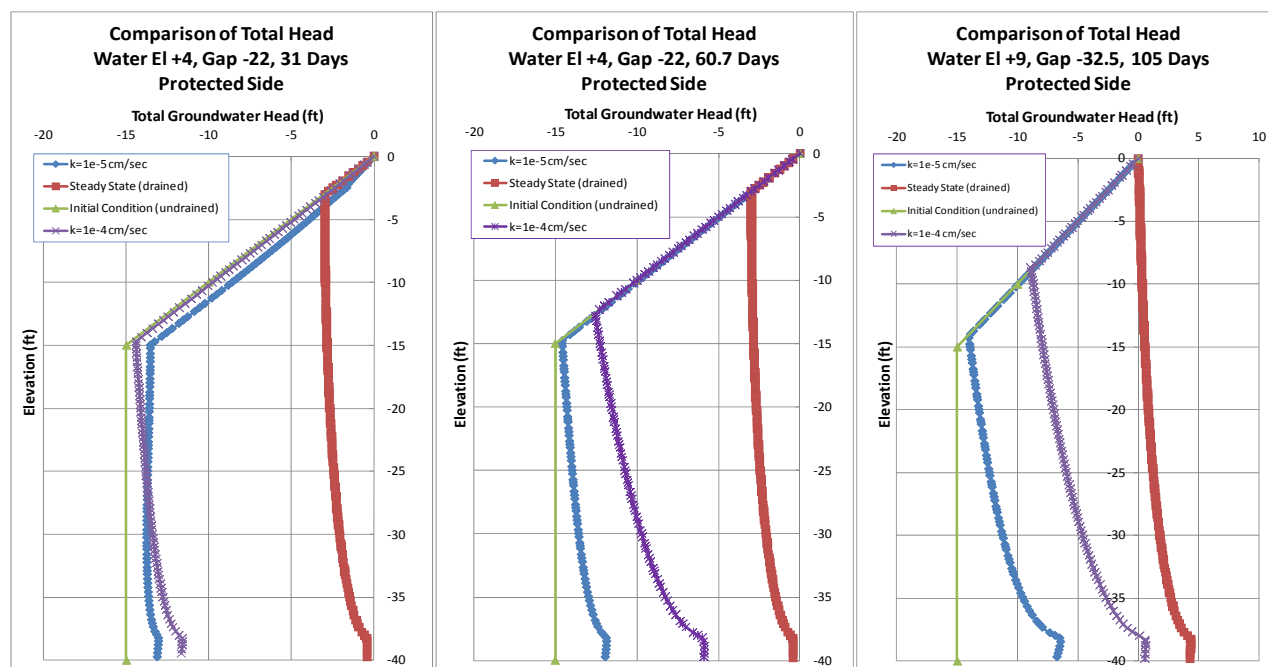


Figure 5.20. Comparison of total head on the protected side (landside) to the bounding initial and steady states for several times and associated water elevations.

value of -15 ft below the water elevation. The total heads existing for the drained condition are shown by the red line. This condition is for the steady-state seepage condition computed by the PLAXFLOW finite element seepage program. The steady-state line is vertical at a specified water elevation along the entire length of the gap. The undrained and drained lines bound the values of total head computed for the two permeabilities. Therefore, how close the actual analysis is to the drained or undrained condition can be compared.

For the flood side, for a water elevation of 4 ft at 30 days, the head values for the two permeabilities are close to each other and progress from a drained condition at the bottom of the gap over to a mostly undrained condition at the bottom of the sheet-pile wall. At 60.7 days the total head values have become more separated, but are still between drained and undrained. At 105 days and a water elevation of 9 ft, the two cases are nearer the drained condition. For any water elevation, the lower permeability is always closer than the higher permeability to the undrained condition.

For the landside, the total heads for the two permeabilities tend to be closer to the undrained condition at higher elevations and tend toward the drained condition toward the tip of the sheet-pile wall. The higher permeability case is closer than the lower permeability case to the drained condition.

Figures 5.21 and 5.22 compare the flood side and landside again along with the computed indicator (R), which shows how close the total head values are to the drained or undrained condition. The R value is computed as shown in Equation 5.6:

$$R = \frac{(H_{ss} - H)}{(H_{ss} - H_o)}, \quad (5.6)$$

where

- H = total head value for a location;
- H_{ss} = total head value for the steady-state condition at a location;
- H_o = total head value for the initial condition at a location.

R varies between 0 for the drained case and 1 for the undrained case. Therefore, R will be closer to 0 for a drained condition and closer to 1 for an undrained condition.

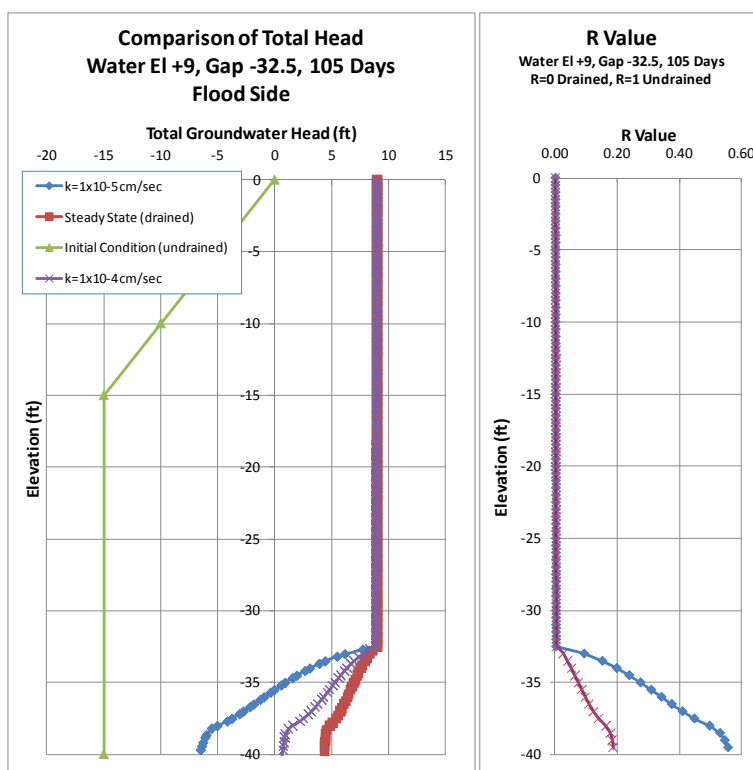


Figure 5.21. Comparison of total heads on the flood side to the drained and undrained conditions for water at el 9 ft.

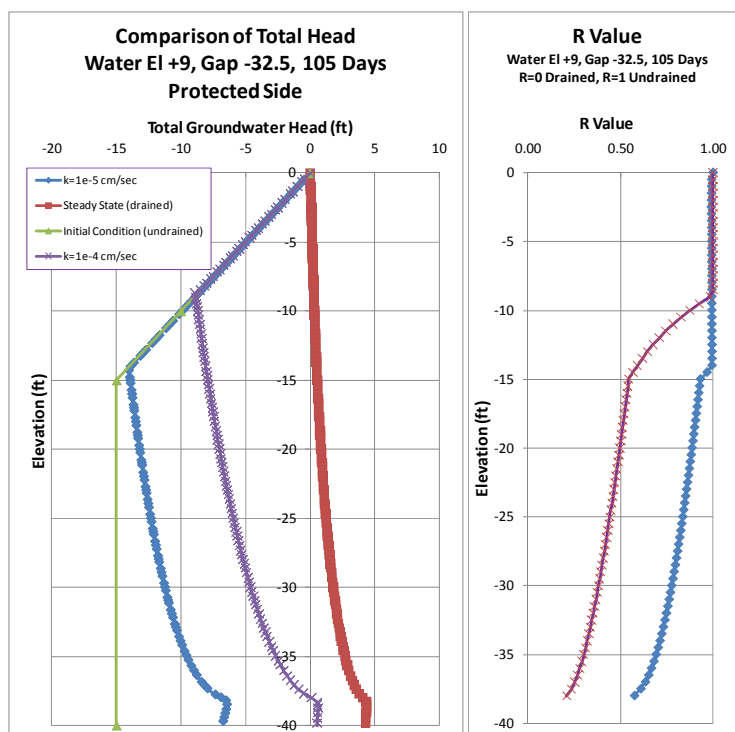


Figure 5.22. Comparison of total heads on the protected side (landside) to the drained and undrained conditions for water at el 9 ft.

5.8.4 Discussion of stresses and displacements

The normal effective stresses adjacent to the wall on the flood side and landside for a period of 31 days are shown in Figure 5.23. The stresses are compared for the two values of permeabilities, and the results show that the stresses at 31 days are relatively close to each other.

The normal effective stresses adjacent to the wall on the flood side and landside for a period of 60.7 days are shown in Figure 5.24. The stresses for the two values of permeability show more differences between them, especially on the flood side. The stresses are larger for the larger permeability.

The relative shear stress for the area around the wall at 105 days is shown in Figure 5.25. The water elevation at this time is 9 ft, and the gap extends to el -32.5. As can be seen from this figure, the relative shear stress (the applied shear stress divided by the maximum shear stress at failure) is largest at the tip of the gap. The region extending from the gap tip up to the surface of the soil has a large relative shear stress and resembles the geometry of an active failure wedge.

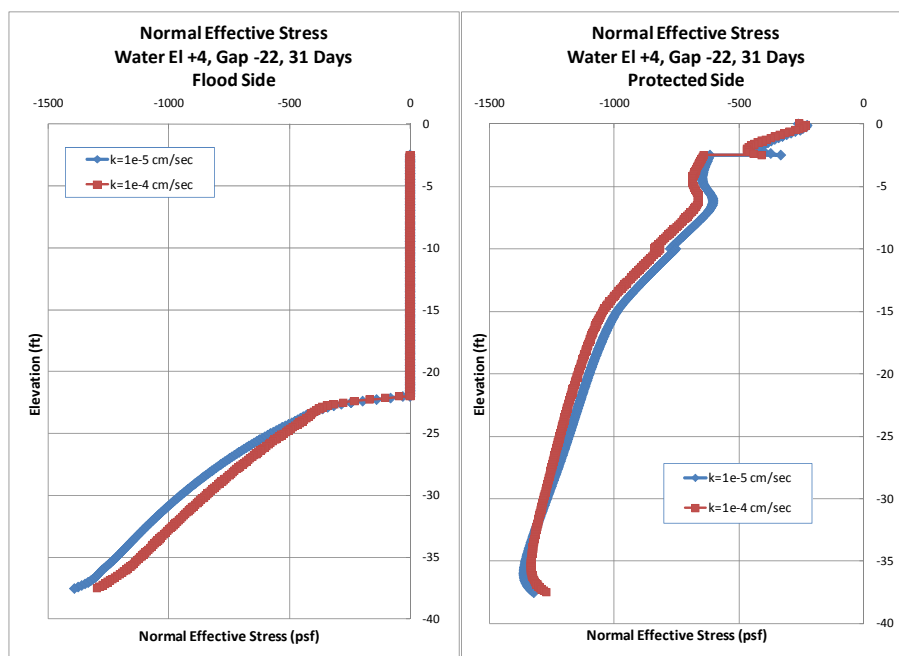


Figure 5.23. Normal effective stresses on the interface elements adjacent to the wall on the flood side and protected side (landside), 31 days.

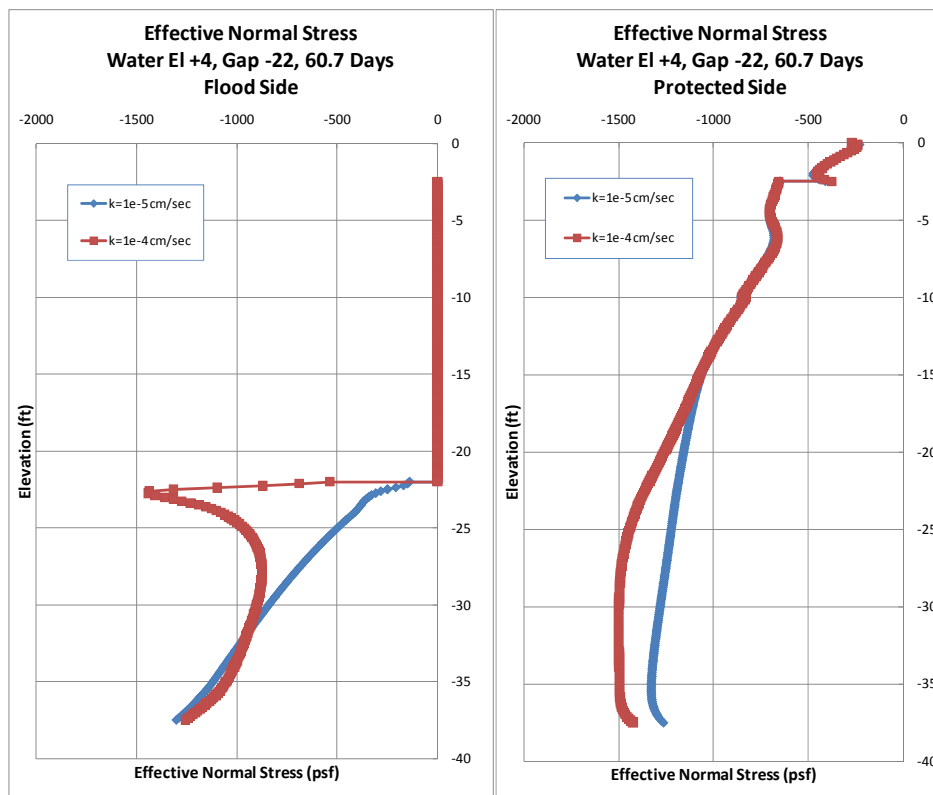


Figure 5.24. Normal effective stresses on the interface elements adjacent to the wall on the flood side and protected side (landside), 60.7 days.

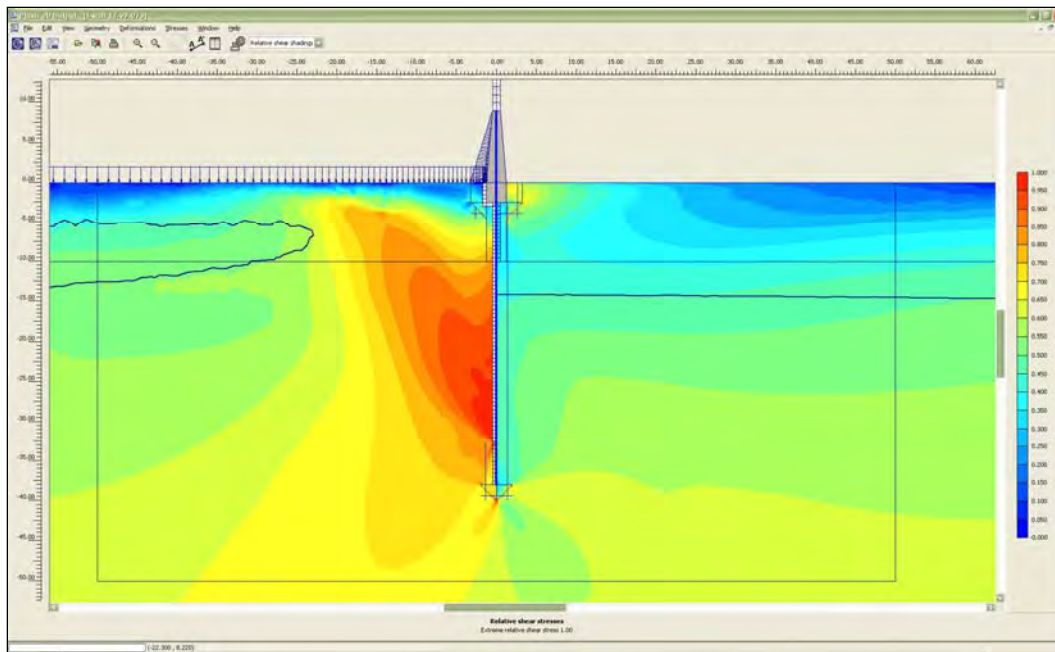


Figure 5.25. Relative shear stress for a water elevation of 9 ft, gap elevation of -32.5 ft, 105 days, and $k_x = 1 \times 10^{-5}$ cm/sec.

The total displacements of the soil and wall are shown in Figure 5.26. These displacements are for a water elevation of 9 ft at 105 days. The soil shows greater movement than the wall. The gap was modeled by inactivating soil elements adjacent to the wall, resulting in a void next to the wall. The soil can be seen essentially to fall into the void.

The maximum movement of the wall at the top of the concrete cap (el 0 ft) is 0.2 ft, as shown in Figure 5.27, for a water elevation of 9 ft. The displacement of the wall consists of horizontal and vertical movements. The tip of the wall actually has moved up and toward the landside. This figure also shows the total horizontal movements of the wall for various water elevations. For each water elevation, the top and bottom of the wall translated laterally.

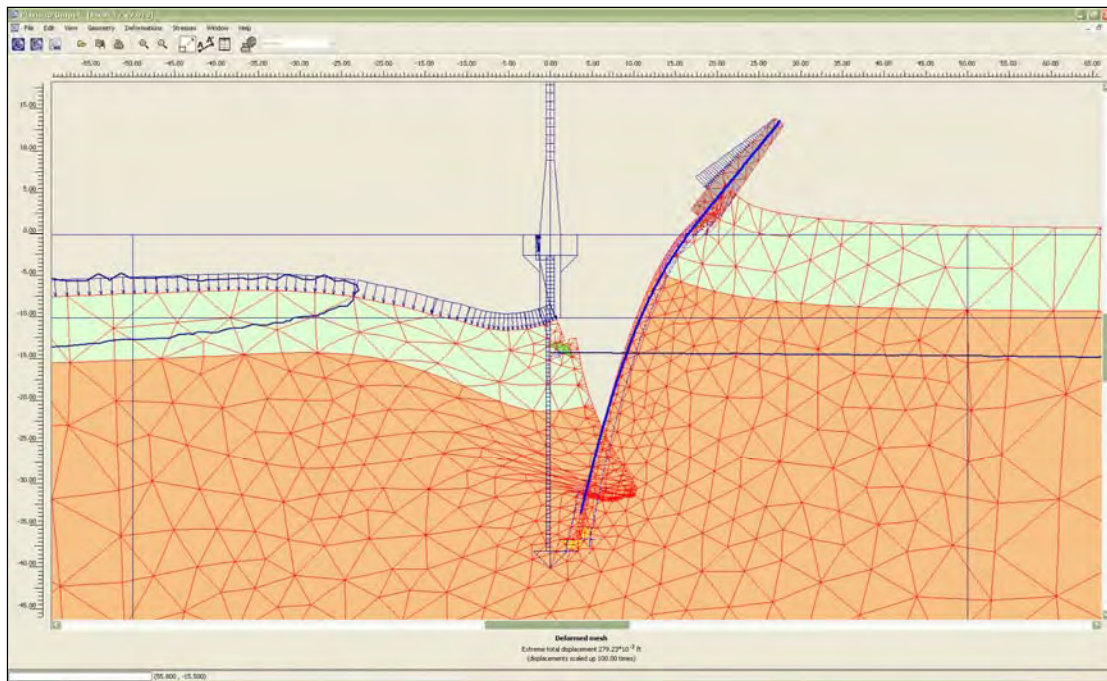


Figure 5.26. Total displacements for a water elevation of 9 ft, gap elevation of -32.5 ft, 105 days, and $k_x = 1 \times 10^{-5}$ cm/sec.

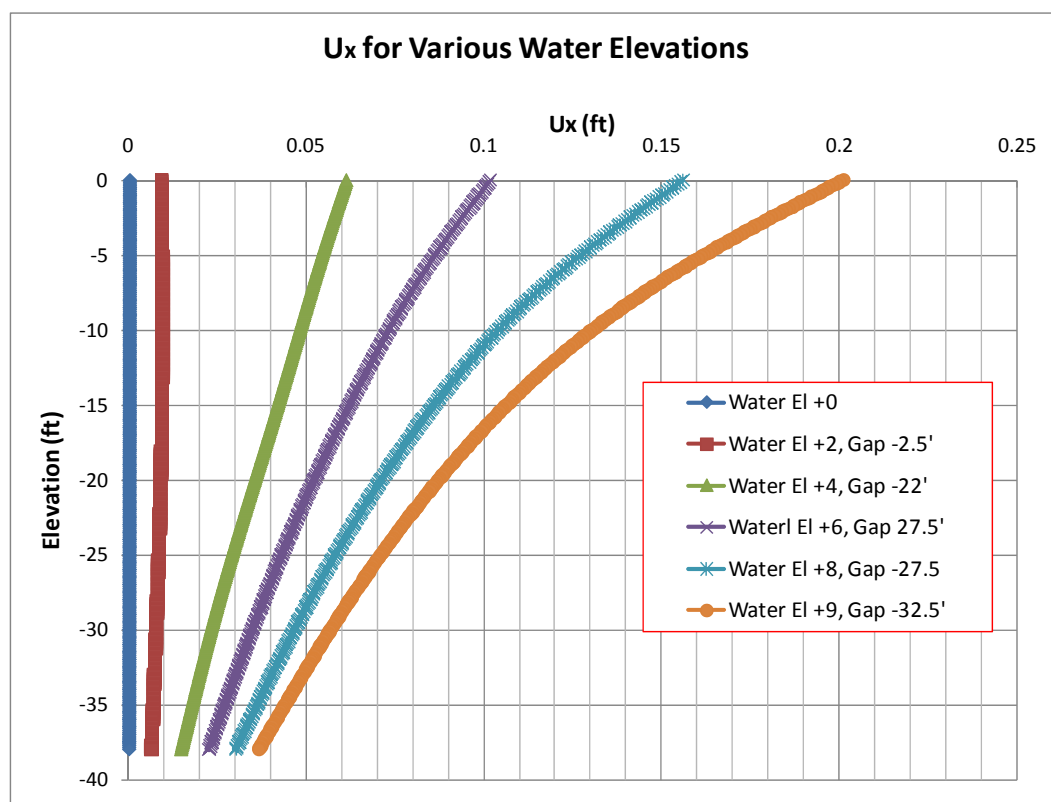


Figure 5.27. Total horizontal pile displacements versus water elevations.

6 Initial Investigation of the Effects of Geometry on I-wall Performance

6.1 Purpose of the analyses

This chapter summarizes the findings of an initial complete nonlinear SSI finite element analysis performed on an I-wall section embedded in a levee section. The focus was to investigate the effects that levee geometry (non-level ground surface) have on the phenomena of gap initiation and propagation along the soil-to-structure interface on the flood side of the I-wall. The effects that levee geometry has on the resulting deformation and stress conditions in the soil regime on both the flood side and landside of the I-wall were examined.

The following sections will describe the soil used in the analyses, the selection of stiffness and shear strength parameters, the conventional design of the I-wall, the analysis procedures employed, and the results of the complete nonlinear SSI analyses.

6.2 Overview of flood-site I-wall being analyzed

The geometry, key profile points and model features, and initial water elevations of the problem analyzed are shown in Figure 6.1. This I-wall on a levee site is a modification of the existing New Tiger Island floodwall in St. Mary Parish, Louisiana. The existing embedded depth for the floodwall is approximately four times the stick-up height of the wall. The I-wall ETL guidance development team requested that the analysis of an I-wall in a levee be made using the New Tiger Island levee geometry and shear strength properties, but with an embedment-to-stick-up height ratio of 2 to 1. The guidance team believed that using this ratio would allow for the investigation of near-limit state conditions.

The soil strata and corresponding undrained shear strength (S_u) values proceeding from the top to the bottom on the landside of Figure 6.2 include: a levee clay centerline region (el 14.8 ft to el 0.6 ft), underlain by a levee clay in the toe region (el 4.6 ft to el -33.0 ft); and, a free field clay material (el 4.6 ft to el -33 ft), underlain by another clay stratum (el -33 ft to EL -45 ft), followed by another clay layer (el -45 ft to el -60 ft), underlain by another clay stratum (el -60 ft to el -80 ft), which mantles a

lower clay deposit that extends to the bottom of the model (el -100 ft). The levee-clay material was assigned a moist unit weight of 105 pcf and a saturated unit weight of 110 pcf, with cohesion of 450 psf.

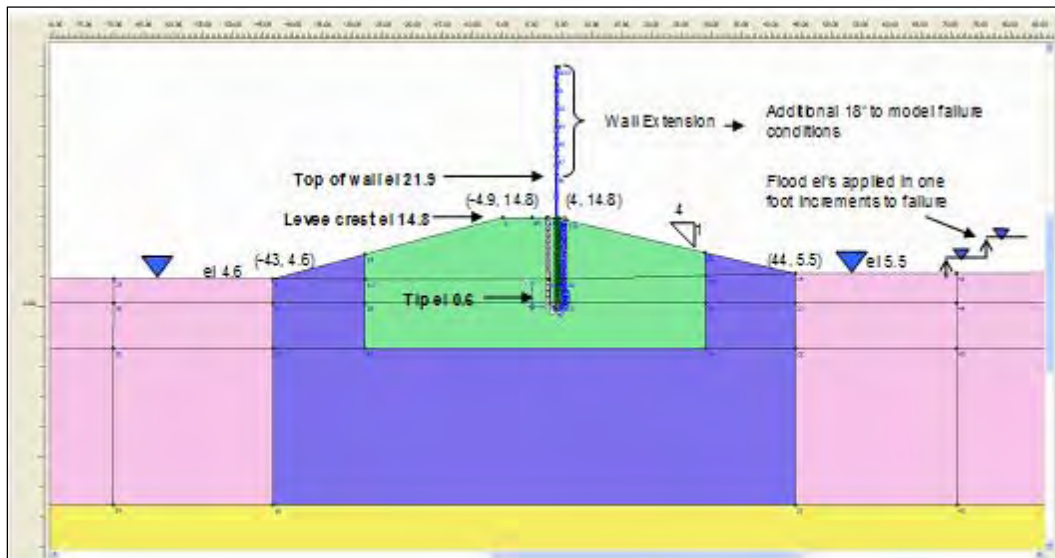


Figure 6.1. Modified New Tiger Island geometry and initial water table elevation of the problem.

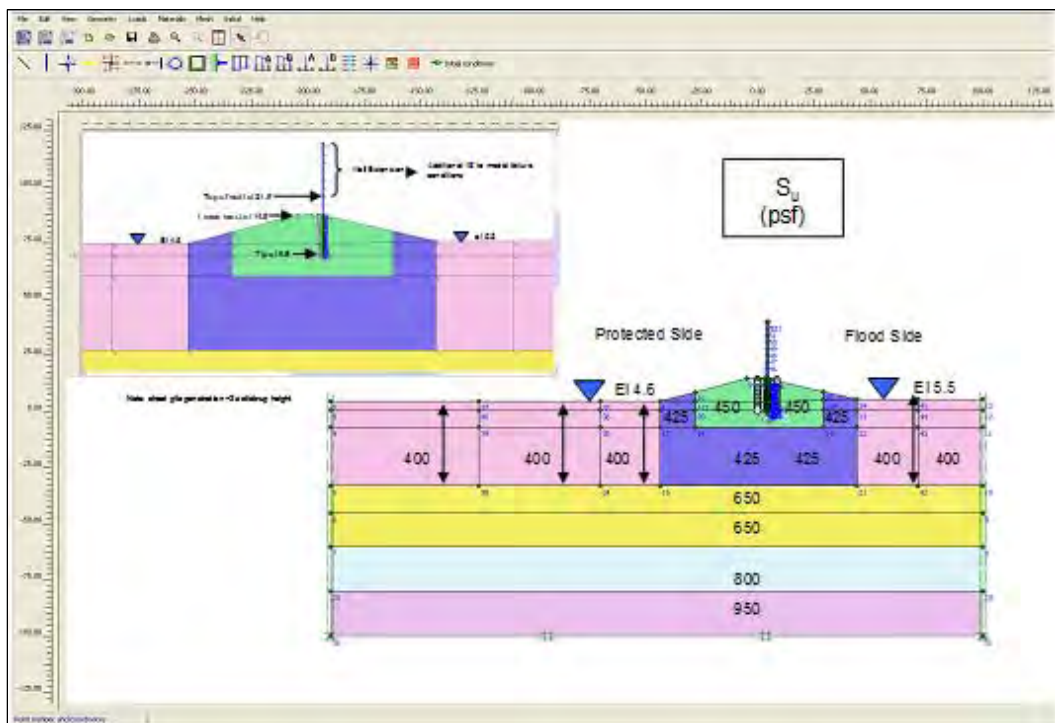


Figure 6.2. Variation in undrained shear strength (S_u) within the soil strata.

The S_u values and soil layering used in the SSI analyses are consistent with those used in recent slope analyses of this cross section. The existing I-wall has a top elevation of 21.9 ft consisting of a concrete cap and PZ 22 sheet pile to tip elevation of 0.6 ft. Multiple soil layers were used in the analyses to account for variation in soil strength and stiffness. The top 40 ft of soil represented an overconsolidated layer, while the underlying soil was assumed to be normally consolidated. The elevation of the soil surface on the landside of the I-wall is el 4.6 ft and on the flood side is el 5.5 ft. The water table for this problem was assumed to be at the landside and flood-side soil surface.

The designation for the soil used in the analysis is clay (CL), based on the Unified Soil Classification System (USCS). This soil has a liquid limit (LL) of less than 50 and a plasticity index of greater than 7 (Figure 2.2). The objective was to have a soil with enough plasticity to hold open a gap along the interface of the flood-side soil and I-wall.

6.3 Shear strength and stiffness values used in the analysis

The total stress (undrained) shear strength parameters were determined using the SHANSEP procedure (Ladd and Foott 1974). It assumes that the soil shear strength can be normalized by the effective overburden pressure. The effective overburden pressure is calculated at midlayer for each of the layers identified in Tables 6.1a to 6.1d for various locations in the 2-D cross section. The ratio of shear strength to effective overburden pressure (S_u/σ'_{vo}) is dependent on the overconsolidation ratio (OCR) and a fitting parameter (m), assumed to be 0.8, as shown in Equation 6.1:

$$\left(\frac{S_u}{\sigma'_{vo}} \right)_{OC} = \left(\frac{S_u}{\sigma'_{vo}} \right)_{NC} \bullet OCR^m, \quad (6.1)$$

where

- $(S_u/\sigma'_{vo})_{NC}$ = ratio of the undrained shear strength to effective overburden pressure for the normally consolidated condition;
- $(S_u/\sigma'_{vo})_{OC}$ = ratio of the undrained shear strength to effective overburden pressure for the over-consolidated condition.

Table 6.1.a. Summary of variations of $E_{u(oc)}$; near free field on landside - Section AA.

Layer			Short-Term (Undrained) Loading								$E_{u(oc)}$, psf
			Depth to Midlayer, ft	σ'_{vo} , psf	OCR	$(S_u/\sigma'_{vo})_{nc}$	$(S_u)_{nc}$, psf	$(S_u)_{oc}$, psf	$(S_u)_{oc}/(S_u)_{nc}$	E_u/S_u	
No.	Top El, ft	Bottom El, ft									
1	4.6	0.6	2	75.2	53.61	0.22	16.5	400	24.18	75	30,000
2	0.6	-7	7.8	293.3	9.78	0.22	64.5	400	6.20	75	30,000
3	-7	-33	24.6	925.0	2.33	0.22	203.5	400	1.97	255	102,000
4	-33	-45	43.6	1639.4	2.09	0.22	360.7	650	1.80	270	175,500
5	-45	-60	57.1	2147.0	1.49	0.22	472.3	650	1.38	292	189,800
6	-60	-80	74.6	2805.0	1.17	0.22	617.1	800	1.13	292	233,600
7	-80	-100	94.6	3557.0	0.95	0.22	782.5	950	0.96	292	277,400

Table 6.1.b. Summary of variations of $E_{u(oc)}$; near landside toe - Section BB.

Layer			Short-Term (Undrained) Loading								$E_{u(oc)}$, psf
			Depth to Midlayer, ft	σ'_{vo} , psf	OCR	$(S_u/\sigma'_{vo})_{nc}$	$(S_u)_{nc}$, psf	$(S_u)_{oc}$, psf	$(S_u)_{oc}/(S_u)_{nc}$	E_u/S_u	
No.	Top El, ft	Bottom El, ft									
1	6.7	4.6	2.	215.3	36.95	0.22	47.4	425	8.97	75	31,875
2	4.6	0.6	6.1	525.7	9.83	0.22	115.6	425	3.67	75	31,875
3	0.6	-7	11.9	801.8	4.44	0.22	176.4	425	2.41	255	74,375
4	-7	-33	28.7	1601.5	1.51	0.22	352.3	425	1.14	270	124,100
5	-33	-45	47.7	2505.9	1.37	0.22	551.3	650	1.18	292	189,800
6	-45	-60	61.2	3148.5	1.01	0.22	692.6	650	0.94	292	189,800
7	-60	-80	78.7	3981.5	0.96	0.22	875.9	800	0.80	292	233,600
8	-80	-100	98.7	4933.5	0.90	0.22	1085.4	950	0.69	292	277,400

Table 6.1.c. Summary of variations of $E_{u(oc)}$; near landside crest - Section CC.

Layer			Short-Term (Undrained) Loading								$E_{u(oc)}$, psf
			Depth to Midlayer, ft	σ'_{vo} , psf	OCR	$(S_u/\sigma'_{vo})_{nc}$	$(S_u)_{nc}$, psf	$(S_u)_{oc}$, psf	$(S_u)_{oc}/(S_u)_{nc}$	E_u/S_u	
No.	Top El, ft	Bottom El, ft									
1	14.8	4.6	5.1	535.5	15.53	0.22	117.8	450	3.82	75	33,750
2	4.6	0.6	12.2	1166.2	5.09	0.22	256.6	450	1.75	145	65,250
3	0.6	-7	18.0	1442.3	3.00	0.22	317.3	450	1.42	230	103,500
4	-7	-33	34.8	2241.9	1.17	0.22	493.3	425	0.81	292	124,100
5	-33	-45	53.8	3146.4	1.237	0.22	692.2	650	0.94	292	189,800
6	-45	-60	67.3	3788.9	0.92	0.22	833.6	650	0.78	292	189,800
7	-60	-80	84.8	4621.9	0.76	0.22	1016.8	800	0.69	292	233,600
8	-80	-100	104.8	5573.9	0.63	0.22	1226.3	950	0.61	292	277,400

Table 6.1.d. Summary of variations of $E_{u(oc)}$; near free field flood side - Section DD.

Layer			Short-Term (Undrained) Loading								$E_{u(oc)}$, psf
			Depth to Midlayer, ft	σ'_{vo} , psf	OCR	$(S_u/\sigma'_{vo})_{nc}$	$(S_u)_{nc}$, psf	$(S_u)_{oc}$, psf	$(S_u)_{oc}/(S_u)_{nc}$	Eu/Su	
No.	Top El, ft	Bottom El, ft									
1	5.5	0.6	2.5	92.2	41.6	0.22	20.3	400	19.94	75	30,000
2	0.6	-7	8.7	327.1	8.53	0.22	71.9	400	5.56	75	30,000
3	-7	-33	25.5	958.8	2.23	0.22	210.9	4005	1.90	240	96,000
4	-33	-45	44.5	1673.2	2.04	0.22	368.1	650	1.77	292	189,800
5	-45	-60	58.0	2180.8	1.46	0.22	479.8	650	1.35	292	189,800
6	-60	-80	75.5	2838.0	1.36	0.22	624.6	800	1.28	292	233,600
7	-80	-100	95.5	3590.0	1.26	0.22	789.9	950	1.20	292	277,400

From Ladd (1991), a value of 0.22 was assigned to $(S_u/\sigma'_v)_{NC}$ and a value of 0.8 for m , based on undrained Direct Simple Shear (DSS) test results. DSS results were chosen because they represented the predominant type of loading stress state of a passive soil wedge. Undrained triaxial compression (TX) tests better represent the loading stress state for an active wedge. Because the passive wedge was deemed more important for the stability of the wall, DSS strengths were used. To compute the effective overburden pressures, 105 pcf was used for the moist unit weight and 110 pcf was used for the saturated unit weight.

To characterize this site, OCR variation with depth was estimated at various sections in the 2-D cross section shown in Figure 6.3. The sections are labeled starting from Section AA near to free field on the landside to Section DD near to free field on the flood side. The OCR is the ratio of the preconsolidation pressure (P'_c) to the effective overburden pressure, σ'_v (P'_c/σ'_v).

Estimates of the variation of OCR with depth were computed using Equation 6.1. and the shear strength profile shown in Figure 6.2. The process.

1. The total stress (undrained) shear strength parameters are determined using the SHANSEP procedure-based Equation 6.1:

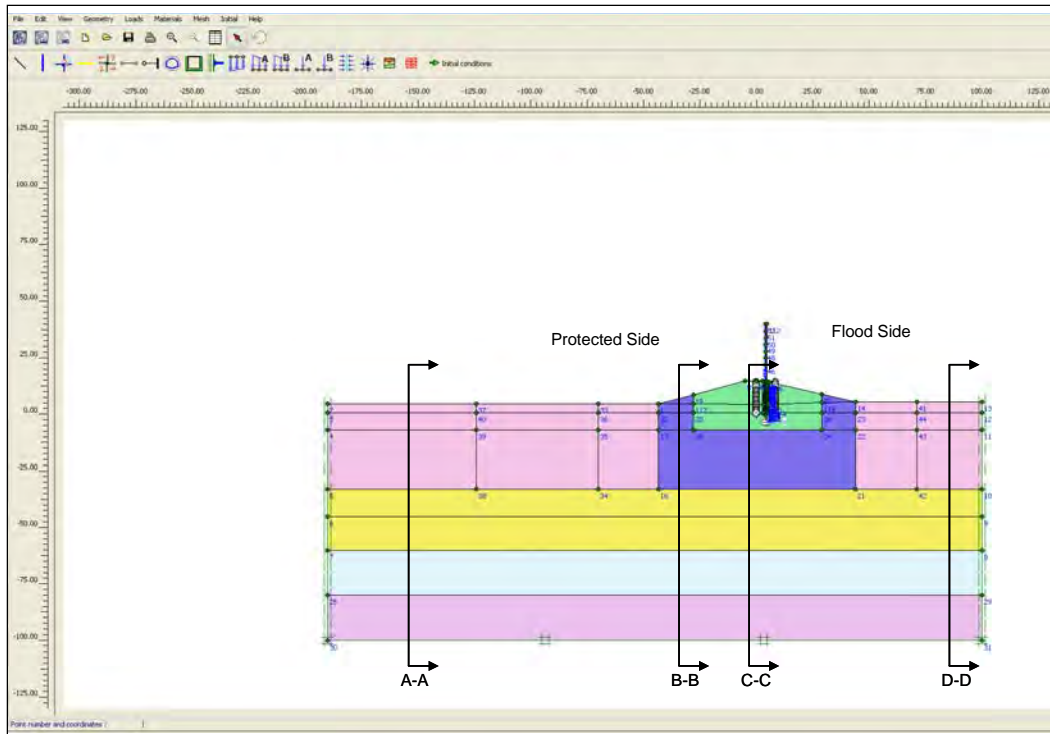


Figure 6.3. Sections used to estimate OCR and undrained stiffness variations.

$$\left(\frac{S_u}{\sigma'_{vo}} \right)_{OC} = \left(\frac{S_u}{\sigma'_{vo}} \right)_{NC} \bullet OCR^m. \quad (6.1)$$

2. Assign $\left(\frac{S_u}{\sigma'_{vo}} \right)_{NC} = 0.22$ and the fitting parameter m equal to 0.8. These values were based on DSS test results that represent the predominant type of loading stress state of a passive soil wedge.
3. Recall that

$$(S_u)_{NC} = \left(\frac{S_u}{\sigma'_{vo}} \right)_{NC} \bullet \sigma'_{vo}, \quad (6.2)$$

where σ'_{vo} is the effective vertical stress computed at the center of each soil layer. Substituting into Equation 6.2 yields

$$S_{u(NC)} = 0.22 \bullet \sigma'_{vo}. \quad (6.3)$$

4. For this finite element analysis, $(S_u)_{OC}$ values were set equal to field values used in slope stability analysis, thus

$$(S_u)_{OC} = \text{field values of } S_u \quad (6.4)$$

Substituting values from Equations 6.3 and 6.4 into Equation 6.1 and solving for the ratio $\left(\frac{(S_u)_{OC}}{(S_u)_{NC}} \right)$ yields:

$$\left(\frac{(S_u)_{OC}}{(S_u)_{NC}} \right) = OCR^{0.8}. \quad (6.5)$$

Solving for OCR yields:

$$OCR = 10^{\frac{10}{8} \cdot \log_{10} \left[\frac{(S_u)_{OC}}{(S_u)_{NC}} \right]}. \quad (6.6)$$

The values of OCR were computed at the center of each layer and are tabulated in Tables 6.1a through 6.1d. The variation of OCR with depth at selected cross section is shown in Figure 6.4. OCR effects (i.e., values greater than 1) are indicated at a depth of approximately 25 ft below the ground surface in the levee crest region and at depths near 60 ft below the ground surface at the other sections.

6.4 Shear strength and stiffness properties used in the complete SSI analysis

A complete SSI analysis of the I-wall section shown in Figure 2.1 was performed using the 2-D version of the PC-based finite element program PLAXIS. A complete SSI analysis is considered to provide the most reasonable estimate for deformation response of a soil-structural system involving nonlinear material behavior. Soil stresses, I-wall deflections, shear forces, and bending moments internal to the sheet piling also are computed in complete SSI analyses. The finite element method employed required certain input material properties for the selected soil constitutive models. The PLAXIS nonlinear Hardening Soil (HS) constitutive model was used to model all soil elements. This constitutive model provides for nonlinear

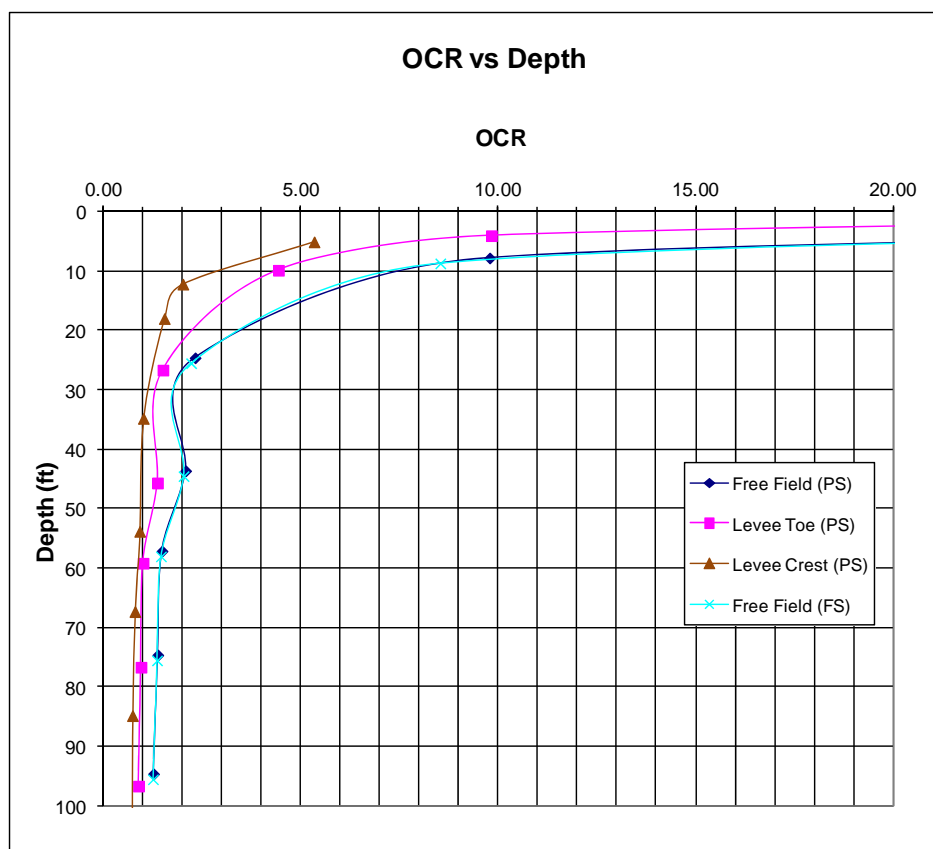


Figure 6.4. Variation in OCR with depth at selected cross sections.

stress-strain response for soil elements during loading. Elastic plate elements were used to model the steel sheet pile and the concrete I-wall section. To process bending moment and shear distribution results more efficiently, plate elements were used to model the concrete I-wall.

PLAXIS can perform analyses in terms of effective or total stress soil strength parameters. For the analysis described herein, total stress soil strength parameters were used to characterize this clay site. The average of values of S_u , assumed to be constant over a given depth, shown in Figure 6.2 also were used in the complete SSI analysis to approximate variation in S_u with depth. The Figure 2.5 correlation by Duncan and Bursey (2007) was used to estimate the variation of undrained secant modulus in clay with depth. The correlation is based on its undrained shear strength, plasticity index, and overconsolidation ratio using Equation 2.2, where: E_{us} is the undrained secant modulus, K is a factor determined from field measurements, and S_u is undrained shear strength.

Tables 6.1.a through 6.1.d summarize the computation of E_{us} with depth using the average values of the given variation of S_u and computed value of OCR using Equation 6.6. Consistent results of increased stiffness values with depth were indicated. These values of E_{us} were used to estimate the variation in the PLAXIS input stiffness parameter (E_{50}^{ref}) at the selected locations in the 2-D cross section. E_{50}^{ref} is a secant modulus at 50 percent of the principal stress difference ($\sigma_1 - \sigma_3$). Figure 6.5 shows the variation of undrained stiffness (E_u) with depth at various cross sections. A comparison of shear strength and stiffness values for various I-wall and levee sections is shown in Table 6.2. It is noted that the shear strength of the levee material for the New Tiger Island I-wall is much less than the shear strengths at other New Orleans sections. Previous studies on I-wall behavior have indicated that low shear strength values in the levee region have implications on numerical analysis results and convergence.

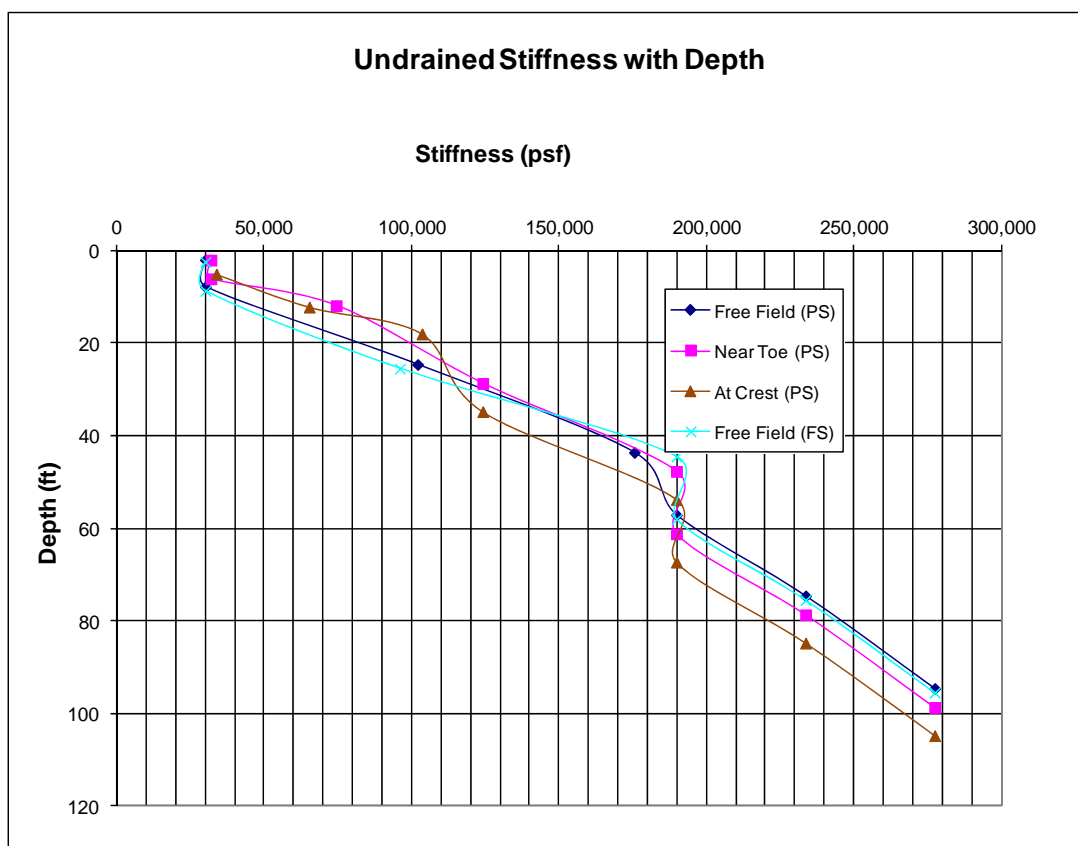


Figure 6.5. Variation in undrained stiffness (E_u) with depth at different modified New Tiger Island I-wall sections.

Table 6.2. Comparison of shear strength (S_u) and stiffness values (E_u) for various New Orleans I-wall and levee sections.

Region	Model					
	17th Street		Orleans		New Tiger Island	
	S_u , psf	E_u , psf	S_u , psf	E_u , psf	S_u , psf	E_u , psf
Levee	900	20,000	1500	72,000	450	33,750
Peat (Foundation)	400	10,000	650	31,200	N/A	N/A
Near Pile Tip	300	2000	650	31,200	450	65,250
Free Field (GS)	300	10,000	400	19,200	400	30,000

Three additional HS parameters were assigned: the unload-reload stiffness (E^{ref}_{ur}), which is set equal to three times E^{ref}_{50} ; the exponent ($m = 0.8$); and the failure ratio ($R_f = 0.9$). Values of the coefficient of friction between the sheet pile and the soil and between the concrete cap and the soil were selected from values published by Potyondy (1961) and are the same ones shown in Table 2.5. The properties of the concrete I-wall section were modeled by elastic plate elements with the same properties given in Tables 2.6 and 2.7. The sheet pile was represented by elastic plate elements with the same properties given in Table 2.8.

6.5 Discussion of finite element analyses

6.5.1 Finite element model

The finite element analysis was performed using the 2-D version of the nonlinear incremental construction finite element program PLAXIS. The finite element mesh used in the analysis is shown in Figure 6.6. Several key modeling features are used. The sheet-pile wall and the concrete I-wall section were modeled by elastic plate elements. Plate elements were used to model the concrete I-wall to process bending moment and shear distribution results more efficiently. Interface elements were placed along both sides of the sheet-pile wall. Extensions of the interface elements are provided at the bottom of the sheet-pile wall at el 0.6 ft. This was done to alleviate stress concentrations that occur at the corners of the geometry during loading. A 2-D element extension was added above the wall to provide for additional flood loading height. The mesh was structured to provide nodal points at 1-ft raises of the water table. The soil elements beside the sheet-pile wall on the flood side were 0.5 ft in height. This allowed for the assignment of 1-ft raises in water and modeling of the gap to within 0.5 foot. The regions of uniform color reflect soil clusters used to define the mesh and assign soil regions with common properties. The mesh

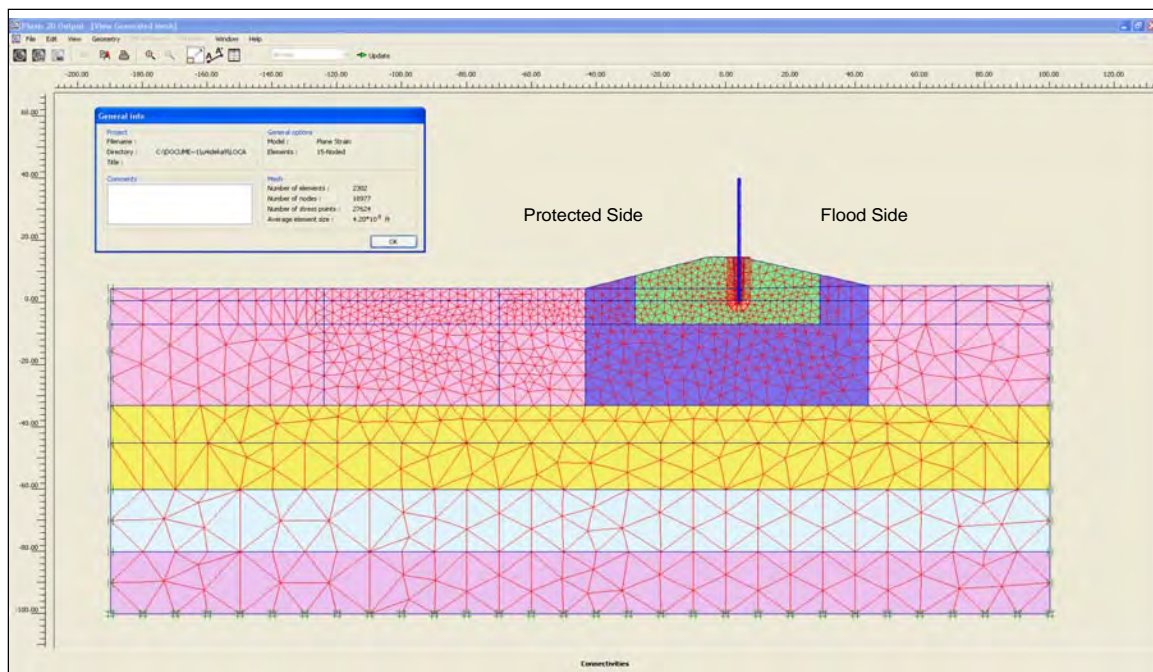


Figure 6.6. PLAXIS finite element mesh of the I-wall, levee, and foundation.

is composed of 23 elements, 18,977 nodes, with 27,624 stress points. The mesh consists of 15-node triangular elements to model the soil, plate elements to model the bending effects of the I-wall and sheet-pile wall, and interface elements to model SSI between the sheet-pile wall and the adjacent soil elements.

6.5.2 Gap initiation and propagation criterion

A hydraulic fracturing criterion is applied to determine whether a gap will develop and if it will spread down the soil-to-I-wall interface. In this procedure of analysis, the total horizontal stress computed by PLAXIS at the ground surface soil-to-I-wall interface is compared to the hydrostatic water pressure developing at the top of the ground surface caused by the presence of the specified flood pool elevation. If the hydrostatic water pressure of the flood pool (the demand) exceeds the total horizontal stress (the capacity), a gap will initiate at the ground surface, along the soil-to-I-wall interface. This criterion is discussed in detail in Chapter 2.

6.6 Results of the finite element analyses

6.6.1 Initial stresses

The initial total stress state within the finite element mesh was established using the Mohr-Coulomb (MC) soil model with steady-state canal water

elevation at el 5.5 ft. and the at-rest soil conditions for a level ground surface. For a nonlevel soil surface, PLAXIS recommends using the gravity loading option. Load input for the gravity loading is specified in PLAXIS by means of the total multiplier method, where gravity loading is applied incrementally until the total multiplier (M_{weight}) equals 1. The stress-strain model was changed to the HS model prior to any additional loading steps. Figure 6.7 shows a plot of exaggerated displacements of the mesh after the material type change to the HS model. The levee material shown in grey and cyan at the toe region compresses the underlying foundation soil. Also, the settlements of the foundation soils generally are symmetric about the I-wall. The resulting computed fraction of mobilized shear strength (referred to as relative shear stress in PLAXIS output) for the initial stress condition is shown in Figure 6.8. The relative shear stress is less than 1 in the levee and foundation soil regions in proximity of the I-wall. These results indicated there is reserved shear strength in these soil regimes at this stage of loading. This is consistent with slope stability results that indicated a stable cross section.

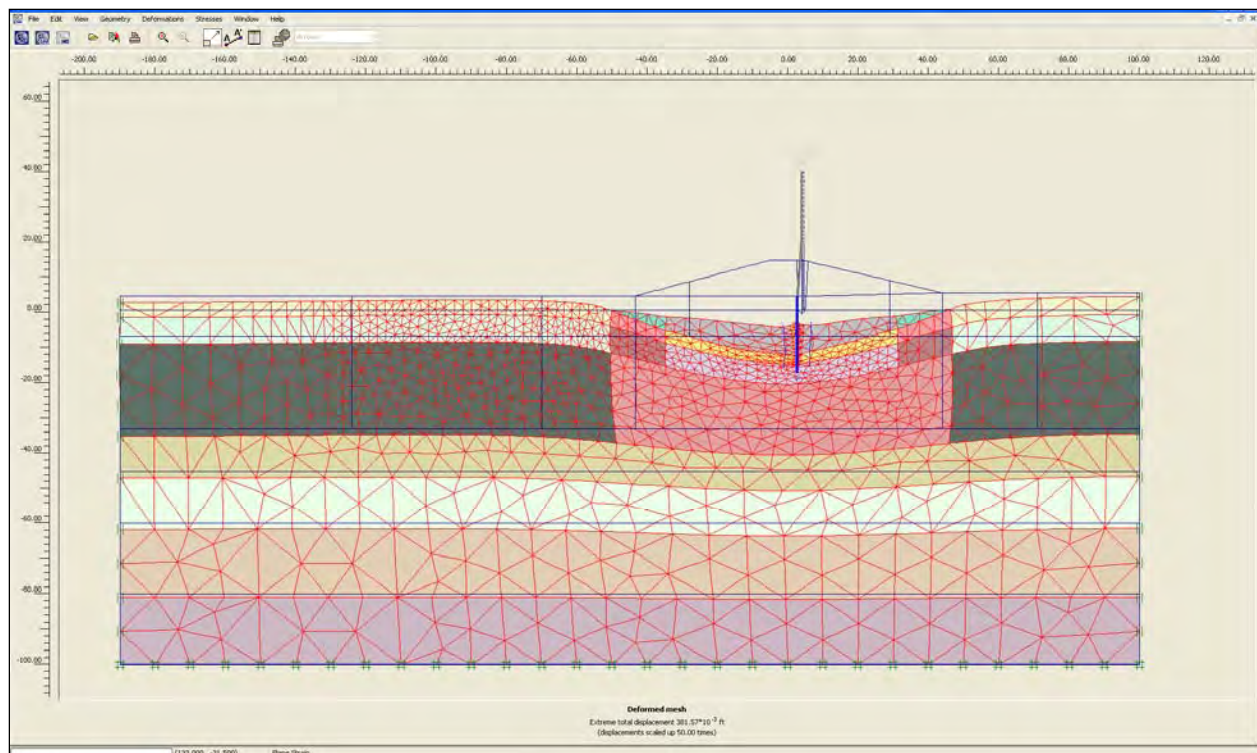


Figure 6.7. Exaggerated displaced mesh plot at initial stress conditions.

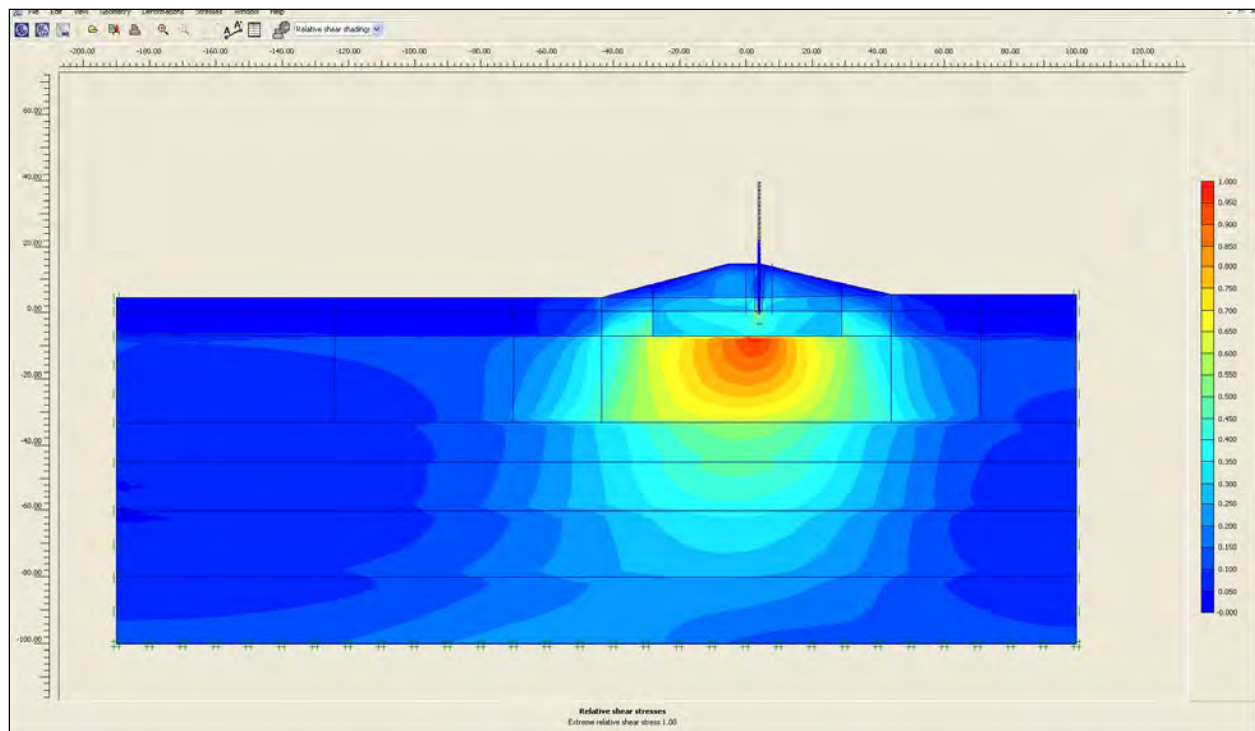


Figure 6.8. Fraction of relative shear stresses at initial conditions.

6.6.2 Gap initiation and propagation results

As stated, the focus of this study was to investigate the phenomena of gap initiation and propagation along the flood side of the soil-to-I-wall interface and to study the effects of gap initiation and propagation on the resulting deformation and stress conditions in the soil regime on both the flood side and landside of the I-wall system. Modeling of the flood loading commenced in the complete SSI analysis after the total initial stresses state was established within the mesh for an assumed steady-state water elevation at the flood-side ground surface (el 5.5 ft). In order to track the formation and propagation of a gap, the flood loading was applied in 1-ft incremental raises of the water level. Hydraulic fracturing criterion is used to estimate a gap formation and its propagation. This procedure compares the total normal earth pressures due to the flood pool acting on the wall at a given depth to the hydrostatic water pressure acting at the corresponding depth. A gap is formed when the total horizontal earth pressure (the capacity) is less than the water pressure due to the flood pool acting at the corresponding depth (the demand). Next, hydrostatic water pressure is applied over the depth of gap, and this hydrostatic water pressure at the new, deeper gap depth is compared to the total horizontal earth pressure. Gap propagation is terminated at the depth at which the demand is less than the capacity. Complete SSI analysis results were examined for various

water elevations and gap depths. Figure 6.9 shows the progression of the gap as the water level against the I-wall is increased. For a rise in flood elevation somewhere between 14.5 and 14.8 ft (i.e., top of levee crest), the gap initiates and propagates to a depth of approximately 4 ft. Then, boundary water pressures are applied to the I-wall, including within the gap, at the flood elevation of 14.8 ft. The gap extends to a depth of 10 ft at water el 16.8 ft. At water el 17.8 ft, the gap extends to a depth of 14.2 ft (tip of sheet pile) and gap elevation remains constant until water el 21.9 ft (top of I-wall).

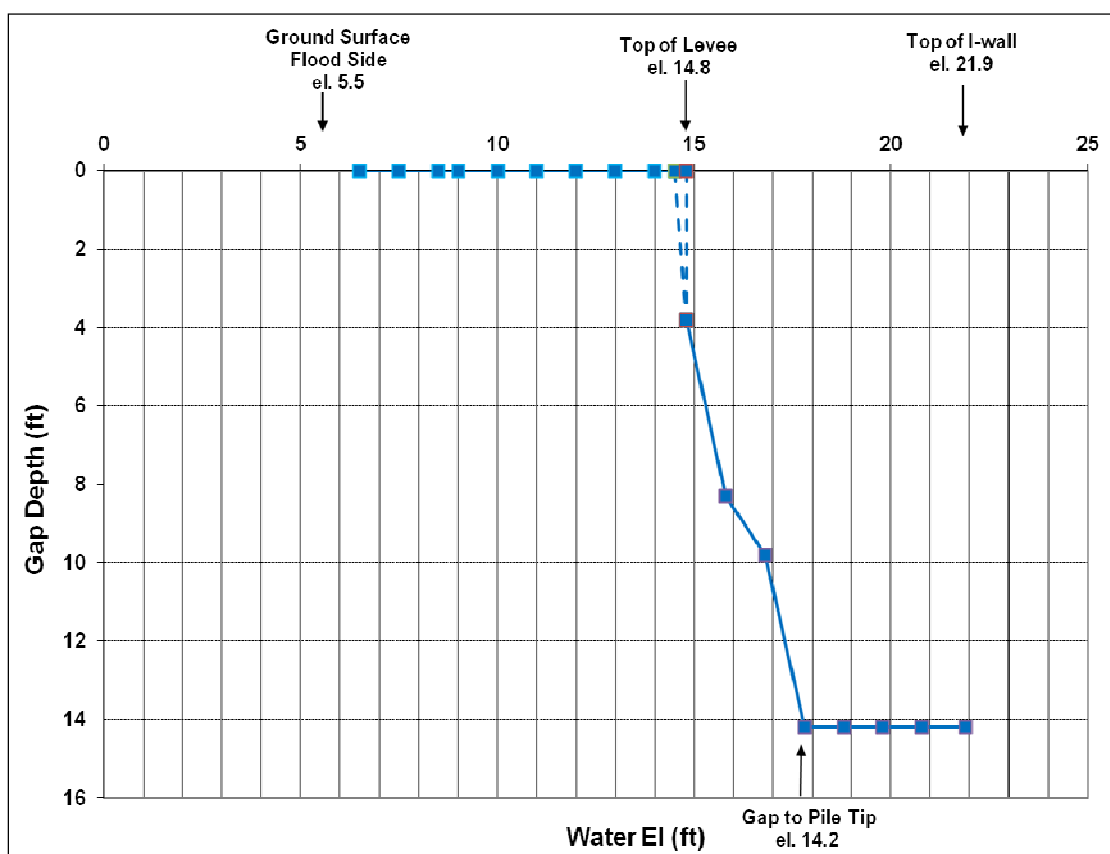


Figure 6.9. Progression of gap versus water elevation.

6.6.3 Discussion of displacements and stresses

The total (exaggerated) nodal displacements within the finite element mesh (both soil and wall) near the I-wall are shown in Figure 6.10. These displacements are for a design water elevation of 21.9 ft (top of the I-wall) with a gap depth to el 0.6 ft (tip of I-wall). Note that the nodal displacements are increased by a factor of 20 to show the deformed mesh relative to its initial position and to show the extent of the gap. The gap is modeled by deactivating the soil elements adjacent to the wall. The general trend of the

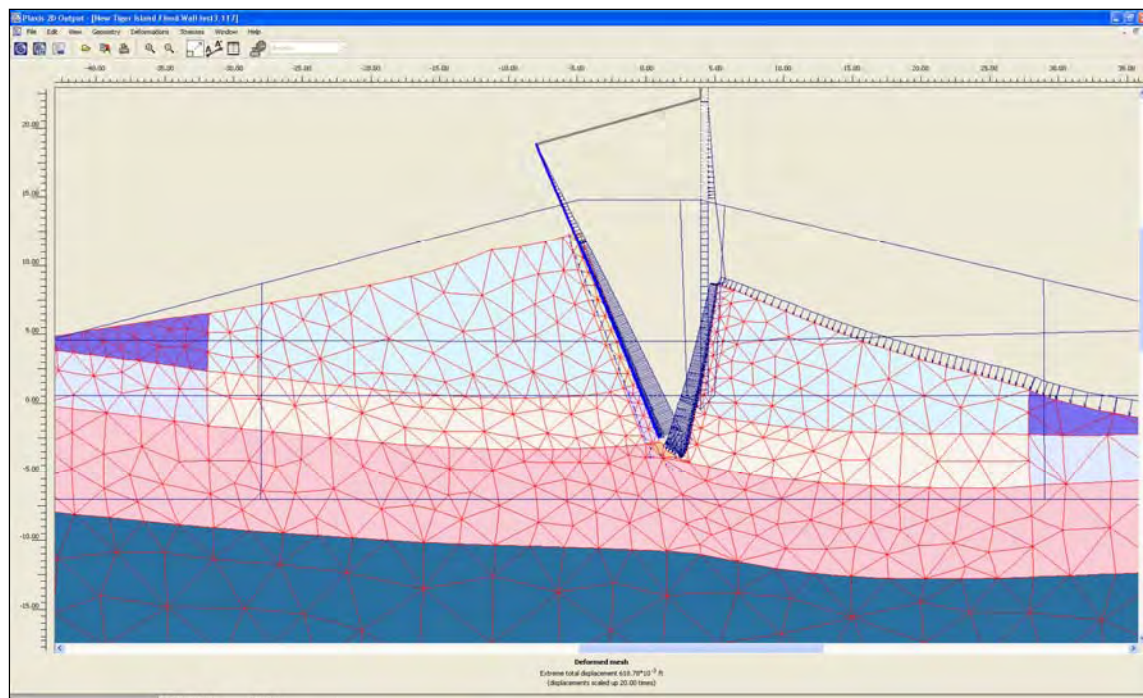


Figure 6.10. Exaggerated deformed mesh after flood elevation to 21.9 ft (top of I-wall), and the gap extends to pile tip (el 0.6 ft).

deflections was toward the landside because of the applied boundary water pressures on the flood side. The wall has a greater movement than the soil at this loading phase. The maximum wall displacement is approximately 7.2 in. at the top of the wall. The displacement of the wall consists of both horizontal and vertical movements. The tip of the wall has moved slightly up and toward the landside.

Figure 6.11 shows a plot of horizontal displacements of I-wall versus floodwater elevation at three points along the wall. The points monitored in the analysis were the top of the I-wall at el 21.9 ft, at the levee crest el 14.8 ft, and at the sheet-pile tip el 0.6 ft. As shown, the deflections of the wall up to flood el 14.8 ft (after gap initiation) consist of very small translation toward the flood side or approximately zero translation. As the water elevation increases, the top of the wall has consistent deformations compared to the ground and much larger deformations than the pile tip. This implies that the wall is undergoing rotation along with translation. However, this analysis did not indicate kickback of the pile tip toward the landside.

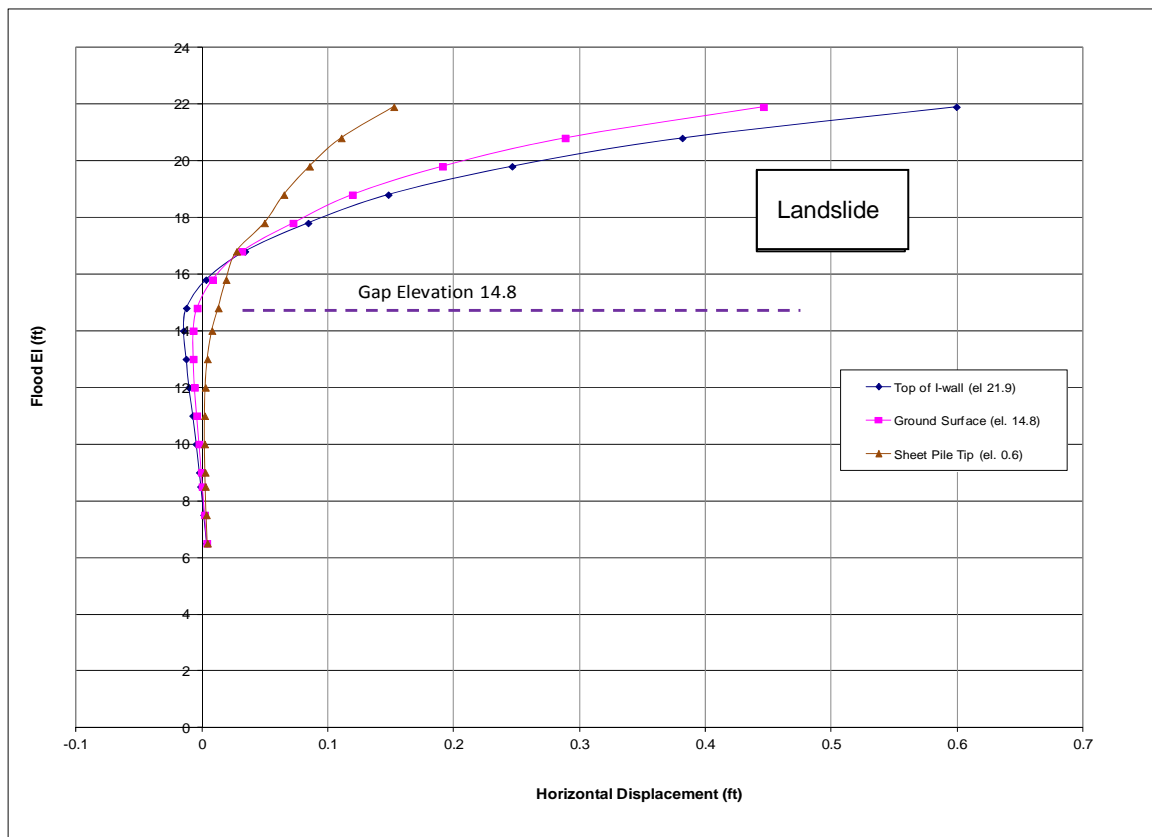


Figure 6.11. Displacement results versus flood elevations at three locations along the wall.

Figure 6.12 shows a plot of relative horizontal displacements of I-wall versus floodwater elevation at the ground surface. Relative displacements were computed at this location to provide results to a companion research effort, HQUSACE (2011), focusing on risk and reliability assessments of I-walls. Relative displacements were computed by subtracting the displacements of the sheet-pile tip from the sheet-pile displacements at the ground surface for a given floodwater elevation. The maximum computed relative horizontal displacement of the wall at the ground was approximately 3.3 in. These computed relative horizontal displacements (U_x) also are reported in Table 6.3.

Figure 6.13 shows a plot of horizontal displacement vectors after the PLAXIS Phi/c reduction procedure. On the flood side, displacements commence near the flood-side toe region and extend downward to an elevation of -30 ft. On the landside, horizontal displacements extend beyond the toe region. The resulting computed factor of safety was equal to 1.595. The zone of large shear strains after the Phi/c reduction load step is shown in Figure 6.14. This region of large shear strains is an indication of this soil regime reaching full mobilization of its available shear strength.

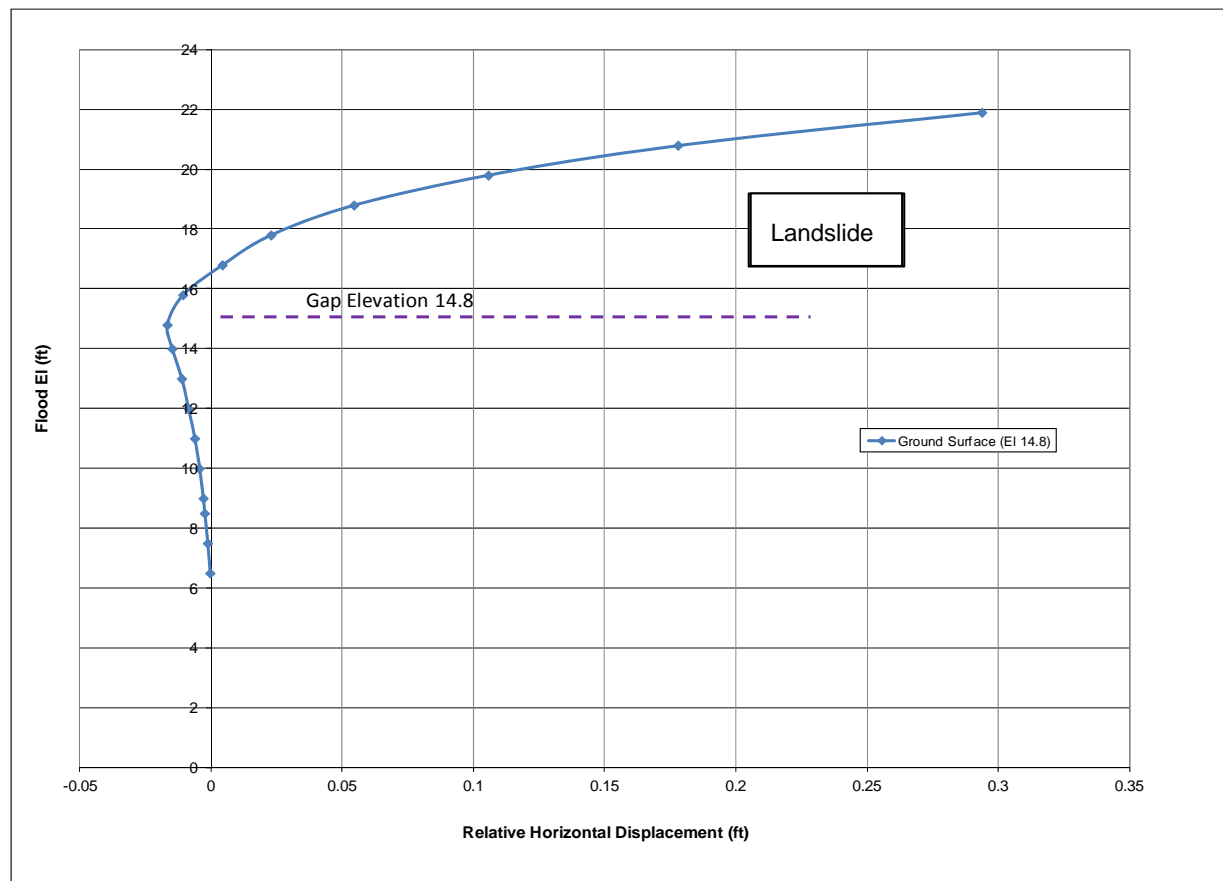


Figure 6.12. Relative horizontal displacement results versus flood elevations at the ground surface.

Figure 6.15 shows the results from the original New Tiger Island slope stability results for a d/h of 4.0. The PLAXIS complete SSI analysis was made of an I-wall embedded in this levee geometry, but possessed a d/h ratio of 2.0 at the request of the ETL guidance development team. Soil shear strengths were unchanged for the PLAXIS analysis. The resulting Figure 6.15 critical slip surface is located deep within the levee foundation soil region with a computed factor of safety equal to 1.68. The PLAXIS analysis of the I-wall with the d/h equal to 2.0 resulted in a computed factor of safety equal to 1.595 by the Φ/c reduction procedure. Observe that the location of the Figure 6.15 critical slip plane has marked similarity to the Figures 6.13 and 6.14 soil regions from the PLAXIS analysis.

Figure 6.16 shows the results from the modified New Tiger Island slope stability results for a d/h of 2.0 using UTexas4. This provided a direct comparison with the PLAXIS complete SSI analysis. The gap was modeled by removing the flood-side soil down to the sheet-pile tip and applying hydrostatic water pressures normal to the I-wall/sheet-pile wall face. The resulting Figure 6.16 critical slip surface is shallower within the levee

foundation soil region, commences at the sheet pile tip and results in a computed factor of safety equal to 1.541. This value is consistent with the PLAXIS analysis result using the Phi/c reduction procedure (i.e., 1.595).

Table 6.3. Summary of relative horizontal displacements (U_x) of I-wall at the ground surface.

U_x at Ground Surface, ft	U_x at Pile Tip, ft	Relative Displacement at Ground Surface, ft	Flood el, ft	Gap depth, ft
0.0039	0.0044	-0.0004	6.5	0
0.0021	0.0035	-0.0014	7.5	0
0.0003	0.0028	-0.0025	8.5	0
-0.0004	0.0026	-0.0030	9	0
-0.0024	0.0022	-0.0045	10	0
-0.0041	0.0022	-0.0063	11	0
-0.0060	0.0027	-0.0087	12	0
-0.0069	0.0043	-0.0112	13	0
-0.0069	0.008	-0.0149	14	0
-0.0038	0.013	-0.0168	14.8	3.8
0.0085	0.0192	-0.0107	15.8	8.3
0.0317	0.0275	0.0042	16.8	9.8
0.0725	0.0497	0.0228	17.8	14.2
0.1196	0.0652	0.0544	18.8	14.2
0.1911	0.0855	0.1056	19.8	14.2
0.2886	0.1107	0.1779	20.8	14.2
0.4462	0.1525	0.2937	21.9	14.2

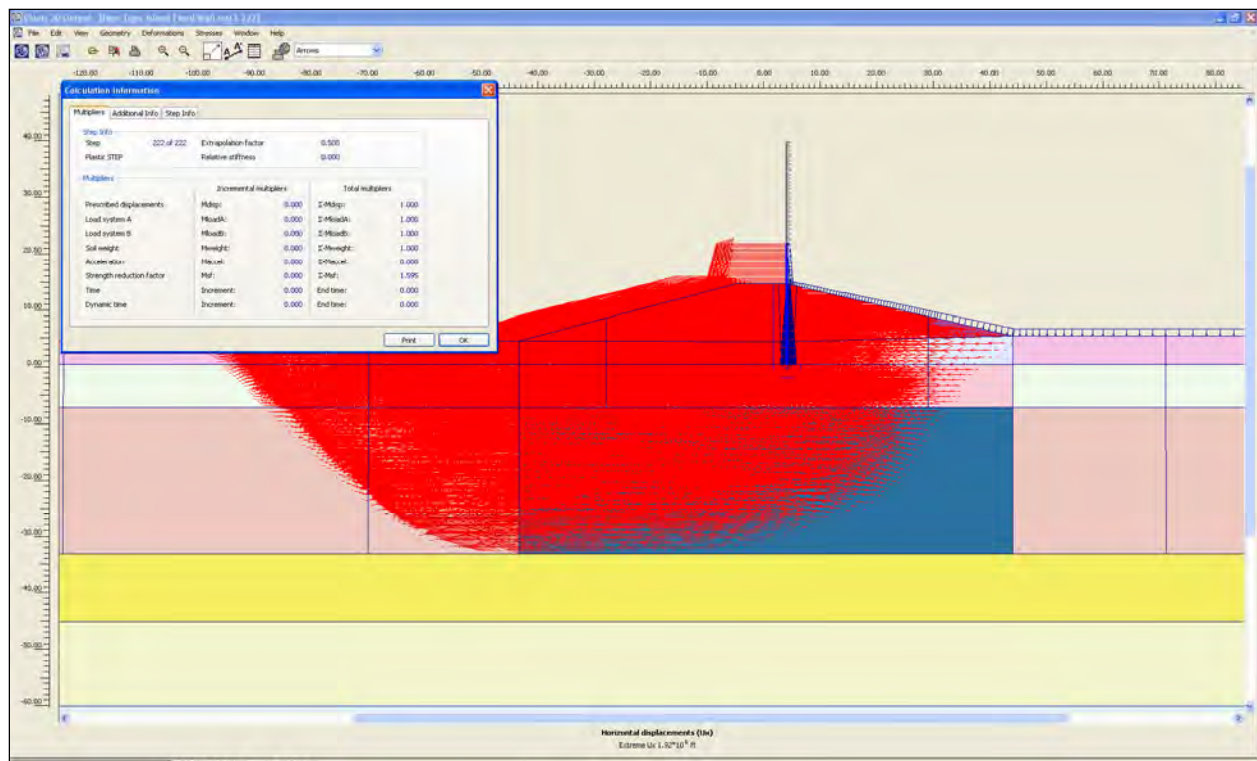


Figure 6.13. Horizontal displacement vectors after Φ/c reduction; computed factor of safety = 1.595, recall: (pile tip at el 0.6) $d/h = 2.0$.

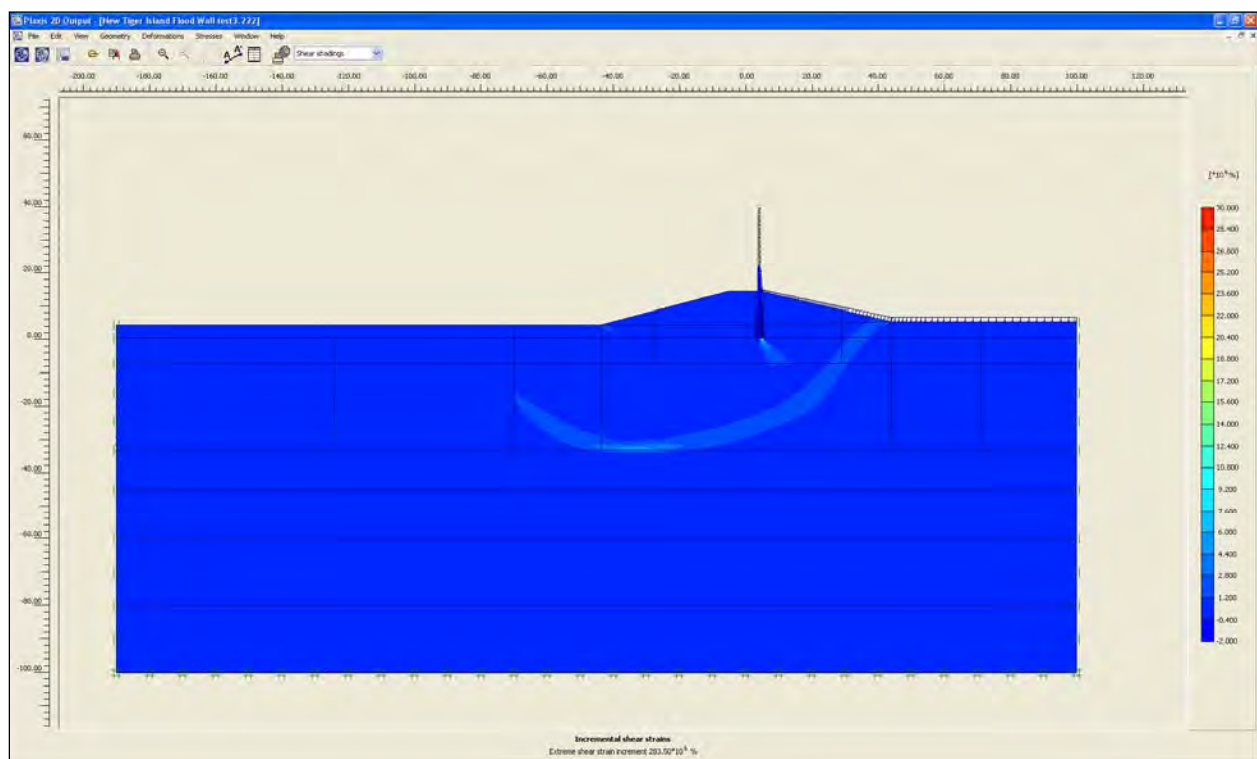


Figure 6.14. Incremental shear strains after Φ/c reduction (computed factor of safety).

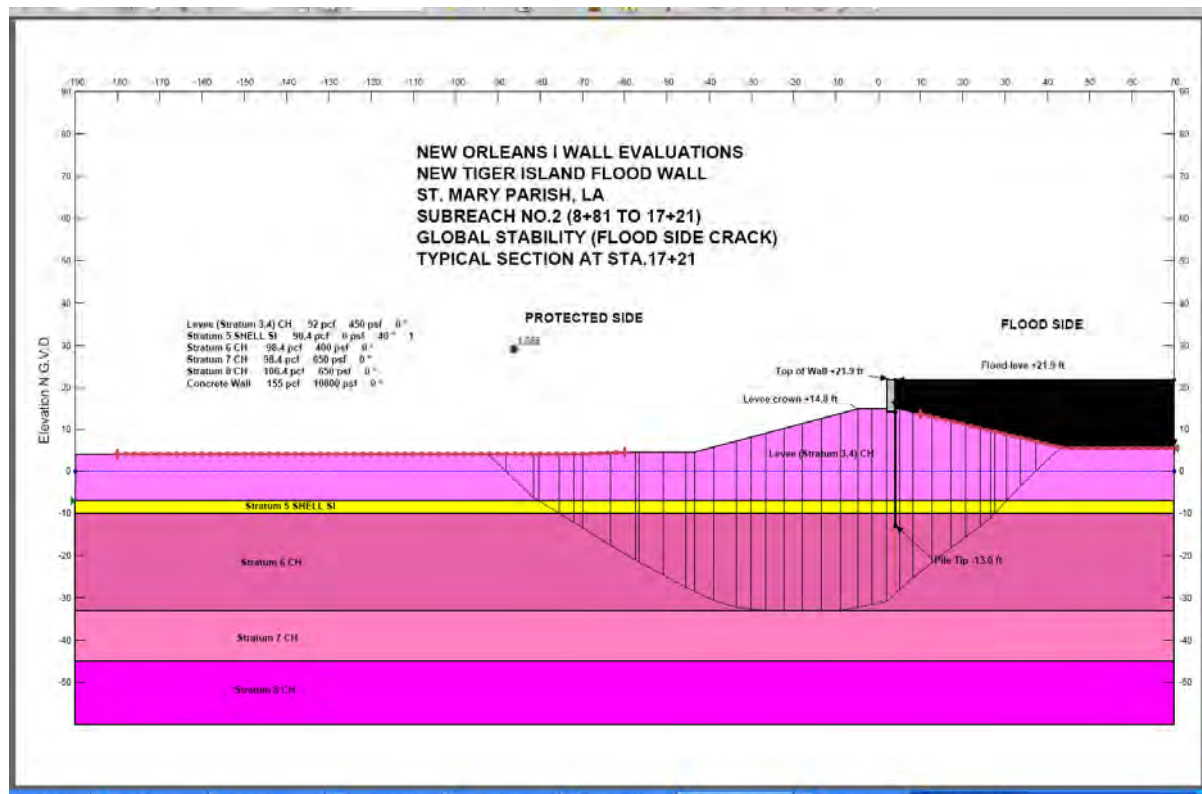


Figure 6.15. Original New Tiger Island floodwall (pile tip at el -13 ft) $d/h = 4.0$; SlopeW results, $FS = 1.68$.

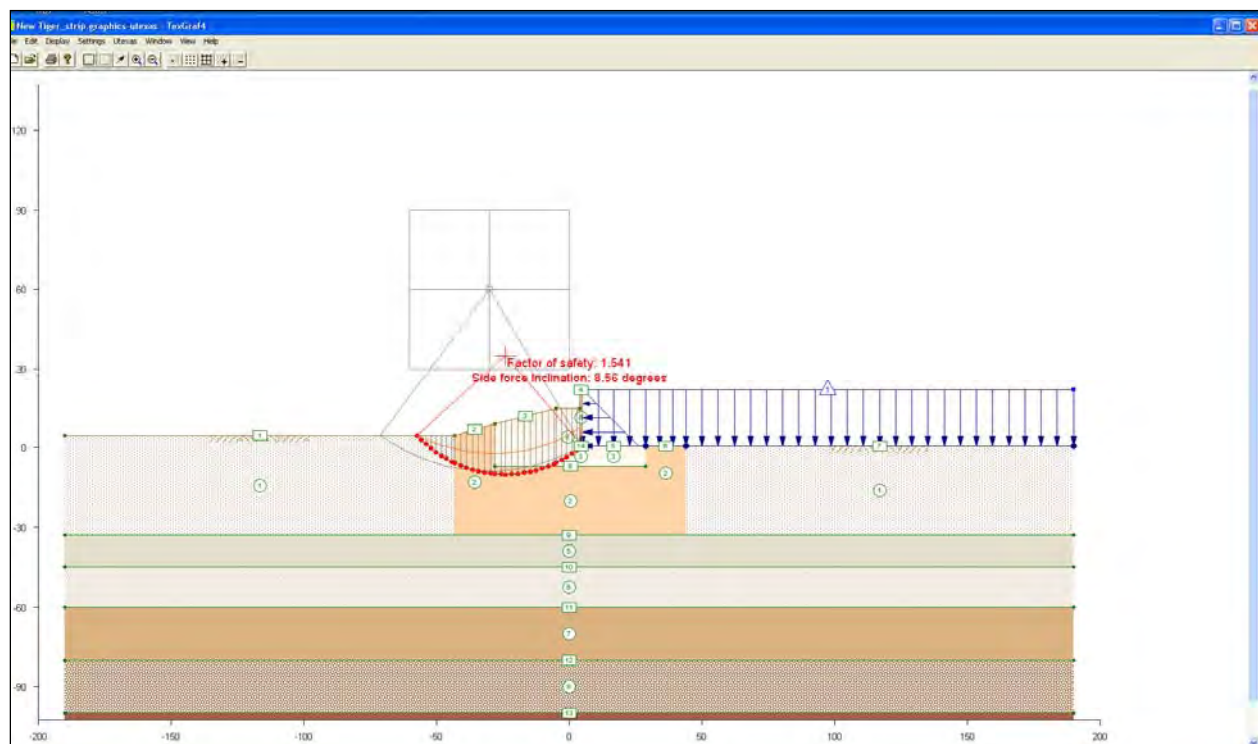


Figure 6.16. UTexas4 slope stability results (flood-side soil removed to sheet-pile tip and hydrostatic water pressures applied to the vertical face of the wall).

7 Summary and Conclusions of the Complete Soil-Structure Interaction (SSI) Analyses of Flood I-walls Embedded in Level Ground

7.1 Summary

7.1.1 Level ground

This study investigates I-walls embedded in level ground consisting of soils that are stronger and stiffer than the fine-grained New Orleans soils that were investigated during the IPET studies. Four different soil sites were investigated using a 2-D complete SSI method of analysis. A complete SSI method of analysis provides the most accurate deformation, soil-to-I-wall interface stress distributions, and gap initiation/propagation results of the analytical tools available. The complete SSI method of analysis involves the use of incremental construction and incremental flood loading of each of the soil sites in a 2-D, nonlinear, finite element method of analysis. This study is restricted to level soil floodwall sites.

The results for mean soil properties are reported in Chapters 2 through 5. The majority of the soil sites investigated consists of fine-grained soils characterized as cohesive soils. One of the sites investigated is characterized as silt with plastic fines.

A focus of the study was to investigate the development of a zone of separation along the flood side of the soil-to-I-wall interface and to study the effects of this zone of separation on the resulting deformation and stress conditions in the soil regime on both the flood side and landside of the I-wall system. A hydraulic fracturing criterion was applied to determine if a gap develops and if it propagates down the soil-to-I-wall interface along the flood side of the I-wall.

Additionally, a series of minimum and maximum strength and stiffness distributions with depth were investigated for two of these soil sites: the overconsolidated clay site (discussed in Chapter 2) and the E-99 clay site (discussed in Chapter 3). The parametric results are summarized in the eight appendices. Appendices A through D discuss the results for the

overconsolidated clay, while Appendices E through H discuss the results for the E99 clay site. I-wall response to flood loading for mean overconsolidated clay soil properties was discussed in Chapter 2. I-wall response to flood loading for mean E99 clay soil properties was discussed in Chapter 3. Chapter 4 discussed I-wall responses to flood loading for a normally consolidated clay site of constant undrained shear strength. Chapter 5 discussed I-wall responses to flood loading for an I-wall embedded in silt containing plastic fines. Chapter 6 summarizes the findings of an initial complete nonlinear SSI finite element analysis performed on an I-wall section embedded in a levee section.

Gap formation, I-wall deformation, earth pressures, and shear and bending moment distributions internal to the I-wall were reported for select flood levels in each of the four series of analyses.

7.1.2 Influence of geometry on I-wall performance

An initial complete nonlinear SSI finite element analysis was performed on an I-wall section embedded in a levee section. The objective of this analysis was to investigate the effects that levee geometry (non-level ground surface) has on the phenomena of gap initiation and propagation along the soil-to-structure interface on the flood side of the I-wall. Additionally, the effects that levee geometry has on the resulting deformation and stress conditions in the soil regime both on the flood side and landside of the I-wall were examined.

Figure 7.1 shows a summary plot of the extent of gap propagation versus floodwater elevation. This plot includes results for the New Tiger Island I-wall and levee site and all the I-walls founded on level ground. In this study, analyses were performed (with incremental raising of the flood elevation) until PLAXIS indicated numerical instability. In order to have the same reference elevation for comparison of the extent of the gap propagation, adjustments were made in the New Tiger Island (levee) computed gap elevations to correspond to the level plane gap elevation results that commenced with a ground surface elevation equal to zero. Therefore, an equivalent gap elevation for the levee was computed by subtracting the levee crest elevation (14.8 ft) from the gap elevation. It is noted that the gap depth is the absolute value of the gap elevation in the figure. Results are presented primarily for sheet-pile depth of penetration to I-wall stick-up height ratio (d/h) corresponding to the design condition (D) of the floodwater

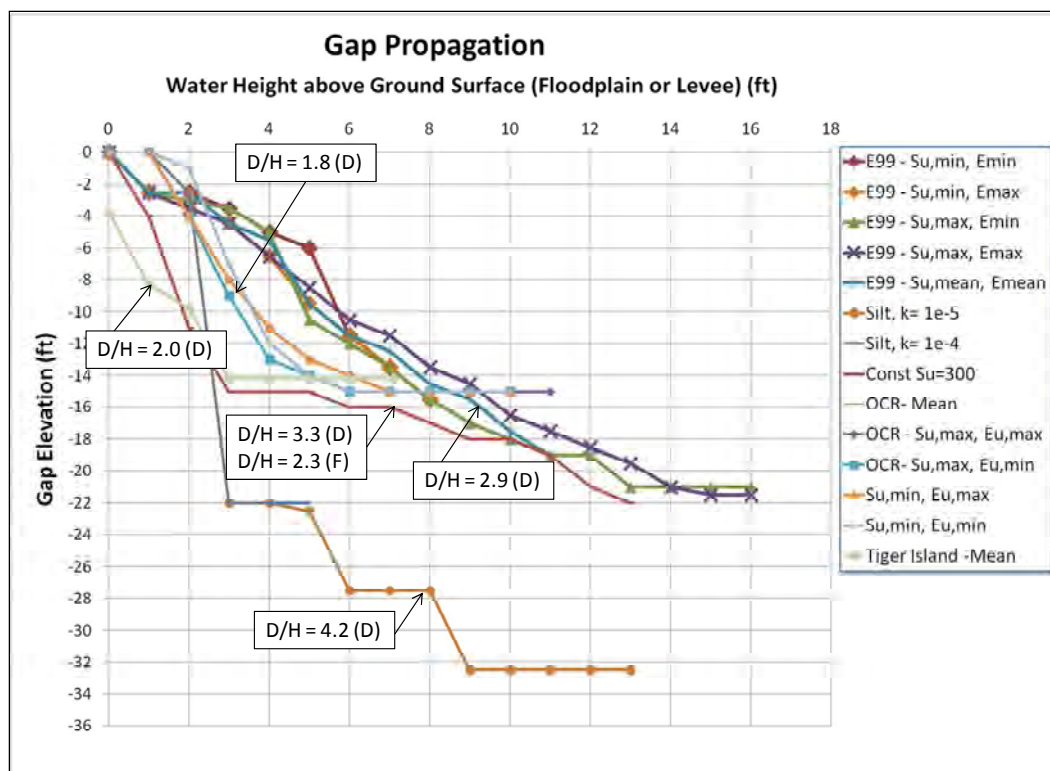


Figure 7.1. Summary of extent of gap propagation for level ground analyses and I-wall in levee analysis (New Tiger Island geometry).

elevation at the top of the wall. An example is that the d/h ratio for the New Tiger Island I-wall and levee site is 2.0. However, for some analyses the floodwater elevation was extended above the existing top of the wall to reach PLAXIS indicated failure condition (F). This would result in a different computed d/h ratio. An example of this case is the I-wall analysis with a constant S_u equal to 300 psf. The design d/h ratio is 3.3, and the d/h ratio corresponding to failure conditions is 2.3. These results indicated that the d/h has an impact on the gap propagation results for these various I-wall systems. For the E-99 and OCR sites, additional parametric analyses were performed for various statistical combinations of soil stiffness and strength values. As shown, there is scatter about the mean results for these two I-wall systems.

Figure 7.2 shows results from analyses using mean values of soil shear strength and stiffness values. The I-wall system had similar values of undrained shear strength in the regions near the I-wall. For a water level at ground surface, results from the levee analysis show a gap propagation to el -4 ft compared to el 0 ft for the level floodplain analyses. These initial results indicate that the levee geometry has some influence on the extent

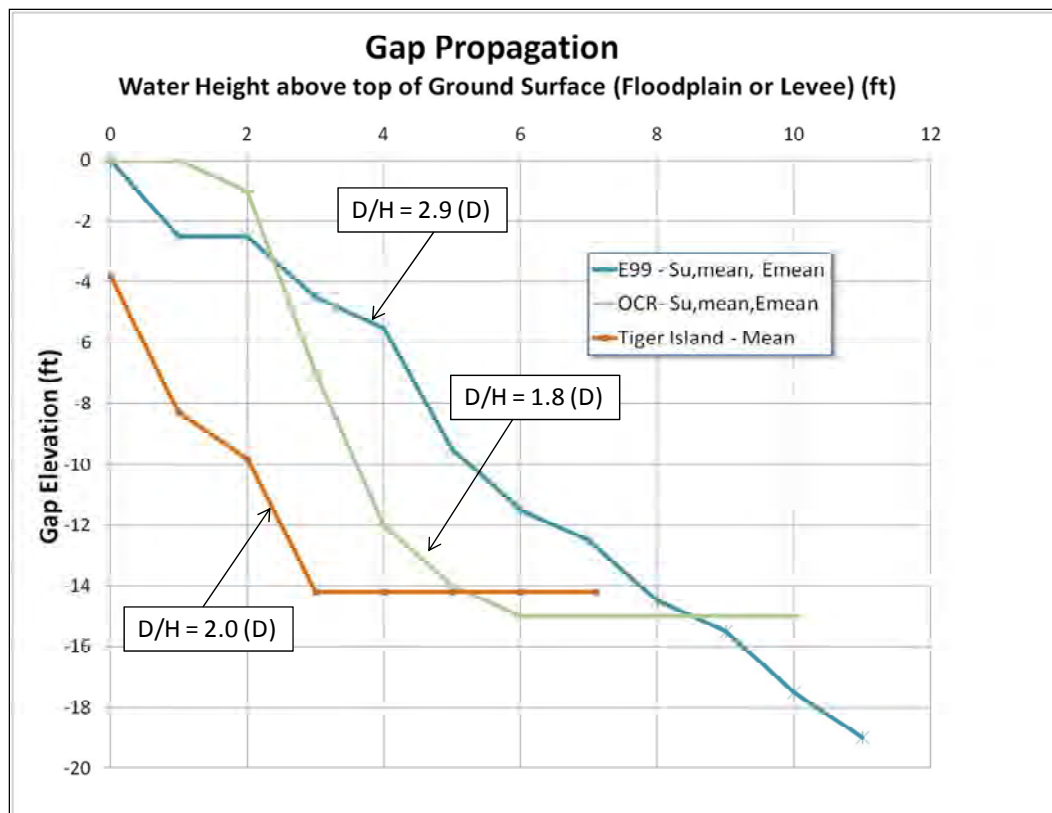


Figure 7.2. Summary of mean analysis result of extent of gap propagation for level ground analyses and I-wall in levee analysis (New Tiger Island geometry).

of gap propagation when compared to the I-walls founded on level ground. Additional analyses are recommended to further support these initial findings as well as to establish the sensitivity of the results to variations in levee slope geometry, I-wall location along the crest of the levee, depth of embedment, and to variations in levee soil shear strength and stiffness values.

7.2 Conclusions

The conclusions are:

- In all I-wall sites assigned, mean soil strength and stiffness properties, gap formation between the I-wall, and the soil is initiated at very low water levels of approximately 2 ft. It does not take a large water level on the I-wall, such as 6 ft, to initiate formation of a gap.
- The five analyses of the overconsolidated clay site indicate that at shallow water level (e.g., 2 to 3 ft) the gap tends to propagate at a higher rate with change in pool elevation for the cases of minimum soil stiffness or minimum soil strength.

- The rate of wall deformation once a gap is formed is relatively slow and constant until the water level reaches approximately 60 percent of the wall height. At that level of flood loading the rate of wall deformation increases, sometimes at a rapid rate.
- For all four I-wall sites, the gap does not penetrate all the way to the bottom of the sheet pile.
- There is a distinct difference in gap propagation relative to the sheet-pile embedment (in the foundation soil) between sheet piles of shorter embedment and sheet piles of longer embedment. In general, the normally consolidated clay sites have lower undrained shear strengths compared to the overconsolidated clay sites. A lower relative shear strength results in the need for a deeper required depth of embedment for I-wall, sheet-pile walls in normally consolidated clays compared to I-walls founded in overconsolidated clays. Thus, longer sheet piles are embedded in normally consolidated clays, while shorter sheet piles are embedded in overconsolidated clays.
- In the shallowest of I-wall embedment soil sites, the overconsolidated clay site (Chapter 2), the gap penetrates to within 1 ft of the sheet-pile wall tip. In that case, the soil wedge between the bottom of the gap and the bottom of the sheet-pile tip serves to arrest the rotation of the I-wall. This sometimes is sometimes referred to as kickback.
- Kickback and the arrest of rotation of the I-wall are harder to observe in the sites with longer piles (i.e., for the normally consolidated clay site, Chapter 4) than in the sites with shorter piles (Chapter 2).
- The gap has been shown to be much more likely to propagate to a limiting depth in the overconsolidated clay site than in the normally consolidated clay site. This likely also is associated with the depth of sheet-pile embedment.
- The surface geometry of the foundation and the I-wall depth of penetration have an influence on the extent of gap propagation for an I-wall system with similar shear strength properties.

References

- AMEC Geomatrix, Inc. 2010. *Report on task 1, I-wall FLAC basic sand model and analysis results, evaluation of phase III numerical models and analysis of I-walls*. Project 14451.000, submitted to U.S. Army Corps of Engineers, Huntington District, February.
- Brandon, T. L., S. G. Wright, and J. M. Duncan. 2008. Analysis of the stability of I-walls with gaps between the I-wall and the levee fill. *Journal of Geotechnical and Geoenvironmental Engineering* 134(5):681-691.
- Brinkgreve, R. B. J., W. Broere, and D. Waterman. 2008. *PLAXIS 2D –Version 9*. The Netherlands: Plaxis B.V.
- Brinkgreve, R. B. J., R. Al-Khoury, and J. M. van Esch. 2006. *PLAXFLOW –Version 1.4*. The Netherlands: Plaxis B.V.
- Clayton, C. R. I., J. Milititsky, and R. I. Woods. 1993. *Earth pressure and earth retaining structures*. 2nd ed. London: Blackie Academic and Professional.
- Craig, R. F. 1997. *Soil mechanics*. 6th ed. New York: Chapman and Hall.
- Dawkins, W. P. 1991. *User's guide: Computer program for design and analysis of sheet-pile walls by classical methods (CWALSHT) including Rowe's Moment Reduction*. Instruction Report ITL-91-1. Vicksburg, MS: U.S. Army Engineer Waterways Experiment Station.
- Duncan, J. M. 1987. Lecture notes on seepage and earth structures, Virginia Tech, September 1987.
- Duncan, J. M., and A. L. Buchignani. 1976. *An engineering manual for settlement studies*. Geotechnical Engineering Report. Berkeley, CA: University of California at Berkeley, 22-28.
- Duncan, J. M., and A. Bursey. 2007. *Soil and rock modulus correlations for geotechnical engineering*. Center for Geotechnical Practice and Research CGPR #4. Blacksburg, VA: Virginia Polytechnic Institute and State University.
- Fredlund, D. G., and H. Rahardjo. 1993. *Soil mechanics for unsaturated soils*, Hoboken, NJ: John Wiley and Sons.
- HQUSACE. 1994. *Design of sheet pile walls*. Engineering Manual 1110-2-2504. Washington, DC: Headquarters, U.S. Army Corps of Engineers.
- HQUSACE. 2011. *Evaluation of I-walls*. Technical Letter 1110-2-575. Washington, DC: Headquarters, U.S. Army Corps of Engineers.
- Independent Panel to Review Cause of Teton Dam Failure. 1976. *Report to U.S. Department of the Interior and the State of Idaho on failure of Teton Dam*. Washington, DC: Superintendent of Documents, U.S. Government Printing Office.

- IPETF. 2007. The Performance- Levees and Floodwall. *Performance Evaluation of the New Orleans and Southeast Louisiana Hurricane Protection System, Final Report of the Interagency Performance Evaluation Task Force*. Vol V. Washington, DC: Interagency Performance Evaluation Task Force.
<https://ipet.wes.army.mil/>
- Jackson, R. B. 1988. *E99 sheet pile wall field load test report*. Technical Report No. 1. Vicksburg, MS: U.S. Army Engineer Division, Lower Mississippi Valley.
- Ladd, C. C. 1991. Stability evaluation during staged construction (22nd Karl Terzaghi Lecture). *ASCE Journal of Geotechnical Engineering*, 117(4):540-615.
- Ladd, C. C., and R. Foott. 1974. A new design procedure for stability of soft clays. *Journal of the Geotechnical Engineering Division*, ASCE, 100(GT7):763-786.
- Leavell, D. A., J. F. Peters, E. V. Edris, and T. L. Holmes. 1989. *Development of finite-element-based design procedure for sheet-pile walls*. Technical Report GL-89-14. Vicksburg, MS: U.S. Army Engineer Waterways Experiment Station.
- Nobari, E. S., K. L. Lee, and J. M. Duncan. 1973. *Hydraulic fracturing in zoned earth and rockfill dams*. Contract Report S-73-2. Vicksburg, MS: U.S. Army Engineer Waterways Experiment Station.
- Oner, M., W. P. Dawkins, R. Mosher, and I. Hallal. 1997. Soil-structure interaction effects in floodwalls. *Electronic Journal of Geotechnical Engineering*.
<http://www.ejge.com/1997/Ppr9707/Ppr9707.htm>.
- PLAXIS. 2012. Essential software for the geotechnical professional.
<http://www.plaxis.nl>.
- Potyondy J. G. 1961. Skin friction between various soils and construction materials. *Geotechnique*, 11(4):339-353.
- Sherard, J. L. 1973. Embankment dam cracking. In *Embankment Dam Engineering-The Casagrande Volume*, New York: John Wiley.
- Sherard, J. L. 1986. Hydraulic fracturing in embankment dams. *ASCE Journal of Geotechnical Engineering*, 112(10):905-927.
- U.S. Army Engineer Division, Lower Mississippi Valley. 1988. *E-99 sheet pile wall field load test*. Technical Report No. 1. Vicksburg, MS: U.S. Army Engineer Division, Lower Mississippi Valley.
- U.S. Army Engineer Research and Development Center. 2012. Computer-aided structural engineering (CASE).
<http://case.army.mil>
- Widjaja, H., J. M. Duncan, and H. B. Seed. 1984. *Scale and time effects in hydraulic fracturing*. Miscellaneous Paper GL-84-10. Vicksburg, MS: U.S. Army Engineer Waterways Experiment Station.

Appendix A: Analyses of I-wall Site Founded in an Overconsolidated Lean Clay Using Minimum Values of Both Undrained Shear Strength (S_u) and Undrained Secant Stiffness (E_u)

A.1 Purpose of analyses

This appendix summarizes the findings of a series of complete nonlinear soil-structure interaction (SSI¹) finite element analyses performed on an I-wall section founded in an overconsolidated lean clay. Minimum values of both undrained shear strength (S_u) and undrained secant stiffness (E_u) are assigned to the clay soils. The focus of this study was to investigate the phenomena of gap initiation and propagation along the soil-to-structure interface on the flood side of the I-wall and to study the effects of gap initiation and propagation on the resulting deformation and stress conditions in the soil regime on both the flood side and landside of the I-wall. The findings of these analyses will be used in a companion research effort focusing on risk and reliability assessments of I-wall systems.

The following sections will describe the soil used in the analyses, the selection of stiffness and shear strength parameters, the conventional design of the I-wall, the analysis procedures employed, and the results of the complete nonlinear SSI analyses.

A.2 Overview of flood-site I-wall being analyzed

The geometry of the problem analyzed is the same wall system shown in Figure 2.1. The site was assumed to be a level plan with a maximum floodwater elevation of 9 ft. Two soil layers were assumed in the analyses. The top 20 ft represented an overconsolidated layer, while the underlying soil was assumed to be normally consolidated. The elevation of the soil surface was assumed to be 0 ft.

¹ Symbols and unusual abbreviations used in this appendix are listed and defined in the Notation, Appendix I.

The I-wall was composed of a sheet-pile wall with the tip at el -16 ft. The top of the I-wall was composed of a concrete cap 2.5 sq ft (i.e., embedment to el -2.5 ft), with the top of the cap level with the ground surface. The wall above the top of the soil was composed of a tapered concrete section 2.5 ft at the base and 1 ft at the top of the wall (el 9 ft). The water table for this problem was at the pile tip (el -16 ft).

A.3 Conventional design of cantilever I-wall and shear strength

The design depth of penetration of the sheet-pile section of the I-wall was determined using the Computer-Aided Structural Engineering (CASE) CWALSHT computer program (U.S. Army Engineer Research and Development Center 2012)¹ and procedures outlined in Headquarters, U.S. Army Corps of Engineers (1994). The computed design depth of penetration of the sheet pile (-16 ft) (refer to Chapter 2) was used in this analysis without consideration of a gap forming between the concrete cap and the soil or between the sheet pile and soil on the flood side of the I-wall. However, note that the finite element analysis for the wall section was conducted for this same -16-ft design depth, and it considered the potential for gap initiation and propagation. It too should be noted that the inclusion of a gap beside the wall also would affect the design depth. This analysis provides useful information for a lower ratio of embedment to flood height. It is important to recognize that the factor of safety for this system, based on complete SSI results for a flood elevation of 9 ft, would not correspond to the factor of safety used for design in CWALSHT because a gap was not assumed in the CWALSHT analysis.

The total stress (undrained) shear strength parameters were determined using the SHANSEP procedure (Ladd and Foott 1974) discussed in Chapter 2. It assumes that the soil shear strength can be normalized by the effective overburden pressure. The effective overburden pressure is calculated at midlayer for each of the layers identified in Table A.1 and using a preflood water table elevation of -16 ft. The ratio of shear strength to effective overburden pressure (S_u/σ'_{vo}) is dependent on the overconsolidation ratio (OCR) and a fitting parameter (m), assumed to be 0.8, as shown in Equation A.1:

¹ Citations in this appendix are in the References at the end of the main text.

Table A.1. Computation of minimum (S_u) variation with depth.

Layer			Short-Term (Undrained) Loading					$S_{u,min,ave}$ psf
			Depth, ft	σ'_{vo} , psf	OCR	$(S_u/\sigma'_{vo})_{oc}$	$S_{u,Min}$, psf	
1	0	-1.5	1	122	7	0.85379	104	104
			2	244	7	0.85379	208	
2	-1.5	-4.5	3	366	7	0.85379	312	312
			4	488	7	0.85379	417	
			5	610	6.4	0.794724	485	
3	-4.5	-7.5	6	732	5.5	0.703984	515	513
			7	854	4.8	0.631343	539	
			8	976	3.6	0.50155	490	
4	-7.5	-11.5	9	1098	2.9	0.421882	463	450
			10	1220	2.3	0.350473	428	
			11	1342	2	0.313398	421	
			12	1464	1.7	0.275189	403	
			13	1586	1.6	0.262161	416	
5	-11.5	-17.5	14	1708	1.4	0.2356	402	418
			15	1830	1.35	0.228844	419	
			16	1952	1.3	0.222038	433	
			17	2011.5	1.25	0.215179	433	
			18	2071	1.2	0.208266	431	
6	-17.5	-20	19	2130.5	1.15	0.201294	429	429
			20	2190	1.1	0.194261	425	
7	-20	-27.5	25	2487.5	1	0.18	448	448
			30	2785	1	0.18	501	
8	-27.5	-40	35	3082.5	1	0.18	555	555
			40	3380	1	0.18	608	
			45	3677.5	1	0.18	662	
			50	3975	1	0.18	716	
9	-40	-60	55	4272.5	1	0.18	769	742
			60	4570	1	0.18	823	
			65	4867.5	1	0.18	876	
10	-60	-80	70	5165	1	0.18	930	956
			75	5462.5	1	0.18	983	
			80	5760	1	0.18	1037	
			85	6057.5	1	0.18	1090	
11	-80	-100	90	6355	1	0.18	1144	1171
			95	6652.5	1	0.18	1197	
			100	6950	1	0.18	1251	

$$\left(\frac{S_u}{\sigma'_{vo}} \right)_{OC} = \left(\frac{S_u}{\sigma'_{vo}} \right)_{NC} \bullet OCR^m, \quad (A.1)$$

where

- $(S_u/\sigma'_{vo})_{OC}$ = ratio of the undrained shear strength to effective overburden pressure for the overconsolidated condition;
 $(S_u/\sigma'_{vo})_{NC}$ = ratio of the undrained shear strength to effective overburden pressure for the normally consolidated condition.

From Ladd (1991), a mean value of 0.22 was assigned to $(S_u/\sigma'_{vo})_{NC}$ (Chapter 2) and a value of 0.8 for m based on undrained Direct Simple Shear (DSS) test results. These data also indicated a standard deviation equal to 0.02 for the $(S_u/\sigma'_{vo})_{NC}$ data. In the computation of the effective overburden pressures, 122 pcf was used for both the moist and the saturated unit weights. The OCR characterization of this site is the same as discussed in Chapter 2 and is shown in Figure 2.3.

The resulting variation in the undrained shear strength (S_u) with depth is shown in blue in Figure A.1. Average values of S_u were estimated to be constant over a given depth, shown in pink in Figure A.1. These constant values are listed for the soil layers in Table A.1 and were used in the complete SSI analysis to approximate variation in S_u with depth.

A.4 Shear strength and stiffness properties used in the complete SSI analysis

A complete SSI analysis of the I-wall section shown in Figure 2.1 was performed using the two-dimensional (2-D) version of the PC-based nonlinear incremental construction finite element program PLAXIS (PLAXIS 2012). The finite element method employed required certain input material properties for the selected soil constitutive models. The PLAXIS nonlinear Hardening Soil (HS) constitutive model was used to model all soil elements. This constitutive model provides for nonlinear stress-strain response for soil elements during loading. Elastic plate elements were used to model the steel sheet pile and the concrete I-wall section. Plate elements were utilized to model the concrete I-wall to process bending moment and shear distribution results more efficiently. Two-dimensional elastic elements were used to represent the concrete cap (the region in which the sheet pile is embedded).

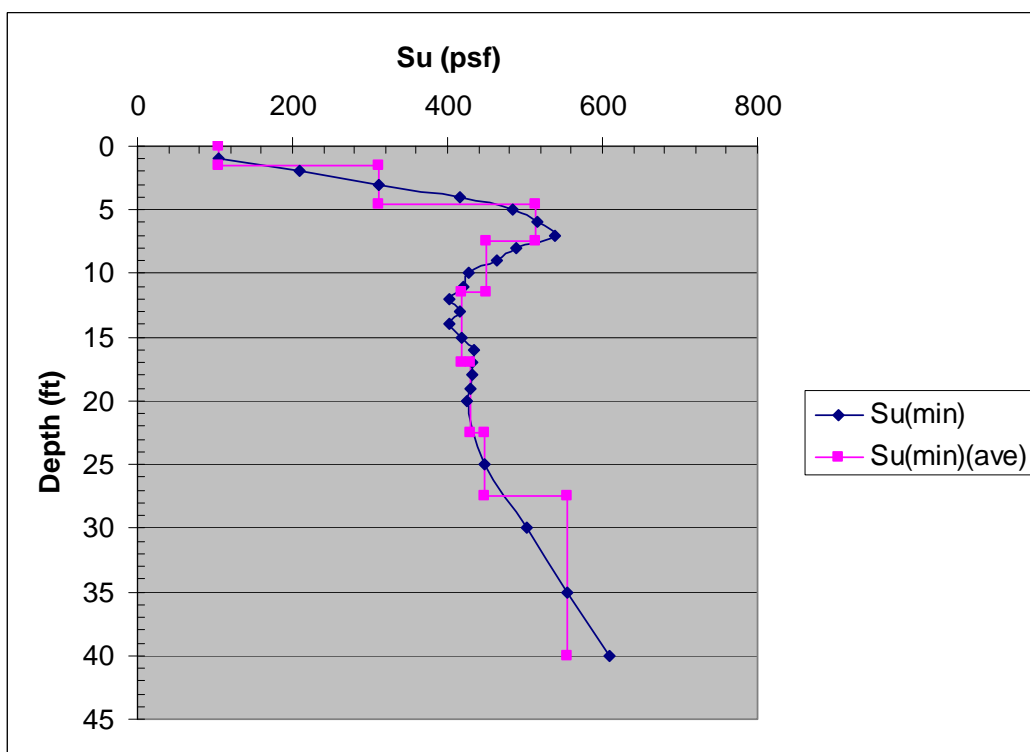


Figure A.1. Variation in minimum computed values of undrained shear strength (S_u) with depth.

Total stress soil strength parameters were used to characterize this over-consolidated lean clay site. An SSI parametric study was conducted to determine a minimum shear strength and stiffness variation (considered near-failure conditions) that resulted in a numerically stable analysis. This was accomplished by using the mean value of 0.22 assigned to $(S_u/\sigma'_v)_{NC}$ in conjunction with a standard deviation of 0.02. The $(S_u/\sigma'_v)_{NC}$ ratio was reduced by one, two, and three standard deviations from the mean value of 0.22 in three separate PLAXIS analyses until both the minimum computed shear strength and stiffness variation resulted in a numerically stable SSI analysis at the design flood elevation of 9 ft. The PLAXIS analysis using the mean minus three standard deviations did not converge. The PLAXIS analysis using the mean minus two standard deviations did converge. The minimum computed ratio $(S_u/\sigma'_v)_{NC}$ was equal to 0.18 and was computed using Equation A.2:

$$\left(\frac{S_u}{\sigma'_v} \right)_{NC-2\sigma} = \left(\frac{S_u}{\sigma'_v} \right)_{NC-mean} - 2\sigma, \quad (A.2)$$

where

$$\left(\frac{S_u}{\sigma_v'} \right)_{NC-mean} = 0.22$$

and σ , the standard deviation, was 0.02.

Additionally, the minimum variation in shear strength with depth was computed using the mean value of 0.22 assigned to $(S_u/\sigma_v')_{NC}$ in conjunction with two times the standard deviation of 0.02. The minimum computed variation in (S_u) also was computed using Equation A.3;

$$S_{u(NC-2\sigma)} = \left[\left(\frac{S_u}{\sigma_v'} \right)_{NC-mean} - 2\sigma \right] \bullet \sigma_v'. \quad (A.3)$$

The resulting minimum variation in stiffness with depth was computed using the results of Equation A.2 and Equation A.4:

$$E_{u(NC-2\sigma)} = \text{constant} \times S_{u(NC-2\sigma)}, \quad (A.4)$$

where constant = E_u/S_u ratios at each elevation listed in Table A.2.

The correlation by Duncan and Buchignani (1976) shown in Figure 2.5 and Equation 2.2 was used to estimate the minimum variation of undrained secant modulus in clay with depth. Table A.2 summarizes the computation of E_{us} with depth using the average values of the variation of S_u with depth from Table A.1 in conjunction with Equation 2.2. These values of E_{us} were used to estimate the variation in the PLAXIS input stiffness parameter (E_{50}^{ref}), which is a secant modulus at 50 percent of the principal stress difference ($\sigma_1 - \sigma_3$). The remaining parameters for soil properties selected to represent the clay (CL) soils used in the PLAXIS finite element analyses were the same as discussed in Chapter 2. Table A.3 shows minimum values of HS constitutive soil parameters used in these analyses. Values of the coefficient of friction between the sheet pile and the soil and between the concrete cap and the soil were the same as referenced in Table 2.5.

Minimum values of adhesion were assigned to the soil along the I-wall-to-soil and sheet-pile-to-soil interfaces in the complete SSI analysis. The minimum value for adhesion was estimated using the one selected for the ratio of adhesion to cohesion (f_c) between the sheet pile and soil and between the concrete and the soil shown in Table 2.5 and Equation 2.3. Substituting the ratio of adhesion to cohesion equal to 0.8 into Equation 2.3 and solving for (C_a) yields Equation A.5:

Table A.2. Computation of minimum undrained secant modulus (E_{us}).

Layer			Short-Term (Undrained) Loading					E_u/S_u	$E_{u,min}$, psf
No.	Top El, ft	Bottom El, ft	Depth, ft	σ'_{vo} , psf	OCR	$(S_u/\sigma'_{vo})_{oc}$	$S_{u,min}$, psf		
1	0	0	1	122	7	0.85379	104	250	26,041
			2	244	7	0.85379	208	250	52,081
2	-1.5	-4.5	3	366	7	0.85379	312	250	78,122
			4	488	7	0.85379	417	250	104,162
			5	610	6.4	0.794724	485	270	130,891
3	-4.5	-7.5	6	732	5.5	0.703984	515	300	154,595
			7	854	4.8	0.631343	539	350	188,708
			8	976	3.6	0.50155	490	450	220,281
4	-7.5	-11.5	9	1098	2.9	0.421882	463	500	231,613
			10	1220	2.3	0.350473	428	550	235,167
			11	1342	2	0.313398	421	580	243,937
			12	1464	1.7	0.275189	403	590	237,698
			13	1586	1.6	0.262161	416	590	245,315
5	-11.5	-17.5	14	1708	1.4	0.2356	402	600	241,443
			15	1830	1.35	0.228844	419	600	251,271
			16	1952	1.3	0.222038	433	600	260,051
			17	2011.5	1.25	0.215179	433	600	259,700
			18	2071	1.2	0.208266	431	600	258,791
6	-17.5	-20	19	2130.5	1.15	0.201294	429	600	257,314
			20	2190	1.1	0.194261	425	600	255,260
7	-20	-27.5	25	2487.5	1	0.18	448	600	268,650
			30	2785	1	0.18	501	600	300,780
8	-27.5	-40	35	3082.5	1	0.18	555	600	332,910
			40	3380	1	0.18	608	600	365,040
			45	3677.5	1	0.18	662	600	397,170
			50	3975	1	0.18	716	600	429,300
9	-40	-60	55	4272.5	1	0.18	769	600	461,430
			60	4570	1	0.18	823	600	493,560
			65	4867.5	1	0.18	876	600	525,690
10	-60	-80	70	5165	1	0.18	930	600	557,820
			75	5462.5	1	0.18	983	600	589,950
			80	5760	1	0.18	1037	600	622,080
			85	6057.5	1	0.18	1090	600	654,210
11	-80	-100	90	6355	1	0.18	1144	600	686,340
			95	6652.5	1	0.18	1197	600	718,470
			100	6950	1	0.18	1251	600	750,600

Table A.3. Minimum HS model strength and stiffness properties for the soil layers.

Layer			c _{ref} lbs/ft ²	E _{50,ref} lbs/ft ²	E _{oed,ref} lbs/ft ²	E _{ur,ref} lbs/ft ²
No.	Top El, ft	Bottom El, ft				
1	0.0	0.0	104	2.60E+04	2.60E+04	7.81E+04
2	-1.5	-4.5	312	7.81E+04	7.81E+04	2.34E+05
3	-4.5	-7.5	513	1.58E+05	1.58E+05	4.74E+05
4	-7.5	-11.5	450	2.33E+05	2.33E+05	6.98E+05
5	-11.5	-17.0	418	2.49E+05	2.49E+05	7.48E+05
6	-17.0	-20.0	429	2.57E+05	2.57E+05	7.71E+05
7	-20.0	-27.5	448	2.69E+05	2.69E+05	8.06E+05
8	-27.5	-40.0	555	3.33E+05	3.33E+05	9.99E+05
9	-40.0	-60.0	742	4.45E+05	4.45E+05	1.34E+06
10	-60.0	-80.0	956	5.74E+05	5.74E+05	1.72E+06
11	-80.0	-100.0	1171	7.02E+05	7.02E+05	2.11E+06

$$(C_a)_{min} = 0.8(C)_{min} = 0.8 (C_{mean} - 2\sigma), \quad (A.5)$$

where

$(C_a)_{min}$ = minimum soil adhesion;

C_{min} = minimum value of cohesion = minimum value of undrained shear strength $(S_u)_{min}$;

C_{mean} = mean value of cohesion = mean value of undrained shear strength $(S_u)_{mean}$;

σ = standard deviation.

The properties of the concrete cap, represented by elastic elements, and the properties of the concrete I-wall section, modeled by elastic plate elements with the properties, were the same as in Tables 2.6 and 2.7, respectively. The sheet pile was represented by elastic plate elements with the same properties as in Table 2.8.

A.5 Discussion of finite element analyses

A.5.1 Conceptual model

The finite element analysis was performed using the 2-D version of the nonlinear incremental construction finite element program PLAXIS. The conceptual model of the finite element mesh is the same as shown in Figure 2.6. The geometry is the same as Figure 2.1. Several special modeling

features were used, including the sheet-pile wall and the concrete I-wall section being modeled by elastic plate elements; interface elements and soil elements beside the sheet-pile wall on the flood side were 1/2 ft in height. These special features are described in Chapter 2.

A.5.2 Gap initiation and propagation criterion

A hydraulic fracturing criterion is applied to determine if a gap will develop and propagate down the soil-to-I-wall interface. In this procedure of analysis, the total horizontal stress computed by PLAXIS at the ground surface soil-to-I-wall interface is compared to the hydrostatic water pressure developing at the top of the ground surface caused by the presence of the specified flood pool elevation. If the hydrostatic water pressure of the flood pool (the demand) exceeds the total horizontal stress (the capacity), a gap will initiate at the ground surface, along the soil-to-I-wall interface. This criterion is discussed in Chapter 2.

A.5.3 Finite element model

Figure A.2 shows a 2-D cross section used to model the variation of undrained shear strength and soil stiffness with depth by the PLAXIS program. The regions of uniform color reflect soil clusters used to define the mesh and assign soil regions with common properties. The inset figure shows the average undrained shear strengths assigned to the upper eight layers based on the minimum S_u values (i.e., mean minus two standard deviations). The finite element mesh used in the analysis is the same as shown in Figure 2.9. The mesh is composed of 4,187 elements and 34,408 nodes with 50,244 stress points. The mesh consists of 15-node triangular elements to model the soil, plate elements to model the bending effects of the I-wall and sheet-pile wall, and interface elements to model SSI between the sheet-pile wall and the adjacent soil elements. The analyses are executed as a plane strain problem. An enlarged view of the area around the wall and its mesh also is shown in Figure 2.10.

A.6 Results of the finite element analyses

A.6.1 Initial stresses

The initial total stress state within the finite element mesh was established using the at-rest soil conditions for a level ground surface. Horizontal

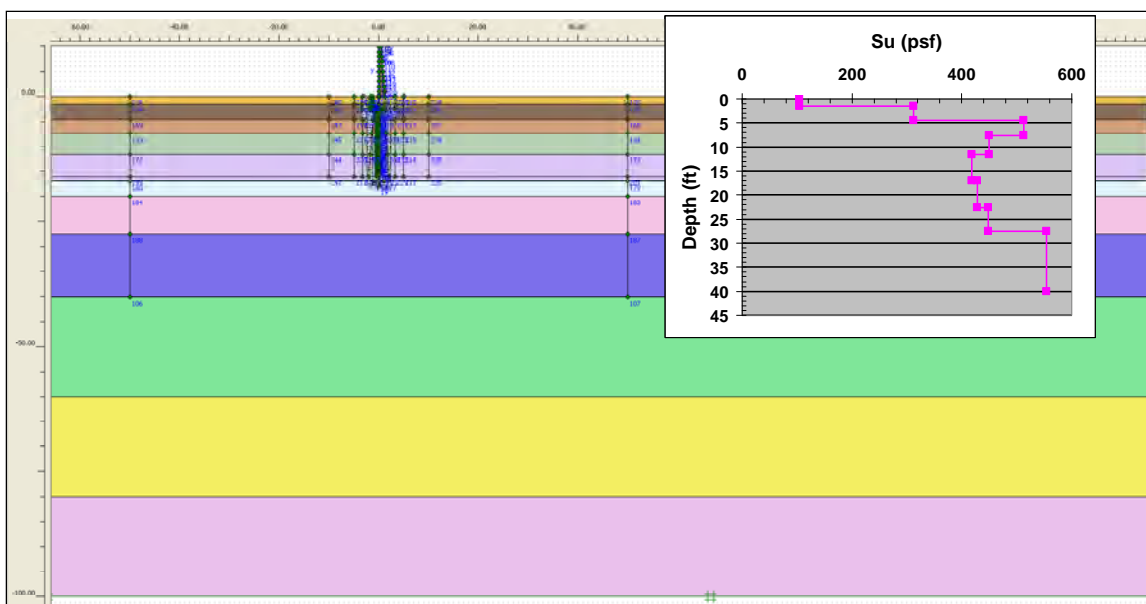


Figure A.2. Two-dimensional (2-D) cross-section model using minimum computed values of undrained shear strength (S_u) used in the SSI analyses.

at-rest soil stresses were estimated using the interrelationship between the at-rest earth pressure coefficient (K_o) and the soil Poisson's ratio (ν) (see Equation 2.4). The assumed groundwater elevation was at the sheet-pile tip (el -16 ft). The assigned values of ν and the corresponding K_o values used to compute the horizontal earth pressures for the initial conditions are summarized in Table 2.9.

For this level ground site, the at-rest stress is computed by multiplying the total overburden pressure for each integration point in every soil element by K_o . Figure A.3 shows the computed fraction of mobilized shear strength (referred to as relative shear stress in PLAXIS output) from the initial total stress condition. The resulting fraction of mobilized shear strength (1.0 indicates full mobilization of shear strength) is less than or equal to 0.77 for all soil clusters. These results indicate reserve shear capacity in the soil regime and, thus, a stable numerical model at this initial stage of construction.

A.6.2 Gap initiation and propagation results

As mentioned, the focus of this study was to investigate the phenomena of gap initiation and propagation along the flood side of the soil-to-I-wall interface and to study the effects of these phenomena on the resulting deformation and stress conditions in the soil regime on both the flood side and landside of the I-wall system.

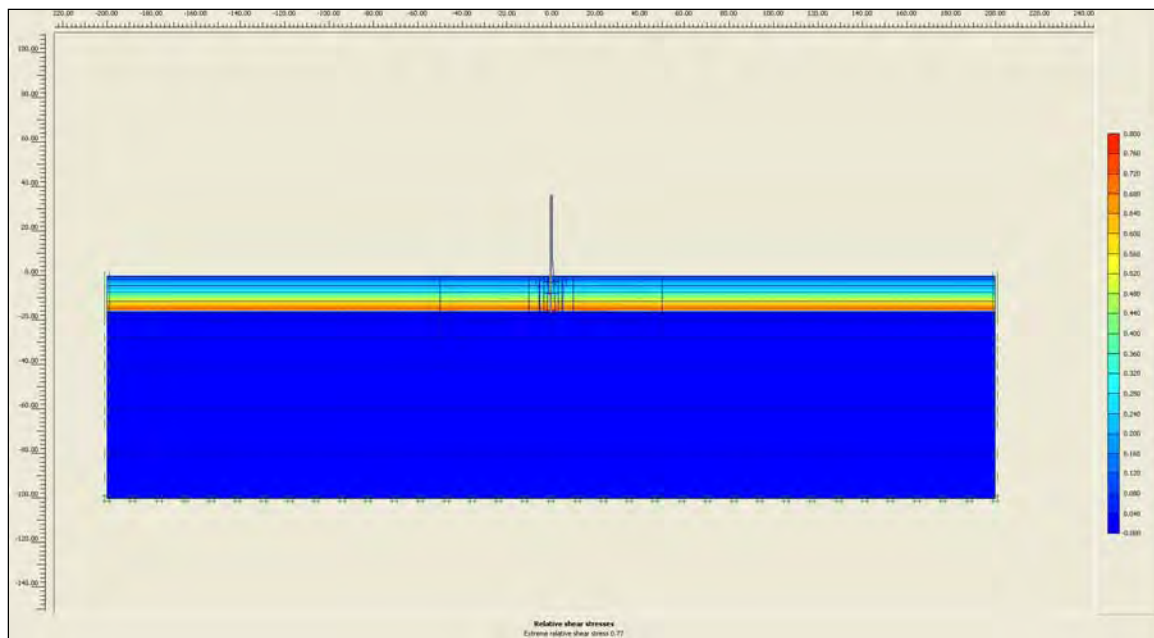


Figure A.3. Fraction of mobilized shear strength for initial conditions using minimum computed values of undrained shear strength (S_u) and undrained stiffness (E_u).

Modeling of the flood loading commenced in the complete SSI analysis after the total initial stress state was established within the mesh for an assumed steady-state water elevation at the ground surface (el 0.0 ft). The flood loading was applied in 1-ft incremental raises of the water level to track the formation and propagation of a gap. The hydraulic fracturing criterion is used to estimate a gap formation and its propagation. This procedure compares the total normal earth pressures, due to the flood pool acting on the wall at a given depth, to the hydrostatic water pressure acting at the corresponding depth. A gap is formed when the total horizontal earth pressure (the capacity) is less than the water pressure, due to the flood pool acting at the corresponding depth (the demand). Next, hydrostatic water pressure is applied over the depth of the gap, and this hydrostatic water pressure at the new, deeper gap depth is compared to the total horizontal earth pressure. Gap propagation is terminated at the depth when the demand is less than the capacity. Complete SSI analysis results were examined for various water elevations and gap depths. Figure A.4 shows the progression of the gap as the water level against the I-wall is increased. As shown, the gap initiates when the water is at the shallow elevation of 2 ft and extends to a depth of -4.0 ft. The gap extends to el -8 ft at a water elevation of 3 ft. At water elevation 6 ft, the gap extends to el -15 ft and remains constant to a water elevation of 9 ft. Observe that the gap is within 1 ft of the sheet-pile tip for floodwater levels at and above el 6 ft.

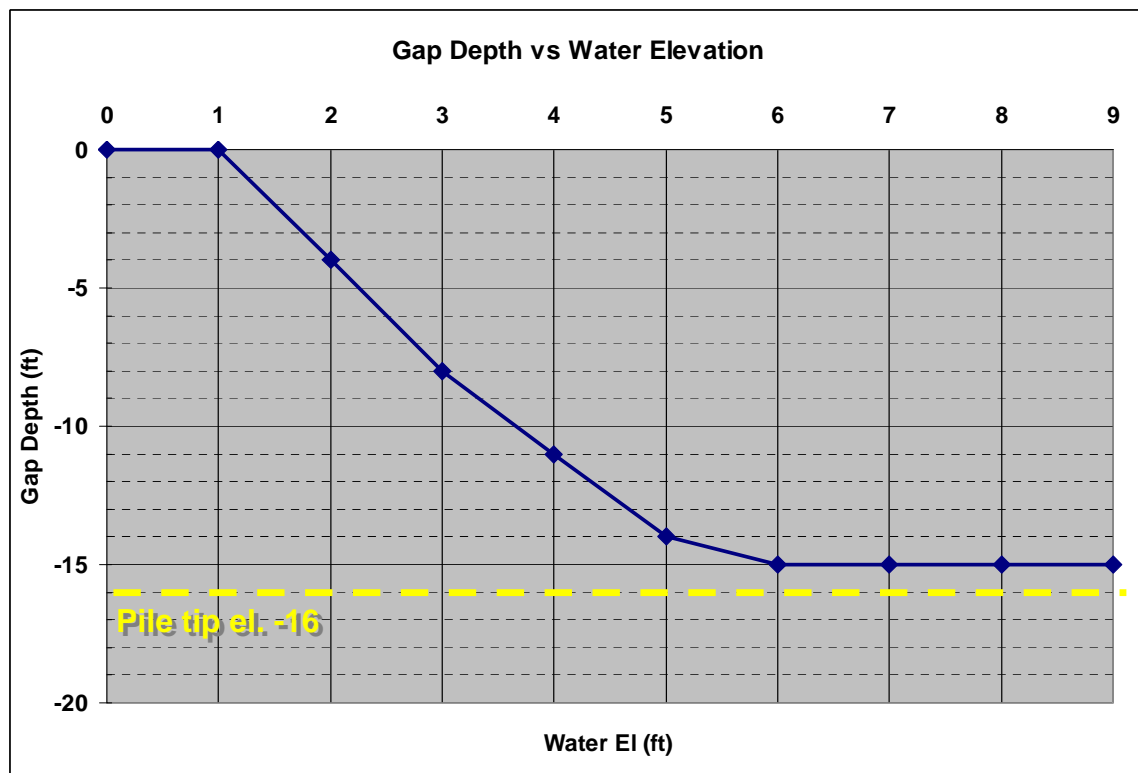


Figure A.4. Progression of gap versus water elevation using minimum computed values of undrained shear strength (S_u) and undrained stiffness (E_u).

A.6.3 Performance of interface elements

The performance of the interface elements was compared to the performance of the soil elements adjacent to the wall to ascertain whether the results for the interface elements could be used to characterize the computed results of the analyses accurately. Figure 2.13 shows that the total horizontal stresses computed within the interface and soil elements agree closely for the selected flood elevation of 2 ft. Therefore, interface element results were used to summarize computed results from this complete SSI analysis.

A.6.4 Discussion of displacements and stresses

The total (exaggerated) nodal displacements within the finite element mesh (both soil and wall) are shown in Figure A.5. These displacements are for the design water elevation of 9 ft with a gap depth to el -15 ft. Note that the nodal displacements are increased by a factor of 50 in this figure to show the deformed mesh relative to its initial position and to show the extent of the gap. The gap is modeled by deactivating the soil elements adjacent to the wall. The general trend of the deflections was toward the

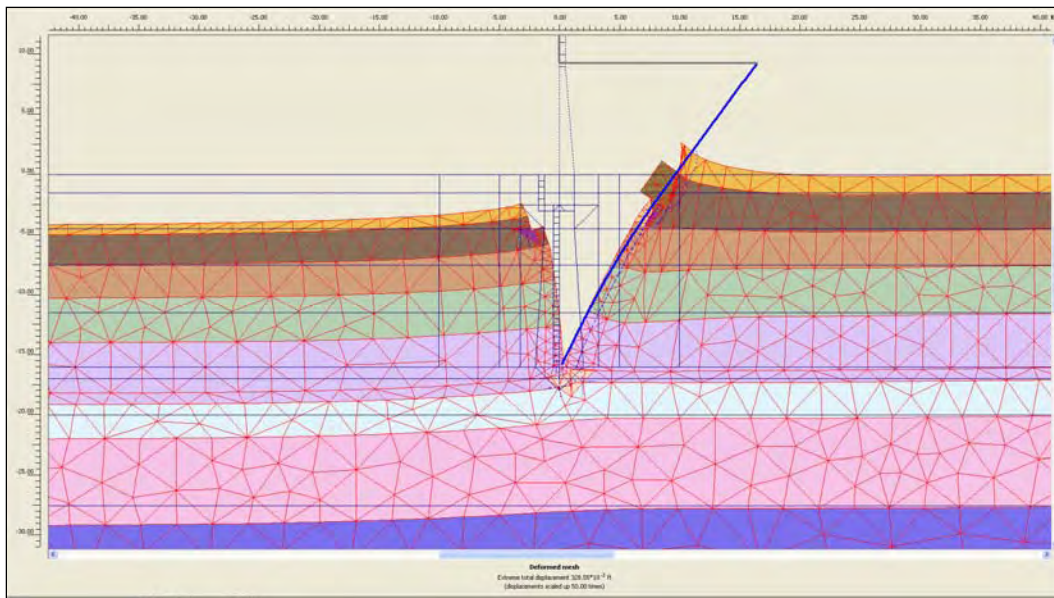


Figure A.5. Total exaggerated displacements for a water elevation of 9 ft and gap elevation of -15 ft using minimum computed values of undrained shear strength (S_u) and undrained stiffness (E_u).

landside because of the applied boundary water pressures on the flood side. The wall had greater movement than the soil at this loading phase. The maximum wall displacement was approximately 4.0 in. at the top of the wall. The displacement of the wall consisted of both horizontal and vertical movements. The tip of the wall actually moved slightly upward and toward the landside.

Figure A.6 shows a plot of horizontal displacements of I-wall versus flood water elevation at three points along the wall. The points monitored in the analysis were the top of the I-wall at el 9 ft, at the ground surface elevation of 0.0 ft, and at the sheet-pile tip elevation of -16 ft. As shown, the deflection of the wall up to a flood elevation of 3 ft (after gap initiation) was primarily uniform translation. As the water elevation increased, the top of the wall experienced larger deformations than those of the ground and much larger deformations than those of the pile tip. This implies that the wall was undergoing rotation along with translation. Also, above water 8 ft, the deflection of the pile tip was directed toward the flood-side soil, which indicates kickback of the pile tip. This behavior is consistent with the behavior assumed in limit equilibrium design procedures for the design of cantilever sheet-pile walls.

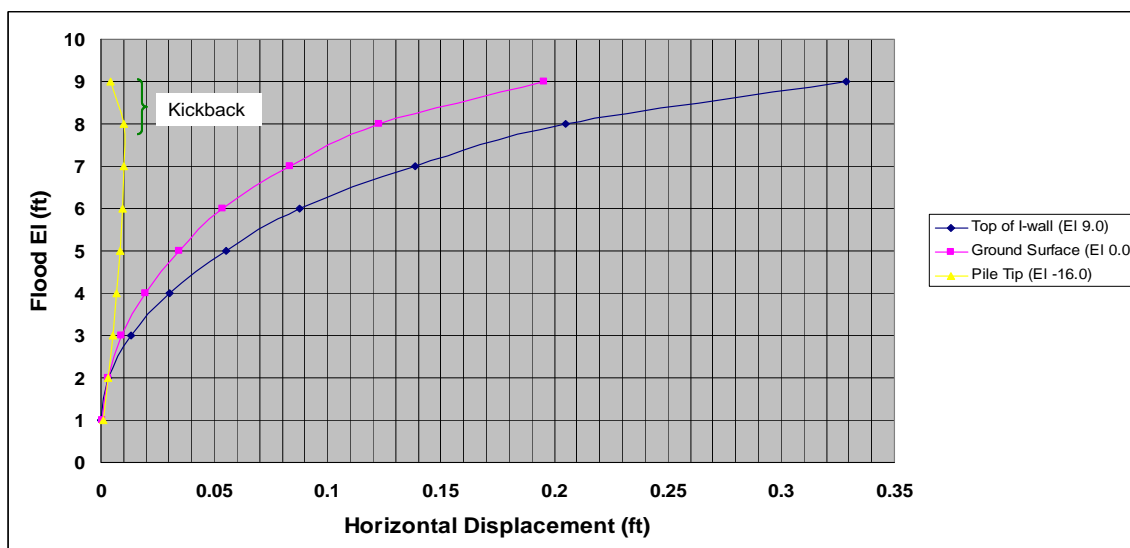


Figure A.6. Horizontal sheet-pile deflection versus water elevation using minimum computed values of undrained shear strength (S_u) and undrained stiffness (E_u).

Figure A.7 shows a plot of relative horizontal displacements of I-wall versus floodwater elevation at the ground surface. Relative displacements were computed at this location to provide results for a companion research effort focusing on risk and reliability assessments of I-walls. Relative displacements were computed by subtracting the displacements of the sheet-pile tip from the sheet-pile displacements at the ground surface for a given floodwater elevation. The maximum computed relative horizontal displacement of the wall at the ground was approximately 2.3 in. for a maximum flood elevation of 9 ft. Computed relative horizontal displacements for this and other flood pool elevations are reported in Table A.4.

The analysis using the mean, best estimate (B.E.), values for S_u and E_u resulted in a maximum computed relative horizontal displacement of approximately 3.3 in. of the wall at the ground (Table 2.10). However, this maximum relative displacement corresponded to a maximum flood elevation of 10 ft. Table A.5 compares the maximum computed relative horizontal displacements from analyses using both the B.E. and minimum values of S_u and E_u . As shown for the flood elevation 9 ft, the maximum computed relative displacement using the minimum values of S_u and E_u was approximately 2.3 in., compared to approximately 2.0 in. using the B.E. values for S_u and E_u . For a 1-ft raise in water level, from 9.0 ft to 10 ft, using the B.E. values for S_u and E_u resulted in an increased relative displacement from 2.0 to 3.3 in. These results imply that an analysis using minimum values of S_u and E_u , if it was numerically stable, likely would compute a maximum relative displacement at the ground surface on the order of 4 in.

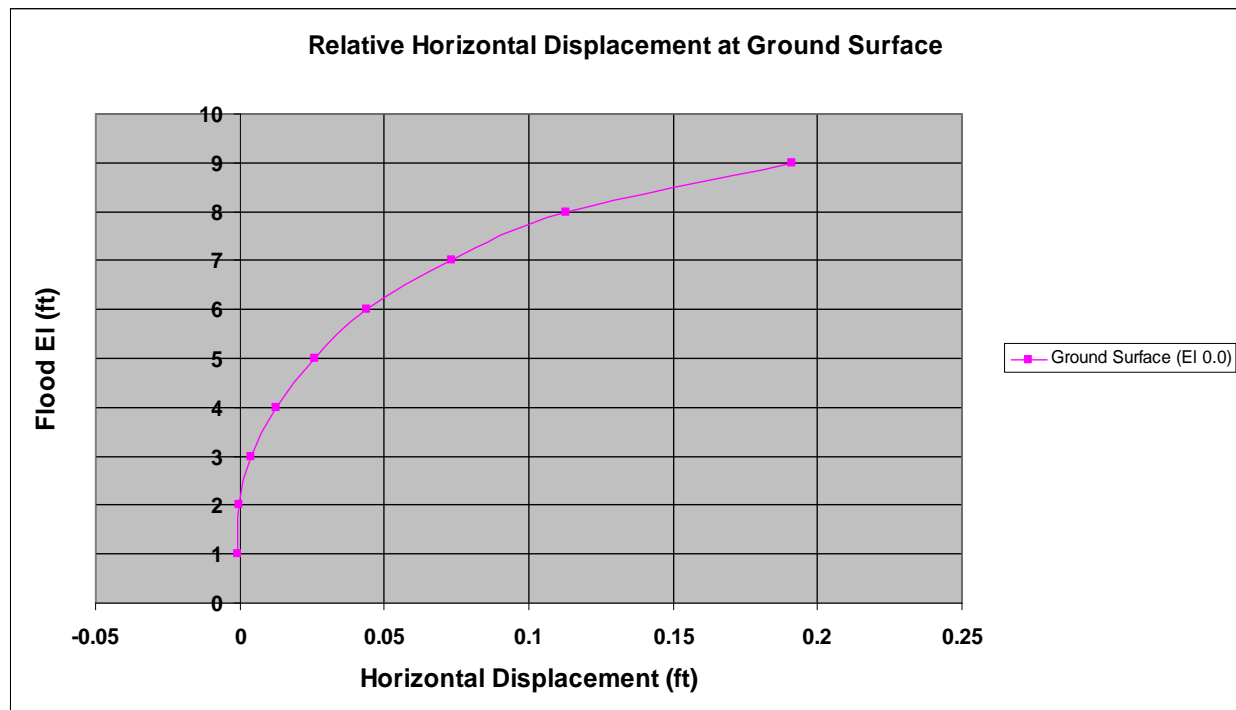


Figure A.7. Relative horizontal sheet-pile deflection at the ground surface el 0 ft versus water surface elevation using minimum computed values of undrained shear strength (S_u) and undrained stiffness (E_u).

Table A.4. Summary of relative horizontal displacements (U_x) of I-wall at the ground surface using minimum computed values of undrained shear strength (S_u) and undrained stiffness (E_u).

U_x at Ground Surface, ft	U_x at PileTip, ft	Relative Displacement at Ground Surface, ft	Flood el, ft	Gap depth, ft
0.0005	0.0012	-0.0007	1	0
0.0031	0.0034	-0.0003	2	4
0.0091	0.0052	0.0040	3	8
0.0194	0.0068	0.0126	4	12
0.0343	0.0084	0.0259	5	14
0.0537	0.0097	0.0440	6	15
0.0835	0.0100	0.0735	7	15
0.1225	0.0098	0.1127	8	15
0.1956	0.0044	0.1912	9	15

Table A.5. Comparison of relative horizontal displacements of I-wall at the ground surface using both the B.E. and minimum values of undrained shear strength (S_u) and undrained stiffness (E_u)

Flood elevation ft	Relative Displacement at Ground Surface ($S_{u(min)}, E_{u(min)}$), ft	Relative Displacement at Ground Surface ($S_{u(B.E.)}, E_{u(B.E.)}$), ft
1	-0.0007	-0.0014
2	-0.0003	-0.0021
3	0.0040	0.0017
4	0.0126	0.0106
5	0.0259	0.0243
6	0.0440	0.0428
7	0.0735	0.0677
8	0.1127	0.1041
9	0.1912	0.1652
10	N/A	0.2751

The total horizontal pressures acting on the interface elements adjacent to the wall on the flood side and landside for two flood elevations (6 ft and 9 ft) and corresponding gap elevation of -15 ft for each flood elevation are shown in Figures A.8 and A.9, respectively. The minimum values of soil adhesion were used in the PLAXIS analysis as well as in the active and passive pressure distributions shown in these figures. These pressure results were compared to limiting stress states (active and passive) for varying factors of safety applied to the undrained shear strength values. The flood elevation of 6 ft corresponds to the shallowest water level at which the gap propagated to el -15 ft. The flood elevation of 9 ft corresponds to both the design water height used in the conventional design and to the peak flood level that was specified in the PLAXIS SSI analysis while maintaining numerical stability.

As shown in Figure A.8 for the flood elevation of 6 ft, the SSI earth pressures on the landside fall between at-rest pressures and passive pressures (with a factor of safety of 1.5) down to el -14 ft. Below el -14 ft, the earth pressures reduce to near-active earth pressure (with a factor of safety of 1.0) at the sheet-pile tip (i.e., at el -16 ft). On the flood side, the complete SSI analysis computes hydrostatic water pressures acting down to the gap tip elevation of -15 ft, which is 1 ft above the pile tip elevation of -16 ft.

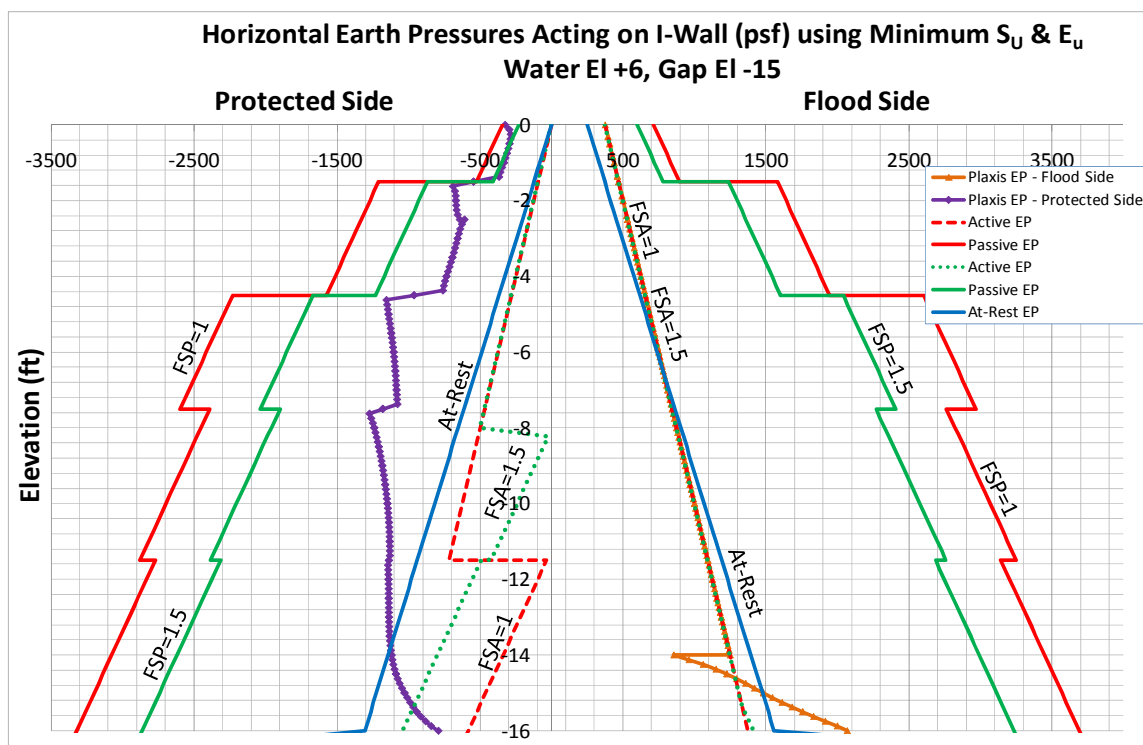


Figure A.8. Comparison of total normal stresses on the interface elements adjacent to the wall on the flood side and protected side (landside) for flood 6 ft and gap el -15 ft using minimum computed values of undrained shear strength (S_u) and undrained stiffness (E_u).

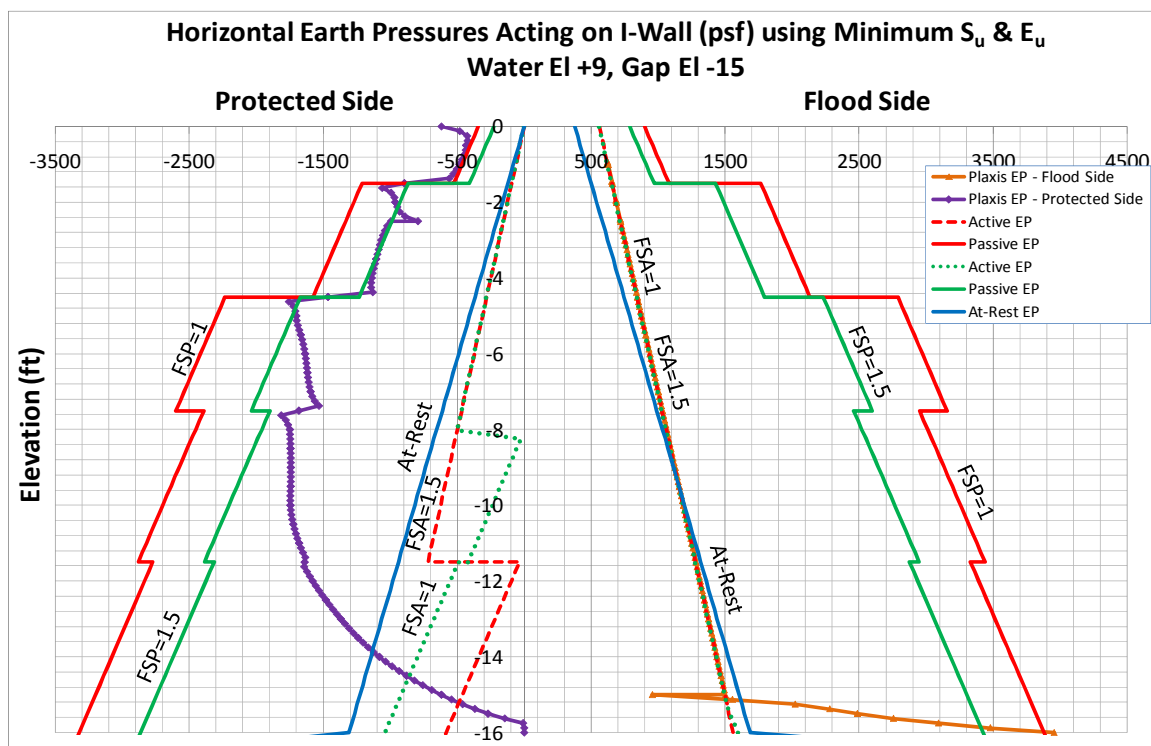
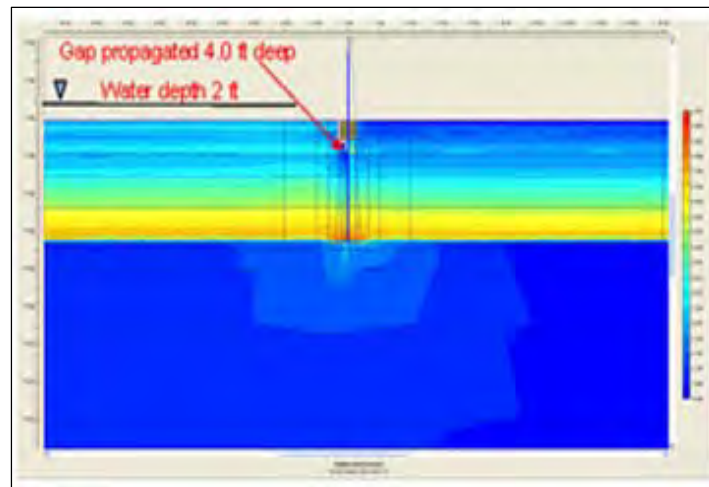


Figure A.9. Comparison of total normal stresses on the interface elements adjacent to the wall on the flood side and protected side (landside) for flood el 9 ft and gap el -15 ft using minimum computed values of undrained shear strength (S_u) and undrained stiffness (E_u).

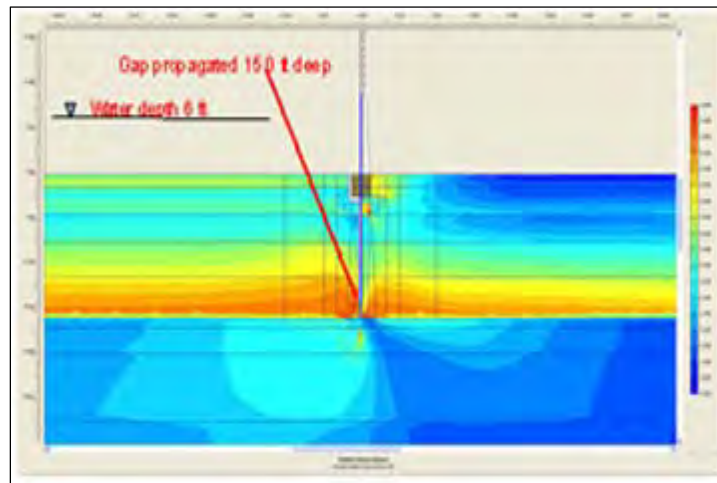
For design and peak flood elevation of 9 ft, the results in Figure A.9 show that on the landside of the wall the complete SSI earth-pressure results more closely match passive earth pressures computed with a factor of safety of 1.5 applied to the undrained shear strength values. On the flood side, the complete SSI analysis computes hydrostatic water pressures acting down to the gap tip elevation of -15 ft, 1 ft above the pile tip elevation of -16 ft. Below the gap tip elevation, the kickback of the I-wall into the flood side soil allows for the comparison of horizontal pressures computed by a complete SSI analysis to limiting earth passive pressures over this 1-ft depth. For all points except the point at el -16 ft, these computed horizontal pressures were less than those limiting passive earth pressure values computed using a factor of safety equal to 1.5. Kickback of the I-wall into the flood-side soil again is observed near the pile tip. This behavior is consistent with conventional force equilibrium procedures.

Computed fractions of mobilized shear strength for select floodwater elevations and gap depths are shown in Figure A.10. Recall that a fraction of mobilized shear strength equal to 1 indicates full mobilization of shear strength. As shown in Figures A.10(a) and A.10(b), for the specified flood elevation and gap depth, there are no regions of full mobilization of shear strength. The maximum fraction of mobilized shear strength in these figures is 0.90. These results indicate reserve shear capacity in the soil regime and, thus, a stable numerical model at these stages of construction. Figure A.10(c), with the design and peak flood depth of 9 ft and gap depth of -15 ft, shows regions of full mobilization of shear strength on the landside near the concrete cap and near the pile tip. However, there is no indication of a fully developed failure mechanism at the stage of loading. An additional loading phase with a flood elevation at 10 ft was attempted, but it resulted in numerical instability.

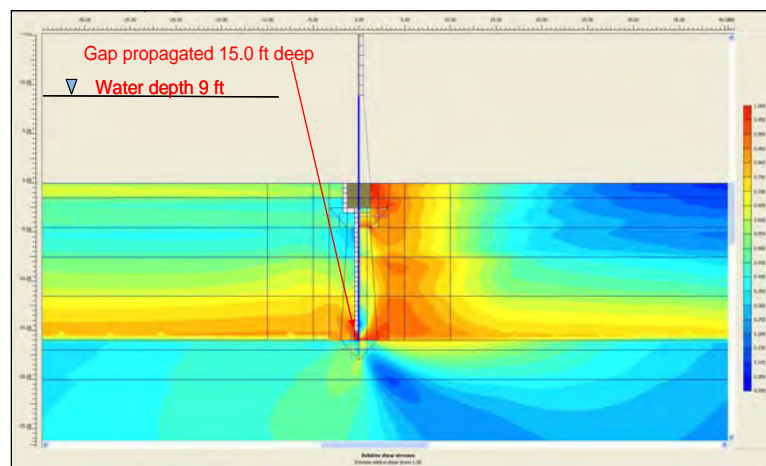
A subsequent PLAXIS analysis was performed at the design and peak flood elevation of 9 ft and gap depth at elevation of -15 ft to compute a factor of safety against a possible rotational failure mechanism. Figure A.6 indicated that the wall was rotating about a point near the pile tip. Figure A.11 shows a failure mechanism based on the PLAXIS Φ/c reduction procedure. The resulting rotational factor of safety was computed to be equal to 1.25. For short-term loading, I-walls are designed using conventional equilibrium procedures with a factor of safety set equal to 1.5 for the soil in the passive region. The factor of safety computed in the passive zone by PLAXIS for this level of loading is equal to 1.25.



a. Water depth 2 ft and gap depth 4 ft.



b. Water depth 6 ft and gap depth 15 ft.



c. Water depth 9 ft and gap depth 15 ft.

Figure A.10. Fractions of mobilized shear strength at various loading phases using minimum computed values of undrained shear strength (S_u) and undrained stiffness (E_u).

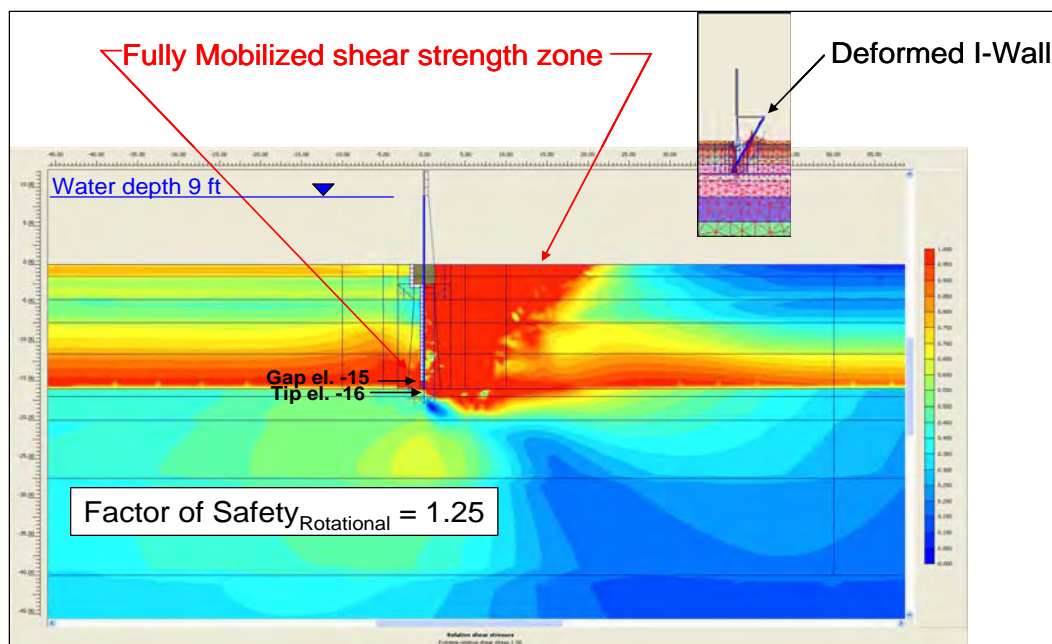


Figure A.11. Rotational factor of safety using Phi/c reduction for design peak flood elevation of 9 ft using minimum computed values of undrained shear strength (S_u) and undrained stiffness (E_u).

Lastly, at intermediate flood elevations less than el 9 ft, rotation of the wall was not indicated. It is believed that the Phi/c reduction procedure would compute factors of safety based on localized shear failures with the active driving wedge only. Similar results were observed using B.E. values of undrained shear strength (S_u) and undrained stiffness (E_u) (refer to Chapter 2). Therefore, for this analysis, the Phi/c reduction procedure was not further used to compute factors of safety resulting from rotational failure mechanisms (as is performed in limit equilibrium procedures) for intermediate flood elevations.

Appendix B: Analyses of I-wall Site Founded in an Overconsolidated Lean Clay Using Minimum Values of Undrained Shear Strength (S_u) and Maximum Values of Undrained Secant Stiffness (E_u)

B.1 Purpose of analyses

This appendix summarizes the findings of a series of complete nonlinear soil-structure interaction (SSI)¹ finite element analyses performed on an I-wall section founded in an overconsolidated lean clay. Minimum values of undrained shear strength (S_u) distribution with depth and maximum values of undrained secant stiffness (E_u) distribution with depth are assigned to the clay soils. This corresponds to mean minus two standard deviations for the S_u distribution and mean plus four standard deviations for the E_u distribution. The focus of this study was to investigate the phenomena of gap initiation and propagation along the soil-to-structure interface on the flood side of the I-wall and to study the effects of gap initiation and propagation on the resulting deformation and stress conditions in the soil regime on both the flood side and landside of the I-wall. The findings of these analyses will be used in a companion research effort focusing on risk and reliability assessments of I-wall systems.

The following sections will describe the soil used in the analyses, the selection of stiffness and shear strength parameters, the conventional design of the I-wall, the procedures employed in the analyses, and the results of the complete nonlinear SSI analyses.

B.2 Overview of flood-site I-wall being analyzed

The geometry of the problem analyzed is the same wall system shown in Figure 2.1. The site was assumed to be a level plan with a maximum floodwater elevation of 9 ft. Two soil layers were assumed in the analyses. The top 20 ft represented an overconsolidated layer, while the underlying

¹ Symbols and unusual abbreviations used in this Appendix are listed and defined in the Notation, Appendix I.

soil was assumed to be normally consolidated. The elevation of the soil surface was assumed to be at 0 ft.

The I-wall is composed of a sheet-pile wall with the tip at el -16 ft. The top of the I-wall is composed of a concrete cap 2.5 sq ft (i.e., embedment to el -2.5 ft), with the top of the cap level with the ground surface. The wall above the top of the soil is composed of a tapered concrete section 2.5 ft at the base and 1 ft at the top of the wall (el 9 ft). The water table for this problem is at the pile tip (el -16 ft).

B.3 Conventional design of cantilever I-wall and shear strength

The design depth of penetration of the sheet-pile section of the I-wall was determined using the Computer-Aided Structural Engineering (CASE) CWALSHT computer program and procedures outlined in Headquarters, U.S. Army Corps of Engineers (1994).¹ The computed design depth of penetration of the sheet pile (-16 ft) (refer to Chapter 2) was used in this analysis without consideration of a gap forming between the concrete cap and the soil or between the sheet pile and soil on the flood side of the I-wall and using the mean S_u distribution with depth given in Chapter 2. However, note that the finite element analysis for the wall section was conducted for this same -16-ft design depth, and it considered the potential for gap initiation and propagation. It too should be noted that the inclusion of a gap beside the wall also would affect the design depth. This analysis provides useful information for a lower ratio of embedment to flood height. It is important to recognize that the factor of safety for this system based on complete SSI results for a flood elevation of 9 ft would not correspond to the factor of safety used for design in CWALSHT because a gap was not assumed in the CWALSHT analysis.

The total stress (undrained) shear strength parameters were determined using the SHANSEP procedure (Ladd and Foott 1974) discussed in Chapter 2. It assumes that the soil shear strength can be normalized by the effective overburden pressure. The effective overburden pressure is calculated at midlayer for each of the layers identified in Table B.1 and using a preflood water table elevation of -16 ft. The ratio of shear strength to effective overburden pressure (S_u/σ'_{vo}) is dependent on the over-consolidation ratio (OCR) and a fitting parameter (m), assumed to be 0.8, as shown in Equation B.1:

¹ Citations in this appendix are in the References at the end of the main text.

Table B.1. Computation of minimum S_u variation with depth.

Layer			Short-Term (Undrained) Loading				
No.	Top el, ft	Bottom el, ft	Depth, ft	σ'_{vo} , psf	OCR	$(S_u/\sigma'_{vo})_{oc}$	$S_{u,min}$, psf
1	0	0	1	122	7	0.85379	104
			2	244	7	0.85379	208
2	-1.5	-4.5	3	366	7	0.85379	312
			4	488	7	0.85379	417
			5	610	6.4	0.794724	485
3	-4.5	-7.5	6	732	5.5	0.703984	515
			7	854	4.8	0.631343	539
			8	976	3.6	0.50155	490
4	-7.5	-11.5	9	1098	2.9	0.421882	463
			10	1220	2.3	0.350473	428
			11	1342	2	0.313398	421
			12	1464	1.7	0.275189	403
			13	1586	1.6	0.262161	416
5	-11.5	-17.5	14	1708	1.4	0.2356	402
			15	1830	1.35	0.228844	419
			16	1952	1.3	0.222038	433
			17	2011.5	1.25	0.215179	433
			18	2071	1.2	0.208266	431
6	-17.5	-20	19	2130.5	1.15	0.201294	429
			20	2190	1.1	0.194261	425
7	-20	-27.5	25	2487.5	1	0.18	448
			30	2785	1	0.18	501
8	-27.5	-40	35	3082.5	1	0.18	555
			40	3380	1	0.18	608
			45	3677.5	1	0.18	662
			50	3975	1	0.18	716
9	-40	-60	55	4272.5	1	0.18	769
			60	4570	1	0.18	823
			65	4867.5	1	0.18	876
10	-60	-80	70	5165	1	0.18	930
			75	5462.5	1	0.18	983
			80	5760	1	0.18	1037
			85	6057.5	1	0.18	1090
11	-80	-100	90	6355	1	0.18	1144
			95	6652.5	1	0.18	1197
			100	6950	1	0.18	1251

$$\left(\frac{S_u}{\sigma'_{vo}} \right)_{OCR} = \left(\frac{S_u}{\sigma'_{vo}} \right)_{NC} \bullet OCR^m, \quad (B.1)$$

where

$(S_u/\sigma'_{vo})_{OCR}$ = ratio of the undrained shear strength to effective overburden pressure for the overconsolidated condition;
 $(S_u/\sigma'_{vo})_{NC}$ = ratio of the undrained shear strength to effective overburden pressure for the normally consolidated condition.

From published values (Ladd 1991), a mean value of 0.22 was assigned to $(S_u/\sigma'_{vo})_{NC}$ (Chapter 2) and a value of 0.8 for m based on Direct Simple Shear (DSS) test results. These data also indicated a standard deviation equal 0.02 for the $(S_u/\sigma'_{vo})_{NC}$ data. In the computation of the effective overburden pressures, 122 pcf was used for both the moist and the saturated unit weights. The OCR characterization of this site is the same as discussed in Chapter 2 and is shown in Figure 2.3.

The resulting variation in the undrained shear strength (S_u) with depth is shown in blue in Figure B.1. Average values of S_u were estimated to be constant over a given depth, as shown in pink in Figure B.1. These constant values for the soil layers are listed in Table B.1 and were used in the complete SSI analysis to approximate variation in S_u with depth.

B.4 Shear strength and stiffness properties used in the complete SSI analysis

A complete SSI analysis of the I-wall section shown in Figure 2.1 was performed using the two dimensional (2-D) version of the PC-based finite element program PLAXIS. The finite element method employed required certain input material properties for the selected soil constitutive models. The PLAXIS nonlinear Hardening Soil (HS) constitutive model was used to model all soil elements. This constitutive model provides for nonlinear stress-strain response for soil elements during loading. Elastic plate elements were used to model the steel sheet-pile and the concrete I-wall sections. In order to process bending moment and shear distribution results more efficiently, plate elements were used to model the concrete I-wall. Two-dimensional elastic elements were used to represent the concrete cap (the region in which the sheet pile is embedded).

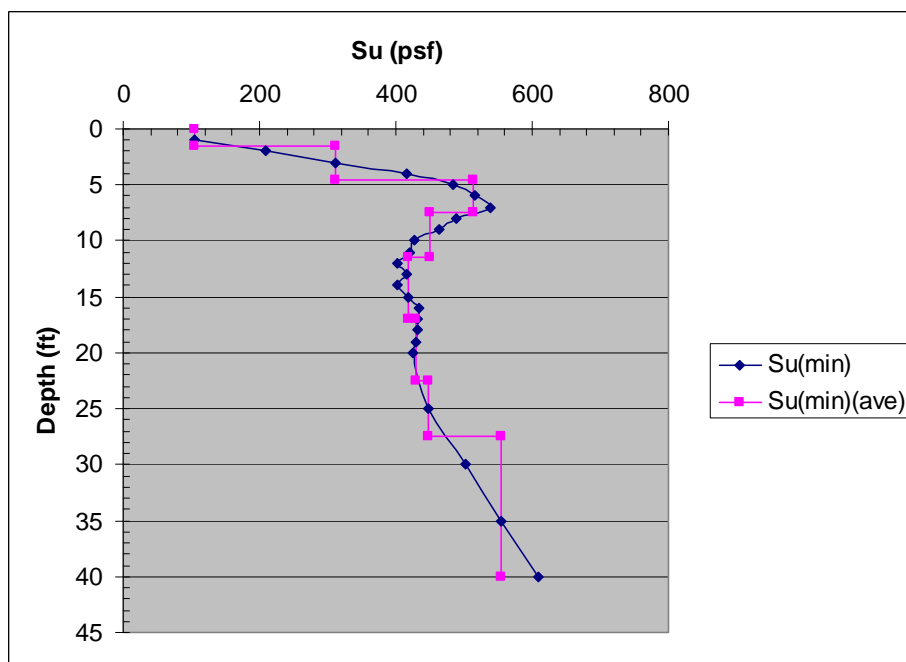


Figure B.1. Variation in minimum computed values of undrained shear strength (S_u) with depth.

Total stress soil strength parameters were used to characterize this over-consolidated lean clay site. An SSI parametric study was conducted to determine a minimum shear strength (considered near-failure conditions) that resulted in a numerically stable analysis. This was accomplished by using the mean value of 0.22 assigned to $(S_u/\sigma_v')_{NC}$ in conjunction with a standard deviation of 0.02. The $(S_u/\sigma_v')_{NC}$ ratio was reduced by one, two, and three standard deviations from the mean value of 0.22 in three separate PLAXIS analyses until the minimum computed shear strength and maximum stiffness variation resulted in a numerically stable SSI analysis at the design flood elevation of 9 ft. The PLAXIS analysis using the mean minus three standard deviations did not converge. The PLAXIS analysis using the mean minus two standard deviations did converge. The minimum computed ratio $(S_u/\sigma_v')_{NC}$ was equal to 0.18 (computed using Equation B.2):

$$\left(\frac{S_u}{\sigma_v'} \right)_{NC-2\sigma} = \left(\frac{S_u}{\sigma_v'} \right)_{NC-mean} - 2\sigma, \quad (B.2)$$

where

$$\left(\frac{S_u}{\sigma_v'} \right)_{NC-mean} = 0.22$$

and σ , the standard deviation, was 0.02.

Additionally, the maximum variation in shear strength with depth was computed using the mean value of 0.22 assigned to $(S_u/\sigma_v')_{NC}$ in conjunction with four times the standard deviation of 0.02. The maximum computed ratio $(S_u/\sigma_v')_{NC}$ was equal to 0.30 and was computed using Equation B.3.

$$\left(\frac{S_u}{\sigma_v'} \right)_{NC+4\sigma} = \left[\left(\frac{S_u}{\sigma_v'} \right)_{NC-mean} + 4\sigma \right]. \quad (B.3)$$

The resulting maximum variation in stiffness with depth was computed using the results of Equation B.3 and Equation B.4:

$$E_{u(NC+4\sigma)} = \text{constant} \times S_{u(NC+4\sigma)}, \quad (B.4)$$

where

$$S_{u(NC+4\sigma)} = \left[\left(\frac{S_u}{\sigma_v'} \right)_{NC-mean} + 4\sigma \right] \bullet \sigma_v'$$

and $\text{constant} = E_u/S_u$ ratios at each elevation listed in Table B.2

The correlation by Duncan and Buchignani (1976), shown in Figure 2.5 and Equation 2.2, was used to estimate the maximum variation of undrained secant modulus in clay with depth. Table B.2 summarizes the computation of E_{us} with depth, using the average values of the variation of S_u with depth from Table B.1 in conjunction with Equation 2.2. These values of E_{us} were used to estimate the variation in the PLAXIS input stiffness parameter E_{50}^{ref} , which is a secant modulus at 50 percent of the principal stress difference $(\sigma_1 - \sigma_3)$. The remaining parameters for soil properties selected to represent the clay (CL) soils used in the PLAXIS finite element analyses were the same as discussed in Chapter 2. Table B.3 shows minimum values of HS constitutive soil parameters used in these analyses. Values of the coefficient of friction between the sheet pile and the soil and between the concrete cap and the soil were the same as referenced in Table 2.5.

Table B.2. Computation of maximum undrained secant modulus (E_{us}).

Layer			Short-Term (Undrained) Loading					Eu/Su	Eu,max, psf
			Depth, ft	σ'_{vo} , psf	OCR	$(S_u/\sigma'_{vo})_{oc}$	$S_{u,max}$, psf		
1	0	0	1	122	7	1.422983	174	250	43,401
			2	244	7	1.422983	347	250	86,802
2	-1.5	-4.5	3	366	7	1.422983	521	250	130,203
			4	488	7	1.422983	694	250	173,604
			5	610	6.4	1.32454	808	270	218,152
3	-4.5	-7.5	6	732	5.5	1.173306	859	300	257,658
			7	854	4.8	1.052239	899	350	314,514
			8	976	3.6	0.835917	816	450	367,135
4	-7.5	-11.5	9	1098	2.9	0.703137	772	500	386,022
			10	1220	2.3	0.584122	713	550	391,946
			11	1342	2	0.52233	701	580	406,561
			12	1464	1.7	0.458649	671	590	396,163
			13	1586	1.6	0.436935	693	590	408,858
5	-11.5	-17.5	14	1708	1.4	0.392666	671	600	402,404
			15	1830	1.35	0.381407	698	600	418,785
			16	1952	1.3	0.370063	722	600	433,418
			17	2011.5	1.25	0.358632	721	600	432,833
			18	2071	1.2	0.347109	719	600	431,318
6	-17.5	-20	19	2130.5	1.15	0.33549	715	600	428,857
			20	2190	1.1	0.323769	709	600	425,433
7	-20	-27.5	25	2487.5	1	0.3	746	600	447,750
			30	2785	1	0.3	836	600	501,300
8	-27.5	-40	35	3082.5	1	0.3	925	600	554,850
			40	3380	1	0.3	1014	600	608,400
			45	3677.5	1	0.3	1103	600	661,950
			50	3975	1	0.3	1193	600	715,500
9	-40	-60	55	4272.5	1	0.3	1282	600	769,050
			60	4570	1	0.3	1371	600	822,600
			65	4867.5	1	0.3	1460	600	876,150
10	-60	-80	70	5165	1	0.3	1550	600	929,700
			75	5462.5	1	0.3	1639	600	983,250
			80	5760	1	0.3	1728	600	1,036,800
			85	6057.5	1	0.3	1817	600	1,090,350
11	-80	-100	90	6355	1	0.3	1907	600	1,143,900
			95	6652.5	1	0.3	1996	600	1,197,450
			100	6950	1	0.3	2085	600	1,251,000

Table B.3. Minimum HS model strength and maximum stiffness properties for the soil layers.

Layer			c_{ref} , lbs/ft ²	$E_{50,ref}$, lbs/ft ²	$E_{oed,ref}$, lbs/ft ²	$E_{ur,ref}$, lbs/ft ²
No.	Top El, ft	Bottom El, ft				
1	0.0	0.0	104	4.34E+04	4.34E+04	1.30E+05
2	-1.5	-4.5	312	1.30E+05	1.30E+05	3.91E+05
3	-4.5	-7.5	513	2.63E+05	2.63E+05	7.90E+05
4	-7.5	-11.5	450	3.88E+05	3.88E+05	1.16E+06
5	-11.5	-17.0	418	4.15E+05	4.15E+05	1.25E+06
6	-17.0	-20.0	429	4.29E+05	4.29E+05	1.29E+06
7	-20.0	-27.5	448	4.48E+05	4.48E+05	1.34E+06
8	-27.5	-40.0	555	5.55E+05	5.55E+05	1.66E+06
9	-40.0	-60.0	742	7.42E+05	7.42E+05	2.23E+06
10	-60.0	-80.0	956	9.56E+05	9.56E+05	2.87E+06
11	-80.0	-100.0	1171	1.17E+06	1.17E+06	3.51E+06

Minimum values of adhesion were assigned to the soil along the I-wall-to-soil and sheet-pile-to-soil interfaces in the complete SSI analysis. The minimum value for adhesion was estimated using the one selected for the ratio of adhesion to cohesion (f_c) between the sheet pile and soil and between the concrete and the soil shown in Table 2.5 and Equation 2.3. Substituting the ratio of adhesion to cohesion equal to 0.8 into Equation 2.3 and solving for $(C_a)_{min}$ yields Equation B.5:

$$(C_a)_{min} = 0.8(C)_{min} = 0.8(C_{mean} - 2\sigma), \quad (B.5)$$

where

$(C_a)_{min}$ = minimum soil adhesion;

C_{min} = minimum value of cohesion = minimum value of undrained shear strength $(S_u)_{min}$;

C_{mean} = mean value of cohesion = mean value of undrained shear strength $(S_u)_{mean}$;

σ = standard deviation.

The properties of the concrete cap represented by elastic elements and the properties of the concrete I-wall section modeled by elastic plate elements with the properties were the same as referenced in Tables 2.6 and 2.7, respectively. The sheet pile was represented by elastic plate elements with the same properties as referenced in Table 2.8.

B.5 Discussion of finite element analyses

B.5.1 Conceptual model

The finite element analysis was performed using the 2-D version of the nonlinear incremental construction finite element program PLAXIS. The conceptual model of the finite element mesh is the same as shown in Figure 2.6. The geometry is the same as in Figure 2.1. Several special modeling features were used, including the sheet-pile wall and the concrete I-wall section being modeled by elastic plate elements. Interface elements and soil elements beside the sheet-pile wall on the flood side were 1/2 ft in height. These special features are described in Chapter 2.

B.5.2 Gap initiation and propagation criterion

A hydraulic fracturing criterion is applied to determine whether a gap will develop and if it will spread down the soil-to-I-wall interface. In this procedure of analysis, the total horizontal stress computed by PLAXIS at the ground surface soil-to-I-wall interface is compared to the hydrostatic water pressure developing at the top of the ground surface caused by the presence of the specified flood pool elevation. If the hydrostatic water pressure of the flood pool (the demand) exceeds the total horizontal stress (the capacity), a gap will initiate at the ground surface, along the soil-to-I-wall interface. This criterion is discussed in Chapter 2.

B.5.3 Finite element model

A 2-D cross section used by the PLAXIS program to model the variation of undrained shear strength and soil stiffness with depth is shown in Figure B.2. The regions of uniform color reflect soil clusters used to define the mesh and assign soil regions with common properties. The inset figure shows the average undrained shear strengths assigned to the upper eight layers and based on the minimum S_u values (i.e., mean minus two standard deviations). The finite element mesh used in the analysis is the same as shown in Figure 2.9. The mesh is composed of 4,187 elements and 34,408 nodes with 50,244 stress points. The mesh consists of 15-node triangular elements to model the soil, plate elements to model the bending effects of the I-wall and sheet-pile wall, and interface elements to model SSI between the sheet-pile wall and the adjacent soil elements. The analyses are executed as a plane strain problem. An enlarged view of the area around the wall and its mesh is shown in Figure 2.10.

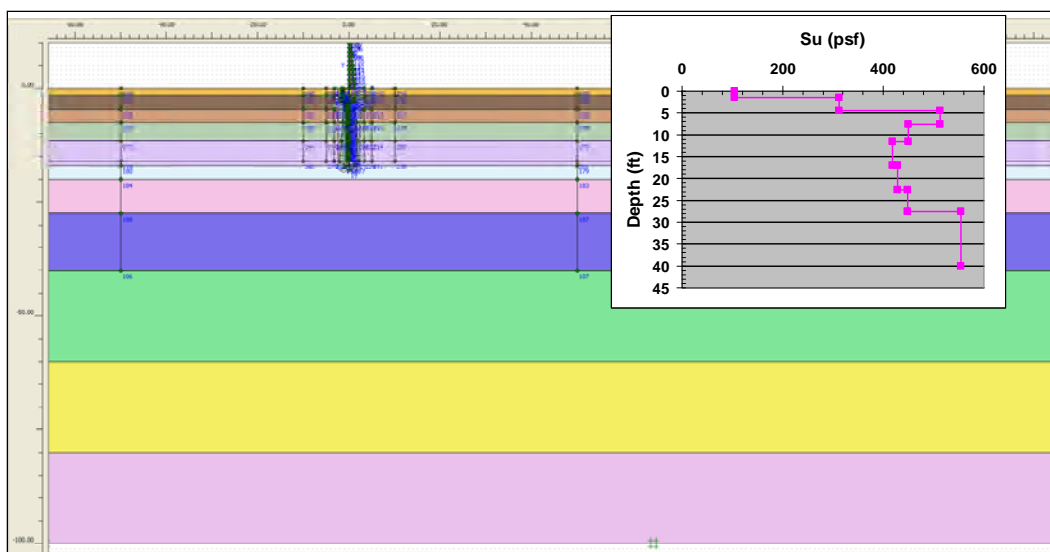


Figure B.2. Two-dimensional (2-D) cross-section model using the minimum computed values of undrained shear strength (S_u) and maximum computed undrained secant stiffness (E_u) used in the SSI analyses.

B.6 Results of the finite element analyses

B.6.1 Initial stresses

The initial total stress state within the finite element mesh was established using the at-rest soil conditions for a level ground surface. Horizontal at-rest soil stresses were estimated using the interrelationship between the at-rest earth pressure coefficient (K_0) and the soil Poisson's ratio (ν) (Equation 2.4). The assumed groundwater elevation was at the sheet-pile tip (el -16 ft). The assigned values of ν and the corresponding (K_0) values used to compute the horizontal earth pressures for the initial conditions are summarized in Table 2.9.

For this level ground site, the at-rest stress is computed by multiplying the total overburden pressure for each integration point in every soil element by K_0 . Figure B.3 shows the computed fraction of mobilized shear strength (referred to as relative shear stress in PLAXIS output) from the initial total stress condition. The resulting fraction of mobilized shear strength (1.0 indicates full mobilization of shear strength) is less than or equal to 0.77 for all soil clusters. These results indicate reserve shear capacity in the soil regime and, thus, a stable numerical model at this initial stage of construction.

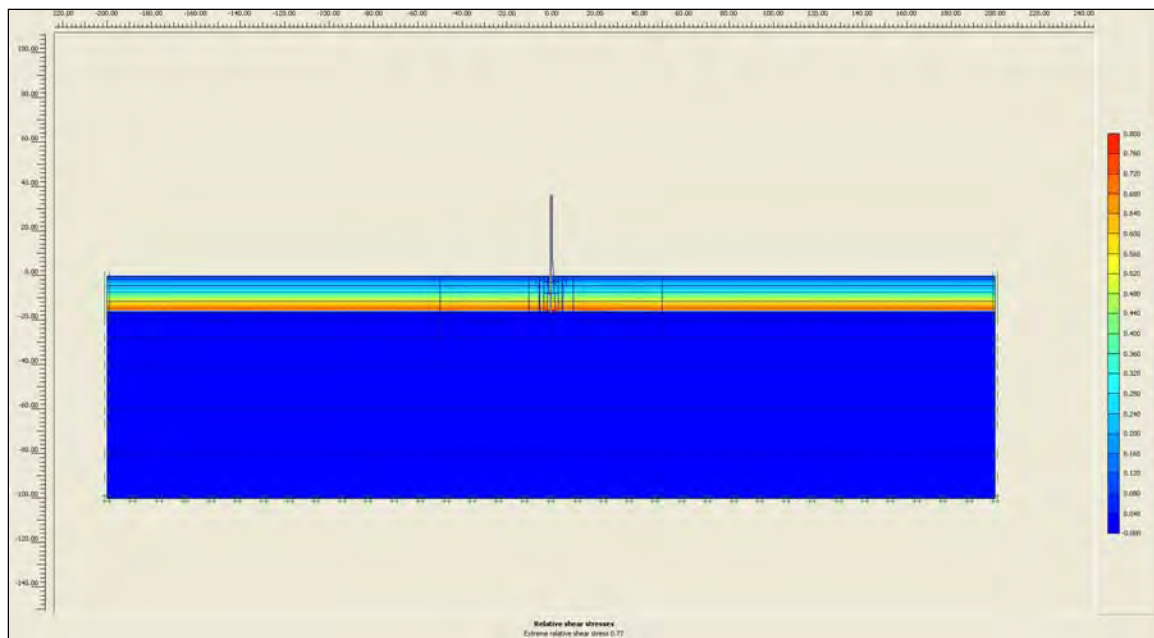


Figure B.3. Fraction of mobilized shear strength for initial conditions using the minimum computed values of undrained shear strength (S_u) and the maximum computed values of undrained secant stiffness (E_u).

B.6.2 Gap initiation and propagation results

The focus of this study was to investigate the phenomena of gap initiation and propagation along the flood side of the soil-to-I-wall interface and the effects of these phenomena on the resulting deformation and stress conditions in the soil regime on both the flood and landside of the I-wall system.

Modeling of the flood loading commenced in the complete SSI analysis after the total initial stress state was established within the mesh for an assumed steady-state water elevation at the ground surface (el 0.0 ft). To track the formation and propagation of a gap, the flood loading was applied in 1-ft incremental raises of the water level. The hydraulic fracturing criterion is used to estimate a gap formation and its propagation. This procedure compares the total normal earth pressures due to the flood pool acting on the wall at a given depth to the hydrostatic water pressure acting at the corresponding depth. A gap is formed when the total horizontal earth pressure (the capacity) is less than the water pressure due to the flood pool acting at the corresponding depth (the demand). Next, hydrostatic water pressure is applied over the depth of gap, and this hydrostatic water pressure at the new, deeper gap depth is compared to the total horizontal earth pressure. Gap propagation is terminated at the depth when the demand is less than

the capacity. Complete SSI analysis results were examined for various water elevations and gap depths. Figure B.4 shows the progression of the gap as the water level against the I-wall is increased. As shown, the gap initiates when the water is at the shallow el 2 ft and extends to a depth of -4.0 ft. The gap extends to el -8 ft at a water elevation of 3 ft. At water el 7 ft, the gap extends to el -15 ft and gap elevation remains constant to a water elevation of 10 ft. Note that the gap is within 1 ft of the sheet-pile tip for floodwater levels at and above el 7 ft. Recall, in the analysis using minimum S_u variations and maximum E_u variations, a floodwater elevation of 6 ft computed a gap that extended to this same elevation of -15 ft.

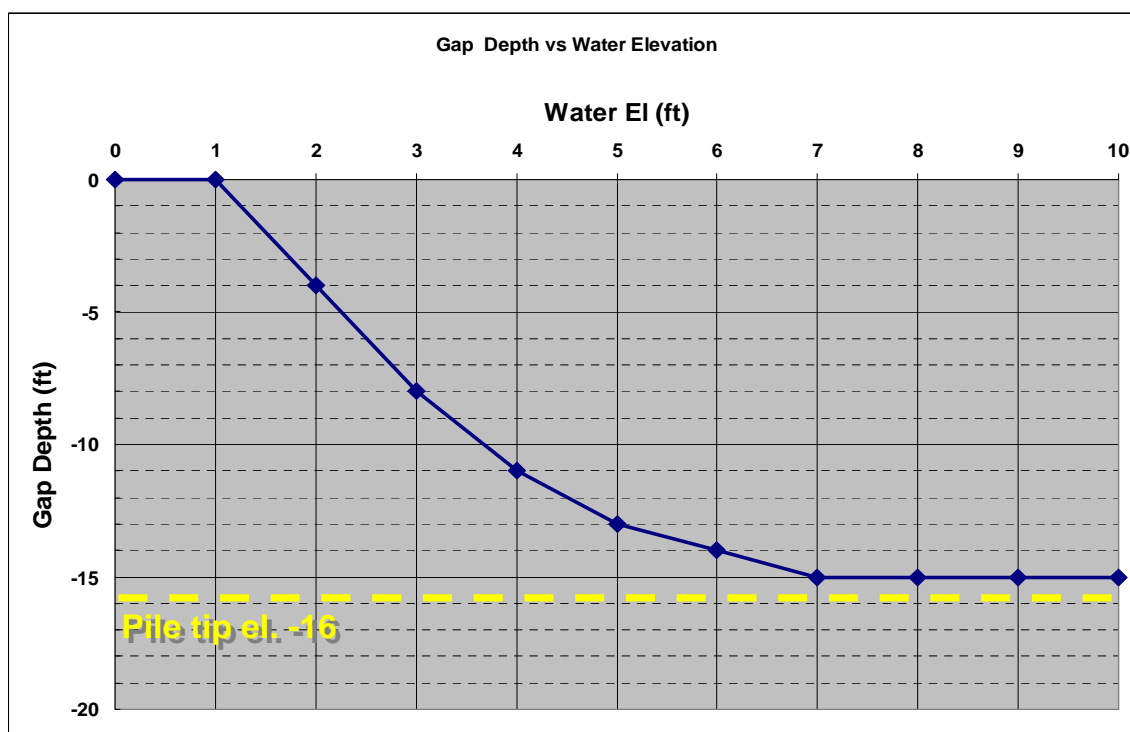


Figure B.4. Progression of gap versus water elevation using the minimum computed values of undrained shear strength (S_u) and the maximum computed values of undrained secant stiffness (E_u).

B.6.3 Performance of interface elements

The performance of the interface elements was compared to the performance of the soil elements adjacent to the wall to ascertain whether the results for the interface elements could be used to characterize the computed results of the analyses accurately. Figure 2.13 shows that the total horizontal stresses computed within the interface and soil elements agree closely for the selected flood elevation of 2 ft. Therefore, interface element results were used to summarize computed results from this complete SSI analysis.

B.6.4 Discussion of displacements and stresses

The total (exaggerated) nodal displacements within the finite element mesh (both soil and wall) are shown in Figure B.5. These displacements are for the design water elevation of 9 ft with a gap depth to el -15 ft. Note that the nodal displacements are increased by a factor of 100 in this figure to show both the deformed mesh relative to its initial position and the extent of the gap. The gap was modeled by deactivating the soil elements adjacent to the wall. The general trend of the deflections was toward the landside because of the applied boundary water pressures on the flood side. The wall had a greater movement than the soil at this loading phase. The maximum wall displacement was approximately 2.5 in. at the top of the wall. The displacement of the wall consisted of both horizontal and vertical movements. The tip of the wall actually moved slightly upward and toward the landside.

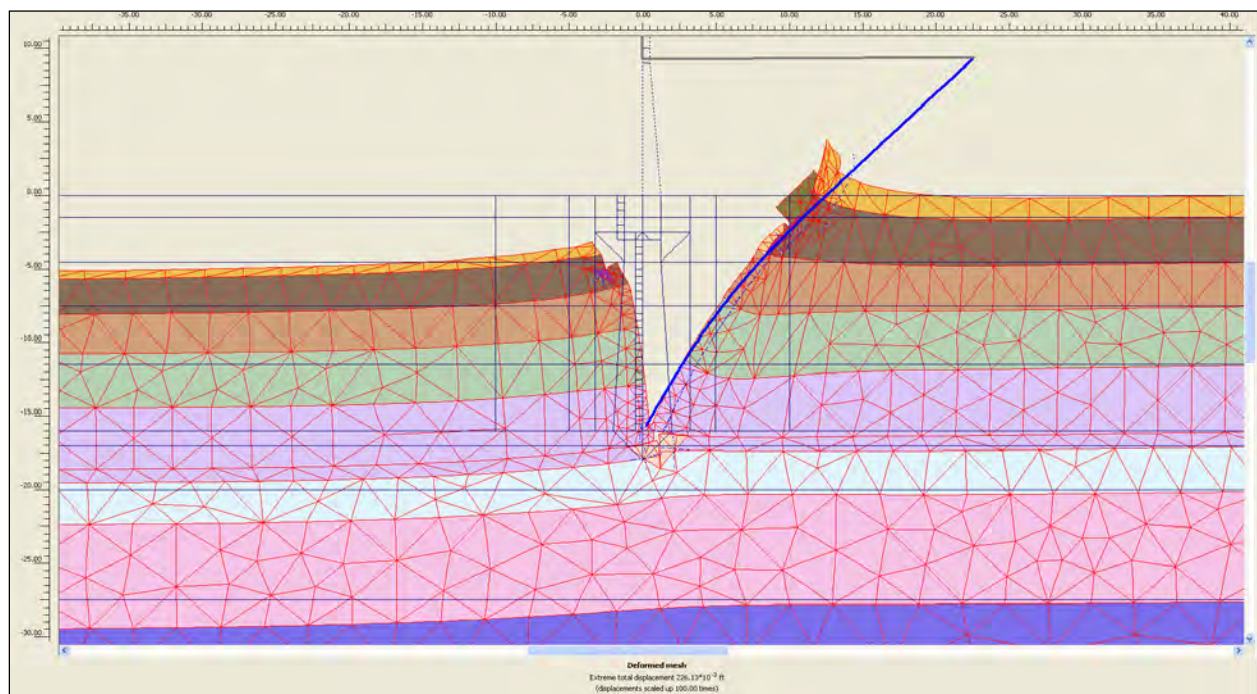


Figure B.5. Total exaggerated displacements for a water elevation of 9 ft and gap elevation of -15 ft using the minimum computed values of undrained shear strength (S_u) and the maximum computed values of undrained secant stiffness (E_u).

Figure B.6 shows a plot of horizontal displacements of I-wall versus flood-water elevation at three points along the wall. The points monitored in the analysis were the top of the I-wall at el 9 ft, at the ground surface el 0 ft, and at the sheet-pile tip el -16 ft. As shown, the deflection of the wall up to flood el 3 ft (after gap initiation) was primarily uniform translation. As

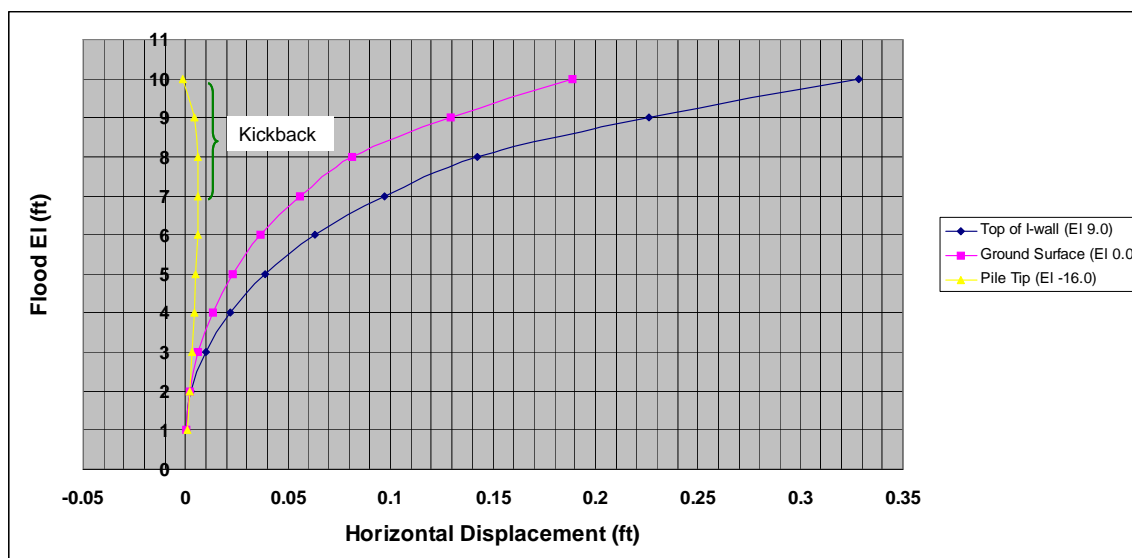


Figure B.6. Horizontal sheet-pile deflection versus water elevation using the minimum computed values of undrained shear strength (S_u) and the maximum computed values of undrained secant stiffness (E_u).

the water elevation increased, the top of the wall experienced larger deformations than those of the ground and much larger deformations than those of the pile tip. This implies that the wall was undergoing rotation along with translation. Also, above water el 7 ft the deflection of the pile tip was directed toward the flood-side soil, which indicates kickback of the pile tip. This behavior is consistent with the behavior assumed in limit equilibrium design procedures for the design of cantilever sheet-pile walls.

Figure B.7 shows a plot of relative horizontal displacements of I-wall versus floodwater elevation at the ground surface. Relative displacements were computed at this location to provide results for a companion research effort focusing on risk and reliability assessments of I-walls. The relative displacements were computed by subtracting the displacements of the sheet-pile tip from the sheet-pile displacements at the ground surface for a given flood-water elevation. The maximum computed relative horizontal displacement of the wall at the ground was approximately 2.3 in. for a maximum flood elevation of 10 ft. Computed relative horizontal displacements for this and other flood pool elevations are reported in Table B.4.

Recall that the analysis using the mean, best estimate (B.E.) values for S_u and E_u resulted in a maximum computed relative horizontal displacement of the wall at the ground of approximately 3.3 in. (Table 2.10). Table B.5 compares the maximum computed relative horizontal displacements from analyses using both the B.E. of S_u and E_u and the minimum S_u and

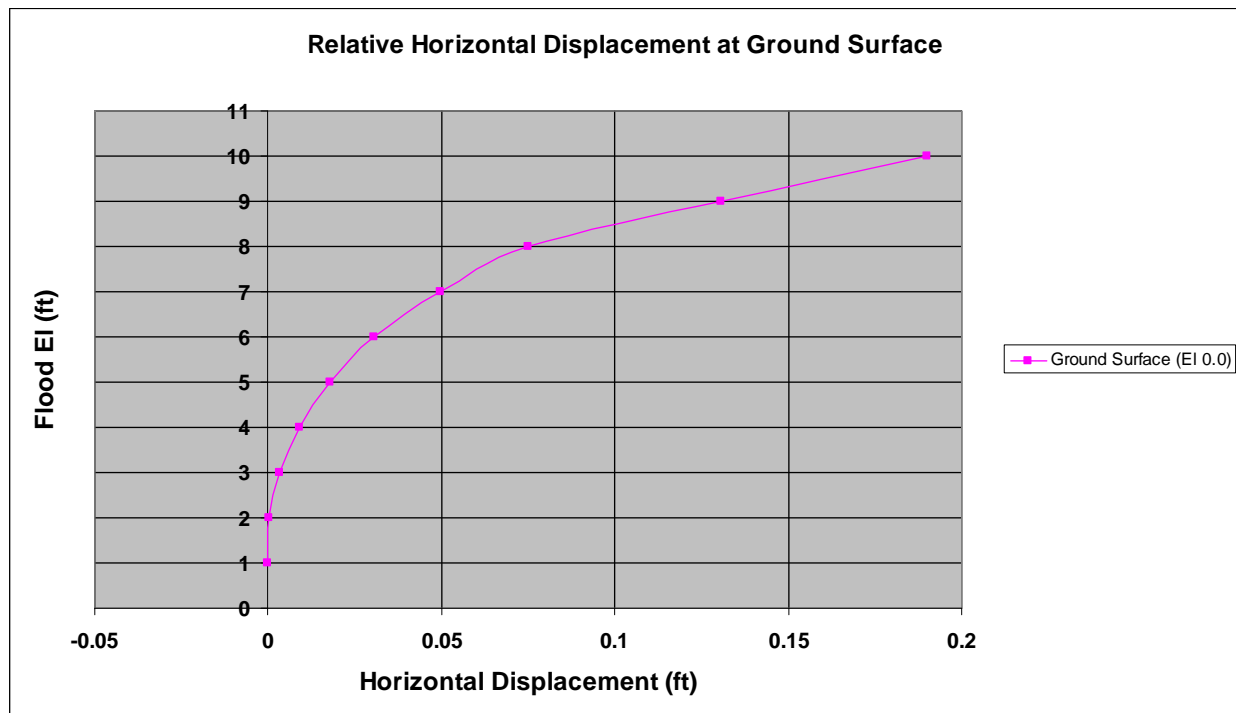


Figure B.7. Relative horizontal sheet-pile deflection at the ground surface el 0 ft versus water elevation using the minimum computed values of undrained shear strength (S_u) and the maximum computed values of undrained secant stiffness (E_u).

Table B.4. Summary of relative horizontal displacements (U_x) of l-wall at the ground surface using minimum computed values of undrained shear strength (S_u) and maximum computed values undrained secant stiffness (E_u).

U_x at Ground Surface, ft	U_x at Pile Tip, ft	Relative Displacement at Ground Surface, ft	Flood Elevation, ft	Gap Depth, ft
0.0003	0.0007	-0.0003	1	0
0.0022	0.0020	0.0001	2	4
0.0063	0.0032	0.0031	3	8
0.0132	0.0042	0.0090	4	11
0.0229	0.0051	0.0178	5	13
0.0364	0.0059	0.0304	6	14
0.0558	0.0062	0.0496	7	15
0.0813	0.0061	0.0751	8	15
0.1293	-0.0013	0.1306	9	15
0.1885	-0.0013	0.1899	10	15

Table B.5. Comparison of relative horizontal displacements of I-wall at the ground surface using both the best-estimate and minimum computed values of undrained shear strength (S_u) and maximum computed values undrained secant stiffness (E_u)

Flood El, ft	Relative Displacement at Ground Surface ($S_{u(min)}, E_{u(max)}$), ft	Relative Displacement at Ground Surface ($S_{u(B.E.)}, E_{u(B.E.)}$), ft
1	-0.0003	-0.0014
2	0.0001	-0.0021
3	0.0031	0.0017
4	0.0090	0.0106
5	0.0178	0.0243
6	0.0304	0.0428
7	0.0496	0.0677
8	0.0751	0.1041
9	0.1306	0.1652
10	0.1899	0.2751

maximum E_u values. As shown for the maximum flood el 10 ft, the maximum computed relative displacement using the minimum values of S_u and maximum values of E_u was equal to approximately 2.3 in., compared to approximately 3.3 in. using the B.E. values for S_u and E_u . The influence of the larger values of soil stiffness resulted in a 30 percent decrease in the computed relative horizontal displacement of the wall at the ground surface.

The total horizontal pressures acting on the interface elements adjacent to the wall on the flood side and landside for three flood elevations (7 ft, 9 ft, and 10 ft) and corresponding gap elevation of -15 ft for each flood elevation are shown in Figures B.8 through B.10, respectively. Minimum values of soil adhesion were used in the PLAXIS analysis as well as in the active and passive pressure distributions shown in these figures. These pressure results were compared to limiting stress states (active and passive) for varying factors of safety applied to the undrained shear strength values. The flood elevation of 7 ft corresponds to the shallowest water level at which the gap propagated to el -15 ft. The flood elevation of 9 ft corresponds to the design water height used in the conventional design. The flood elevation of 10 ft corresponds to the peak flood level that was specified in the PLAXIS SSI analysis while maintaining numerical stability.

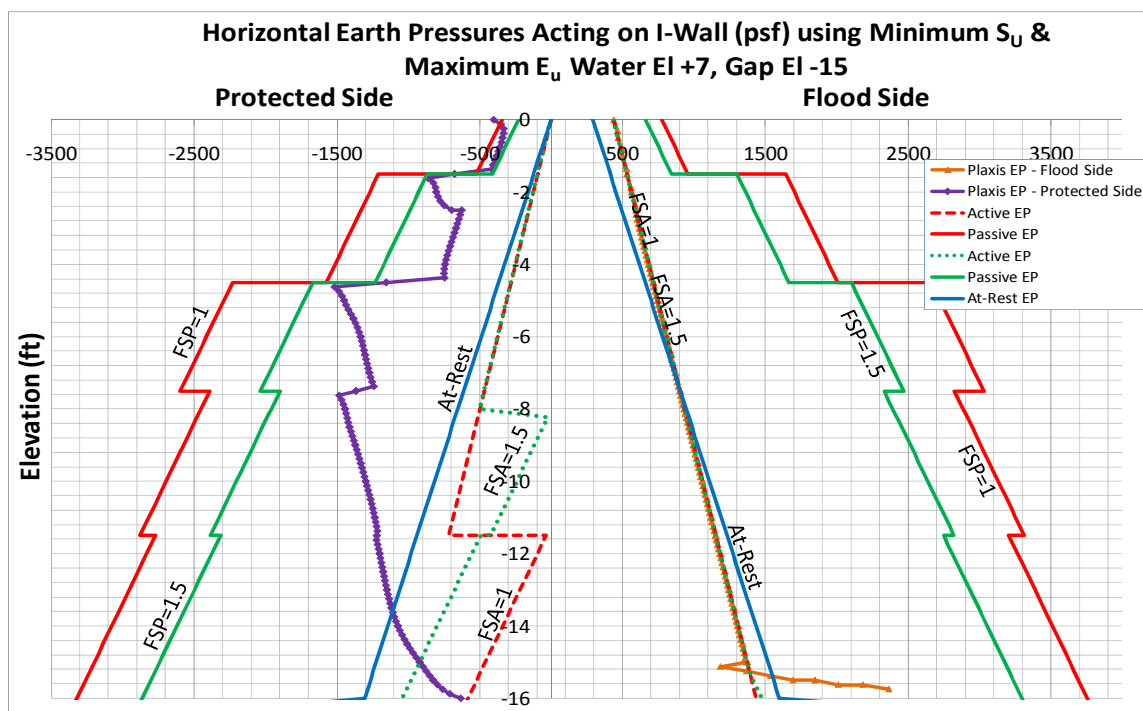


Figure B.8. Comparison of total normal stresses on the interface elements adjacent to the wall on the flood side and protected side (landside) for flood el 7 ft and gap el -15 ft using the minimum computed values of undrained shear strength (S_u) and the maximum computed values of undrained secant stiffness (E_u).

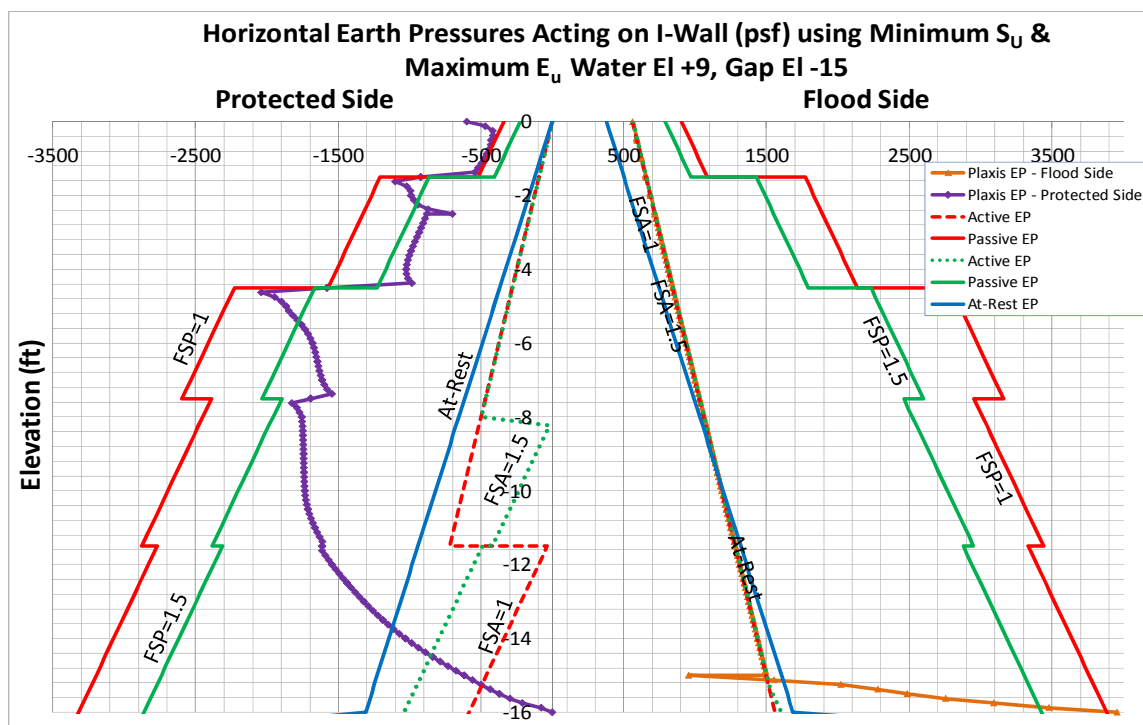


Figure B.9. Comparison of total normal stresses on the interface elements adjacent to the wall on the flood side and protected side (landside) for flood el 9 ft and gap el -15 ft using the minimum computed values of undrained shear strength (S_u) and the maximum computed values of undrained secant stiffness (E_u).

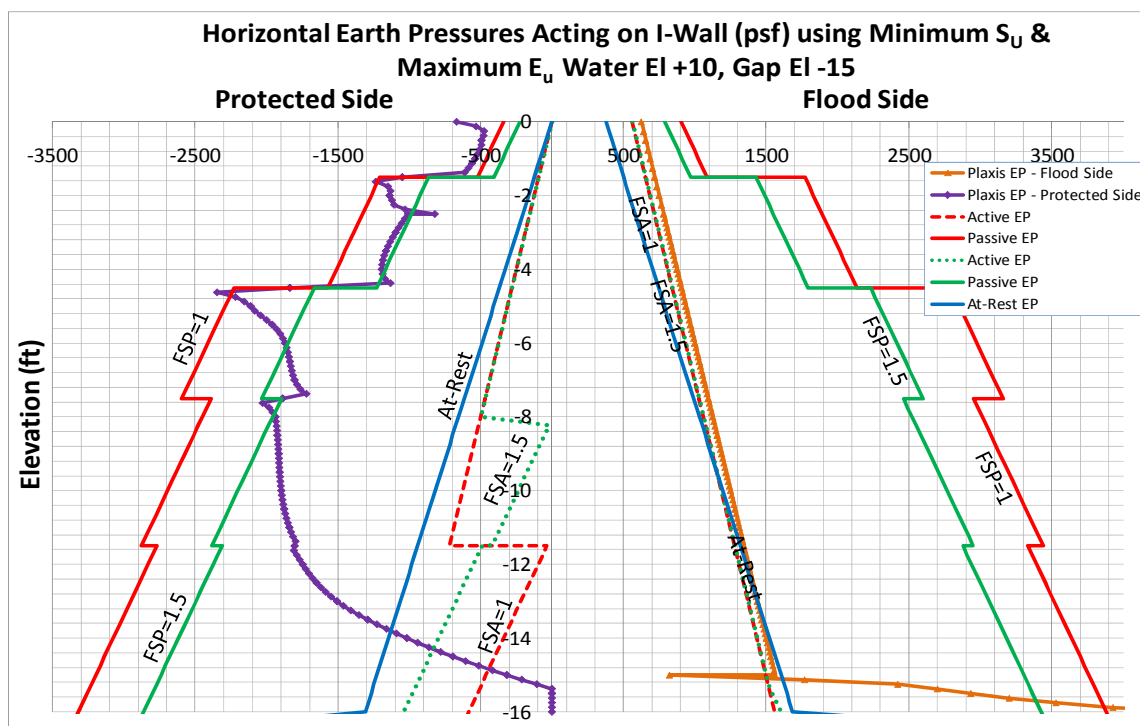


Figure B.10. Comparison of total normal stresses on the interface elements adjacent to the wall on the flood side and protected side (landside) for flood el 10 ft and gap el -15 ft using the minimum computed values of undrained shear strength (S_u) and the maximum computed values of undrained secant stiffness (E_u).

As shown in Figure B.8 for the flood elevation of 7 ft, the SSI earth pressures on the landside fall between at-rest pressures and passive pressures beginning at el -2 ft (with a factor of safety of 1.5) down to el -14 ft. Below el -14 ft, the earth pressures reduce to near-active earth pressure (with a factor of safety of 1.0) at the sheet-pile tip (i.e., at el -16 ft). On the flood side, the complete SSI analysis computes hydrostatic water pressures acting down to the gap tip elevation of -15 ft, which is 1 ft above the pile tip el -16 ft.

In Figure B.9, for the design flood el 9 ft, the results show that on the landside of the wall the complete SSI earth pressures more closely match passive earth pressures computed with a factor of safety of 1.0 applied to the undrained shear strength values, except for the upper 2 ft (el 0 ft to el -2 ft). On the flood side, the complete SSI analysis computes hydrostatic water pressures acting down to the gap tip elevation of -15 ft, 1 ft above the pile tip el -16 ft. Below the gap tip elevation, the kickback of the I-wall into the flood-side soil allows for the comparison of horizontal pressures computed by complete SSI analysis to limiting earth passive pressures over this 1-ft depth. For all points, except the point at el -16 ft, these computed horizontal pressures were less than those limiting passive earth pressure values computed using a factor of safety equal to 1.5. Kickback of

the I-wall into the flood-side soil again is observed near the pile tip. Figure B.10 shows the horizontal pressure results for the peak elevation of 10 ft. On the landside, the pressure results more closely match the passive pressures (with a factor of safety of 1.0) down to el -2.5 ft because of the increased flood loading. Below el -2.5 ft, the SSI earth pressures on the landside fall between at-rest pressures and passive pressures (with a factor of safety of 1.5) down to el -14 ft. Below el -14 ft, the earth pressures reduce to near-active earth pressure (with a factor of safety of 1.0) at the sheet-pile tip (at el -16 ft). Again, the complete SSI analysis computes hydrostatic water pressures acting on the flood side, down to the gap tip elevation of -15 ft. Kickback of the I-wall into the flood-side soil again is observed near the pile tip. This behavior is consistent with conventional force equilibrium procedures.

Computed fractions of mobilized shear strength for selected floodwater elevations and gap depths are shown in Figure B.11. Recall that a fraction of mobilized shear strength equal to 1 indicates full mobilization of shear strength. As shown in Figures B.11(a) and B.11(b), for the specified flood elevation and gap depth, there are no regions of full mobilization of shear strength. These results indicate reserve shear capacity in the soil regime and, thus, a stable numerical model at these stages of construction. Figure B.11(c), with the design flood depth of 9 ft and gap el depth of -15 ft, shows small regions of full mobilization of shear strength on the landside near the concrete cap. However, there is no indication of a fully developed failure mechanism at the stage of loading. Figure B.11(d), with peak flood elevation of 10 ft and gap depth of -15 ft, shows larger regions of full mobilization of shear strength. An additional loading phase with a flood elevation at 11 ft was attempted, but it resulted in numerical instability.

A subsequent PLAXIS analysis was performed at the peak flood elevation of 10 ft and gap depth at an elevation of -15 ft to compute a factor of safety against a possible rotational failure mechanism. Figure 2.16 indicated that the wall was rotating about a point near the pile tip. Figure B.12 shows a failure mechanism based on the PLAXIS Phi/c reduction procedure. The resulting rotational factor of safety was computed to be 1.03. However, at intermediate flood elevations, less than 10 ft, rotation of the wall was not indicated, and it is believed that the Phi/c reduction procedure would compute factors of safety based on localized shear failures with the active driving wedge only. Therefore, for this analysis, the Phi/c reduction procedure was not further used to compute factors of safety resulting from rotational failure mechanisms (as is performed in limit equilibrium procedures) for intermediate flood elevations.

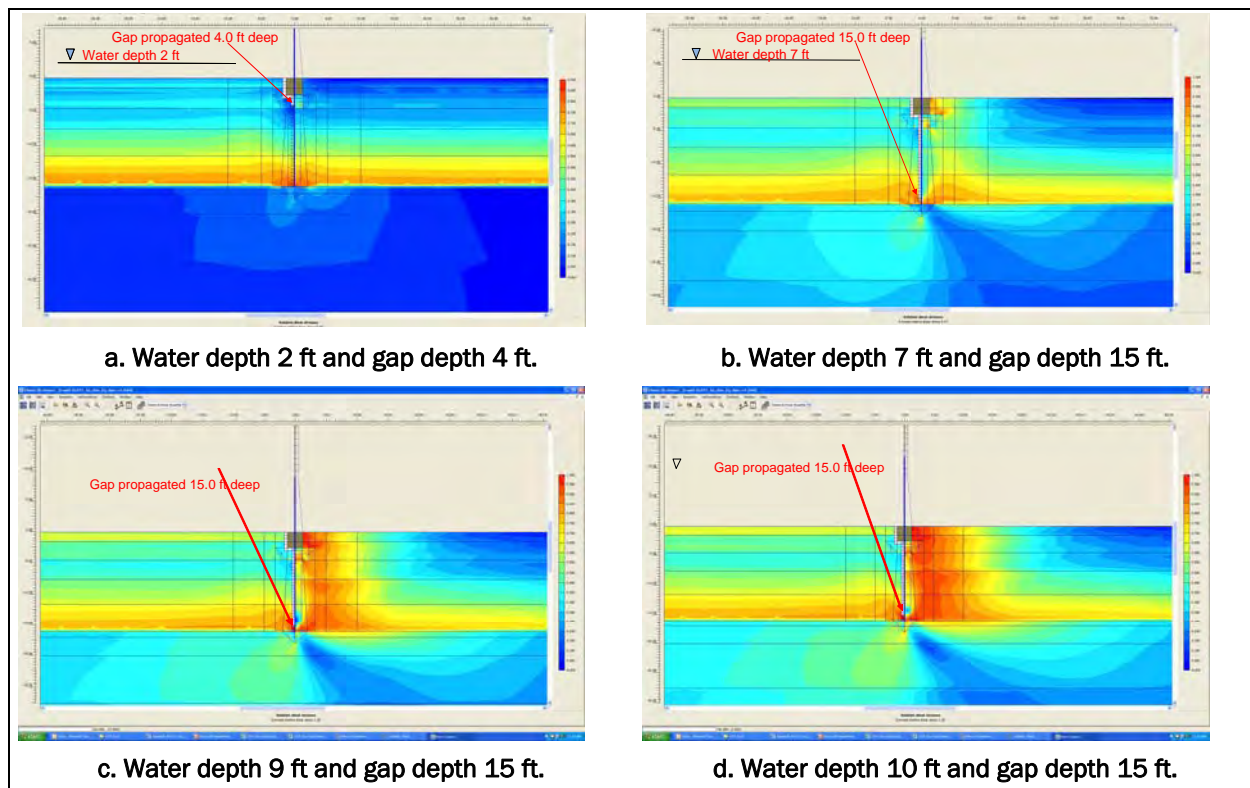


Figure B.11. Fraction of mobilized shear strength at various loading phases using minimum computed values of undrained shear strength (S_u) and the maximum computed values of undrained secant stiffness (E_u).

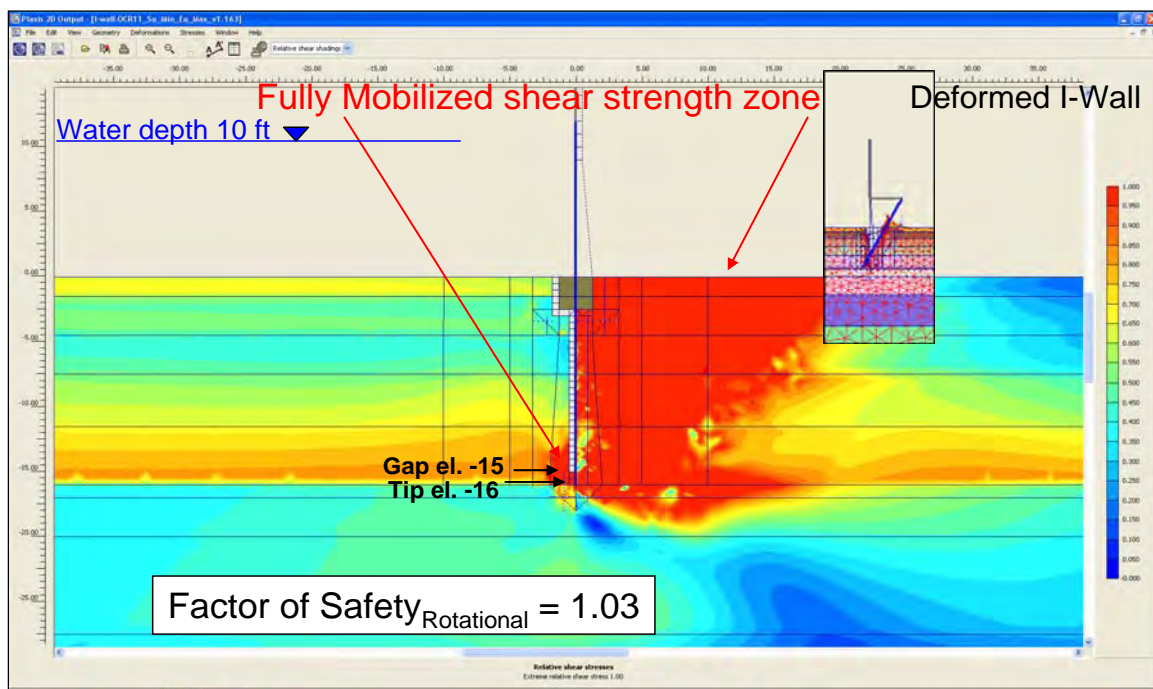


Figure B.12. Rotational factor of safety using Phi/c reduction for design peak flood elevation of 10 ft using minimum computed values of undrained shear strength (S_u) and the maximum computed values of undrained secant stiffness (E_u).

Appendix C: Analyses of I-wall Site Founded in an Overconsolidated Lean Clay Using Maximum Values of Undrained Shear Strength (S_u) and Minimum Values of Undrained Secant Stiffness (E_u)

C.1 Purpose of analyses

This appendix summarizes the findings of a series of complete nonlinear soil-structure interaction (SSI¹) finite element analyses performed on an I-wall section founded in an overconsolidated lean clay. Maximum values of undrained shear strength (S_u) distribution with depth and minimum values of undrained secant stiffness (E_u) distribution with depth are assigned to the clay soils. This corresponds to mean plus four standard deviations for the S_u distribution and mean minus two standard deviations for the E_u distribution. The focus of this study was to investigate the phenomena of gap initiation and propagation along the soil-to-structure interface on the flood side of the I-wall and to study the effects of gap initiation and propagation on the resulting deformation and stress conditions in the soil regime on both the flood side and landside of the I-wall. The findings of these analyses will be used in a companion research effort focusing on risk and reliability assessments of I-wall systems.

The following sections will describe the soil used in the analyses, the selection of stiffness and shear strength parameters, the conventional design of the I-wall, the analysis procedures employed, and the results of the complete nonlinear SSI analyses.

C.2 Overview of flood-site I-wall being analyzed

The geometry of the problem analyzed is the same wall system shown in Figure 2.1. The site was assumed to be a level plan with a maximum floodwater elevation of 9 ft. Two soil layers were assumed in the analyses. The top 20 ft represented an overconsolidated layer, while the underlying

¹ Symbols and unusual abbreviations used in this appendix are listed and defined in the Notation, Appendix I.

soil was assumed to be normally consolidated. The elevation of the soil surface was assumed to be at 0 ft.

The I-wall was composed of a sheet-pile wall with the tip at el -16 ft. The top of the I-wall was composed of a concrete cap 2.5 sq ft (i.e. embedment to el -2.5 ft), with the top of the cap level with the ground surface. The wall above the top of the soil was composed of a tapered concrete section 2.5 ft at the base and 1 ft at the top of the wall (el 9 ft). The water table for this problem was at the pile tip (el -16 ft).

C.3 Conventional design of cantilever I-wall and shear strength

The design depth of penetration of the sheet-pile section of the I-wall was determined using the Computer-Aided Structural Engineering (CASE) CWALSHT computer program (U.S. Army Engineer Research and Development Center 2012) and procedures outlined in Headquarters, U.S. Army Corps of Engineers (1994).¹ The computed design depth of penetration of the sheet pile (-16 ft) (refer to Chapter 2) was used in this analysis without consideration of a gap forming between the concrete cap and the soil or between the sheet pile and soil on the flood side of the I-wall and using the mean S_u distribution with depth given in Chapter 2. However, note that the finite element analysis for the wall section was conducted for this same -16-ft design depth, and it considered the potential for gap initiation and propagation. It too should be noted that the inclusion of a gap beside the wall also would affect the design depth. This analysis provides useful information for a lower ratio of embedment to flood height. It is important to recognize that the factor of safety for this system based on complete SSI results for a flood elevation of 9 ft would not correspond to the factor of safety used for design in CWALSHT because a gap was not assumed in the CWALSHT analysis.

The total stress (undrained) shear strength parameters were determined using the SHANSEP procedure (Ladd and Foott 1974) discussed in Chapter 2. It assumes that the soil shear strength can be normalized by the effective overburden pressure. The effective overburden pressure is calculated at midlayer for each of the layers identified in Table C.1 and using a preflood water table elevation of -16 ft. The ratio of shear strength to effective overburden pressure (S_u/σ'_{vo}) is dependent on the overconsolidation ratio (OCR) and a fitting parameter (m), assumed to be 0.8, as shown in Equation C.1:

¹ Citations in this appendix are in the References at the end of the main text.

Table C.1. Computation of maximum S_u variation with depth.

Layer			Short-Term (Undrained) Loading				
			Depth, ft	σ'_{vo} , psf	OCR	$(S_u/\sigma'_{vo})_{oc}$	$S_{u,max}$, psf
No.	Top El, ft	Bottom El, ft					
1	0	-1.5	1	122	7	1.422983	174
			2	244	7	1.422983	347
2	-1.5	-4.5	3	366	7	1.422983	521
			4	488	7	1.422983	694
			5	610	6.4	1.32454	808
3	-4.5	-7.5	6	732	5.5	1.173306	859
			7	854	4.8	1.052239	899
			8	976	3.6	0.835917	816
4	-7.5	-11.5	9	1098	2.9	0.703137	772
			10	1220	2.3	0.584122	713
			11	1342	2	0.52233	701
			12	1464	1.7	0.458649	671
			13	1586	1.6	0.436935	693
5	-11.5	-17.5	14	1708	1.4	0.392666	671
			15	1830	1.35	0.381407	698
			16	1952	1.3	0.370063	722
			17	2011.5	1.25	0.358632	721
			18	2071	1.2	0.347109	719
6	-17.5	-20	19	2130.5	1.15	0.33549	715
			20	2190	1.1	0.323769	709
7	-20	-27.5	25	2487.5	1	0.3	746
			30	2785	1	0.3	836
8	-27.5	-40	35	3082.5	1	0.3	925
			40	3380	1	0.3	1014
			45	3677.5	1	0.3	1103
			50	3975	1	0.3	1193
9	-40	-60	55	4272.5	1	0.3	1282
			60	4570	1	0.3	1371
			65	4867.5	1	0.3	1460
10	-60	-80	70	5165	1	0.3	1550
			75	5462.5	1	0.3	1639
			80	5760	1	0.3	1728
			85	6057.5	1	0.3	1817
11	-80	-100	90	6355	1	0.3	1907
			95	6652.5	1	0.3	1996
			100	6950	1	0.3	2085

$$\left(\frac{S_u}{\sigma'_{vo}} \right)_{OCR} = \left(\frac{S_u}{\sigma'_{vo}} \right)_{NC} \bullet OCR^m, \quad (C.1)$$

where

- $(S_u/\sigma'_{vo})_{OCR}$ = ratio of the undrained shear strength to effective overburden pressure for the overconsolidated condition;
 $(S_u/\sigma'_{vo})_{NC}$ = ratio of the undrained shear strength to effective overburden pressure for the normally consolidated condition.

From Ladd (1991), a mean value of 0.22 was assigned to $(S_u/\sigma'_{vo})_{NC}$ (Chapter 2), and a value of 0.8 was used for m based on undrained Direct Simple Shear (DSS) test results. These data also indicated a standard deviation equal to 0.02 for the $(S_u/\sigma'_{vo})_{NC}$. In the computation of the effective overburden pressures, 122 pcf was used for both the moist and the saturated unit weights. The OCR characterization of this site is the same as discussed in Chapter 2 and shown in Figure 2.3.

The resulting maximum variation in the undrained shear strength (S_u) with depth is shown in blue in Figure C.1. Average maximum values of S_u were estimated to be constant over a given depth, as shown in pink in Figure C.1. These constant values are listed for the soil layers in Table C.1 and were used in the complete SSI analysis to approximate variation in S_u with depth.

C.4 Shear strength and stiffness properties used in the complete SSI analysis

A complete SSI analysis of the I-wall section shown in Figure 2.1 was performed using the two dimensional (2-D) version of the PC-based finite element program PLAXIS. The finite element method employed required certain input material properties for the selected soil constitutive models. The PLAXIS nonlinear Hardening Soil (HS) constitutive model was used to model all soil elements. This constitutive model provides for nonlinear stress-strain response for soil elements during loading. Elastic plate elements were used to model the steel sheet pile and the concrete I-wall section. Plate elements were used to model the concrete I-wall to process bending moment and shear distribution results more efficiently. Two-dimensional elastic elements were used to represent the concrete cap (the region in which the sheet pile is embedded).

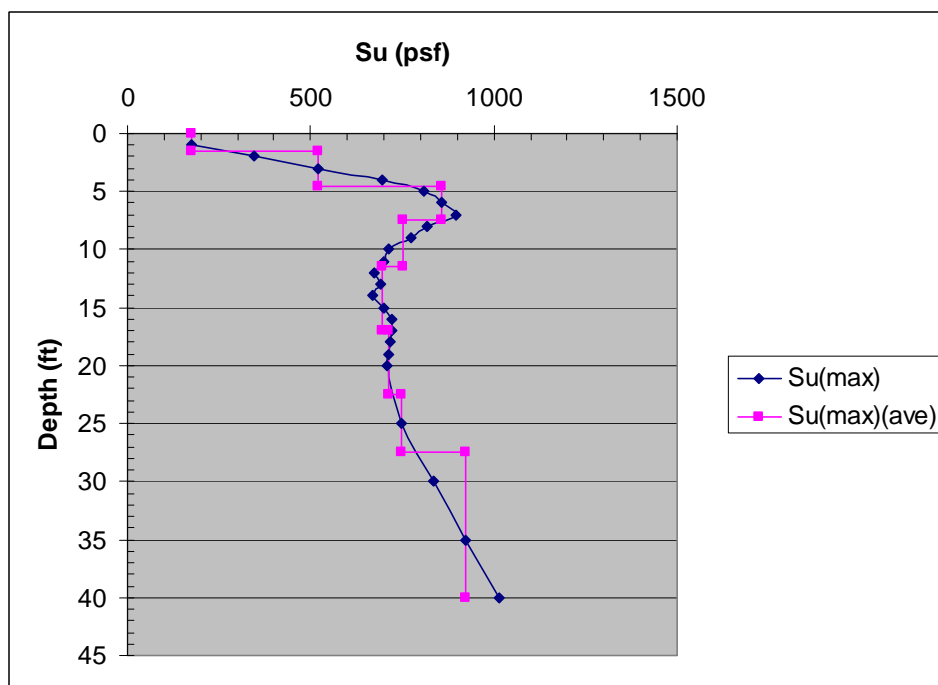


Figure C.1. Variation in maximum computed values of undrained shear strength (S_u) with depth.

Total stress soil strength parameters were used to characterize this over-consolidated lean clay site. An SSI parametric study was conducted to determine the minimum variation in the undrained secant stiffness in conjunction with a maximum variation in shear strength with depth that resulted in a numerically stable analysis. The minimum variation in stiffness was obtained by using the mean value of 0.22 assigned to $(S_u/\sigma'_v)_{NC}$ with a standard deviation equal to 0.02. The $(S_u/\sigma'_{vo})_{NC}$ ratio reduced by two standard deviations was selected based on the findings of Appendix A (using both minimum variations in shear strength and stiffness). The PLAXIS analysis using the mean minus two standard deviations at the design flood elevation of 9 ft converged. The minimum computed ratio $(S_u/\sigma'_v)_{NC}$ was equal to 0.18 (computed using Equation C.2):

$$\left(\frac{S_u}{\sigma'_v} \right)_{NC-2\sigma} = \left(\frac{S_u}{\sigma'_v} \right)_{NC-mean} - 2\sigma, \quad (C.2)$$

where

$$S_{u(NC-2\sigma)} = \left[\left(\frac{S_u}{\sigma'_v} \right)_{NC-mean} - 2\sigma \right] \bullet \sigma'_v,$$

with

$$\left(\frac{S_u}{\sigma'_v} \right)_{NC-mean} = 0.22$$

and σ , the standard deviation, was 0.02.

The resulting minimum variation in stiffness with depth was computed using the results of Equation C.2 and Equation C.3:

$$E_{u(NC-2\sigma)} = \text{constant} \times S_{u(NC-2\sigma)}, \quad (C.3)$$

where $\text{constant} = E_u/S_u$ ratios at each elevation listed in Table C.2.

Additionally, the maximum variation in shear strength with depth was computed using the mean value of 0.22 assigned to $(S_u/\sigma'_v)_{NC}$ in conjunction with four times the standard deviation of 0.02. The maximum computed ratio $(S_u/\sigma'_v)_{NC}$ was equal to 0.30 and was computed using Equation C.4:

$$\left(\frac{S_u}{\sigma'_v} \right)_{NC+4\sigma} = \left[\left(\frac{S_u}{\sigma'_v} \right)_{NC-mean} + 4\sigma \right], \quad (C.4)$$

where

$$S_{u(NC+4\sigma)} = \left[\left(\frac{S_u}{\sigma'_v} \right)_{NC-mean} + 4\sigma \right] \bullet \sigma'_v.$$

The correlation by Duncan and Buchignani (1976) shown in Figure 2.5 and Equation 2.2 were used to estimate the minimum variation of undrained secant modulus in clay with depth. Table C.2 summarizes the computation of the undrained secant modulus (E_{us}) with depth using the average values of the variation of S_u with depth from Table C.1 in conjunction with Equation 2.2. These values of E_{us} were used to estimate the variation in the PLAXIS input stiffness parameter (E_{50}^{ref}), which is a secant modulus at 50 percent of the principal stress difference ($\sigma_1 - \sigma_3$). The remaining parameters for soil properties selected to represent the clay (CL) soils used in the

Table C.2. Computation of minimum undrained secant modulus (E_{us}).

Layer			Short-Term (Undrained) Loading					E_u/S_u	$E_{u,min}$, psf
No.	Top El, ft	Bottom El, ft	Depth, ft	σ'_{vo} , psf	OCR	$(S_u/\sigma'_{vo})_{OC}$	$S_{u,min}$, psf		
1	0	-1.5	1	122	7	0.85379	104	250	26,041
			2	244	7	0.85379	208	250	52,081
			3	366	7	0.85379	312	250	78,122
2	-1.5	-4.5	4	488	7	0.85379	417	250	104,162
			5	610	6.4	0.794724	485	270	130,891
			6	732	5.5	0.703984	515	300	154,595
3	-4.5	-7.5	7	854	4.8	0.631343	539	350	188,708
			8	976	3.6	0.50155	490	450	220,281
			9	1098	2.9	0.421882	463	500	231,613
4	-7.5	-11.5	10	1220	2.3	0.350473	428	550	235,167
			11	1342	2	0.313398	421	580	243,937
			12	1464	1.7	0.275189	403	590	237,698
			13	1586	1.6	0.262161	416	590	245,315
			14	1708	1.4	0.2356	402	600	241,443
5	-11.5	-17.5	15	1830	1.35	0.228844	419	600	251,271
			16	1952	1.3	0.222038	433	600	260,051
			17	2011.5	1.25	0.215179	433	600	259,700
			18	2071	1.2	0.208266	431	600	258,791
6	-17.5	-20	19	2130.5	1.15	0.201294	429	600	257,314
			20	2190	1.1	0.194261	425	600	255,260
7	-20	-27.5	25	2487.5	1	0.18	448	600	268,650
			30	2785	1	0.18	501	600	300,780
8	-27.5	-40	35	3082.5	1	0.18	555	600	332,910
			40	3380	1	0.18	608	600	365,040
			45	3677.5	1	0.18	662	600	397,170
			50	3975	1	0.18	716	600	429,300
9	-40	-60	55	4272.5	1	0.18	769	600	461,430
			60	4570	1	0.18	823	600	493,560
			65	4867.5	1	0.18	876	600	525,690
10	-60	-80	70	5165	1	0.18	930	600	557,820
			75	5462.5	1	0.18	983	600	589,950
			80	5760	1	0.18	1037	600	622,080
			85	6057.5	1	0.18	1090	600	654,210
11	-80	-100	90	6355	1	0.18	1144	600	686,340
			95	6652.5	1	0.18	1197	600	718,470
			100	6950	1	0.18	1251	600	750,600

PLAXIS finite element analyses were the same as discussed in Chapter 2. Table C.3 shows the values of HS constitutive soil parameters used in this analysis. Values of the coefficient of friction between the sheet pile and the soil and between the concrete cap and the soil were the same as referenced in Table 2.5.

Table C.3. Maximum HS model strength and minimum stiffness properties for the soil layers.

Layer			c_{ref} , lb/ft ²	$E_{50,ref}$, lb/ft ²	$E_{oed,ref}$, lb/ft ²	$E_{ur,ref}$, lb/ft ²
No.	Top El, ft	Bottom El, ft				
1	0.0	0.0	174	2.60E+04	2.60E+04	7.81E+04
2	-1.5	-4.5	521	7.81E+04	7.81E+04	2.34E+05
3	-4.5	-7.5	855	1.58E+05	1.58E+05	4.74E+05
4	-7.5	-11.5	750	2.33E+05	2.33E+05	6.98E+05
5	-11.5	-17.0	696	2.49E+05	2.49E+05	7.48E+05
6	-17.0	-20.0	714	2.57E+05	2.57E+05	7.71E+05
7	-20.0	-27.5	746	2.69E+05	2.69E+05	8.06E+05
8	-27.5	-40.0	925	3.33E+05	3.33E+05	9.99E+05
9	-40.0	-60.0	1237	4.45E+05	4.45E+05	1.34E+06
10	-60.0	-80.0	1594	5.74E+05	5.74E+05	1.72E+06
11	-80.0	-100.0	1951	7.02E+05	7.02E+05	2.11E+06

Minimum values of adhesion were assigned to the soil along the I-wall-to-soil and sheet-pile-to-soil interfaces in the complete SSI analysis. The minimum value for adhesion was estimated using the one selected for the ratio of adhesion to cohesion (f_c) between the sheet pile and soil and between the concrete and the soil shown in Table 2.5 and Equation 2.3. Substituting the ratio of adhesion to cohesion equal to 0.8 into Equation 2.3 and solving for $(C_a)_{min}$ yields Equation C.5:

$$(C_a)_{min} = 0.8(C)_{min} = 0.8(C_{mean} - 2\sigma), \quad (C.5)$$

where

$(C_a)_{min}$ = minimum soil adhesion;

C_{min} = minimum value of cohesion = minimum value of undrained shear strength $(S_u)_{min}$;

C_{mean} = mean value of cohesion = mean value of undrained shear strength $(S_u)_{mean}$;

σ = standard deviation.

The properties of the concrete cap represented by elastic elements and the properties of the concrete I-wall section modeled by elastic plate elements with the properties were the same as referenced in Tables 2.6 and 2.7. The sheet pile was represented by elastic plate elements with the same properties as referenced in Table 2.8.

C.5 Discussion of finite element analyses

C.5.1 Conceptual model

The finite element analysis was performed using the 2-D version of the nonlinear incremental construction finite element program PLAXIS. The conceptual model of the finite element mesh is the same as shown in Figure 2.6. The geometry is the same as in Figure 2.1. Several special modeling features were used, including the sheet-pile wall and the concrete I-wall section being modeled by elastic plate elements; the interface elements and soil elements beside the sheet-pile wall on the flood side were 0.5 ft in height. These special features are described in Chapter 2.

C.5.2 Gap initiation and propagation criterion

A hydraulic fracturing criterion is applied to determine whether a gap will develop and if it propagates down the soil-to-I-wall interface. In this procedure of analysis, the total horizontal stress (computed by PLAXIS) at the ground surface soil-to-I-wall interface is compared to the hydrostatic water pressure developing at the top of the ground surface caused by the presence of the specified flood pool elevation. If the hydrostatic water pressure of the flood pool (the demand) exceeds the total horizontal stress (the capacity), a gap will initiate at the ground surface, along the soil-to-I-wall interface. This criterion is discussed in Chapter 2.

C.5.3 Finite element model

Figure C.2 shows a 2-D cross section used to model the variation of undrained shear strength and soil stiffness with depth by the PLAXIS program. The regions of uniform color reflect soil clusters used to define the mesh and assign soil regions with common properties. The inset figure shows the average undrained shear strengths assigned to the upper eight layers based on the maximum S_u values (i.e., mean plus four standard deviations). The finite element mesh used in the analysis is the same as shown in Figure 2.9. The mesh is composed of 4,187 elements and

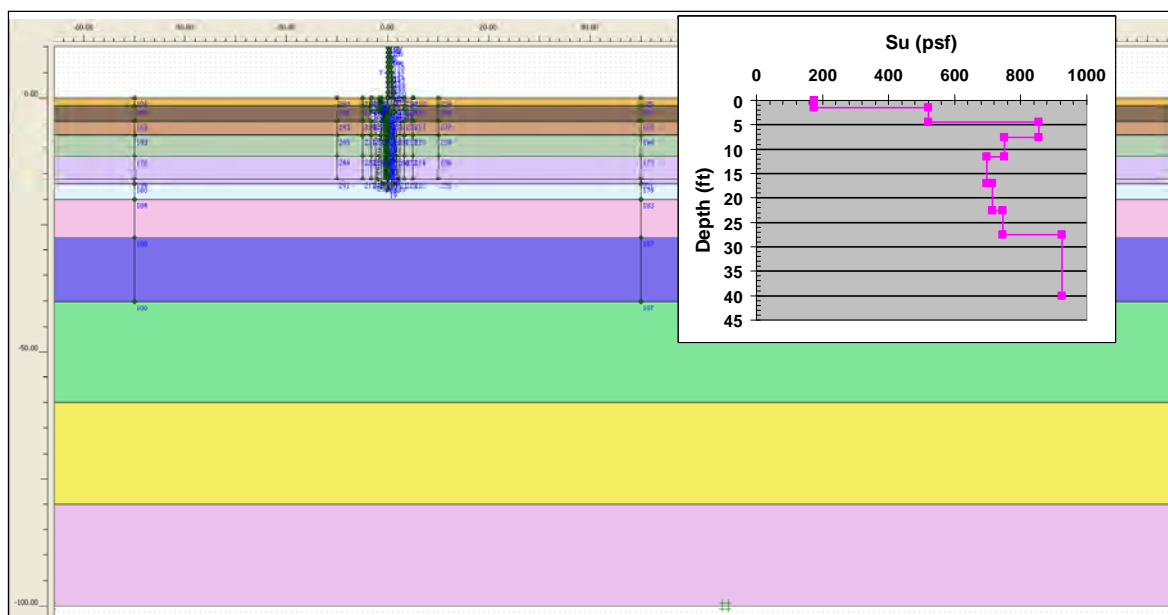


Figure C.2. Two-dimensional (2-D) cross-section model using the maximum computed values of undrained shear strength (S_u) and minimum computed undrained secant stiffness (E_u) used in the SSI analyses.

34,408 nodes with 50,244 stress points. The mesh consists of 15-node triangular elements to model the soil, plate elements to model the bending effects of the I-wall and sheet-pile wall, and interface elements to model SSI between the sheet-pile wall and the adjacent soil elements. The analyses are executed as a plane strain problem. An enlarged view of the area around the wall and its mesh is shown in Figure 2.10.

C.6 Results of the finite element analyses

C.6.1 Initial stresses

The initial total stress state within the finite element mesh was established using the at-rest soil conditions for a level ground surface. Horizontal at-rest soil stresses were estimated using the interrelationship between the at-rest earth pressure coefficient (K_o) and the soil Poisson's ratio (ν) (Equation 2.4). The assumed groundwater elevation was at the sheet-pile tip (el -16 ft). The assigned values of ν and the corresponding K_o values used to compute the horizontal earth pressures for the initial conditions are summarized in Table 2.9.

For this level ground site, the at-rest stress is computed by multiplying the total overburden pressure for each integration point in every soil element by K_o . Figure C.3 shows the computed fraction of mobilized shear strength (referred to as relative shear stress in PLAXIS output) from the initial

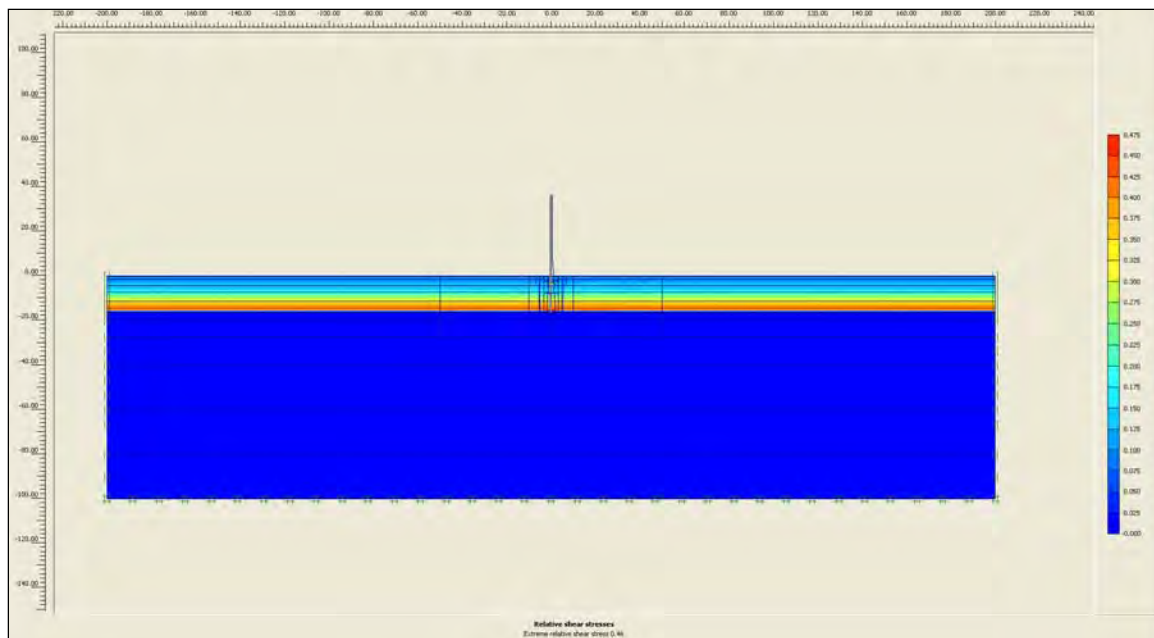


Figure C.3. Fraction of mobilized shear strength for initial conditions using the maximum computed values of undrained shear strength (S_u) and the minimum computed values of undrained secant stiffness (E_u).

total stress condition. The resulting fraction of mobilized shear strength (1.0 indicates full mobilization of shear strength) is less than or equal to 0.46 for all soil clusters. These results indicate considerable reserve shear capacity in the soil regime and, thus, a stable numerical model at this initial stage of construction.

C.6.2 Gap initiation and propagation results

The focus of this study was to investigate the phenomena of gap initiation and propagation along the flood side of the soil-to-I-wall interface and to study the effects of these phenomena on the resulting deformation and stress conditions in the soil regime on both the flood side and landside of the I-wall system.

Modeling of the flood loading commenced in the complete SSI analysis after the total initial stresses state was established within the mesh for an assumed steady-state water elevation at the ground surface (el 0.0 ft). To track the formation and propagation of a gap, the flood loading was applied in 1-ft incremental raises of the water level. The hydraulic fracturing criterion is used to estimate a gap formation and its propagation. This procedure compares the total normal earth pressures due to the flood pool acting on the wall at a given depth to the hydrostatic water pressure acting

at the corresponding depth. A gap is formed when the total horizontal earth pressure (the capacity) is less than the water pressure due to the flood pool acting at the corresponding depth (the demand). Next, hydrostatic water pressure is applied over the depth of the gap and this hydrostatic water pressure at the new, deeper gap depth is compared to the total horizontal earth pressure. Gap propagation is terminated at the depth when the demand is less than the capacity. Complete SSI analysis results were examined for various water elevations and gap depths.

Figure C.4 shows the progression of the gap as the water level against the I-wall is increased. As shown, the gap initiates when the water is at the shallow elevation of 2 ft and extends to a depth of -4.0 ft. The gap extends to el -9 ft at a water elevation of 3 ft and to el -13 ft at a water elevation of 4 ft. At water el 6 ft, the gap extends to el -15 ft, and gap elevation remains constant until a water elevation of 10 ft. Note that the gap is within 1 ft of the sheet-pile tip for floodwater levels at and above el 6 ft. The previous analysis, using minimum S_u variations, maximum E_u variations, and the same floodwater elevation of 6 ft, computed a gap that extended to this same elevation of -15 ft. However, for this analysis, using maximum S_u variations and minimum E_u variations computed deeper gap propagation at shallower water levels (i.e., 3 ft and 4 ft) compared to the analysis using minimum S_u variations and maximum E_u variations (Appendix B).

C.6.3 Performance of interface elements

The performance of the interface elements was compared to the performance of the soil elements adjacent to the wall to ascertain whether the results for the interface elements could be used to characterize the computed results of the analyses accurately. Figure 2.13 shows that the total horizontal stresses computed within the interface and soil elements agree closely for the selected flood elevation of 2 ft. Therefore, interface element results were used to summarize computed results from this complete SSI analysis.

C.6.4 Discussion of displacements and stresses

The total exaggerated nodal displacements within the finite element mesh (both soil and wall) are shown in Figure C.5. These displacements are for the design water elevation of 9 ft with a gap depth to el -15 ft. Note that the nodal displacements are increased by a factor of 100 in this figure to show

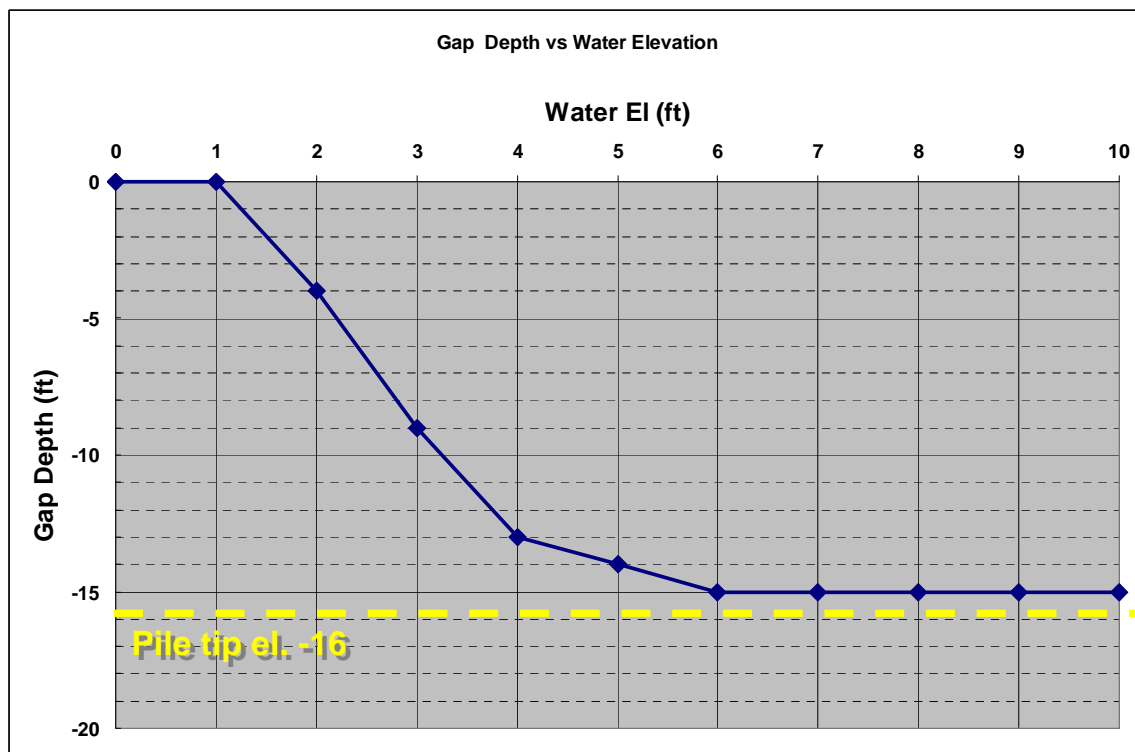


Figure C.4. Progression of gap versus water elevation using the maximum computed values of undrained shear strength (S_u) and the minimum computed values of undrained secant stiffness (E_u).

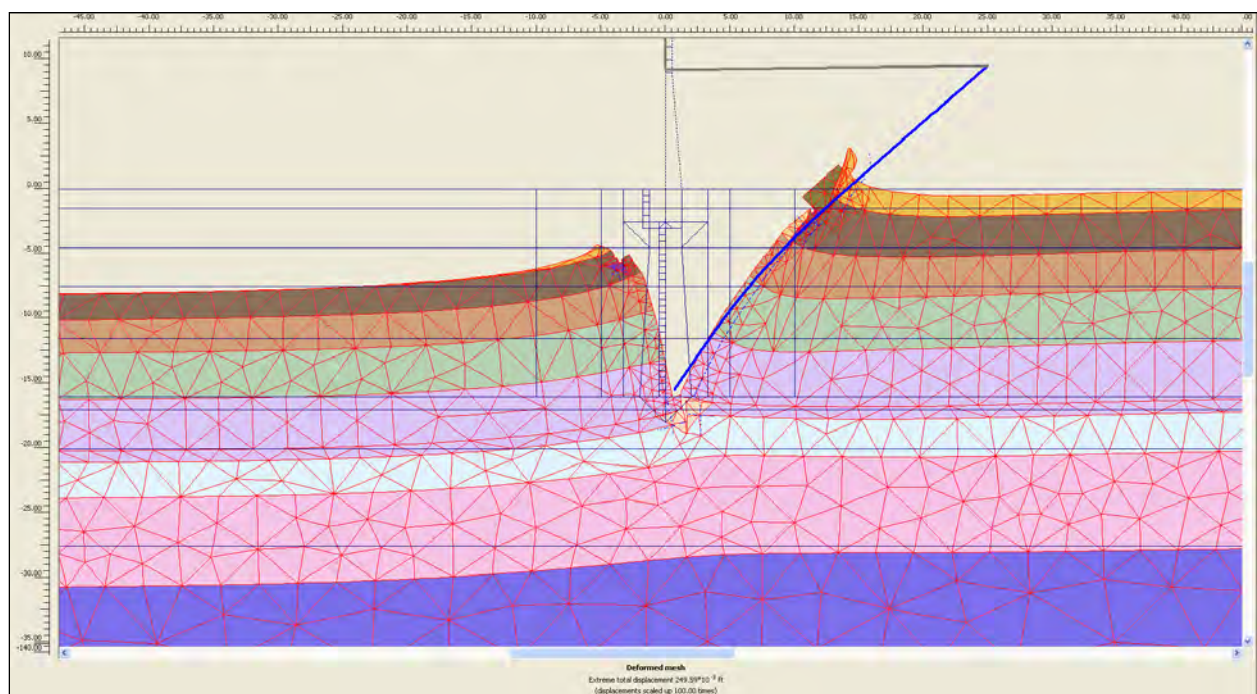


Figure C.5. Total exaggerated displacements for a water elevation of 9 ft and gap elevation of -15 ft using the maximum computed values of undrained shear strength (S_u) and the minimum computed values of undrained secant stiffness (E_u).

the deformed mesh relative to its initial position and to show the extent of the gap. The gap is modeled by deactivating the soil elements adjacent to the wall. The general trend of the deflections was toward the landside because of the applied boundary water pressures on the flood side. The wall has a greater movement than the soil at this loading phase. The maximum wall displacement is approximately 3.0 in. at the top of the wall. The displacement of the wall consists of both horizontal and vertical movements. The tip of the wall has moved slightly upward and toward the landside.

Figure C.6 shows a plot of horizontal displacements of I-wall versus flood-water elevation at three points along the wall. The points monitored in the analysis were the top of the I-wall at el 9 ft, at the ground surface el 0 ft, and at the sheet-pile tip el -16 ft. As shown, the deflection of the wall up to flood el 3 ft (after gap initiation) was primarily uniform translation. As the water elevation increased, the top of the wall had larger deformations compared with those of the ground and much larger deformations than those of the pile tip. This implies that the wall was undergoing rotation along with translation. Also, above water el 7 ft the deflection of the pile tip was directed toward the flood-side soil, which indicates kickback of the pile tip. This behavior is consistent with the behavior assumed in limit equilibrium design procedures for the design of cantilever sheet-pile walls.

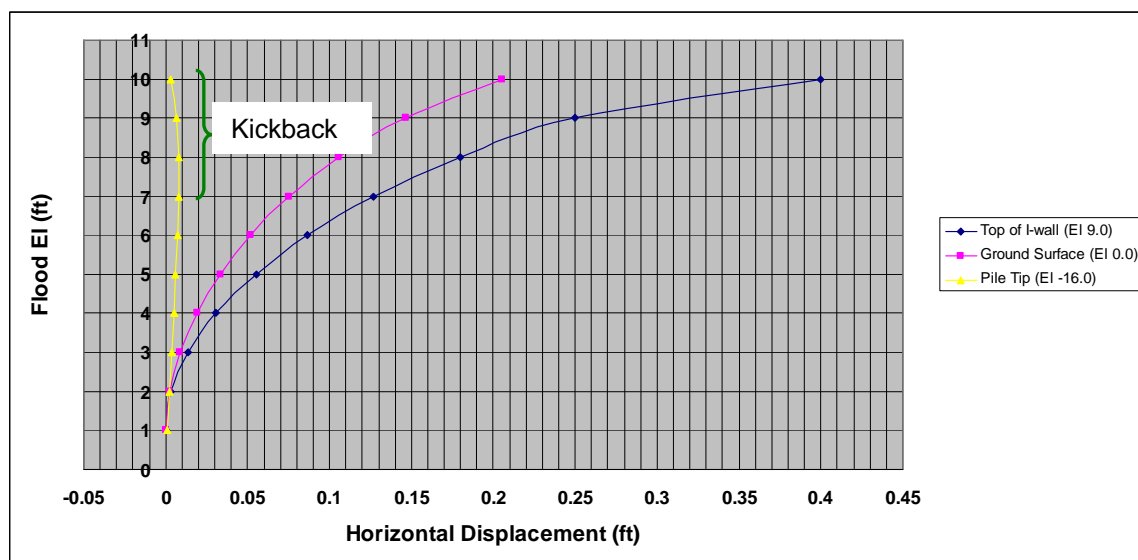


Figure C.6. Horizontal sheet-pile deflection versus water elevation using the maximum computed values of undrained shear strength (S_u) and the minimum computed values of undrained secant stiffness (E_u).

Figure C.7 shows a plot of relative horizontal displacements of I-wall versus floodwater elevation at the ground surface. Relative displacements were computed at this location to provide results for a companion research effort focusing on risk and reliability assessments of I-walls. The relative displacements were computed by subtracting the displacements of the sheet-pile tip from the sheet-pile displacements at the ground surface for a given floodwater elevation. The maximum computed relative horizontal displacement of the wall at the ground was approximately 2.4 in. for a maximum flood elevation of 10 ft. Computed relative horizontal displacements for this and other flood pool elevations are reported in Table C.4.

The analysis using the mean, best estimate (B.E.), values for S_u and E_u resulted in a maximum computed relative horizontal displacement of the wall at the ground of approximately 3.3 in. (Table 2.10). Table C.5 compares the maximum computed relative horizontal displacements from analyses using both the B.E. of S_u and E_u ; and maximum S_u and minimum E_u values. As shown for the maximum flood el 10 ft, the maximum computed relative displacement using the maximum values of S_u and minimum values of E_u was approximately equal to 2.4 in., compared to approximately 3.3 in.

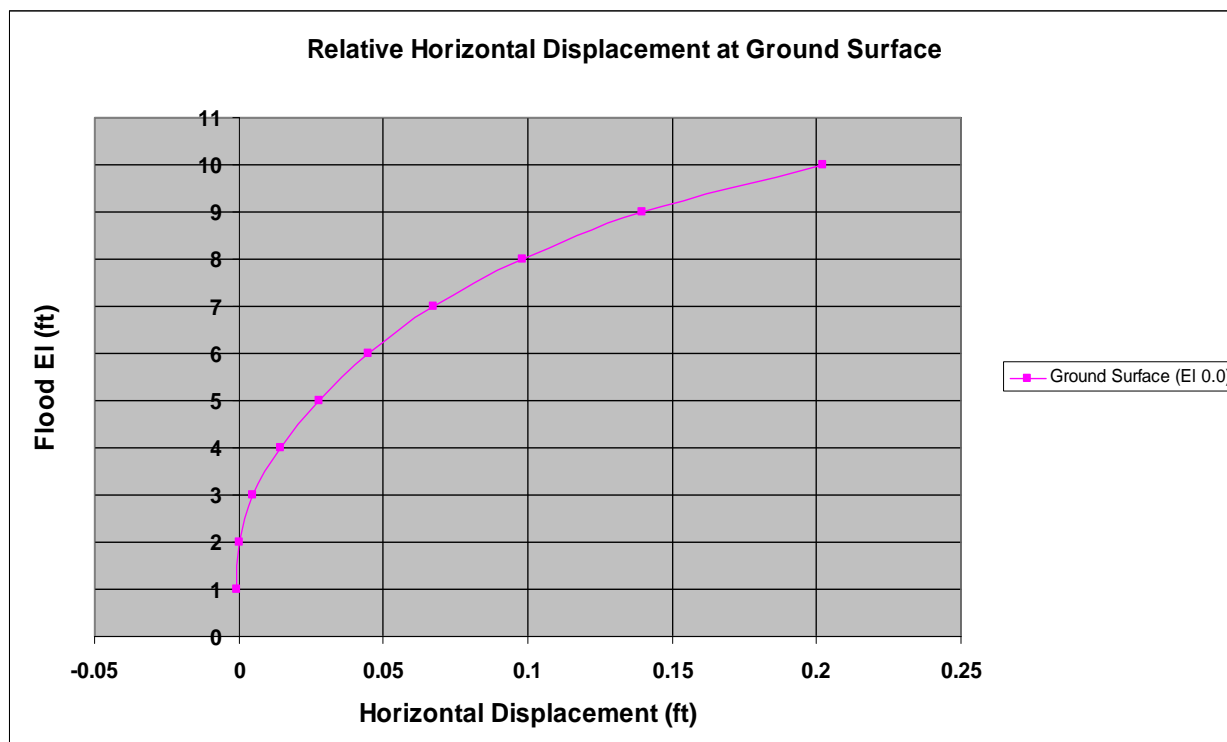


Figure C.7. Relative horizontal sheet-pile deflection at the ground surface el 0.0 versus water elevation using the maximum computed values of undrained shear strength (S_u) and the minimum computed values of undrained secant stiffness (E_u).

Table C.4. Summary of relative horizontal displacements (U_x) of I-wall at the ground surface using maximum computed values of undrained shear strength (S_u) and minimum computed values undrained secant stiffness (E_u).

U_x at Ground Surface, ft	U_x at Pile Tip, ft	Relative Displacement at Ground Surface, ft	Flood EI, ft	Gap Depth, ft
0.0003	0.0007	-0.0003	1	0
0.0022	0.0020	0.0001	2	4
0.0063	0.0032	0.0031	3	8
0.0132	0.0042	0.0090	4	11
0.0229	0.0051	0.0178	5	13
0.0364	0.0059	0.0304	6	14
0.0558	0.0062	0.0496	7	15
0.0813	0.0061	0.0751	8	15
0.1293	-0.0013	0.1306	9	15
0.1885	-0.0013	0.1899	10	15

Table C.5. Comparison of relative horizontal displacements of I-wall at the ground surface using both the best estimate and maximum computed values of undrained shear strength (S_u) and minimum computed values undrained secant stiffness (E_u).

Flood EI, ft	Relative Displacement at Ground Surface ($S_{u(min)}, E_{u(max)}$), ft	Relative Displacement at Ground Surface ($S_{u(B.E.)}, E_{u(B.E.)}$), ft
1	-0.0003	-0.0014
2	0.0001	-0.0021
3	0.0031	0.0017
4	0.0090	0.0106
5	0.0178	0.0243
6	0.0304	0.0428
7	0.0496	0.0677
8	0.0751	0.1041
9	0.1306	0.1652
10	0.1899	0.2751

using the B.E. values for S_u and E_u . The influence of the larger values of soil shear strengths resulted in an approximately 27 percent decrease in the computed relative horizontal displacement of the wall at the ground surface.

The total horizontal pressures acting on the interface elements adjacent to the wall on the flood side and landside for three flood elevations (6 ft, 9 ft, and 10 ft) and corresponding gap elevation of -15 ft for each flood elevation are shown in Figures C.8 through C.10, respectively. Minimum values of soil

adhesion were used in the PLAXIS analysis as well as in the active and passive pressure distributions shown in these figures. These pressure results were compared to limiting stress states (active and passive) for varying factors of safety applied to the undrained shear strength values. The flood elevation of 6 ft corresponds to the shallowest water level to which the gap propagated at el -15 ft. The flood elevation of 9 ft corresponds to the design water height used in the conventional design. The flood elevation of 10 ft corresponds to the peak flood level that was specified in the PLAXIS SSI analysis while maintaining numerical stability.

As shown in Figure C.8 for the flood elevation of 6 ft, the SSI earth pressures on the landside fall between at-rest pressures and passive pressures beginning at el -2 ft (with a factor of safety of 1.5) down to el -13 ft. Below el -13 ft, the earth pressures reduce to near active (with a factor of safety of 1.0) near the sheet-pile tip (at el -16 ft). On the flood side, the complete SSI analysis computes hydrostatic water pressures acting down to the gap tip elevation of -15 ft, which is 1 ft above the pile tip elevation of -16 ft.

In Figure C.9 for the design flood el 9 ft, the results show that on the landside of the wall the complete SSI earth pressures results more closely match passive earth pressures computed with a factor of safety of 1.0 applied to the undrained shear strength values for the upper 2 ft (el 0 ft to el -2 ft). The SSI earth pressures on the landside fall between at-rest pressures and passive pressures beginning at el -5 ft (with a factor of safety of 1.5) down to el -13 ft. On the flood side, the complete SSI analysis computes hydrostatic water pressures acting down to the gap tip elevation of -15 ft, 1 ft above the pile tip el -16 ft. Below the gap tip elevation, the kickback of the I-wall into the flood-side soil allows for the comparison of horizontal pressures computed by complete SSI analysis to limiting earth passive pressures over this 1-ft depth. For all points except the point at el -16 ft, these computed horizontal pressures were less than those limiting passive earth pressure values computed using a factor of safety equal to 1.5. Kickback of the I-wall into the flood-side soil again is observed near the pile tip.

Figure C.10 shows the horizontal pressure results for the peak elevation of 10 ft. On the landside, the pressure results more closely match the passive pressures (with a factor of safety of 1.0) down to el -2.5 ft because of the increased flood loading. Below el -2.5 ft and -6.0 ft, the SSI earth pressure results more closely match passive earth pressures computed with a factor

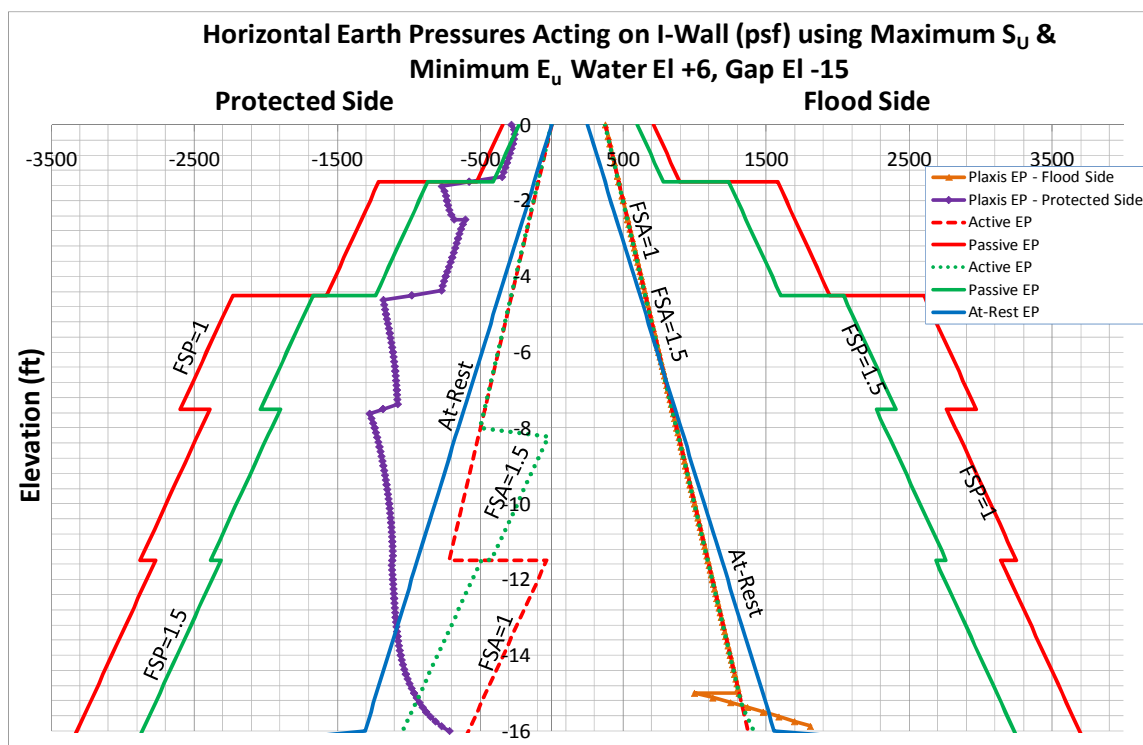


Figure C.8. Comparison of total normal stresses on the interface elements adjacent to the wall on the flood side and protected side (landside) for flood el 6 and gap el -15 using the maximum computed values of undrained shear strength (S_u) and the minimum computed values of undrained secant stiffness (E_u).

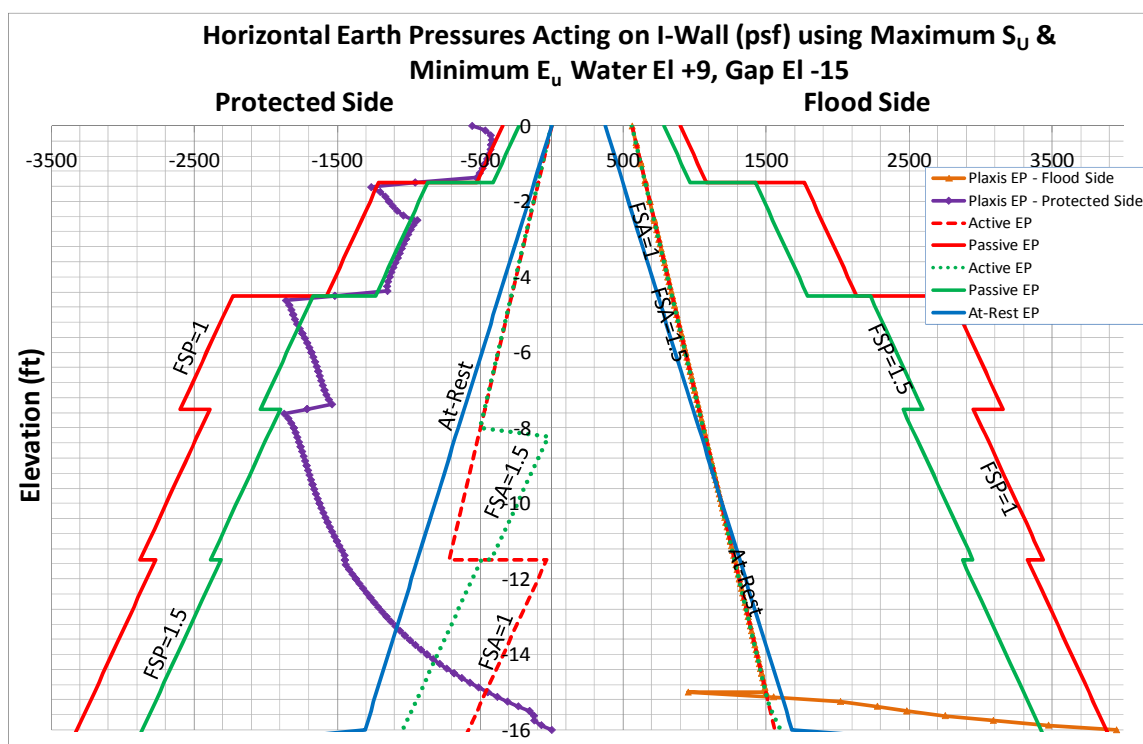


Figure C.9. Comparison of total normal stresses on the interface elements adjacent to the wall on the flood side and protected side (landside) for flood el 9 ft and gap el -15 ft using the maximum computed values of undrained shear strength (S_u) and the minimum computed values of undrained secant stiffness (E_u).

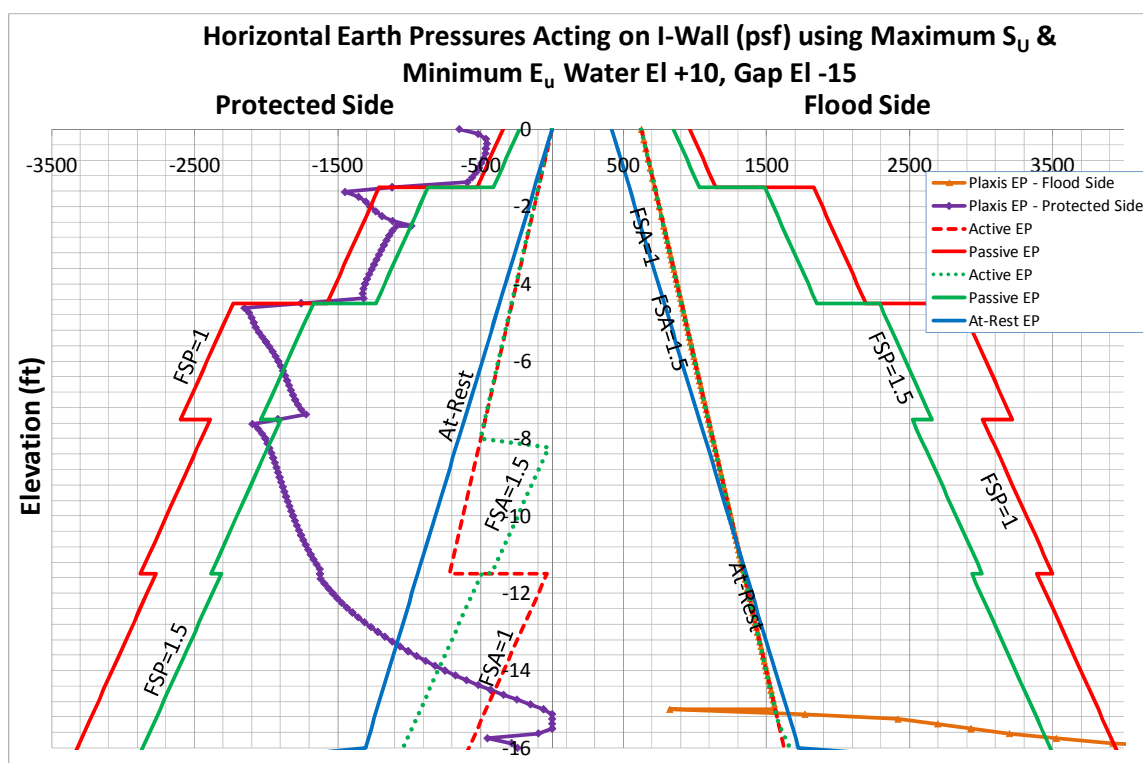


Figure C.10. Comparison of total normal stresses on the interface elements adjacent to the wall on the flood side and protected side (landside) for flood el 10 ft and gap el -15 ft using the maximum computed values of undrained shear strength (S_u) and the minimum computed values of undrained secant stiffness (E_u).

of safety of 1.5 applied to the undrained shear strength values. Below el -6.0 ft, the SSI earth pressures on the landside fall between at-rest pressures and passive pressures (with a factor of safety of 1.5) down to el -14 ft. Below el -14 ft, the earth pressure reduces to near-active earth pressure (with a factor of safety of 1.0) at the sheet-pile tip (at el -16 ft). Again, the complete SSI analysis computes hydrostatic water pressures acting on the flood side, down to the gap tip elevation of -15 ft. Kickback of the I-wall into the flood-side soil again is observed near the pile tip. This behavior is consistent with conventional force equilibrium procedures.

Computed fractions of mobilized shear strength for selected floodwater elevations and gap depths are shown in Figure C.11. A fraction of mobilized shear strength equal to 1 indicates full mobilization of shear strength. As shown in Figures C.11(a) and (b), for the specified flood elevation and gap depth, there are no regions of full mobilization of shear strength. These results indicate reserve shear capacity in the soil regime and, thus, a stable numerical model at these stages of construction. Figure C.11(c), with the design flood depth of 9 ft and gap depth of -15 ft, showed small regions of full mobilization of shear strength on the landside near the concrete cap.

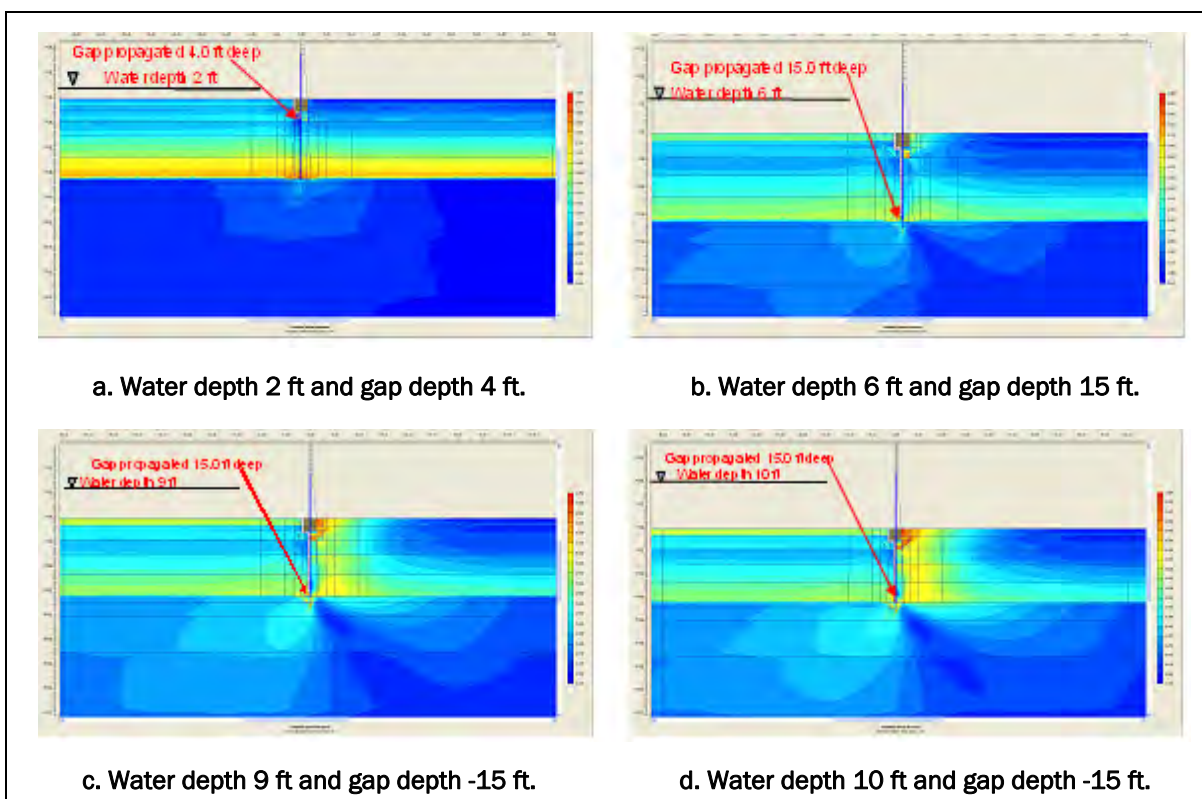


Figure C.11. Fraction of mobilized shear strength at various loading phases using maximum computed values of undrained shear strength (S_u) and the minimum computed values of undrained secant stiffness (E_u).

However, there is no indication of a fully developed failure mechanism at the stage of loading. Figure C.11(d), with peak flood elevation of 10 ft and gap depth of -15 ft, showed larger regions of full mobilization of shear strength. An additional loading phase with a flood elevation at 11 ft was attempted, but it resulted in numerical instability. A subsequent PLAXIS analysis was performed at the peak flood elevation of 10 ft and gap depth at elevation of -15 ft to compute a factor of safety against a possible rotational failure mechanism.

Figure 2.18 indicated that the wall was rotating about a point near the pile tip. Figure C.12 shows a failure mechanism based on the PLAXIS Phi/c reduction procedure. The resulting rotational factor of safety was computed to be equal to 1.6. However, at intermediate flood elevations, less than el 10 ft, rotation of the wall was not indicated. It is believed that the Phi/c reduction procedure would compute factors of safety based on localized shear failures with the active driving wedge only. Therefore, for this analysis, the Phi/c reduction procedure was not used further to compute factors of safety resulting from rotational failure mechanisms (as is performed in limit equilibrium procedures) for intermediate flood elevations.

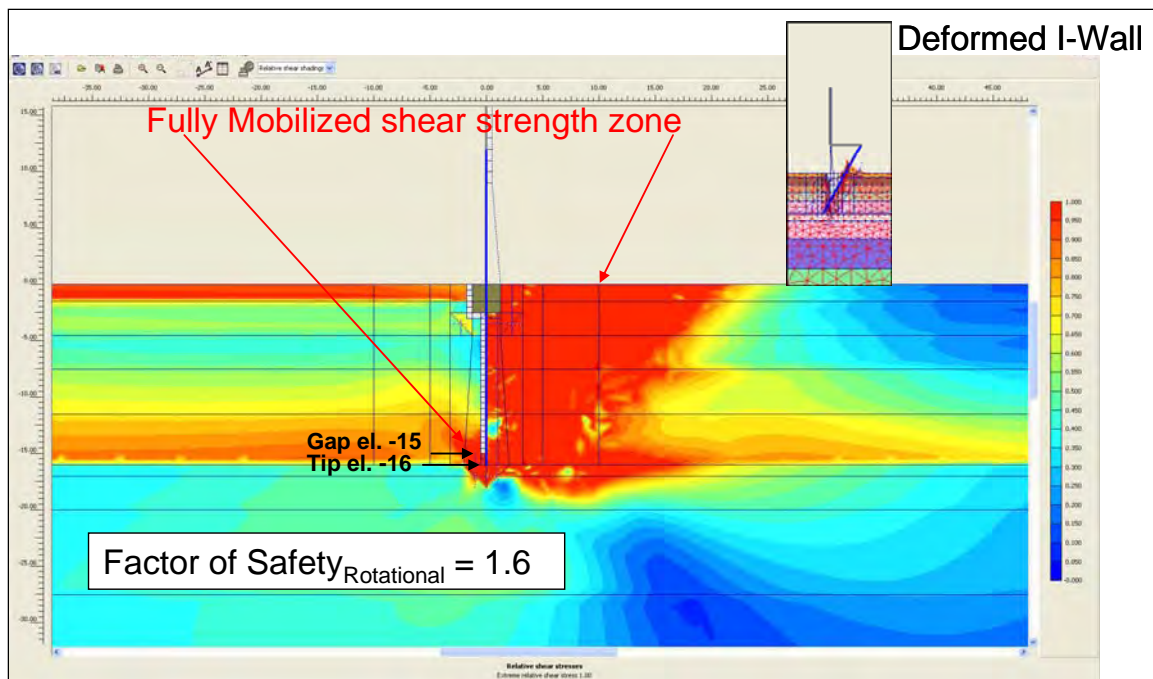


Figure C.12. Rotational factor of safety using Phi/c reduction for design peak flood elevation of 10 ft using maximum computed values of undrained shear strength (S_u) and the minimum computed values of undrained secant stiffness (E_u).

Appendix D: Analyses of I-wall Site Founded in an Overconsolidated Lean Clay Using Maximum Values of Undrained Shear Strength (S_u) and Maximum Values of Undrained Secant Stiffness (E_u)

D.1 Purpose of analyses

This appendix summarizes the findings of a series of complete nonlinear soil-structure interaction (SSI¹) finite element analyses performed on an I-wall section founded in an overconsolidated lean clay. Maximum values of undrained shear strength (S_u) distribution with depth and maximum values of undrained secant stiffness (E_u) distribution with depth are assigned to the clay soils. This corresponds to mean plus four standard deviations for both the S_u distribution and the E_u distribution. The focus of this study was to investigate the phenomena of gap initiation and propagation along the soil-to-structure interface on the flood side of the I-wall and to study the effects of gap initiation and propagation on the resulting deformation and stress conditions in the soil regime on both the flood side and landside of the I-wall. The findings of these analyses will be used in a companion research effort focusing on risk and reliability assessments of I-wall systems.

The following sections will describe the soil used in the analyses, the selection of stiffness and shear strength parameters, the conventional design of the I-wall, the analysis procedures employed, and the results of the complete nonlinear SSI analyses.

D.2 Overview of flood-site I-wall being analyzed

The geometry of the problem analyzed is the same wall system shown in Figure 2.1. The site was assumed to be a level plan with a maximum floodwater elevation of 9 ft. Two soil layers were assumed in the analyses. The top 20 ft represented an overconsolidated layer, while the underlying soil was assumed to be normally consolidated. The elevation of the soil surface was assumed to be at 0 ft.

¹ Symbols and unusual abbreviations used in this appendix are listed and defined in the Notation, Appendix I.

The I-wall was composed of a sheet-pile wall with the tip at el -16 ft. The top of the I-wall was composed of a concrete cap 2.5 sq ft (i.e. embedment to el -2.5 ft) with the top of the cap level with the ground surface. The wall above the top of the soil was composed of a tapered concrete section 2.5 ft at the base and 1 ft at the top of the wall (el 9 ft). The water table for this problem was at the pile tip (el -16 ft).

D.3 Conventional design of cantilever I-wall and shear strength

The design depth of penetration of the sheet-pile section of the I-wall was determined using the Computer-Aided Structural Engineering (CASE) CWALSHT computer program (U.S. Army Engineer Research and Development Center 2012) and procedures outlined in Headquarters, U.S. Army Corps of Engineers (1994).¹ The computed design depth of penetration of the sheet pile (-16 ft) (refer to Chapter 2) was used in this analysis without consideration of a gap forming between the concrete cap and the soil or between the sheet pile and soil on the flood side of the I-wall and using the mean S_u distribution with depth given in Chapter 2. However, note that the finite element analysis for the wall section was conducted for this same -16-ft design depth, and it considered the potential for gap initiation and propagation. It too should be noted that the inclusion of a gap beside the wall also would affect the design depth. This analysis provides useful information for a lower ratio of embedment to flood height. It is important to recognize that the factor of safety for this system based on complete SSI results for a flood elevation of 9 ft would not correspond to the factor of safety used for design in CWALSHT because a gap was not assumed in the CWALSHT analysis.

The total stress (undrained) shear strength parameters were determined using the SHANSEP (Stress History and Normalized Soil Engineering Properties) procedure (Ladd and Foott 1974) discussed in Chapter 2. It assumes that the soil shear strength can be normalized by the effective overburden pressure. The effective overburden pressure is calculated at midlayer for each of the layers identified in Table D.1 and using a preflood water table elevation of -16 ft. The ratio of shear strength to effective overburden pressure (S_u/σ'_{vo}) is dependent on the overconsolidation ratio (OCR) and a fitting parameter (m), assumed to be 0.8, as shown in Equation D.1.

¹ Citations in this appendix are in the References at the end of the main text.

Table D.1. Computation of maximum S_u variation with depth.

Layer			Short-Term (Undrained) Loading				
No.	Top El, ft	Bottom El, ft	Depth, ft	σ'_{vo} , psf	OCR	$(S_u/\sigma'_{vo})_{oc}$	$S_{u,max}$, psf
1	0	-1.5	1	122	7	1.422983	174
			2	244	7	1.422983	347
2	-1.5	-4.5	3	366	7	1.422983	521
			4	488	7	1.422983	694
			5	610	6.4	1.32454	808
3	-4.5	-7.5	6	732	5.5	1.173306	859
			7	854	4.8	1.052239	899
			8	976	3.6	0.835917	816
4	-7.5	-11.5	9	1098	2.9	0.703137	772
			10	1220	2.3	0.584122	713
			11	1342	2	0.52233	701
			12	1464	1.7	0.458649	671
			13	1586	1.6	0.436935	693
5	-11.5	-17.5	14	1708	1.4	0.392666	671
			15	1830	1.35	0.381407	698
			16	1952	1.3	0.370063	722
			17	2011.5	1.25	0.358632	721
			18	2071	1.2	0.347109	719
6	-17.5	-20	19	2130.5	1.15	0.33549	715
			20	2190	1.1	0.323769	709
7	-20	-27.5	25	2487.5	1	0.3	746
			30	2785	1	0.3	836
8	-27.5	-40	35	3082.5	1	0.3	925
			40	3380	1	0.3	1014
			45	3677.5	1	0.3	1103
			50	3975	1	0.3	1193
9	-40	-60	55	4272.5	1	0.3	1282
			60	4570	1	0.3	1371
			65	4867.5	1	0.3	1460
10	-60	-80	70	5165	1	0.3	1550
			75	5462.5	1	0.3	1639
			80	5760	1	0.3	1728
			85	6057.5	1	0.3	1817
11	-80	-100	90	6355	1	0.3	1907
			95	6652.5	1	0.3	1996
			100	6950	1	0.3	2085

$$\left(\frac{S_u}{\sigma'_{vo}} \right)_{OC} = \left(\frac{S_u}{\sigma'_{vo}} \right)_{NC} \bullet OCR^m, \quad (D.1)$$

where

$(S_u/\sigma'_{vo})_{OC}$ =ratio of the undrained shear strength to effective overburden pressure for the overconsolidated condition;

$(S_u/\sigma'_{vo})_{NC}$ =ratio of the undrained shear strength to effective overburden pressure for the normally consolidated condition.

From published values (Ladd 1991), a mean value of 0.22 was assigned to $(S_u/\sigma'_v)_{NC}$ (Chapter 2) and a value of 0.8 for m based on undrained Direct Simple Shear (DSS) test results. These data also indicated a standard deviation equal to 0.02 for the $(S_u/\sigma'_{vo})_{NC}$. In the computation of the effective overburden pressures, 122 pcf was used for both the moist and the saturated unit weights. The OCR characterization of this site is the same as discussed in Chapter 2 and shown in Figure 2.3.

The resulting maximum variation in the undrained shear strength ($S_{u,max}$) with depth is shown in Figure D.1. Average maximum values of the undrained shear strength ($S_{u,max,ave}$) were estimated to be constant over a given depth as shown in Figure D.1. These constant values are listed for the soil layers in Table D.1 and were used in the complete SSI analysis to approximate variation in S_u with depth.

D.4 Shear strength and stiffness properties used in the complete SSI analysis

A complete SSI analysis of the I-wall section shown in Figure 2.1 was performed using the two dimensional (2-D) version of the PC-based finite element program PLAXIS. The finite element method employed required certain input material properties for the selected soil constitutive models. The PLAXIS nonlinear Hardening Soil (HS) constitutive model was used to model all soil elements. This constitutive model provides for nonlinear stress-strain response for soil elements during loading. Elastic plate elements were used to model the steel sheet pile and the concrete I-wall section. To process bending moment and shear distribution results more efficiently, plate elements were used to model the concrete I-wall. Two-dimensional elastic elements were used to represent the concrete cap (the region in which the sheet pile is embedded).

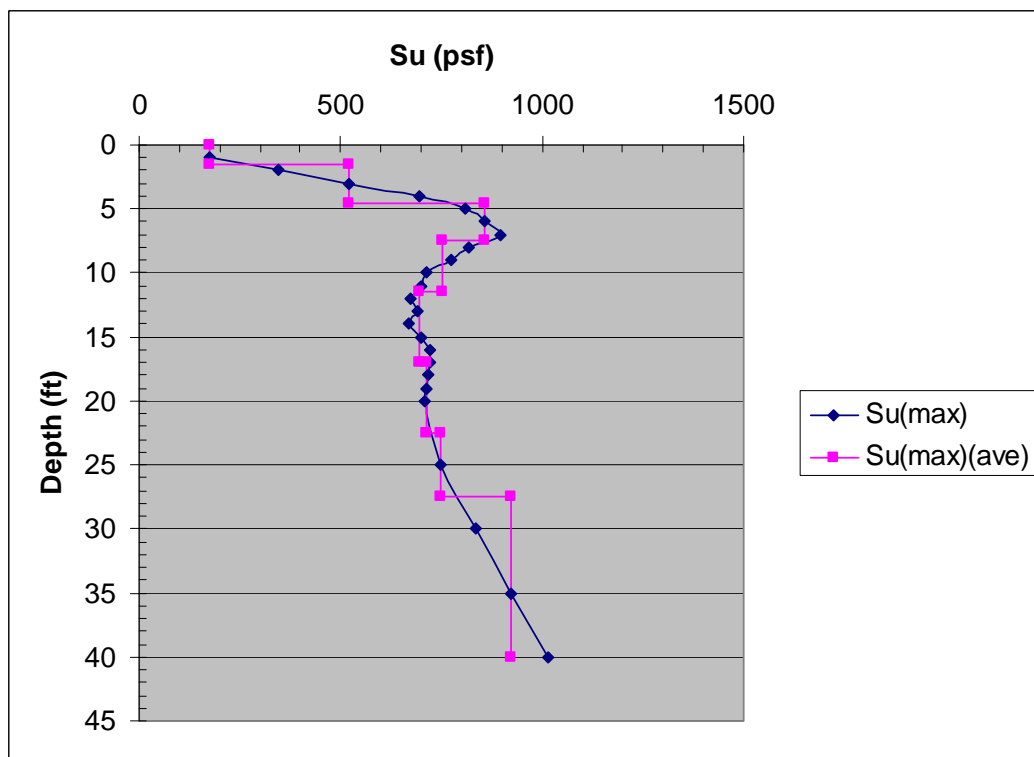


Figure D.1. Variation in maximum computed values of undrained shear strength (S_u) with depth.

Total stress soil strength parameters were used to characterize this over-consolidated lean clay site. An SSI parametric study was conducted to determine the maximum variation in the undrained secant stiffness in conjunction with a maximum variation in shear strength with depth that resulted in a numerically stable analysis. The maximum variation in stiffness was obtained by using the mean value of 0.22 assigned to $(S_u/\sigma'_v)_{NC}$ in conjunction with a standard deviation of 0.02. The $(S_u/\sigma'_v)_{NC}$ ratio was increased by four standard deviations. This mean plus four standard deviations using the PLAXIS analysis at the design flood elevation of 9 ft converged. The maximum computed ratio $(S_u/\sigma'_v)_{NC}$ was equal to 0.30 (computed using Equation D.2):

$$\left(\frac{S_u}{\sigma'_v} \right)_{NC+4\sigma} = \left(\frac{S_u}{\sigma'_v} \right)_{NC-mean} + 4\sigma, \quad (D.2)$$

$$\text{where } S_{u(NC+4\sigma)} = \left[\left(\frac{S_u}{\sigma'_v} \right)_{NC-mean} + 4\sigma \right] \bullet \sigma'_v,$$

$$\text{with } \left(\frac{S_u}{\sigma'_v} \right)_{NC-mean} = 0.22,$$

and σ , the standard deviation = 0.02.

The resulting maximum variation in stiffness with depth was computed using the results of Equation D.2 and Equation D.3:

$$E_{u(NC+4\sigma)} = \text{constant} \times S_{u(NC+4\sigma)} \quad (\text{D.3})$$

and constant = E_u/S_u ratios at each elevation listed in Table D.2.

Additionally, the maximum variation in shear strength with depth was computed using the mean value of 0.22 assigned to $(S_u/\sigma'_v)_{NC}$ in conjunction with four times the standard deviation of 0.02. The maximum computed ratio $(S_u/\sigma'_v)_{NC}$ was equal to 0.30 and was computed using Equation D.4:

$$\left(\frac{S_u}{\sigma'_v} \right)_{NC+4\sigma} = \left[\left(\frac{S_u}{\sigma'_v} \right)_{NC-mean} + 4\sigma \right], \quad (\text{D.4})$$

$$\text{where } S_{u(NC+4\sigma)} = \left[\left(\frac{S_u}{\sigma'_v} \right)_{NC-mean} + 4\sigma \right] \bullet \sigma'_v.$$

The Figure 2.5 correlation by Duncan and Buchignani (1976) and Equation 2.2 were used to estimate the minimum variation of undrained secant modulus in clay with depth. Table D.2 summarizes the computation of E_{us} with depth using the average values of the variation of S_u with depth from Table D.1 in conjunction with Equation 2.2. These values of E_{us} were used to estimate of the variation in the PLAXIS input stiffness parameter (E_{50}^{ref}), which is a secant modulus at 50 percent of the principal stress difference ($\sigma_1 - \sigma_3$). The remaining parameters for soil properties selected to represent the clay (CL) soils used in the PLAXIS finite element analyses were the same as discussed in Chapter 2. Table D.3 shows the values of HS constitutive soil parameters used in this analysis. Values of the coefficient of friction between the sheet pile and the soil and between the concrete cap and the soil were the same as referenced in Table 2.5.

Table D.2. Computation of maximum undrained secant modulus (E_{us}).

Layer			Short-Term (Undrained) Loading					E_u/S_u	$E_{u,max}$, psf
			Depth, ft	σ'_{vo} , psf	OCR	$(S_u/\sigma'_{vo})_{oc}$	$S_{u,max}$, psf		
1	0	-1.5	1	122	7	1.422983	174	250	43,401
			2	244	7	1.422983	347	250	86,802
			3	366	7	1.422983	521	250	130,203
2	-1.5	-4.5	4	488	7	1.422983	694	250	173,604
			5	610	6.4	1.32454	808	270	218,152
			6	732	5.5	1.173306	859	300	257,658
3	-4.5	-7.5	7	854	4.8	1.052239	899	350	314,514
			8	976	3.6	0.835917	816	450	367,135
			9	1098	2.9	0.703137	772	500	386,022
4	-7.5	-11.5	10	1220	2.3	0.584122	713	550	391,946
			11	1342	2	0.52233	701	580	406,561
			12	1464	1.7	0.458649	671	590	396,163
5	-11.5	-17.5	13	1586	1.6	0.436935	693	590	408,858
			14	1708	1.4	0.392666	671	600	402,404
			15	1830	1.35	0.381407	698	600	418,785
6	-17.5	-20	16	1952	1.3	0.370063	722	600	433,418
			17	2011.5	1.25	0.358632	721	600	432,833
			18	2071	1.2	0.347109	719	600	431,318
7	-20	-27.5	19	2130.5	1.15	0.33549	715	600	428,857
			20	2190	1.1	0.323769	709	600	425,433
			25	2487.5	1	0.3	746	600	447,750
8	-27.5	-40	30	2785	1	0.3	836	600	501,300
			35	3082.5	1	0.3	925	600	554,850
			40	3380	1	0.3	1014	600	608,400
9	-40	-60	45	3677.5	1	0.3	1103	600	661,950
			50	3975	1	0.3	1193	600	715,500
			55	4272.5	1	0.3	1282	600	769,050
10	-60	-80	60	4570	1	0.3	1371	600	822,600
			65	4867.5	1	0.3	1460	600	876,150
			70	5165	1	0.3	1550	600	929,700
11	-80	-100	75	5462.5	1	0.3	1639	600	983,250
			80	5760	1	0.3	1728	600	1,036,800
			85	6057.5	1	0.3	1817	600	1,090,350
			90	6355	1	0.3	1907	600	1,143,900
			95	6652.5	1	0.3	1996	600	1,197,450
			100	6950	1	0.3	2085	600	1,251,000

Table D.3. Maximum HS model strengths and maximum stiffness properties for the soil layers.

Layer			C_{ref} , lbs/ft ²	$E_{50,ref}$, lbs/ft ²	$E_{oed,ref}$, lbs/ft ²	$E_{ur,ref}$, lbs/ft ²
No.	Top El, ft	Bottom El, ft				
1	0.0	-1.5	174	4.34E+04	4.34E+04	1.30E+05
2	-1.5	-4.5	521	1.30E+05	1.30E+05	3.91E+05
3	-4.5	-7.5	855	2.63E+05	2.63E+05	7.90E+05
4	-7.5	-11.5	750	3.88E+05	3.88E+05	1.16E+06
5	-11.5	-17.0	696	4.15E+05	4.15E+05	1.25E+06
6	-17.0	-20.0	714	4.29E+05	4.29E+05	1.29E+06
7	-20.0	-27.5	746	4.48E+05	4.48E+05	1.34E+06
8	-27.5	-40.0	925	5.55E+05	5.55E+05	1.66E+06
9	-40.0	-60.0	1237	7.42E+05	7.42E+05	2.23E+06
10	-60.0	-80.0	1594	9.56E+05	9.56E+05	2.87E+06
11	-80.0	-100.0	1951	1.17E+06	1.17E+06	3.51E+06

Minimum values of adhesion were assigned to the soil along the I-wall-to-soil and sheet-pile-to-soil interfaces in the complete SSI analysis. The minimum value for adhesion was estimated using the one selected for the ratio of adhesion to cohesion (f_c) between the sheet pile and soil and between the concrete and the soil shown in Table 2.5 and Equation 2.3. Substituting the ratio of adhesion to cohesion equal to 0.8 into Equation 2.3 and solving for $(C_a)_{min}$, yields Equation D.5:

$$(C_a)_{min} = 0.8(C)_{min} = 0.8 (C_{mean} - 2\sigma), \quad (D.5)$$

where

$(C_a)_{min}$ = minimum soil adhesion;

C_{min} = minimum value of cohesion = minimum value of undrained shear strength ($S_{u,min}$);

C_{mean} = mean value of cohesion = mean value of undrained shear strength ($S_{u,mean}$);

σ = standard deviation.

The properties of the concrete cap represented by elastic elements and the properties of the concrete I-wall section modeled by elastic plate elements with the properties were the same as referenced in Tables 2.6 and 2.7, respectively. The sheet pile was represented by elastic plate elements with the same properties as referenced in Table 2.8.

D.5 Discussion of finite element analyses

D.5.1 Conceptual model

The finite element analysis was performed using the 2-D version of the nonlinear incremental construction finite element program PLAXIS. The conceptual model of the finite element mesh is the same as shown in Figure 2.6. The geometry is the same as in Figure 2.1. Several special modeling features were used including the sheet-pile wall and the concrete I-wall section being modeled by elastic plate elements. Interface elements and soil elements beside the sheet-pile wall on the flood side were 0.5 ft in height. These special features are described in Chapter 2.

D.5.2 Gap initiation and propagation criterion

A hydraulic fracturing criterion is applied to determine if a gap develops and if it spreads down the soil-to-I-wall interface. In this procedure of analysis, the total horizontal stress (computed by PLAXIS) at the ground surface soil-to-I-wall interface is compared to the hydrostatic water pressure developing at the top of the ground surface caused by the presence of the specified flood pool elevation. If the hydrostatic water pressure of the flood pool (the demand) exceeds the total horizontal stress (the capacity), a gap will initiate at the ground surface, along the soil-to-I-wall interface. This criterion is discussed in Chapter 2.

D.5.3 Finite element model

A 2-D cross section used to model the variation of undrained shear strength and soil stiffness with depth by the PLAXIS program is shown in Figure D.2. The regions of uniform color reflect soil clusters used to define the mesh and assign soil regions with common properties. The inset figure shows the average undrained shear strengths assigned to the upper eight layers based on the maximum S_u values (i.e., mean plus four standard deviations). The finite element mesh used in the analysis is the same as shown in Figure 2.9. The mesh is composed of 4,187 elements, 34,408 nodes, and 50,244 stress points. The mesh consists of 15-node triangular elements to model the soil, plate elements to model the bending effects of the I-wall and sheet-pile wall, and interface elements to model SSI between the sheet-pile wall and the adjacent soil elements. The analyses are executed as a plane strain problem. An enlarged view of the area around the wall and its mesh are shown in Figure 2.10.

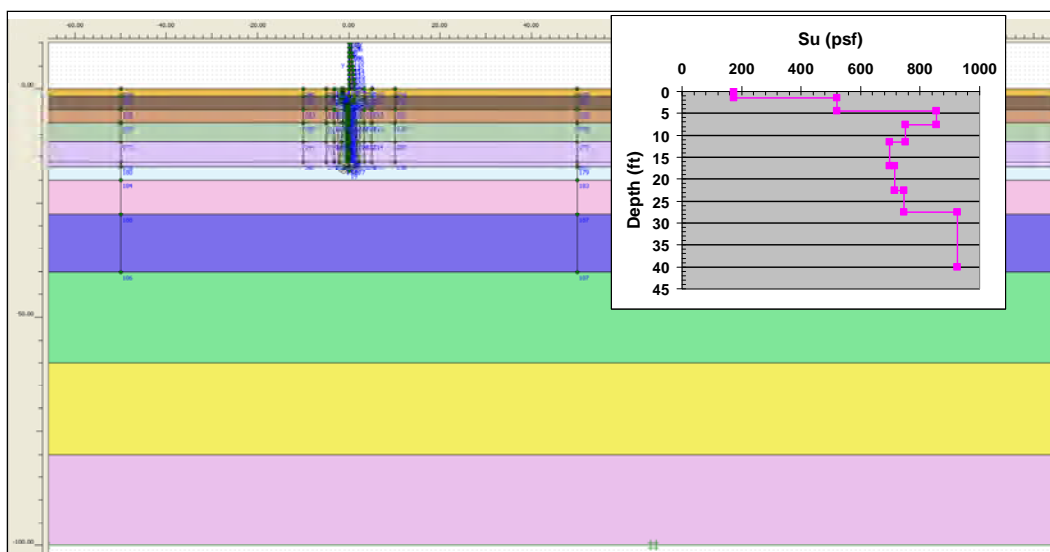


Figure D.2. Two-dimensional (2-D) cross-section model using the maximum computed values of undrained shear strength (S_u) and maximum computed undrained secant stiffness (E_u) used in the SSI analyses.

D.6 Results of the finite element analyses

D.6.1 Initial stresses

The initial total stress state within the finite element mesh was established using the at-rest soil conditions for a level ground surface. Horizontal at-rest soil stresses were estimated using the interrelationship between the at-rest earth pressure coefficient (K_o) and the soil Poisson's ratio (ν) (Equation 2.4). The assumed groundwater elevation was at the sheet-pile tip (el -16 ft). The assigned values of ν and the corresponding K_o values used to compute the horizontal earth pressures for the initial conditions are summarized in Table 2.9.

For this level ground site, the at-rest stress is computed by multiplying the total overburden pressure for each integration point in every soil element by K_o . Figure D.3 shows the computed fraction of mobilized shear strength (referred to as relative shear stress in PLAXIS output) from the initial total stress condition. The resulting fraction of mobilized shear strength (1.0 indicates full mobilization of shear strength) is less than or equal to 0.46 for all soil clusters. These results indicate considerable reserve shear capacity in the soil regime and, thus, a stable numerical model at this initial stage of construction.

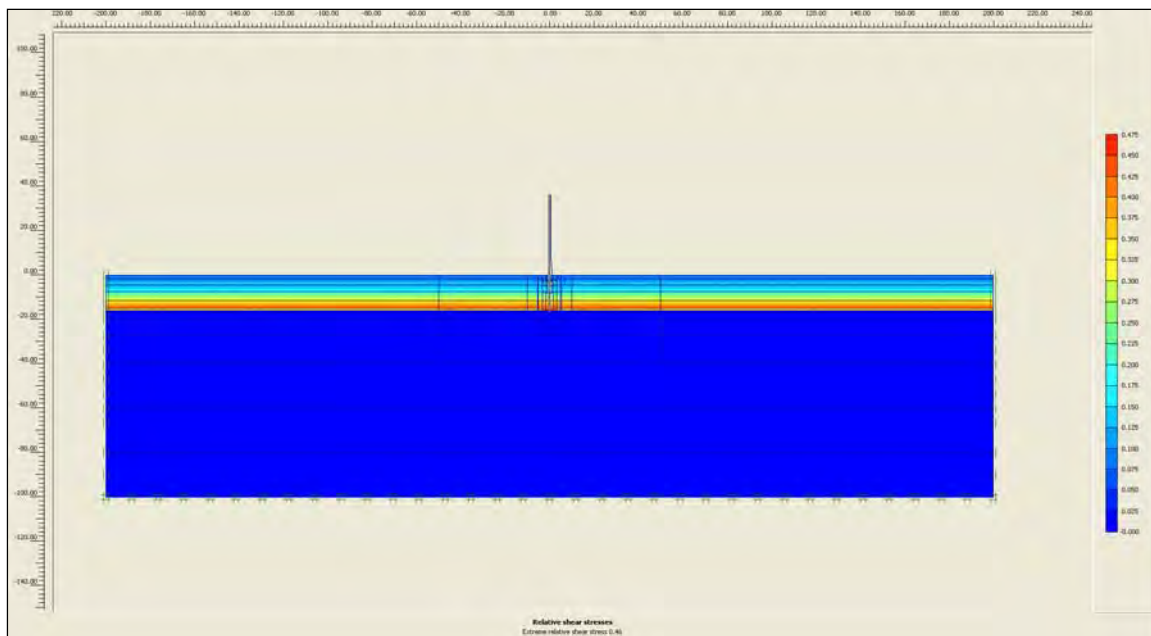


Figure D.3. Fraction of mobilized shear strength for initial conditions using the maximum computed values of undrained shear strength (S_u) and the maximum computed values of undrained secant stiffness (E_u).

D.6.2 Gap initiation and propagation results

The focus of this study was to investigate the phenomena of gap initiation and propagation along the flood side of the soil-to-I-wall interface and to study the effects of gap initiation and propagation on the resulting deformation and stress conditions in the soil regime on both the flood side and landside of the I-wall system.

Modeling of the flood loading commenced in the complete SSI analysis after the total initial stress state was established within the mesh for an assumed steady-state water elevation at the ground surface (el 0.0 ft). The flood loading was applied in 1-ft incremental raises of the water level to track the formation and propagation of a gap. The hydraulic fracturing criterion is used to estimate a gap formation and its propagation. This procedure compares the total normal earth pressures due to the flood pool acting on the wall at a given depth to the hydrostatic water pressure acting at the corresponding depth. A gap is formed when the total horizontal earth pressure (the capacity) is less than the water pressure due to the flood pool acting at the corresponding depth (the demand). Next, hydrostatic water pressure is applied over the depth of the gap, and this hydrostatic water pressure at the new, deeper gap depth is compared to the total horizontal earth pressure. Gap propagation is terminated at the depth when the

demand is less than the capacity. Complete SSI analysis results were examined for various water elevations and gap depths. Figure D.4 shows the progression of the gap as the water level against the I-wall is increased. As shown, the gap initiates when the water is at the shallow el 2 ft and extends to a depth of -4.0 ft. The gap extends to el -8 ft at a water elevation of 3 ft and to el -11 ft at a water elevation of only 4 ft. At water el 6 ft, the gap extends to el -14 ft. At water el 7 ft, the gap extends to el -15 ft, and gap elevation remains constant until a water elevation of 11 ft. Note that the gap is within 1 ft of the sheet-pile tip for floodwater levels at and above el 7 ft. In the previous analyses (Appendices A through C) the gap propagated to this same elevation of 15 ft. However, at shallower water levels and depending on the S_u variations and E_u variations, differences in computed gap propagation were observed.

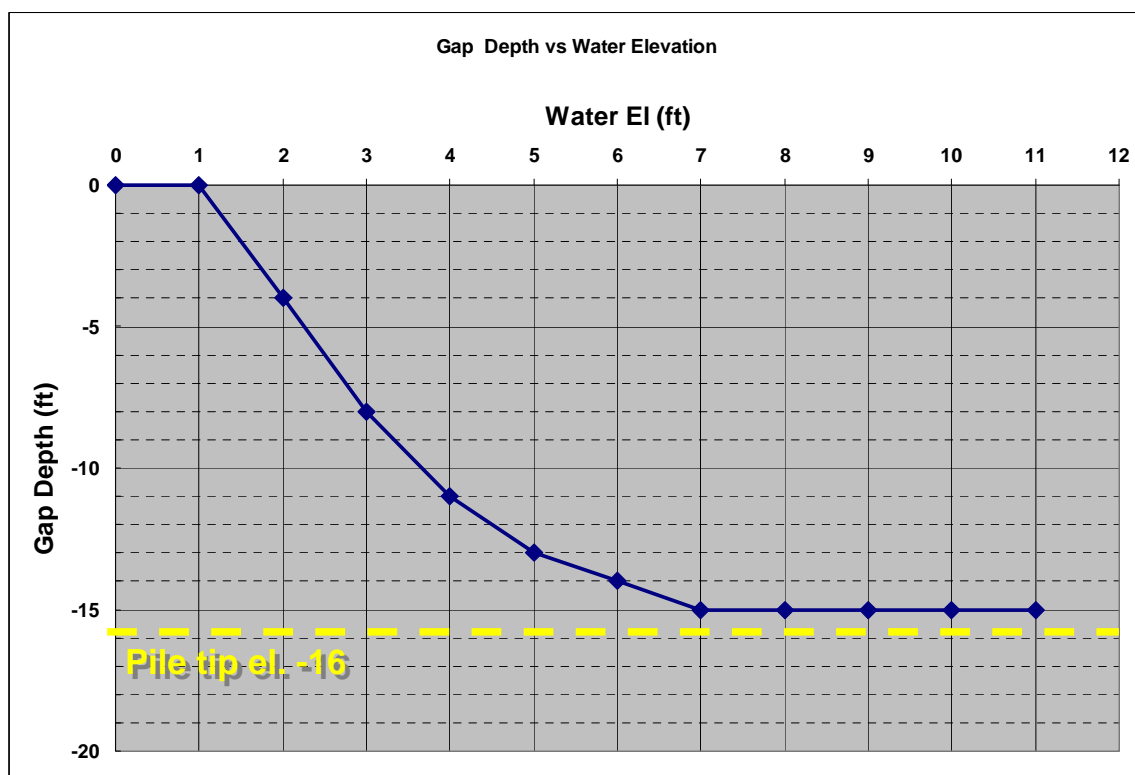


Figure D.4. Progression of gap versus water elevation using the maximum computed values of undrained shear strength (S_u) and the maximum computed values of undrained secant stiffness (E_u).

D.6.3 Performance of interface elements

The performance of the interface elements was compared to the performance of the soil elements adjacent to the wall to ascertain whether the results for the interface elements could be used to accurately characterize the computed results of the analyses. Figure 2.16 showed that the total

horizontal stresses computed within the interface and soil elements agree closely for the selected flood elevation of 2 ft. Therefore, interface element results were used to summarize computed results from this complete SSI analysis.

D.6.4 Discussion of displacements and stresses

The total (exaggerated) nodal displacements within the finite element mesh (both soil and wall) are shown in Figure D.5. These displacements are for the design water elevation of 9 ft with a gap depth to el -15 ft. Note that the nodal displacements are increased by a factor of 100 in this figure to show the deformed mesh relative to its initial position and to show the extent of the gap. The gap is modeled by deactivating the soil elements adjacent to the wall. The general trend of the deflections was toward the landside because of the applied boundary water pressures on the flood side. The wall had a greater movement than the soil at this loading phase. The maximum wall displacement was approximately 2.0 in. at the top of the wall. The displacement of the wall consisted of both horizontal and vertical movements. The tip of the wall moved slightly upward and toward the landside.

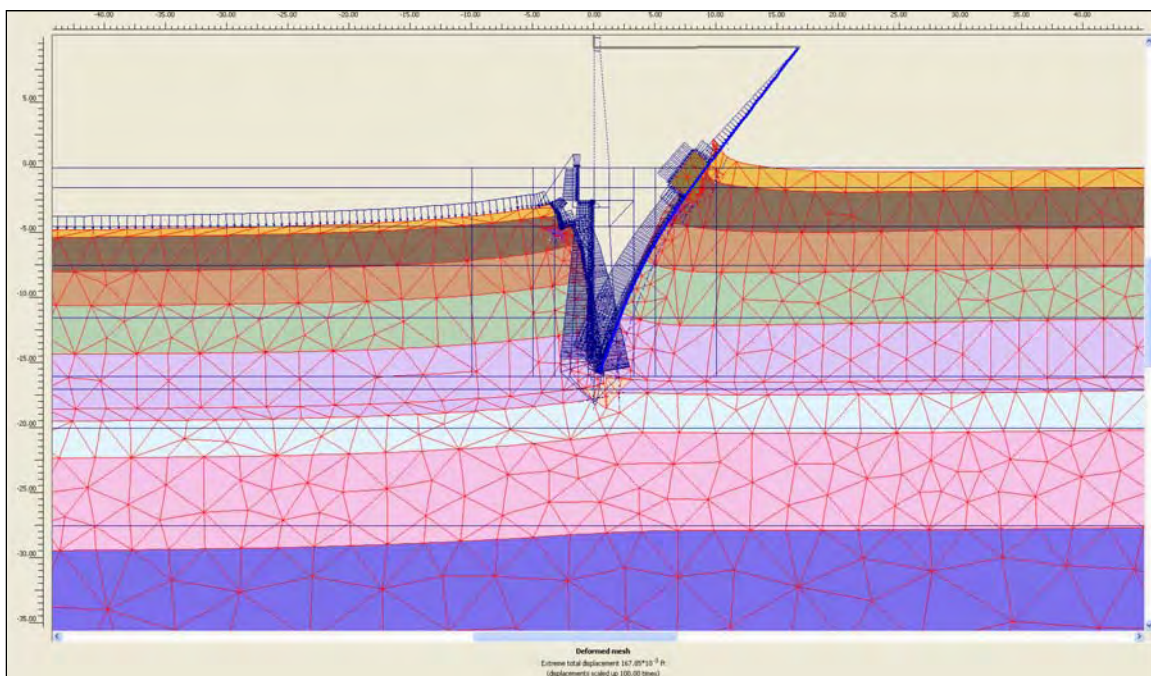


Figure D.5. Total exaggerated displacements for a water elevation of 9 ft and gap elevation of -15 ft using the maximum computed values of undrained shear strength (S_u) and the maximum computed values of undrained secant stiffness (E_u).

Figure D.6 shows a plot of horizontal displacements of I-wall versus flood water elevation at three points along the wall. The points monitored in the analysis were the top of the I-wall at el 9 ft, the ground surface at el 0.0 ft, and the sheet-pile tip at el -16 ft. As shown, the deflection of the wall up to flood el 3 ft (after gap initiation) is primarily uniform translation. As the water elevation increased, the top of the wall had larger deformations than those of the ground and much larger deformations than those of the pile tip. This implies that the wall was undergoing rotation along with translation. Also, above water el 9 ft, the deflection of the pile tip was directed toward the flood-side soil, which indicates kickback of the pile tip. This behavior is consistent with the behavior assumed in limit equilibrium design procedures for the design of cantilever sheet-pile walls.

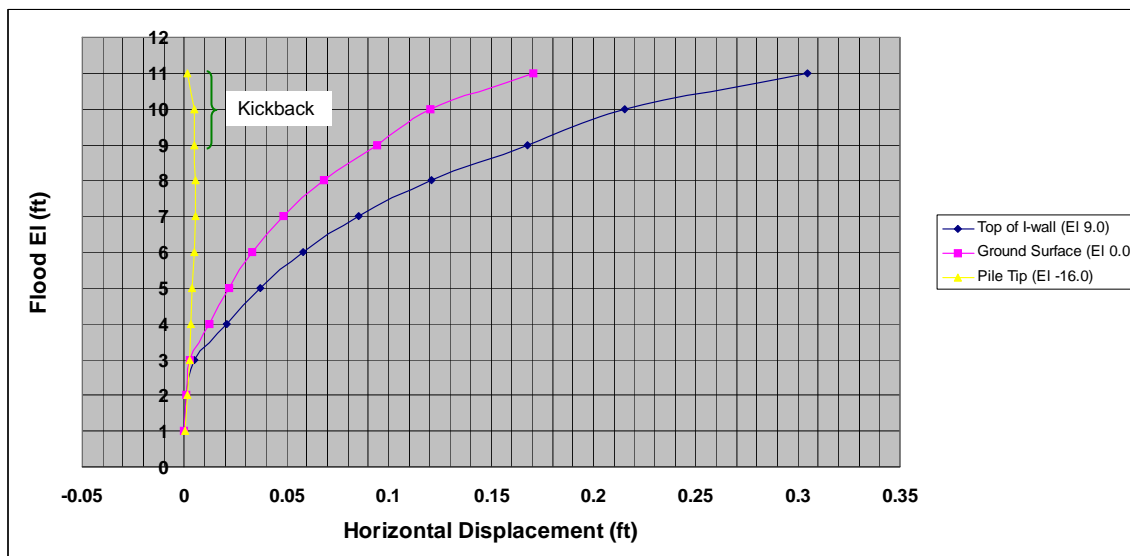


Figure D.6. Horizontal sheet-pile deflection versus water elevation using the maximum computed values of undrained shear strength (S_u) and the maximum computed values of undrained secant stiffness (E_u).

Figure D.7 shows a plot of relative horizontal displacements of I-wall versus floodwater elevation at the ground surface. Relative displacements were computed at this location to provide results for a companion research effort focusing on risk and reliability assessments of I-walls. The relative displacements were computed by subtracting the displacements of the sheet-pile tip from the sheet-pile displacements at the ground surface for a given flood-water elevation. The maximum computed relative horizontal displacement of the wall at the ground was approximately 2.0 in. for a maximum flood elevation of 11 ft. Computed relative horizontal displacements for this and other flood pool elevations are reported in Table D.4.

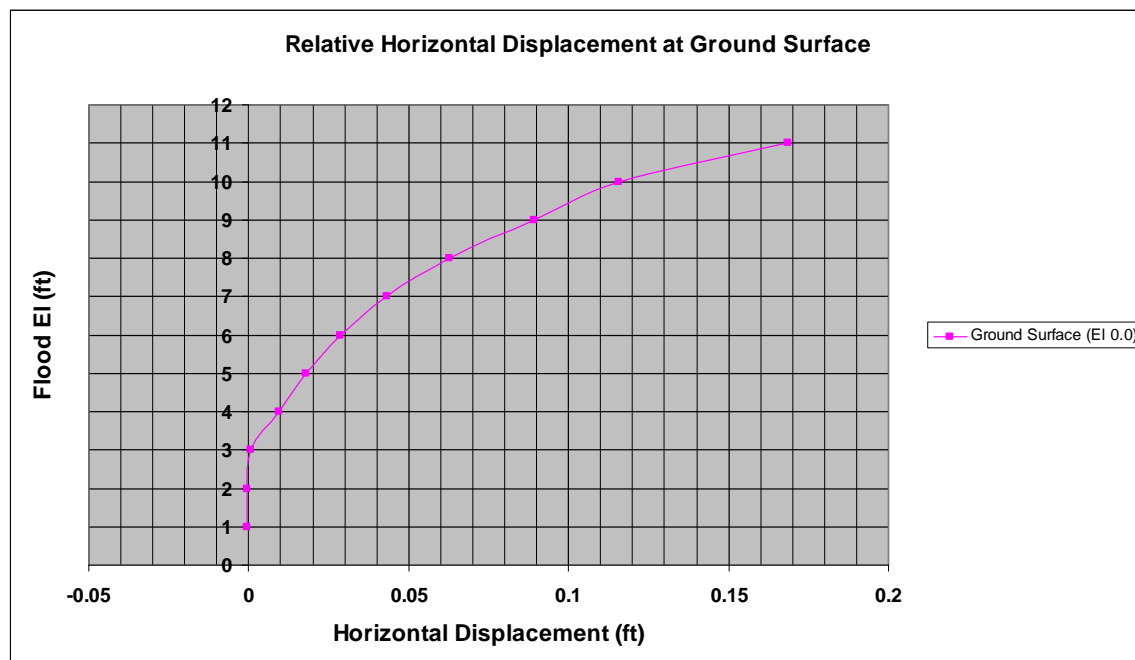


Figure D.7. Relative horizontal sheet-pile deflection at the ground surface el 0 ft versus water elevation using the maximum computed values of undrained shear strength (S_u) and the maximum computed values of undrained secant stiffness (E_u).

Table D.4. Summary of relative horizontal displacements (U_x) of I-wall at the ground surface using maximum computed values of undrained shear strength (S_u) and maximum computed values undrained secant stiffness (E_u).

U_x at Ground Surface, ft	U_x at Pile Tip, ft	Relative Displacement at Ground Surface, ft	Flood El, ft	Gap Depth, ft
-0.0001	0.0005	-0.0006	1	0
0.0007	0.0015	-0.0007	2	4
0.0028	0.0023	0.0005	3	8
0.0124	0.0030	0.0093	4	11
0.0217	0.0038	0.0178	5	13
0.0333	0.0046	0.0287	6	14
0.0485	0.0052	0.0432	7	15
0.0683	0.0054	0.0629	8	15
0.0943	0.0050	0.0894	9	15
0.1203	0.0046	0.1157	10	15
0.1705	0.0017	0.1687	11	15

The analysis using the mean, best estimate (B.E.), values for S_u and E_u resulted in a maximum computed relative horizontal displacement of the wall at the ground of approximately 3.3 in. (Table 2.10). Table D.5 compares the maximum computed relative horizontal displacements from analyses

using both the B.E. of S_u and E_u and maximum S_u and maximum E_u values. As shown for the maximum flood el 11 ft, the maximum computed relative displacement using the maximum values of both S_u and E_u was approximately equal to 2.0 in. The analysis using the B.E. values for S_u and E_u did not converge at flood el 11 ft. However, at flood el 10 ft, the maximum computed relative displacement using the maximum values of both S_u and E_u was approximately equal to 1.4 in., compared to approximately 3.3 in. using the B.E. values for S_u and E_u . The influence of the larger values of both soil shear strength and stiffness resulted in an approximately 60 percent decrease in the computed relative horizontal displacement of the wall at the ground surface.

Table D.5. Comparison of relative horizontal displacements of I-wall at the ground surface using both the B.E. and maximum computed values of undrained shear strength (S_u) and maximum computed values undrained secant stiffness (E_u).

Flood El, ft	Relative Displacement at Ground Surface ($S_{u(max)}, E_{u(max)}$), ft	Relative Displacement at Ground Surface ($S_{u(B.E.)}, E_{u(B.E.)}$), ft
1	-0.0006	-0.0014
2	-0.0007	-0.0021
3	0.0005	0.0017
4	0.0093	0.0106
5	0.0178	0.0243
6	0.0287	0.0428
7	0.0432	0.0677
8	0.0629	0.1041
9	0.0894	0.1652
10	0.1157	0.2751
11	0.1687	N/A

The total horizontal pressures acting on the interface elements adjacent to the wall on the flood side and landside for two flood elevations (9 ft and 11 ft) and corresponding gap elevation of -15 ft for each flood elevation are shown in Figures D.8 and D.9, respectively. Minimum values of soil adhesion were used in the PLAXIS analysis as well as in the active and passive pressure distributions shown in these figures. These pressure results were compared to limiting stress states (active and passive) for varying factors of safety applied to the undrained shear strength values. The flood elevation of 9 ft corresponds with the design water height used in the conventional design.

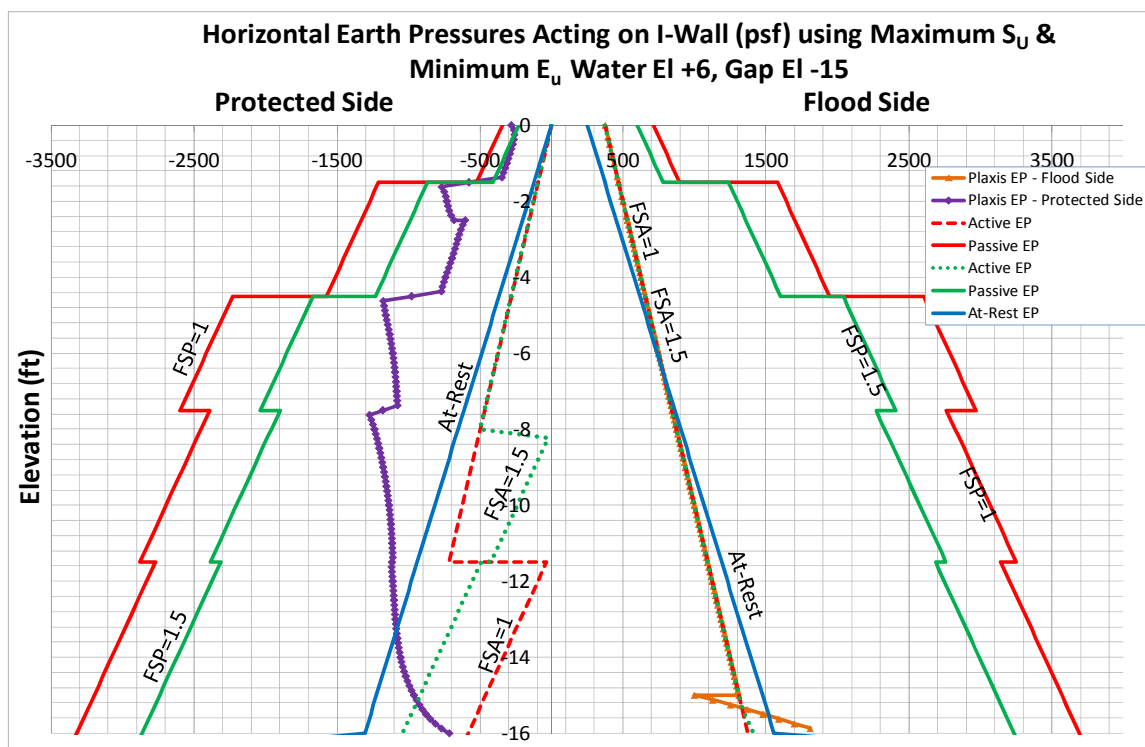


Figure D.8. Comparison of total normal stresses on the interface elements adjacent to the wall on the flood side and protected side (landside) for flood el 9 ft and gap el -15 ft using the maximum computed values of undrained shear strength (S_u) and the maximum computed values of undrained secant stiffness (E_u).

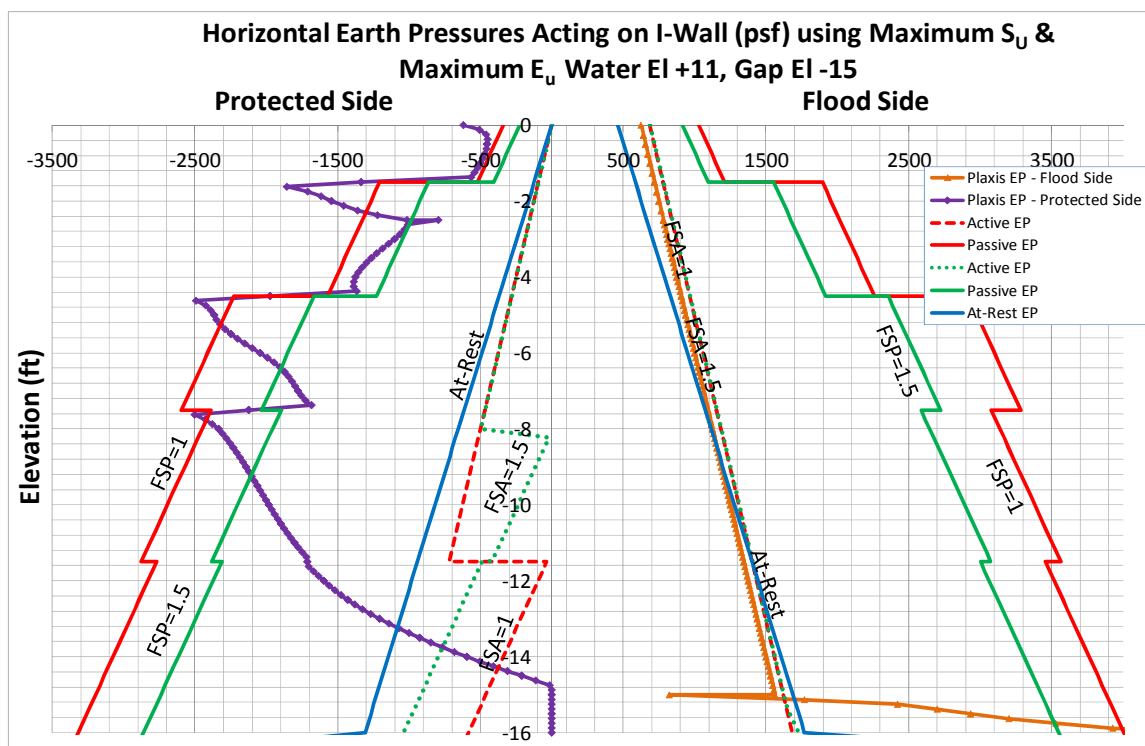


Figure D.9. Comparison of total normal stresses on the interface elements adjacent to the wall on the flood side and protected side (landside) for flood el 11 ft and gap el -15 ft using the maximum computed values of undrained shear strength (S_u) and the maximum computed values of undrained secant stiffness (E_u).

As shown in Figure D.8 for the flood elevation of 9 ft, the SSI earth pressures on the landside fall between at-rest pressures and passive pressures beginning at el -2 ft (with a factor of safety of 1.5) down to el -13 ft. Below el -13 ft, the earth pressures reduce to near-active earth pressure (with a factor of safety of 1.0) near the sheet-pile tip (i.e., at el -16 ft). On the flood side, the complete SSI analysis computes hydrostatic water pressures acting down to the gap tip elevation of -15 ft, which is 1 ft above the pile tip elevation of -16 ft. Below the gap tip elevation, the kickback of the I-wall into the flood-side soil allows for the comparison of horizontal pressures computed by complete SSI analysis to limiting earth passive pressures over this 1-ft depth. For all points except the one at el -16 ft, these computed horizontal pressures were less than those limiting passive earth pressure values computed using a factor of safety equal to 1.5. Kickback of the I-wall into the flood-side soil again is observed near the pile tip.

Figure D.9 shows the horizontal pressure results for the peak flood elevation of 11 ft. On the landside, the pressure results more closely match the passive pressures (with a factor of safety of 1.0) down to el -2.5 ft because of the increased flood loading. Between el -2.5 ft and -6.0 ft, the SSI earth pressure results more closely match passive earth pressures computed with a factor of safety of 1.5 applied to the undrained shear strength values. Between el -6.0 ft and -10 ft, the SSI earth pressures on the landside fall between passive pressures with a factor of safety of 1.0 and passive pressures with a factor of safety of 1.5. Below el -10 ft and down to el -14 ft, the SSI earth pressures on the landside fall between at-rest pressures and passive pressures (with a factor of safety of 1.5) down to el -14 ft. Below el -14 ft, the earth pressure reduces to near-active earth pressure (with a factor of safety of 1.0) at the sheet-pile tip (el -16 ft). Again, the complete SSI analysis computes hydrostatic water pressures acting on the flood side down to the gap tip elevation of -15 ft. Kickback of the I-wall into the flood-side soil again is observed near the pile tip. This behavior is consistent with conventional force equilibrium procedures.

Computed fractions of mobilized shear strength for selected floodwater elevations and gap depths are shown in Figure D.10. A fraction of mobilized shear strength equal to 1 indicates full mobilization of shear strength. As shown in Figures D.10(a) and (b), for the specified flood elevation and gap depth, there are no regions of full mobilization of shear strength. These results indicate reserve shear capacity in the soil regime and, thus, a stable numerical model at these stages of construction.

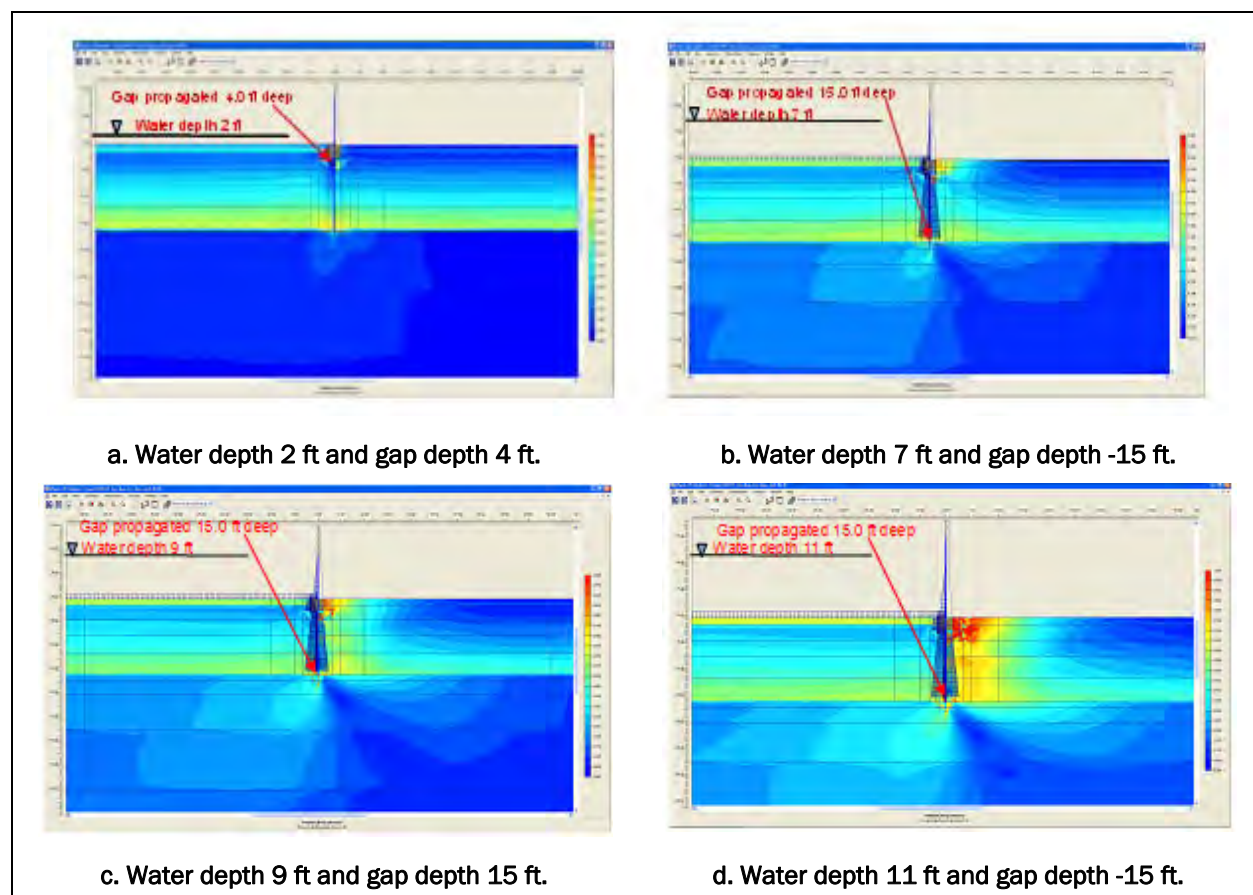


Figure D.10. Fraction of mobilized shear strength at various loading phases using maximum computed values of undrained shear strength (S_u) and the maximum computed values of undrained secant stiffness (E_u).

Figure D.10(c), with the design flood depth of 9 ft and gap depth of -15 ft, shows regions of full mobilization of shear strength on the landside adjacent to and just below the concrete cap. However, there is no indication of a fully developed failure mechanism at the stage of loading. Figure D.10d, with peak flood elevation of 11 ft and gap depth of -15 ft, shows larger regions of full mobilization of shear strength on the passive side of the cap region. An additional loading phase with a flood elevation at 12 ft was attempted, but it resulted in numerical instability.

A subsequent PLAXIS analysis was performed at the peak flood elevation of 11 ft and gap depth at elevation of -15 ft to compute a factor of safety against a possible rotational failure mechanism. Figure 2.16 indicated that the wall was rotating about a point near the pile tip.

Figure D.11 shows a failure mechanism based on the PLAXIS Phi/c reduction procedure. The resulting rotational factor of safety was computed to be 1.35. However, at intermediate flood elevations, less than el 9 ft, rotation of

the wall was not indicated, and it is believed that the Phi/c reduction procedure would compute factors of safety based on localized shear failures with the active driving wedge only. Therefore, for this analysis, the Phi/c reduction procedure was not further used to compute factors of safety resulting from rotational failure mechanisms (as is performed in limit equilibrium procedures) for intermediate flood elevations.

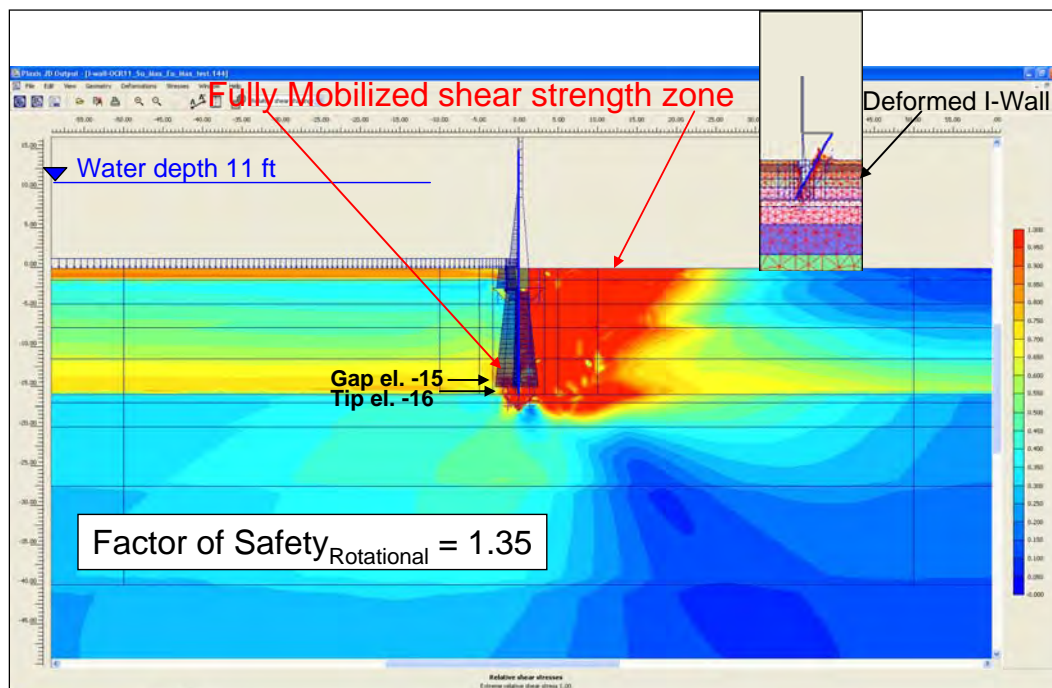


Figure D.11. Rotational factor of safety using Phi/c reduction for design peak flood elevation of 10 ft using maximum computed values of undrained shear strength (S_u) and the maximum computed values of undrained secant stiffness (E_u).

Appendix E: Analyses of E-99 Sheet-pile Wall Field Load Test Using Minimum Values of Both Undrained Shear Strength (S_u) and Undrained Secant Stiffness (E_u)

E.1 Purpose of analyses

This appendix summarizes the results of nonlinear soil-structure interaction (SSI¹) finite element analyses of the E-99 sheet-pile wall field load test described by Jackson (1988).² The analyses included the formation and propagation of a gap beside the sheet-pile wall on the flood side. The gap affected the resulting deformation and stress conditions of the soil regime on both the flood side and landside of the I-wall. The analyses were part of a parametric study determining the effects of the undrained shear strength (S_u) and undrained secant stiffness (E_u) on the deformation and gap formation characteristics of the system. For the analysis described in this appendix, minimum values of the undrained shear strength and undrained secant stiffness were selected.

The following sections will describe the soil used in the analyses, the selection of stiffness and shear strength parameters, the conventional analysis and design of the I-wall, the analysis procedures employed, and the results of the finite element analyses.

E.2 Overview of problem analyzed

The E-99 field load test consisted of a 200-ft section of floodwall constructed on the landside berm of the Item E-99 East Atchafalaya Basin Protection Levee (EABPL) on Avoca Island just south of Morgan City, Louisiana. The test was performed between July and September of 1985 (Jackson 1988).

The soil geometry, maximum water height, and pile geometry of the field load test are shown in Figure 3.1. The sheet pile is located on the landside

¹ Symbols and unusual abbreviations used in this appendix are listed and defined in the Notation, Appendix I.

² Citations in this appendix are in the References at the end of the main text.

of the existing levee. The water loading was applied between the existing levee and the sheet-pile wall. The geometry was idealized as shown in Figure 3.2 and is assumed to be a flat (level) site. The top of the sheet-pile wall was at el 14.5 ft¹, and the tip of the sheet-pile wall was at el -16.5 ft. The elevation of the top soil layer was at 6.5 ft. The I-wall system is described in Chapter 3, Section 3.2.

The soils at the site were clays of high plasticity designated as CH, clay of high plasticity, in the Unified Soil Classification System (USCS). From the classification chart shown in Figure 3.4, the plasticity index of a CH material has a value of 22 percent and greater. The soil was normally consolidated with liquid limits between 76 and 114 percent and natural water contents between 40 and 80 percent.

For the analyses described in this appendix, the permeability of the clay layers was assumed to be small enough that the soil would not become fully saturated as the floodwater level was increased. Therefore, as shown in Figure 3.2, two zones of soil were considered in the analysis: a partially saturated zone above water table el 4 ft and a saturated zone of soil below the water table.

E.3 Material properties used for parametric analysis

The analyses described in this appendix are one case study in a set of parametric analyses varying the values of S_u and E_u . The values used for the analysis described in this appendix correspond to the minimum values of (S_u) and (E_u). The material properties used in the analysis described in Chapter 3 are denoted and treated as the mean values. Actually, they are the values used for the design of the I-wall, which differ slightly from the mean values computed from laboratory test data.

The undrained shear strengths of the clay layers were determined from unconsolidated undrained (UU) and unconfined compression (UC) tests. These design values, shown in Table 3.1, were used to perform an undrained short-term design of the wall. The material property values consist of the saturated (γ_{sat}) and moist (γ_{moist}) unit weights of the soil, the undrained shear strength (S_u), and adhesion (c_a). The angles of internal friction (ϕ) and wall friction (δ) were zero because this is an undrained

¹ All elevations cited in this appendix are in feet referred to the National Geodetic Vertical Datum (NGVD).

analysis. The same value of the unit weight was used for both saturated and moist conditions. Adhesion was used in the total stress analysis using values cited in Potyondy (1961) for a cohesive soil against rough steel, and is equal to 0.8 times the undrained shear strength ($c_a = 0.8 \cdot S_u$).

The laboratory test data were used to compute mean (μ) and standard deviation (σ) values for the soil layers. These values are shown in Table E.1. The column labeled Plate 9 corresponds to the design values assumed in the E-99 field test report (Jackson 1988). As can be seen from Table E.1, the design values are slightly different from the mean values computed from test data. The design values were used in the finite element analysis discussed in Chapter 3. The mean values shown in Table E.1 were computed based on a limited number of tests, and it was felt that the design values provided a better estimate of the strengths. The coefficients of variation (COV) for the clay layers computed from test data also are shown in Table E.1. Because Layer 2 had only two data points, the COV for this layer was deemed to be too low and, therefore, was adjusted to a higher value. The last column in Table E.1 shows the values of the COVs used in this analysis.

Table E.1. Mean and standard deviation values for the clay layers.

Layer	Top El, ft	Bottom El, ft	Plate 9 S_u , psf	Mean μ , psf	Standard Deviation (σ), psf	COV, %	COV, % for Analyses
1	6.5	-1	200	285	74	37.2	37
2	-1	-5	500	580	50	2.4	10
3	-5	-14	350	362	70	20.2	20
4	-14	-29	500	476	175	34.6	35

Using the COVs for the soil layers listed in Table E.1, σ was computed for each layer. These values for σ were used to compute minimum values of S_u ($S_{u,min}$) and E_u ($E_{u,min}$). The minimum value of S_u was computed as shown in Equation E.1:

$$S_{u,min} = S_{u,mean} - X \bullet \sigma. \quad (\text{E.1})$$

The variable (x) in Equation E.1 represents a multiple of the standard deviation. The design values of S_u listed in Table E.1 were used as the $S_{u,mean}$ values.

The value of the minimum E_u was computed as:

$$E_{u,min} = E_{ref} = KS_{u,min}, \quad (E.2)$$

where E_{ref} is the reference stiffness needed for the Mohr-Coulomb (MC) soil model and K is defined as

$$K = \frac{E_{u,min}}{S_{u,min}} \quad (E.3)$$

The value of K in Equation E.3 is taken from a chart developed by Duncan and Buchignani (1976) relating the plasticity index and the overconsolidation ratio to the dimensionless factor K . The same value of K of 200 used in the analysis of Chapter 3 was used for this analysis.

The intent of this analysis was to use the smallest values of S_u and E_u possible and still keep the design condition of the water at the top of the wall at el 14.5 ft numerically stable. The multiple of the standard deviation was varied to find the largest multiple at which the design condition was still stable (i.e., the factor of safety was greater than 1.0). The loading in PLAXIS, a two-dimensional (2-D) nonlinear incremental construction finite element program, was applied in one construction step and the gap propagation was not tracked in these analyses. PLAXIS applies the load increment in many substeps for convergence. Previous experience with I-wall analyses has shown that the results are comparable between a complete analysis tracking the gap progression and this simplified procedure, as long as the gap depth does not vary greatly and unloading of the system does not occur. A constant gap elevation of -10 ft was used. This is the same gap elevation used in the analysis described in Chapter 3. The factor of safety was computed using a Phi/c reduction analysis within PLAXIS. The results of these analyses are shown in Table E.2. The largest multiple of the standard deviation that was acceptable was determined to be 1.6.

Table E.2. Factors of safety for various multiples of the standard deviation.

	Multiples of Standard Deviation			
	-1.5	-1.6	-1.75	-2
FS	1.105	1.06	0.881	Design case would not run

The multiple of 1.6 was used in Equation E.1 to compute the minimum S_u . The minimum value of E_u was computed using a K value of 200 and $S_{u,min}$ in Equation E.2. These minimum values are shown in Table E.3. Also shown in the table are the maximum values of these parameters used in subsequent parametric analyses.

Table E.3. Material properties for analyses.

Layer	Elevation			S_u		Design Values		Min Values		Max Values	
								$S_{u,mean}-1.60*\sigma$		$S_{u,mean}+4*\sigma$	
	Top, ft	Bottom, ft	γ_{sat} , pcf	COV, %	σ	Mean S_u , psf	E_u , psf	S_u , psf	E_u , psf	S_u , psf	E_u , psf
1	6.5	-1	104	37	74	200	40,000	82	16,320	496	99,200
2	-1	-5	107	10	50	500	300,000	420	84,000	700	140,000
3	-5	-14	106	20	70	350	210,000	238	47,600	630	126,000
4	-14	-19	104	35	175	500	300,000	220	44,000	1200	240,000
5	-19	-29	101	35	175	500	300,000	220	44,000	1200	240,000
6	-29	-44	100	35	193	550	330,000	242	48,400	1320	264,000
7	-44	-72	100	35	236	675	405,000	297	59,400	1620	324,000
8	-72	-100	100	35	324	925	555,000	407	81,400	2220	444,000

E.4 Conventional analysis of cantilever I-wall

E.4.1 Criteria for gap initiation and propagation

Two different criteria, one for the flood side of the sheet-pile wall and another for the landside, were used to determine whether a gap initiates in the soil adjacent to the sheet-pile wall and how far the gap will propagate. A hydraulic fracturing criterion was used for the flood side of the I-wall, and a negative horizontal stress criterion was used for the landside. Both of these criteria are discussed in more detail in Chapter 3, Section 3.3.3.

E.4.2 Computed gap depth

CWALSHT (U.S. Army Engineer Research and Development Center 2012) uses the negative horizontal stress criterion discussed in Section 3.3.3 to compute whether a gap forms in the soil. Negative computed earth pressures imply that the soil-to-sheet-pile interface is in tension. Because the soil-to-sheet-pile interface cannot sustain a tensile load, the soil is assumed to form a gap, and CWALSHT sets any negative (tensile) earth pressures to zero. CWALSHT applies water pressures within a gap below the input water level. If the gap is above the water level, CWALSHT does not fill the gap with water.

E.4.3 Total stress analysis with CWALSHT

CWALSHT always computes effective stresses based on the input material properties and the level of the water in the soil. For problems involving all

clay layers, a total stress (short-term) analysis with $c = S_u$ and $\phi = 0$, where c is cohesion, can be performed with CWALSHT by inputting the actual soil geometry and water levels. This gives a correct total stress analysis because, even though CWALSHT computes effective stresses based on the input water levels, the pore pressures are added to the effective stresses to arrive at total stresses. Because the value of the horizontal earth pressure coefficient is equal to 1.0 for a soil with only cohesion, the total stress computed in this manner is correct. The determination of the depth of the gap also conforms to the hydraulic fracturing criterion described in Section 3.3.3. This is because CWALSHT computes effective stresses and uses the effective stresses to determine the tensile zone. The hydraulic fracturing criterion uses total stresses and compares these to static pore pressures, a process that produces equivalent numerical results. Horizontal earth pressures are computed as described in Section 3.3.2.

E.4.4 CWALSHT analysis results

The elevation of the tip of the sheet pile for this analysis was -16.5 ft. A short-term analysis was performed with CWALSHT using the minimum material properties as given in Table E.3. The results of analyses performed with CWALSHT are shown in Table E.4.

Table E.4. Results of analysis computations using CWALSHT.

Analysis Case		S_u , psf	Φ , deg	Adhesion, psf	Wall Friction, deg	Elevation of Bottom of Gap, ft	Elevation of Tip of Sheet Pile		
							FS_{Active}	$FS_{Passive}$	El, ft
1	Short-term with water levels	Minimum values	0	0	0	2.5	1	0.76	-16.5
2	Short-term with water levels	Minimum values	0	$0.8 \cdot S_u$	0	Below wall	1	1.1	-16.5

Cases 1 and 2 were modeled with the actual soil layer geometry with input water levels as described in Section E.4.3. Both Case 1 and Case 2 used a factor of safety applied to the active earth pressures (FS_{Active}) of 1.0. Case 1 did not include adhesion and resulted in a factor of safety on the passive earth pressures ($FS_{Passive}$) equal to 0.76. The gap extended down to el 2.5 ft. Case 2 included adhesion and resulted in a $FS_{Passive}$ of 1.1. The gap in this case extended below the tip of the sheet pile.

E.5 PLAXIS finite element analyses

E.5.1 Conceptual model

The finite element analyses were performed with PLAXIS. The conceptual model of the finite element mesh is shown in Figure 3.7. The geometry is the same as explained previously, but several modeling features should be noted. The sheet-pile wall was represented by plate elements. Interface elements were placed on both sides of the plate elements from the ground surface down to the tip of the sheet pile. To alleviate stress concentrations at the corners of the geometry, both horizontal and vertical extensions of the interface elements were provided at the tip of the sheet-pile wall at el -16.5 ft. A plate element extension and dummy soil elements were added above the wall to provide for additional loading height if needed. The mesh was structured to provide node points at 1-ft raises of the water table. The soil elements beside the sheet-pile wall on the flood side were 0.5 ft in height. This enabled the inputting of 1-ft raises in water and modeling of the gap to within 0.5 ft.

E.5.2 Finite element mesh

The finite element mesh used in the analyses is shown in Figures 3.8 and 3.9. The mesh is composed of 2,396 elements and 19,917 nodes with 28,752 stress points. The type and number of elements used in the mesh are shown in Table 3.3. The mesh consists of 15-node triangular elements to model the soil, 5-node plate elements to model the sheet-pile wall, and 5-node interface elements to model the SSI effects between the sheet-pile wall and the adjacent soil elements. The problem was run as a plane strain problem.

E.5.3 Total stress analysis procedure in PLAXIS

The E-99 field test was analyzed using total unit weights of the soil and boundary water pressures to perform a short-term (undrained) analysis using PLAXIS. All materials were designated as drained, which in PLAXIS terminology means that no excess pore-water pressures will be generated because of applied loads. The general phreatic surface was used in PLAXIS to apply the boundary water pressures on the soil surface and within the gap. All soil layers were associated with a cluster phreatic surface that was input below the minimum elevation of the mesh. Because the water surface was below all soil layers, no internal water pressures were generated within the soil layers. This procedure results in a total stress analysis with the

computed effective stresses being equal to the total stresses (i.e., no internal pore pressures are present).

It was assumed that the permeability of the soil was small enough that any time-dependent effects such as seepage could be ignored and that the undrained shear strengths could be used to determine the behavior of the system.

E.5.4 Tracking the progression of the gap

The I-wall deflects as the flood loading increases, and eventually a gap forms beside the I-wall on the flood side of the wall. The gap begins at the ground surface and progresses downward as shown in Figure 3.10. The gap along the flood side of the I-wall-to-soil interface is modeled by deactivating soil clusters (elements), effectively creating a void beside the wall. As water pressures are applied within this void, the gap progresses downward. Modeling of the flood loading commenced in the finite element analysis after the total initial stress state was computed based on an assumed steady-state water elevation of 4 ft. The flood loading was applied in 1-ft incremental raises of the water level in order to track the formation and propagation of the gap.

The criterion used to estimate the formation and propagation of the gap is based on the hydraulic fracturing concept discussed in Chapter 3, Section 3.3.3. The procedure used to estimate the gap depth:

1. For each rise in water level, the total horizontal stresses against the sheet-pile wall are compared against the hydrostatic water pressures acting on the wall given the current water elevation. A gap is formed when the horizontal earth pressure is less than the water pressure at a given depth.
2. Soil elements are deactivated within the computed region of the gap, and hydrostatic water pressures are applied within the deactivated elements.
3. The analysis is rerun for the current water level, and Steps 1 and 2 are repeated until the depth of the gap ceases to increase.
4. The water level is increased, and Steps 1 through 3 are repeated. The water level is raised until instability in the analyses is encountered.

E.5.5 Shear strength and stiffness properties used in the finite element analyses

The finite element analyses described in this appendix were performed using the PLAXIS finite element program. The MC soil model was used for

the soil elements. This model uses an elastic-perfectly plastic stress-strain relationship. Elastic plate elements were used to model the steel sheet pile, and interface elements were used to capture the soil-structure interaction effects between the sheet-pile wall and the soil. PLAXIS can perform analyses using either effective or total stress soil parameters. For the analyses described herein, total stress soil parameters were used.

Figure 3.11 shows the material numbering and soil layering used in the finite element analyses. The soil was divided into layers below the tip of the pile to provide for an increasing undrained shear strength and stiffness below the elevation of the pile tip. See Chapter 3, Section 3.4.5, for discussion of the properties assumed for the soil, pile, and interface elements.

The undrained shear strength (S_u) and undrained reference stiffness (E_{ref}) of the clay layers used in this parametric analysis are computed as described in Section E.3 and shown in Table E.5. The remaining material property values consist of the saturated (γ_{sat}) and moist (γ_{moist}) unit weights of the soil, angle of internal friction (ϕ), dilation angle (Ψ), unload/reload Poisson's ratio (ν), and the interface strength ($R_{interface}$).

Table E.5. Strength and stiffness properties for the soil layers used in the MC soil model for the case of a minimum S_u and minimum E_{ref} .

Material Number	Material Description	γ_{moist} , lb/ft ³	γ_{sat} , lb/ft ³	S_u , lb/ft ²	E_{ref} , lb/ft ²	ν	$R_{interface}$
1	Clay_1_6.5_200_Rinit=0.8	104	104	82	16,320	0.4	0.8
2	Clay_2_4_200_Rinit=0.8	104	104	82	16,320	0.495	0.8
3	Clay_3_-1_500_Rinit=0.8	107	107	420	84,000	0.495	0.8
4	Clay_4_-5_350_Rint=0.8	106	106	238	47,600	0.495	0.8
5	Clay_5_-14_500_Rinit=0.8	104	104	220	44,000	0.495	0.8
6	Clay_5a_-14_500_Rinit=1.0	104	104	220	44,000	0.495	1
7	Clay_6_-19_500_Rinit=0.8	101	101	220	44,000	0.495	0.8
8	Clay_7_-29_550_Rinit=0.8	100	100	242	48,400	0.495	0.8
9	Clay_8_-44_675_Rinit=0.8	100	100	297	59,400	0.495	0.8
10	Clay_9_-72_925_Rinit=0.8	100	100	407	81,400	0.495	0.8

Note: properties are given for drained material, with the angle of internal friction for the soil (ϕ) and the dilation angle (Ψ) set to 0, as this is a total stress analysis.

The ($R_{interface}$) value is from values cited by Potyondy (1961) as discussed in Chapter 3, Section 3.3.4. This controls the amount of adhesion along the

soil-to-wall interface. Material 6 in Table E.5 has a $R_{interface}$ value of 1.0 because this material represents a soil-to-soil interface.

E.5.6 Initial stresses

The initial total stress state within the finite-element mesh was established using the at-rest soil conditions for a level ground surface. Horizontal at-rest soil stresses were estimated using the relationship between the at-rest earth pressure coefficient (K_o) and the soil's Poisson's ratio (ν) given in Equation 3.14.

The assumed groundwater elevation was at 4 ft. Table 3.9 lists a summary of the K_o values used to compute the horizontal earth pressures for the initial conditions. The Poisson's ratio for the partially saturated soil layer was 0.4, which corresponds to a K_o of 0.67. This value is less than the value for a fully saturated material, which has a K_o of 1.0.

E.5.7 Performance of interface elements

The performance of the interface elements was examined to determine if the normal stresses in the interface elements corresponded closely to the normal stresses in the adjacent soil elements. As discussed in Chapter 3, Section 3.4.7, and shown in Figure 3.14, the stresses within the interface elements agreed very closely with the stresses in the adjacent soil elements and that the processing of results could be done using either data set. The results presented in this appendix use the stresses extracted from the soil elements adjacent to the sheet-pile wall.

E.5.8 Progression of gap propagation for MC analyses

Figure E.1 shows the progression of the gap as the water level against the I-wall is increased from 1 ft (el 7.5 ft) up to 8 ft (el 14.5 ft). The gap initiates at a water elevation of 7.5 ft and extends to a depth of 4 ft. The gap propagation essentially follows a parabolic path with the rate of gap depth increasing as the water elevation increases. The black dotted line in Figure E.1 is a parabolic fit to the gap depths at the various water elevations. The depth of the gap extends to el -9 ft at water el 14.5 ft. The tip of the sheet pile is at el -16.5 ft.

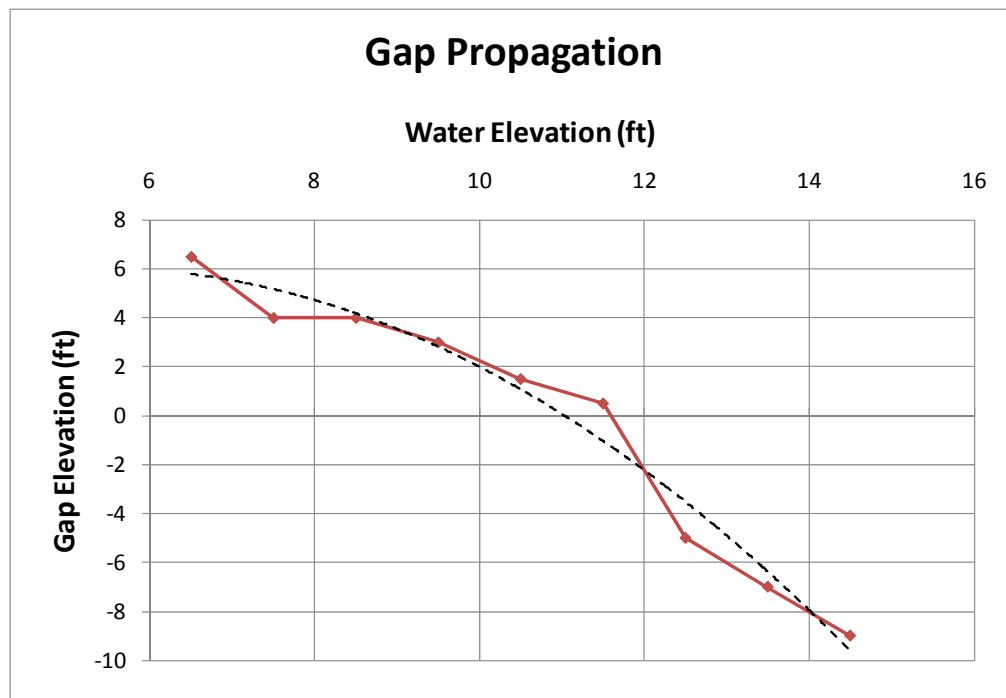


Figure E.1. Progression of gap versus water elevation along flood side of I-wall.

E.5.9 Sheet-pile wall displacements for MC model

Figure E.2 shows the horizontal displacements of the sheet-pile wall for various water elevations. The horizontal displacements at the top of the pile increase with increasing water elevation as seen from Figure E.2. For the last water elevation of 14.5 ft, the displacements at the top of the pile double for a 1-ft rise in water. From Table E.6, the displacement of the top of the sheet pile for a water elevation of 14.5 ft is 18.7 in., while the displacement at the ground surface is 14.5 in.

Also as shown in Figure E.2, the displacements of the tip were relatively constant with an increasing water elevation and progressively translated into the landside of the I-wall. The displacements of the tip can be seen to decrease slightly for a water elevation of 14.5 ft and to kick back into the flood side. The maximum tip displacement was 4.5 in. at a water elevation of 13.5 ft, and the tip moved back into the landside 0.3 in. at a water elevation of 14.5 ft.

A Φ/c reduction analysis performed for water el 14.5 ft resulted in a factor of safety of 1.06.

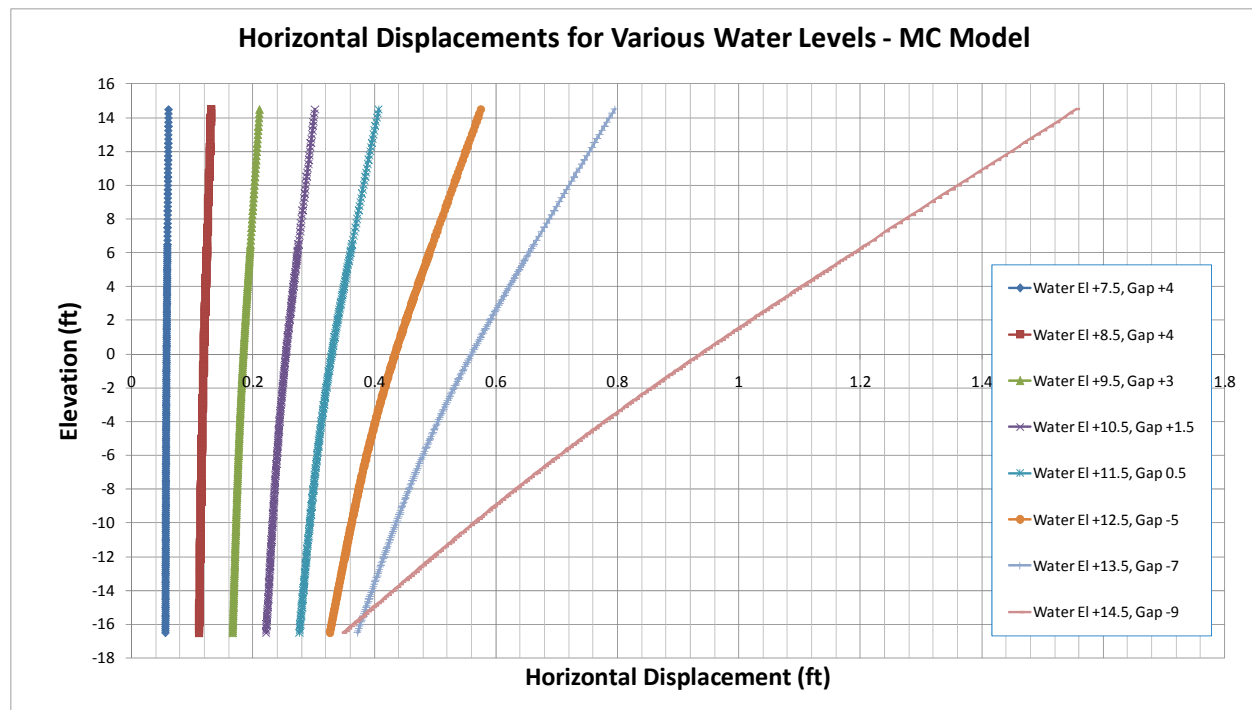


Figure E.2. Sheet-pile horizontal displacements for various water elevations.

Table E.6. Pile displacements for MC model.

Water El	Top of I-Wall, el 14.5 ft		Ground Surface, el 6.5 ft		Tip of Sheetpile, el -16.5 ft		Relative Pile Displacement at Ground Surface, Ground Surface minus Tip Displacement	
	ft	in	ft	in	ft	in	ft	in
6.5	0.0000	0.0000	0.0000	0.0000	0.0000	0.0000	0.0000	0.0000
7.5	0.0609	0.7303	0.0590	0.7082	0.0558	0.6693	0.0032	0.0389
8.5	0.1314	1.5764	0.1245	1.4941	0.1114	1.3369	0.0131	0.1572
9.5	0.2111	2.5329	0.1961	2.3530	0.1668	2.0018	0.0293	0.3512
10.5	0.3021	3.6254	0.2751	3.3017	0.2219	2.6625	0.0533	0.6392
11.5	0.4068	4.8811	0.3632	4.3582	0.2765	3.3180	0.0867	1.0402
12.5	0.5755	6.9056	0.4956	5.9478	0.3268	3.9211	0.1689	2.0267
13.5	0.7954	9.5451	0.6629	7.9549	0.3719	4.4631	0.2910	3.4918
14.5	1.5553	18.6637	1.2096	14.5155	0.3482	4.1790	0.8614	10.3366

Values of horizontal displacements for the sheet pile at the top, ground surface, and tip are tabulated in Table E.6 and displayed in Figure E.3. As shown in Figure E.3, the pile tip displacements increased by a constant amount until finally reducing and kicking back into the flood side.

Figure E.4 shows the relative displacement of the sheet pile at the ground surface, which is computed as the displacement of the sheet pile at the ground surface minus the displacement of the tip of the sheet pile. There is almost a threefold increase in relative horizontal displacement at the ground surface for the last 1-ft rise in water.

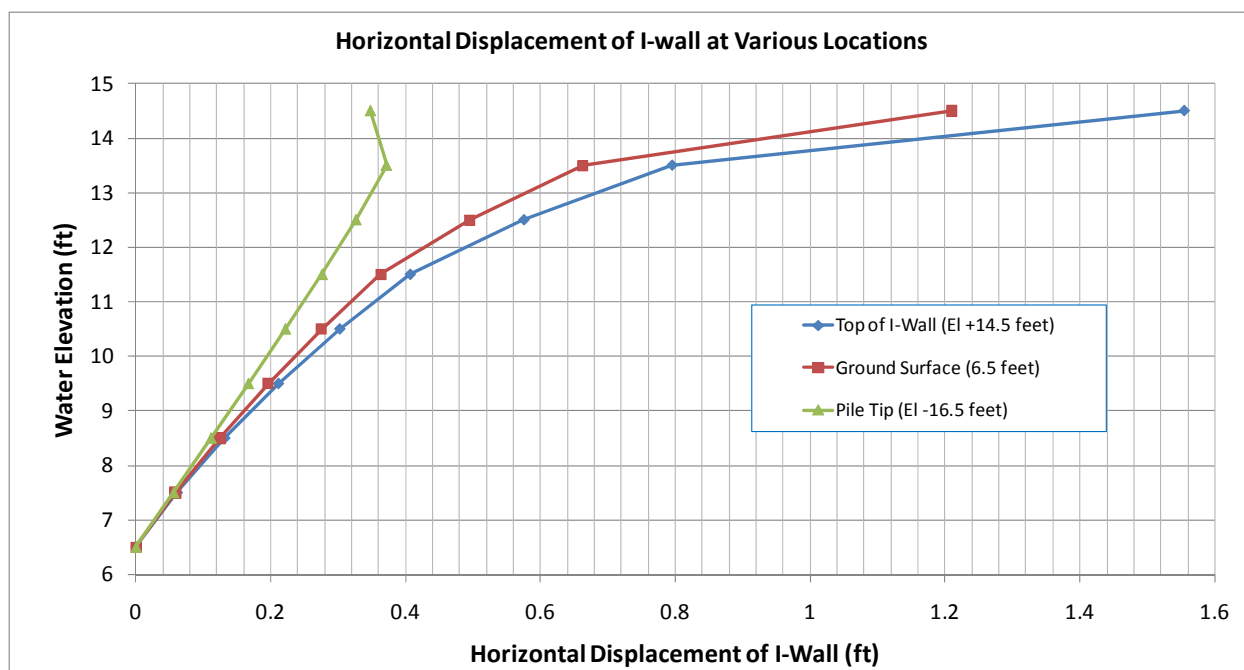


Figure E.3. Sheet-pile horizontal displacements for selected locations.

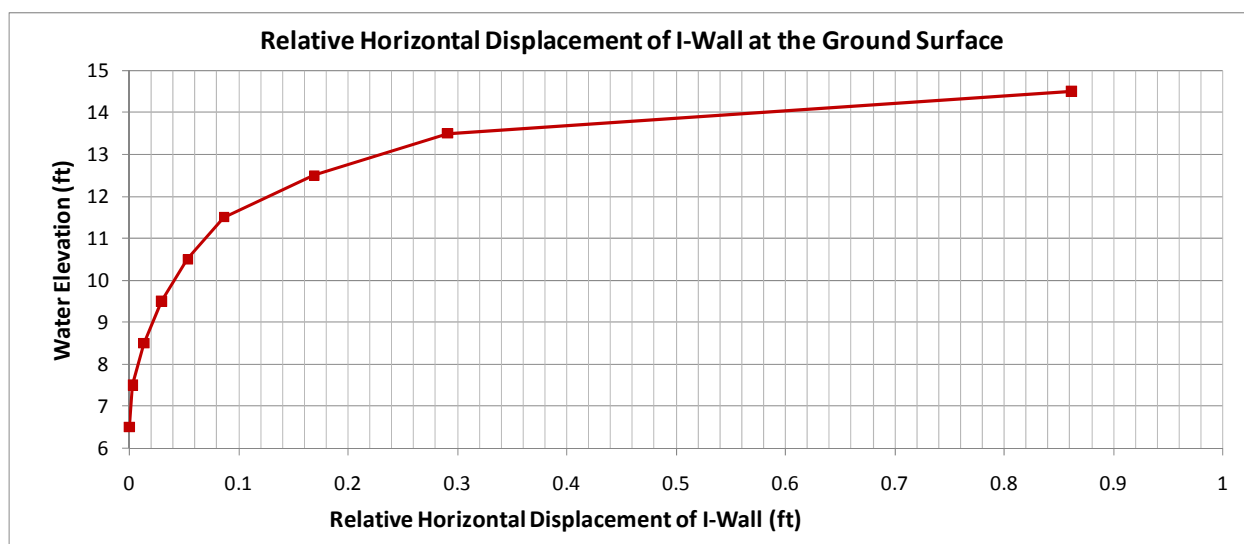


Figure E.4. Relative horizontal displacements of the sheet pile at the ground surface.

E.5.10 Total displacements of finite element mesh for maximum water condition

Figures E.5 and E.6 show the total deflection of the finite element mesh for water el 14.5 ft. The gap at this water height propagated down to el -9 ft. There is some settlement on the flood side of the wall and some heave on the landside as shown in Figure E.6.

The left side of Figure E.7 shows the total incremental displacements for water el 14.5 ft. The incremental displacements give the movements during the last increment of loading; that is, the last part of the load that completes the total load added to the system. From Figure E.7, for water el 14.5 ft, the soil is moving downward on the flood side and upward on the landside. Figure E.8 shows the total displacements of the system for the applied loads. The displacements are similar to those of Figure E.7 but display more horizontal movement.

E.5.11 Moments in sheet-pile wall for MC model

Moments in the sheet pile for various water elevations are compared in Figure E.9. The moment increases as the water elevation increases and reaches a maximum at water el 14.5 ft. The moment for water el 14.5 ft is 30,274 ft-lb at el -4.3 ft. The moment at water el 12.5 ft is 14,363 ft-lb at el -3.0 ft.

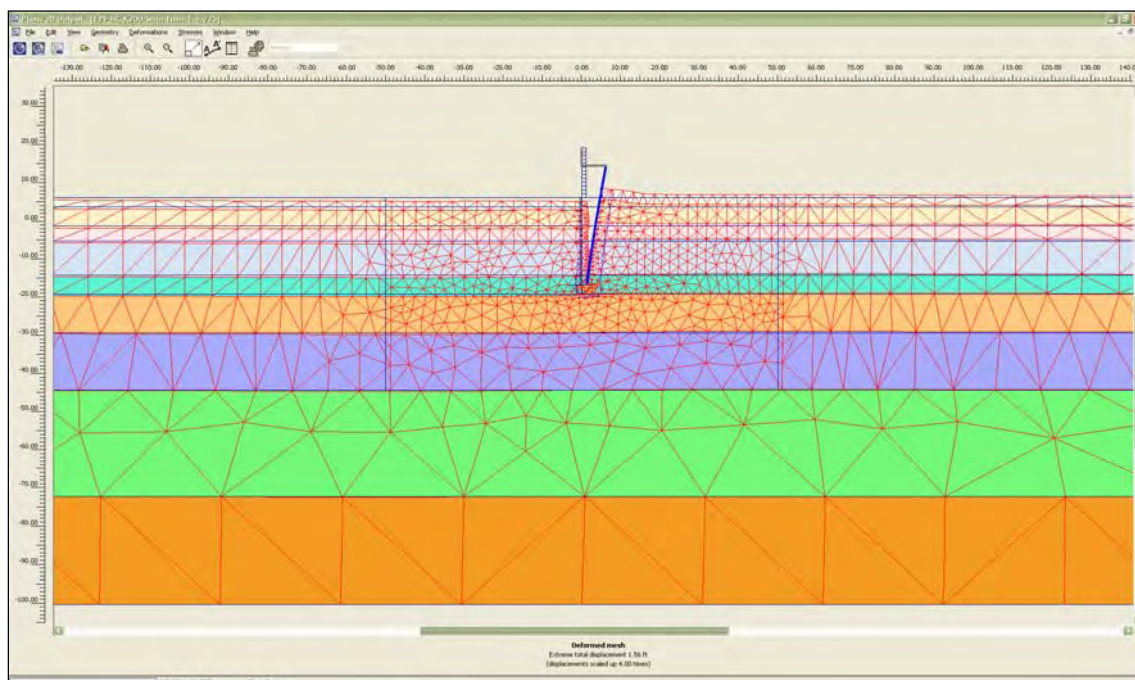


Figure E.5. Total displacements for water el 14.5 ft and gap tip el -9 ft.

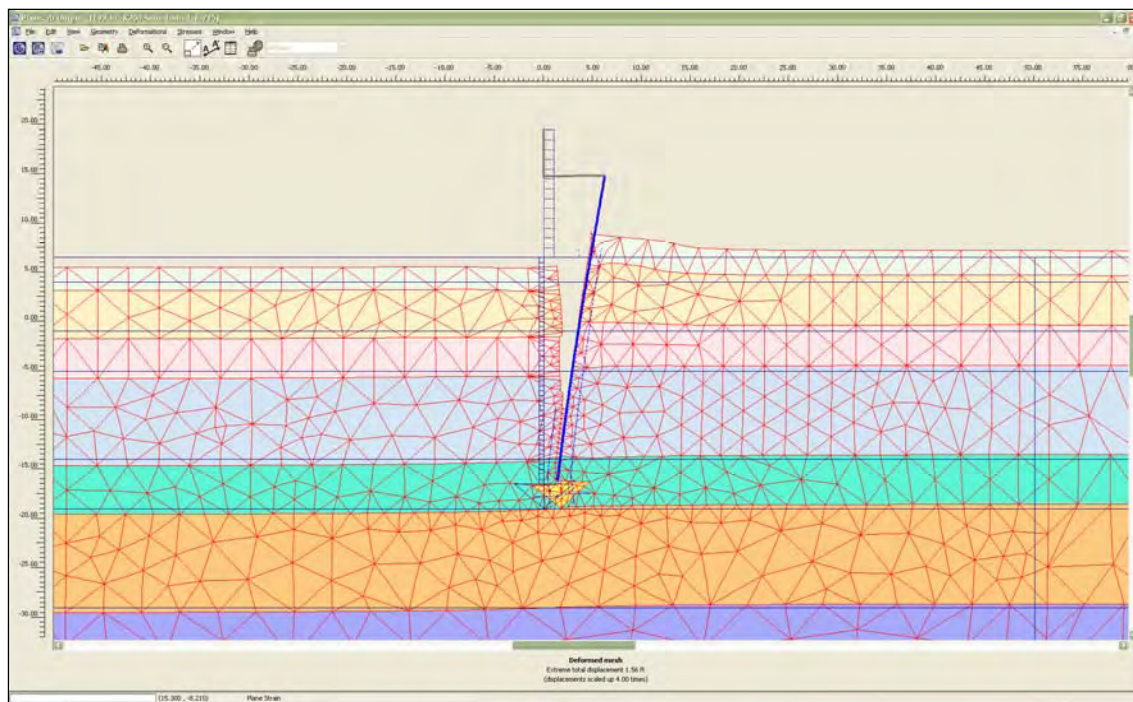


Figure E.6. Enlarged view of total displacements for water el 14.5 ft and gap tip el -9 ft.

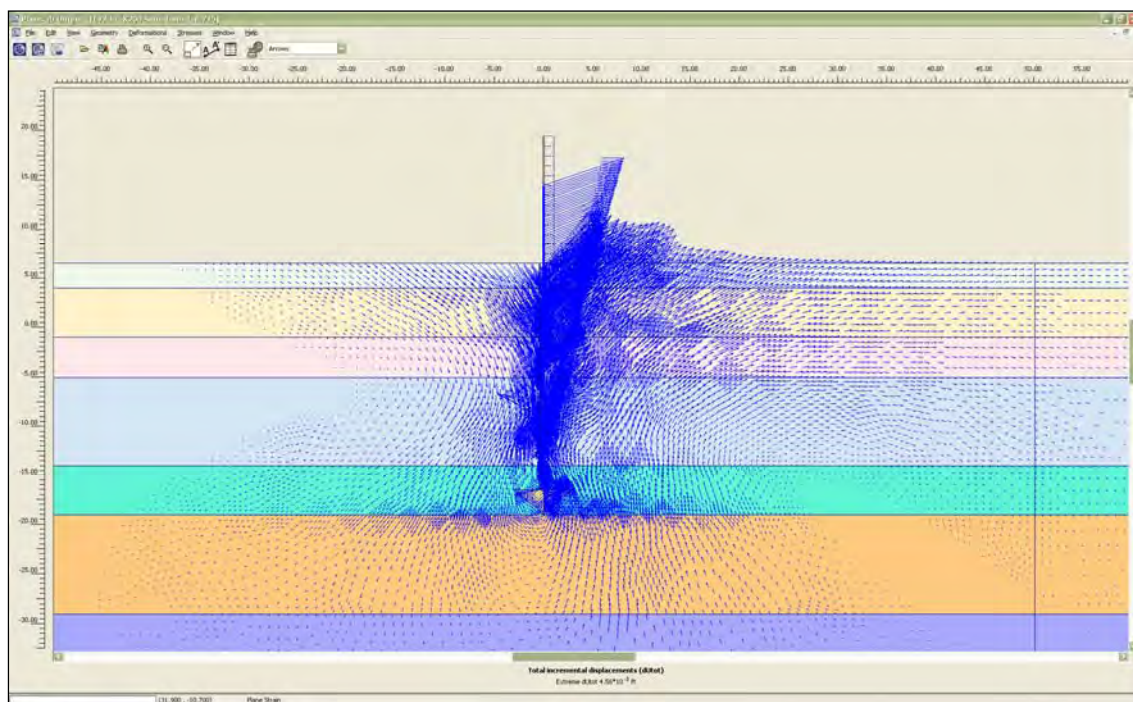


Figure E.7. Vectors of total incremental displacements showing the movement of the soil during the final increment of loading.

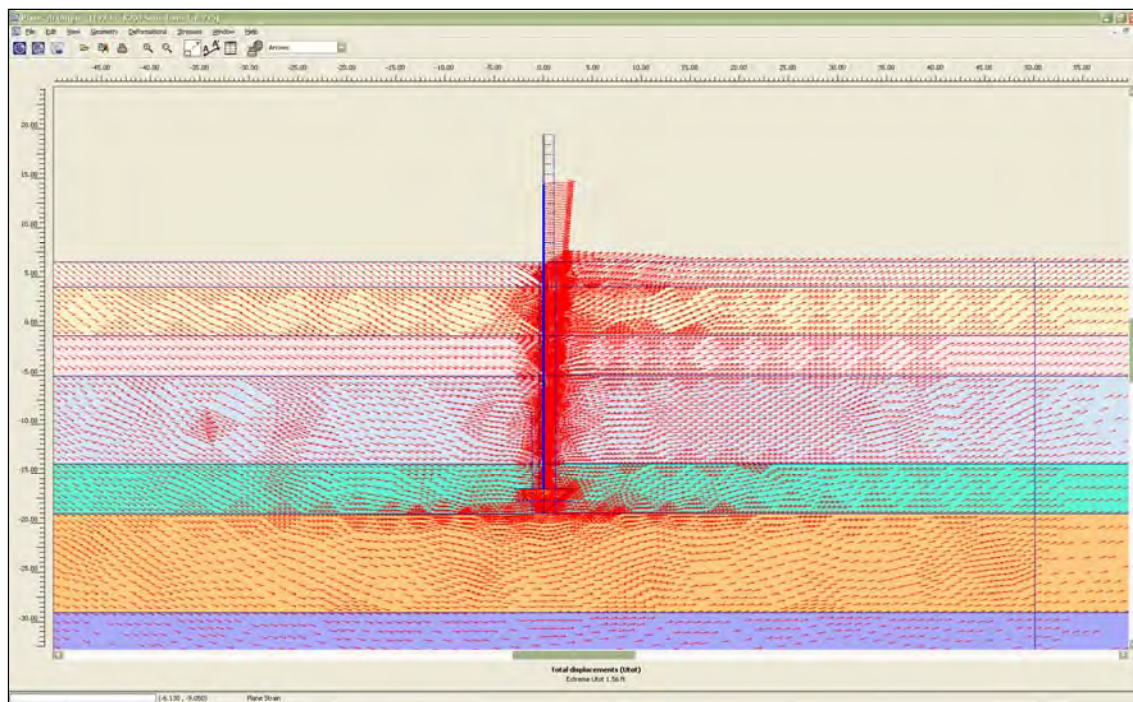


Figure E.8. Vectors of total displacements showing the movement of the soil.

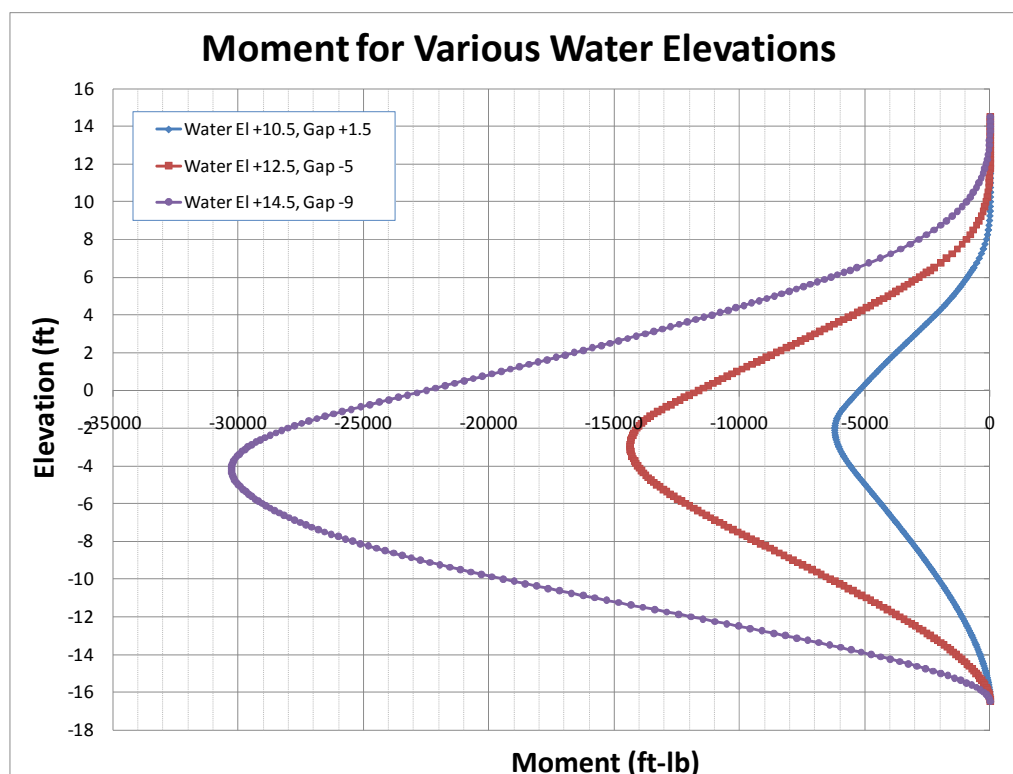


Figure E.9. Comparison of moments at various water elevations.

E.5.12 Shear stresses in soil for MC model

Figures E.10 through E.12 show the relative shear stress in the soil for various water elevations and the associated gap depths. The relative shear stress is a measure of the shear stress in the soil compared to the maximum available shear stress at failure. The shear stress in the soil increases as the water elevation increases. The shear stress increases in the upper unsaturated layer first, then progresses downward toward the tip of the pile. The shear stresses are greatest on the landside of the sheet-pile wall and at the bottom of the gap. For a water elevation of 14.5 ft, as shown in Figure E.12, the highly stressed region extends to the tip of the sheet pile.

E.5.13 Horizontal earth pressures for MC model

For Figures E.13 through E.15, the flood side is on the right side of the figure and the landside is on the left. This corresponds with the input convention CWALSHT uses.

Figures E.13 and E.14 compare the horizontal earth pressures from PLAXIS acting against the sheet-pile wall to the limiting active and passive earth pressures computed using adhesion as discussed in Chapter 3, Section 3.3.2. The value of adhesion used is 80 percent of the cohesion as discussed in Chapter 3, Section 3.3.4. The limiting earth pressures in the figures are

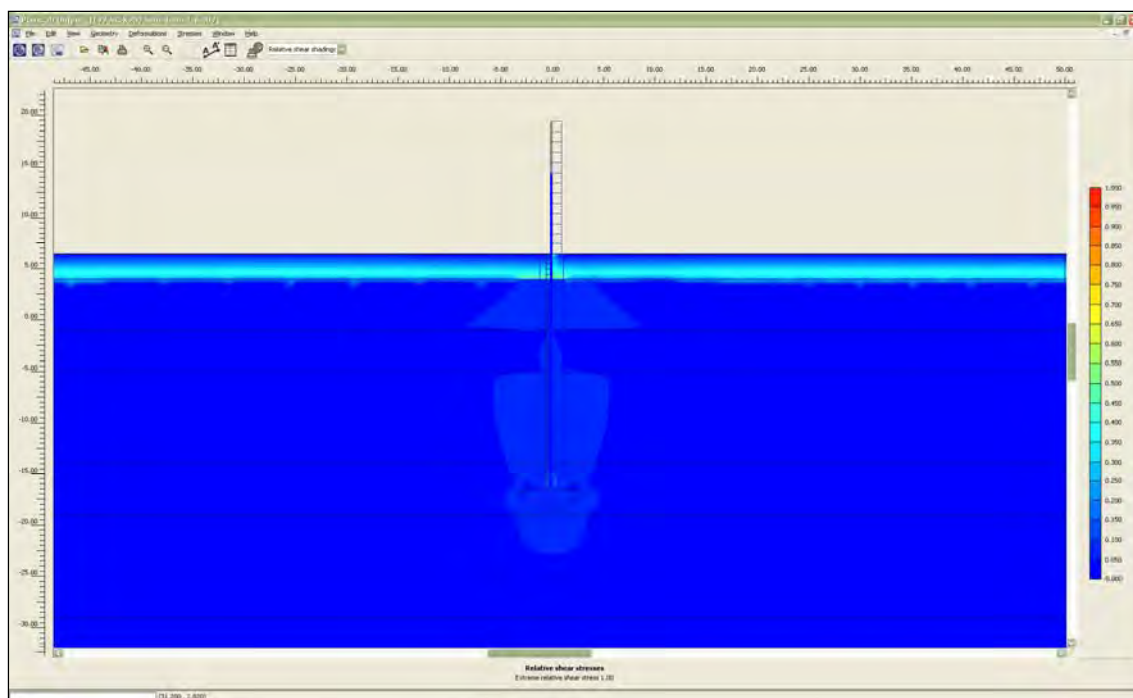


Figure E.10. Relative shear stress after placement of I-wall.

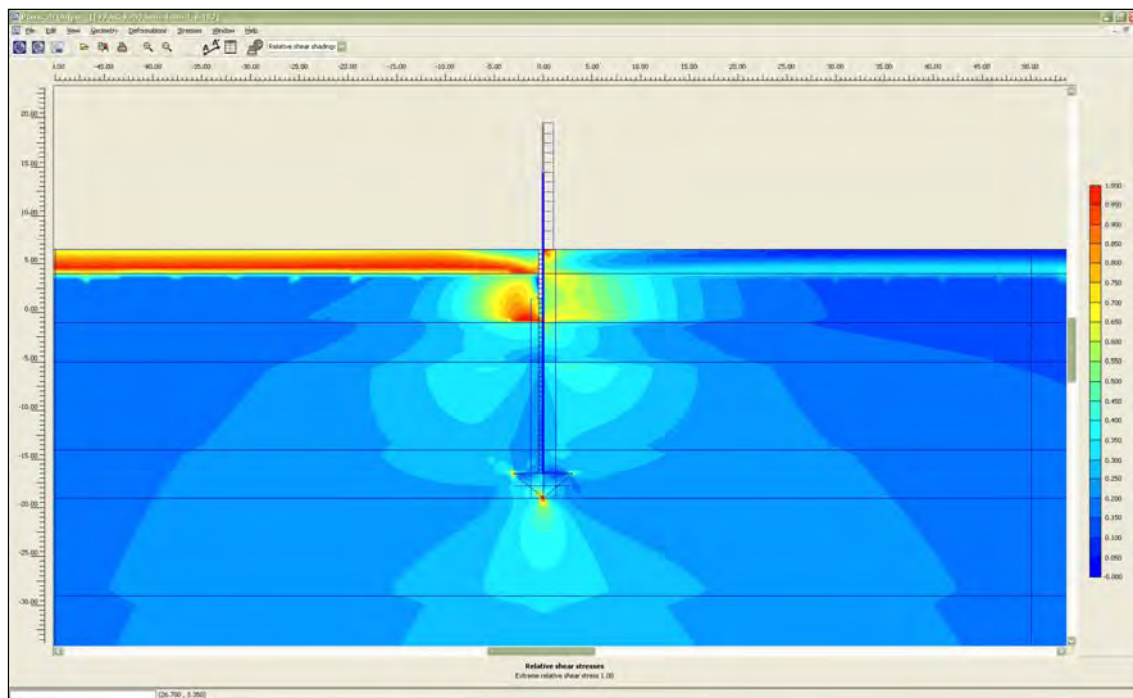


Figure E.11. Relative shear stress for water at el 10 ft and gap tip el 1.5 ft.

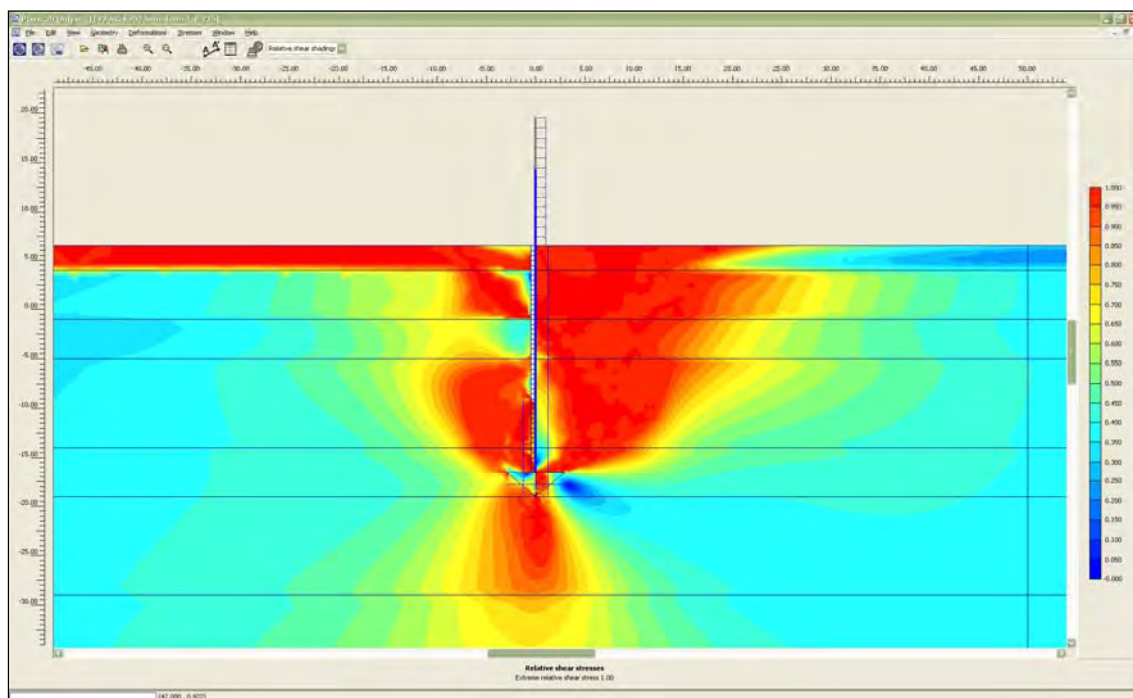


Figure E.12. Relative shear stress for water at el 14.5 ft and gap tip el -9 ft.

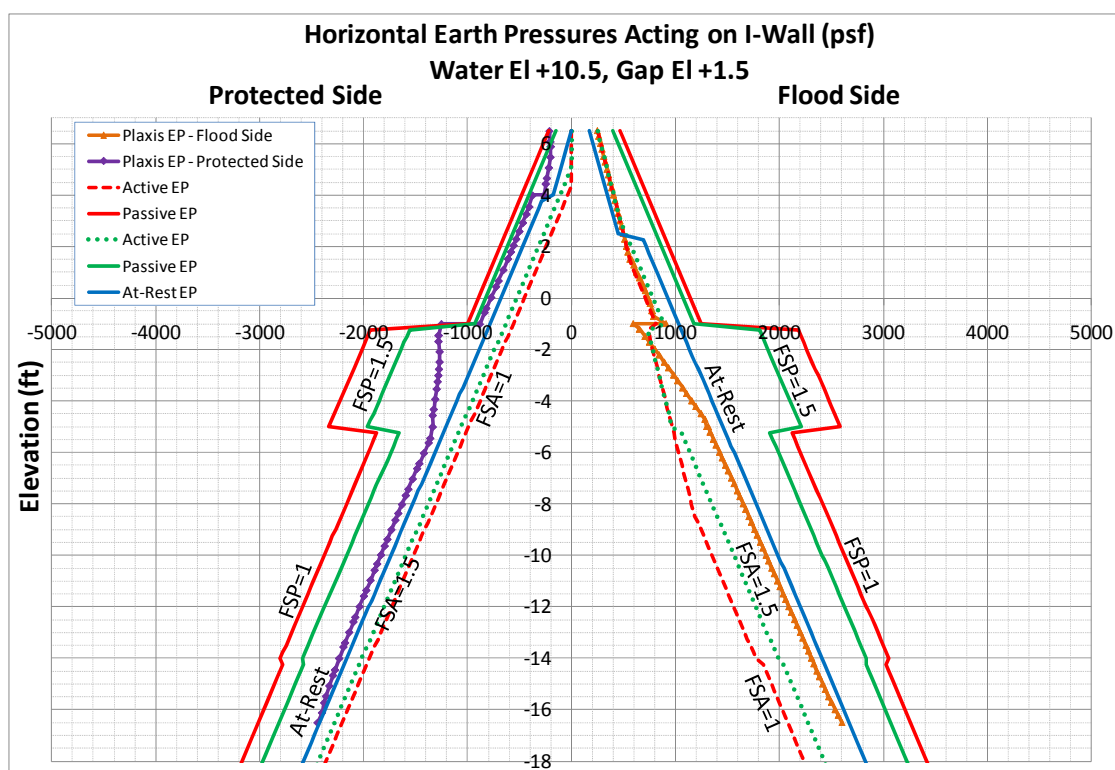


Figure E.13. Horizontal earth pressures for water el 10.5 ft and gap tip el 1.5 ft.

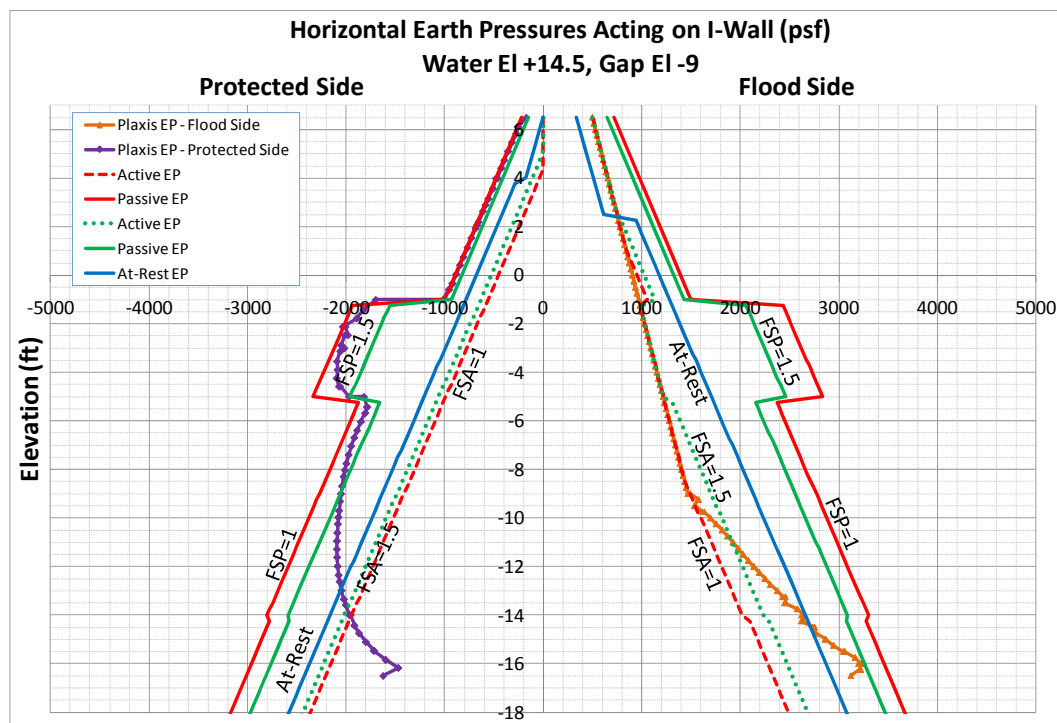


Figure E.14. Horizontal earth pressures for water el 14.5 ft and gap tip el -9 ft.

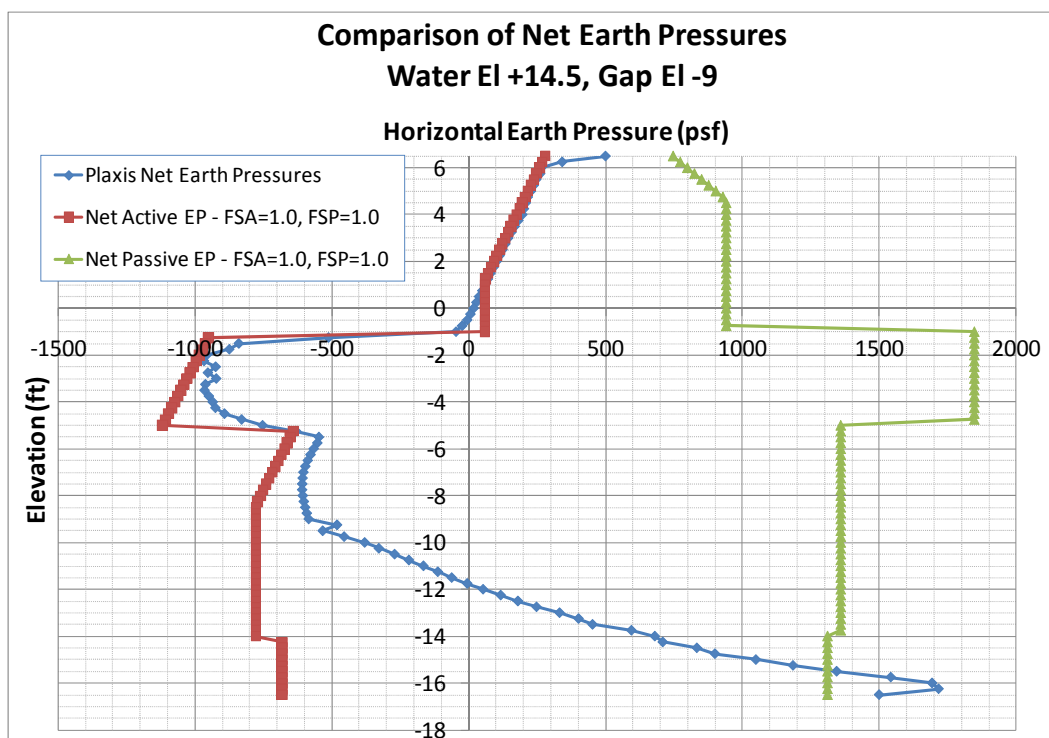


Figure E.15. Comparison of net earth pressures computed from limiting earth pressures and PLAXIS results for water el 14.5 ft.

computed for factors of safety of 1.0 and 1.5. A factor of safety of 1.0 results in full active and passive earth pressures, while a factor of safety of 1.5 results in increased active and decreased passive earth pressures. The results from PLAXIS are compared to the earth pressures computed by CWALSH using limiting earth pressures computed using two different factors of safety. This allows a comparison of the PLAXIS earth pressures to values computed from conventional design procedures.

Figure E.13 displays the earth pressures for water el 10.5 ft and gap tip el 1.5 ft. For the flood side, the pressures are equal to hydrostatic pressures down to the bottom of the gap. Below the gap, the pressures are close to at-rest earth pressures computed using the assumed values of K_o given in Table 3.9. On the landside, the earth pressures are very close to passive earth pressures computed using a factor of safety of 1.5 at elevations above -1 ft. Below -1 ft, the earth pressures are close to at-rest earth pressures.

Figure E.14 shows the earth pressures for water el 14.5 ft. The gap in this case extends to el -9 ft. The earth pressures on the flood side are equal to hydrostatic pressures down to the bottom of the gap. Below the gap, the earth pressures are less than the at-rest condition because the wall moved

from the soil. On the landside, above el -5 ft, the earth pressures are almost equal to the fully passive earth pressures computed using a factor of safety of 1.0. Below -5 ft, the pressures decrease with depth and become less than active earth pressures computed using a factor of safety of 1.0.

Figure E.15 compares the net earth pressures computed using limiting earth pressures and the results from PLAXIS for water el 14.5 ft. The limiting earth pressures were computed using a factor of safety of 1.0 for both the active and passive earth pressures for both the flood side and landside of the wall. Net pressures were compared for this water elevation because the movements of the wall were sufficient to produce values of full active and passive earth pressures. As can be seen from the figure, the net earth pressures on the landside compare fairly well to the net active earth pressures. Toward the tip of the pile, the net earth pressures transition from the net active to the net passive earth pressures and compare fairly well.

Appendix F: Analyses of E-99 Sheet-pile Wall Field Load Test Using Minimum Values of Undrained Shear Strength (S_u) and Maximum Values of Undrained Secant Stiffness (E_u)

F.1 Purpose of analyses

This appendix summarizes the results of nonlinear soil-structure interaction (SSI)¹ finite element analyses of the E-99 sheet-pile wall field load test described by Jackson (1988).² The analyses included the formation and propagation of a gap beside the sheet-pile wall on the flood side. The gap affected the resulting deformation and stress conditions of the soil regime on both the flood side and landside of the I-wall. The analyses were part of a parametric study determining the effects of the undrained shear strength (S_u) and undrained secant stiffness (E_u) on the deformation and gap formation characteristics of the system. For the analysis described in this appendix, minimum values of the undrained shear strength and maximum values of undrained secant stiffness were selected.

The following sections will describe the soil used in the analyses, the selection of stiffness and shear strength parameters, the conventional analysis and design of the I-wall, the analysis procedures employed, and the results of the finite element analyses.

F.2 Overview of problem analyzed

The E-99 field load test consisted of a 200-ft section of floodwall constructed on the landside berm of the Item E-99 East Atchafalaya Basin Protection Levee (EABPL) on Avoca Island just south of Morgan City, Louisiana. The test was performed between July and September of 1985 (Jackson 1988).

The soil geometry, maximum water height, and pile geometry of the field load test are shown in Figure 3.1. The sheet pile is located on the landside of

¹ Symbols and unusual abbreviations used in this appendix are listed and defined in the Notation, Appendix I.

² Citations in this appendix are in the References at the end of the main text.

the existing levee. The water loading was applied between the existing levee and the sheet-pile wall. The geometry was idealized as shown in Figure 3.2 and is assumed to be a flat (level) site. The top of the sheet-pile wall was at el 14.5 ft¹, and the tip of the sheet-pile wall was located at el -16.5-ft. The elevation of the top soil layer was at 6.5 ft. The I-wall system is described in Chapter 3, Section 3.2.

Soils at the site were clays of high plasticity, designated as CH in the Unified Soil Classification System (USCS). From the classification chart shown in Figure 3.4, the plasticity index of a CH material has a value of 22 percent and greater. The soil was normally consolidated with liquid limits between 76 and 114 percent and natural water contents between 40 and 80 percent.

For the analyses described in this appendix, the permeability of the clay layers was assumed to be small enough that the soil would not become fully saturated as the floodwater level was increased. Therefore, as shown in Figure 3.2, two zones of soil are considered in the analysis: a partially saturated one above the water table elevation of 4 ft and a saturated one of soil below the water table.

F.3 Material properties used for parametric analysis

The analysis described in this appendix is one in a set of parametric analyses varying the values of S_u and E_u . The values used for the analysis described in this appendix correspond with the minimum values of S_u and the maximum values of E_u . The material properties used in the analysis described in Chapter 3 are denoted and treated as the mean values. Actually, they are the values used for the design of the I-wall that differ slightly from the mean values computed from laboratory test data.

The undrained shear strengths of the clay layers were determined from unconsolidated undrained (UU) and unconfined compression (UC) tests. These design values, shown in Table 3.1, were used to perform an undrained short-term design of the wall. The material property values consist of the saturated (γ_{sat}) and moist (γ_{moist}) unit weights of the soil, the undrained shear strength (S_u) and adhesion (c_a). The angle of internal friction (ϕ) and wall friction (δ) were zero because this is an undrained analysis. The same value of the unit weight was used for both saturated

¹ All elevations cited in this appendix are in feet referred to the National Geodetic Vertical Datum (NGVD).

and moist conditions. Adhesion was used in the total stress analysis using values cited in Potyondy (1961) for a cohesive soil against rough steel, and is equal to 0.8 times the undrained shear strength ($c_a = 0.8 * S_u$).

The laboratory test data was used to compute mean (μ) and standard deviation (σ) values for the soil layers. These values are shown in Table F.1. The column labeled Plate 9 corresponds with the design values assumed in the E-99 field test report (Jackson 1988). As can be seen from Table F.1, the design values are slightly different from the mean values computed from test data. The design values were used in the finite element analysis discussed in Chapter 3. The mean values shown in Table F.1 were computed based on a limited number of tests, and it was felt that the design values provided a better estimate of the strengths. The coefficients of variation (COV) for the clay layers computed from test data are shown in Table F.1. Because Layer 2 had only two data points, the COV for this layer was deemed too low and, therefore, was adjusted to a higher value. The last column in Table F.1 shows the values of the COVs used in this analysis.

Table F.1. Mean and standard deviation values for the clay layers.

Layer	Top El, ft	Bottom El, ft	Plate 9 S_u , psf	Mean μ , psf	Standard Deviation σ , psf	COV, %	COV % for Analyses
1	6.5	-1	200	285	74	37.2	37
2	-1	-5	500	580	50	2.4	10
3	-5	-14	350	362	70	20.2	20
4	-14	-29	500	476	175	34.6	35

Using the COVs for the soil layers, as shown in Table F.1, the standard deviations (σ) for each layer was computed. These standard deviations were used to compute minimum and maximum values of S_u and E_u .

The minimum value of S_u ($S_{u,min}$) was computed as shown in Equation F.1:

$$S_{u,min} = S_{u,mean} - x_{min} \bullet \sigma. \quad (F.1)$$

The variable (x_{min}) in Equation F.1 represents a multiple of the standard deviation. The design values of S_u listed in Table F.1 were used as the $S_{u,mean}$ values. The value of the minimum E_u ($E_{u,min}$) was computed as:

$$E_{u,min} = E_{ref} = KS_{u,min}, \quad (F.2)$$

where E_{ref} is the reference stiffness needed for the Mohr-Coulomb (MC) soil model and K is defined as:

$$K = \frac{E_{u,min}}{S_{u,min}}. \quad (F.3)$$

The maximum value of S_u ($S_{u,max}$) was computed as shown in Equation F.4:

$$S_{u,max} = S_{u,mean} + x_{max} \bullet \sigma. \quad (F.4)$$

The variable (x_{max}) in Equation F.4 represents a multiple of the standard deviation and does not equal x_{min} .

The value of the maximum E_u ($E_{u,max}$) was computed as:

$$E_{u,max} = E_{ref} = KS_{u,max}. \quad (F.5)$$

In Equation F.5, E_{ref} is the reference stiffness needed for the MC soil model and K is defined as:

$$K = \frac{E_{u,max}}{S_{u,max}}. \quad (F.6)$$

The value of K in Equation F.6 was taken from a chart developed by Duncan and Buchignani (1976) relating the plasticity index and the overconsolidation ratio (OCR) to the dimensionless factor K . The same value of (K) of 200 used in the analysis of Chapter 3 was used for this analysis.

The intent of analyses described in Appendix E was to use the lowest values of S_u and E_u possible and still keep the design condition of the water at the top of the wall at el 14.5 numerically stable. The multiple of the standard deviation was varied to find the largest multiple at which the design condition was still stable (i.e., the factor of safety was greater than 1.0). The loading in PLAXIS, a two-dimensional (2-D) nonlinear incremental construction finite element program, was applied in one construction step, and the gap propagation was not tracked in these analyses. PLAXIS applies the load increment in many substeps for convergence. Previous experience with I-wall analyses has shown that the results are comparable between a

complete analysis tracking the gap progression and this simplified procedure, as long as the gap depth does not vary greatly and unloading of the system does not occur. A constant gap elevation of -10 ft was used. This is the same gap elevation used in the analyses described in Chapter 3. The factor of safety was computed using a Φ/c reduction analysis within PLAXIS. Based on the results of these analyses, shown in Table F.2, the largest multiple of the standard deviation that was acceptable was determined to be 1.6.

Table F.2. Factors of safety for various multiples of the standard deviation.

	Multiples of Standard Deviation			
	-1.5	-1.6	-1.75	-2
FS	1.105	1.06	0.881	Design case would not run

The intent of the analyses in this appendix was to use the smallest values of S_u and largest values of E_u possible to ascertain the effects on the gap initiation and propagation and subsequent height of water loading that is possible while the analysis remained numerically stable. The multiple of 1.6 was used in Equation F.1 to compute the minimum S_u . The minimum value of E_u was computed using a K value of 200 and $S_{u,min}$ in Equation F.2. The maximum values of S_u were computed using a multiple of 4 in Equation F.4. This resulted in a maximum value of S_u that was used in Equation F.5 to compute the maximum value of E_u . Equation F.6 with a K value of 200 and the value of $S_{u,max}$ was used to compute the maximum value of E_u . The use of four standard deviations in Equation F.4 was deemed to result in the largest values possible of both S_u and E_u . The minimum and maximum values of S_u and E_u computed in this fashion are shown in Table F.3.

Table F.3. Material properties for analyses.

Layer	Elevation			S_u		Design Values		Min Values		Max Values	
	Top, ft	Bottom, ft	γ_{sat} , pcf	COV, %	σ	Mean S_u , psf	E_u , psf	$S_{u,mean}-1.60*\sigma$		$S_{u,mean}+4*\sigma$	
								S_u , psf	E_u , psf	S_u , psf	E_u , psf
1	6.5	-1	104	37	74	200	40,000	82	16,320	496	99,200
2	-1	-5	107	10	50	500	300,000	420	84,000	700	140,000
3	-5	-14	106	20	70	350	210,000	238	47,600	630	126,000
4	-14	-19	104	35	175	500	300,000	220	44,000	1200	240,000
5	-19	-29	101	35	175	500	300,000	220	44,000	1200	240,000
6	-29	-44	100	35	193	550	330,000	242	48,400	1320	264,000
7	-44	-72	100	35	236	675	405,000	297	59,400	1620	324,000
8	-72	-100	100	35	324	925	555,000	407	81,400	2220	444,000

F.4 Conventional analysis of cantilever I-wall

F.4.1 Criteria for gap initiation and propagation

Two different criteria, one for the flood side of the sheet-pile wall and another for the landside, are used to determine whether a gap initiates in the soil adjacent to the sheet-pile wall and how far the gap will propagate. A hydraulic fracturing criterion is used for the flood side of the I-wall, and a negative horizontal stress criterion is used for the landside. Both of these criteria are discussed in Chapter 3, Section 3.3.3.

F.4.2 Computed gap depth

CWALSHT (U.S. Army Engineer Research and Development Center 2012) uses the negative horizontal stress criterion discussed in Section 3.3.3 to compute whether a gap forms in the soil. Negative computed earth pressures imply that the soil-to-sheet-pile interface is in tension. Because the soil-to-sheet-pile interface cannot sustain a tensile load, the soil is assumed to form a gap, and CWALSHT sets any negative (tensile) earth pressures to zero. CWALSHT applies water pressures within a gap below the input water level. If the gap is above the water level, CWALSHT does not fill the gap with water.

F.4.3 Total stress analysis with CWALSHT

CWALSHT always computes effective stresses based on the input material properties and the level of the water in the soil. For problems involving all clay layers, a total stress (short-term) analysis with $c = S_u$ and $\phi = 0$, where c is cohesion, can be performed with CWALSHT by inputting the actual soil geometry and water levels. This gives a correct total stress analysis because, even though CWALSHT computes effective stresses based on the input water levels, the pore pressures are added to the effective stresses to arrive at total stresses. Because the value of the horizontal earth pressure coefficient is equal to 1.0 for a soil with only cohesion, the total stress computed in this manner is correct. The determination of the depth of the gap also conforms to the hydraulic fracturing criteria described in Section 3.3.3. This is because CWALSHT computes effective stresses and uses the effective stresses to determine the tensile zone. The hydraulic fracturing criterion uses total stresses and compares these to static pore pressures, a process that produces equivalent numerical results. Horizontal earth pressures are computed as described in Section 3.3.2.

F.4.4 CWALSHT analysis results

The elevation of the tip of the sheet pile for this analysis was -16.5 ft. A short-term analysis was performed with CWALSHT using the minimum material properties as given in Table F.3. The results of analyses performed with CWALSHT are shown in Table F.4.

Table F.4. Results of analysis computations using CWALSHT.

Analysis Case		S_u , psf	Φ , deg	Adhesion, psf	Wall Friction, deg	Elevation of Bottom of Gap, ft	Elevation of Tip of Sheet Pile		
							FS_{Active}	$FS_{Passive}$	EI, (ft)
1	Short-term with water levels	Minimum values	0	0	0	2.5	1	0.76	-16.5
2	Short-term with water levels	Minimum values	0	$0.8 \cdot S_u$	0	Below wall	1	1.1	-16.5

Cases 1 and 2 were modeled with the actual soil layer geometry with input water levels as described in Section F.4.3. Both Case 1 and Case 2 used a factor of safety applied to the active earth pressures (FS_{Active}) of 1.0. Case 1 did not include adhesion and resulted in a factor of safety on the passive earth pressures ($FS_{Passive}$) equal to 0.76. The gap extended down to el 2.5 ft. Case 2 included adhesion and resulted in a $FS_{Passive}$ of 1.1. The gap in this case extended below the tip of the sheet pile.

F.5 PLAXIS finite element analyses

F.5.1 Conceptual model

The finite element analyses were performed with PLAXIS. The conceptual model of the finite element mesh is shown in Figure 3.7. The geometry is the same as explained previously, but several modeling features should be noted. The sheet-pile wall was represented by plate elements. Interface elements were placed on both sides of the plate elements from the ground surface down to the tip of the sheet pile. To alleviate stress concentrations at the corners of the geometry, both horizontal and vertical extensions of the interface elements were provided at the tip of the sheet-pile wall at el -16.5 ft. A plate element extension and dummy soil elements were added above the wall to provide for additional loading height if needed. The mesh was structured to provide node points at 1-ft raises of the water table. The soil elements beside the sheet-pile wall on the flood side were 0.5 ft in height. This enabled the inputting of 1-ft raises in water and modeling of the gap to within 0.5 ft.

F.5.2 Finite element mesh

The finite element mesh used in the analyses is shown in Figures 3.8 and 3.9. The mesh is composed of 2,396 elements and 19,917 nodes, with 28,752 stress points. The type and number of elements used in the mesh are shown in Table 3.3. The mesh consists of 15-node triangular elements to model the soil, 5-node plate elements to model the sheet-pile wall, and 5-node interface elements to model the soil-structure interaction effects between the sheet-pile wall and the adjacent soil elements. The problem was run as a plane strain problem.

F.5.3 Total stress analysis procedure in PLAXIS

The E-99 field test was analyzed using total unit weights of the soil and boundary water pressures to perform a short-term (undrained) analysis using PLAXIS. All materials were designated as drained, which in PLAXIS terminology means that no excess pore-water pressures will be generated because of applied loads. The general phreatic surface was used in PLAXIS to apply the boundary water pressures on the soil surface and within the gap. All soil layers were associated with a cluster phreatic surface that was input below the minimum elevation of the mesh. Because the water surface was below all soil layers, no internal water pressures were generated within the soil layers. This procedure resulted in a total stress analysis with the computed effective stresses being equal to the total stresses (i.e., no internal pore pressures are present).

It was assumed that the permeability of the soil was small enough that any time-dependent effects such as seepage could be ignored and that the undrained shear strengths could be used to determine the behavior of the system.

F.5.4 Tracking the progression of the gap

The I-wall deflects as the flood loading increases, and eventually a gap forms beside the I-wall on the flood side of the wall. The gap begins at the ground surface and progresses downward as shown in Figure 3.10. The gap along the flood side of the I-wall-to-soil interface is modeled by deactivating soil clusters (elements), effectively creating a void beside the wall. As water pressures are applied within this void, the gap progresses downward. Modeling of the flood loading commenced in the finite element analysis after the total initial stress state was computed based on an

assumed steady state water elevation of 4 ft. The flood loading was applied in 1-ft incremental raises of the water level in order to track the formation and propagation of the gap.

The criterion used to estimate the formation and propagation of the gap is based on the hydraulic fracturing concept discussed in Chapter 3, Section 3.3.3. The procedure used to estimate the gap depth:

1. For each rise in water level, the total horizontal stresses against the sheet-pile wall are compared against the hydrostatic water pressures acting on the wall given the current water elevation. A gap is formed when the horizontal earth pressure is less than the water pressure at a given depth.
2. Soil elements are deactivated within the computed region of the gap, and hydrostatic water pressures are applied within the deactivated elements.
3. The analysis is rerun for the current water level, and Steps 1 and 2 are repeated until the depth of the gap ceases to increase.
4. The water level is increased, and Steps 1 through 3 are repeated. The water level is raised until instability in the analyses is encountered.

F.5.5 Shear strength and stiffness properties used in the finite element analyses

The finite element analyses described in this appendix were performed using the PLAXIS finite element program. The MC soil model was used for the soil elements. This model uses an elastic-perfectly plastic stress-strain relationship. Elastic plate elements were used to model the steel sheet pile, and interface elements were used to capture the soil-structure interaction effects between the sheet-pile wall and the soil. PLAXIS can perform analyses using either effective or total stress soil parameters. For the analyses described herein, total stress soil parameters were used.

Figure 3.11 shows the material numbering and soil layering used in the finite element analyses. The soil was divided into layers below the tip of the pile to provide for an increasing undrained shear strength and stiffness below the elevation of the pile tip. See Chapter 3, Section 3.4.5, for a more detailed discussion of the properties assumed for the soil, pile, and interface elements.

The undrained shear strength (S_u) and undrained reference stiffness (E_{ref}) of the clay layers used in this parametric analysis are computed as described in Section F.3 and shown in Table F.5. The remaining material property

values consist of the saturated (γ_{sat}) and moist (γ_{moist}) unit weights of the soil, angle of internal friction (ϕ), dilation angle (Ψ), unload/reload Poisson's ratio (ν), and the interface strength ($R_{interface}$).

Table F.5. Strength and stiffness properties for the soil layers used in the MC soil model for the case of a minimum (S_u) and maximum (E_{ref}).

Material Number	Material Description	γ_{moist} , lb/ft ³	γ_{sat} , lb/ft ³	S_u , lb/ft ²	E_{ref} , lb/ft ²	ν	$R_{interface}$
1	Clay_1_6.5_200_Rinit=0.8	104	104	82	99,200	0.4	0.8
2	Clay_2_4_200_Rinit=0.8	104	104	82	99,200	0.495	0.8
3	Clay_3_1_500_Rinit=0.8	107	107	420	140,000	0.495	0.8
4	Clay_4_5_350_Rinit=0.8	106	106	238	126,000	0.495	0.8
5	Clay_5_14_500_Rinit=0.8	104	104	220	240,000	0.495	0.8
6	Clay_5a_14_500_Rinit=1.0	104	104	220	240,000	0.495	1
7	Clay_6_19_500_Rinit=0.8	101	101	220	240,000	0.495	0.8
8	Clay_7_29_550_Rinit=0.8	100	100	242	264,000	0.495	0.8
9	Clay_8_44_675_Rinit=0.8	100	100	297	324,000	0.495	0.8
10	Clay_9_72_925_Rinit=0.8	100	100	407	444,000	0.495	0.8

Note: properties are given for drained material, with the angle of internal friction for the soil (ϕ) and the dilation angle (Ψ) set to 0, as this is a total stress analysis.

The $R_{interface}$ value is from values cited by Potyondy (1961) as discussed in Chapter 3, Section 3.3.4. This controls the amount of adhesion along the soil-to-wall interface. Material 6 in Table F.5 has an $R_{interface}$ value of 1.0 because this material represents a soil-to-soil interface.

F.5.6 Initial stresses

The initial total stress state within the finite element mesh was established using the at-rest soil conditions for a level ground surface. Horizontal at-rest soil stresses were estimated using the relationship between the at-rest earth pressure coefficient (K_o) and the soil's Poisson's ratio (ν) given in Equation 3.14.

The assumed groundwater elevation was at 4 ft. Table 3.9 summarizes the K_o values used to compute the horizontal earth pressures for the initial conditions. The Poisson's ratio for the partially saturated soil layer was 0.4, which corresponds to a K_o of 0.67. This value is less than the value for a fully saturated material, which has a K_o of 1.0.

F.5.7 Performance of interface elements

The performance of the interface elements was examined to determine if the normal stresses in the interface elements corresponded closely to the normal stresses in the adjacent soil elements. As discussed in Chapter 3, Section 3.4.7, and shown in Figure 3.14, the stresses within the interface elements agree very closely with the stresses in the adjacent soil elements, and the processing of results could be done using either data set. The results presented in this appendix use the stresses extracted from the soil elements adjacent to the sheet-pile wall.

F.5.8 Progression of gap propagation for MC analyses

Figure F.1 shows the progression of the gap as the water level against the I-wall is increased from 1 ft (el 7.5 ft) to 8 ft (el 14.5 ft). The gap initiates at water el 7.5 ft and extends to a depth of 4 ft. The gap propagation essentially follows a linear path with the gap depth increasing as the water elevation increases. The black dotted line in Figure F.1 is a linear fit to the gap depths at the various water elevations. The depth of the gap extends to el -9 ft at water el 14.5 ft. The tip of the sheet pile is at el -16.5 ft.

F.5.9 Sheet-pile wall displacements for MC model

Figure F.2 shows the horizontal displacements of the sheet-pile wall for various water elevations. The horizontal displacements at the top of the pile increase with an increasing water elevation as seen from Figure F.2. For the last water elevation of 14.5 ft, the displacements at the top of the pile double for a 1-ft rise in water. From Table F.6, the displacement of the top of the sheet pile for water el 14.5 ft is 7.4 in., while the displacement at the ground surface is 5.3 in.

Also in Figure F.2, the displacements of the tip are relatively constant with an increasing water elevation and progressively translate into the landside of the I-wall. The displacements of the tip can be seen to decrease slightly for water el 14.5 and to kick back into the flood side. The maximum tip displacement is 0.86 in. at water el 13.5 ft, and the tip moves back into the landside 0.13 in. at water el 14.5 ft.

A Φ/c reduction analysis performed for water el 14.5 ft resulted in a factor of safety of 1.06.

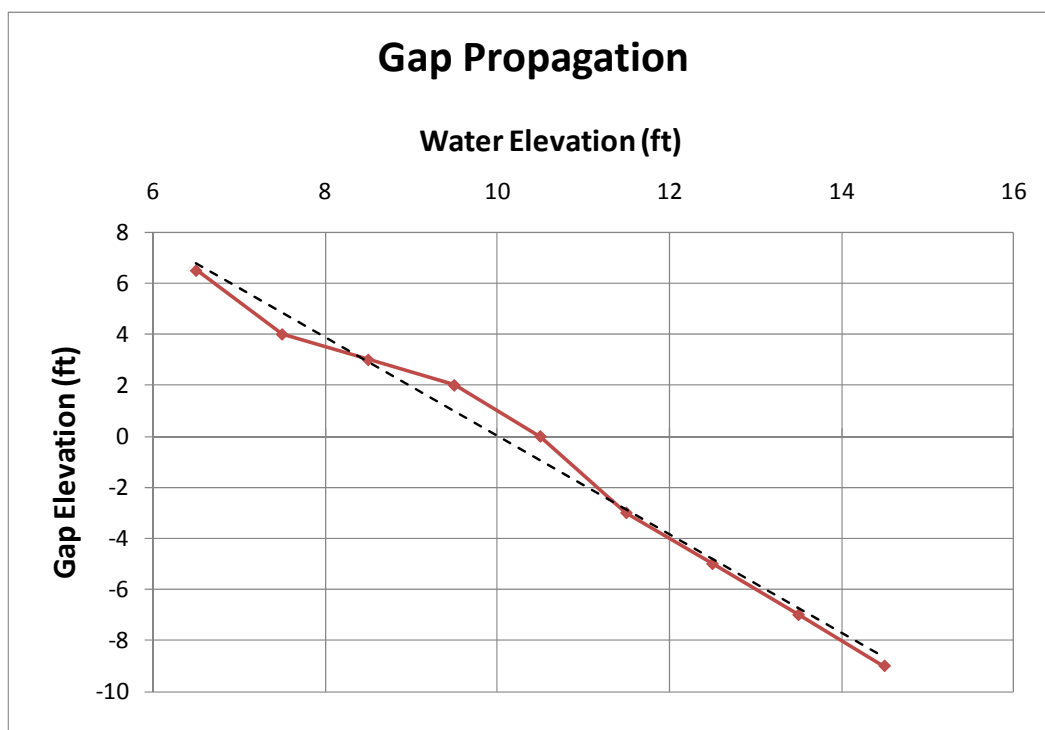


Figure F.1. Progression of gap versus water elevation along flood side of I-wall.

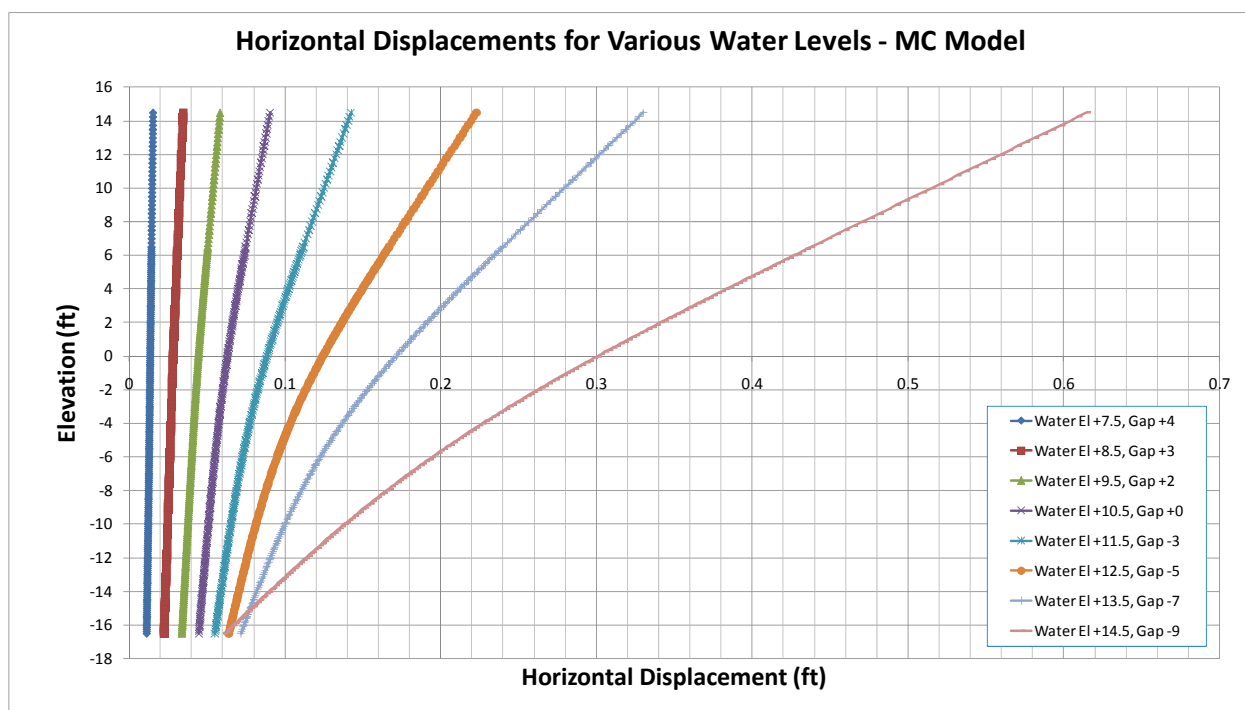


Figure F.2. Sheet-pile horizontal displacements for various water elevations.

Table F.6. Pile displacements for MC model.

Water El ft	Top of I-Wall, el 14.5 ft		Ground Surface, el 6.5 ft		Tip of Sheet Pile, el -16.5 ft		Relative Pile Displacement at Ground Surface, Ground Surface Minus Tip Displacement	
	ft	in.	ft	in.	ft	in.	ft	in.
7.5	0.0154	0.1847	0.0144	0.1722	0.0112	0.1345	0.0031	0.0378
8.5	0.0347	0.4167	0.0311	0.3729	0.0224	0.2692	0.0086	0.1037
9.5	0.0583	0.7002	0.0504	0.6044	0.0336	0.4037	0.0167	0.2007
10.5	0.0905	1.0859	0.0748	0.8978	0.0447	0.5368	0.0301	0.3611
11.5	0.1424	1.7094	0.1117	1.3398	0.0551	0.6615	0.0565	0.6783
12.5	0.2229	2.6751	0.1669	2.0022	0.0640	0.7680	0.1028	1.2342
13.5	0.3302	3.9619	0.2399	2.8793	0.0716	0.8593	0.1683	2.0200
14.5	0.6149	7.3784	0.4377	5.2525	0.0610	0.7318	0.3767	4.5207

Values of horizontal displacements for the sheet pile at the top, ground surface, and tip are tabulated in Table F.6 and displayed in Figure F.3. As shown in Figure F.3, the pile tip displacements increase by a constant amount until reducing and kicking back into flood side. Figure F.4 shows the relative displacement of the sheet pile at the ground surface, which is computed as the displacement of the sheet pile at the ground surface minus the displacement of the tip of the sheet pile. There is approximately a twofold increase in relative horizontal displacement at the ground surface for the last 1-ft rise in water.

F.5.10 Total displacements of finite element mesh for maximum water condition

Figures F.5 and F.6 show the total deflection of the finite element mesh for water el 14.5 ft. The gap at this water height propagated down to el -9 ft. There is some settlement on the flood side of the wall and some heave on the landside as shown in Figure F.6.

Figure F.7 shows the total incremental displacements for water el 14.5 ft. The incremental displacements give the movements during the last increment of loading, that is, the last part of the load that completes the total load added to the system. In Figure F.7 for water el 14.5 ft, the soil is moving down on the flood side and up on the landside. Figure F.8 shows the total displacements of the system for the applied loads. The displacements are similar to those of Figure F.7 but display more horizontal movement.

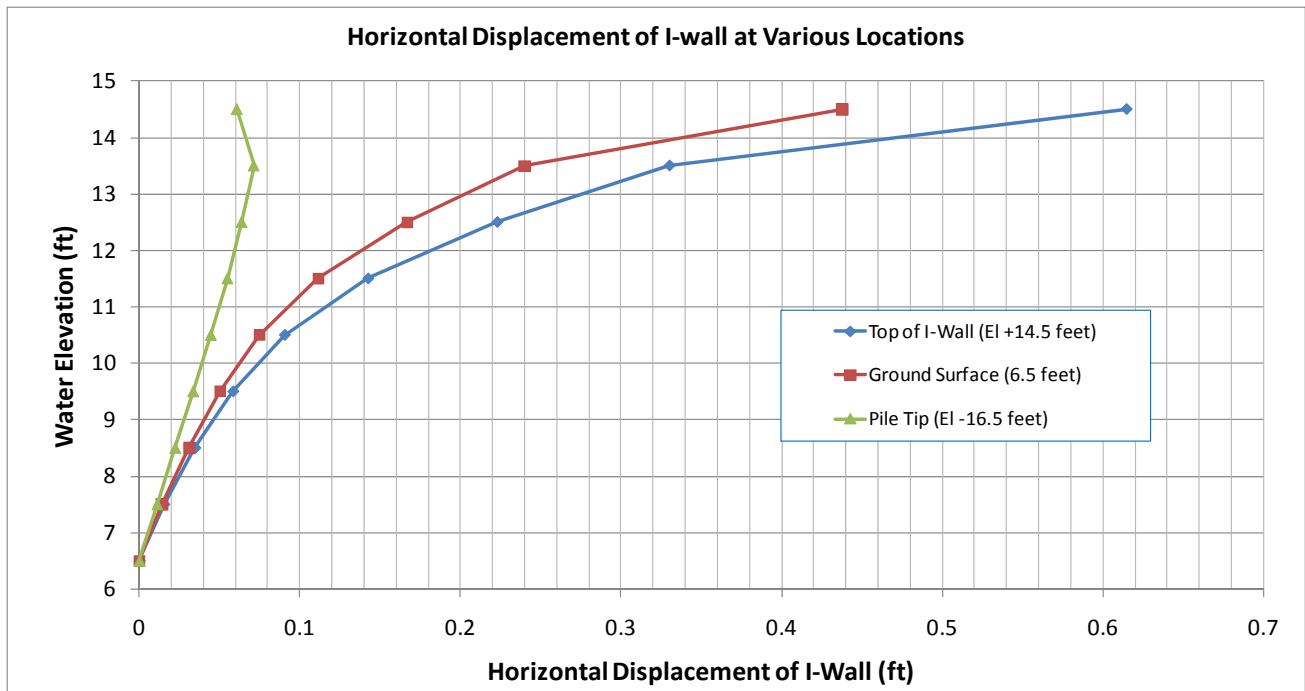


Figure F.3. Sheet-pile horizontal displacements for selected locations.

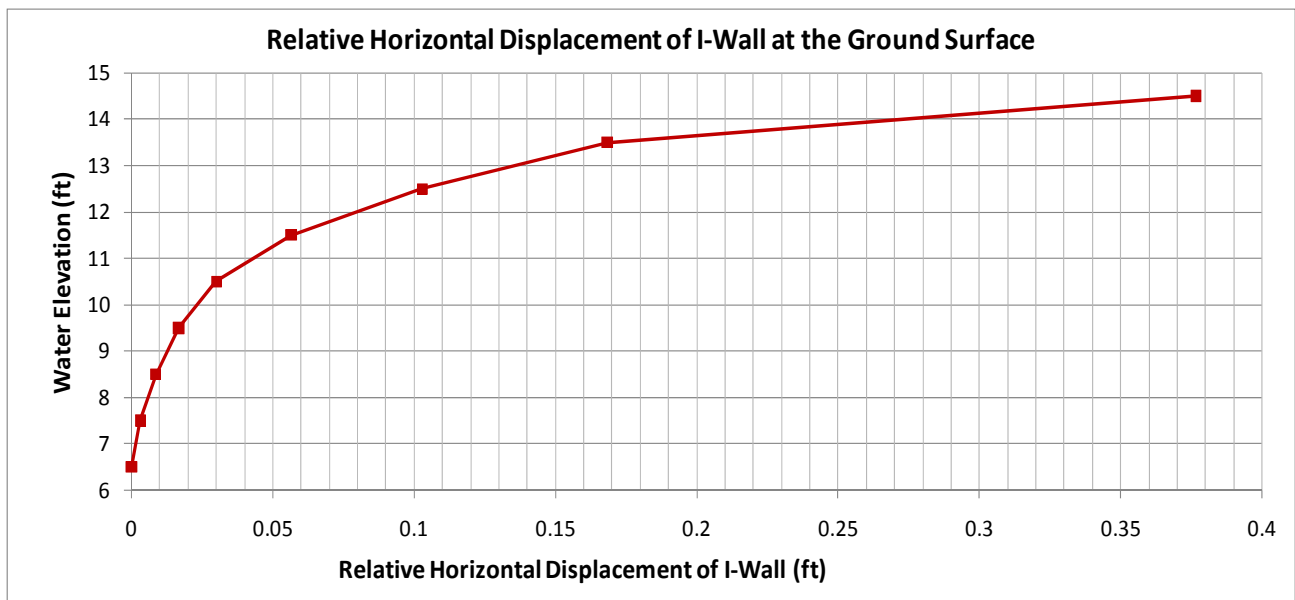


Figure F.4. Relative horizontal displacements of the sheet pile at the ground surface.

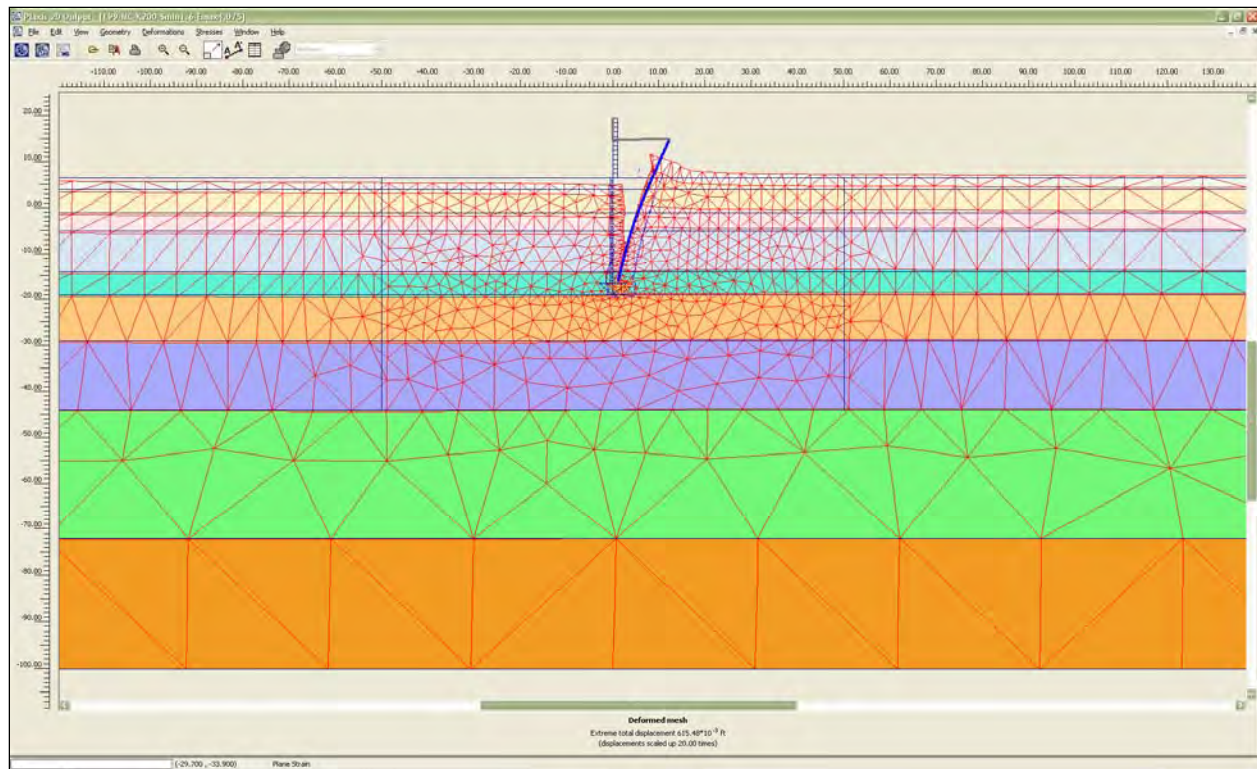


Figure F.5. Total displacements for water el 14.5 ft and gap tip el -9 ft.

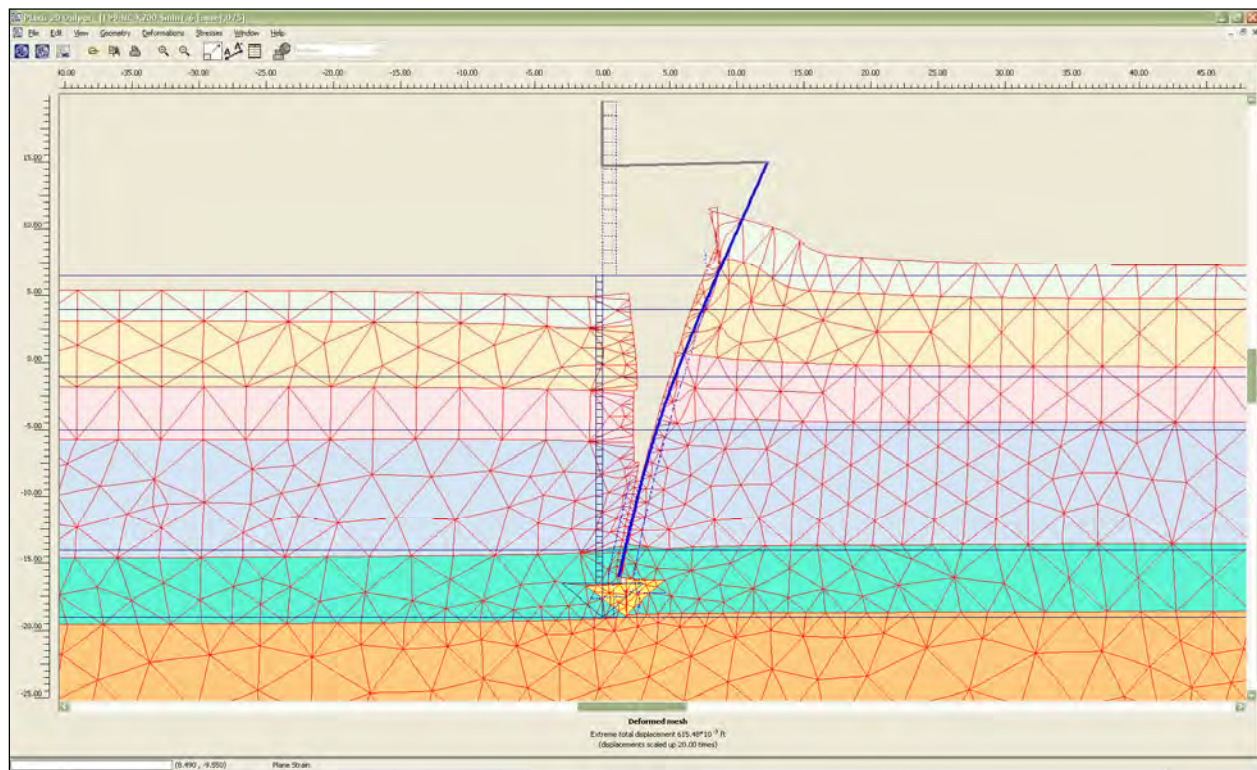


Figure F.6. Enlarged view of total displacements for water el 14.5 ft and gap tip el -9 ft.

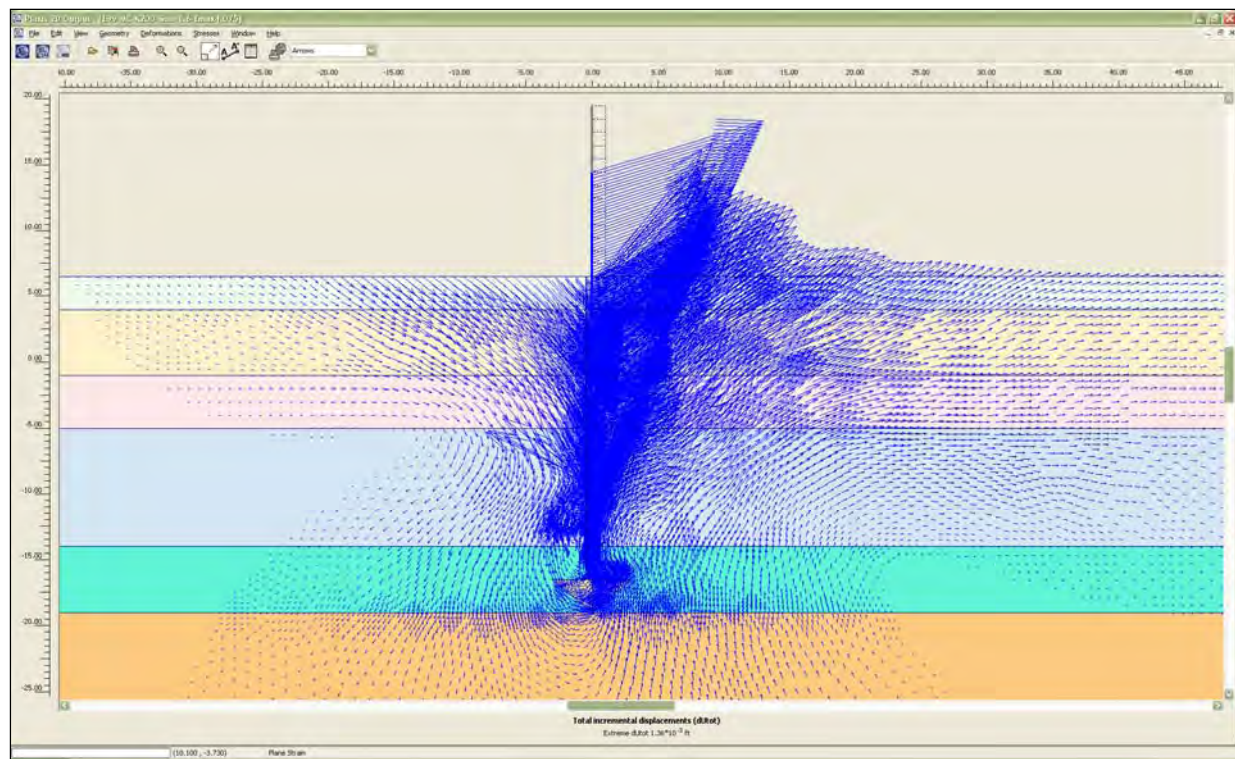


Figure F.7. Vectors of total incremental displacements showing the movement of the soil during the final increment of loading.

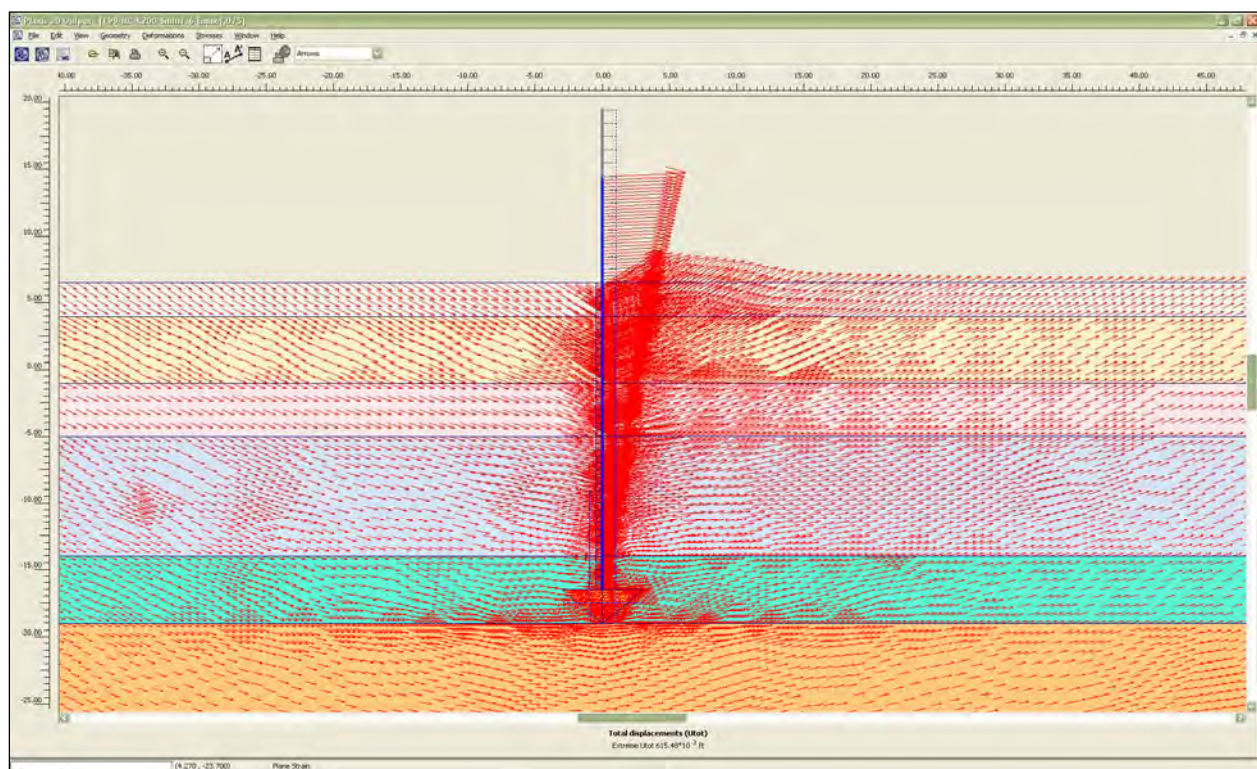


Figure F.8. Vectors of total displacements showing the movement of the soil.

F.5.11 Moments in sheet-pile wall for MC model

Moments in the sheet pile for various water elevations are shown in Figure F.9. The moment increases as the water elevation increases and reaches a maximum at water el 14.5 ft. The moment for water el 14.5 ft is 30,197 ft-lb at el -4.6 ft. The moment at water el 12.5 ft is 13,470 ft-lb at el -3.0 ft.

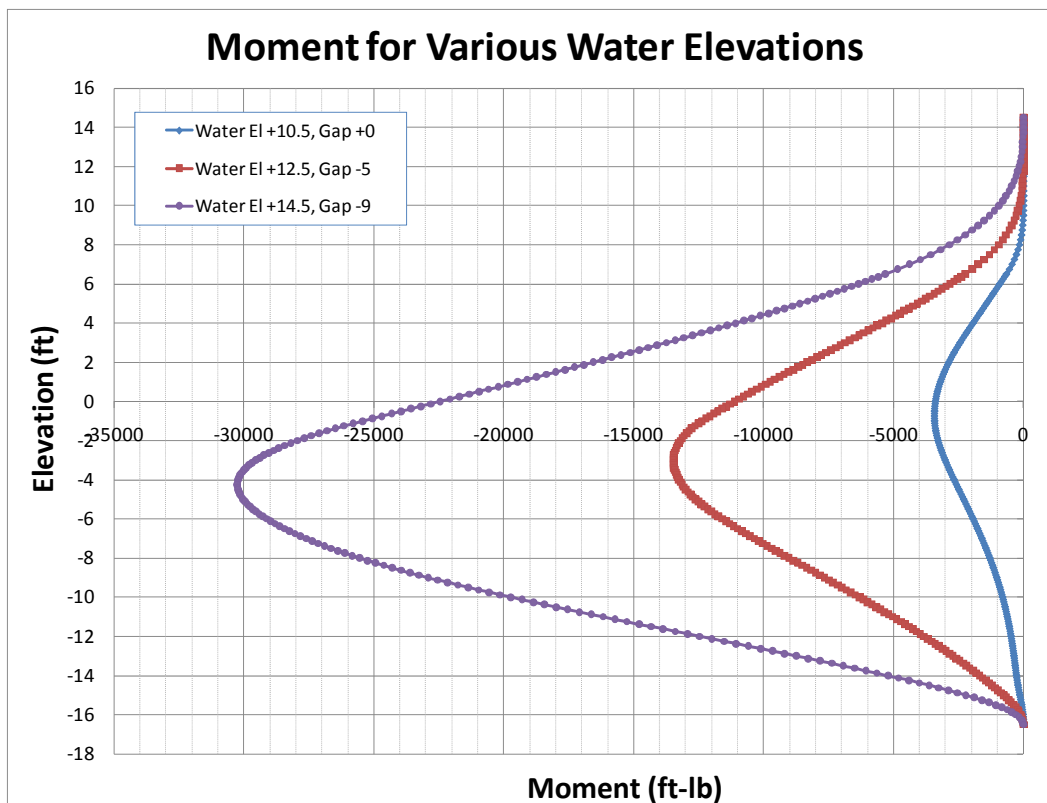


Figure F.9. Comparison of moments at various water elevations.

F.5.12 Shear stresses in soil for MC model

Figures F.10 through F.12 show the relative shear stress in the soil for various water elevations and the associated gap depths. The relative shear stress is a measure of the shear stress in the soil compared to the maximum available shear stress at failure. The shear stress in the soil increases as the water elevation increases. The shear stress increases in the upper unsaturated layer first then progresses down toward the tip of the pile. The shear stresses are greatest on the landside of the sheet-pile wall and at the bottom of the gap. For water el 14.5 ft, as shown in Figure F.12, the highly stressed region extends to the tip of the sheet pile.

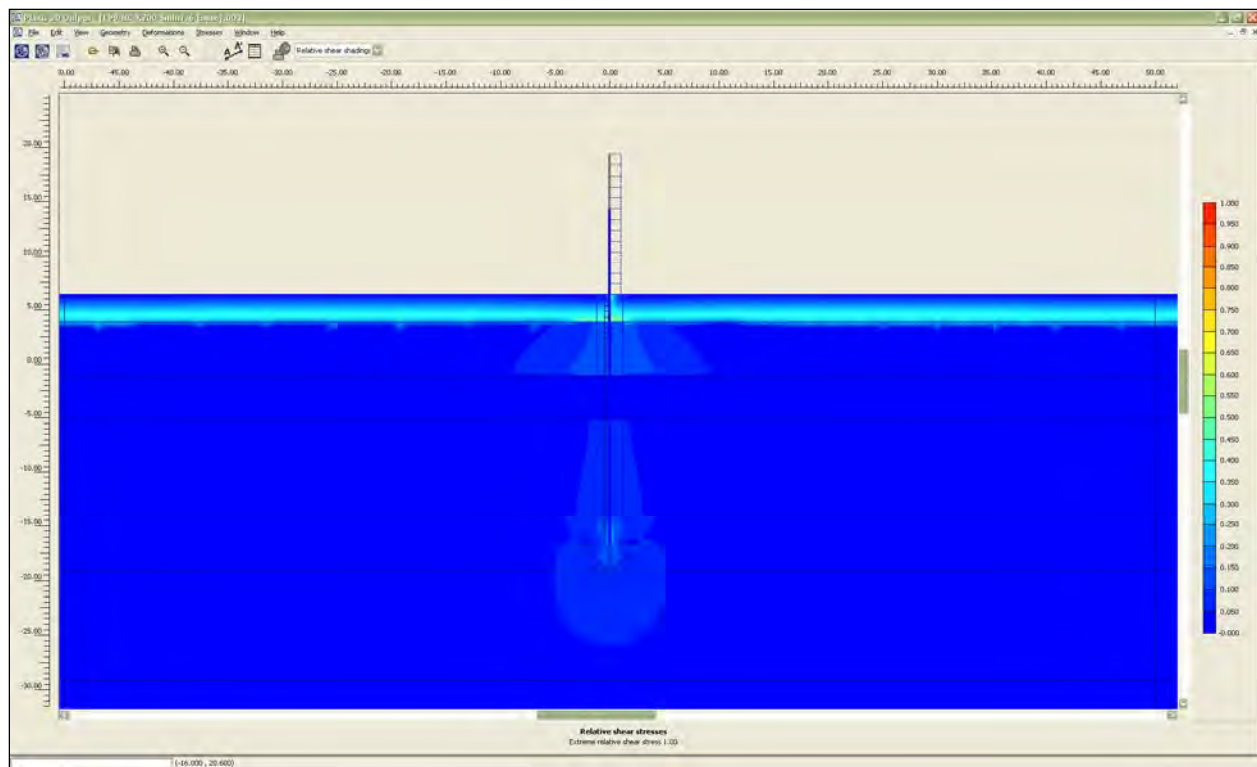


Figure F.10. Relative shear stress after placement of I-wall.

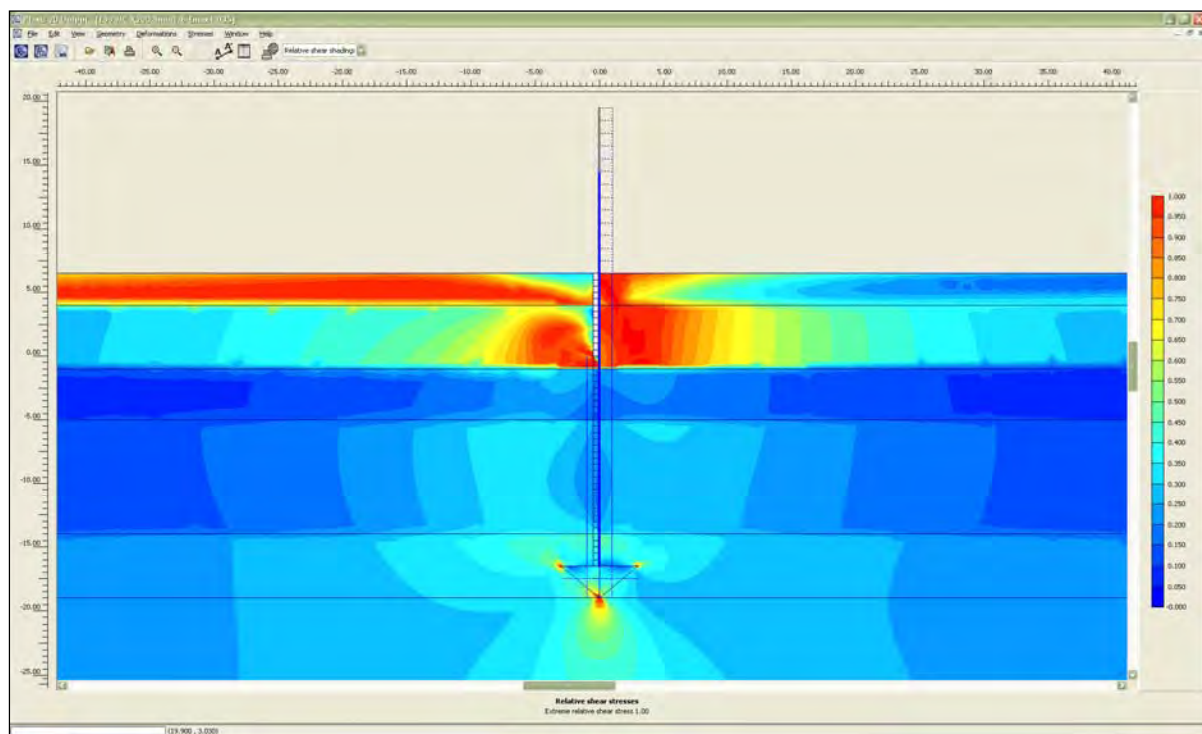


Figure F.11. Relative shear stress for water at el 10.5 ft and gap tip at el 0 ft.

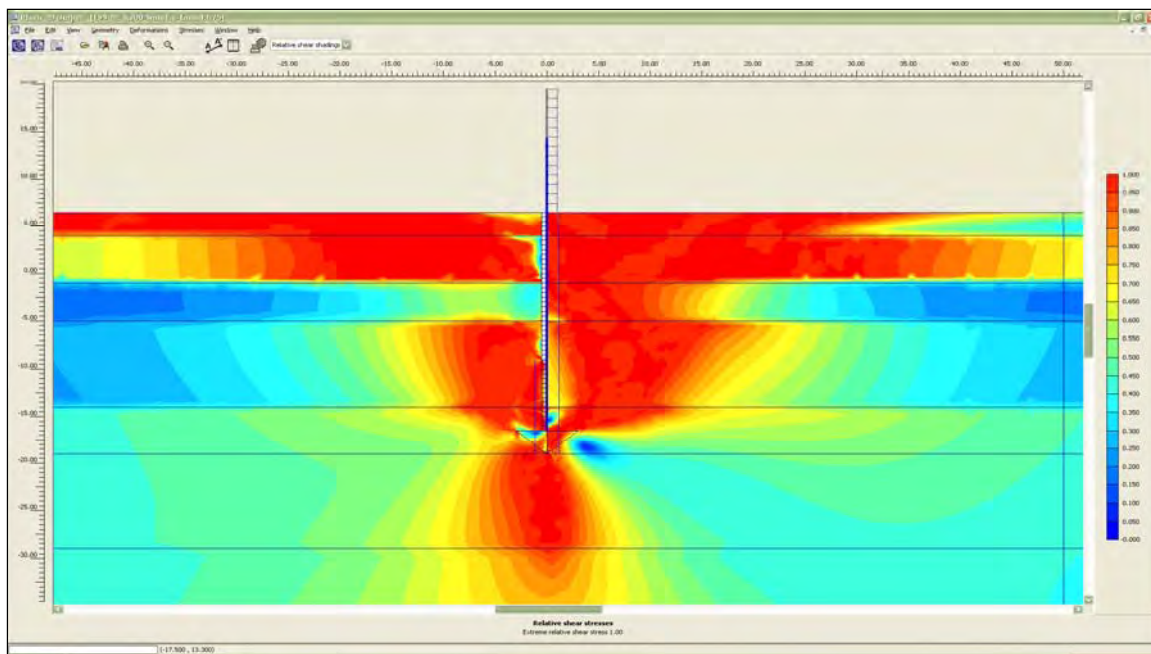


Figure F.12. Relative shear stress for water at el 14.5 ft and gap tip at el -9 ft.

F.5.13 Horizontal earth pressures for MC model

For Figures F.13 through F.15, the flood side is on the right side of the figure and the landside is on the left. This corresponds to the input convention CWALSHT uses.

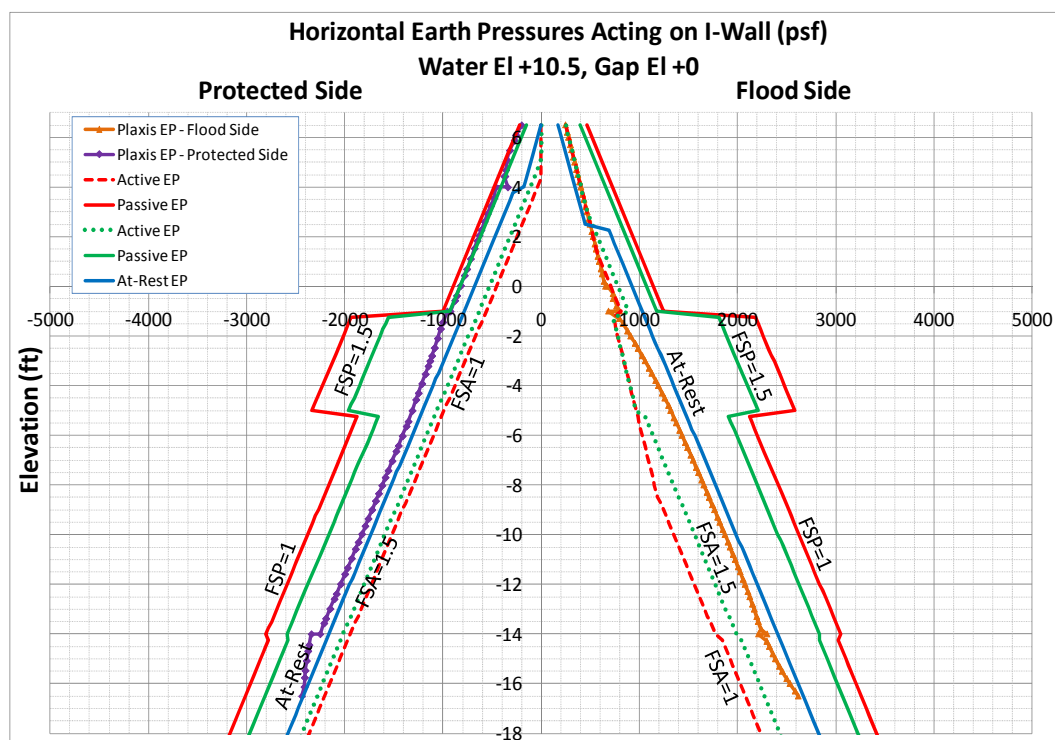


Figure F.13. Horizontal earth pressures for water el 10.5 ft and gap tip el 0 ft.

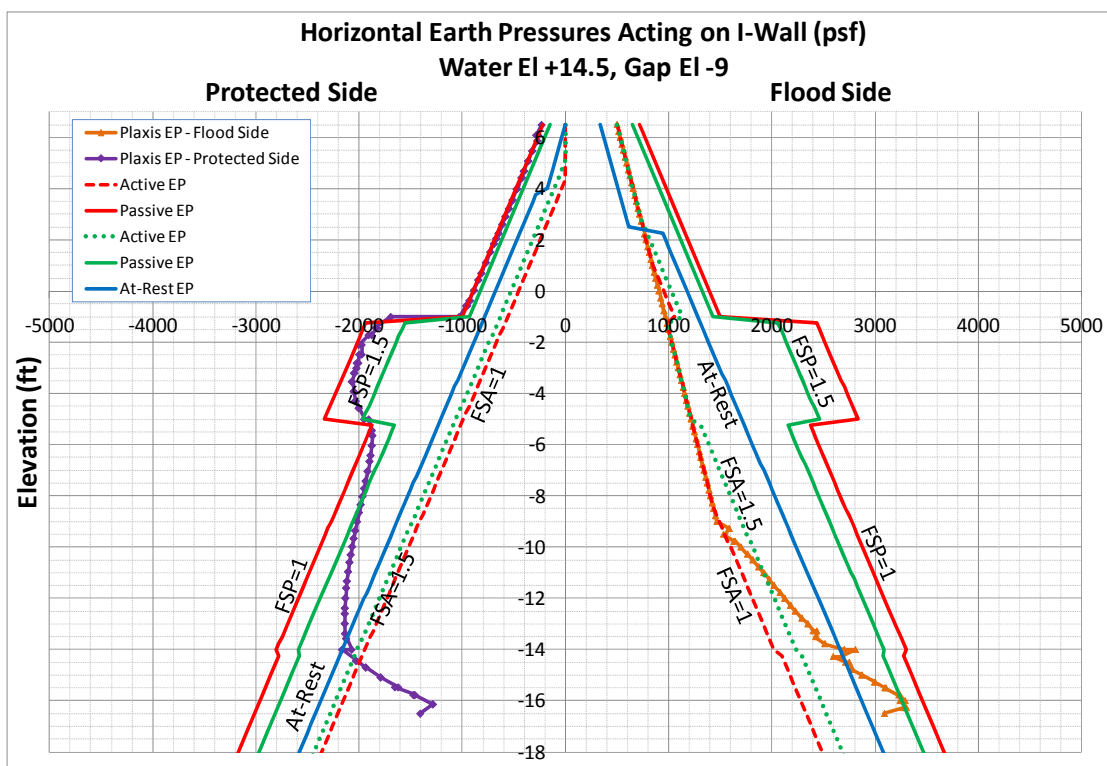


Figure F.14. Horizontal earth pressures for water el 14.5 ft and gap tip el -9 ft.

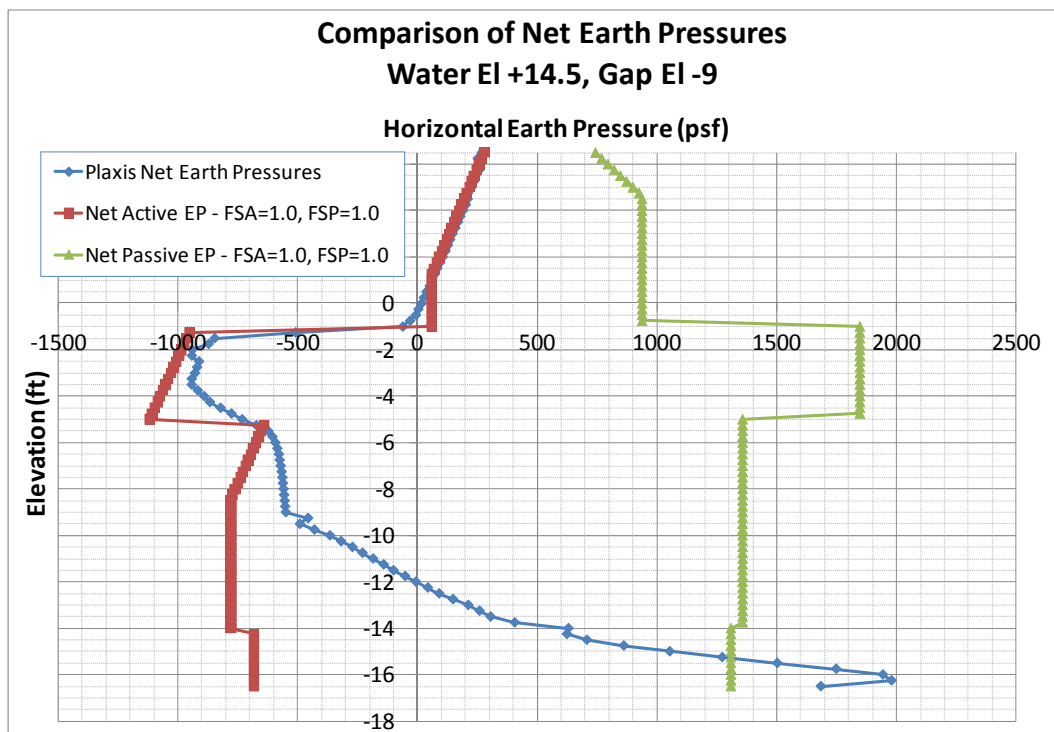


Figure F.15. Comparison of net earth pressures computed from limiting earth pressures and PLAXIS results for water el 14.5 ft.

Figures F.13 and F.14 compare the horizontal earth pressures acting against the sheet-pile wall and calculated using PLAXIS to the limiting active and passive earth pressures computed using adhesion as discussed in Chapter 3, Section 3.3.2. The value of adhesion used is 80 percent of the cohesion as discussed in Chapter 3, Section 3.3.4. The limiting earth pressures in the figures are computed for factors of safety equal to 1.0 and 1.5. A factor of safety of 1.0 results in full active and passive earth pressures, while a factor of safety of 1.5 results in increased active and decreased passive earth pressures. Comparing the earth pressures in this manner allows a comparison of the PLAXIS earth pressures to values computed from conventional design procedures.

Figure F.13 displays the earth pressures for water el 10.5 ft and gap tip el 0 ft. For the flood side, the pressures are equal to hydrostatic pressures down to the bottom of the gap. Below the gap, the pressures are close to at-rest earth pressures computed using the assumed values of K_o given in Table 3.9. On the landside, the earth pressures are very close to passive earth pressures computed using a factor of safety of 1.5 at elevations above -1 ft. Below -1 ft, the earth pressures are close to at-rest earth pressures.

Figure F.14 shows results for water el 14.5 ft. The gap in this case extends to el -9 ft. The earth pressures on the flood side are equal to hydrostatic pressures down to the bottom of the gap. Below the gap, the earth pressures are less than the at-rest condition because of the wall moving away from the soil. The earth pressures increase closer to the tip of the sheet pile to passive pressure values computed using a factor of safety of 1.5. On the landside, above el -5 ft, the earth pressures are almost equal to the fully passive earth pressures computed using a factor of safety of 1.0. Below -5 ft, the pressures decrease with depth and become less than active earth pressures computed using a factor of safety of 1.0.

Figure F.15 compares the net earth pressures computed using limiting earth pressures and the results from PLAXIS for water el 14.5 ft. The limiting earth pressures were computed using a factor of safety of 1.0 for both the active and passive earth pressures for both the flood side and landside of the wall. Net pressures were compared for this water elevation because the movements of the wall were sufficient to produce values of full active and passive earth pressures. As can be seen from the figure, the net earth pressures on the landside compare fairly well to the net active earth pressures. Toward the tip of the pile, the net earth pressures transition from the net active to the net passive earth pressures. The magnitudes of the net earth pressures are larger than the net passive pressures.

Appendix G: Analyses of E-99 Sheet-pile Wall Field Load Test Using Maximum Values of Undrained Shear Strength (S_u) and Minimum Values of Undrained Secant Stiffness (E_u)

G.1 Purpose of analyses

This appendix summarizes the results of nonlinear soil-structure interaction (SSI)¹ finite element analyses of the E-99 sheet-pile wall field load test as described by Jackson (1988).² The analyses included the formation and propagation of a gap beside the sheet-pile wall on the flood side. The gap affected the resulting deformation and stress conditions of the soil regime on both the flood side and landside of the I-wall. The analyses were part of a parametric study determining the effects of the undrained shear strength (S_u) and undrained secant stiffness (E_u) on the deformation and gap formation characteristics of the system. For the analysis described in this appendix, maximum values of the undrained shear strength and minimum values of undrained secant stiffness were selected.

The following sections will describe the soil used in the analyses, the selection of stiffness and shear strength parameters, the conventional analysis and design of the I-wall, the analysis procedures employed, and the results of the finite element analyses.

G.2 Overview of problem analyzed

The E-99 field load test consisted of a 200-ft section of floodwall constructed on the landside berm of the Item E-99 East Atchafalaya Basin Protection Levee (EABPL) on Avoca Island just south of Morgan City, Louisiana. The test was performed between July and September of 1985 (Jackson 1988).

The soil geometry, maximum water height, and pile geometry of the field load test are shown in Figure 3.1. The sheet pile is located on the landside

¹ Symbols and unusual abbreviations used in this appendix are listed and defined in the Notation, Appendix I.

² Citations in this appendix are in the References at the end of the main text.

of the existing levee. The water loading was applied between the existing levee and the sheet-pile wall. The geometry was idealized as shown in Figure 3.2 and is assumed to be a flat (level) site. The top of the sheet-pile wall was at el 14.5 ft¹, and the tip of the sheet-pile wall was at el -16.5 ft. The elevation of the top soil layer was at 6.5 ft. The I-wall system is described in Chapter 3, Section 3.2.

The soils at the site were clays of high plasticity, designated as CH in the Unified Soil Classification System (USCS). From the classification chart shown in Figure 3.4, the plasticity index of a CH material has a value of 22 and greater. The soil was normally consolidated with liquid limits between 76 and 114 percent and natural water contents between 40 and 80 percent.

For the analyses described in this appendix, the permeability of the clay layers was assumed to be small enough that the soil would not become fully saturated as the floodwater level was increased. Therefore, as shown in Figure 3.2, two zones of soil were considered in the analysis: a partially saturated one above the water table el 4 ft and a saturated one below the water table.

G.3 Material properties used for parametric analysis

The analysis described in this appendix is one in a set of parametric analyses varying the values of S_u and E_u . The values used for the analysis in this appendix correspond to the maximum values of S_u and the minimum values of E_u . The material properties used in the analysis described in Chapter 3 are denoted and treated as the mean values. In actuality, they are the values used for the design of the I-wall that differ slightly from the mean values computed from laboratory test data.

The undrained shear strengths of the clay layers were determined from unconsolidated undrained (UU) and unconfined compression (UC) tests. These design values, shown in Table 3.1, were used to perform an undrained, short-term design of the wall. The material property values consist of the saturated (γ_{sat}) and moist (γ_{moist}) unit weights of the soil, the undrained shear strength (S_u), and adhesion (c_a). The angle of internal friction (ϕ) and wall friction (δ) were zero because this is an undrained analysis. The same value of the unit weight was used for both saturated

¹ All elevations cited in this Appendix are in feet referred to the National Geodetic Vertical Datum (NGVD).

and moist conditions. Adhesion was used in the total stress analysis using values cited in Potyondy (1961) for a cohesive soil against rough steel and is equal to 0.8 times the undrained shear strength ($c_a = 0.8 * S_u$).

The laboratory test data were used to compute mean (μ) and standard deviation (σ) values for the soil layers. These values are shown in Table G.1. The column labeled Plate 9 corresponds to the design values assumed in the E-99 field test report (Jackson 1988). As can be seen from Table G.1, the design values are slightly different from the mean values computed from test data. The design values were used in the finite element analysis discussed in Chapter 3. The mean values shown in Table G.1 were computed based on a limited number of tests, and it was felt that the design values provided a better estimate of the strengths. The coefficients of variation (COV) for the clay layers computed from test data also are shown in Table G.1. Because Layer 2 had only two data points, the COV for this layer was deemed to be too low and, therefore, was adjusted to a higher value. The last column in Table G.1 shows the values of the COVs used in this analysis.

Table G.1. Mean and standard deviation values for the clay layers.

Layer	Top El, ft	Bottom El, ft	Plate 9 S_u , psf	Mean μ , psf	Standard Deviation σ , psf	COV, %	COV % for Analyses
1	6.5	-1	200	285	74	37.2	37
2	-1	-5	500	580	50	2.4	10
3	-5	-14	350	362	70	20.2	20
4	-14	-29	500	476	175	34.6	35

Using the COVs for the soil layers listed in Table G.1, σ was computed for each layer. These standard deviations were used to compute minimum and maximum values of S_u and E_u .

The minimum value of S_u ($S_{u,min}$) was computed as shown in Equation G.1:

$$S_{u,min} = S_{u,mean} - x_{min} \bullet \sigma. \quad (G.1)$$

The variable (x_{min}) in Equation G.1 represents a multiple of the standard deviation. The design values of S_u listed in Table G.1 were used as the $S_{u,mean}$ values. The value of the minimum E_u ($E_{u,min}$) was computed as:

$$E_{u,min} = E_{ref} = KS_{u,min}, \quad (G.2)$$

where E_{ref} is the reference stiffness needed for the Mohr-Coulomb (MC) soil model and K is defined as:

$$K = \frac{E_{u,min}}{S_{u,min}}. \quad (G.3)$$

The maximum value of S_u ($S_{u,max}$) was computed as shown in Equation G.4:

$$S_{u,max} = S_{u,mean} + x_{max} \bullet \sigma. \quad (G.4)$$

The variable (x_{max}) in Equation G.4 represents a multiple of the standard deviation and does not equal x_{min} .

The value of the maximum E_u ($E_{u,max}$) was computed as:

$$E_{u,max} = E_{ref} = KS_{u,max}. \quad (G.5)$$

In Equation G.5, E_{ref} is the reference stiffness needed for the MC soil model and K is defined as:

$$K = \frac{E_{u,max}}{S_{u,max}}. \quad (G.6)$$

The value of K in Equation G.6 was taken from a chart developed by Duncan and Buchignani (1976) relating the plasticity index and the over-consolidation ratio (OCR) to the dimensionless factor K . The same value of (K) of 200 used in the analysis of Chapter 3 was used for this analysis.

The intent of the analyses described in Appendix E was to use the lowest values of S_u and E_u possible and still keep the design condition of the water at the top of the wall at el 14.5 ft numerically stable. The multiple of the standard deviation was varied to find the largest multiple at which the design condition was still stable (i.e., the factor of safety was greater than 1.0). The loading in PLAXIS, a two-dimensional (2-D) nonlinear incremental construction finite element program (PLAXIS 2012), was applied in one construction step, and the gap propagation was not tracked in these

analyses. PLAXIS applies the load increment in many substeps for convergence. Previous experience with I-wall analyses has shown that the results are comparable between a complete analysis tracking the gap progression and this simplified procedure, as long as the gap depth does not vary greatly and no unloading of the system occurs. A constant gap elevation of -10 ft was used. This is the same gap elevation used in the analysis described in Chapter 3. The factor of safety was computed using a Phi/c reduction analysis within PLAXIS. The results of these analyses are shown in Table G.2, and the largest multiple of the standard deviation that was acceptable was determined to be 1.6.

Table G.2. Factors of safety for various multiples of the standard deviation.

	Multiples of Standard Deviation			
	-1.5	-1.6	-1.75	-2
FS	1.105	1.06	0.881	Design case would not run

The intent of the analyses in this appendix was to use the largest values of S_u and smallest values of E_u possible to ascertain the effects on the gap initiation and propagation and subsequent height of water loading possible while the analysis remained numerically stable. The multiple of 1.6 was used in Equation G.1 to compute the minimum S_u . Equation G.2 with a value of 200 for K and the minimum value of S_u was used to compute the minimum value of E_u . The maximum values of S_u were computed using a multiple of 4 in Equation G.4. This resulted in a maximum value of S_u that was used in Equation G.5 to compute the maximum value of E_u . Equation G.6 with a value of 200 for K and the maximum value of S_u was used to compute the maximum value of E_u . The use of four standard deviations in Equation G.4 was deemed to result in the largest values possible of both S_u and E_u . The minimum and maximum values of S_u and E_u computed in this fashion are shown in Table G.3.

G.4 Conventional analysis of cantilever I-wall

G.4.1 Criteria for gap initiation and propagation

Two different criteria, one for the flood side and another for the landside, are used to determine whether a gap initiates in the soil adjacent to the sheet-pile wall and how far the gap will propagate. A hydraulic fracturing criterion is used for the flood side of the I-wall, and a negative horizontal stress criterion is used for the landside. Both of these criteria are discussed in Chapter 3, Section 3.3.3.

Table G.3. Material properties for analyses.

Layer	Elevation			S_u		Design Values		Min Values		Max Values	
								$S_{u,mean}-1.60*\sigma$		$S_{u,mean}+4*\sigma$	
	Top, ft	Bottom, ft	γ_{sat} , pcf	COV, %	σ	Mean S_u , psf	E_u , psf	S_u , psf	E_u , psf	S_u , psf	E_u , psf
1	6.5	-1	104	37	74	200	40,000	82	16,320	496	99,200
2	-1	-5	107	10	50	500	300,000	420	84,000	700	140,000
3	-5	-14	106	20	70	350	210,000	238	47,600	630	126,000
4	-14	-19	104	35	175	500	300,000	220	44,000	1200	240,000
5	-19	-29	101	35	175	500	300,000	220	44,000	1200	240,000
6	-29	-44	100	35	193	550	330,000	242	48,400	1320	264,000
7	-44	-72	100	35	236	675	405,000	297	59,400	1620	324,000
8	-72	-100	100	35	324	925	555,000	407	81,400	2220	444,000

G.4.2 Computed gap depth

CWALSHT (U.S. Army Engineer Research and Development Center 2012) uses the negative horizontal stress criterion discussed in Section 3.3.3 to compute whether a gap forms in the soil. Negative computed earth pressures imply that the soil-to-sheet-pile interface is in tension. Because the soil-to-sheet-pile interface cannot sustain a tensile load, the soil is assumed to form a gap, and CWALSHT sets any negative (tensile) earth pressures to zero. CWALSHT applies water pressures within a gap below the input water level. If the gap is above the water level, CWALSHT does not fill the gap with water.

G.4.3 Total stress analysis with CWALSHT

CWALSHT always computes effective stresses based on the input material properties and the level of the water in the soil. For problems involving all clay layers, a total stress (short-term) analysis with $c = S_u$ and $\phi = 0$, where c is cohesion, can be performed with CWALSHT by inputting the actual soil geometry and water levels. This gives a correct total stress analysis because, even though CWALSHT computes effective stresses based on the input water levels, the pore pressures are added to the effective stresses to arrive at total stresses. Because the value of the horizontal earth pressure coefficient is equal to 1.0 for a soil with only cohesion, the total stress computed in this manner is correct. The determination of the depth of the gap also conforms to the hydraulic fracturing criteria described in Section 3.3.3. This is because CWALSHT computes effective stresses and uses the

effective stresses to determine the tensile zone. The hydraulic fracturing criterion uses total stresses and compares these to static pore pressures, a process that produces equivalent numerical results. Horizontal earth pressures are computed as described in Section 3.3.2.

G.4.4 CWALSHT analysis results

The elevation of the tip of the sheet pile for this analysis was -16.5 ft. A short-term analysis was performed with CWALSHT, using the maximum material properties as given in Table G.3. The results of analyses performed with CWALSHT are shown in Table G.4.

Table G.4. Results of analysis computations using CWALSHT.

Analysis Case		S_u , psf	Adhesion, psf	Water El, ft	El, of Bottom of Gap, ft	Elevation of Tip of Sheet Pile		
						FS_{Active}	$FS_{Passive}$	El, ft
1	Short-term with water levels	Max values	0	14.5	Below wall	1	2.78	-16.5
2	Short-term with water levels	Max values	$0.8 \cdot S_u$	14.5	Below wall	1	3.68	-16.5
3	Short-term with water levels	Max values	0	22.5	Below wall	1	0.68	-16.5
4	Short-term with water levels	Max values	$0.8 \cdot S_u$	22.5	Below wall	1	0.91	-16.5

For Cases 1 through 4, the factor of safety applied to the active earth pressures (FS_{Active}) was 1.0, while the factor of safety applied to the passive earth pressures ($FS_{Passive}$) varied. Cases 1 through 4 were modeled with the actual soil layer geometry with input water levels as described in Section G.4.3. Cases 1 and 2 were for a water elevation of 14.5 ft, which is the elevation of the top of the wall. Case 1 did not include adhesion and resulted in a factor of safety on the passive earth pressures ($FS_{Passive}$) equal to 2.78. The gap extended below the tip of the sheet pile. Case 2 included adhesion and resulted in a value for $FS_{Passive}$ of 3.68. The gap in this case also extended below the tip of the sheet pile. Cases 3 and 4 were for water el 22.5 ft (8 ft above the top of the wall). Case 3 did not include adhesion and resulted in a value for $FS_{Passive}$ of 0.68. The gap extended below the tip of the sheet pile. Case 4 included adhesion and resulted in a value for $FS_{Passive}$ of 0.91. The gap also extended below the tip of the sheet pile.

G.5 PLAXIS finite element analyses

G.5.1 Conceptual model

The finite element analyses were performed with PLAXIS. The conceptual model of the finite element mesh is shown in Figure 3.7. The geometry is the same as explained previously, but several modeling features should be noted. The sheet-pile wall was represented by plate elements. Interface elements were placed on both sides of the plate elements, from the ground surface down to the tip of the sheet pile. To alleviate stress concentrations at the corners of the geometry, both horizontal and vertical extensions of the interface elements were provided at the tip of the sheet-pile wall at el -16.5 ft. A plate element extension and dummy soil elements were added above the wall to provide for additional loading height if needed. The mesh was structured to provide node points at 1-ft raises of the water table. The soil elements beside the sheet-pile wall on the flood side were 0.5 ft in height. This enabled the inputting of 1-ft raises in water and modeling of the gap to within 0.5 ft.

G.5.2 Finite element mesh

The finite element mesh used in the analyses is shown in Figures 3.8 and 3.9. The mesh is composed of 2,396 elements and 19,917 nodes with 28,752 stress points. The type and number of elements used in the mesh are shown in Table 3.3. The mesh consists of 15-node triangular elements to model the soil, 5-node plate elements to model the sheet-pile wall, and 5-node interface elements to model the soil-structure interaction effects between the sheet-pile wall and the adjacent soil elements. The problem was run as a plane strain problem.

G.5.3 Total stress analysis procedure in PLAXIS

The E-99 field test was analyzed using total unit weights of the soil and boundary water pressures to perform a short-term (undrained) analysis using PLAXIS. All materials were designated as drained, which in PLAXIS terminology means that no excess pore-water pressures will be generated because of applied loads. The general phreatic surface was used in PLAXIS to apply the boundary water pressures on the soil surface and within the gap. All soil layers were associated with a cluster phreatic surface that was input below the minimum elevation of the mesh. Because the water surface was below all soil layers, no internal water pressures were generated within the soil layers. This procedure resulted in a total stress analysis with the

computed effective stresses being equal to the total stresses (i.e., no internal pore pressures are present).

It was assumed that the permeability of the soil was small enough that any time-dependent effects such as seepage could be ignored and that the undrained shear strengths could be used to determine the behavior of the system.

G.5.4 Tracking the progression of the gap

The I-wall deflects as the flood loading increases, and eventually a gap forms beside the I-wall on the flood side of the wall. The gap begins at the ground surface and progresses downward as shown in Figure 3.10. The gap along the flood side of the I-wall-to-soil interface is modeled by deactivating soil clusters (elements), effectively creating a void beside the wall. As water pressures are applied within this void, the gap progresses downward. Modeling of the flood loading commenced in the finite element analysis after the total initial stress state was computed based on an assumed steady-state water elevation of 4 ft. The flood loading was applied in 1-ft incremental raises of the water level in order to track the formation and propagation of the gap.

The criterion used to estimate the formation and propagation of the gap is based on the hydraulic fracturing concept discussed in Chapter 3, Section 3.3.3. The procedure used to estimate the gap depth:

1. For each rise in water level, the total horizontal stresses against the sheet-pile wall are compared against the hydrostatic water pressures acting on the wall, given the current water elevation. A gap is formed when the horizontal earth pressure is less than the water pressure at a given depth.
2. Soil elements are deactivated within the computed region of the gap, and hydrostatic water pressures are applied within the deactivated elements.
3. The analysis is rerun for the current water level, and Steps 1 and 2 are repeated until the depth of the gap ceases to increase.
4. The water level is increased, and Steps 1 through 3 are repeated. The water level is raised until instability in the analyses is encountered.

G.5.5 Shear strength and stiffness properties used in the finite element analyses

The finite element analyses described in this appendix were performed using the PLAXIS finite element program. The MC soil model was used for

the soil elements. This model uses an elastic-perfectly plastic stress-strain relationship. Elastic plate elements were used to model the steel sheet pile, and interface elements were used to capture the soil-structure interaction effects between the sheet-pile wall and the soil. PLAXIS can perform analyses using either effective or total stress soil parameters. For the analyses described herein, total stress soil parameters were used.

Figure 3.11 shows the material numbering and soil layering used in the finite element analyses. The soil was divided into layers below the tip of the pile to provide for an increasing undrained shear strength and stiffness below the elevation of the pile tip. See Chapter 3, Section 3.4.5, for discussion of the properties assumed for the soil, pile, and interface elements.

The undrained shear strength (S_u) and undrained reference stiffness (E_{ref}) of the clay layers used in this parametric analysis are computed as described in Section G.3 and the results shown in Table G.5. The remaining material property values consist of the saturated (γ_{sat}) and moist (γ_{moist}) unit weights of the soil, angle of internal friction (ϕ), dilation angle (Ψ), unload/reload Poisson's ratio (ν), and the interface strength ($R_{interface}$).

Table G.5. Strength and stiffness properties for the soil layers used in the MC soil model for the case of a maximum (S_u) and minimum (E_{ref}).

Material Number	Material Description	γ_{moist} , lb/ft ³	γ_{sat} , lb/ft ³	S_u , lb/ft ²	E_{ref} , lb/ft ²	ν	$R_{interface}$
1	Clay\1_6.5_200_Rinit=0.8	104	104	496	16,320	0.4	0.8
2	Clay\2_4_200_Rinit=0.8	104	104	496	16,320	0.495	0.8
3	Clay\3_-1_500_Rinit=0.8	107	107	700	84,000	0.495	0.8
4	Clay\4_-5_350_Rint=0.8	106	106	630	47,600	0.495	0.8
5	Clay\5_-14_500_Rinit=0.8	104	104	1200	44,000	0.495	0.8
6	Clay\5a_-14_500_Rinit=1.0	104	104	1200	44,000	0.495	1
7	Clay\6_-19_500_Rinit=0.8	101	101	1200	44,000	0.495	0.8
8	Clay\7_-29_550_Rinit=0.8	100	100	1320	48,400	0.495	0.8
9	Clay\8_-44_675_Rinit=0.8	100	100	1620	59,400	0.495	0.8
10	Clay\9_-72_925_Rinit=0.8	100	100	2220	81,400	0.495	0.8

Note: properties are given for drained material, with the angle of internal friction for the soil ϕ and the dilation angle (Ψ) set to 0, as this is a total stress analysis.

The $R_{interface}$ value is from values cited by Potyondy (1961) as discussed in Chapter 3, Section 3.3.4. This controls the amount of adhesion along the soil-to-wall interface. Material 6 in Table G.5 has an $R_{interface}$ value of 1.0 because this material represents a soil-to-soil interface.

G.5.6 Initial stresses

The initial total stress state within the finite element mesh was established using the at-rest soil conditions for a level ground surface. Horizontal at-rest soil stresses were estimated using the relationship between the at-rest earth pressure coefficient (K_o) and the soil Poisson's ratio (ν) given in Equation 3.14.

The assumed groundwater elevation was at 4 ft. Table 3.9 summarizes the K_o values used to compute the horizontal earth pressures for the initial conditions. The Poisson's ratio for the partially saturated soil layer was 0.4, which corresponds to a K_o of 0.67. This value is less than the value for a fully saturated material, which has a K_o of 1.0.

G.5.7 Performance of interface elements

The performance of the interface elements was examined to determine if the normal stresses in the interface elements corresponded closely to the normal stresses in the adjacent soil elements. As discussed in Chapter 3, Section 3.4.7, and shown in Figure 3.14, the stresses within the interface elements agree very closely with the stresses in the adjacent soil elements and the processing of results could be done using either data set. The results presented in this appendix use the stresses extracted from the soil elements adjacent to the sheet-pile wall.

G.5.8 Progression of gap propagation for MC analyses

Figure G.1 shows the progression of the gap as the water level against the I-wall is increased from 1 ft (el 7.5 ft) to 16 ft (el 22.5 ft). The gap initiates at water el 7.5 ft and extends to a depth of 4 ft. The gap propagation follows essentially a linear path, with the gap depth increasing as the water elevation increases to 14.5 ft. The black dotted line in Figure G.1(a) is a linear fit to the gap depths at the various water elevations. The depth of the gap extends to el -9 ft at water el 14.5 ft. The tip of the sheet pile is at el -16.5 ft. The gap extends to a depth of -14.5 ft at water el 22.5 ft as shown in Figure G.1(b). The rate of the gap depth decreases for water elevations above 14.5 ft and follows a more parabolic path as shown by the black dotted line in Figure G.1(b).

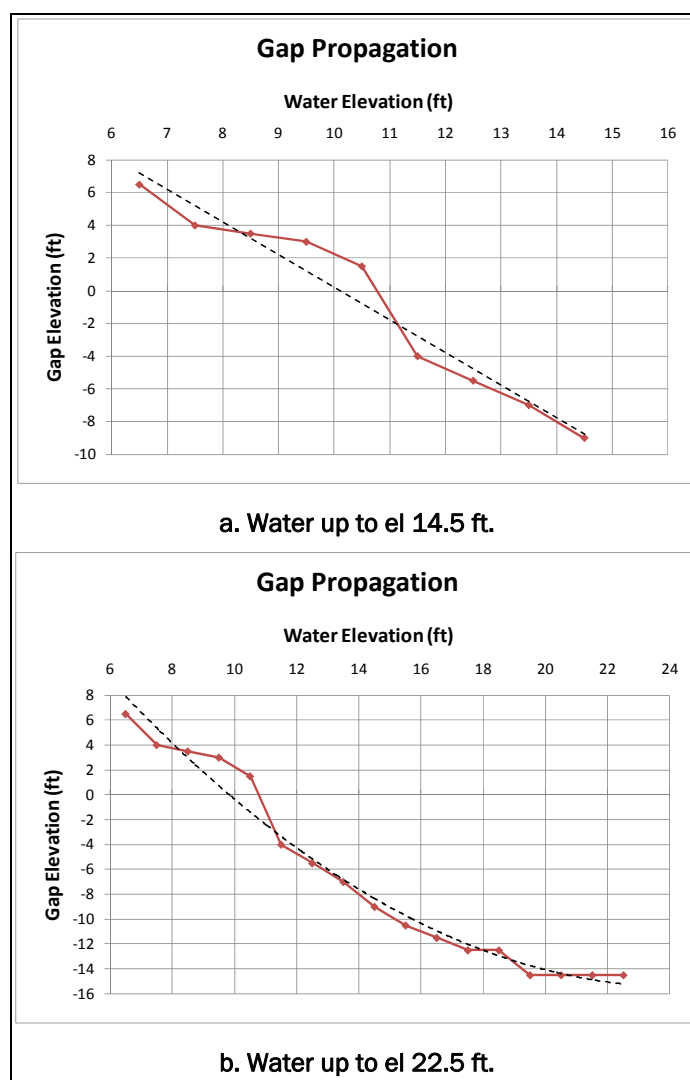


Figure G.1. Progression of gap versus water elevation along flood side of I-wall.

G.5.9 Sheet-pile wall displacements for MC model

Figure G.2 shows the horizontal displacements of the sheet-pile wall for various water elevations. The horizontal displacements at the top of the pile rise with an increasing water elevation as seen from Figure G.2. The rate of increase of the displacement also rises with an increasing water level. For the last water elevation of 22.5 ft, the displacements at the top of the pile increase by a factor of 1.7 for a 1-ft rise in water. From Table G.6, the displacement of the top of the sheet pile for water el 22.5 ft is 62.2 in., while the displacement at the ground surface is 47.2 in.

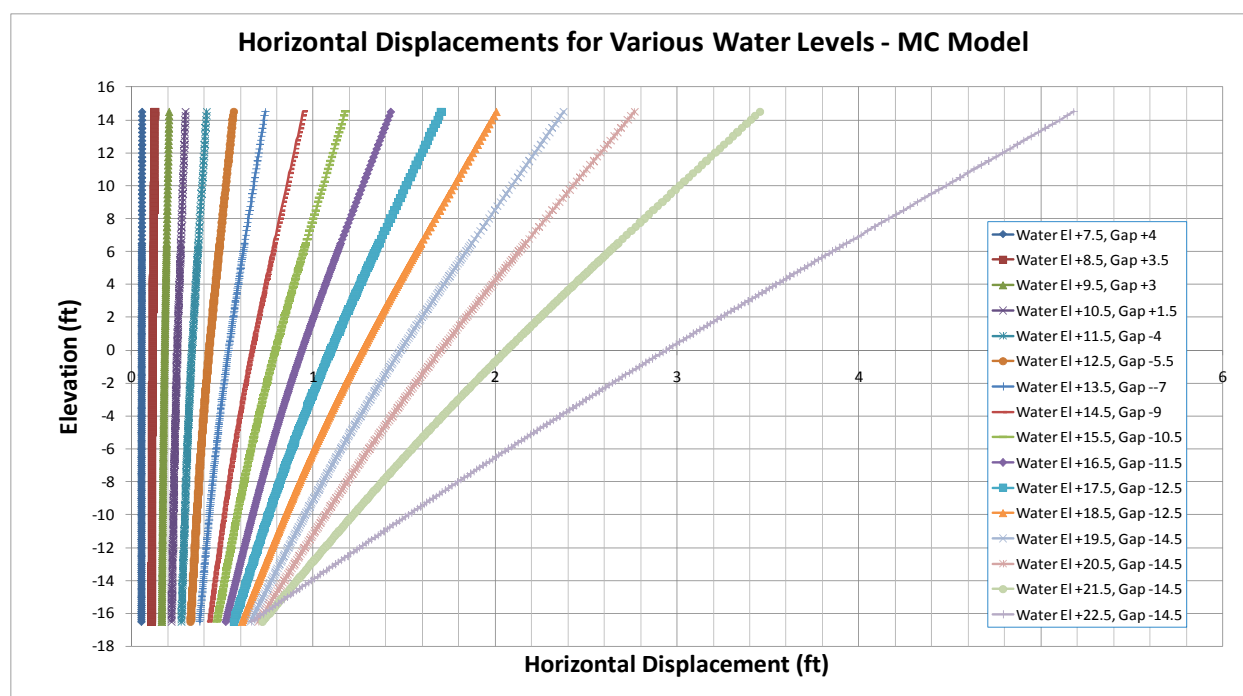


Figure G.2. Sheet-pile horizontal displacements for various water elevations.

Table G.6. Pile displacements for MC model.

Water El	Top of I-Wall, el 14.5		Ground Surface, el 6.5		Tip of Sheetpile, el -16.5		Relative Pile Displacement at Ground Surface, Ground Surface minus Tip Displacement	
ft	ft	in.	ft	in.	ft	in.	ft	in.
6.5	0.0000	0.0000	0.0000	0.0000	0.0000	0.0000	0.0000	0.0000
7.5	0.0600	0.7203	0.0585	0.7019	0.0558	0.6702	0.0026	0.0317
8.5	0.1295	1.5543	0.1233	1.4799	0.1116	1.3387	0.0118	0.1412
9.5	0.2084	2.5012	0.1944	2.3328	0.1671	2.0048	0.0273	0.3280
10.5	0.2987	3.5845	0.2729	3.2749	0.2221	2.6652	0.0508	0.6097
11.5	0.4151	4.9812	0.3693	4.4314	0.2760	3.3119	0.0933	1.1195
12.5	0.5626	6.7508	0.4869	5.8425	0.3269	3.9233	0.1599	1.9193
13.5	0.7369	8.8425	0.6230	7.4762	0.3760	4.5122	0.2470	2.9639
14.5	0.9458	11.3497	0.7835	9.4018	0.4237	5.0842	0.3598	4.3176
15.5	1.1775	14.1295	0.9604	11.5252	0.4710	5.6521	0.4894	5.8731
16.5	1.4246	17.0955	1.1492	13.7901	0.5185	6.2216	0.6307	7.5686
17.5	1.7044	20.4522	1.3621	16.3458	0.5649	6.7792	0.7972	9.5666
18.5	2.0050	24.0603	1.5908	19.0902	0.6098	7.3171	0.9811	11.7731
19.5	2.3769	28.5229	1.8727	22.4730	0.6556	7.8667	1.2172	14.6063
20.5	2.7671	33.2048	2.1677	26.0125	0.7002	8.4021	1.4675	17.6104
21.5	3.4549	41.4585	2.6755	32.1060	0.7211	8.6535	1.9544	23.4526
22.5	5.1824	62.1888	3.9318	47.1814	0.6605	7.9265	3.2712	39.2549

Also as shown in Figure G.2, the displacements of the tip are relatively constant with an increasing water elevation and progressively translate into the landside of the I-wall. The displacements of the tip can be seen to decrease slightly for water el 22.5 ft and to kick back into the flood side. The maximum tip displacement was 8.7 in, at water el 21.5 ft, and the tip moved back into the landside 0.7 in. at water el 22.5 ft.

A Φ/c reduction analysis performed for water el 14.5 ft resulted in a factor of safety of 3.46. A Φ/c reduction analysis performed also for the maximum water elevation of 22.5 ft resulted in a factor of safety of 1.04.

Values of horizontal displacements for the sheet pile at the top, ground surface, and tip are tabulated in Table G.6 and displayed in Figure G.3. As shown in Figure G.3, the pile tip displacements increase by a constant amount until reducing and kicking back into the flood side.

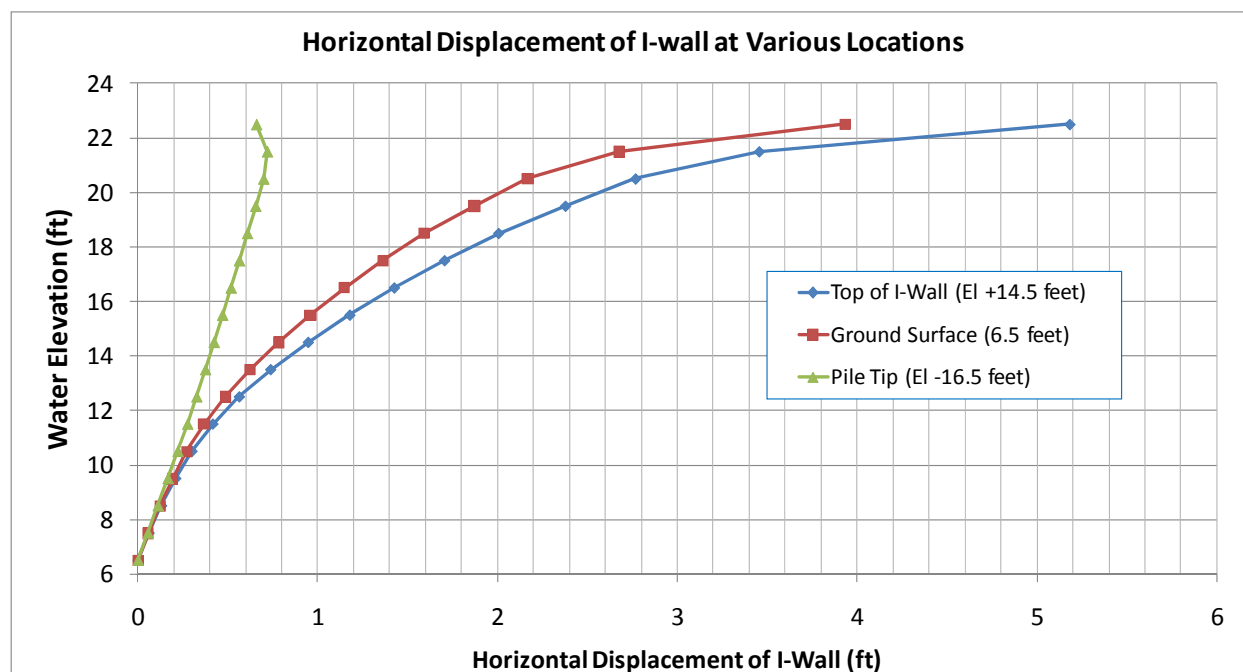


Figure G.3. Sheet-pile horizontal displacements for selected locations.

Figure G.4 shows the relative displacements of the sheet pile at the ground surface, computed as the displacement of the sheet pile at the ground surface minus the displacement of the tip of the sheet pile. There is a 1.7 times increase in relative horizontal displacement at the ground surface for the last 1-ft rise in water.

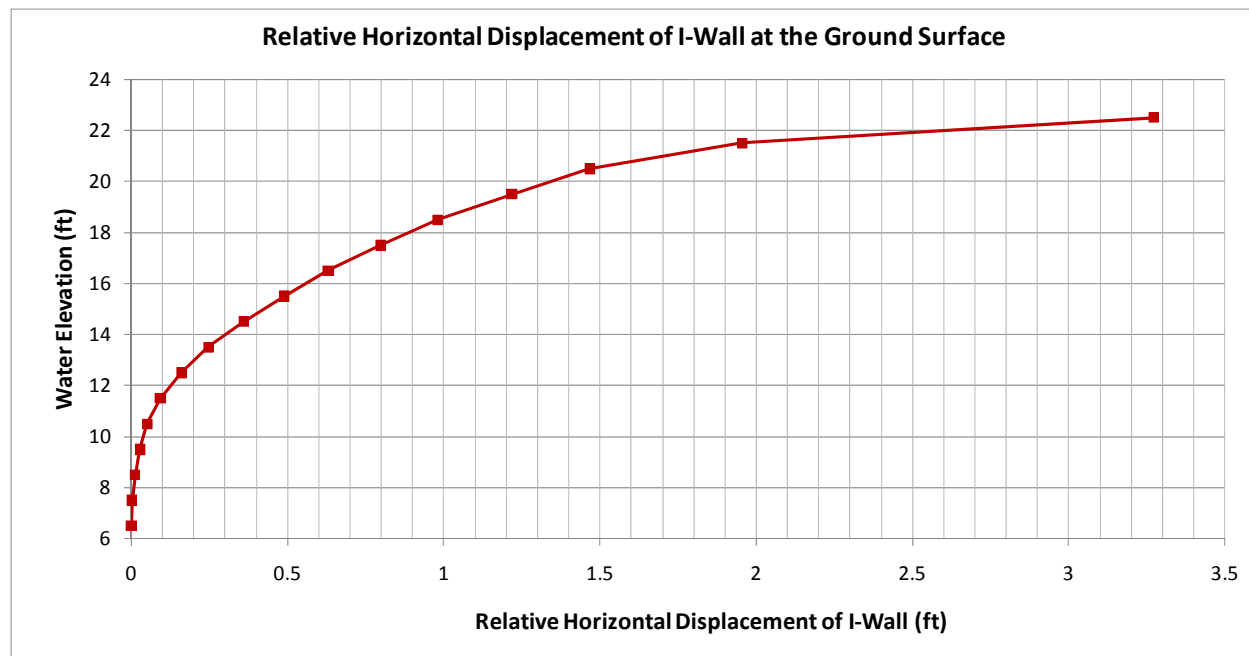


Figure G.4. Relative horizontal displacements of the sheet pile at the ground surface.

G.5.10 Total displacements of finite element mesh for maximum water condition

Figures G.5 and G.6 show the total deflection of the finite element mesh for water el 22.5. The gap at this water height propagated down to el -14.5 ft. There is some settlement on the flood side of the wall and some heave on the landside as shown in Figure G.6.

Figure G.7 shows the total incremental displacements for water el 22.5 ft. The incremental displacements give the movements during the last increment of loading, that is, the last part of the load that completes the total load added to the system. From Figure G.7, for water el 22.5 ft, the soil is moving down on the flood side and up on the landside. Also, at el -15 ft a zone of soil exhibits a rotational behavior consistent with the tip of the sheet pile moving back into the flood side. Figure G.8 shows the total displacements of the system for the applied loads. The displacements are similar to those of Figure G.7 but display more horizontal movement.

G.5.11 Moments in sheet-pile wall for MC model

Figure G.9 compares moments in the sheet pile for various water elevations. The moment increases as the water elevation increases and reaches a maximum at water el 22.5 ft. The moment for water el 14.5 ft is 23,139 ft-lb at el -3.1 ft. The moment at water el 22.5 ft is 60,250 ft-lb at el -3.6 ft.

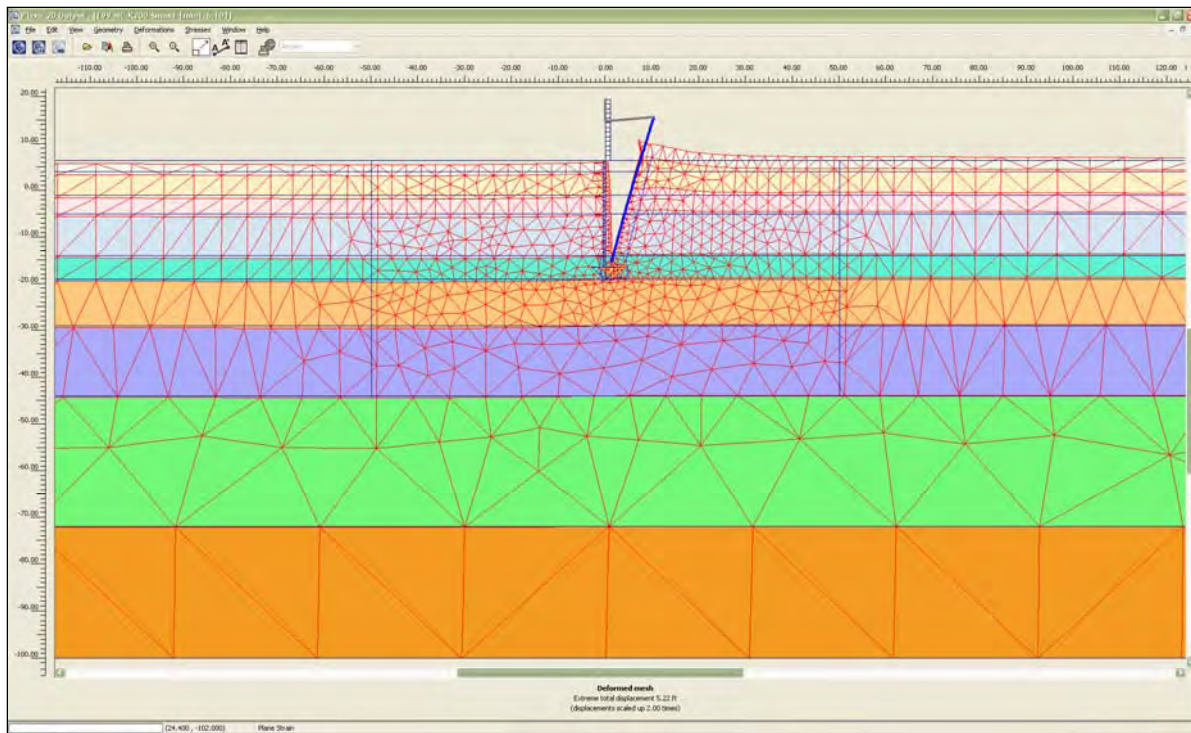


Figure G.5. Total displacements for water el 22.5 ft and gap tip el -14.5 ft.

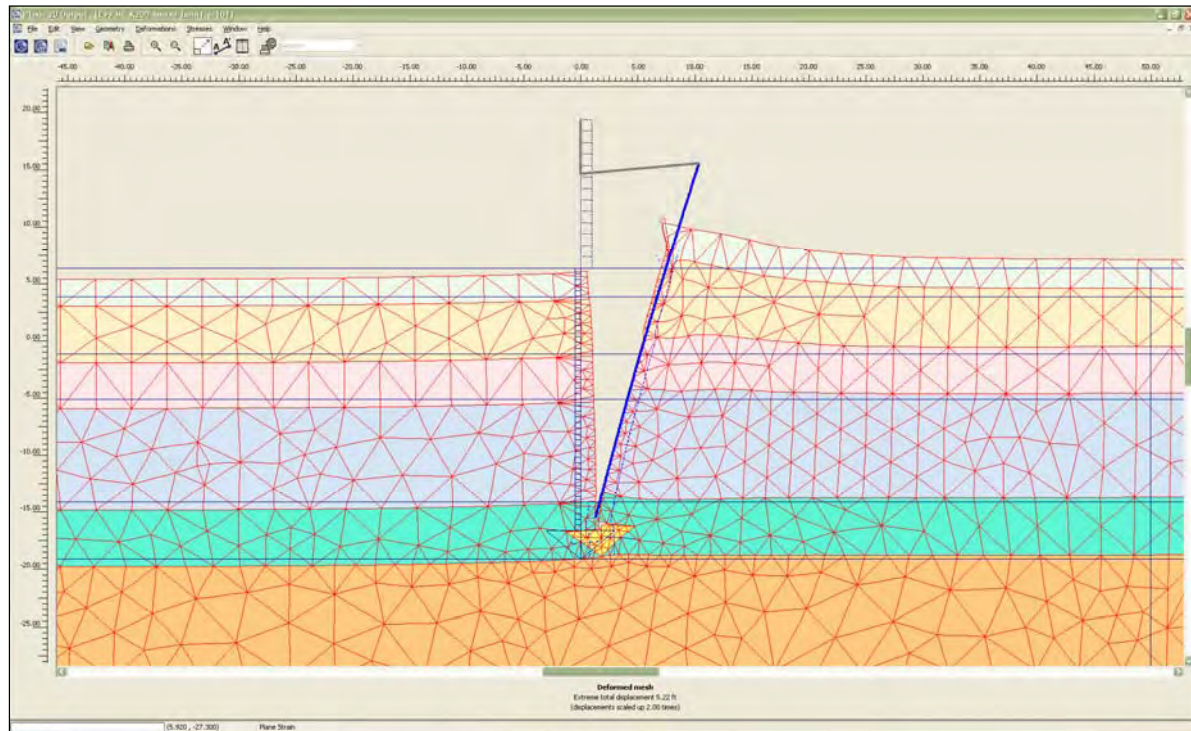


Figure G.6. Enlarged view of total displacements for water el 22.5 ft and gap tip el -14.5 ft.

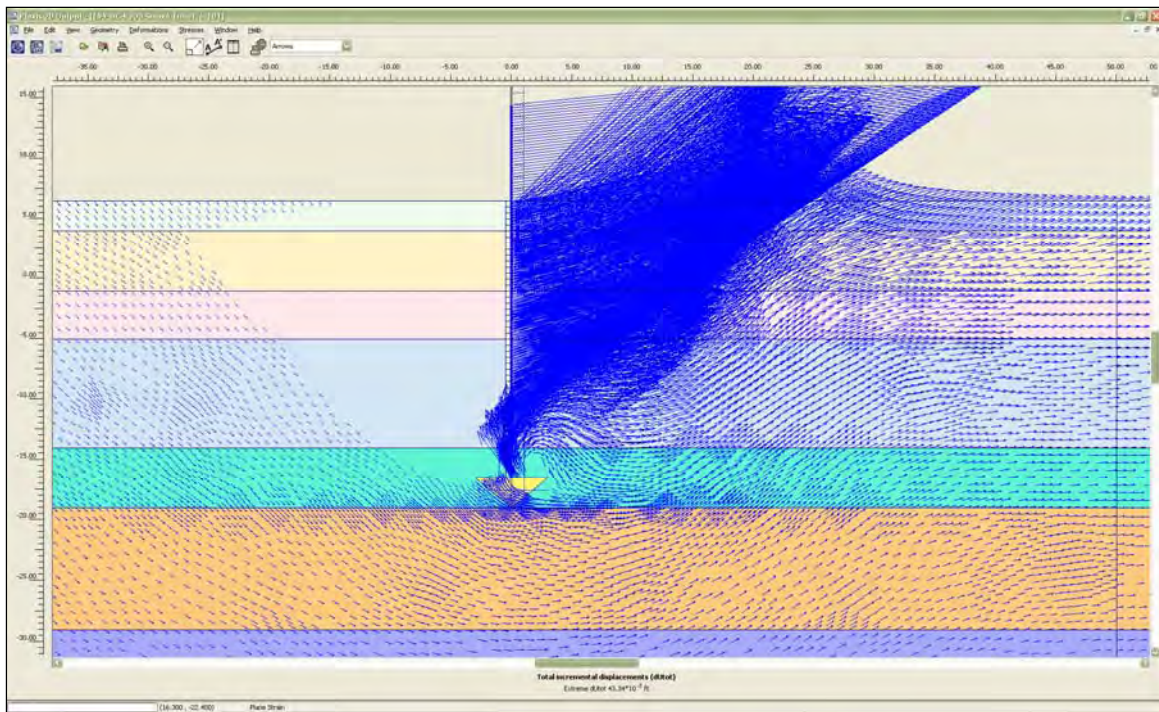


Figure G.7. Vectors of total incremental displacements showing the movement of the soil during the final increment of loading.

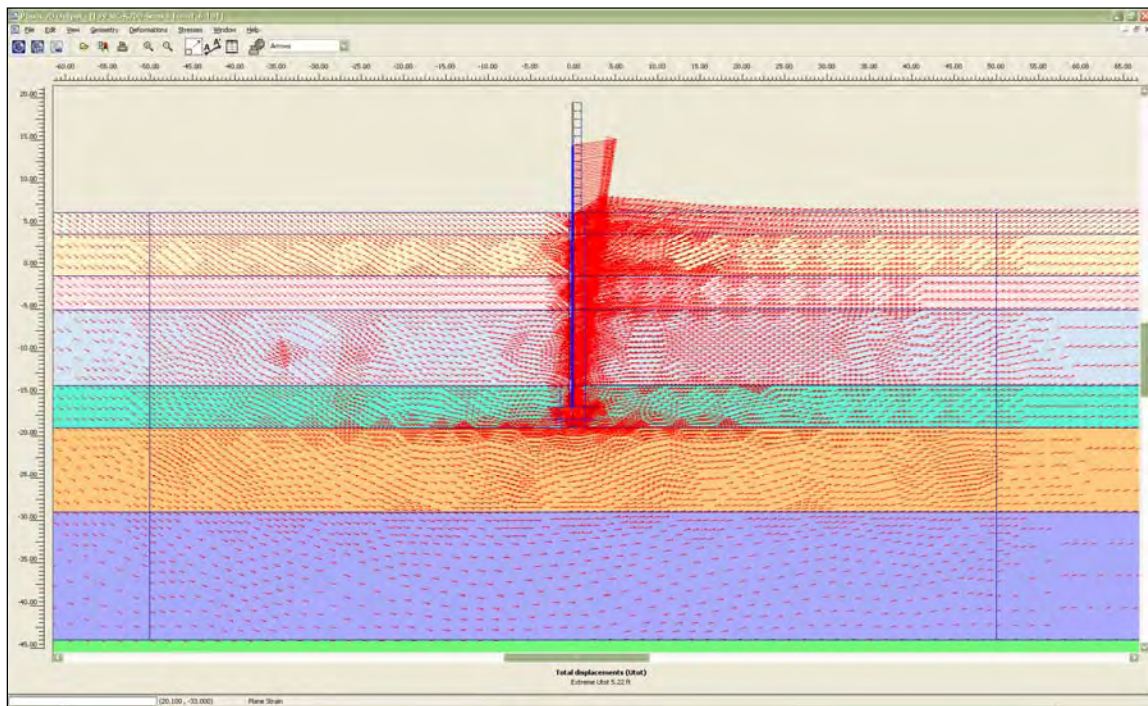


Figure G.8. Vectors of total displacements showing the movement of the soil.

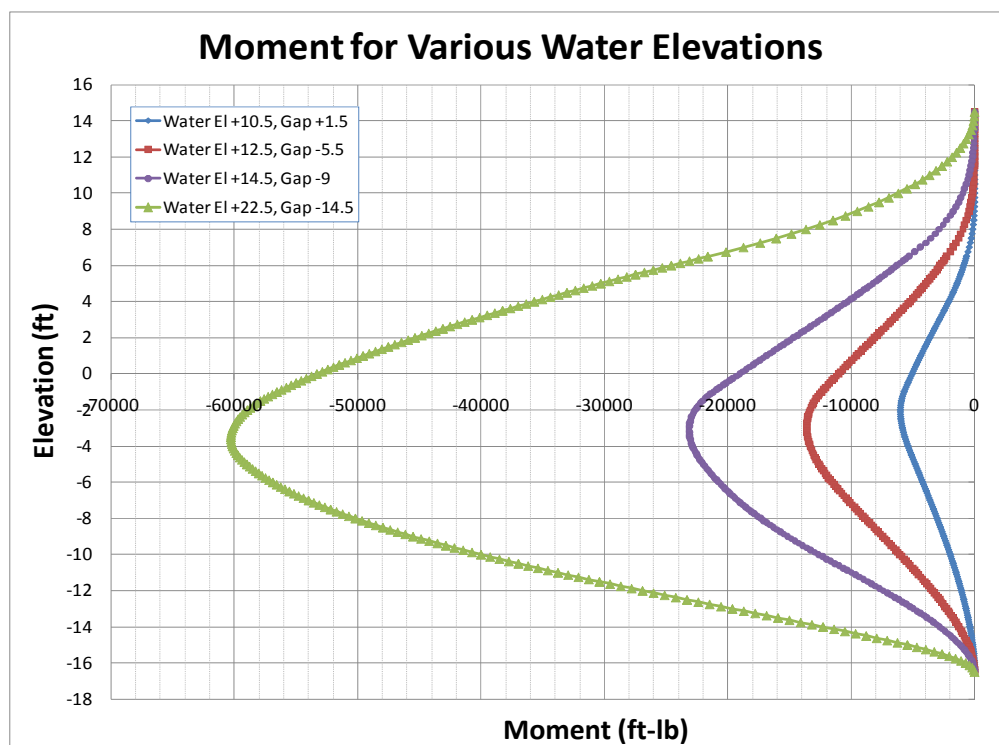


Figure G.9. Comparison of moments at various water elevations.

G.5.12 Shear stresses in soil for MC model

Figures G.10 through G.12 show the relative shear stress in the soil for various water elevations and the associated gap depths. The relative shear stress is a measure of the shear stress in the soil compared to the maximum available shear stress at failure. The shear stress in the soil increases as the water elevation increases. The shear stress increases in the upper unsaturated layer first, then progresses down toward the tip of the pile. The shear stresses are greatest on the landside of the sheet-pile wall and at the bottom of the gap. For water el 22.5 ft, as shown in Figure G.12, the highly stressed region extends almost to the tip of the sheet pile.

G.5.13 Horizontal earth pressures for MC model

For Figures G.13 through G.15, the flood side is on the right side of the figure and the landside is on the left. This corresponds to the input convention CWALSHT uses.

Figures G.13 and G.14 compare the horizontal earth pressures from PLAXIS acting against the sheet-pile wall to the limiting active and passive earth pressures computed using adhesion as discussed in Chapter 3, Section 3.3.2. The value of adhesion used is 80 percent of the cohesion as discussed

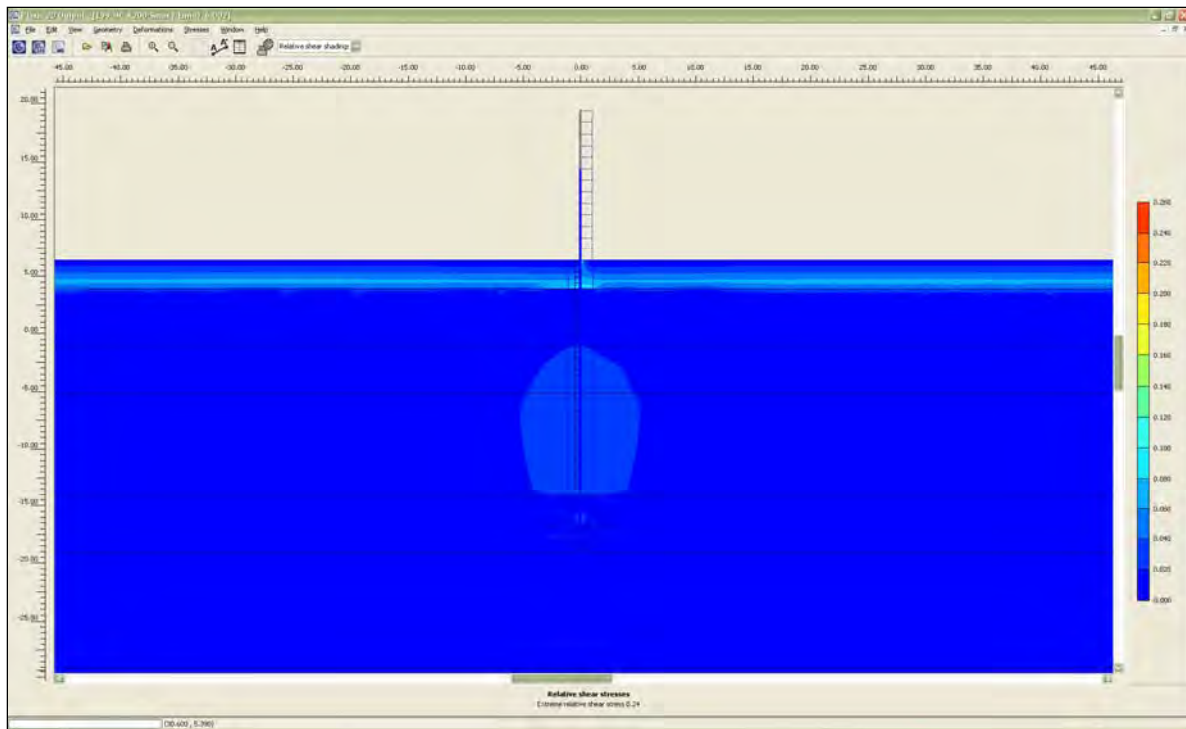


Figure G.10. Relative shear stress after placement of I-wall.

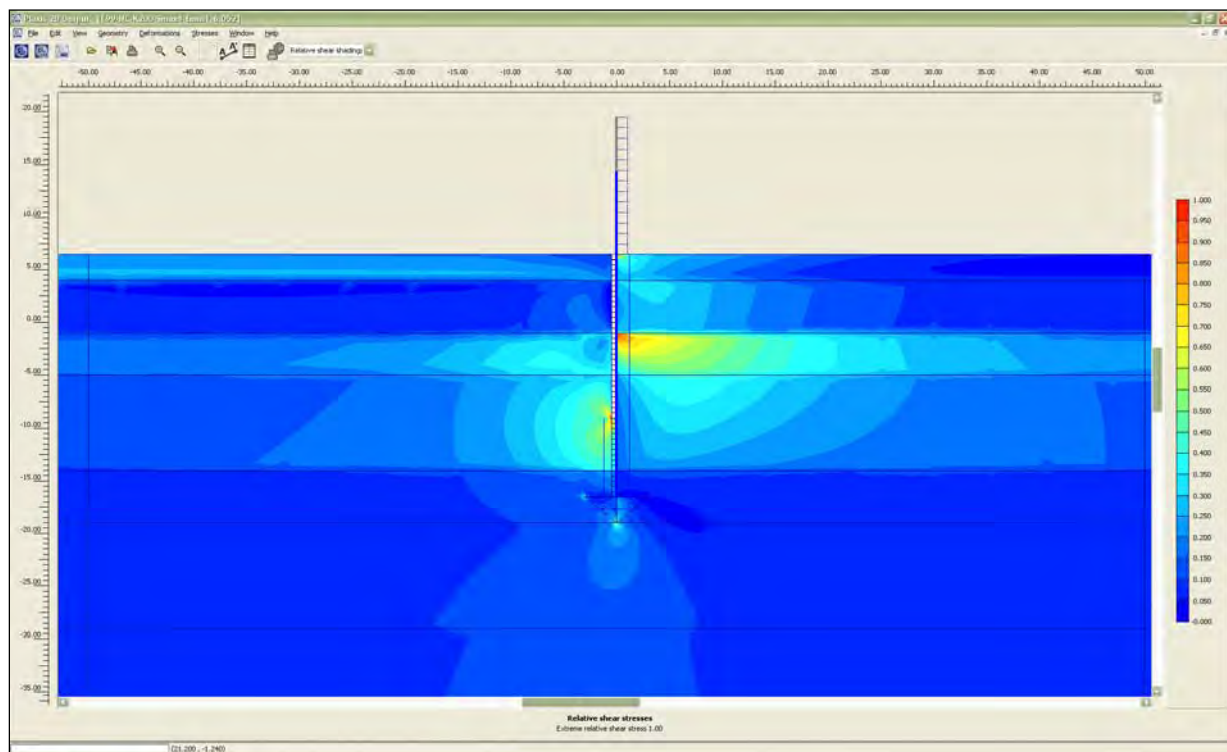


Figure G.11. Relative shear stress for water at el 14.5 ft and gap tip el -9 ft.

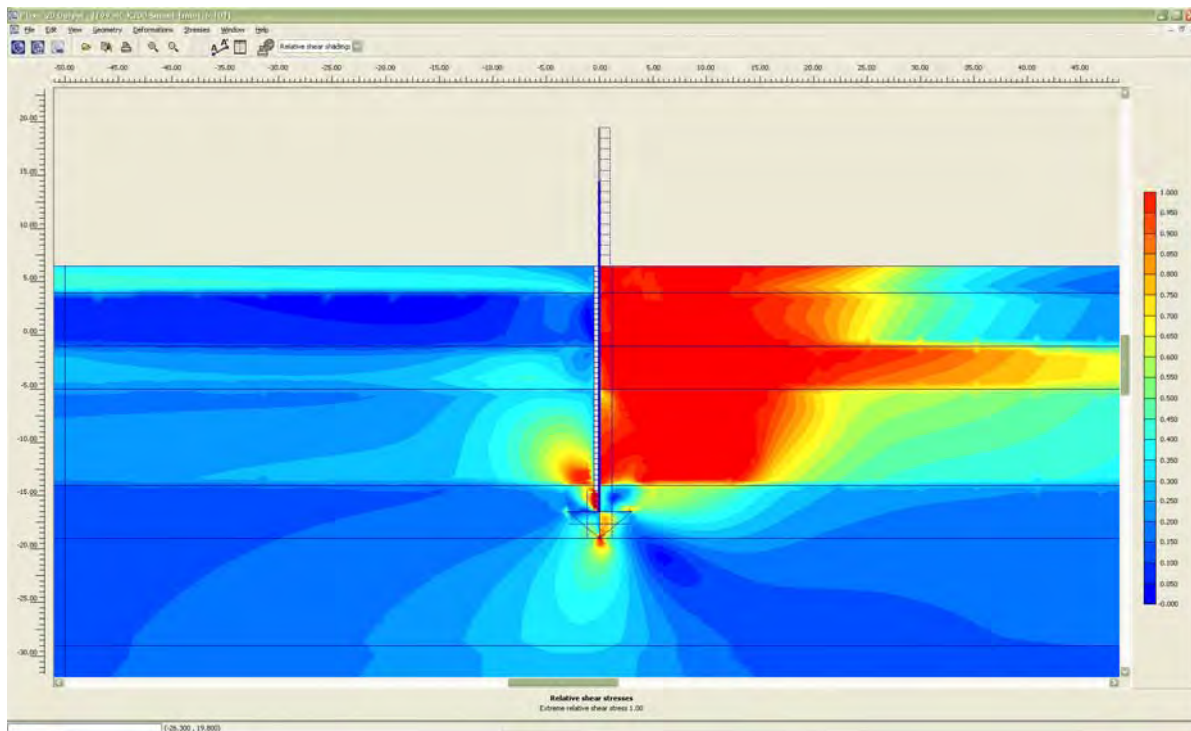


Figure G.12. Relative shear stress for water at el 22.5 ft and gap tip el -14.5 ft.

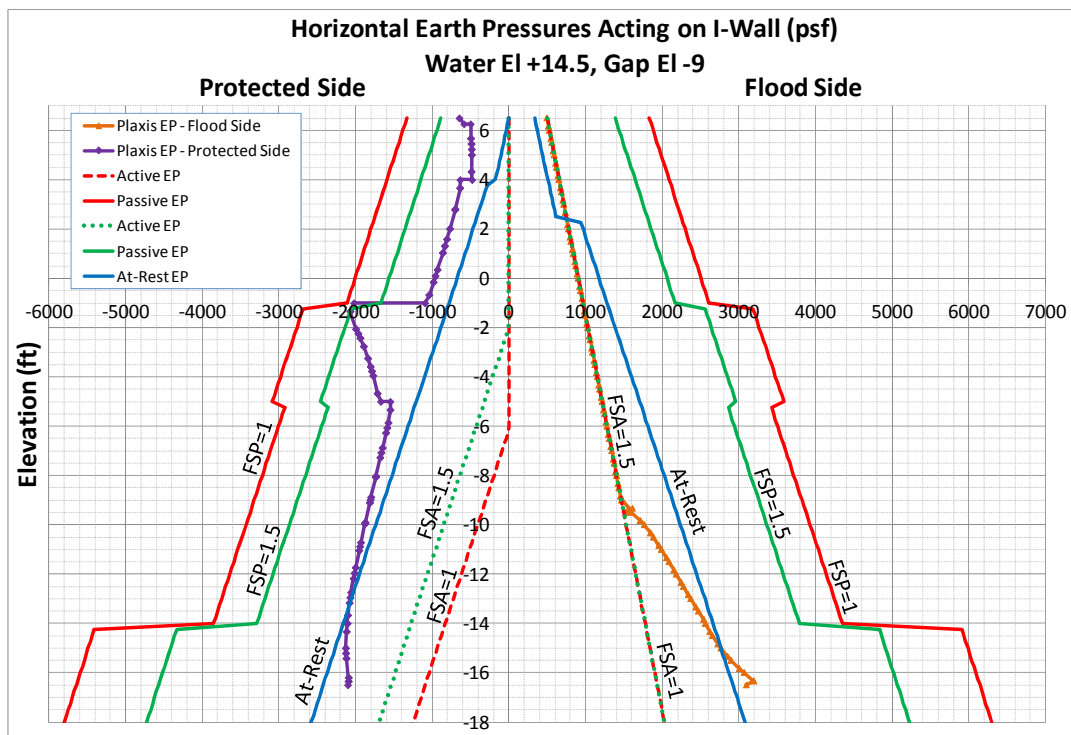


Figure G.13. Horizontal earth pressures for water el 14.5 ft and gap tip el -9 ft.

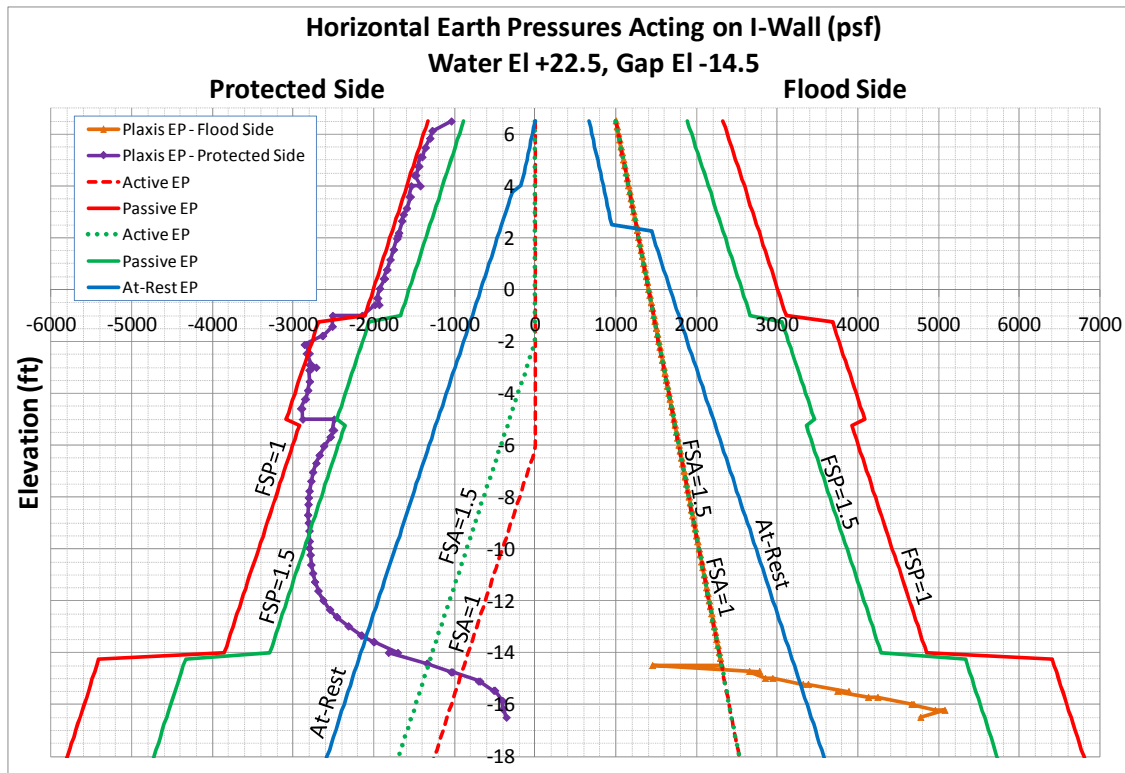


Figure G.14. Horizontal earth pressures for water el 22.5 ft and gap tip el -14.5 ft.

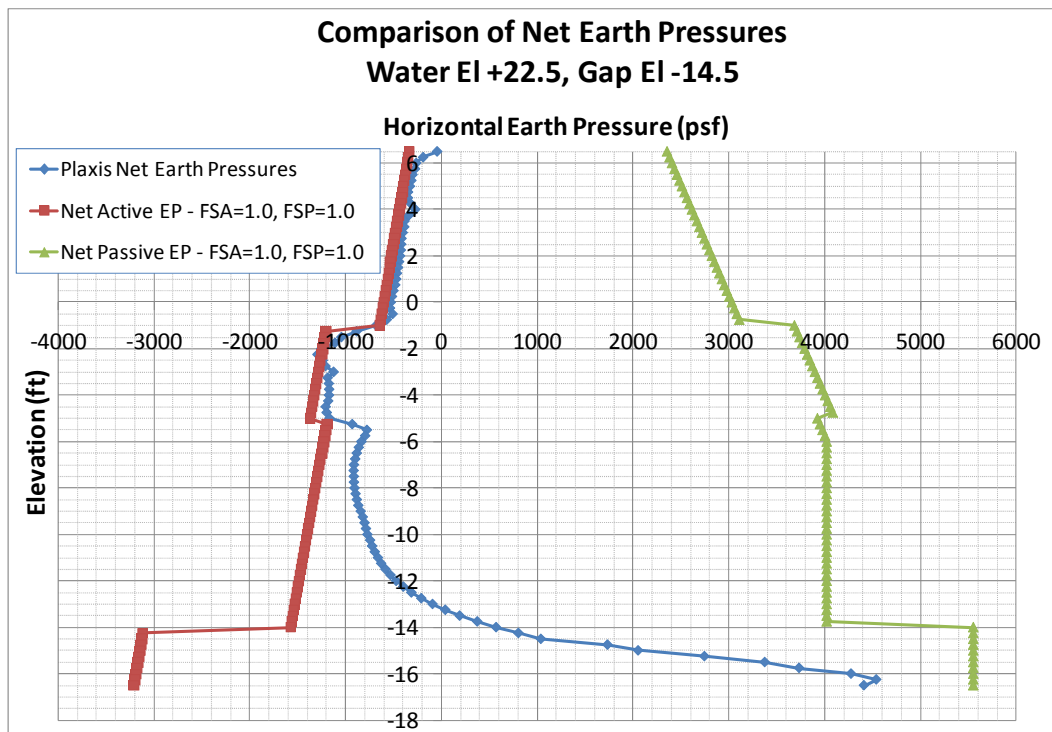


Figure G.15. Comparison of net earth pressures computed from limiting earth pressures and PLAXIS results for water el 22.5 ft.

in Chapter 3, Section 3.3.4. The limiting earth pressures in the figures are computed for factors of safety equal to 1.0 and 1.5. A factor of safety of 1.0 results in full active and passive earth pressures, while a factor of safety of 1.5 results in increased active and decreased passive earth pressures. The results from PLAXIS are compared to the earth pressures computed by CWALSHT using limiting earth pressures computed using two different factors of safety. Comparing the earth pressures in this manner allows a comparison of PLAXIS earth pressures to values computed from conventional design procedures.

Figure G.13 displays the earth pressures for water el 14.5 ft and gap tip el -9 ft. For the flood side, the pressures are equal to hydrostatic pressures down to the bottom of the gap. Below the gap, the pressures are close to at-rest earth pressures computed using the assumed values of K_o given in Table 3.9. On the landside, the earth pressures are close to at-rest for elevations above -1 ft. Below -1 ft, the pressures approach the passive earth pressures computed using a factor of safety of 1.5 and decrease with depth to values close to at-rest pressures.

Figure G.14 displays the earth pressures for water el 22.5 ft. The gap in this case extends to el -14.5 ft. The earth pressures on the flood side are equal to hydrostatic pressures down to the bottom of the gap. Below the gap, the earth pressures are lower than the at-rest condition because the wall has moved away from the soil. The earth pressures increase closer to the tip of the sheet pile to passive pressure values computed using a factor of safety of 1.5. On the landside, above el -5 ft, the earth pressures are almost equal to the fully passive earth pressures computed using a factor of safety of 1.0. Below -5 ft, the pressures decrease with depth and become less than active earth pressures computed using a factor of safety of 1.0.

Figure G.15 compares the net earth pressures computed using limiting earth pressures and the results from PLAXIS for water el 22.5 ft. The limiting earth pressures were computed using a factor of safety of 1.0 for both the active and passive earth pressures for both the flood side and landside of the wall. Net pressures were compared for this water elevation because the movements of the wall were sufficient to produce values of full active and passive earth pressures. As can be seen from the figure, the net earth pressures on the landside compare fairly well to the net active earth pressures. Toward the tip of the pile, the net earth pressures transition from the net active to the net passive earth pressures. The net earth pressures are slightly lower than the net passive pressures.

Appendix H: Analyses of E-99 Sheet-pile Wall Field Load Test Using Maximum Values of Undrained Shear Strength (S_u) and Maximum Values of Undrained Secant Stiffness (E_u)

H.1 Purpose of analyses

This appendix summarizes the results of nonlinear soil-structure interaction (SSI)¹ finite element analyses of the E-99 sheet-pile wall field load test described by Jackson (1988).² The analyses included the formation and propagation of a gap beside the sheet-pile wall on the flood side. The gap affected the resulting deformation and stress conditions of the soil regime on both the flood side and landside of the I-wall. The analyses were part of a parametric study determining the effects of the undrained shear strength (S_u) and undrained secant stiffness (E_u) on the deformation and gap formation characteristics of the system. For the analyses described in this appendix, maximum values of the undrained shear strength and undrained secant stiffness were selected.

The following sections will describe the soil used in the analyses, the selection of stiffness and shear strength parameters, the conventional analysis and design of the I-wall, the procedures employed in the analyses, and the results of the finite element analyses.

H.2 Overview of problem analyzed

The E-99 field load test consisted of a 200-ft section of floodwall constructed on the landside berm of the Item E-99 East Atchafalaya Basin Protection Levee (EABPL) on Avoca Island just south of Morgan City, Louisiana. The test was performed between July and September of 1985 (Jackson 1988).

The soil geometry, maximum water height, and pile geometry of the field load test are shown in Figure 3.1. The sheet pile is located on the landside

¹ Symbols and unusual abbreviations used in this appendix are listed and defined in the Notation, Appendix I.

² Citations in this appendix are in the References at the end of the main text.

of the existing levee. The water loading was applied between the existing levee and the sheet-pile wall. The geometry was idealized as shown in Figure 3.2 and is assumed to be a flat (level) site. The top of the sheet-pile wall was at el 14.5 ft¹, and the tip of the sheet-pile wall was at el -16.5 ft. The elevation of the top soil layer was at 6.5 ft. The I-wall system is described in Chapter 3, Section 3.2.

The soils at the site were clays of high plasticity, designated as CH in the Unified Soil Classification System (USCS). From the classification chart shown in Figure 3.4, the plasticity index of a CH material has a value of 22 and greater. The soil was normally consolidated with liquid limits between 76 and 114 percent and natural water contents between 40 and 80 percent.

For the analyses explained in this chapter, the permeability of the clay layers was assumed to be small enough that the soil would not become fully saturated as the floodwater level was increased. Therefore, as shown in Figure 3.2, two zones of soil were considered in the analyses: a partially saturated one above the water table elevation of 4 ft and a saturated one below the water table.

H.3 Material properties used for parametric analyses

The analyses described in this appendix is one in a set of parametric analyses varying the values of S_u and E_u . The values used for the analyses described in this appendix correspond to the maximum values of S_u and the maximum values of E_u . The material properties used in the analyses described in Chapter 3 are denoted and treated as the mean values. Actually, they are the values used for the design of the I-wall that differ slightly from the mean values computed from laboratory test data.

The undrained shear strengths of the clay layers were determined from unconsolidated undrained (UU) and unconfined compression (UC) tests. These design values, shown in Table 3.1, were used to perform an undrained, short-term design of the wall. The material property values consist of the saturated (γ_{sat}) and moist (γ_{moist}) unit weights of the soil, the undrained shear strength (S_u), and adhesion (c_a). The angle of internal friction (ϕ) and wall friction (δ) were zero because this is an undrained analysis. The same value of the unit weight was used for both saturated

¹ All elevations cited in this appendix are in feet referred to the National Geodetic Vertical Datum (NGVD).

and moist conditions. Adhesion was used in the total stress analysis using values cited in Potyondy (1961) for a cohesive soil against rough steel and is equal to 0.8 times the undrained shear strength ($c_a = 0.8 * S_u$).

The laboratory test data was used to compute mean (μ) and standard deviation (σ) values for the soil layers. These values are shown in Table H.1. The column labeled Plate 9 corresponds to the design values assumed in the E-99 field test report (Jackson 1988). As can be seen from Table H.1, the design values are slightly different from the mean values computed from test data. Design values were used in the finite element analysis discussed in Chapter 3. Mean values shown in Table H.1 were computed based on a limited number of tests, and it was felt that the design values provided a better estimate of the strengths. The coefficients of variation (COV) for the clay layers computed from test data are shown in Table H.1. Because Layer 2 had only two data points, the COV for this layer was deemed to be too low and, therefore, was adjusted to a higher value. The last column in Table H.1 shows the values of the COVs used in this analysis.

Table H.1. Mean and standard deviation values for the clay layers.

Layer	Top El, ft	Bottom El, ft	Plate 9 S_u , psf	Mean μ , psf	Standard Deviation σ , psf	COV, %	COV % for Analyses
1	6.5	-1	200	285	74	37.2	37
2	-1	-5	500	580	50	2.4	10
3	-5	-14	350	362	70	20.2	20
4	-14	-29	500	476	175	34.6	35

Using the COVs for the soil layers listed in Table H.1, σ was computed for each layer. These values for σ were used to compute maximum values of S_u and E_u .

The maximum value of S_u ($S_{u,max}$) was computed as shown in Equation H.1:

$$S_{u,max} = S_{u,mean} + X_{max} \bullet \sigma. \quad (H.1)$$

The variable (X_{max}) in Equation H.1 represents a multiple of the standard deviation. The design values of S_u listed in Table F.1 were used as the $S_{u,mean}$ values. The value of the maximum E_u ($E_{u,max}$) was computed as:

$$E_{u,max} = E_{ref} = K S_{u,max}, \quad (H.2)$$

where E_{ref} is the reference stiffness needed for the Mohr-Coulomb (MC) soil model and K is defined as:

$$K = \frac{E_{u,max}}{S_{u,max}}. \quad (H.3)$$

The value of K in Equation H.3 is taken from a chart developed by Duncan and Buchignani (1976) relating the plasticity index and the overconsolidation ratio (OCR) to the dimensionless factor (K). The same value of K of 200 used in the analysis of Chapter 3 was used for these analyses.

The intent of these analyses was to use the largest values of S_u and E_u possible to ascertain the effects on the gap initiation and propagation and subsequent height of water loading possible while the analyses remained numerically stable. The maximum values of S_u were computed using a multiple of 4 in Equation H.1. This resulted in a maximum value of S_u that was used in Equation H.2 to compute the maximum value of E_u . Equation H.3, with a K value of 200 and the value of $S_{u,max}$, was used to compute the maximum value of E_u . The use of four standard deviations in Equation H.1 was deemed to result in the largest values possible of both S_u and E_u . The maximum values of S_u and E_u computed in this fashion are shown in Table H.2.

Table H.2. Material properties for analyses.

Layer	Elevation			S_u		Design Values		Min Values		Max Values	
								$S_{u,mean}-1.60*\sigma$		$S_{u,mean}+4*\sigma$	
	Top, ft	Bottom, ft	γ_{sat} , pcf	COV, %	σ	Mean (S_u), psf	E_u , psf	S_u , psf	E_u , psf	S_u , psf	E_u , psf
1	6.5	-1	104	37	74	200	40,000	82	16,320	496	99,200
2	-1	-5	107	10	50	500	300,000	420	84,000	700	140,000
3	-5	-14	106	20	70	350	210,000	238	47,600	630	126,000
4	-14	-19	104	35	175	500	300,000	220	44,000	1200	240,000
5	-19	-29	101	35	175	500	300,000	220	44,000	1200	240,000
6	-29	-44	100	35	193	550	330,000	242	48,400	1320	264,000
7	-44	-72	100	35	236	675	405,000	297	59,400	1620	324,000
8	-72	-100	100	35	324	925	555,000	407	81,400	2220	444,000

H.4 Conventional analysis of cantilever I-wall

H.4.1 Criteria for gap initiation and propagation

Two different criteria, one for the flood side and another for the landside, were used to determine whether a gap will initiate in the soil adjacent to the sheet-pile wall and how far the gap will propagate. A hydraulic fracturing criterion was used for the flood side of the I-wall, and a negative horizontal stress criterion was used for the landside of the I-wall. Both of these criteria are discussed in Chapter 3, Section 3.3.3.

H.4.2 Computed gap depth

CWALSHT (U.S. Army Engineer Research and Development Center 2012) uses the negative horizontal stress criteria discussed in Section 3.3.3 to compute whether a gap forms in the soil. Negative computed earth pressures imply that the soil-to-sheet-pile interface is in tension. Because the soil-to-sheet-pile interface cannot sustain a tensile load, the soil is assumed to form a gap, and CWALSHT sets any negative (tensile) earth pressures to zero. CWALSHT applies water pressures within a gap below the input water level. If the gap is above the water level, CWALSHT does not fill the gap with water.

H.4.3 Total stress analysis with CWALSHT

CWALSHT always computes effective stresses based on the input material properties and the level of the water in the soil. For problems involving all clay layers, a total stress (short-term) analysis with $c = S_u$ and $\phi = 0$, where c is cohesion, can be performed with CWALSHT by inputting the actual soil geometry and water levels. This gives a correct total stress analysis because, even though CWALSHT computes effective stresses based on the input water levels, the pore pressures are added to the effective stresses to arrive at total stresses. Because the value of the horizontal earth pressure coefficient is equal to 1.0 for a soil with only cohesion, the total stress computed in this manner is correct. The determination of the depth of the gap also conforms to the hydraulic fracturing criterion described in Section 3.3.3. This is because CWALSHT computes effective stresses and uses to determine the tensile zone. The hydraulic fracturing criterion uses total stresses and compares these to static pore pressures, a process that produces equivalent numerical results. Horizontal earth pressures are computed as described in Section 3.3.2.

H.4.4 CWALSHT analysis results

The elevation of the tip of the sheet pile for this analysis was -16.5 ft. A short-term analysis was performed with CWALSHT using the maximum material properties as given in Table H.2. The analyses performed with CWALSHT are shown in Table H.3.

Table H.3. Results of analysis computations using CWALSHT.

Analysis Case		S_u , psf	Adhesion, psf	Water El, ft	El of Bottom of Gap, ft	Elevation of Tip of Sheet Pile		
						FS_{Active}	$FS_{Passive}$	El, ft
1	Short-term with water levels	Max values	0	14.5	Below wall	1	2.78	-16.5
2	Short-term with water levels	Max values	$0.8 \cdot S_u$	14.5	Below wall	1	3.68	-16.5
3	Short-term with water levels	Max values	0	22.5	Below wall	1	0.68	-16.5
4	Short-term with water levels	Max values	$0.8 \cdot S_u$	22.5	Below wall	1	0.91	-16.5

For Cases 1 through 4, the factor of safety applied to the active earth pressures (FS_{Active}) was 1.0, while the factor of safety applied to the passive earth pressures ($FS_{Passive}$) varied. Cases 1 through 4 were modeled with the actual soil layer geometry with input water levels as described in Section H.4.3. Cases 1 and 2 used water el 14.5, which was the elevation of the top of the wall. Case 1 did not include adhesion and resulted in a factor of safety on the passive earth pressures ($FS_{Passive}$) equal to 2.78. The gap extended below the tip of the sheet pile. Case 2 did include adhesion and resulted in an $FS_{Passive}$ of 3.68. The gap in this case also extended below the tip of the sheet pile. Cases 3 and 4 were for water el 22.5 ft (8 ft above the top of the wall). Case 3 did not include adhesion and resulted in an $FS_{Passive}$ of 0.68. The gap extended below the tip of the sheet pile. Case 4 did include adhesion and resulted in an $FS_{Passive}$ of 0.91. The gap also extended below the tip of the sheet pile.

H.5 PLAXIS finite element analyses

H.5.1 Conceptual model

The finite element analyses were performed with PLAXIS, a two-dimensional (2-D) nonlinear incremental construction finite element

program (PLAXIS 2012). The conceptual model of the finite element mesh is shown in Figure 3.7. The geometry is the same as explained previously, but several modeling features should be noted. The sheet-pile wall was represented by plate elements. Interface elements were placed on both sides of the plate elements from the ground surface down to the tip of the sheet pile. To alleviate stress concentrations at the corners of the geometry, both horizontal and vertical extensions of the interface elements were provided at the tip of the sheet-pile wall at el -16.5 ft. A plate element extension and dummy soil elements were added above the wall to provide for additional loading height if needed. The mesh was structured to provide node points at 1-ft raises of the water table. The soil elements beside the sheet-pile wall on the flood side were 0.5 ft in height. This enabled the inputting of 1-ft raises in water and modeling of the gap to within 0.5 ft.

H.5.2 Finite element mesh

The finite element mesh used in the analyses is shown in Figures 3.8 and 3.9. The mesh is composed of 2,396 elements and 19,917 nodes, with 28,752 stress points. The type and number of elements used in the mesh are shown in Table 3.3. The mesh consists of 15-node triangular elements to model the soil, 5-node plate elements to model the sheet-pile wall, and 5-node interface elements to model the soil-structure interaction effects between the sheet-pile wall and the adjacent soil elements. The problem was run as a plane strain problem.

H.5.3 Total stress analysis procedure in PLAXIS

The E-99 field test was analyzed using total unit weights of the soil and boundary water pressures to perform a short-term (undrained) analysis using PLAXIS. All materials were designated as drained, which in PLAXIS terminology means that no excess pore-water pressures will be generated because of applied loads. The general phreatic surface was used in PLAXIS to apply the boundary water pressures on the soil surface and within the gap. All soil layers were associated with a cluster phreatic surface that was input below the minimum elevation of the mesh. Because the water surface was below all soil layers, no internal water pressures were generated within the soil layers. This procedure results in a total stress analysis with the computed effective stresses being equal to the total stresses (i.e., no internal pore pressures are present).

It was assumed that the permeability of the soil was small enough that any time-dependent effects such as seepage could be ignored and that the undrained shear strengths could be used to determine the behavior of the system.

H.5.4 Tracking the progression of the gap

The I-wall deflects as the flood loading increases, and eventually a gap forms beside the I-wall on the flood side of the wall. The gap begins at the ground surface and progresses downward as shown in Figure 3.10. The gap along the flood side of the I-wall-to-soil interface is modeled by deactivating soil clusters (elements), effectively creating a void beside the wall. As water pressures are applied within this void, the gap progresses downward. Modeling of the flood loading commenced in the finite element analysis after the total initial stress state was computed based on an assumed steady-state water elevation of 4 ft. The flood loading was applied in 1-ft incremental raises of the water level in order to track the formation and propagation of the gap.

The criterion used to estimate the formation and propagation of the gap is based on the hydraulic fracturing concept discussed in Chapter 3, Section 3.3.3. The procedure used to estimate the gap depth:

1. For each rise in water level, the total horizontal stresses against the sheet-pile wall are compared against the hydrostatic water pressures acting on the wall given the current water elevation. A gap is formed when the horizontal earth pressure is less than the water pressure at a given depth.
2. Soil elements are deactivated within the computed region of the gap, and hydrostatic water pressures are applied within the deactivated elements.
3. The analysis is rerun for the current water level, and Steps 1 and 2 are repeated until the depth of the gap ceases to increase.
4. The water level is increased, and Steps 1 through 3 are repeated. The water level is raised until instability in the analyses is encountered.

H.5.5 Shear strength and stiffness properties used in the finite element analyses

The finite element analyses described in this appendix were performed using the PLAXIS finite element program. The MC soil model was used for the soil elements. This model uses an elastic-perfectly plastic stress-strain relationship. Elastic plate elements were used to model the steel sheet pile,

and interface elements were used to capture the soil-structure interaction effects between the sheet-pile wall and the soil. PLAXIS can perform analyses using either effective or total stress soil parameters. For the analyses described herein, total stress soil parameters were used.

Figure 3.11 shows the material numbering and soil layering used in the finite element analyses. The soil was divided into layers below the tip of the pile to provide for an increasing undrained shear strength and stiffness below the elevation of the pile tip. See Section 3.4.5 for discussion of the properties assumed for the soil, pile, and interface elements.

The undrained shear strength (S_u) and undrained reference stiffness (E_{ref}) of the clay layers used in this parametric analysis are computed as described in Section H.3 and shown in Table H.4. The remaining material property values consist of the saturated (γ_{sat}) and moist (γ_{moist}) unit weights of the soil, angle of internal friction (ϕ), dilation angle (Ψ), unload/reload Poisson's ratio (ν), and the interface strength ($R_{interface}$).

Table H.4. Strength and stiffness properties for the soil layers used in the MC soil model for the case of a maximum (S_u) and (E_{ref}).

Material Number	Material Description	γ_{moist} , lb/ft ³	γ_{sat} , lb/ft ³	S_u , lb/ft ²	E_{ref} , lb/ft ²	ν	$R_{interface}$
1	Clay\1_6.5_200_Rinit=0.8	104	104	496	99200	0.4	0.8
2	Clay\2_4_200_Rinit=0.8	104	104	496	99200	0.495	0.8
3	Clay\3_1_500_Rinit=0.8	107	107	700	140000	0.495	0.8
4	Clay\4_5_350_Rint=0.8	106	106	630	126000	0.495	0.8
5	Clay\5_-14_500_Rinit=0.8	104	104	1200	240000	0.495	0.8
6	Clay\5a_-14_500_Rinit=1.0	104	104	1200	240000	0.495	1
7	Clay\6_-19_500_Rinit=0.8	101	101	1200	240000	0.495	0.8
8	Clay\7_-29_550_Rinit=0.8	100	100	1320	264000	0.495	0.8
9	Clay\8_-44_675_Rinit=0.8	100	100	1620	324000	0.495	0.8
10	Clay\9_-72_925_Rinit=0.8	100	100	2220	444000	0.495	0.8

Note: properties are given for drained material, with the angle of internal friction for the soil (ϕ) and the dilation angle (Ψ) set to 0, as this is a total stress analysis.

The $R_{interface}$ value is from values cited by Potyondy (1961) as discussed in Chapter 3, Section 3.3.4. This controls the amount of adhesion along the soil-to-I-wall interface. Material 6 in Table H.4 has an $R_{interface}$ value of 1.0 because this material represents a soil-to-soil interface.

H.5.6 Initial stresses

The initial total stress state within the finite element mesh was established using the at-rest soil conditions for a level ground surface. Horizontal at-rest soil stresses were estimated using the relationship between the at-rest earth pressure coefficient (K_o) and the soil's Poisson's ratio (ν) given in Equation 3.14

The assumed groundwater elevation was at 4 ft. Table 3.9 shows a summary of the K_o values used to compute the horizontal earth pressures for the initial conditions. The Poisson's ratio for the partially saturated soil layer was 0.4, which corresponds to a K_o of 0.67. This value is less than the value for a fully saturated material, which has a K_o of 1.0.

H.5.7 Performance of interface elements

The performance of the interface elements was examined to determine if the normal stresses in the interface elements corresponded closely to the normal stresses in the adjacent soil elements. As discussed in Chapter 3, Section 3.4.7, and shown in Figure 3.14, the stresses within the interface elements agreed very closely with the stresses in the adjacent soil elements, and the processing of results could be done using either data set. The results presented in this appendix use the stresses extracted from the soil elements adjacent to the sheet-pile wall.

H.5.8 Progression of gap propagation for MC analyses

Figure H.1 shows the progression of the gap as the water level against the I-wall is increased from 1 ft (el 7.5 ft) up to 16 ft (el 22.5 ft). The gap initiates at water el 7.5 ft and extends to a depth of 4 ft. The gap propagation essentially follows a linear path, with the gap depth increasing as the water elevation increases up to el 14.5 ft. The black dotted line in Figure H.1 is a cubic fit to the gap depths at the various water elevations but is essentially linear up to water el 14.5 ft. The depth of the gap extends to el -7 ft at water el 14.5 ft. Recall that the tip of the sheet pile is at el -16.5 ft. The gap extends to a depth of -15 ft at water el 22.5 ft as shown in Figure H.1. The rate of the gap depth decreases for water elevations above 14.5 ft and follows the cubic fit as shown by the black dotted line in Figure H.1.

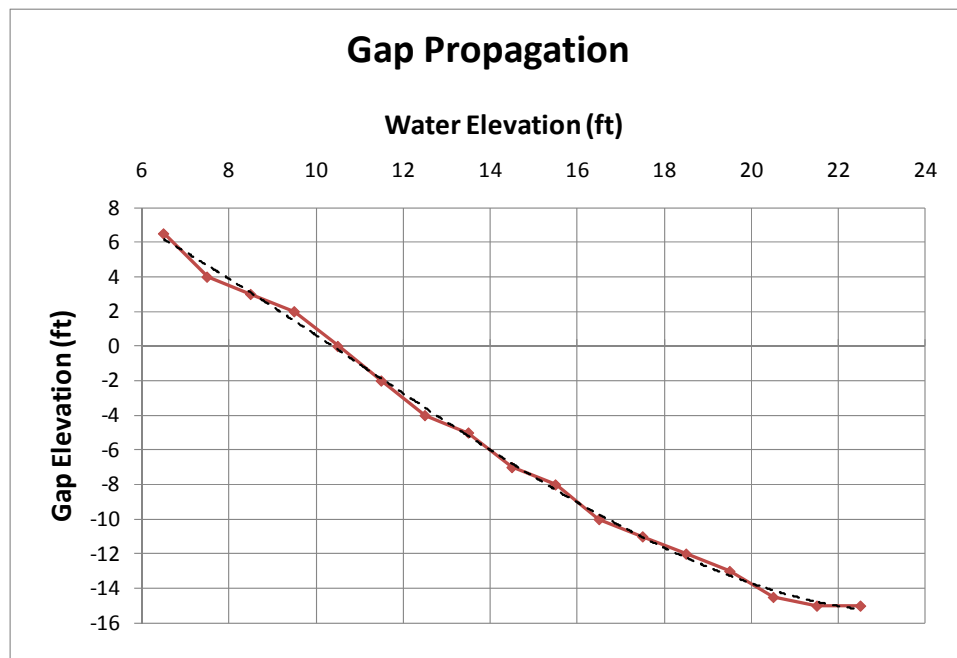


Figure H.1. Progression of gap versus water elevation along flood side of I-wall.

H.5.9 Sheet-pile wall displacements for MC model

Figure H.2 shows the horizontal displacements of the sheet-pile wall for various water elevations. The horizontal displacements at the top of the pile increase with rising water elevation as seen from Figure H.2. The rate of increase of the displacement also increases with an increasing water level. For the last water elevation of 22.5 ft, the displacements at the top of the pile increase by a factor of 1.5 for a 1-ft rise in water. From Table H.5, the displacement of the top of the sheet pile for water el 22.5 ft is 19.2 in., while the displacement at the ground surface is 13.6 in.

Also as shown in Figure H.2, the displacements of the tip are relatively constant with an increasing water elevation and progressively translate into the landside of the I-wall. The displacements of the tip can be seen to decrease slightly for water el 22.5 ft and to kick back into the flood side. The maximum tip displacement was 1.7 in. at water el 21.5 ft, and the tip moved back into the landside 0.28 in. at water el 22.5 ft.

A Phi/c reduction analysis performed for water el 14.5 ft resulted in a factor of safety of 3.48. A Phi/c reduction analysis also performed for the maximum water el 22.5 ft resulted in a factor of safety of 1.03.

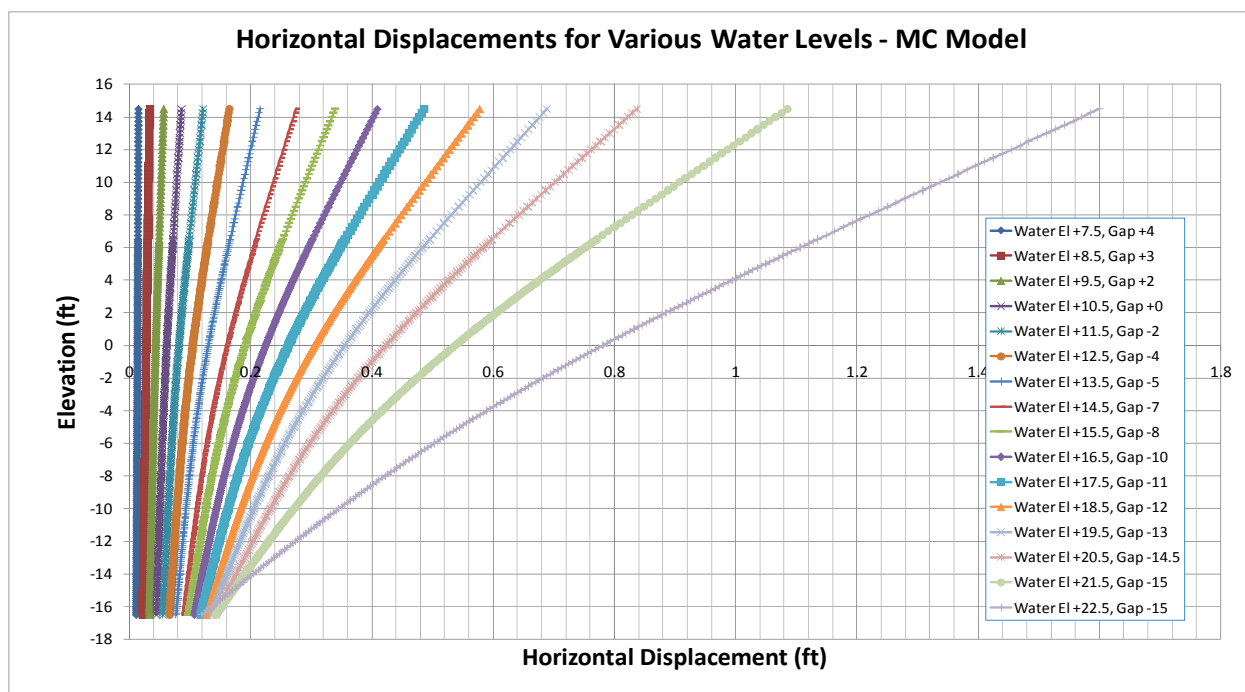


Figure H.2. Sheet-pile horizontal displacements for various water elevations.

Table H.5. Pile displacements for MC model.

Water Elevation	Top of I-Wall, el 14.5 ft		Ground Surface, el 6.5 ft		Tip of Sheet Pile, el -16.5 ft		Relative Pile Displacement at Ground Surface, Ground Surface Minus Tip Displacement	
ft	ft	in.	ft	in.	ft	in.	ft	in.
7.5	0.0149	0.1790	0.0141	0.1690	0.0112	0.1346	0.0029	0.0344
8.5	0.0338	0.4061	0.0306	0.3668	0.0225	0.2694	0.0081	0.0974
9.5	0.0572	0.6861	0.0497	0.5963	0.0337	0.4041	0.0160	0.1922
10.5	0.0862	1.0343	0.0722	0.8670	0.0448	0.5377	0.0274	0.3293
11.5	0.1219	1.4623	0.0989	1.1871	0.0558	0.6698	0.0431	0.5173
12.5	0.1650	1.9805	0.1304	1.5645	0.0666	0.7997	0.0637	0.7648
13.5	0.2155	2.5864	0.1664	1.9966	0.0772	0.9263	0.0892	1.0703
14.5	0.2747	3.2963	0.2080	2.4959	0.0876	1.0512	0.1204	1.4447
15.5	0.3393	4.0718	0.2531	3.0373	0.0978	1.1730	0.1554	1.8642
16.5	0.4098	4.9176	0.3025	3.6299	0.1080	1.2956	0.1945	2.3343
17.5	0.4867	5.8403	0.3561	4.2729	0.1179	1.4143	0.2382	2.8586
18.5	0.5777	6.9329	0.4190	5.0283	0.1272	1.5268	0.2918	3.5014
19.5	0.6890	8.2684	0.4956	5.9473	0.1357	1.6287	0.3599	4.3187
20.5	0.8373	10.0478	0.5981	7.1775	0.1432	1.7181	0.4550	5.4594
21.5	1.0858	13.0292	0.7710	9.2522	0.1428	1.7139	0.6282	7.5383
22.5	1.6005	19.2054	1.1348	13.6181	0.1194	1.4326	1.0155	12.1854

Values of horizontal displacements for the sheet pile at the top, ground surface, and tip are tabulated in Table H.5 and displayed in Figure H.3. As shown in Figure H.3, the pile tip displacements increase by a constant amount until reducing and kicking back into the flood side. Figure H.4 shows the relative displacement of the sheet pile at the ground surface, which is computed as the displacement of the sheet pile at the ground surface minus the displacement of the tip of the sheet pile. There is a 1.5 times increase in relative horizontal displacement at the ground surface for the last 1-ft rise in water.

H.5.10 Total displacements of finite element mesh for maximum water condition

Figures H.5 and H.6 show the total deflection of the finite element mesh for water el 22.5 ft. The gap at this water height propagated down to el -14.5 ft. Figure H.6 shows some settlement on the flood side of the wall and some heave on the landside.

Figure H.7 shows the total incremental displacements for water el 22.5 ft. The incremental displacements give the movements during the last increment of loading; that is, the last part of the load that completes the total load added to the system. From Figure H.7, for water el 22.5 ft, the soil is moving downward on the flood side and upward on the landside. Also, a zone of soil at el -15 ft exhibits a rotational behavior consistent with the tip of the sheet pile moving back into the flood side. Figure H.8 shows the total displacements of the system for the applied loads. The displacements are similar to those in Figure H.7 but display more horizontal movement.

H.5.11 Moments in sheet-pile wall for MC model

Moments in the sheet pile for various water elevations are compared in Figure H.9. The moment increases as the water elevation increases and reaches a maximum at water el 22.5 ft. The maximum moment for water el 14.5 ft is 12,942 ft-lb at el -2.25 ft. The maximum moment at water el 22.5 ft is 60,007 ft-lb at el -3.5 ft.

H.5.12 Shear stresses in soil for MC model

Figures H.10 through H.12 show the relative shear stress in the soil for various water elevations and the associated gap depths. The relative shear stress is a measure of the shear stress in the soil compared to the maximum

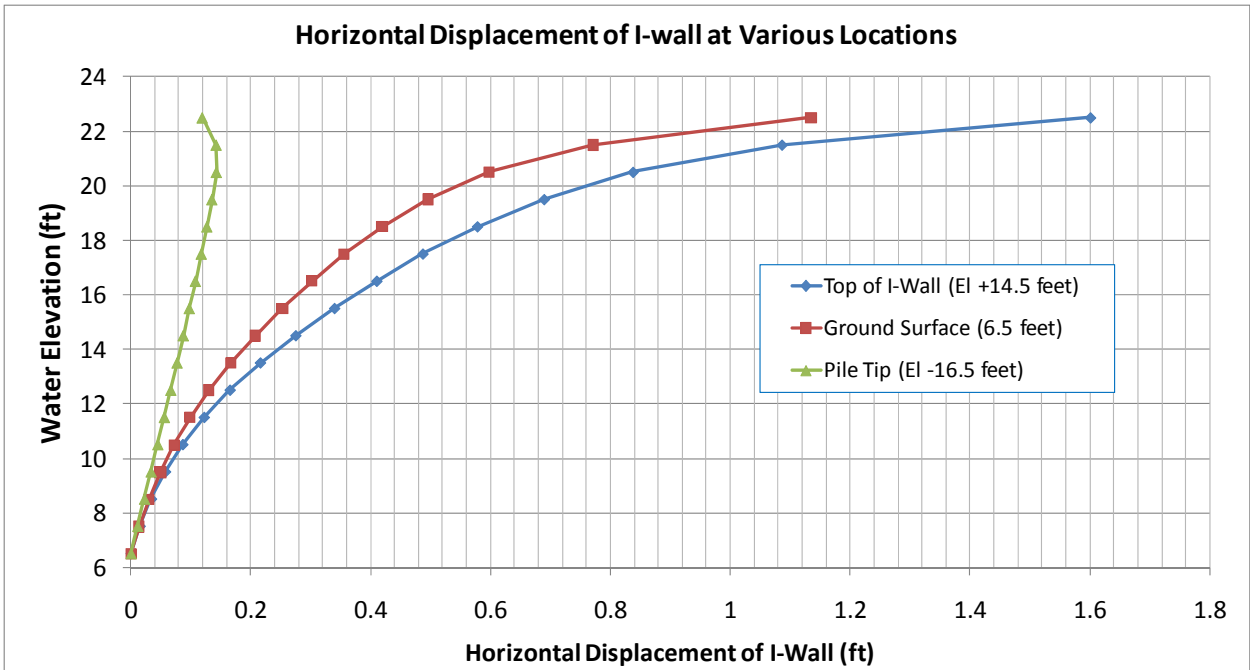


Figure H.3. Sheet-pile horizontal displacements for selected locations.

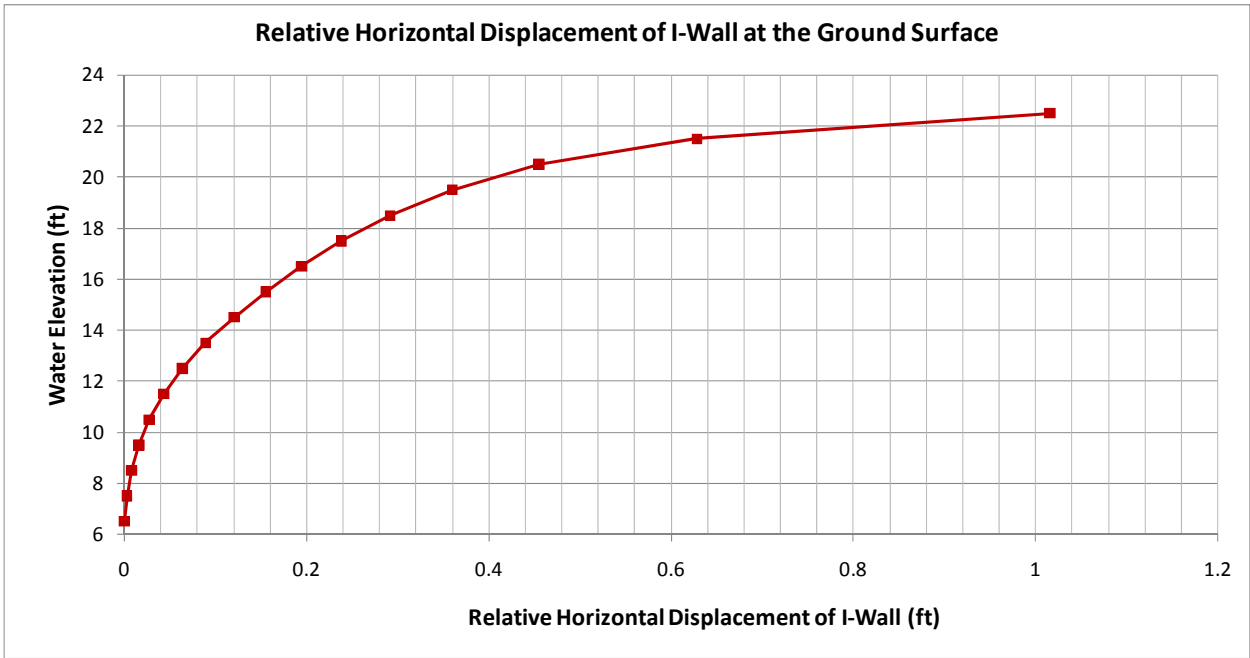


Figure H.4. Relative horizontal displacements of the sheet pile at the ground surface.

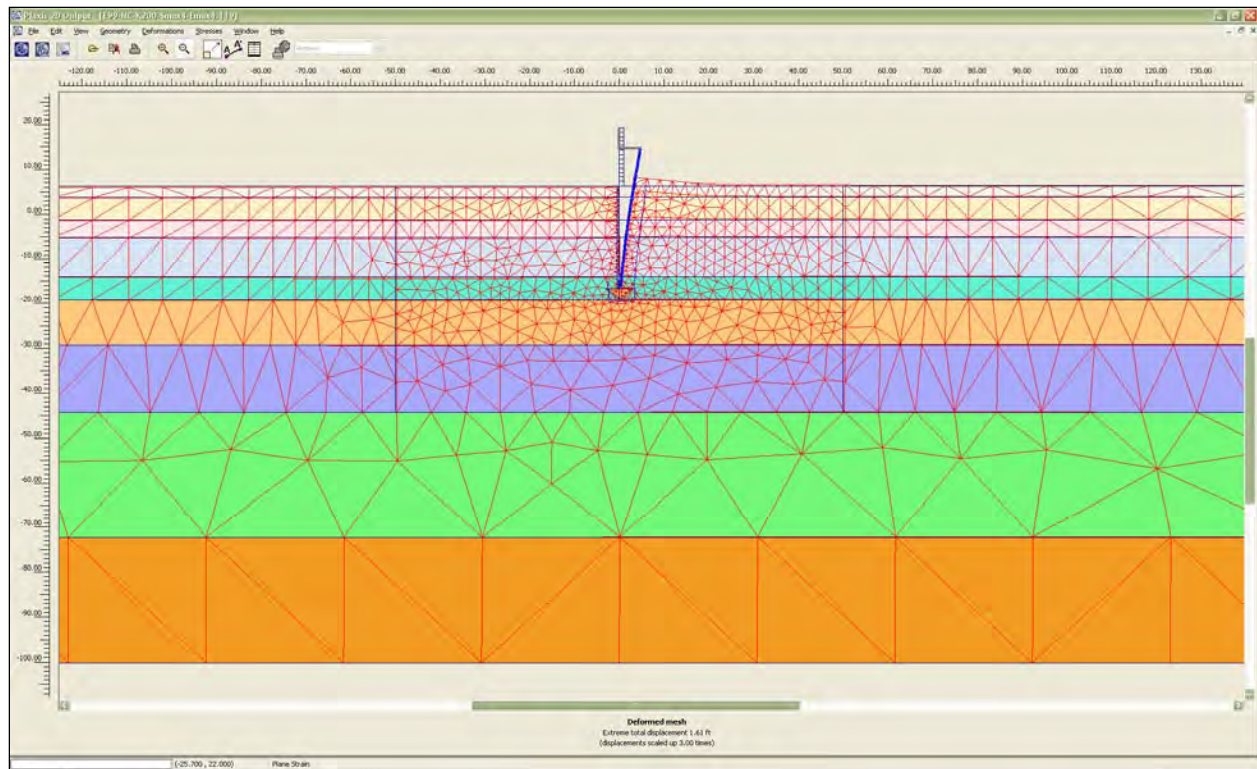


Figure H.5. Total displacements for water el 22.5 ft and gap tip el -15 ft.

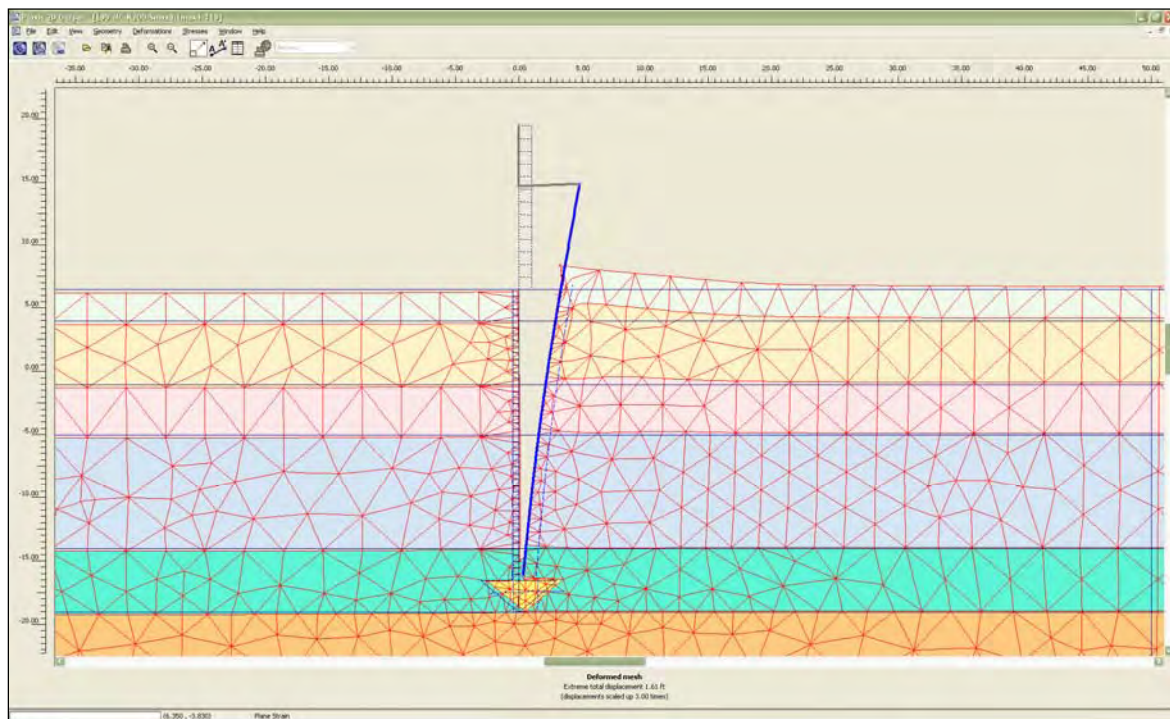


Figure H.6. Enlarged view of total displacements for a water elevation of 22.5 ft and a gap tip elevation of -15 ft.

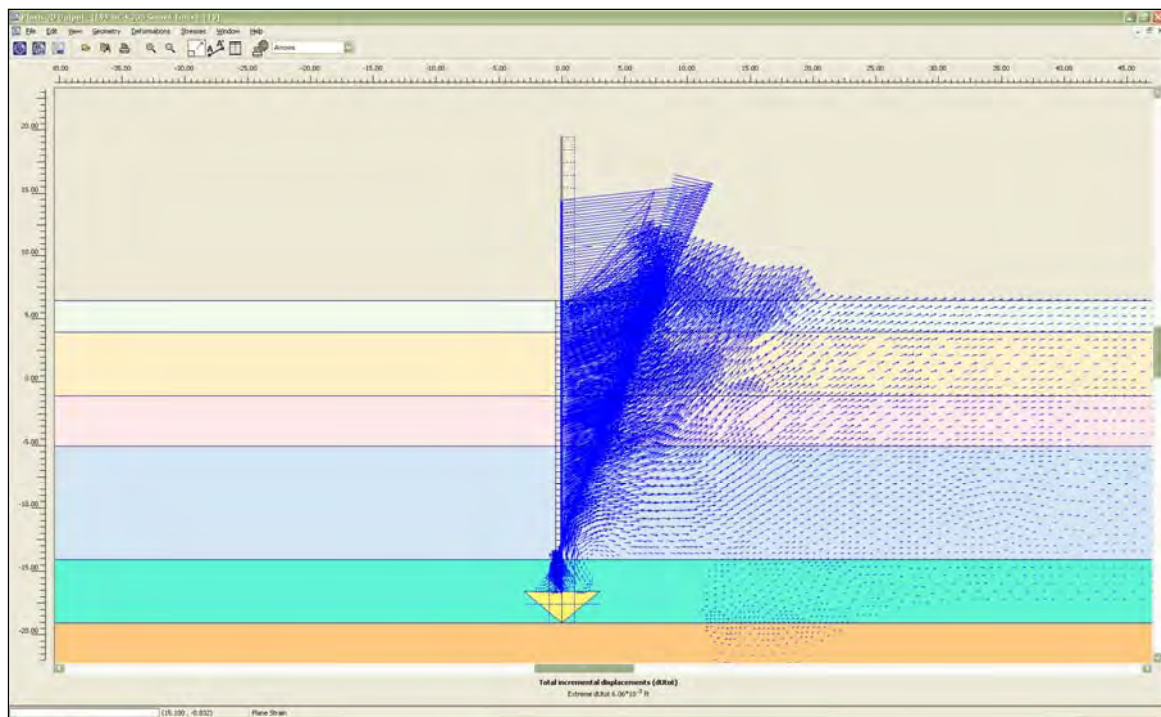


Figure H.7. Vectors of total incremental displacements showing the movement of the soil during the final increment of loading.

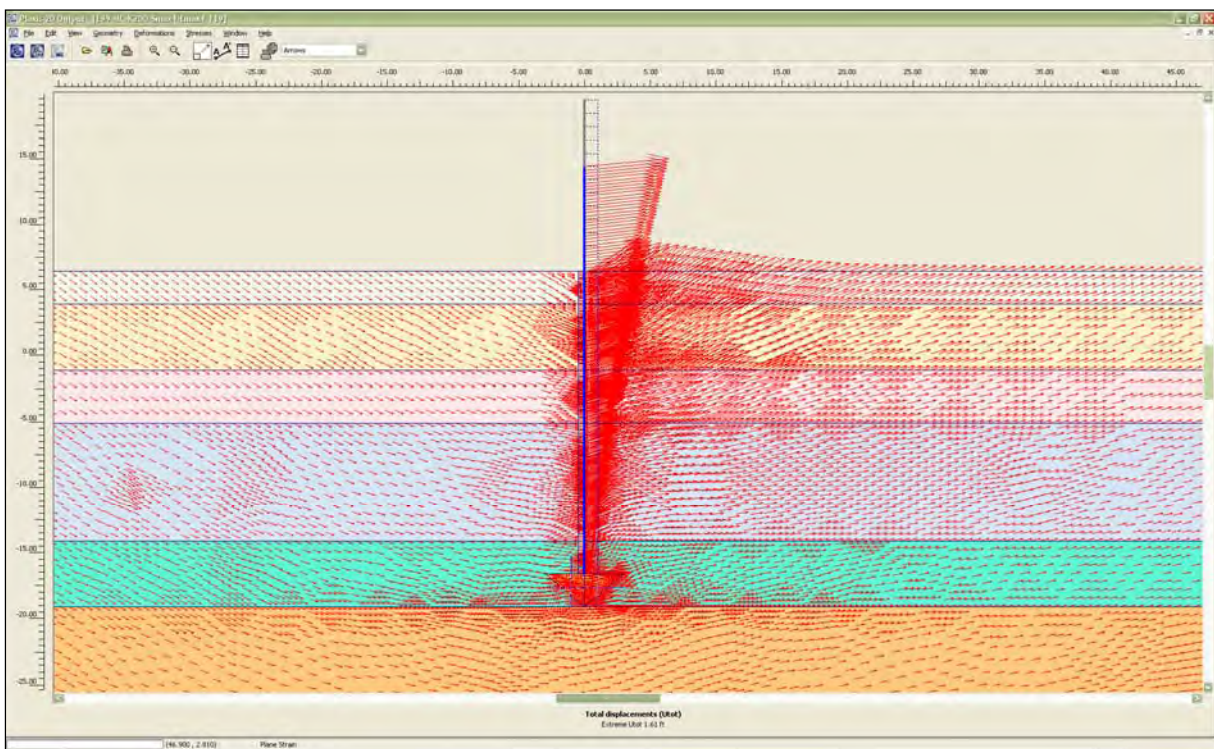


Figure H.8. Vectors of total displacements showing the movement of the soil.

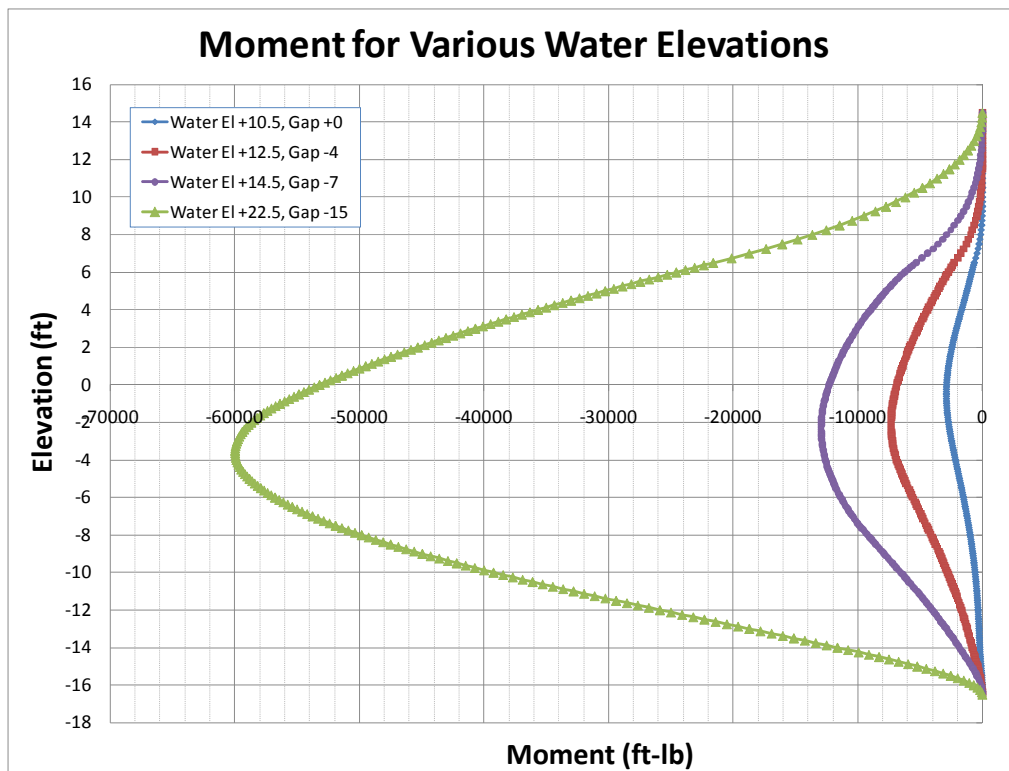


Figure H.9. Comparison of moments at various water elevations.

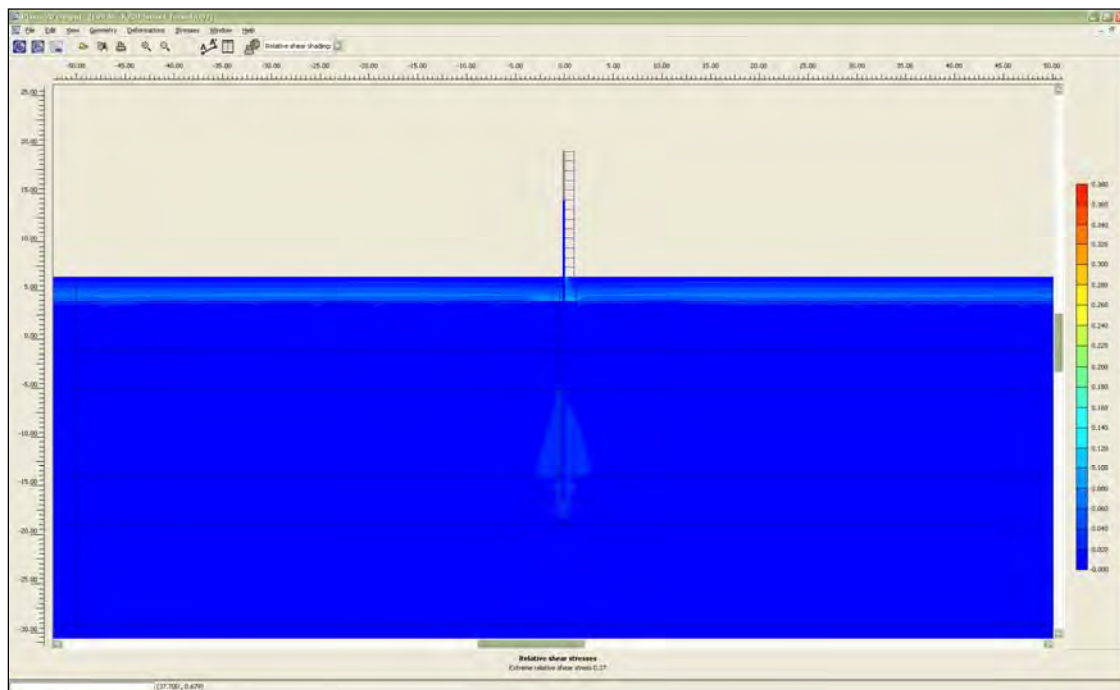


Figure H.10. Relative shear stress after placement of I-wall.

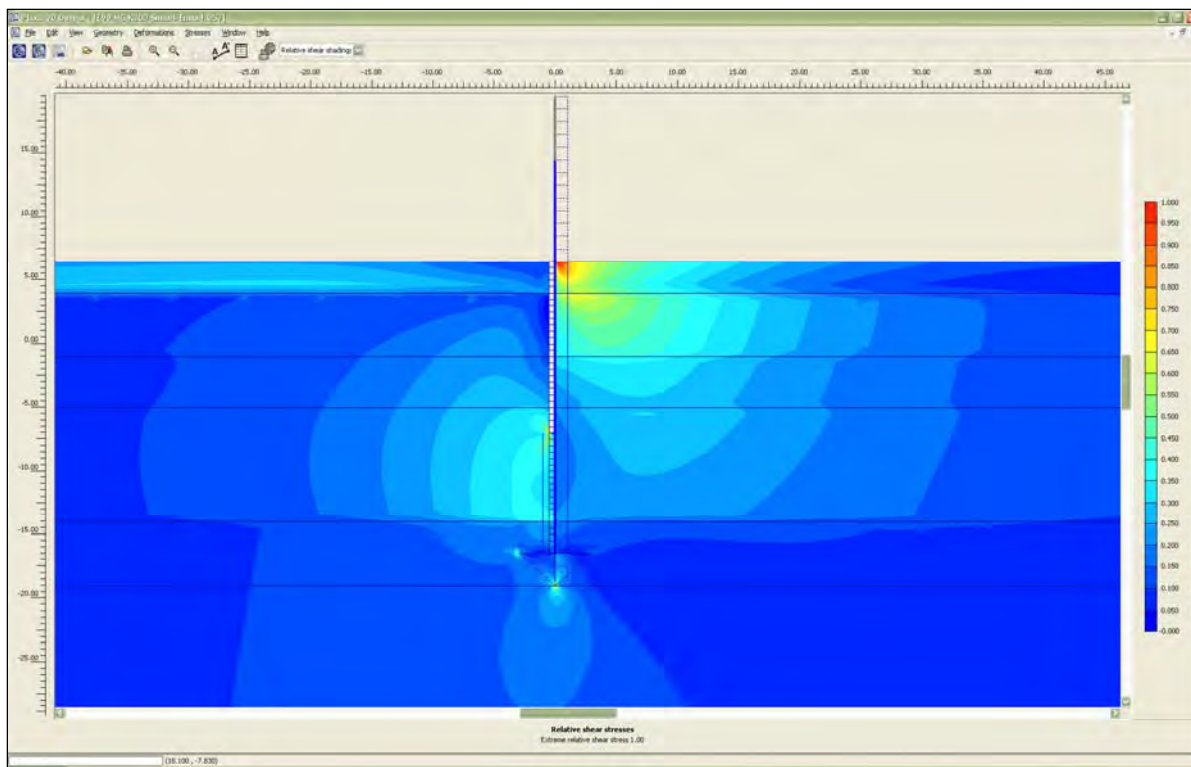


Figure H.11. Relative shear stress for water at el 14.5 ft and gap tip el -7 ft.

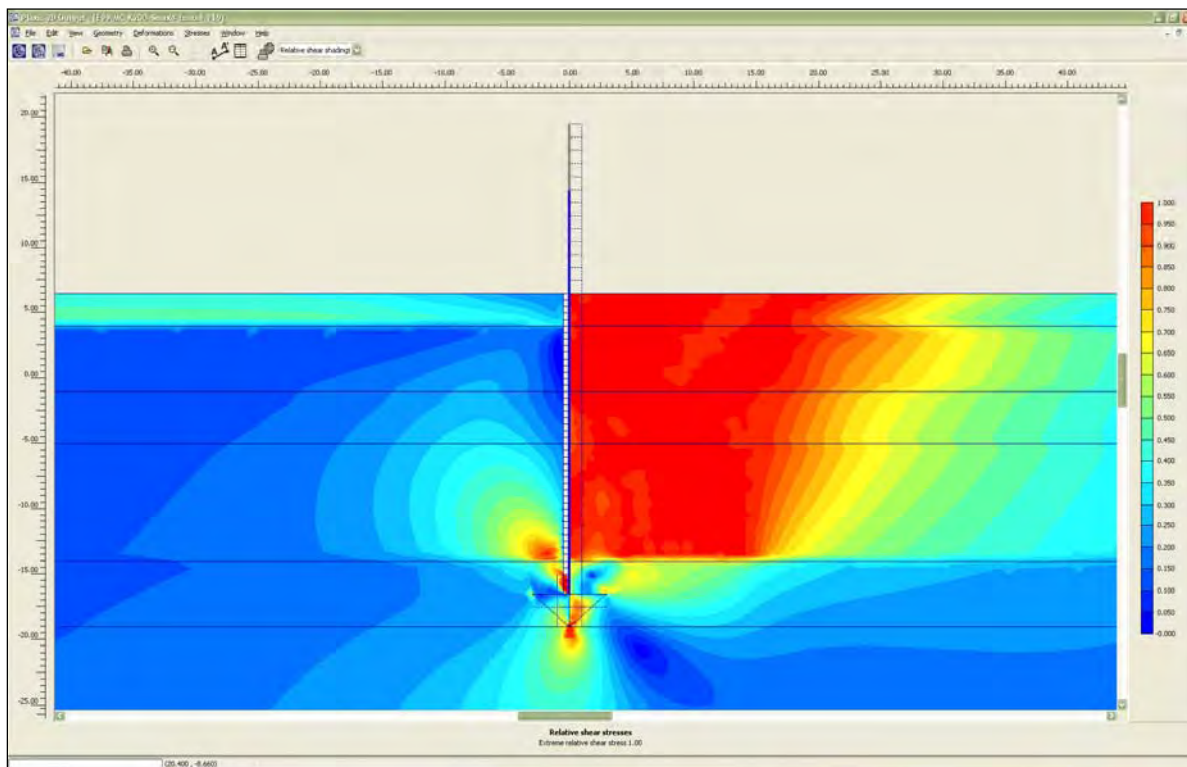


Figure H.12. Relative shear stress for water at el 22.5 ft and gap tip el -15 ft.

available shear stress at failure. The shear stress in the soil increases as the water elevation increases. The shear stress increases in the upper unsaturated layer first, then progresses downward toward the tip of the pile. The shear stresses are greatest on the landside of the sheet-pile wall and at the bottom of the gap. As shown in Figure H.12, for water el 22.5 ft the highly stressed region extends almost to the tip of the sheet pile.

H.5.13 Horizontal earth pressures for MC model

For Figures H.13 through H.15, the flood side is on the right side of the figure and the landside is on the left. This corresponds to the input convention CWALSHT uses.

Figures H.13 and H.14 compare the horizontal earth pressures from PLAXIS acting against the sheet-pile wall to the limiting active and passive earth pressures computed using adhesion as discussed in Chapter 3, Section 3.3.2. The value of adhesion used is 80 percent of the cohesion as discussed in Chapter 3, Section 3.3.4. The limiting earth pressures in the figures are computed for factors of safety equal to 1.0 and 1.5. A factor of safety of 1.0 results in full active and passive earth pressures, while a factor of safety of 1.5 results in increased active and decreased passive earth pressures. Comparing the earth pressures in this manner allows a comparison of PLAXIS earth pressures to values computed from conventional design procedures.

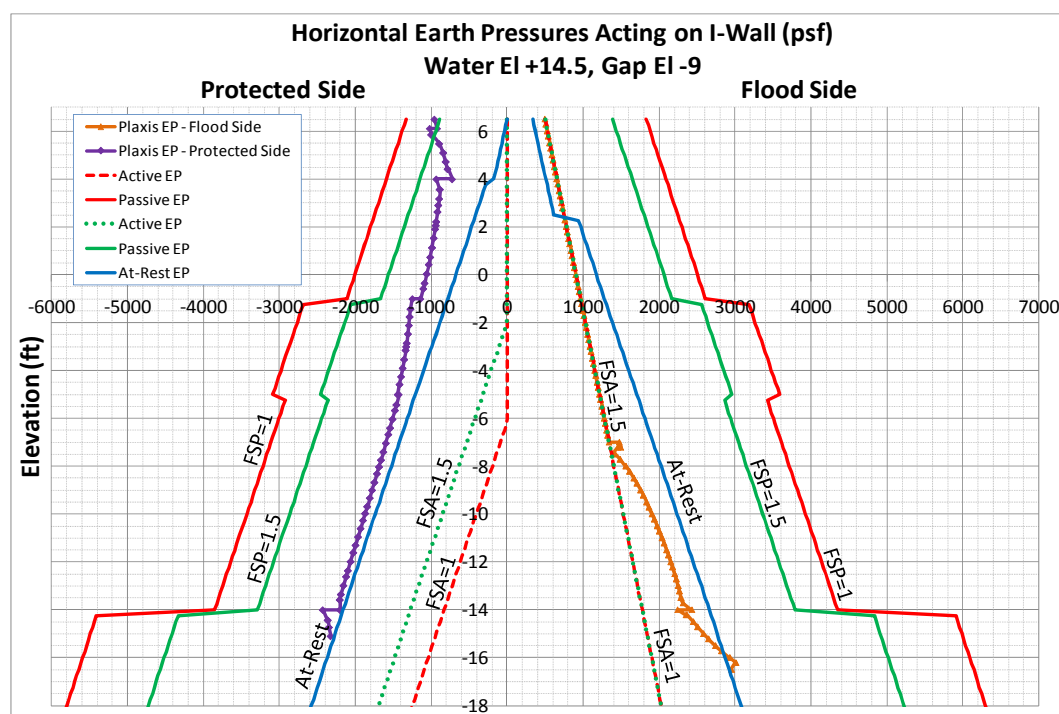


Figure H.13. Horizontal earth pressures for water el 14.5 ft and gap tip el -7 ft.

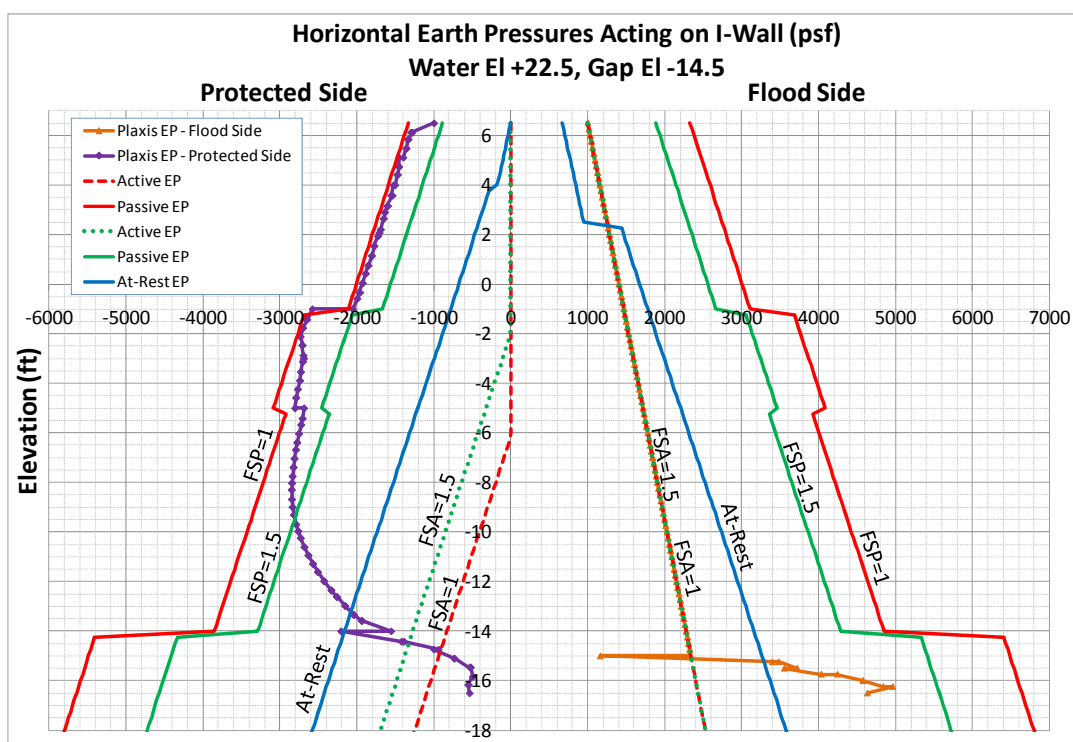


Figure H.14. Horizontal earth pressures for water el 22.5 ft and gap tip el -15 ft.

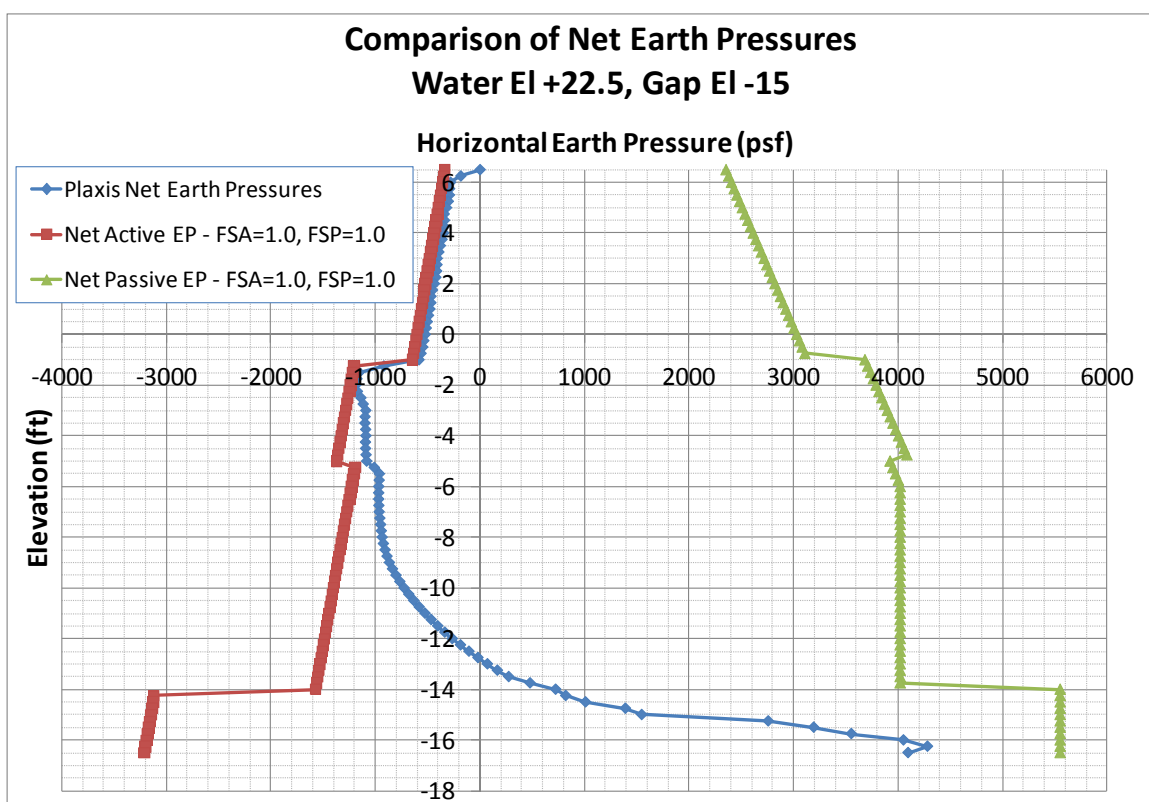


Figure H.15. Comparison of net earth pressures computed from limiting earth pressures and PLAXIS results for water el 22.5 ft.

Figure H.13 displays the earth pressures for water el 14.5 ft and gap tip el -7 ft. For the flood side, the pressures are equal to hydrostatic pressures down to the bottom of the gap. Below the gap, the pressures are close to at-rest earth pressures computed using the assumed values of K_o given in Table 3.9. On the landside, the earth pressures are close to passive earth pressures computed using a factor of safety of 1.5 at el 6.5 ft and decrease with depth to values close to at-rest earth pressures at the tip of the sheet pile.

Figure H.14 shows horizontal earth pressures for water el 22.5 ft. The gap in this case extends to el -15 ft. The earth pressures on the flood side are equal to hydrostatic pressures down to the bottom of the gap. Below the gap, the earth pressures are lower than the at-rest condition caused by the wall moving away from the soil. The earth pressures increase closer to the tip of the sheet pile to passive pressure values computed using a factor of safety of 1.5. On the landside, above el -5 ft, the earth pressures are almost equal to the fully passive earth pressures computed using a factor of safety of 1.0. Below -5 ft, the pressures decrease with depth and become lower than active earth pressures computed using a factor of safety of 1.0.

Figure H.15 compares the net earth pressures computed using limiting earth pressures and the results from PLAXIS for water el 22.5 ft. The limiting earth pressures were computed using a factor of safety of 1.0 for both the active and passive earth pressures for both the flood side and landside of the wall. Net pressures were compared for this water elevation because the movements of the wall were sufficient to produce values of full active and passive earth pressures. As can be seen from the figure, the net earth pressures on the landside compare fairly well to the net active earth pressures. Toward the tip of the pile, the net earth pressures transition from the net active to the net passive earth pressures. The magnitudes of the net earth pressures are slightly less than that of the net passive pressures.

Appendix I: Notation

B.E.	best estimate
c	cohesion
c_a	adhesion
$(C_a)_{min}$	minimum soil adhesion
C_{mean}	mean value of cohesion = mean value of undrained shear strength $(S_u)_{mean}$
C_{min}	minimum value of cohesion = minimum value of undrained shear strength $(S_u)_{min}$
c_{ref}	cohesion
COV	coefficient of variation
d_c	depth of gap
DSS	Direct Simple Shear
EA	axial stiffness
EI	flexural rigidity
$E_{50,ref}$	secant modulus at 50 percent of the principal stress difference $(\sigma_1 - \sigma_3)$
$E_{ur,ref}$	unload-reload stiffness, an assigned hardening soil parameter, which is in the range of three to five times E_{50}^{ref}
$E_{oed,ref}$	oedometer reference stiffness; tangent stiffness modulus at a reference vertical stress equal to p_{ref}
E_{ref}	reference stiffness needed for the Mohr-Coulomb soil model
E_u	undrained secant stiffness
$E_{u,min}$	minimum undrained secant stiffness
$E_{u,max}$	maximum undrained secant stiffness
E_{us}	undrained secant modulus
f_c	adhesion (c_a) divided by the cohesion (c) of the soil

f_{cmax}	maximum ratio of adhesion (c_a) divided by the cohesion (c) of the soil
FS_{Active}	factor of safety applied to the active earth pressures
$FS_{Passive}$	factor of safety applied to the passive earth pressures
FSA	factor of safety applied to active earth pressures
FSP	factor of safety applied to passive earth pressures
H	total head value for a location
H_o	total head value for the initial condition at a location
H_{ss}	total head value for the steady state condition at a location
HS	hardening soil
I	moment of inertia
k	permeability of a soil or hydraulic conductivity (units of length/time)
k_r	relative permeability with respect to the water phase (ranges in value between 0.0 and 1.0)
k_s	coefficient of permeability with respect to the water phase at saturation of 100 percent (units of length/time)
k_w	coefficient of permeability with respect to the water phase (units of length/time)
k_x	horizontal permeability (units of length/time)
k_y	vertical permeability (units of length/time)
K	a factor determined from field measurements and shown in Figure 2.5
K_a	active earth pressure coefficient
K_o	at-rest earth pressure coefficient
K_p	passive earth pressure coefficient
K_r	relative permeability
K_w	water coefficient of permeability
m	fitting parameter
OCR	overconsolidation ratio

p_{pref}	reference pressure
P'_c	preconsolidation pressure
q	surcharges on the soil surface (units of force/length ²)
r	adhesion factor
R	computed indicator that shows how close the total head values are to the drained or undrained condition
R_f	failure ratio
$R_{interface}$	interface strength
S	Section modulus
SSI	soil-structure interaction
S_e	the effective saturation (ranges in value between 0.0 and 1.0)
S_r	residual saturation
S_s	saturation at the maximum moisture content
S_u	undrained shear strength
$S_{u,min}$	minimum undrained shear strength
$S_{u,max}$	maximum undrained shear strength
$(S_u/\sigma'_{vo})_{NC}$	ratio of the undrained shear strength to effective overburden pressure for the normally consolidated condition
$(S_u/\sigma'_{vo})_{OC}$	ratio of the undrained shear strength to effective overburden pressure for the over-consolidated condition
2-D	two-dimensional
TX	triaxial compression
w	weight of sheet-pile per unit area (units of force/length ²)
x	multiple of the standard deviation
x_{min}	multiple of the standard deviation resulting in the minimum undrained shear strength
x_{max}	multiple of the standard deviation resulting in the maximum undrained shear strength
z	the depth at which the pressure is computed, (units of length)

δ	wall friction
γ	the saturated or moist unit weight of the soil for a total stress analysis and the buoyant unit weight for an effective stress analysis (units of force/length ³)
γ_{moist}	moist unit weight of the soil
γ_{sat}	saturated unit weight of the soil
γ_{unsat}	moist or unsaturated unit weight of the soil
ν	Poisson's ratio
ν_{ur}	unload/reload Poisson's ratio
σ	standard deviation
σ_{ha}	horizontal active earth pressure
σ_{hp}	horizontal passive earth pressure
σ_3'	confining stress
σ_v'	effective overburden pressure
ϕ	angle of internal friction
ϕ_p	matric suction head
ϕ_u	undrained angle of internal friction
ψ	dilation angle

REPORT DOCUMENTATION PAGE				Form Approved OMB No. 0704-0188	
Public reporting burden for this collection of information is estimated to average 1 hour per response, including the time for reviewing instructions, searching existing data sources, gathering and maintaining the data needed, and completing and reviewing this collection of information. Send comments regarding this burden estimate or any other aspect of this collection of information, including suggestions for reducing this burden to Department of Defense, Washington Headquarters Services, Directorate for Information Operations and Reports (0704-0188), 1215 Jefferson Davis Highway, Suite 1204, Arlington, VA 22202-4302. Respondents should be aware that notwithstanding any other provision of law, no person shall be subject to any penalty for failing to comply with a collection of information if it does not display a currently valid OMB control number. PLEASE DO NOT RETURN YOUR FORM TO THE ABOVE ADDRESS.					
1. REPORT DATE (DD-MM-YYYY) September 2012		2. REPORT TYPE Final		3. DATES COVERED (From - To)	
4. TITLE AND SUBTITLE Flood and Coastal Storm Damage Reduction Program: Complete Soil-Structure Interaction (SSI) Analyses of I-walls Embedded in Level Ground During Flood Loading				5a. CONTRACT NUMBER	
				5b. GRANT NUMBER	
				5c. PROGRAM ELEMENT NUMBER	
6. AUTHOR(S) Michael E. Pace, Kevin Abraham, and Robert M. Ebeling				5d. PROJECT NUMBER	
				5e. TASK NUMBER	
				5f. WORK UNIT NUMBER	
7. PERFORMING ORGANIZATION NAME(S) AND ADDRESS(ES) Information Technology Laboratory U.S. Army Engineer Research and Development Center 3909 Halls Ferry Road Vicksburg, MS 39180-6199				8. PERFORMING ORGANIZATION REPORT NUMBER ERDC/ITL TR-12-4	
9. SPONSORING / MONITORING AGENCY NAME(S) AND ADDRESS(ES) U.S. Army Corps of Engineers				10. SPONSOR/MONITOR'S ACRONYM(S) USACE	
				11. SPONSOR/MONITOR'S REPORT NUMBER(S)	
12. DISTRIBUTION / AVAILABILITY STATEMENT Approved for public release; distribution is unlimited.					
13. SUPPLEMENTARY NOTES					
14. ABSTRACT <p>This report extends the 2007 investigation of I-wall performance during flood loading to I-walls located in regions of the United States outside New Orleans, Louisiana. Specifically, this study investigates I-walls embedded in level ground consisting of four different soils that are stronger and stiffer than the fine-grained New Orleans soils that were inspected during the 2007 Interagency Performance Evaluation Task Force (IPET) study. A focus of the study summarized in this report is the investigation of the development of a zone of separation along the flood side of the soil-to-I-wall interface. The effects of this zone of separation on the resulting deformation and stress conditions in the soil regime on both the flood side and landside of the I-wall system were then examined. This study is restricted to level soil flood wall sites. The landside is referred to as the protected side in some figures in this report.</p> <p>This investigation relies on a complete soil-structure interaction (SSI) method of analysis. In this procedure, the soil foundation, I-wall, and interface between the I-wall and the soil (on both sides of the I-wall) all are modeled using finite elements; both the soil and interface properties are modeled as nonlinear materials; and flood loadings are incrementally raised to the design flood pool elevation. A hydraulic fracturing criterion is applied to determine if a gap develops on the flood side of the I-wall and if it propagates down the soil-to-I-wall interface during the incremental flood loadings.</p> <p>Soil stresses, the level of mobilized shear strength, gap depth, I-wall deflections, shear forces, and bending moments internal to the sheet piling are computed in the complete SSI analyses at the incremental flood elevations.</p> <p>Results presented in this report will be used to prepare a U.S. Army Corps of Engineers (USACE) guidance document for flood I-walls.</p>					
15. SUBJECT TERMS Complete soil-structure interaction (SSI) analysis I-walls			Levees Hurricane Katrina Flood and Coastal Storm Damage Reduction Program Water Resources Infrastructure Research Program		
16. SECURITY CLASSIFICATION OF:			17. LIMITATION OF ABSTRACT	18. NUMBER OF PAGES 371	19a. NAME OF RESPONSIBLE PERSON
a. REPORT Unclassified	b. ABSTRACT Unclassified	c. THIS PAGE Unclassified			19b. TELEPHONE NUMBER (include area code)